Md. Nazrul Islam
André van Amstel *Editors*

India II: Climate Change Impacts, Mitigation and Adaptation in Developing Countries

Springer

Springer Climate

Springer Climate is an interdisciplinary book series dedicated to climate research. This includes climatology, climate change impacts, climate change management, climate change policy, regional climate studies, climate monitoring and modeling, palaeoclimatology etc. The series publishes high quality research for scientists, researchers, students and policy makers. An author/editor questionnaire, instructions for authors and a book proposal form can be obtained from the Publishing Editor. **Now indexed in Scopus® !**

Md. Nazrul Islam • André van Amstel
Editors

India II: Climate Change Impacts, Mitigation and Adaptation in Developing Countries

🖋 Springer

Editors
Md. Nazrul Islam
Department of Geography and
Environment
Jahangirnagar University
Savar, Dhaka, Bangladesh

André van Amstel
Environmental Systems Analysis (ESA) Group
Wageningen University (WUR)
Amerongen, The Netherlands

Dedicated
To my only daughter
SABABA MOBASHIRA ISLAM
(Only daughter of Professor Dr. Md. Nazrul Islam)

Preface

Climate diplomacy is the practice and process of creating a international climate change regimen and ensuring its effective operation. Climate change is now among the key drivers that perpetuate poverty in the coastal region of the Bay of Bengal. The Intergovernmental Panel on Climate Change (IPCC) concludes South Asia and the Coastal Region of Bay of Bengal as among the world's most vulnerable regions. The second chapter attempts to understand the significant changes of LULC cover and identify the changing pattern of natural vegetation due to innumerable cyclonic storm surges along the coastal areas of the Indian Sundarbans using multi-temporal, remotely sensed data. For this purpose, three Landsat 8 satellite imageries, including January, May, and December 2021, have been selected to perform the supervised image classification. Thus, normalized difference vegetation index (NDVI), soil adjusted vegetation index (SAVI), and land surface water index (LSWI) have also been taken into consideration to identify the crop health pattern of the study area before and after super cyclonic storms. Currently, the incidence of floods are increasing due to the variability of the weather and the variable nature and amount of rainfall. There are many rivers in the Duars and Barind region of West Bengal and its lowlands, which cause severe flooding during the monsoon season. However, due to the changing and complex nature of this flood, it is not possible to measure and predict it. This article highlights flood susceptibility and vulnerability zones along the Mahananda river basin through the frequency ratio (FR) model. Flood-prone areas along the Mahananda river basin have been identified, using various parameters and machine learning algorithms. The flood susceptibility model has also been validated using the receiver operating characteristic curve (ROC). The flood vulnerable map constructed with the FR model is very accurate for this river basin with strong positive relation.

Many coastal lands have been converted into inland fisheries due to saltwater intrusion. The land use and land cover have been classified using the supervised classification technique and maximum likelihood algorithm. 13.73 km^2 of agricultural land was decreased and 13.45 km^2 of the inland fishery was increased in this

study location. The relationship with land surface temperature (LST) and normalized difference salinity index (NDSI) showed a high negative correlation, the R^2 value was 0.45. The build-up land also increased 8.3 km^2 in the Gosaba area. Basically, south, south-east, and eastern parts of this area have been identified for huge soil salinity during field survey, and also the spectral indicators show such results. Results were helpful for administrators, local planers, and agricultural departments for delineation of sustainable food security of this area. The fifth chapter of this book shows that the Pindar basin is situated at higher ranges of the Kumaun Himalayas and comparatively less worked from climate change point of view. This basin's main glaciers are Pindari, Kafni, Bidalgwar, Mrigthuni, and Buriagal. The current trend of the surrounding basins shows that a majority of glaciers have sustained a decrease in this area at an accelerating rate. It is evident from the analysis that the average retreat rate of Pindar glacier was higher at 38.19 m/year from 2000 to 2010 but reduced to 55.41 m/year during 2010–2018.

Snow cover fraction or the fractional snow cover is the fraction of an area covered with snow against the total area. Today, Climate change became an issue throughout the World that proportionally affects the snow cover. Surface water and ground water is used for agricultural, industrial, and domestic purposes. Rainfall and corresponding runoff generated are important hydrological processes which depend on the local physiographic, climatic, and biotic factors. Remotely sensed data provides valuable and real-time spatial information on natural resources and physical parameters. Due to climate change and human interference with the river systems, flood risk has also increased. Flood losses can be reduced by proper floodplain management. Watershed means a naturally occurring hydrologic unit that contributes storm runoff to a single waterway classified on the basis of its geographical area. The present study investigates the anthropogenic factors that shift the ecological status (ES) of wetlands in the SKD because fewer surveys work. Seventy-five chosen wetlands were surveyed by a range of methods at five different districts, such as Alappuzha, Ernakulam, Kottayam, Thrissur, and Palakkad district. Results revealed that mostly hydrologically isolated wetlands, few semi-parched over in the summer. Dominant forms of wetlands were 5 acres in size. The human disturbance scores (HDS) showed that wetlands mainly in the Alappuzha district were high impacted (HI), followed by wetlands in Palakkad district, which were mid impacted (MI). However, the rest of the wetlands in other districts were the least impacted (LI) category. Overall, the population around the wetland habitat was 500 individuals were common in all wetlands. The Pearson correlation results revealed a statistically significant, positive interaction between the wetland habitat population and the HDS scores noted in riverine ($r = 48,.058$, $p <= 0.687$) and palustrine wetlands ($r = 13,.817$, $p > 0.000$).

Strom water management under climatic vulnerability is gaining significant attention in urban areas of the world. The analysis and design of urban storm water drainage/channel/stream/nallah system under non-stationary extreme rainfall intensity is a challenging task in any area. Apart from this, more attention is required to develop possible methods and techniques for alternate design of storm drains in fast growing urbanization. This research describes hydrological and hydraulic

comparison between storm water management model (SWMM) and modified rational method (MRM) for design peak discharge and forecast peak flow estimation in a Mega Industrial Park (MIP), Bidkin, Aurangabad, India. The Intergovernmental Panel on Climate Change (IPCC) CMIP5 models of Representative Concentration Pathways (RCP 2.6, RCP 4.5, RCP 6 and RCP 8.5) are used for the future climate change scenarios. Remote sensing data is used for land use and land cover types like water and vegetation area detection. Land surface temperature (LST) is an essential aspect in global climate change studies, calculating radiation budgets, heat balance studies, and also estimating the climate change scenario on a particular area. Landsat multi-temporal imageries in the period between 2000 and 2020 are used to identify the water area change in southern parts of North 24 Parganas district, West Bengal. The results from the field are based on 50 household surveys, where farmers above 40 years were selected based on purposive random sampling. Focused group discussions were also held with a group of age-old farmers apart from the interview schedule. The data collected was later validated with the meteorological data available from the regional center to see how scientific the locals' perception was. The results from the study highlight that people perceive climate change as a real threat to agriculture based on their experience and local knowledge.

Gridded rainfall data of 0.50×0.50 resolution has been investigated to draw a conclusion regarding long-term dimensional and temporal trends on an annual and seasonal scale in the state located in Southern India. The various statistical methods such as Mann-Kendall trend test and Theil Sen's slope test were adopted to analyze the data besides departure analysis, which was performed to determine the extent of precipitation deficit and for ascertaining the drought years. The change point year has been ascertained to be 1956 by homogeneity test for the state. The annual mean precipitation was estimated to be 1069 mm. Precipitation is an essential component of the hydrological cycle, and its variability is the principal determinant of irrigation practices and other water developmental works. In the present study, gridded rainfall values of $0.5° \times 0.5°$ resolution spanning 115 years (1901–2015) were taken for the recently formed Telangana state in India for analysis of annual and seasonal variability. The average annual precipitation varied between 691.64 and 1141.01 mm. The north and north-eastern regions of Telangana were the most fed regions during the monsoon season, contributing 79% of the annual rainfall. Further, the departure analysis of rainfall revealed 14 excess years, 77 normal years, 22 deficient years, and 2 scanty years for the state. Mann–Kendall test and Sen's slope test revealed an overall significant positive trend in most grid points, and the slope of the trend was lower in the northern regions for the annual rainfall series. Monsoon (89%) and post-monsoon series (59%) depicted a significantly positive trend. Climate change has put tremendous impact on the environment in the current scenario. The consequences are extensive consequences on atmosphere, agronomy, water resources, biome, natural reserves, budget, biodiversity, and social security. Odisha, lying on the eastern coast of India along the Bay of Bengal, with a coastline of 480 kilometers, is always vulnerable to climate change in terms of heavy storm like cyclones, beach erosion, coastal flooding, storm swell, and denudation. This state has scores of agro climatic sectors which require improvement in the shape of diverse reworking

approaches keeping pace with the on-going scenario of climate change. Adaptation strategies such as agriculture, fisheries and animal husbandry, water, health, and coastal and disaster risk management have been formulated looking at vulnerability, food security, and other parameters.

Savar, Dhaka, Bangladesh   Md. Nazrul Islam

Amerongen, The Netherlands   André van Amstel

Contents

About the Editors

Md. Nazrul Islam is a permanent professor in the Department of Geography and Environment at Jahangirnagar University, Savar, Dhaka, Bangladesh. Prof. Nazrul has completed his PhD from the University of Tokyo, Japan. Besides, he has completed 2-year standard JSPS postdoctoral research fellowship at the University of Tokyo, Japan. Prof. Nazrul's fields of interest are environmental and ecological modeling; climate change impact on aquatic ecosystem; modeling of phytoplankton transition; harmful algae; marine ecosystems dealing with hydrodynamic ecosystems coupled model on coastal seas, bays, and estuaries; and application of computer based programming for numerical simulation modeling. Prof. Nazrul is an expert on scientific research techniques and methods to develop the models for environmental systems analysis research. Prof. Nazrul also visited as an invited speaker several foreign universities in Japan, the USA, Australia, UK, Canada, China, South Korea, Germany, France, the Netherlands, Taiwan, Malaysia, Singapore, and Vietnam. Prof. Nazrul has been awarded "Best Young Researcher Award" by the International Society of Ecological Modeling (ISEM) for his outstanding contribution to the field of ecological modeling, 2013, Toulouse, France, and he has also been awarded "Best Paper Presenter Award 2010" by SautaiN in Kyoto, Japan. He has also been awarded the "Best Poster Presenter Award" in the Techno Ocean Conference, Kobe City Exhibition Hall, Kobe, Japan.

Prof. Nazrul has made more than 40 scholarly presentations in more than 20 countries around the world, authored more than 140 peer-reviewed articles, and written 17 books and research volumes. Currently, Prof. Nazrul has published an excellent textbook entitled *Environmental Management of Marine Ecosystems* jointly with Prof. Sven Erik Jorgensen by the CRC press (Taylor & Francis). He has also currently published several excellent book volume entitled: *Bangladesh I*

& II: Climate Change Impacts, Mitigation and Adaptation in Developing Countries, *India I: Climate Change Impacts, Mitigation and Adaptation in Developing Countries* Springer Publication, the Netherlands & Germany. Prof. Nazrul is currently serving as an ***executive editor-in-chief*** of the journal *Modeling Earth Systems and Environment*, Springer International Publications (Journal no. 40808). E-mail: nazrul_geo@juniv.edu

André van Amstel is an assistant professor at Wageningen University and Research, the Netherlands. Andre studied physical geography and planning in Amsterdam and has a long-standing expertise in integrated environmental assessment. He contributed to the development of Integrated Model to Assess the Global Environment at the Institute of Public Health and the Environment in the Netherlands. He is particularly interested in the global environment and the risk of a runaway greenhouse effect by methane from melting of the permafrost in the Arctic. Andre contributed to the IPCC 2006 Guidelines on Agriculture, Forestry and Land use and as such contributed the Nobel Peace Prize 2007 for Al Gore and the IPCC. Since 2014, he is a member of the Nordforsk Scientific Advisory Board for the Arctic Council of Ministers on Arctic Integrated Environmental Research. E-mail: andre.vanamstel@wur.nl

Chapter 1
Climate Change Diplomacy, Adaptation, and Mitigation Strategies in South Asian Countries: A Critical Review

Md. Nazrul Islam, Sahanaj Tamanna, Md. Noman, Al Rabby Siemens, S. M. Rashedul Islam, and Md. Shahriar Islam

Abstract Climate diplomacy is the strategy and technique for building and implementing an international environmental framework, which is now one of the leading reasons for deprivation in the Bay of Bengal's coastal belt. South Asia and the Bay of Bengal Coastal Region are among the highly endangered regions due to climate change impact and natural clamaties, according to the Intergovernmental Panel on Climate Change (IPCC). Southeast Asia will be one of the world's most vulnerable regions to climate change unless countries make dramatic cuts in greenhouse gas pollution and ensuring to reduce the environmental degration. Global warming poses a threat to food security, hobbles economic growth, prompts political instability, and catalyzes pandemics like Covid-19 severity. The government and policy makers are trying to fix the climate issues and to develop some mitigation strategies but the initiatives are not working well. Because the initiatives are based on the belief that considerable ideological commitment is required at the international, regional, and county level in South Asian nations in order to further enhance awareness of environmental disruption and security and to obtain support for preventative measures. Climate change might have a significant influence in South Asia, and then it will affect regions in different ways depending on how it is perceived spatially and temporally. The region encompasses several different climatic conditions spread over a wide and diverse geographic area. Landscapes in the region include arid areas subject to severe droughts, low-lying coastal areas subject to flooding and coastal erosion, islands whose survival is challenged by the expected sea-level rise, tropical zones subject to increasingly frequent and devastating cyclones, and mountainous ranges affected by the melting of glaciers. Apart from

Md. N. Islam (✉) · Md. Noman · A. R. Siemens · S. M. R. Islam · Md. S. Islam
Department of Geography and Environment, Jahangirnagar University, Savar, Dhaka, Bangladesh
e-mail: nazrul_geo@juniv.edu

S. Tamanna
Bangladesh Environmental Modeling Alliance (BEMA), A Non-Profit Research Organization, Dhaka, Bangladesh

taking early steps for climate change adaptation, South Asian country has enacted any laws or regulations to directly address climate change adaptation. Despite the considerable progress that the Government of Bangladesh and the Bangladeshi people have made, they face continuous challenges associated with climate change. Though the SAARC has taken several initiatives on regional cooperation in the areas relating to climate change that have a bearing on adaptation, India can still play a vital role to develop a smart policy for climate change adaptive capacity in South Asia.

Introduction

South Asian countries are among the most vulnerable globally to the impacts of climate change. Extreme climate-related events-heatwaves, storms, floods, fires and droughts affect more than half of the region's population every year and continue to burden South Asian countries' economies (Unicef 2021). Bangladesh, India and Pakistan are among those most at risk of the impacts of climate change, threatening their health, education, and protection, according to a new UNICEF report launched today. In addition Nepal and Sri Lanka are among the top 65 countries most impacted globally. The hydrologic cycle is becoming more intense as a consequence of global warming. Across many areas, this means heavy rainfall and floods, and also more extreme droughts (Ghazi et al. 2016; Gogoni et al. 2017; Edge 2020). It has an impact on precipitation pattern. Precipitation is expected to increase in upper latitudes, whereas it is expected to reduce in the subtropics (Shah 2009; Shidore 2020; Maizland 2021). Climate change will have a negative influence on many people's health and lives. Extreme events and deteriorating circumstances are likely to force many individuals to relocate, either partially or totally, to another hamlet, municipality, province, or country (Bhattacharyya and Michael 2012; Parvaiz 2021). Through the International Solar Alliance (ISA), the Kigali Amendment to the Montreal Protocol, the International Coalition for Disaster Resilient Infrastructure (CDRI), and the Leadership Group for Industry Transition, India is leading global efforts to create reasonable environmental standards (Skodvin 2000; Aggarwal et al. 2013; Singh et al. 2016). Rate of deforestation, particularly in the Bay of Bengal region, is having an effect on economy, farming, and ecosystems, as well as limiting economic prospects for the rural population (Revi 2008; Rong 2010; Ojha et al. 2014; Akram and Hamid 2014; Anon 2018; Bhatta 2019; Basumatary 2020; Huq 2021). Coastline and mountainside soil degradation in South Asia will accelerate in the next decades as a result of increased extreme weather events caused by climate change (Boykoff 2010; Bhatta and Aggarwal 2016; Khanna et al. 2017). Though India's electricity sector has been the main source of greenhouse gases emission, the country's industries and oil consumption have also seen considerable increases in CO_2 production as the economy picks up (Lal 2004; Cruz et al. 2007; Singh 2016).

Consequently, India came in number 10 with a score of 63.98 out of 100. India is placed 27th out of 57 countries in the field of renewable energy (Karmacharya 2007; Kumar and Viswanathan 2012; Abbas et al. 2016; Ahsan et al. 2018; Klare 2020; Aggarwal 2008). Energy has established as the leading source of greenhouse gases, contributing approximately two of total output, trailed by agricultural (20%) and industrial activities (10%) (Garg et al. 2007; Milkoreit 2015).

The climate change impact mitigation and adaptation operations are based on the belief that strong political commitment at the international, regional, and local levels is essential to further develop knowledge of the subject and stability and to obtain support for prevention (Ojha 2012; Carius et al. 2017). If one considers an entity, the Bay of Bengal Initiative for Multi-Sectoral Technical and Economic Cooperation (BIMSTEC), a regional multilateral independent organization in 1997, provides a good foundation for dealing with these issues how we can mitigate the climate change impact by the regional cooperation (Kumar and Parikh 1998; Smit et al. 1999; Mirza 2007; Laborde et al. 2012; Mall et al. 2019). However, BIMSTEC's aim of deepening regional cooperation will be more likely to accomplish if its representatives (Bangladesh, Bhutan, India, Myanmar, Nepal, Sri Lanka, and Thailand) prioritize the organization, provide enough resources, or implement reforms to strengthen its strengths (Table 1.1) (Boykoff 2010; Dinda 2014; Bhatta and Aggarwal 2016; Khanna et al. 2017; Dutta 2020).

The Himalayan Ranges go through the northern section of the peninsula of India, and the Bay of Bengal runs through the southeast. The Indian Ocean surrounds it to the southern part, and the Arabian Sea encircles it to the southwest (Karmacharya et al. 2007; Alam and Dash 2011). The surface area is approximately 3,280,000 km^2. Climate patterns differ greatly from one place to the next (Singh and Abdullah 2016). Whereas the regional climate has a significant impact on the temperature gradient between different seasons in the northern province, the climate in the coastal areas is moderate all year with plenty of precipitation (Lal et al. 2010; Sharma and Tomar 2010). Precipitation pattern differs from one place to the next. Average rainfall varies greatly, ranging from 13 mm to 1187 mm. Bangladesh is particularly bordered to the northwest, north, and northeast by India. To the southeast, it shares a border with Myanmar, while to the south, it confronts the Bay of Bengal (Alam and Hamid 2014). The Himalayan peaks border the country to the north, and even the Tropic of Cancer cuts across the country's midsection. It has a land area of around 147,570 km^2 (Karmacharya 2007; Kumar and Viswanathan 2012; Abbas et al. 2016; Ahsan et al. 2018; Klare 2020; Aggarwal 2008). Bangladesh is largely a low-elevation flat plain, with the exception of the Northern Province, which is limited by the Himalayan Mountain range, as well as the northeastern and southeastern parts, which are bordered by hill areas. Eighty percent of the country is in the floodplain of three river systems (Boykoff 2010; Bhatta and Aggarwal 2016; Khanna et al. 2017).

Table 1.1 Scenarios of climate change in India and possible mitigation options

Sl.	Changes in the climate	Informed materials	Yield materials	Action materials	Sources/ references
1	Excessive temperature	Greenhouse effect has already been affecting India.	The west coasts of India and southern India are expected to experience a change to high-temperature climatic zones, which would have considerable agricultural implications.	Need to action for mitigation and adaptation with natural hazards and disasters that are occurred frequently.	Chaudhary and Aryal (2009) and Das and Bandyopadhyay (2015)
2	Precipitation patterns	After the 1950s, there has been a decrease in monsoon precipitation.	The summer monsoon of India will become exceedingly uncertain if mean global temperatures climb by 2 °C.	Developments to hydrometeorological weather prediction systems, as well as the construction of flood warning systems.	Smit et al. (2000) and Agarwal et al. (2021)
3	Droughts	Research shows that portions of South Asia have been harsher, with an increasing number of droughts, since the 1970s.	Agricultural production is anticipated to plummet by the 2040s as a result of excessive temperatures.	Drought-resistant crops developed through research and innovation can help mitigate several of the harmful effects.	Sathaye et al. (2006), Ravi (2008) and Ojha (2012)
4	Underground water	Rain-fed agricultural production accounts for more than 60% of India's farming, making the country extremely reliant on	Increased demand for water from a population explosion, more sophisticated lifestyles, as well as the services sector and industries, is	It will be necessary to promote the optimal use of groundwater supplies.	Tänzler (2018) and Sharma (2021)

Table 1.1 (continued)

Sl.	Changes in the climate	Informed materials	Yield materials	Action materials	Sources/ references
		underground water.	predicted to decline significantly.		
5	Ice melting	Polar ice caps in the Karakoram range and the northwestern Himalayas are melting at an alarming rate.	Streams in the Indus and Brahmaputra are projected to climb in the spring-time when-ever the snows melt, then decrease in the late spring and summer.	To profit from greater river flows in the spring and mitigate for decreased flows later, significant expansions in water-holding capacity would be required.	Sahu and Mishra (2013) and Zafarullah and Huque (2018)
6	The increas-ing of the ocean level	Mumbai appears to have the world's greatest pop-ulation exposed to catastrophic floods, with major por-tions of the city established on reclaimed land below the high-tide level.	Ocean warming, tropical storms, and riverine floods are all threats to Kolkata and Mumbai, which are both densely inhabited regions.	Where necessary, coastal embankments may need to be constructed, and coastal regulation zone codes will need to be applied consistently.	Kumar (2014) and Singh et al. (2021)

How Will Climate Change Affect South Asia?

Changes in climate could have a significant influence in South Asia and will impact countries differently. The region encompasses several different climatic conditions spread over a wide and diverse physiographic and geographic area (Kumar 2014; Akram and Hamid 2014; Anon 2018; BHatta 2019; Basumatary 2020; Huq 2021; Singh et al. 2021). Landscapes in the region include arid areas subject to severe droughts, low-lying delta, coastal areas subject to flooding and coastal erosion, islands whose continued existence is affected by the projected rising of the sea level, tropical zones subject to increasingly frequent and devastating cyclones, and mountainous ranges affected by the melting of glaciers (Mirza and Ahmad 2005; Agarwal et al. 2021). The Intergovernmental Panel on Climate Change (IPCC) assessment gives a bleak outlook for South Asia, projecting warmer temperatures,

extended monsoon seasons, and more droughts as total global warming rises by about 1.5 °C within the next 20 years (IPCC 2001, 2007; Chaudhary and Aryal 2009). Coast regions in Bangladesh, India, Pakistan, and Sri Lanka are all threatened by rising water levels or flooding. Afghanistan, Bhutan, and Nepal, which are landlocked, are facing temperature increases, drought, and melting glaciers (IPCC 2001, 2007; Chaudhary and Aryal 2009; Ahmed et al. 2019). The Maldives, a densely packed island country, is located in a territory and may be inundated in the not-too-distant period.

Because many of its countries' populations reside along the coast, they are more vulnerable to sea-level rise and extreme weather events, and the South-Asia region is one of the most vulnerable to the effects of climate change (Boykoff 2010; Bhatta and Aggarwal 2016; Khanna et al. 2017). The region is often regarded very extremely vulnerable to environmental disasters because of its dense population and significant poverty levels. According to a 2009 World Bank research, more than half of South Asians have been affected by at least one natural catastrophe in the previous two decades, resulting in the deaths of more than 200,000 people and losses of more than US$45 billion (Isaksen and Stokke 2014). In the long run, however, the consequence of glacier melting on Bhutan and Nepal, as well as rising sea levels on the Maldives, is projected to grow increasingly acute (Sterrett 2011; Agarwal et al. 2021).

And according to the World Bank, approximately 700 million people, or close to half of South Asia's inhabitants, have been impacted by at least one climate-related catastrophe in the recent decade. According to the research tank German Watch's 2020 Global Climate Risk Index, India and Pakistan are among the 20 countries most affected by climate change in the twenty-first century (IPCC 2001, 2007; Chaudhary and Aryal 2009).

The Himalayas sustained the greatest losses as a result of these abrupt meltwater pulses, but there is no quantitative assessment of GLOF (Glacier Lake Outburst Floods) risk. The peak discharge for a certain return time is used to express the threat from Himalayan glacier lakes. GLOF hazard is three times higher in the Eastern Himalayas than in any other Himalayan area (Karmacharya 2007; Kumar and Viswanathan 2012; Abbas et al. 2016; Ahsan et al. 2018; Klare 2020; Aggarwal 2008). GLOF threat is determined by the extent of the predictability of lake outbursts and the expansion of glacial lakes which should be better recognized in flood hazard analyses. Considering the rising trends in population, construction, and hydroelectric developments in the Himalayan highlands, estimates of future danger from meteorological floods must account for high runoffs during lake outbursts (Stalley 2013; Veh et al. 2019). The climatic vulnerability of the territory poses a security risk. As water scarcity worsens, tensions between India, Pakistan, and China over shared rivers are likely to rise. The Indus River, which flows downstream from Indian-controlled Kashmir, is Pakistan's principal supply of surface water (Kugelman 2021). Global warming might deepen the complaints of Pakistani Baloch militants and Indian Naxalite terrorists, who both accuse governments of stealing water and other essential materials (Akram and Hamid 2014; Anon 2018; BHatta 2019; Basumatary 2020; Huq 2021).

However, widespread climate-induced migration might be the most powerful destabilizing factor. Without proper climate-friendly government actions and mitigation strategies, a 2018 World Bank report predicts roughly 40 million climate migrants in South Asia by 2050, along with more than 13 million in Bangladesh only. Despite these restrictions, the report estimates that approximately 20 million climate migrants would be displaced by 2050 (Karmacharya 2007; Kumar and Viswanathan 2012; Abbas et al. 2016; Ahsan et al. 2018; Klare 2020; Aggarwal 2008). Additionally, rural-to-urban migration may result in resource shortages in cities, increasing the likelihood of radicalism among those who lack basic necessities. According to the IPCC assessment, urbanization will exacerbate heat waves and floods. Ethnic Pashtuns escaping floods in Pakistan, Muslims uprooted by drought in India, and Rohingya refugees fleeing flooded towns in Bangladesh might exacerbate communal violence and bloodshed (Taheripour et al. 2018; Kugelman 2021).

Climate Change Impact and Vulnerability in India

Climate change is one of today's most difficult concerns that must be addressed. Climate change-related dangers such as sea-level rise, storm surge, floods, and coastal erosion threaten the metropolis (Sathaye et al. 2006; Ravi 2008; Ojha 2012). Climate change threatens all 612 districts of India, but 100 districts, primarily in the nation's east, are particularly susceptible. As per this comprehensive risk assessment, 123.35 km^2 (24%) of Mumbai's areas are classed as composite vulnerable (Murthy et al. 2011; Tänzler 2018; Sharma 2021). They are typically found around the seaside. Within the risk zones, inland flood-affected areas from previous floods cover 37.13 km^2, accounting for about 30% of the defined most susceptible regions (Boykoff 2010; Bhatta and Aggarwal 2016; Khanna et al. 2017; Arora-Desai 2021). Built-up, barren, woodland, vegetation, and mangrove zones are among the remaining susceptible places. The greatest concerning impact would be in the 44 km^2 of built-up areas, which account for around 35% of the sensitive zones (Venkateswarlu and Shanker 2009). According to the Intergovernmental Panel on Climate Change, global temperatures have already risen to 1.1 °C over preindustrial levels and are expected to rise to 1.5 °C in the next two decades (IPCC 2001, 2007; Chaudhary and Aryal 2009). Global warming is predicted to have a bigger influence on India in the future, with an increase in the frequency, severity, and length of heat waves. The monsoon may become more erratic. Droughts and floods may become more common. More sea-level rise may occur in the Indian Ocean. Tropical cyclones may also become more regular (Jat et al. 2016; Khadka 2018; Kreutzer 2017; Jayaram 2021; Khalae 2021).

The IPCC working group report issues dire warnings about global climate risks. The predicted two-degree rise in global temperatures may occur sooner than expected. It has the potential to have a significant influence on India, particularly in agriculture, health, and water security. India is faced with the task of dealing with such consequences. The very next two decades will be critical (Murthy et al. 2013;

Xie and Jia 2017; Saryal 2018). The southern zone of India is the most vulnerable to extreme climate events and their compounding impacts, followed by the eastern, western, northern, north-eastern and central zones. 59 and 41 per cent of the total districts in the eastern and western zones of India are highly vulnerable to extreme cyclone events (Boykoff 2010; Bhatta and Aggarwal 2016; Khanna et al. 2017; Mohanty and Wadhawan 2021). Due to low per capita income, social inequality, and a large reliance on agriculture, India is particularly vulnerable to high heat. Heat stress will cause India to lose 5.8% of its working hours by 2050, equating to 34 million full-time jobs out of a total of 80 million worldwide (Unicef 2021). Agriculture and construction, India's two largest jobs, would face the brunt of this productivity loss (Mirza 2007; Sahu and Mishra 2013; Zafarullah and Huque 2018). Over the last 5 years, India's overall standing on the index has shifted. However, it has always been the country with one of the five largest economic losses as a result of climate change. It has also recorded the highest number of deaths as a result of extreme weather events in four of the last 5 years.

Vulnerabilities and Adaptive Strategies in Developing Countries

South Asia's adaptability policies have already been fragmented thus far, with no clear link connecting national climate change plans and strategies and current disaster risk reduction, agricultural, and other related policies (Boykoff 2010; Bhatta and Aggarwal 2016; Khanna et al. 2017). This mismatch is due in part to a lack of fundamental clarity and in part to the continuous argument over what constitutes adaptation and what defines excellent, long-term development (Table 1.2). And there is agreement across South Asia that climate change will have a significant impact, there is still a lack of awareness at the local level about what those consequences would be but also how people can adapt. This knowledge has been impeded by a paucity of meteorological data and modeling (Karmacharya 2007; Kumar and Viswanathan 2012; Abbas et al. 2016; Ahsan et al. 2018; Klare 2020; Aggarwal 2008). South Asia is facing major threats from rising sea levels and an increase in the frequency of natural disasters, such as floods, drought, cyclone, storms, and monsoon irregularities.

Rapid urbanization has further aggravated the issue, which may soon become deplorable as a result of massive inflow of 'climate refugees' to ill-equipped cities (Jat et al. 2016; Khadka 2018; Kreutzer 2017; Jayaram 2021; Khalae 2021). It is not yet too late to be gloomy; instead, swift and effective interventions in places where South Asia is susceptible can make a huge impact. To deal with the realities of climate change, mitigation and adaptation methods at the global, regional, and local levels are required. South Asian nations may better negotiate with the international community if they act as a unit (Islam et al. 2009). Numerous international nongovernmental organizations (NGOs) have begun to build CCA programs in

Table 1.2 Evolving approaches to climate change adaptation and mitigation strategies in developing countries in South Asia

Feature	1990s	2000s	2010s	2020
Ultimate intent	Mitigating the risks and consequences of climate change.	Minimizing the risks and uncertainty associated with climate change.	Reducing climate risks and impacts with socioeconomic improvements.	Taking steps to mitigate the dangers and create a worldwide co-operation to do so.
			Taking use of socioeconomic progress to mitigate climate risks and effects.	To ensure ecological restoration.
Encompassing area	Using a sector-based strategy and focusing on a single place.	Approach is sector-based, although adaptability is incorporated into sectoral planning.	Approaches that are cross-sectoral and cross-border have begun.	Over time and place, a global mindset, attitude, and strategy are developing.
Main focus	Protective measures include coping methods and the protection of individuals who are most sensitive to climate threats and have limited adaptive ability.	Coping mechanisms and the avoidance of harmful measures as a result of threats to climate-sensitive livelihoods.	Building adaptive capability, modifying social interactions to counteract prejudice, and underlying social and political vulnerability are all transformative concepts Nair (2019).	Adapting to living in a changing environment entails making adjustments to the current or anticipated future climate. The focus is to lessen our vulnerability to climate change's negative consequences (Sudan 2019).
Operations	Activities seek to address impacts exclusively associated with climate change: Provision of social services and social transfers (food/cash), including safety nets.	Climate risk management: Efforts aimed at incorporating climate-related data into judgment.	Building reaction capacities: Actions aim to create stable problem-solving mechanisms.	To create adaption programs that cover various aspects of environmental and sustainable development, such as the use of renewable energy sources.
			Addressing the causes of vulnerability: Efforts aimed at reducing poverty and other nonclimatic stresses that put individuals at risk.	

Source: After modified and adopted from Rasul and Sharma (2014), Davies et al. (2013) and Calow et al. (2011)

various South Asian nations. From 'stand-alone' initiatives to making adjustments to climate change that are fully integrated into development programs, these programs and methodologies differ greatly (Sterrett 2021).

Current State of Climate Change Adaptation and Mitigation Strategies in South Asia

South Asian countries have advanced to different degrees in their adaptation to climate change in relation to nonstructural interventions, structural resilience building, fiscal actions, financial actions, and risk management. First, all South Asian countries have developed a national climate change action plan and disaster management (Jat et al. 2016; Khadka 2018; Kreutzer 2017; Jayaram 2021; Khalae 2021). These nonstructural interventions involve developing guidelines and operating frameworks and action plans to help guide both ex-ante resilience building and postdisaster resilience (Akram and Hamid 2014; Anon 2018; BHatta 2019; Basumatary 2020; Huq 2021). These plans are quite granular in nature, invariably containing sectoral action plans for each vulnerable sector. Sri Lanka is the only South Asian country to have officially released its National Adaptation Plan (NAP), while the rest have made progress toward parts of the process (UNCCC 2019). Some countries like India have also encouraged their states to prepare their own action plans and are requiring them to be revised at regular intervals.

Nonstructural Interventions and Structural Resilience Building

Dams, flood levies, ocean wave barriers, earthquake-resistant structures, and evacuation shelters are all common structural techniques for disaster risk reduction. Building regulations, land-use planning legislation and their enforcement, research and assessment, information resources, and public awareness programs are all examples of nonstructural approaches (Karmacharya 2007; Kumar and Viswanathan 2012; Abbas et al. 2016; Ahsan et al. 2018; Klare 2020; Aggarwal 2008). Note that the term 'structural' is used in a more limited meaning in civil and structural engineering to refer only to the load-bearing structure, with other components such as wall cladding and interior fittings being referred to as 'non-structural' (UNDDR 2020).

Apart from taking early steps for climate change adaptation, South Asian country has enacted any laws or regulations to directly address climate change adaptation. Examples of such policies in other countries include National Building Codes that stipulate natural-disaster-proof physical infrastructure and land regulations to prevent land degradation (Jat et al. 2016; Khadka 2018; Kreutzer 2017; Jayaram 2021; Khalae 2021). Starting in 2019, both Sri Lanka and the Maldives have taken

initiatives to strengthen the safety and resilience of their built environment through participation in the Building Regulation for Resilience (BRR) Program. As part of the program, the current level of building regulatory capacity of both countries will be assessed, and tailored recommendations will be provided and incorporated into the existing regulatory framework (Karmacharya 2007; Kumar and Viswanathan 2012; Abbas et al. 2016; Ahsan et al. 2018; Klare 2020; Aggarwal 2008). Utilizing such programs and updating the laws and regulations could play a critical role in building adaption capital. In addition, none of the South Asian countries have a cohesive and holistic climate risk financing strategy (Akram and Hamid 2014; Anon 2018; BHatta 2019; Basumatary 2020; Huq 2021). Resilience building would require consistent spending over the next decades that would be facilitated by formulating a financing roadmap.

Fiscal Actions and Policies for Climate Change

Most South Asian countries have limited fiscal space to deal with natural disasters and other climate change shocks to the economy. With potentially increasing frequency and severity of natural disasters due to climate change, coping with shocks such as the COVID-19 pandemic and other crisis situations will become more challenging (Akram and Hamid 2014; Anon 2018; BHatta 2019; Basumatary 2020; Huq 2021). Some South Asian countries have established contingent budgets or reserve funds to cover disaster expenses, usually financed by annual appropriations and drawn down in the event of a disaster. An example is Bhutan's Druk Gyalpo Relief Fund of about US\$ 1.5 million funded through annual budget appropriations by the Ministry of Finance (The World Bank 2020).

For risk-reduction purposes, a majority of the South Asian countries have started to allocate budget or create a resilience fund for adaptation building. An example is Bangladesh's Climate Fiscal Framework (CFF) where about 2% of the national budget was allocated to resilient infrastructure building in 2017 (Akram and Hamid 2014; Anon 2018; BHatta 2019; Basumatary 2020; Huq 2021; IMF 2021). Alternatively, the Maldives levied a green tax of US\$6 per person per day from resorts, vessels, and hotels and US\$3 per person per day from guest houses from 2016, and this revenue could be used for resilience building. However, besides Bangladesh and Nepal, monitoring and tracking climate-related expenditures in the national budget system can be improved across South Asia (CPI 2018; GFLAC and UNDP 2018). This public financial management (PFM) tool would help the governments identify financing gaps, effectively mobilize investment to attain the national action plans, evaluate the climate financing activities, and improve accountability (Karmacharya 2007; Kumar and Viswanathan 2012; Abbas et al. 2016; Ahsan et al. 2018; Klare 2020; Aggarwal 2008). Finally, given the capacity constraints in South Asian countries, adaptation strategies are likely to be cost-effective and efficient when built into, funded from, and made an integral part of the existing schemes and

programs, rather than trying to create new ones and find additional resources for the same.

Financial Actions and Risk Management in South Asia

South Asian countries generally have an underinsurance problem whereby few people have adequate protection in the event of natural disasters. Sri Lanka has the only public national insurance program in South Asia, the National Natural Disaster Insurance Scheme (NNDIS) launched in 2016 (Karmacharya 2007; Kumar and Viswanathan 2012; Abbas et al. 2016; Ahsan et al. 2018; Klare 2020; Aggarwal 2008). The NNDIS covers properties of all uninsured households and small businesses for up to SLRs 2.5 million for damages caused by natural disasters, excluding drought, and lives for SLRs 100,000 per person (UN 2020). Besides the Sri Lankan case, microinsurance for households and farmers is the most common instrument across the region, and these schemes tend to be run by private or nongovernmental organizations with financial sustainability, transparency, and solvency issues (Linnerooth-Bayer and Mechler 2009; Tripathi and Mishra 2017).

Furthermore, no South Asian government has implemented a sovereign parametric insurance plan or issued catastrophe bonds (Cat bonds) to address the rising costs of climate change. A catastrophe bond is an instrument that pays the issuer if a certain disaster risk occurs (Polacek 2018). This lack of take-up in insurance can primarily be attributed to the high costs and high barriers to access. Pooling insurance or issuance of Cat bond by multiple countries in a region like that of Pacific Alliance Countries Cat Bonds (Chile, Colombia, Mexico, and Peru) can overcome these challenges through economies of scale for insurers, better costs, and diversification for investors (World Bank 2018).

A comparison of the present flood management systems of the three nations is made based on a thorough assessment, and a framework for long-term flood control in the region is proposed (Ashrit et al. 2001; Bansal and Datta 2013, Bhatt et al. 2020; Lazard and Youngs 2021). Bangladesh has been able to build an efficient governance system to address flood dangers, but Pakistan's flood management strategy is mostly inadequate. Missing linkages in policy development and planning procedures, as well as a lack of institutional coordination, are mostly to blame for this deficiency. Bangladesh and India appear to have benefitted from scientific assistance in developing flood management plans (Abbas et al. 2015; Ahmed et al. 2019). Due to its relatively big and sophisticated financial capital market, India is the only country with an active green bond market (Jat et al. 2016; Khadka 2018; Kreutzer 2017; Jayaram 2021; Khalae 2021). While projects are funded with climate benefits, there is a lack of clarity in the banking industry about what constitutes green funding. The Central Bank of Sri Lanka developed a Roadmap for Sustainable Finance in 2019 to address this issue, and this could serve as a model for other South Asian countries that are looking to expand and standardize green financing.

Even within green financing, encouraging projects on climate-change adaptation can help to accelerate resilience building through the private sector.

South Asian countries are making significant headway in adjusting to the new realities of climate change on a piecemeal basis. However, there are insufficient monitoring and tracking of their adaptation spending, as well as a lack of integrated plans to fulfill all of their objectives. Learning and implementing 'best practices' and adaption experiences from other areas and nations will also be critical (Agarwal et al. 2021).

Regional Cooperation in Climate Change

Regional cooperation is among the key principles of sustainable development as exhorted in the Rio Declaration on Environment and Development. As noted by Shukla et al. (2019), the most convincing argument for regional cooperation lies in its potential to sustain economic growth through the regional deployment of shared human, natural, and environmental resources. Countries in a region share the rivers, water bodies, forests, biological and natural resources, as well as culture (Shukla 2003; Rahman 2007; Srivastava 2010). At the same time, countries are diverse in terms of resource endowments, economic development, skill, and institutional capacities, and therefore have different capacities to tackle a problem like climate change. Regional cooperation aids in exploiting the complementarities that exist between the nations in a region to achieve win–win outcomes in terms of development, adaptation, and also mitigation (Shukla 2003; Rahman 2007; Srivastava 2010; Subedi 2010; Devkota 2013; Zafarullah and Huque 2018). This is all true for the South Asian region, given the shared vulnerabilities of the countries to climate change as well as the possibility of exploiting the complementarities of the countries in dealing with the problems.

The SAARC (South Asian Association for Regional Cooperation) has taken several initiatives on regional cooperation in the areas relating to climate change that have a bearing on adaptation. Since 1987, the Heads of State or Government of SAARC at successive summits have reiterated the need to strengthen and intensify regional cooperation to preserve, protect, and manage the diverse and fragile ecosystems of the region, including the need to address the challenges posed by climate change and natural disasters (Subedi 2010; Devkota 2013; Zafarullah and Huque 2018; Rattani 2018a, b). The meetings of the SAARC Environment Ministers and the Technical Committee are the key mechanisms to guide and facilitate the agenda of cooperation. The numerous directives issued by successive SAARC Summits and meetings of the SAARC Environment Ministers provided continued impetus for strengthening and intensifying regional cooperation toward adaptation and building resilience (Thapa 2013). Furthermore, four regional centers have been created to address the diverse aspects of the environment, climate change, and natural disasters, and constitute a framework of SAARC institutions to address climate-related risks and vulnerabilities in the region (Devkota 2013; Zafarullah and Huque 2018). A

brief description of these regional centers and the roles played by them is provided below:

SAARC Disaster Management Centre (SDMC) was founded in 2006 in New Delhi, India, in the context of the December 2004 Indian Ocean Tsunami. Its charter calls for the establishment and enhancement of a regional disaster management system. It also plans to use the regional center to identify and define action objectives for member countries (Rattani 2018a, b).

SAARC Meteorological Research Centre (SMRC) was established in 2005 in Dhaka, Bangladesh, to offer a regional base for weather forecasting and monitoring (Karim 2020). One of the Center's main objectives is to establish a network in member nations that can facilitate data gathering and forecasting (Subedi 2010; Devkota 2013; Zafarullah and Huque 2018).

SAARC Forestry Centre (SFC), a company based in Taba, Bhutan, commenced operations in 2008. It has been researching mountain ecology and creating novel forest resource management approaches. It also has a defined regional focus, collecting data from member states and acting as a clearinghouse for information pertaining to forests and mountains (Centre 2013).

SAARC Coastal Zone Management Centre (SCZMC) was founded in 2005 and is based in Male, Maldives. Since its inception, it has served as SAARC's primary institution for promoting regional integration in coastal zone planning, management, and sustainable development, as well as research, training, and public awareness (Shukla 2003; Rahman 2007; Srivastava 2010).

Can India Lead the Fight Against Climate Change in South Asia?

Climate change has finally taken center stage on the agendas of global fora, and rightly so. All countries, from the United States to China, have reaffirmed their commitment to combatting it. India, too, has taken a tough stance against climate change and is on an amazing path to meet its NDCs (Nationally Determined Contributions) in compliance with the Paris Agreement (Karmacharya 2007; Kumar and Viswanathan 2012; Abbas et al. 2016; Ahsan et al. 2018; Klare 2020; Aggarwal 2008; Rana and Ilina 2021). However, because climate change has transboundary consequences, combating it necessitates collaborative effort. South Asian genecology's sensitivity makes cooperation all the more essential (Dasgupta et al. 2020). Whereas the Indo-Pak conflict has slowed progress via SAARC (South Asian Association for Regional Cooperation), India has recently expressed fresh interest in developing the BIMSTEC (Bay of Bengal Initiative for Multi-Sectoral Technical Cooperation) (Mirza and Ahmed 2005; Sathaye et al. 2006; India Go 2008; Milkoreit 2015). In the future, India may use the BIMSTEC platform to advocate for stronger cooperative action against climate change. Besides combating climate change, migratory steps against climate disasters are crucial too. In the past,

India launched a 'BIMSTEC Disaster Management Exercise,' and it now has a fully operational 'BIMSTEC Centre for Weather and Climate,' which aims to offer early warnings of catastrophes (Ashrit et al. 2001; Bansal and Datta 2013, Bhatt et al. 2020; Lazard and Youngs 2021). Another noteworthy observation is that India's approach to Humanitarian Assistance and Disaster Relief (HADR) has always been centered around its immediate neighborhood, with more than two-thirds of it being directed to South Asia. India readily gives humanitarian help in the form of rescue operations and relief funding in times of humanitarian disasters induced by climate change (ranging from tsunamis to cyclones).

As the countries of South Asia are quickly developing and particularly sensitive to climate change, whatever occurs there will have a significant impact (Karmacharya 2007; Kumar and Viswanathan 2012; Abbas et al. 2016; Ahsan et al. 2018; Klare 2020; Aggarwal 2008). If we cannot properly address the climatic concerns here, there is little hope for the rest of the globe. South Asia is among the most sensitive regions to the effects of climate change increased rates of population expansion and natural resource degradation, as well as relatively high rates of poverty and food insecurity (Sivakumar 2010). The capacity to make a difference comes with the privilege of being the region's largest economy by far. Climate change and global warming have offered India with once-in-a-lifetime chance to aid in the restoration of its ecology and realign regional collaboration and integration toward a more sustainable route to climate change survival (Iwasaki et al. 2009). The region's adaptive reaction does not have to be limited to treating the symptoms of challenges to old economic patterns. Regional economic diversification that is more efficient can produce totally new patterns and supporting infrastructure to replace them.

In terms of climate policy and politics, India is a major player. Although its position on international climate problems has shifted over time, it has remained an active participant. India has become a testing ground for strategies that integrate climate issues into development as a consequence of an interacting link between domestic policy and foreign concepts (Ashrit et al. 2001; Bansal and Datta 2013, Bhatt et al. 2020; Lazard and Youngs 2021). This article looks at how India's politics and climate policy have changed through time. It starts by looking over how India's perception and attitudes about climate change have changed through time, focusing on ethics, climatic effects, India's energy revolution, conservation, and absorption (Dubash et al. 2018). India has cause to be cautious about climate change's effects. Its big population is reliant on climate-sensitive industries like agricultural development for survival. Any decrease in water accessibility due to glacier retreat, rainfall variability, and severe floods in specific places would endanger food security and nutrition, cause the disappearance of ecosystems, including species that support the livelihoods of rural households, and have a negative impact on the coastal region due to sea-level rise and the steadily increasing frequency of extreme events (GWP 2011; Dubash 2013; Belis et al. 2015; Kumar et al. 2016; Bhatta et al. 2017). In contrast to these consequences, achieving critical national objectives relating to environment, healthcare, energy usage, and other systems will have ramifications.

To put it another way, policymakers must move quickly to adapt to climate concerns. South Asia's rising countries have already evolved a strategy for adaptation. State and subnational action plans have been formed in certain countries, such as India, enabling for the inclusion of climate change mitigation and adaptation alternatives into local projects and facility development. Understanding the risks and vulnerabilities of sector and area development projects and programs, as well as adopting socially, environmentally, and economically feasible adaptation and mitigation strategies, are all necessary for increasing resistance to the effects of climate change.

Bangladesh–India Joint Collaboration

Climate change is a serious regional concern for South Asia, which is one of the most vulnerable places to climate disaster (GWP 2011; Dubash 2013; Belis et al. 2015; Kumar et al. 2016; Bhatta et al. 2017). Collective actions for a regional solution will have several benefits, including the pooling of material resources, the sharing of collective information and know-how, capacity-building initiatives, and greater efficacy of activities. The area can potentially attract more climate money through collaborative initiatives. The fight against climate change in South Asia, like anywhere else, is also a fight to protect lives and preserve livelihoods. Merely bilateral solutions will not suffice. A revised regional approach is the need of the hour, and India has the potential to lead it (Rana and Ilina 2021). These really are clear indicators that Bangladesh and India should work together to overcome such severe climate consequences and to strengthen their adaptability and resiliency. Despite multiple pronouncements on climate change and various regional centers for collaboration in research and data collecting, the SAARC (South Asian Association for Regional Cooperation) has not been very productive during the previous two decades (Karmacharya 2007; Kumar and Viswanathan 2012; Abbas et al. 2016; Ahsan et al. 2018; Klare 2020; Aggarwal 2008). Clearly, political will in the area has not been sufficient to overcome the technological barriers to establishing an effective regional platform to tackle climate effects and adaptation (Khan et al. 2021). It's a win scenario for both nations since, in addition to financial assistance, a collaborative push for the Sundarbans is likely to result in a high level of climate adaption plans for the region, probably the most extensive among offshore regions.

Because Bangladesh has a relatively limited amount of high land to which individuals may migrate, relocation to India is the next best choice. With India suffering population pressures in low-lying coastal regions, this new situation creates issues for both administrations (Pandey 2011). The two neighbors must perform cooperative research on the impact of forced migration due to sea-level rise, the number of persons who will be relocated, and potential remedies. India, for example, might identify regions where climate refugees could be housed (GWP 2011; Dubash 2013; Belis et al. 2015; Kumar et al. 2016; Bhatta et al. 2017). India and Bangladesh will have to investigate the prospect of climate refugees migrating from India to other areas of the world (Rahman et al. 2007; Pandey 2011). These

climate refugees should be given with basic necessities such as food, clothing, and medical treatment. The current UN convention on the status of refugees, which dates from 1951, only applies to individuals who fear or escape persecution; it's doesn't apply to persons who cross national boundaries as a consequence of climate change. In view of the current scenario, both nations should together petition the UN to broaden the definition of refugees (Pandey 2011).

India–Sri Lanka Joint Collaboration

India, the home of one of the oldest civilizations, is the largest country in South Asia. It has wide diversity in language, culture, religion, etc. In world politics, India is developing as a worldwide force. India has seven nations on its borders (GWP 2011; Dubash 2013; Belis et al. 2015; Kumar et al. 2016; Bhatta et al. 2017). Pakistan, Bangladesh, China, Afghanistan, Nepal, Bhutan, and Myanmar are the seven nations. India maintains close bilateral ties with Bangladesh, Nepal, and Sri Lanka. Sri Lanka is a 65,525-km^2-large island in the Indian Ocean off the coast of India (Taheripour et al. 2018). The Indian Ocean, the Gulf of Mannar, and the Palk Strait, as well as India and the Maldives, all border Sri Lanka (Edge 2020). Sri Lanka has a history of robust bilateral relation with India. But in recent times, Sri Lanka has become more dependent on China for several economic reasons. Sri Lanka's dependency on China weakens its relationship with India.

India and Sri Lanka have such a long history of cognitive, social, spiritual, and linguistic exchange, and their connection dates back more than 2500 years. Economic cooperation has increased, and collaboration in the spheres of development, education, culture, and defense has increased (GWP 2011; Dubash 2013; Belis et al. 2015; Kumar et al. 2016; Bhatta et al. 2017). Both nations have a broad awareness of significant international concerns (Indian Ministry of External Affairs 2021). But there is another issue which connects India and Sri Lanka, and that is climate change. Climate change is a global problem. But it is affecting South Asian region most comparing other parts of the world. Both India and Sri Lanka are facing a diverse variety of problems because of climate change (Fig. 1.1).

As Sri Lanka is a small tropical island, there is no considerable annual change in temperature due to latitude. Altitude, on the other hand, can cause large regional temperature variations. Average rainfall is decreasing in recent times (Krishnan et al. 2020). Floods and droughts are extreme occurrences showing increasing intensity and frequency (Mfasia 2020). The Asian region is experiencing a 1 to 3 mm/year rise in sea level, which is slightly higher than global norms (Cruz et al. 2007). The above evidences prove that the problems due to climate change cannot be mitigated single-handedly. A united effort can bring fruitful result to make an efficient mitigation plan. Both India and Sri Lanka are susceptible to the effects of climate change (GWP 2011; Dubash 2013; Belis et al. 2015; Kumar et al. 2016; Bhatta et al. 2017). A joint collaboration can bring an impactful result. A pathway to joint collaboration is possible as follows: (a) A proper settlement planning should be made to mitigate the negative impacts of rising sea level; (b) both countries should construct a climate
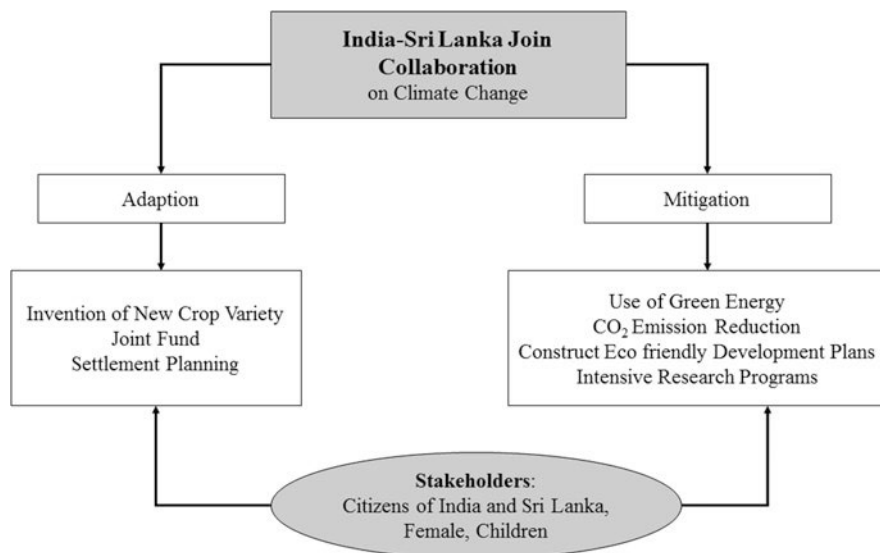
Fig. 1.1 India–Sri Lanka joint collaboration for developing the adaptation and mitigation strategies of climate change impact

refugee fund to properly face the future climate refugee problem; (c) both India and Sri Lanka should give incentives to the green energy sectors (a united effort can make this successful); and (d) intensive joint research programs should be launched by both India and Sri Lanka (Mahe 2019).

India–Nepal Joint Collaboration

Countries in South Asia have been the most sensitive to the consequences of climate change on a massive level. The Himalayas' proximity to this area, particularly in Nepal, Bhutan, and India, has created a notable topographical feature here (SAARC 2008; Wani et al. 2013; Nepal and Shrestha 2015; Roy 2017; Bagale 2020). Every year, more than half of the region's population is affected by extreme climate-related events such as increasing temperatures, floods, storms, wildfires, and droughts, imposing a strain on the economy of South Asian countries (Prabhakar and Shaw 2007; Singh and Abdullah 2016). So some cooperation, i.e., working with someone to create something new or solve a problem, might be a good way to address these challenges. For example, India and Nepal have had long-standing social, historical, diplomatic, political, and economic ties as well as on climate change (O'Brien et al. 2004; Pandey and Jha 2012). Regardless of the fact South Asia is sensitive to climate change, there are various issues among the governments for a variety of reasons, including political, prejudice, and inconceivable elements. Sarada Agreement (1920), Kosi Agreement (1954), Gandak Agreement (1959), and Mahakali Treaty

are only a few of the water accords that the two South Asian neighbors have signed (1996). Nepal is chastised inside the nation for failing to secure its advantages and alleging that all accords favor India (Pittock 2011; Roy 2017; Bagale 2020). The 1850-km combined India–Nepal border passes across five Indian states: Sikkim, West Bengal, Bihar, Uttar Pradesh, and Uttarakhand. The Indian side, on the other hand, says that Nepal's water concerns have become overly politicized which is the cause for the country's failure to reap the advantages of these accords (Bagale 2020).

The Eastern Himalayas are home to a wide variety of plants and animals. Climate change is having an influence on India's, Nepal's, and Bhutan's forests, which are three of the most significant nations in the Himalayan area (Fig. 1.2). Climate change is expected to have a severe influence on forests, resulting in an increase in pest infestations, invasions, and changes in forest types (Nenow 2021). Previously, these areas' efforts were mostly focused on mitigation, but the need to research and foster adaptation has now become clear (Wani et al. 2013; Nepal and Shrestha 2015; Roy 2017). India and Nepal are preparing to sign a memorandum of understanding on environmental preservation, encompassing transborder landscape management and a focus on tigers, elephants, and rhinoceros (SAARC 2008; Wani et al. 2013; Nepal and Shrestha 2015; Roy 2017; Bagale 2020). The 1850-kilometer combined India–Nepal border passes across five Indian states: Sikkim, West Bengal, Bihar, Uttar Pradesh, and Uttarakhand. Several transboundary animal habitats can be found along the shared border (Aggarwal et al. 2019). Although certain stages are stated, there might be a vast number of actions that both parties can take. Nepal and India have a shared orientation to bilateral and global organizations, and so collaborate on most major international problems in the United Nations, the Non-Aligned Movement, and other international forums (Nepal and Shrestha 2015; Roy 2017). Additionally, both nations have been heavily involved in the regional and subregional frameworks of SAARC (South Asian Association for Regional Cooperation), BIMSTEC (Bay of Bengal Initiative for Multi-Sectoral Technical and Economic Cooperation), and Bangladesh, Bhutan, India, and Nepal (BBIN) developed regions in order to
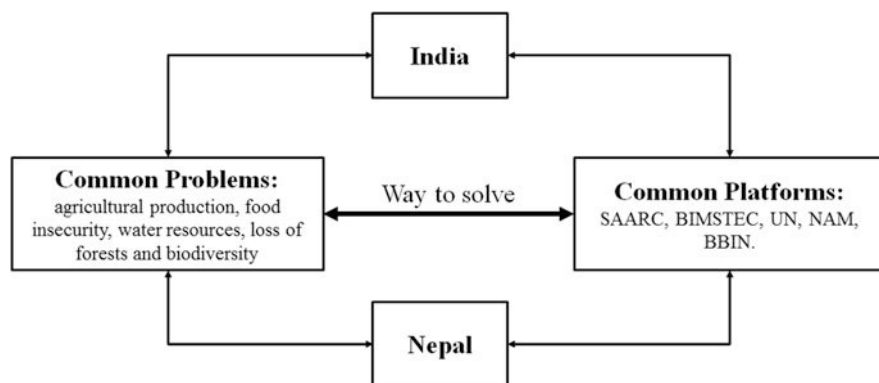
Fig. 1.2 India–Nepal joint collaboration for developing climate change mitigation and adaptation strategies

improve collaboration and economic integration by combining the region's opportunities and interrelatedness (Nepal and Shrestha 2015; Roy 2017).

India–Bhutan Joint Collaboration

India and Bhutan have signed a Memorandum of Understanding (MoU) to improve their environmental collaboration. The signing of the Memorandum of Understanding, according to Union Minister of Environment, Forests, and Climate Change Prakash Javadekar, will open up new channels of bilateral collaboration in areas such as climate change, waste management, and so on (India GO 2011a; Team 2021). The MoU was signed virtually on behalf of India by Prakash Javadekar, Minister of External Affairs and Chairperson of the National Environment Commission Lyonpo, and on behalf of Bhutan by Dr. Tandi Dorji, Minister of Foreign Affairs and Chairperson of the National Environment Commission Lyonpo (India GO 2011b).

According to ministry officials, the MoU between India's Ministry of Environment and Bhutan's National Environment Commission will increase technological, scientific, and management skills, as well as expand environmental cooperation sectors, resulting in a mutually beneficial partnership (Karmacharya 2007; Kumar and Viswanathan 2012; Abbas et al. 2016; Ahsan et al. 2018; Klare 2020; Aggarwal 2008). The Memorandum of Understanding will serve as a venue for bettering Indian–Bhutanese collaboration and encouraging and sharing best practices in areas including air pollution control, waste management, chemical management, and climate change. It also allows the establishment of collaborative ventures in mutually beneficial sectors (Massen 2011; Kumar and Geneletti 2015; Polacek 2018; Lacombe et al. 2019; Team 2021). The MoU serves as a venue for Indian and Bhutanese collaboration and support, as well as the exchange of best practices in areas such as air pollution control, waste management, chemical management, and climate change (Fig. 1.3). It also enables the formation of joint ventures in mutually
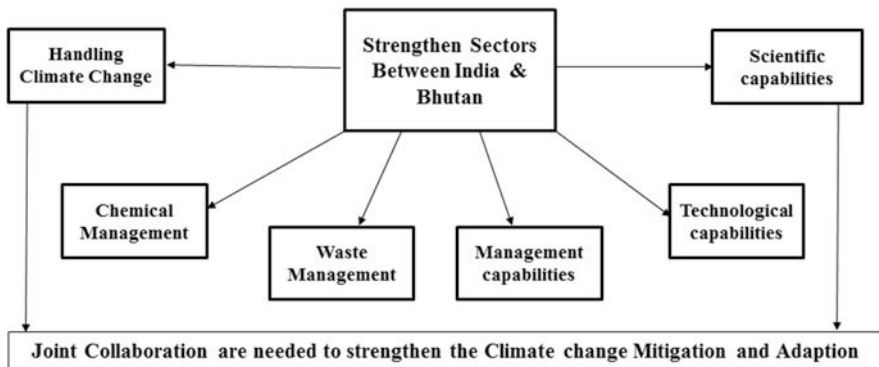
Fig. 1.3 Joint collaboration between India and Bhutan on climate change impact mitigation and adaptation strategies

beneficial sectors. The MoU will also improve technological, scientific, and managerial capabilities, as well as expand environmental cooperation, in order to forge a mutually beneficial partnership between the two countries (Ministry of Environment 2021). India and Bhutan have symbiotic connections, with India expressing a desire to collaborate on environmental issues such as climate change (Rasul and Sharma 2016; Tripathi 2021). The Memorandum of Understanding lays the groundwork for future cooperation and support between India and Bhutan. There will be an exchange of best practices in waste management, air pollution, climate change, chemical management, and other areas. The inked Memorandum of Understanding will also allow for cooperative initiatives in areas of mutual interest (Karmacharya 2007; Kumar and Viswanathan 2012; Klare 2020; Aggarwal 2008). It will improve scientific, technical, and managerial skills (Tripathi 2021). Because the two nations are close allies who are dedicated to climate action, a healthy planet, and a sustainable future, the MoU between India and Bhutan is regarded as a crucial step that will add impetus to the good bilateral ties. The MoU is designed to foster stronger institutional ties between actors engaged in the environmental sector in India and Bhutan (Nenow 2021).

India–Maldives Joint Collaboration

For decades, the Maldives has been seen as a leader in the fight against climate change. Coastal erosion, sea-level rise, saltwater intrusion, and changes in monsoon patterns, which alter rainfall, are all concerns that take time to emerge due to the archipelago's lower elevation. As a result, migration has long been proposed as a way of population adjustment (Stojanov et al. 2016). India's climate is classified under monsoon-type. South and Southeast Asia have this sort of climate. There are, nevertheless, differences in climate patterns inside the region. Climate change is a legitimate cause for worry in India since it threatens the attainment of critical national development goals such as socioeconomic growth, social equity, health, energy supply and usage, and infrastructural facilities.

According to the circumstances at 2010, Maldives will become a carbon-neutral nation within ten-year MOU with the Maldives on climate change and other matters but added that the island needed India's assistance in gaining access to new technologies and data on renewable energy in order to combat climate change (Hindu 2010; Massen 2011; Kumar and Geneletti 2015; Polacek 2018; Lacombe et al. 2019). Both stakeholders will collaborate and work together to preserve their widely recognized ecosystems, address the Maldives and Indian Islands' system vulnerabilities to climate change, strengthen coastal research, and, to the greatest extent possible, coordinate their response in international platforms to research and develop environmental protection and adaptation programs (India 2021). So, the two neighboring countries combine hands and make crucial decisions over the course of a year, and these partnerships are led by the governments of India and the Maldives. Though there have been administrative changes in the two nations, the basic motivation to combat climate change has not changed.

India–Pakistan Joint Collaboration

South Asia is both a major donor and a major victim of climate change. This analysis looks at the region's vulnerabilities, as well as government pledges to cut emissions and strategies to adapt to a changing climate (Massen 2011; Kumar and Geneletti 2015; Polacek 2018; Lacombe et al. 2019). As one of the most vulnerable regions to climate change, there appears to be a pressing need to continue to pursue policies that reduce the region's contribution to global warming and adapt to the consequences of more frequent extreme weather events, ocean warming, and less predictable rainfall and agricultural production through international cooperation (India 2011; Agarwal et al. 2021). The majority of Pakistan is dry to semiarid climatically, with substantial geographical and temporal diversity in climatic indices. Monsoon rains account for 59% of yearly rainfall in Pakistan, making them the country's primary hydro-meteorological source (Farooqi et al. 2005). The impact of climate change and as India and Pakistan are both directly or indirectly affected by global warming, sea levels are predicted to increase and Himalayan glaciers to melt at a quicker than usual rate (Ruffini 2018; Ahsan 2019). More frequent and severe flooding is expected as a result of these consequences. In South Asia, as well as India and Pakistan, climate change is projected to result in decreased rainfall. Such an outcome would be terrible, especially because summer rains account for 90% of India's entire water supply (Shidore 2020). Increased catastrophic flooding and greater temperatures along the Indus River suggest that climate change will create instability between the river's riparian states, India and Pakistan.

However, both India and Pakistan have vowed to be part of the developing international agreement on the need to confront climate change challenges, and they do not have any intergovernmental climate change mechanisms (Rasul and Sharma 2020). Both are parties to the 2015 Paris Agreement, which arose from the United Nations Climate Change Conference in Paris in November–December 2015, which concentrated on climatic concerns and represented the participating nations' commitments to developing solutions (Aggarwal and Sivakumar 2010; Kumar 2014; Anbumozhi 2017; IMF 2021). A parliamentary committee in India has suggested that the government update a 61-year-old agreement with Pakistan in order to account for the consequences of climate change and pollution, particularly on the Indus River, which the two countries share. Renegotiation was necessary to build a framework that tackles 'urgent challenges like as climatic changes, greenhouse effect, and environmental consequence evaluation' on water supply in the Indus basin, according to the committee's report delivered in August 2021 (Parvaiz 2021).

Is India Doing Enough to Combat Climate Change?

Climate change is one of the most pressing global challenges of our day. Recent incidents have vividly demonstrated our increasing vulnerability to climate change's repercussions (Aggarwal and Sivakumar 2010; Kumar 2014; Anbumozhi 2017; IMF

2021). Climate change will impact agriculture, putting food security in jeopardy, as well as sea-level rise and accelerated coastal erosion, increased intensity of natural disasters, species extinction, and the spread of vector-borne diseases (Pandve 2009). The Intergovernmental Panel on Climate Change (IPCC) observed in its fourth assessment report that the earth's climate system has changed on a global and regional scale since the preindustrial era (Massen 2011; Kumar and Geneletti 2015; Polacek 2018; Lacombe et al. 2019). Global mean temperature might climb anywhere between 1.4 and 5.8 °C by 2100. India is one of the most vulnerable countries to climate change (Panda 2009). Climate change is already having a negative influence on this country. One of the most major potential impacts of climate change on India is changes in the monsoon pattern. The average monsoon strength and variability are expected to rise in general, according to numerous studies (Kumar and Parikh 1998; Smit et al. 1999; Mirza 2007; Laborde et al. 2012; Mall et al. 2019). Alongside agriculture, evidence suggests that climate change would have an impact on the occurrence of climate extremes such as cyclones, droughts, and floods in India (Kumar and Parikh 1998; Smit et al. 1999; Mirza 2007; Laborde et al. 2012; Mall et al. 2019). On June 30, 2008, over a year after it was announced, India issued its long-awaited National Action Plan on Climate Change (NAPCC) to mitigate and adapt to climate change. The action plan lays out a series of initiatives that will help India achieve both development and climate change-related goals at the same time. A variety of actions are included in the National Action Plan on Climate Change (NAPCC). It is divided into eight missions, as follows (Pandve 2009; Hsu et al. 2015).

National Solar Mission

To make solar energy competitive with fossil fuels in India, this project aims to promote its use. It will encourage research and development in order to increase the efficiency and affordability of solar power and energy storage technologies.

National Mission for Enhanced Energy Efficiency

The goal of this project is to increase energy efficiency in India's home, commercial, and industrial sectors by establishing an enabling policy environment and supporting innovative business models (Massen 2011; Kumar and Geneletti 2015; Polacek 2018; Lacombe et al. 2019).

National Mission for Sustainable Habitat

The goal of this project is to promote sustainable urban design in India by policy, infrastructure, and research interventions in areas such as buildings, waste management, water resources, and transportation (Rattani, An Analysis on India's National Action Plan on Climate Change 2018a).

National Water Mission

The goal is to maintain a long-term supply of water through saving water, reducing waste, and ensuring an equal distribution of water resources across India (Rattani, An Analysis on India's National Action Plan on Climate Change 2018a).

National Mission for Strategic Knowledge and Climate Change

With the use of research and communication-based efforts, the goal is to develop a complete knowledge system that informs and supports climate change action in India (Rattani, An Analysis on India's National Action Plan on Climate Change 2018a).

National Mission for Sustainable Agriculture

The goal of this project is to improve agriculture's sustainability, productivity, remuneration, and climate resilience in India. Capacity building, research, infrastructural, and institutional interventions in the Indian agricultural industry would help to attain these objectives (Rattani, An Analysis on India's National Action Plan on Climate Change 2018a).

National Mission for Green India

The goal of this project is to maintain, enhance, and restore forests while also responding to climate change with suitable adaptation and mitigation efforts. It aims to increase green cover while focusing on a variety of ecosystem services, including biodiversity, water, biomass, mangroves, wetlands, and essential habitats, as well as carbon sequestration as a side effect (Rattani, An Analysis on India's National Action Plan on Climate Change 2018a).

Conclusion

India, the world's third-largest carbon emitter after China and the United States, has maintained that it is on track to meet its Paris climate agreement target to decrease its carbon footprint by 33% to 35% by 2030 compared to 2005 levels. According to some analysts, the impact of global warming on India's environment has resulted in climate disasters. The expected rise in precipitation, melting glaciers, and expanding oceans have the potential to significantly impact the Indian climate, increasing the frequency of floods, hurricanes, and storms. Climate change consequences in India might result in an additional 50 million poor people by 2040, according to the report, due to falling earnings, higher food prices, and slower economic growth (Aggarwal and Sivakumar 2010; Kumar 2014; Anbumozhi 2017; IMF 2021). The process of creating changes in ecological, social, or economic systems in response to real or expected climatic stimuli, as well as their ramifications or consequences, is known as adaptation. Climate adaptation refers to changes in procedures, policies, or structures to mitigate or counteract potential harms or to take advantage of opportunities related to climate change. It entails making changes to lessen a community's, region's, or activity's susceptibility to climate change and variability. The people of India, Bangladesh, Maldives, and Sri Lanka are the most vulnerable to climate change impacts. But other countries like Pakistan, Afghanistan, Nepal, and Bhutan are not free from risk. Climate change is a problem which has a deep root. It will not only affect the most vulnerable regions but the less vulnerable regions too. Already the countries less vulnerable to climate change are experiencing some severe impacts. So, climate change resilience plan in the Bay of Bengal region is totally worthless without the participation of the citizens of South Asian nations.

References

Abbas A et al (2015) An overview of flood mitigation strategy and research support in South Asia: implications for sustainable flood risk management. Int J Sustain Dev World Ecol 23:98–111

Abbas A, Al-Amer AM, Laoui T, Al-Marri MJ, Nasser MS, Khraisheh M, Atieh MA (2016) Heavy metal removal from aqueous solution by advanced carbon nanotubes: critical review of adsorption applications. Sep Purif Technol 157:141–161

Agarwal R, Balasundharam V, Blagrave P, Gudmundsson R, Mousa R (2021) Climate change in South Asia: further need for mitigation and adaptation. IMF Working Papers, 2021 (217)

Aggarwal PK (2008) Global climate change and Indian agriculture: impacts, adaptation and mitigation. Indian J Agric Sci 78(11):911

Aggarwal PK, Sivakumar MV (2010) Global climate change and food security in South Asia: an adaptation and mitigation framework. In: Climate change and food security in South Asia. Springer, Dordrecht, pp 253–275

Aggarwal P, Pathak H, Kumar S, Sharma P (2013) South Asia perspectives on climate change and agriculture: adaptation options. Handbook of climate change and agroecosystems. In: ICP series on climate change impacts, adaptation, and mitigation, 2, pp 209–222

Aggarwal P, Vyas S, Thornton P, Campbell BM, Kropff M (2019) Importance of considering technology growth in impact assessments of climate change on agriculture. Glob Food Sec 23: 41–48

Ahmed AU, Appadurai AN, Neelormi S (2019) Status of climate change adaptation in South Asia region. In: Status of climate change adaptation in Asia and the Pacific. Springer, Cham, pp 125–152

Ahsan A (2019) Pakistan and India face common threats. Climate change is the biggest one, September 18. Retrieved from Dawn https://www.dawn.com/news/1505534

Ahsan MA, Katla SK, Islam MT, Hernandez-Viezcas JA, Martinez LM, Díaz-Moreno CA et al (2018) Adsorptive removal of methylene blue, tetracycline and Cr (VI) from water using sulfonated tea waste. Environ Technol Innov 11:23–40

Akram N, Hamid A (2014) Climate change and human security in South Asia. Forensic Sci Int 26(2):801–808

Alam K, Dash S (2011) Climate change in the coast of Bay of Bengal: impact, resilience and implication – summary report. Concern Worldwide

Anbumozhi V (2017) Coping with globalization and climate change: lessons learned from pro-poor business in South Asia. In: Corporations and sustainability. Routledge, pp 104–116

Anon (2018) An analysis of India's National Action Plan on climate change. In: Coping with climate change. Center for Science and Environment, New Delhi, p 9

Ashrit R, Kumar KR, Kumar KK (2001) ENSO-monsoon relationships in a greenhouse warming scenario. The American Geophysical Union, Pune

Arora-Desai P (2021, June 24) Mumbai to have its own climate action plan by October. Hindustan Times. https://www.hindustantimes.com/cities/mumbai-news/mumbai-to-have-its-own-climate-action-plan-by-october-101624562450737.html

Bagale DR (2020) Nepal–India water cooperation: consequences of mutuality or hegemony? Water Policy 22(6):1098–1108

Bansal A, Datta S (2013) The impact of climate change in South Asia. In: South Asian security. Routledge, pp 234–250

Basumatary R (2020) Are migrant sending households better off? Evidence from a flood Prone District in North-Eastern India. Asian Man Int J 14(1):77–86

Belis D, Joffe P, Kerremans B, Qi Y (2015) China, the United States and the European Union: multiple bilateralism and prospects for a new climate change diplomacy. Carbon Clim Law Rev 9(3):203–218

Bhatt M, Patel RB, Gleason K, Pandya M (2020) Disaster risk reduction and climate change adaptation in South Asia. In: Oxford research encyclopedia of natural hazard science

Bhatta M (2019) Challenges and opportunities in South Asia. In: New futures for South Asia. Routledge India, pp 21–34

Bhatta GD, Aggarwal PK (2016) Coping with weather adversity and adaptation to climatic variability: a cross-country study of smallholder farmers in South Asia. Clim Dev 8(2):145–157

Bhatta GD, Ojha HR, Aggarwal PK, Sulaiman VR, Sultana P, Thapa D et al (2017) Agricultural innovation and adaptation to climate change: empirical evidence from diverse agro-ecologies in South Asia. Environ Dev Sustain 19(2):497–525

Bhattacharyya A, Michael W (2012) Climate change, migration, and conflict in South Asia: rising tensions and policy options across the subcontinent, Asia-Pacific, Foreign Policy and Security, India

Boykoff M (2010) Indian media representations of climate change in a threatened journalistic ecosystem. Clim Chang 99(1–2):17

Calow R, Bonsor H, Jones L, O'Meally S, MacDonald A, Kaur N (2011) Climate change, water resources and WASH: a scoping study. Overseas Development Institute

Carius N, Speck M, Laub K (2017, March) Regional impact assessment: a methodology to measure the regional value added of trans-sectoral urban planning. In: International conference on smart and sustainable planning for cities and regions. Springer, Cham, pp 253–265

Centre SF (2013) History of SAARC Forestry Centre (SFC): Bhutan. Retrieved from http://www.sfc.org.bt/; http://www.sfc.org.bt/about_us.html

Chaudhary P, Aryal KP (2009) Global warming in Nepal: challenges and policy imperatives. J For Livelihood 8(1):5–14

Climate Policy Initiative (CPI) (2018) Global climate finance: an updated view 2018, CPI works in places that provide the most potential for policy impact including Brazil, Europe, India, Indonesia, and the United States

Cruz RV, Harasawa H, Lal M, Wu S, Anokhin Y, Punsalmaa B, Li CNH (2007) Asia. Climate change 2007: impacts, adaptation and vulnerability, Contribution of Working Group II to the Fourth Assessment Report of the Intergovernmental Panel on Climate Change. Cambridge University Press, Cambridge, pp 469–506

Das K, Bandyopadhyay KR (2015) Climate change adaptation in the framework of regional cooperation in South Asia. Carbon Clim Law Rev 9(1):40–54

Dasgupta S, Wheeler D, Sobhan MI, Bandyopadhyay S, Nishat A, Paul T (2020) Coping with climate change vulnerability in the Sundarbans: lessons from multidisciplinary studies. International Development in F

Davies A, Thompson KA, Giri K, Kafatos G, Walker J, Bennett A (2013) Testing the efficacy of homemade masks: would they protect in an influenza pandemic? Disaster Med Public Health Prep 7(4):413–418

Devkota DC (2013) Regional cooperation: key to climate change adaptation in HKH region. Nepal J Environ Sci 1:27–35

Dinda S (2014) Climate change: an emerging trade opportunity in South Asia. South Asian J Macroecon Public Finance 3(2):221–239

Dubash NK (2013) The politics of climate change in India: narratives of equity and cobenefits. Wiley Interdiscip Rev Clim Chang 4(3):191–201

Dubash N, Khosla R, Kelkar U, Lele S (2018) Annual review of environment and resources. In: India and climate change: evolving ideas and increasing policy engagement, pp 395–424

Dutta S (2020) India offers support to Maldives green energy plan. [Online] Available at https://timesofindia.indiatimes.com/business/india-business/india-offers-support-to-maldives-green-energy-plan/articleshow/79468392.cms

Edge G (2020) Retrieved from global EDGE https://globaledge.msu.edu/countries/sri-lanka

Farooqi AB, Khan AH, Mir H (2005) Climate change perspective in Pakistan. Pak J Meteorol:12

Garg A, Shukla PR, Kapshe M (2007) From climate change impacts to adaptation: a development perspective for India. Nat Resour Forum 31(2):132–141

GFLAC and UNDP (2018). Conducted a review of domestic data sources for climate finance flows in recipient countries which you can access at: https://www.climatefinancedevelopmenteffectiveness.org/sites/default/files/GFLAC-Web.pdf

Ghazi TW, Muniruzzaman ANM, Singh AK (2016) Climate change & security in South Asia. Global Military Advisory Council on Climate Change(GMACC)

Gogoi E, Bahadur AV, del Rio CR (2017) Mainstreaming adaptation to climate change within governance systems in South Asia: an analytical framework and examples from practice. ACT Learning Paper

GWP (2011) Climate change, food and water security in south. Global Water Partnership and International Water Management

Hindu T (2010) Maldives wants India's help in climate change battle. [Online] Available at https://www.thehindu.com/news/national/Maldives-wants-Indiarsquos-help-in-climate-change-battle/article16815781.ece

Hsu A, Moffat AS, Weinfurter AJ, Schwartz JD (2015) Towards a new climate diplomacy. Nat Clim Chang 5(6):501–503

https://www.natureasia.com/en/nindia/article/10.1038/nindia.2021.121

Huq S (2021). https://www.thedailystar.net. [Online] Available at https://www.thedailystar.net/opinion/politics-climate-change/news/vulnerable-countries-take-the-lead-tackling-climate-change-2129341. Accessed 31 Oct 2021

IMF (2021) Fiscal policies for climate change and a green recovery. [Online]

India (2011). https://mea.gov.in/. [Online] Available at https://mea.gov.in/in-focus-article.htm?1 8785/Brief+on+SAARC. Accessed 31 Oct 2021

India (2021) India, Bhutan sign mou for cooperation on climate change, waste management. India News, New Delhi

India GO (2011a) Ministry of External Affairs, Government of India, November 12. Retrieved from mea.gov.in https://mea.gov.in/bilateral-documents.htm?dtl/5407/Framework+Agreement+on +Cooperation+for+Development+between+India+and+Maldives

India GO (2011b) Ministry of External Affairs, Government of India. [Online] Available at https:// mea.gov.in/bilateral-documents.htm?dtl/5407/Framework+Agreement+on+Cooperation+for +Development+between+India+and+Maldives

India GO (2008) National action plan on climate change

Indian Ministry of External Affairs (2021) Retrieved from Ministry of External Affairs, Government of India, June 01 https://www.mea.gov.in/Portal/ForeignRelation/Brief_on_India_for_ website.pdf

IPCC (2001) Climate change 2001: the scientific basis. Contribution of Working Group to the Third Assessment Report of the Intergovernmental Panel on Climate Change. Cambridge University Press, Cambridge

IPCC (2007) Working Group II Contribution to the Intergovernmental Panel on Climate Change Fourth Assessment Report. Climate change 2007: climate change impacts, adaptation and vulnerability. Cambridge University Press, Cambridge

Isaksen KA, Stokke K (2014) Changing climate discourse and politics in India. Climate change as challenge and opportunity for diplomacy and development. Geoforum 57:110–119

Islam N, Sultan S, Afroz (2009) Climate change and South Asia: what makes the region most vulnerable?. University Library of Munich, Germany, MPRA Paper

Iwasaki S, Razafindrabe B, Shaw R (2009) Fishery livelihoods and adaptation to climate change: a case study of Chilika lagoon, India. Mitig Adapt Strateg Glob Chang 14(4):339–355

Jat ML, Dagar JC, Sapkota TB, Govaerts B, Ridaura SL, Saharawat YS et al (2016) Climate change and agriculture: adaptation strategies and mitigation opportunities for food security in South Asia and Latin America. Adv Agron 137:127–235

Jayaram D (2021) India's climate diplomacy towards the EU: from Copenhagen to Paris and beyond. In: EU-India relations: the strategic partnership in the light of the European Union global strategy, pp 201–226

Karim MH, Sardar Shahraki A, Kiani Ghalesard S, Fahimi F (2020) Management challenges and adaptations with climate change in Iran forests. Caspian J Environ Sci 18(1):81–91

Karmacharya JL (2007) Maximizing benefits from hydropower: a Nepal case. Hydro Nepal J Water Energy Environ 1:29–34

Karmacharya J, Shrestha A, Shrestha ML (2007) Climate change scenarios for South Asia and Central Himalayan region based on GCM ensemble. Department of Hydrology and Meteorology, Kathmandu

Khadka NS (2018). https://www.bbc.com/. [Online] Available at https://www.bbc.com/news/ world-asia-india-58155294. Accessed 31 Oct 2021

Khalae MK (2021) Water wars: how is climate change, specifically water scarcity, affecting existing dynamics between India and its neighbors? Doctoral dissertation, Boston University

Khan NA, Gao Q, Abid M, Shah AA (2021) Mapping farmers' vulnerability to climate change and its induced hazards: evidence from the rice-growing zones of Punjab, Pakistan. Environ Sci Pollut Res 28(4):4229–4244

Khanna J, Medvigy D, Fueglistaler S et al (2017) Regional dry-season climate changes due to three decades of Amazonian deforestation. Nat Clim Chang 7:200–204. https://doi.org/10.1038/ nclimate3226

Klare MT (2020) Climate change, water scarcity, and the potential for interstate conflict in South Asia. J Strateg Secur 13(4):109–122

Kreutzer P (2017) Ten principles of operational diplomacy: a framework. Association for Diplomatic Studies and Training

Krishnan R, Sanjay J, Gnanaseelan C, Mujumdar M, Kulkarni A, Chakraborty S (2020) Assessment of climate change over the Indian region. Government of India

Kugelman M (2021) Foreign policy. [Online] Available at https://foreignpolicy.com/2021/08/12/south-asia-climate-ipcc-report-front-lines/. Accessed 12 Aug 2021

Kumar C (2014) Climate change in South Asia: a framework of sustainable development and human security. J Environ Pollut Hum Health 2(5):100–109

Kumar P, Geneletti D (2015) How are climate change concerns addressed by spatial plans? An evaluation framework, and an application to Indian cities. Land Use Policy 42:210–226

Kumar K, Parikh J (1998) Climate change impacts on Indian agriculture: a Ricardian approach. The World Bank, Washington, DC

Kumar KK, Viswanathan B (2012) Weather variability and agriculture: implications for long and short-term migration in India. Centre for Development Economics Department of Economics, Delhi School of Economics

Kumar P, Geneletti D, Nagendra H (2016) Spatial assessment of climate change vulnerability at city scale: a study in Bangalore, India. Land Use Policy 58:514–532

Laborde D, Lakatos C, Nelson G, Robertson R, Thomas M, Yu W, Jansen HG (2012) Climate change and agriculture in South Asia. World Bank

Lacombe G, Chinnasamy P, Nicol A (2019) Review of climate change science, knowledge and impacts on water resources in South Asia. International Water Management Institute (IWMI)

Lal R (2004) Soil and water resources of South Asia in an uncertain climate. In: Sustainable agriculture and the international rice-wheat system. CRC Press, pp 43–59

Lal R, Sivakumar MV, Faiz SMA, Rahman AM, Islam KR (eds) (2010) Climate change and food security in South Asia. Springer

Lazard O, Youngs R (2021) The EU and climate security: toward ecological diplomacy. Carnegie Europe, 12

Linnerooth-Bayer J, Mechler R (2009) Insurance against losses from natural disasters in developing countries, New York, NY

Mahe DJ (2019) Asia adaptation and resilience, July 24. Retrieved from climate-diplomacy https://climate-diplomacy.org/magazine/conflict/why-has-climate-change-adaptation-become-more-important-ever-india

Maizland L (2021). https://www.cfr.org/. [Online] Available at https://www.cfr.org/backgrounder/paris-global-climate-change-agreements. Accessed 29 Oct 2021

Mall RK, Srivastava RK, Banerjee T, Mishra OP, Bhatt D, Sonkar G (2019) Disaster risk reduction including climate change adaptation over South Asia: challenges and ways forward. Int J Dis Risk Sci 10(1):14–27

Massen FABEG (2011) Accurate estimation of CO(2) background level from near ground measurements at non-mixed environments. In: The economic, social and political elements of climate change. Springer, pp 509–522

mfasia (2020). https://mfasia.org/. [Online] Available at: https://mfasia.org/mfa_programs/advocacy/south-asian-association-for-regional-cooperation/. Accessed 31 Oct 2021

Milkoreit M (2015) Science and climate change diplomacy: cognitive limits and the need to reinvent science communication. In: Science diplomacy: new day or false dawn? pp 109–131

Ministry of Environment FA (2021) India and Bhutan sign MOU for developing cooperation in the areas of environment. PIB Delhi, Delhi

Mirza M (2007) Climate change, adaptation and adaptive governance in water sector in South Asia. Phys Sci Basis:1–19

Mirza MMQ, Ahmad QK (2005) Climate change and water resources in South Asia: an introduction. Climate change and water resources in South Asia. AA Balkema Publishers (Taylor & Francis Group), London, pp 1–8

Mohanty A, Wadhawan S (2021) Mapping India's climate vulnerability: a district-level assessment. New Delhi: Council on Energy, Environment and Water, Council on Energy, Environment and Water Sanskrit Bhawan, A-10, Qutab Institutional Area, Aruna Asaf Ali Marg, New Delhi – 110067

Murthy IK, Tiwari R, Ravindranath NH (2011) Climate change and forests in India: adaptation opportunities and challenges. Mitig Adapt Strateg Glob Chang 16(2):161

Murthy IK, Gupta M, Tomar S, Munsi M, Tiwari R, Hegde GT, Ravindranath NH (2013) Carbon sequestration potential of agroforestry systems in India. J Earth Sci Clim Change 4(1):1–7

Nair S (2019) Jagran josh. [Online] Available at https://www.jagranjosh.com/current-affairs/current-affairs-18-march-2019-digest-3-india-maldives-sign-three-agreements-iit-iisc-collaborate-on-climate-change-initiative-1552910226-1

Nenow (2021) India and Bhutan sign MoU on cooperation in environment sector, June 29. Retrieved from https://nenow.in/; https://nenow.in/top-news/india-and-bhutan-sign-mou-on-cooperation-in-environment-sector.html

Nepal S, Shrestha AB (2015) Impact of climate change on the hydrological regime of the Indus, Ganges and Brahmaputra river basins: a review of the literature. Int J Water Resour Dev 31(2):201–218

O'Brien K, Leichenko R, Kelkar U, Venema H, Aandahl G, Tompkins H et al (2004) Mapping vulnerability to multiple stressors: climate change and globalization in India. Glob Environ Chang 14(4):303–313

Ojha VP (2012) Climate change mitigation strategies in South Asia. In: Routledge handbook of South Asian economics. Routledge, pp 329–342

Ojha HR, Sulaiman VR, Sultana P, Dahal K, Thapa D, Mittal N, Aggarwal P (2014) Is South Asian agriculture adapting to climate change? Evidence from the Indo-Gangetic Plains. Agroecol Sustain Food Syst 38(5):505–531

Panda A (2009) Assessing vulnerability to climate change in India. Economic & Political Weekly

Pandey P (2011) United Service Institution of India and has been researching on Indo-Bangladesh water issues. She contributes this article specially for RSIS Commentaries. https://www.rsis.edu.sg/rsis-publication/rsis/1599-india-bangladesh-relations-ne/#.YX6k4mBBzIU

Pandey R, Jha S (2012) Climate vulnerability index-measure of climate change vulnerability to communities: a case of rural Lower Himalaya, India. Mitig Adapt Strateg Glob Chang 17(5):487–506

Pandve HT (2009) India's National Action Plan on climate change. Indian J Occup Environ Med 13:17–19

Parvaiz A (2021) India, Pakistan cross-border water treaty needs climate change revision. [Online] Available at https://www.natureasia.com/en/nindia/article/10.1038/nindia.2021.121

Pittock J (2011) National climate change policies and sustainable water management: conflicts and synergies. Ecol Soc 16(2):25

Polacek A (2018) Catastrophe bonds: a primer and retrospective. Chicago Fed Letter

Prabhakar SVRK, Shaw S (2007) Climate change adaptation implications for drought risk mitigation: a perspective for India. Springer

Rahman K (2007) Studies on free radicals, antioxidants, and co-factors. Clin Interv Aging 2(2):219

Rahman AA, Alam M, Alam SS, Uzzaman MR, Rashid M, Rabbani G (2007) Risks, vulnerability and adaptation in Bangladesh. Human Development Report, 8

Rana MMP, Ilina IN (2021) Climate change and migration impacts on cities: lessons from Bangladesh. Environ Chall 5:100242

Rasul G, Sharma E (2014) Understanding the poor economic performance of Bihar and Uttar Pradesh, India: a macro-perspective. Reg Stud Reg Sci 1(1):221–239

Rasul G, Sharma B (2016) The nexus approach to water–energy–food security: an option for adaptation to climate change. Clim Pol 16(6):682–702

Rasul G, Sharma B (2020) Water, food, and energy nexus in South Asia: implications for adaption to climate change. In: Handbook of climate change adaptation

Rattani V (2018a) An analysis on India's National Action Plan on climate change. In: Rattani V (ed) Coping with climate change. Center for Science and Environment, New Delhi, p 9

Rattani V (2018b) Coping with climate change: an analysis of India's national action plan on climate change. Centre for Science and Environment, New Delhi

Revi A (2008) Climate change risk: an adaptation and mitigation agenda for Indian cities. Environ Urban 20(1):207–229

Rong F (2010) Understanding developing country stances on post-2012 climate change negotiations: comparative analysis of Brazil, China, India, Mexico, and South Africa. Energy Policy 38(8):4582–4591

Roy AKD (2017) An investigation into the major environment and climate change policy issues in southwest coastal Bangladesh. Int J Clim Change Strategies Manage

Ruffini PB (2018) The Intergovernmental Panel on Climate Change and the science-diplomacy nexus. Global Pol 9:73–77

SAARC (2008) SAARC action plan on climate change, (Adopted by the SAARC Ministerial Meeting on Climate Change), Bangladesh, Dhaka, 3 July 2008

Sahu NC, Mishra D (2013) Analysis of perception and adaptability strategies of the farmers to climate change in Odisha, India. APCBEE Procedia 5:123–127

Saryal R (2018) Climate change policy of India: modifying the environment. South Asia Res 38(1): 1–19

Sathaye J, Shukla PR, Ravindranath NH (2006) Climate change, sustainable development and India: global and national concerns. Curr Sci 90:314–325

Shah T (2009) Climate change and groundwater: India's opportunities for mitigation and adaptation. Environ Res Lett 4(3):035005

Sharma A (2021) DW, October 28. Retrieved from DW https://www.dw.com/en/cop26-what-is-india-doing-to-combat-climate-change/a-59653129

Sharma D, Tomar S (2010) Mainstreaming climate change adaptation in Indian cities. Environ Urban 22(2):451–465

Shidore S (2020) Climate change and the India-Pakistan rivalry. The Council on Strategic Risks

Shukla PR (2003) Climate change and India: vulnerability assessment and adaptation. Universities Press

Shukla R, Agarwal A, Sachdeva K, Kurths J, Joshi PK (2019) Climate change perception: an analysis of climate change and risk perceptions among farmer types of Indian Western Himalayas. Clim Chang 152(1):103–119

Singh AK (2016) Climate change and conflict for water a threat to peace and security in South Asia. In: Climate change and its implications on crop production and food security, 1

Singh SP, Abdullah H (2016) Historic arguments and transboundary disputes on water conflict in South Asia. J Def Secur 7(1):40-III

Singh M, Rao M, Butler CD (2016) Climate change, health and future well-being in South Asia. In: Climate change and human health scenario in South and Southeast Asia. Springer, Cham, pp 11–27

Singh BB, Singh M, Singh D (2021) An overview of climate change over South Asia: observations, projections, and recent advances. In: Practices in regional science and sustainable regional development, pp 263–277

Sivakumar MV (2010) Climate change and food security in South Asia. Springer, Dordrecht

Skodvin T (2000) Structure and agent in the scientific diplomacy of climate change. In: Structure and agent in the scientific diplomacy of climate change. Springer, Dordrecht, pp 225–233

Smit B, Burton I, Klein JR, Street R (1999) The science of adaptation: a framework for assessment. Kluwer Academic Publications, Dordrecht

Smit B, Pilifosova O, Burton I, Challenger B, Huq S, Klein R, Yohe G (2000) Adaptation to climate change in the context of sustainable development and equity. IPCC

Srivastava SK (2010) A framework for regional cooperation on integration of disaster risk reduction and climate change adaptation in South Asia. In: Climate change and food security in South Asia. Springer, Dordrecht, pp 569–584

Stalley P (2013) Principled strategy: the role of equity norms in China's climate change diplomacy. Glob Environ Polit 13(1):1–8

Sterrett C (2011) Review of climate change adaptation practices in South Asia. Oxfam Policy Pract Clim Change Resilien 7(4):65–164

Sterrett C (2021) Review of climate change adaptation practices in South Asia

Stojanov R, Duží B, Kelman I, Němec D, Prochá D (2016) Local perceptions of climate change impacts and migration patterns in Malé, Maldives. Geogr J 183(4):70–385

Subedi J (2010) Climate change adaptation in Nepal: issues and strategies. In: Climate change adaptation and disaster risk reduction: an Asian perspective. Emerald Group Publishing Limited

Sudan FK (2019) Addressing climate change and energy security through energy cooperation: challenges and opportunities in South Asia. In: Achieving energy security in Asia: diversification, integration and policy implications, pp 3–30

Taheripour F, Hertel TW, Gopalakrishnan BN, Sahin S, Markandya A, Mitra BK, Prasad V (2018) Climate change and water scarcity: growing risks for agricultural based economies in South Asia. In: Routledge handbook of sustainable development in Asia. Routledge, pp 104–132

Tänzler D (2018) Climate diplomacy and peace. In: Routledge handbook of environmental conflict and peacebuilding. Routledge, pp 295–305

Team C (2021) India, Bhutan sign MoU to boost environmental cooperation, June 21. Retrieved from https://www.constructionworld.in/; https://www.constructionworld.in/policy-updates-and-economic-news/india%2D%2Dbhutan-sign-mou-to-boost-environmental-cooperation/27808

Thapa A (2013) Does private school competition improve public school performance? The case of Nepal. Int J Educ Dev 33(4):358–366

The World Bank (2020). https://ppp.worldbank.org/. [Online] Available at https://ppp.worldbank.org/public-private-partnership/overview/ppp-objectives. Accessed 31 Oct 2021

Tripathi S (2021) India and Bhutan ink MoU for developing cooperation in the areas of environment. Jagran Josh, New Delhi

Tripathi A, Mishra AK (2017) Knowledge and passive adaptation to climate change: an example from Indian farmers. Clim Risk Manag 16:195–207

UN (2020). https://www.un.org/. [Online] Available at https://www.un.org/en/un75/climate-crisis-race-we-can-win. Accessed 31 Oct 2021

United Nations Climate Change Annual Report (UNCCC) (2019) United Nations framework convention on climate change, the Kyoto protocol and the Paris agreement. ISBN: 978–92–9219-190-0

UNDDR (2020) Structural and non-structural measures. [Online] Available at https://www.undrr.org/terminology/structural-and-non-structural-measures

Unicef (2021). www.unicef.org. [Online] Available at https://www.unicef.org/bangladesh/en/press-releases/children-four-south-asian-countries-extremely-high-risk-impacts-climate-crisis. Accessed 31 Oct 2021

Veh G, Korup O, Walz A (2019) Hazard from Himalayan glacier lake outburst floods. Natl Acad Sci 117(2):907–912

Venkateswarlu B, Shanker AK (2009) Climate change and agriculture: adaptation and mitigation stategies. Indian J Agron 54(2):226–230

Wani AM, Raj AJ, Kanwar M (2013) Impact of climate change on forests of eastern Himalayas and adaptation strategies for combating it. Int J Agric For 3(3):98–104

Workingabroad (2018). https://www.workingabroad.com/. [Online] Available at https://www.workingabroad.com/travel/india-climate-and-geography/. Accessed 31 Oct 2021

Xie L, Jia S (2017) Diplomatic water cooperation: the case of Sino-India dispute over Brahmaputra. Int Environ Agreem Politics Law Econ 17(5):677–694

Zafarullah H, Huque AS (2018) Climate change, regulatory policies and regional cooperation in South Asia. Public Administration and Policy

Chapter 2
Impact of Frequent Cyclonic Storms on Land Use and Land Cover Changes Along the Coastal Areas of Indian Sundarban

Prosenjit Kayal and Indrajit Roy Chowdhury

Abstract The Sundarban region has been considered as a 'World Heritage Site' by IUCN since 1987 and a 'Biosphere Reserve' by UNESCO since 1989 (Chaudhuri and Choudhury, Mangrove of the Sundarban, India, vol 1, no 1. IUCN- The World Conservation Union, Bangkok, pp 7–1). Since 1870 onwards, due to excessive human interaction and frequent coastal storm surges, Sundarban has become more vulnerable. As a result, these natural calamities may directly impact on the extinction of species, increasing rate of siltation, loss of agricultural land, inundation of saline water in the low lying areas, change of chemical properties of soil which lead to rapid land use and land cover changes (Datta and Deb, Geo-spatial Inf Sci 15(4): 241–250). The present study attempts to understand the significant changes of LULC cover and identify the changing pattern of natural vegetation due to innumerable cyclonic storm surges along the coastal areas of Indian Sundarban using multi-temporal, remotely sensed data. For this purpose, three Landsat 8 satellite imageries, including January, May and December 2021, have been selected to perform the supervised image classification. Thus, Normalized Difference Vegetation Index (NDVI), Soil Adjusted Vegetation Index (SAVI) and Land Surface Water Index (LSWI) were also taken into consideration to identify the crop health pattern of the study area before and after a super cyclonic storm. Several statistical techniques, including weighted rank score, aggregate rank score, chi-square techniques, have been incorporated into the study. The results of the study indicate massive changes have occurred in the LULC cover and also on the vegetation health status due to the super cyclonic storm.

Keywords Natural hazards · Cyclone · Land cover change · Vegetation health · Indian Sundarbans

P. Kayal (✉) · I. R. Chowdhury
Department of Geography and Applied Geography, University of North Bengal,
Raja Rammohunpur, West Bengal, India

Introduction

In the tropical and subtropical region, the most fertile ecosystems are Mangroves. They belong within the intertidal zones of Indian coastlines, primarily depending on local climatic conditions. Mangrove covers 75% of tropical coastlines throughout the world and supports approximately 80 species of flora and 1300 faunal species (Datta and Deb 2012). However, recently the mangroves of the Sundarban region are showing a declining trend globally in terms of biodiversity. The Sundarban, which is the world's largest mangrove forest, extending from India to Bangladesh, is facing a similar problem (Datta et al. 2010). Sundarban is located at the land-sea interface where the morphology is fragile, and the elevation is low, i.e. 7.5 m, which makes it vulnerable to periodic disturbance by cyclones, tidal surge and floods (Richardson and Everitt 1992). It is frequently struck by devastating cyclones due to sharing 260 km of long shoreline with the Bay of Bengal that is documented as the ideal ground for 6–10% of global cyclone formation (Debnath 2018).

Land use and land cover change is a dynamic phenomenon which directly influences environmental issues including, natural calamities. Owing to the advancements of geospatial technology and easy availability of remote sensing data from various sources, monitoring and mapping land use and land cover changes can be achieved in a more precise way (Priyadarshini et al. 2019). Nowadays, remote sensing is extensively used to identify the land use and land cover changes in the coastal environment induced by cyclonic storms.

The adverse impacts of cyclones in the Sundarban region have long been observed, some of them are listed below (Table 2.1)

Table 2.1 Information regarding some selected Cyclonic Storms in Sundarban Region

Name of the tropical cyclones	Name given by	Date of occurrence	Associated impacts
Bhola	–	November, 1970	As reported by The Ware, the Cyclone Bhola made a severe impact, including the deaths of 5 lakh (500,000) people; in the Ganga delta region, many low lying islands have been washed away due to the occurring of flood associated with storm surges. It also devastated croplands (Naeem 2020).
Sidr	Oman	November, 2007	The number of deaths associated with the Sidr cyclone is 3447 (Khan 2007). According to the report of Save, the total number of children deaths related to this Cyclone is between 3100 and 10,000.
Rashmi	Srilanka	October, 2008	As an immediate impact of this Cyclone, 15 people were killed, and thousands of homes were also damaged. In addition to destroying farm land, trees were uprooted and along with electric posts (Ahmed 2008).

(continued)

Table 2.1 (continued)

Name of the tropical cyclones	Name given by	Date of occurrence	Associated impacts
Aila	Maldives	25th May, 2009	Around 1 lakh (100,000) people became homeless due to this cyclonic storm. In addition, at least a hundred embankments were damaged (PTI 2013).
Viyaru	Srilanka	16–17th May, 2013	It made a significant impact in northern Indonesia, Bangladesh and Myanmar. According to the report of the International Federation of Red Cross and Red Crescent Societies (2013), this Cyclone, damaged approx. 50,000 homes were devastated in Bangladesh.
Komen	Thailand	29th July, 2015	According to the IMD report (2015) the cyclonic storm Komen killed 83 people, more than 10,000 livestock and approx. 3.6 lakh (360,000) houses were damaged.
Roanu	Maldives	21st May, 2016	Although it had a severe impact in Bangladesh and Sri Lanka, it also affected the Indian states of Tamil Nadu, Andhra Pradesh, Kerala and Odisha (Yadav 2016).
Mora	Thailand	29th May, 2017	It left a profound impact on the Maldah District of West Bengal. The Mora cyclone killed two people, wounded 50 and damaged around 6000 houses. Fruits, orchards and food grain were also severely affected (Pal 2017).
Fani	Bangladesh	4th May, 2019	The Fani cyclone severely affected Odisha, West Bengal, Assam in India and Bangladesh (Kumar et al., 2020). Fani in India killed 72 people; 64 in Odisha (Adil 2019).
Bulbul	Pakistan	5th November, 2019	Odisha and West Bengal in India were the worst affected by this Cyclone. According to the Times of India (2019), 10 people were killed from West Bengal, and the number of affected families is approx. 2.73 lakh.
Amphan	Thailand	20th May, 2020	Amphan made landfall near Bakkhali in West Bengal at 2:30 p.m. (Chowdhuri 2020). It killed 72 in West Bengal; 15 from Kolkata (Singh 2020).

Source: Prepared by the researchers based on secondary data

In this present study, an attempt has been made to understand the significant changes that have occurred in land use and land cover. In addition, we identify the changing pattern of crops, as well as vegetation health due to innumerable cyclonic storm surges along the coastal areas of Indian Sundarban, especially to analyse the impact of Super Cyclone Amphan (20 May, 2020) using multi-temporal remote sensing data.

Super Cyclone Amphan
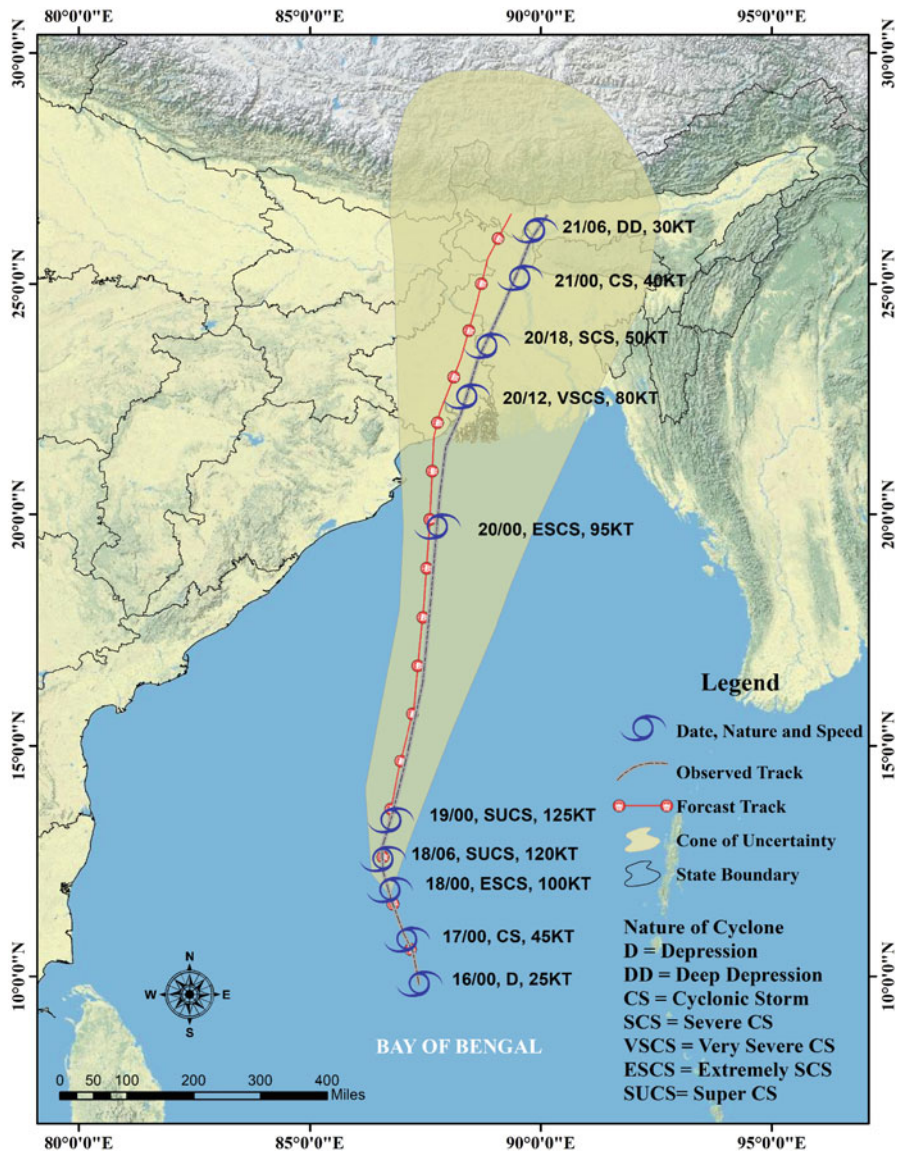
Fig. 2.1 Observed and forecast tracking SuCS AMPHAN. (Source: IMD Report 22nd May, 2020)

The Super Cyclonic Storm (SuCS) "AMPHAN" was the second SuCS over the Bay of Bengal (BoB), after the Odisha SuCS in 1999 (UNICEF, West Bengal). IMD constantly forecast since 16 May that Cyclone Amphan would make landfall on the coast of West Bengal as a very severe cyclonic storm (VSCS) having wind speed of 155–165 km/h gusting to 180 km/h on 20 May (World Meteorological Organization) (Indian Meteorological Department 2020) (Fig. 2.1). On May 20, SuCS Amphan

made landfall on the West Bengal coast resulting in 86 deaths and suffering more than 10 million people. Eastern India and adjacent districts of Bangladesh experienced this super Cyclone (Singh 2020). As per the Post Cyclone landfall survey conducted by Area Cyclone Warning Centre, commonly known as ACWC of Kolkata, it can been seen that South & North 24 Parganas and adjacent areas of East Medinipur Districts of West Bengal experienced tides up to 15 feet high resulting in inundation of the low lying areas of these districts. This SuCS Amphan had a severe impact on land use and land cover condition and as well as on livelihood of the local people. Thus, this research work has been wholly developed based on the impact associated with only SuCS Amphan.

Literature Review

Several researchers have conducted studies on cyclonic storms and their associated impact on the environment. Among them Rahman et al. (2017) investigated the impacts of cyclonic storm Aila on the mangrove forest of the Sundarban region in Bangladesh, Datta and Deb (2012) identified the coastal land use/land cover changes in the Indian Sunderban using remotely sensed data, Mishra and Panigrahi (2014) studied the impact of the storm on the south Odisha coast, Kar and Bandhyopadhyay (2015) analysed Tropical storm Aila in the Gosaba Block of Indian Sundarban, Srinivasa (2015) (Scanlon et al. 2002) investigated the impact of tropical cyclone Hudhud on the coastal region of Visakhapatnam, Hossain and Karlson (2017) investigated the Land Cover Change in the Sundarbans Caused by Cyclone Roanu, Debnath (2018) examined the land use and land cover change detection of the Gosaba Island of the Indian Sundarban, Gupta et al. (2018) investigated the impact of climate change on tropical cyclones frequency and intensity on Indian coasts, Priyadarshini et al. (2019) identified the land cover change dynamics of the Gaja cyclone in coastal Tamil Nadu, Sarkhel et al. (2019) pointed out the impact on the Coastal Belts of Odisha, and Ghosh and Mistri (2020) explored the coastal agriculture and its challenges on the Gosaba Island of Indian Sundarban.

Objectives

The entire study has been based on two major objectives:

- To understand the changes in land use and land cover condition along the coastal areas of Indian Sundarbans before and after SuCS Amphan .
- To identify the changing pattern and condition of crop health and natural vegetation before and after SuCS Amphan in the study area.

Study Area

The Sundarban region is considered to be the world's largest mangrove ecosystem hub. Several works of literature have been reviewed and indicated that approximately 106 deltas can be found in this region (WBFD, Govt. of West Bengal). Among them, 54 islands are considered to be the human habitat zone. Several rivers and creeks characterize this region. This region is rich in biodiversity. In this research work, the coastal blocks of south 24 Parganas districts, including Sagar, Kakdwip, Namkhana, Patharpratima, Mathurapur-II, Kultali, Basanti and Gosaba, are taken into consideration as the study area because these regions are located in the extreme coastal region and are the worst affected in the Sundarban region during cyclone conditions (Map 2.1).

The latitudinal and longitudinal extension of the study area is 21° 36′ 22″ North to 22° 26′ 32″ North and 88° 12′ 23″ East to 89° 17′ 24″ East. This studied region is bounded by Kulpi, Mathurapur-I Joynagar-I and II Canning-I, Canning-II C.D. blocks and North 24 Parganas District in the north, Bangladesh in the east, Hooghly River in the west and Bay of Bengal in the south.
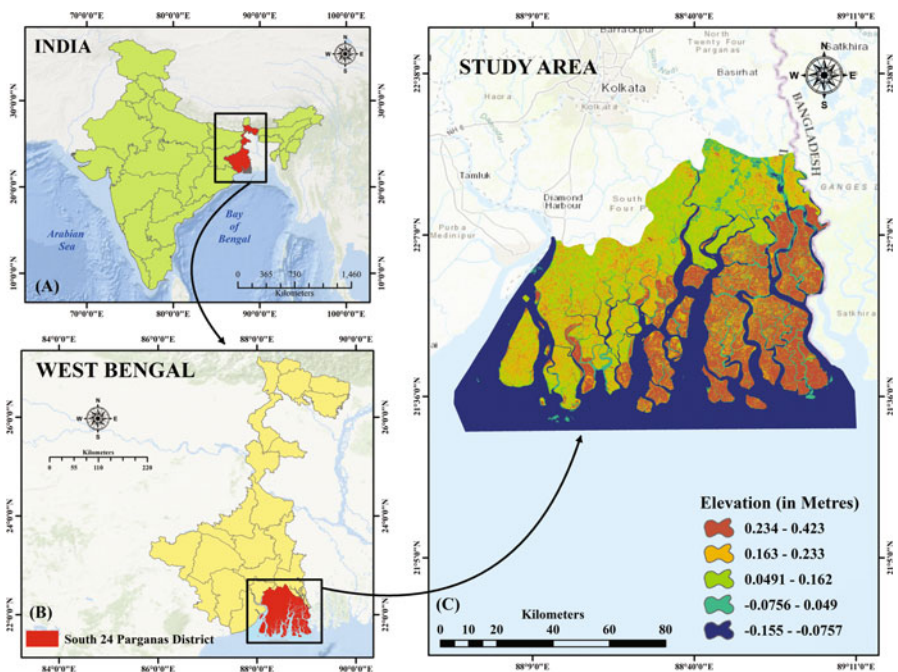
Map 2.1 Location map of West Bengal in India (**A**), Location map of South 24 Parganas district in West Bengal (**B**), Elevation map of the study area (**C**)
Source: Compiled from NATMO, Primary Census Abstract, 2011 Government of West Bengal, Prepared by the Researchers

According to the 2011 census of India, 1,601,021 persons reside in the study area; most of them are subsistence farmers and fishers. It is exciting to know that this region still has substantial mangrove forest despite the vast population present in this study area. This is possible because of the active participation of the Forest Department (FD) of the State Government and community-based Forest Protection Committees (FPCs) of Joint Forest Management (JFM) programme taken by the Government of India during the 1980s (Datta and Deb 2012). Currently, due to the rapid reduction of mangrove forests, residents are shifting towards brackish water aquaculture. Still, the villagers are substantially dependent on the products derived from mangroves, making it possible to manage the Sundarban mangrove forest and associated landscapes sustainably.

Data Base and Methodology

Satellite Data

The present research work has been conducted based on secondary data. A supervised image classification technique has been applied with a maximum likelihood algorithm based on three Landsat 8 satellite images, one pre-Amphan (January, 2020) and two post-Amphan satellite images to understand the land use and land cover changes (May and December, 2020). These satellite images have been downloaded from USGS websites. The detailed information of these satellite imageries is given below (Table 2.2). Figure 2.2 illustrates the details methodological flow diagram of the present study.

Normalized Difference Vegetation Index (NDVI)

It is the most extensively used techniques in vegetation health analysis (Morawitz et al. 2006). The essential principle of NDVI lies in the fact that the reflection difference of two-band combinations, which are NIR and RED, creates an image indicating the status of green plants (Datta and Deb 2012).

Table 2.2 Detailed information of the satellite imageries

Date of data acquisition	Spacecraft ID/Sensor	Data Type	Path	Row	Projection	Datum	UTM Zone	Spatial resolution
01/01/2020 17/01/2020	Landsat 8	OLI/ TIRS	138	045	UTM	WGS84	45N	MS 30m/ PAN 15m
08/05/2020 24/05/2020	Landsat 8	OLI/ TIRS	138	045	UTM	WGS84	45N	MS 30m/ PAN 15m
2/12/2020 18/12/2020	Landsat 8	OLI/ TIRS	138	045	UTM	WGS84	45N	MS 30m/ PAN 15m

Source: USGS Platform, Computed by the Researchers
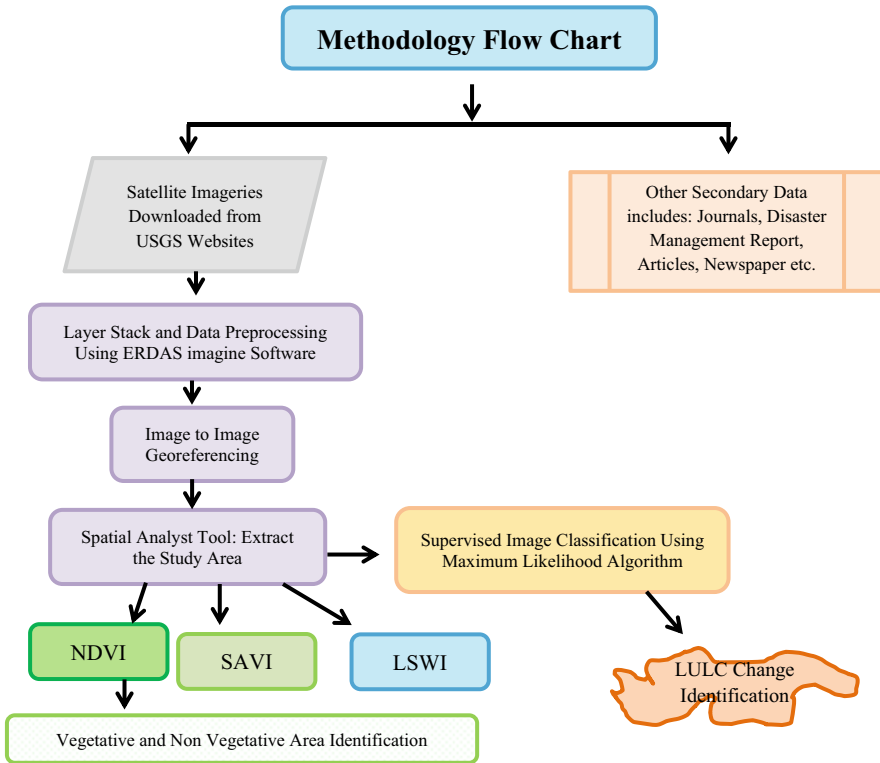
Fig. 2.2 Methodology flow chart. (Source: Computed by the Researchers)

Table 2.3 NDVI range and concern objects

Range of NDVI value	Name of the objects
−0.1	Water body
0	Bare soil, rock, sand, snow or cloud
0.2–0.3	Shrub and grassland
0.3–0.5	Sparse and unhealthy forest
>0.5	Dense and healthy forest

Source: Bid (2016)

To examine the vegetative and non-vegetative area, the NDVI technique has been implemented in three different multitemporal satellite images, i.e. January, May and December 2020. To calculate each pixel of NDVI classes, the raster calculator tool of ArcGIS 10.4 (ESRI 2015) has been used. Generally, the NDVI values range from −1 to 1, and each value indicates different objects. These are discussed in Table 2.3.

Soil Adjusted Vegetation Index (SAVI)

According to the United States Geological Survey (USGS), SAVI is used basically to correct NDVI, which is affected by soil brightness in the less dense vegetation areas. SAVI can be calculated by using the ratio between RED and Near-Infrared band with the help of SA soil brightness correction factor (L), which is defined as 0.5 to accommodate most land cover types.

Land Surface Water Index (LSWI)

The Land Surface Water Index (LSWI) is derived from the NIR and SWIR reflectance of the satellite imageries. The difference in waterlogged areas, as well as flood condition created by SuCS Amphan in the study area, can be easily represented with the help of LSWI.

The mathematical transformations for the different indices which are taken into consideration are discussed in Table 2.4.

Several secondary data sources, including Newspaper report, Article, Journal, Disaster management report published by the Government of West Bengal, and so on also, have been taken into consideration. Several statistical techniques, including percentage analysis, weighted rank score, aggregate rank score, average calculation, chi-square etc., are incorporated for the analysis of the study. ArcGIS 10.4 (ESRI 2015) and ERDAS Imagine 2014 software has been used with the help of a raster calculator tool to calculate the NDVI, SAVI and LSWI values.

Table 2.4 Remote sensing derived indices used in the study

Indices	Equation	Explanation	References
1. Normalized difference vegetation index (NDVI)	$NDVI = \frac{(NIR-RED)}{(NIR+RED)}$	NIR = Band 5 RED = Band 4 in Landsat 8 satellite imageries	Malik et al. (2019)
2. Soil Adjusted Vegetation Index (SAVI)	$SAVI = \frac{(NIR-RED)}{(NIR+RED+L)} * (1+L)$	NIR = Band 5 RED = Band 4 in Landsat 8 satellite imageries and L = 0.5 as per (Richardson and Everitt, 1992)	Huete (1988)
3. Land Surface Water Index (LSWI)	$LSWI = \frac{(NIR-SWIR)}{(NIR+SWIR)}$	NIR = Band 5 SWIR = Band 6 in Landsat 8 satellite imageries	Bofana et al. (2020)

Source: Computed by the Researchers

Result and Discussion

Land Use and Land Cover Analysis

In this research work, to understand the land use and land cover condition of the study area mainly from the pre- and post-Amphan period, three land use and land cover maps have been prepared, as shown in Map 2.2, 2.3 and 2.4. The result of these maps can be understood by the following cartograms (Fig. 2.3). This figure represents the Aerial Distribution of Different LULC Classes in January, 2020. The
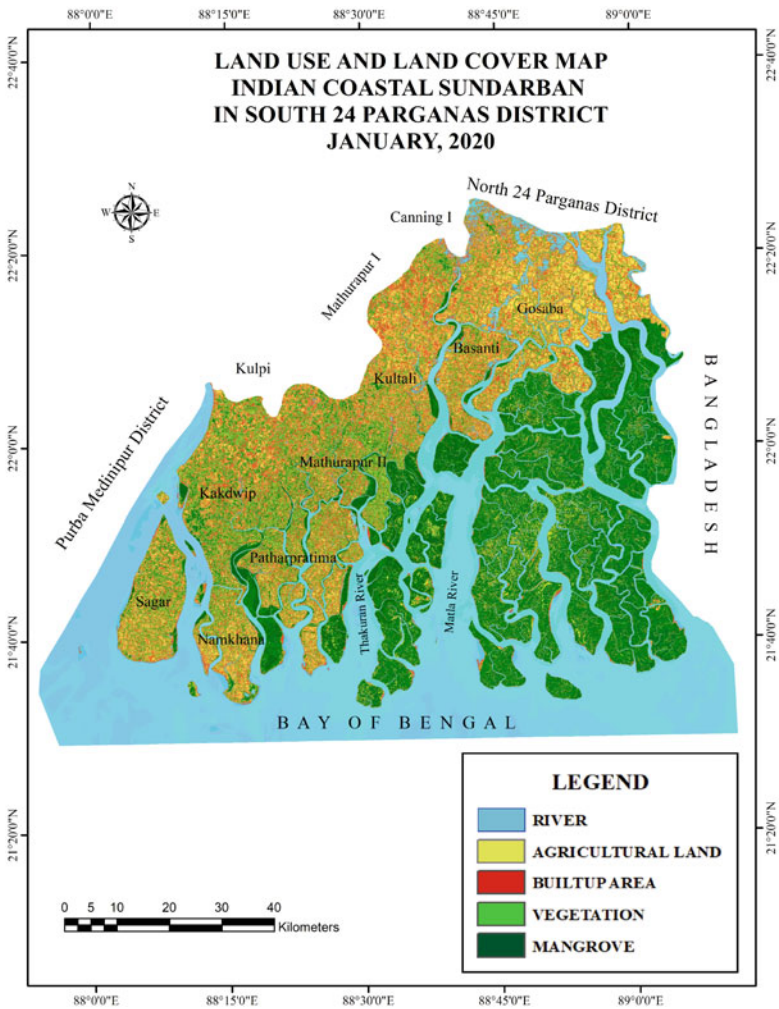
Map 2.2 Land use and land cover map in January 2020
Source: Compiled from USGS Platform and Prepared by the Researchers
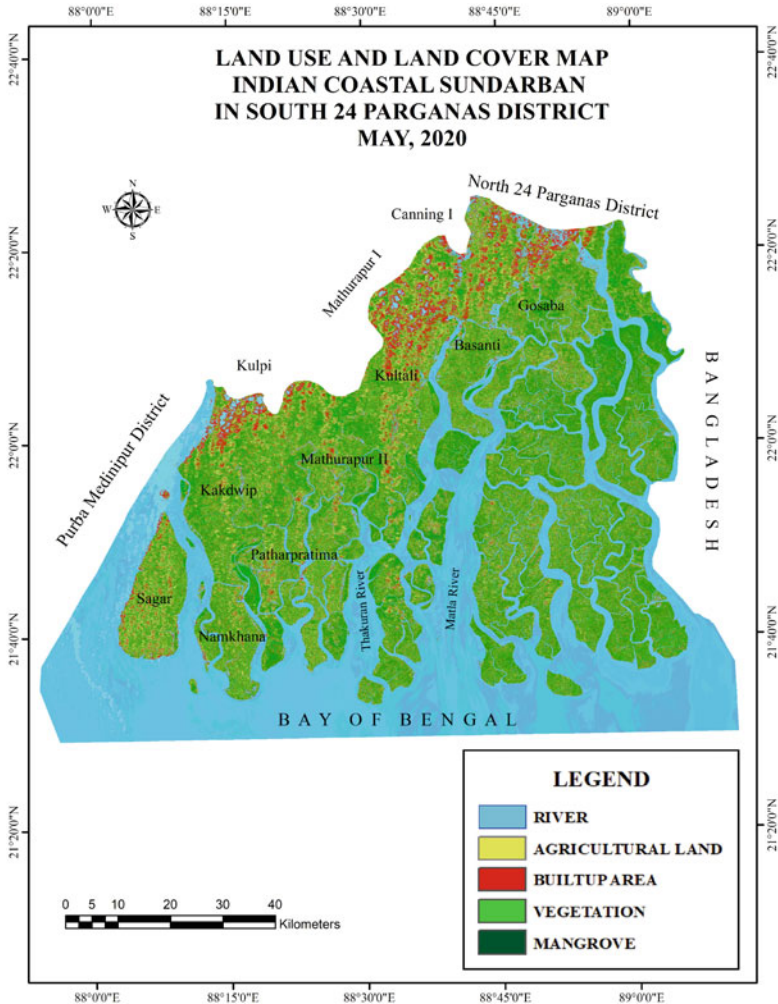
Map 2.3 Land use and land cover map in May 2020
Source: Compiled from USGS Platform and Prepared by the Researchers

entire map has been divided into five land use and land cover classes: river, agricultural land, built-up area, vegetation cover, and mangrove area. The percentage-wise aerial coverage of each land use and land cover class can be understood from Table 2.5. Here it can be seen that the river occupies the maximum percentage of areal coverage, that is, 42.29%, followed by mangrove area covered by 17.83% of the region: agricultural land, built-up area and vegetation cover occupy 14.69%, 11.92% and 13.27%, respectively.
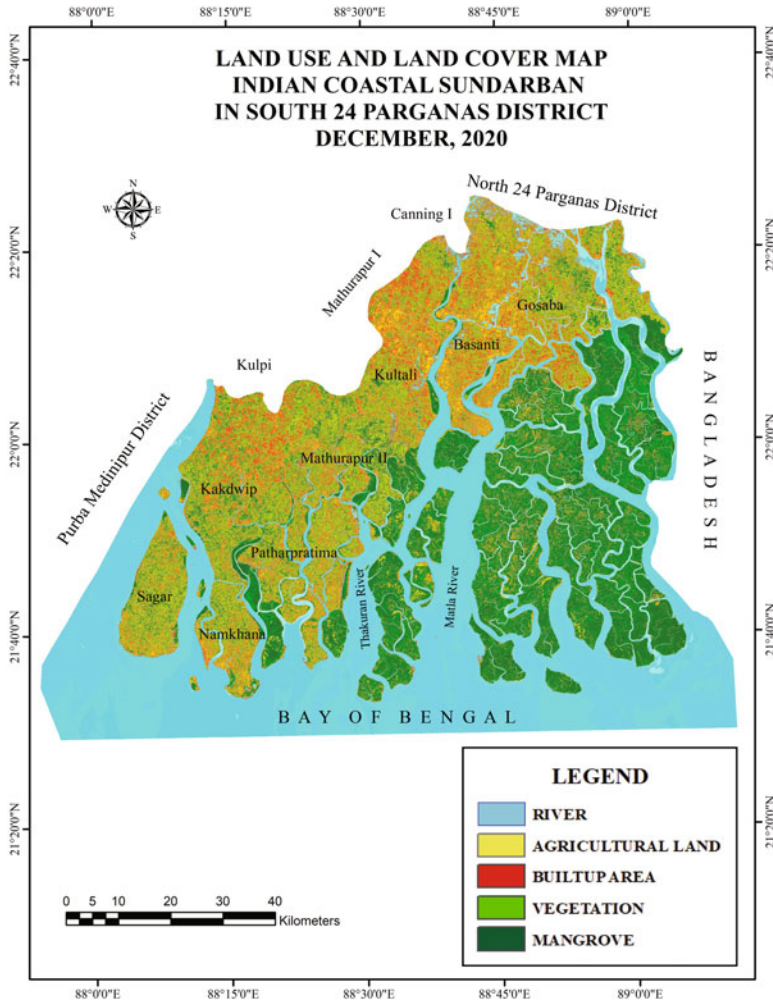
Map 2.4 Land use and land cover map in December 2020
Source: Compiled from USGS Platform and Prepared by the Researchers

Figure 2.4 represents the aerial distribution of different land use and land cover classes of May, 2020. Here similar classification can be seen of five land use and land cover classes, including river, agricultural land, built-up area, vegetation cover and mangrove area. The percentage-wise aerial coverage of each land use and land cover class can be seen in Table 2.6. Here it can be seen that the river occupies the maximum percentage of areal coverage that is 43.73%, followed by mangrove area covered by 16%. Agricultural land, built-up area and vegetation cover occupy 12.42, 14.31 and 13.54%, respectively.

Fig. 2.3 Aerial distribution of different land use and land cover classes (January 2020)
Source: Prepared by the Researchers

Aerial Distribution of Different LULC Classes (January, 2020)
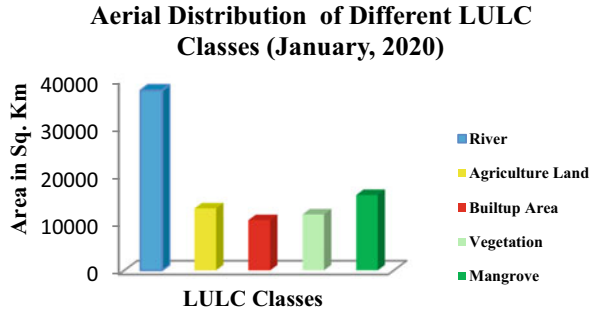
Table 2.5 Aerial distributions of LULC classes of January 2020

LULC Classes	Area in Sq. Km	Area in percentage
River	37,802.52	42.29
Agriculture land	13,127.84	14.69
Built-up area	10,651.36	11.92
Vegetation	11,863.58	13.27
Mangrove	15,940.19	17.83
Total	89,385.48	100.00

Source: Prepared by the Researchers

Fig. 2.4 Aerial distribution of different land use and land cover classes (May 2020)
Source: Prepared by the Researchers

Aerial Distribution of Different LULC Classes (May, 2020)
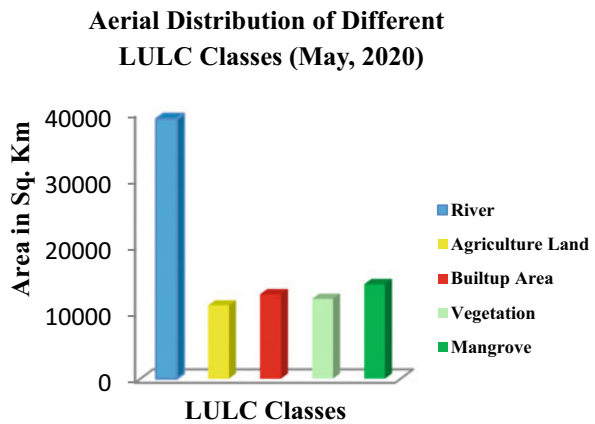
Table 2.6 Aerial distributions of LULC classes of May 2020

LULC classes	Area in Sq. Km	Area in percentage
River	39,085	43.73
Agriculture land	11,102	12.42
Built-up area	12,794	14.31
Vegetation	12,100	13.54
Mangrove	14,305	16.00
Total	89,385	100.00

Source: Prepared by the Researchers

Fig. 2.5 Aerial distribution
of different land use and
land cover classes
(December 2020)
Source: Prepared by the
Researchers

**Aerial Distribution of Different
LULC Classes (December, 2020)**
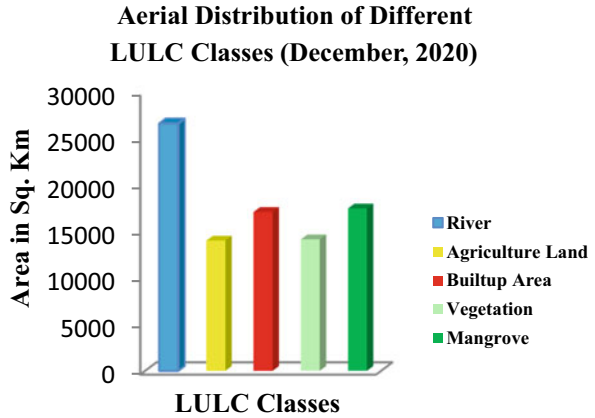
Table 2.7 Aerial distribu-
tions of LULC classes of
December, 2020

LULC classes	Area in Sq. Km	Area in percentage
River	26633.45	34.80
Agriculture land	14018.97	15.68
Built-up area	17097.29	17.13
Vegetation	14150.48	15.83
Mangrove	17485.29	19.56
Total	89385.48	100.00

Source: Prepared by the Researchers

Figure 2.5 represents the aerial distribution of different land use and land cover
classes of December 2020. We can see the similar classification of five land use and
land cover classes, including river, agricultural land, built-up area, vegetation cover
and mangrove area. The percentage-wise aerial coverage of each land use and land
cover class are shown in Table 2.7. Here it can be seen that the river occupies the
maximum percentage of areal coverage at 34.80%, followed by mangrove area
covered by 19.56%. Agricultural land, built-up area and vegetation cover occupy
15.68, 17.13 and 15.83%, respectively.

Land Use and Land Cover Change Detection Analysis

Table 2.8 indicates the land use land cover change detection. From this table, it can
be seen that the area covered by each land use and land cover class fluctuates
throughout the year. The area occupied by the river during January is 37.29%, and
during May, it is much higher due to excessive rainfall associated with SuCS
Amphan. During December, it again illustrates the usual scenario. In the case of
agricultural land during January, it occupies 14.69%. A decreasing trend is
represented during May due to the inundation of low lying agricultural land, and it
occupies 15.68% of the area during December. Owing to excessive population

Table 2.8 Aerial distributions of LULC classes from January to December, 2020

LULC classes	Area in percentage		
	January 2020	May 2020	December 2020
River	37.29	43.73	34.8
Agriculture land	14.69	12.42	15.68
Built-up area	11.92	14.31	19.13
Vegetation	13.27	13.54	15.83
Mangrove	17.83	16	19.56

Source: Prepared by the Researchers

Table 2.9 Calculation of weighted rank score of area occupied by water bodies in January, May and December 2020

Months	Water bodies (area in sq. km)	Rank	Level	Weight	Weighted rank score
January	37,802.520	2	0.897	0.632	1.265
May	39,084.970	3	1.000		1.897
December	26,633.440	1	0.000		1.124
			Σ = 1.897		

Source: Computed by the Researchers

Table 2.10 Calculation of weighted rank score of area occupied by agricultural land in January, May and December 2020

Months	Agricultural land (area in sq. km)	Rank	Level	Weight	Weighted rank score
January	13,127.840	2	0.692	0.564	1.128
May	11,102.170	1	0.000		0.564
December	14,028.970	3	1.000		1.692
			Σ = 1.692		

Source: Computed by the Researchers

pressure in this study area, the built-up area reflects a significantly increasing trend throughout time. The percentage of vegetation cover is quite similar during January and May, but in December, the areal extension becomes larger. From this chart, it is clear that SuCS Amphan severely impacted the mangrove of the Sundarban region. As a result, it reflects a decreasing trend from January to May.

Five weighted rank score values have been calculated based on the individual land use and land cover classes to understand the changes that occurred from January to December 2020. Table 2.9 represents the weighted rank score of area occupied by water bodies in January, May and December 2020. Here the weighted rank score value is the maximum during May (1.897) due to excessive rainfall associated with SuCS Amphan and the waterlogging scenario of the study area. Table 2.10 represents the weighted rank score of the area occupied by agricultural land in January, May and December 2020. Here the result shows that during December, the space

occupied by agricultural land is the maximum (1.692) followed by January (1.128), which indicated that the low lying agricultural fields of the study area became inundated during May. As a result, this particular time frame reflects the minimum aerial coverage. Table 2.11 shows the weighted rank score of the area occupied by the built-up area throughout the year 2020. This calculation highlighted that the built-up area is the maximum during December (1.332). It is the minimum during January (0.444) because of the rapid growth rate of the population of the study area. Tables 2.12 and 2.13 provide the weighted rank score of the space occupied by vegetation and mangrove cover in January, May and December 2020, respectively. This calculation significantly indicated that maximum changes have occurred in the aerial distribution of mangrove cover during December (1.514) due to the overall impact of SuCS Amphan, including storm surges, flooding, and inundation of saline water. With the help of the aggregate rank score (Table 2.14) technique, the individual land use and land cover classes have been ranked based on the three months which are taken into consideration. With the help of the cartographic

Table 2.11 Calculation of weighted rank score of area occupied by built-up area in January, May and December 2020

Months	Built-up Area (area in sq. km)	Rank	Level	Weight	Weighted rank score
January	10,651.360	1	0.000	0.444	0.444
May	12,793.530	2	0.332		0.888
December	17,097.290	3	1.000		1.332
			$\Sigma = 1.332$		

Source: Computed by the Researchers

Table 2.12 Calculation of weighted rank score of area occupied by vegetation in January, May and December 2020

Months	Vegetation (area in sq. km)	Rank	Level	Weight	Weighted rank score
January	11863.575	1	0.000	0.368	0.368
May	12100.281	2	0.104		0.736
December	14150.481	3	1.000		1.104
			$\Sigma = 1.103$		

Source: Computed by the Researchers

Table 2.13 Calculation of weighted rank score of area occupied by mangrove in January, May and December 2020

Months	Mangrove (area in sq. km)	Rank	Level	Weight	Weighted rank score
January	15,940.187	2	0.514	0.505	1.009
May	14,304.539	1	0.000		0.505
December	17,485.287	3	1.000		1.514
			$\Sigma = 1.514$		

Source: Computed by the Researchers

Table 2.14 Calculation of aggregate rank score of different land use and land cover classes in January, May and December 2020

Months	Weighted rank score of water bodies	Rank	Weighted rank score of agricultural land	Rank	Weighted rank score of built-up area	Rank	Weighted rank score of vegetation	Rank	Weighted rank score of mangrove	Rank	Aggregate rank score
January	1.264	2	1.128	2	0.444	1	0.368	1	1.009	2	1.6
May	1.897	3	0.564	1	0.888	2	0.736	2	0.505	1	1.8
December	1.124	1	1.692	3	1.332	3	1.104	3	1.514	3	2.6

Source: Computed by the Researchers
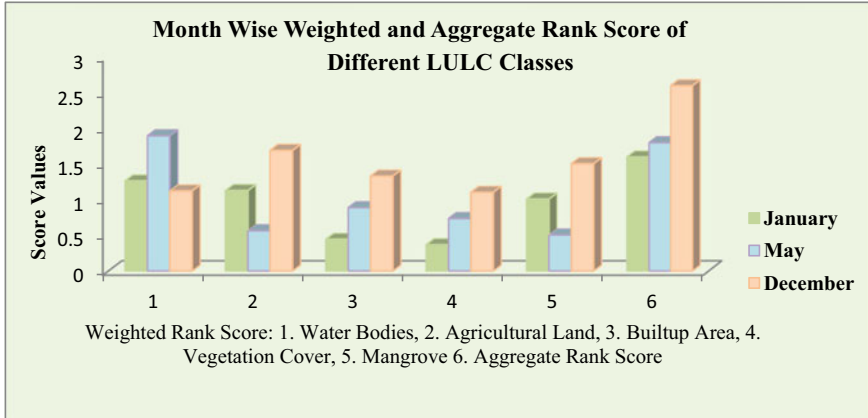
Fig. 2.6 Month wise weighted and aggregate rank score of different land use and land cover classes
Source: Prepared by the Researchers

technique, the result is displayed in Fig. 2.6. The work shows little change from January to May, and it is quite high from May to December for each land use and land cover class. From this, it can be concluded that SuCS Amphan made significant changes in land use and land cover condition of the coastal Sundarban region of the south 24 Parganas district.

Accuracy Assessment

With the help of ground reference data, accuracy assessments were performed on the LULC maps. To depict the pre LULC situation of the study area, a pilot survey has been conducted on the knowledgeable persons in local communities (Datta and Deb 2012). Here the theoretical error matrices have been produced for each of the LULC classes of three multi-temporal classified images. To understand the strength of accuracy of the image classification Kappa coefficient (Rwanga et al. 2017) has been calculated based on the formula given below:

$$K = \frac{N\sum_{i=1}^{r} x_{ii} - \sum_{i=1}^{r}(x_i + Xx_{+1})}{N^2 - \sum_{i=1}^{r}(x_{ii}Xx_{+1})}$$

where r = number of rows and columns in error matrix, N = total number of observations (pixels), X_{ii} = observation in row i and column i, $Xi+$ = marginal total of row i, and $X+i$ = marginal total of column i.

Overall Kappa coefficients have been represented in Table 2.15 for images of January, May and December, which were 0.879, 0.809 and 0.906, respectively.

Table 2.15 Accuracy assessments of different land use and land cover classes in January, May and December 2020

LULC classes	January 2020		May 2020		December 2020	
	Producer's accuracy (in %)	User accuracy (in %)	Producer's accuracy (in %)	User accuracy (in %)	Producer's accuracy (in %)	User accuracy (in %)
Water bodies	86.96	76.92	83.33333	86.2069	84.62	88.00
Agriculture land	93.75	86.07	81.96721	75.18797	91.51	85.09
Built-up area	89.71	98.39	81.39535	82.35294	86.36	91.57
Vegetation	89.72	94.12	85.43689	88	94.85	95.83
Mangrove	90.58	91.91	90.90909	94.89051	98.46	99.22
Overall accuracy (%)	90.848		85.330		92.841	
Kappa coefficient	0.879		0.809		0.906	

Source: Computed by the Researchers following the Rwanga et al. (2017) method

Similarly, the overall accuracy was 90.848, 85.330 and 92.841% for those three images, respectively. From the Kappa coefficient rating criteria, it can be understood that the three images had satisfactory accuracy levels (Rwanga et al. 2017). Among the five LULC classes, the maximum producer of accuracy is found in the agricultural land and dense mangrove class of LULC among the three selected imageries.

The maximum values were attained in the built-up area and thick mangrove land use class as per the user accuracy. The overlap areas between agricultural land and vegetation class of LULC show the utmost confusion and misinterpretation.

Vegetation Health Analysis

Normalized Difference Vegetation Index (NDVI)

The greenness of vegetation is easily pointed out with the help of NDVI (Bid 2016). It is an easier way of representing crop health condition (Kunkel et al. 2011; Scanlon et al. 2002). The NDVI is one of the essential numerical indicators (Demirel et al. 2010; Ricotta et al. 1999; Zhang et al. 2009) which are capable of dealing with the productivity of vegetation (Malo and Nicholson 1990) and providing the scientific information regarding the vegetative and non-vegetative areal coverage. Three normalized difference vegetation index maps (Maps 2.5, 2.6 and 2.7) have been prepared for January 2020, May 2020 and December 2020 to identify the changing pattern and condition of crop health as well as natural vegetation before and after SuCS Amphan in the study area.
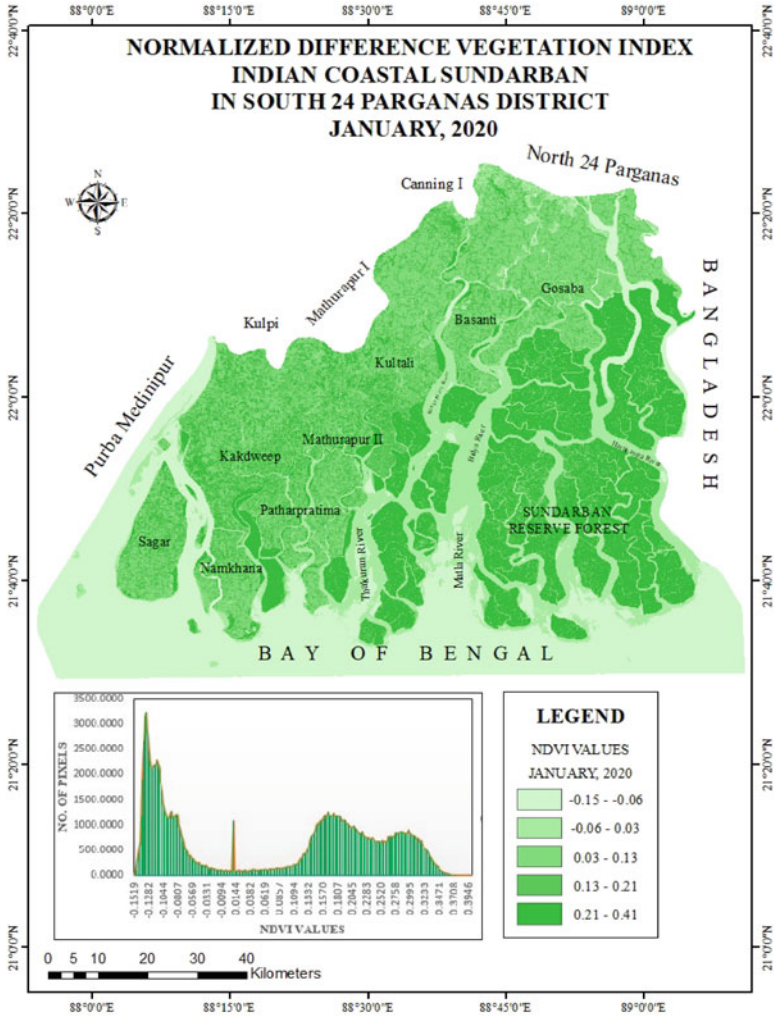
Map 2.5 NDVI map of the study area in January 2020
Source: Compiled from USGS Platform and Prepared by the Researchers

The area of each NDVI class, including very low, low, moderate, high and very high, has been calculated using ArcGIS software from January to December 2020. The result is reflected in the Fig. 2.7. From this diagram, it can be interpreted that the very low class of NDVI, which is generally represented as a water body, shows an increasing trend from January to May and again shows a decreasing trend from May to December. The low class of NDVI generally represents the bare soil, rock and sand, which offers a negative trend throughout the year. The moderate class shows fluctuation of aerial cover throughout the year. The high class shows a similar trend
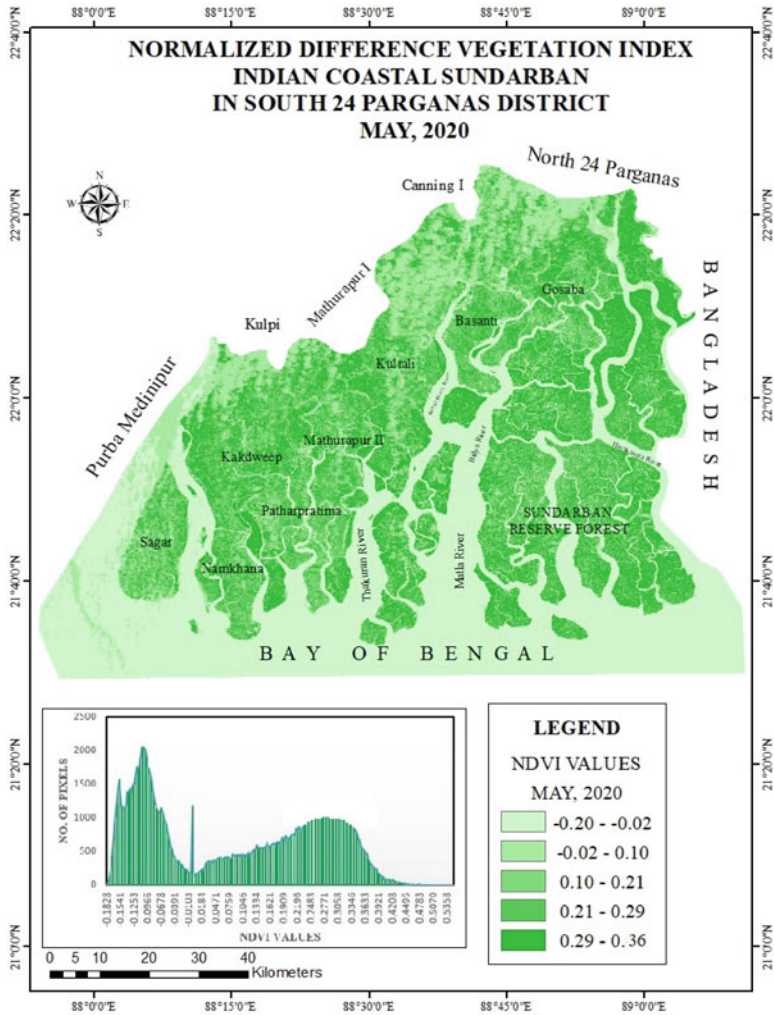
Map 2.6 NDVI map of the study area in May 2020
Source: Compiled from USGS Platform and Prepared by the Researchers

and the very high class represents mangrove areas as per the study area, and it can be seen that from January to May, it shows a negative direction and from May to December a small increase.

Soil Adjusted Vegetation Index (SAVI)

The information extracted from the processed image (Map 2.8) is based on the SAVI, which shows the spatial concentration of vegetation in the coastal blocks of
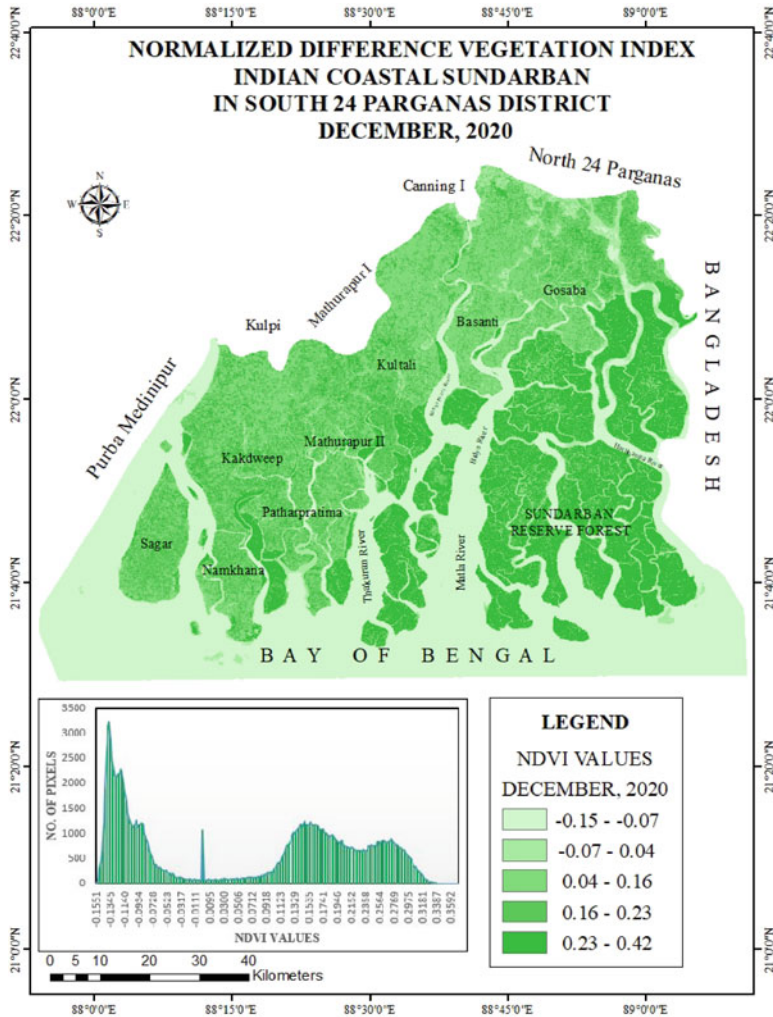
Map 2.7 NDVI map of the study area in December 2020
Source: Compiled from USGS Platform and Prepared by the Researchers

the Sundarban region. The acquisition date 1.1.2020 to 17.01.2020, selected for the study, is January 2020, available from the USGS website and appropriation Landsat 8, which belongs to the pre-Amphan category. Therefore, the southeastern part and few scattered southwestern parts of the studied blocks signify a high SAVI value (0.349–0.634), indicating dense vegetation concentration. This region falls under the Sundarban thick forest cover region dense mangrove cover areas.

The northeastern part of the Gosaba block has a medium SAVI value (-0.234 to -0.349). This region is occupied by vegetation cover, and water bodies fragment the
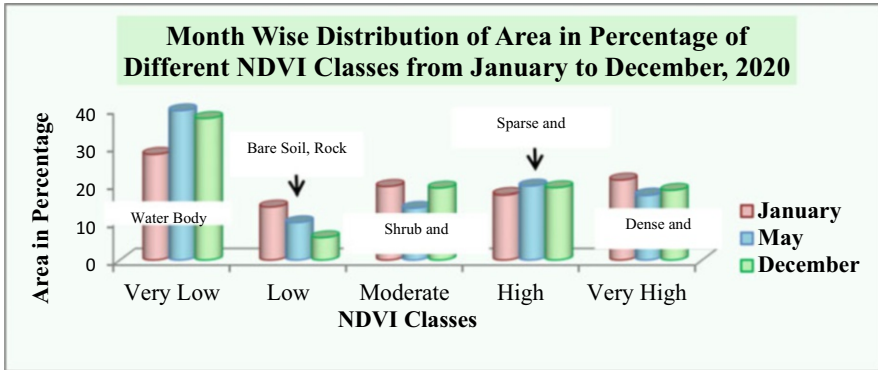
Fig. 2.7 Month wise distribution of area (in percentage) of different NDVI classes from January to December 2020
Source: Prepared by the Researchers

maximum part of the block. However, the western and southwestern coastal blocks showing very low SAVI values (−0.232 to −0.113) automatically show declining vegetative areas as it is built-up, open land and agricultural land.

Map 2.9 shows the spatial concentration of vegetation in the selected coastal blocks of the Indian Sundarban region, which is created based on the extracted information from May 2020 satellite imageries. Here it can be easily noticed that the northeastern and southeastern parts of the studied blocks signify a high SAVI values (ranging from 0.325 to 0.703), indicating the maximum concentration of dense vegetation. The northwestern, southwestern and middle part of the studied blocks, including Sagar, Namkhana, Patharpratima, Kultali, Mathurapur-II blocks, signify low to very low SAVI values (ranging from −0.013 to 0.109 and −214 to −0.013, respectively), denoting sparse vegetation concentration and relatively high soil reflectance due to the presence of built-up area, agricultural land, fallow land and open fields.

Land Surface Water Index (LSWI)

The LSWI uses the shortwave infrared (SWIR), band four, and the NIR belongs to band 5 of Landsat 8 satellite imagery regions of the electromagnetic spectrum. Shortwave infrared generally absorbed a minimal amount of liquid water, and LSWI very efficiently depicts the liquid moisture present in the vegetative area and its association with soil (Chandrasekar et al. 2010).

The information extracted from the processed image December 2020, which is the post-Amphan category map (Map 2.10), is based on the SAVI, which shows the spatial concentration of vegetation area in the coastal blocks of the Indian Sundarban region. It has been marked out that the southeastern part of the studied blocks
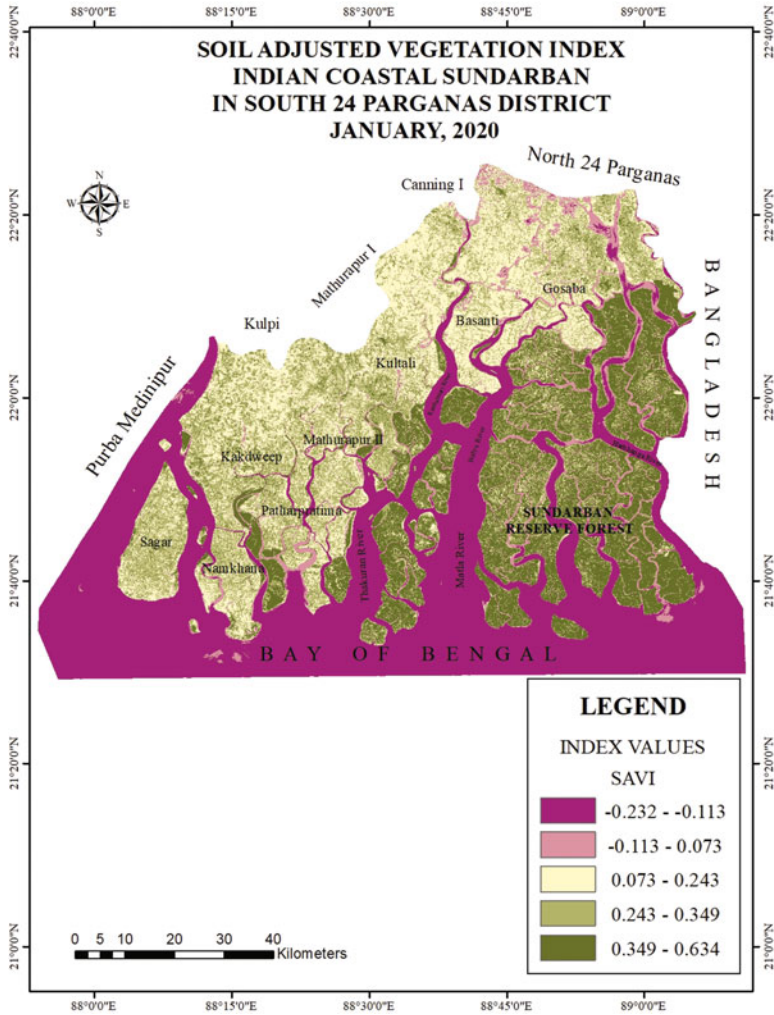
Map 2.8 SAVI map of the study area in January 2020
Source: Compiled from USGS Platform and Prepared by the Researchers

signifies a high SAVI value (ranging from 0.349 to 0.634), which represents the maximum concentration of dense vegetation due to the presence of thick mangrove forest cover. It is the minimum in the western part due to the attention of non-vegetative areas where the reflection from the soil is more than the remaining areas of the studied blocks.

The information extracted from the processed image (Maps 2.11, 2.12 and 2.13) is based on the Land Surface Water Index (LSWI), which shows the spatial concentration of surface water in the coastal blocks of the Sundarban region. From these three maps, it can be seen that the southeastern part and a few scattered southwestern
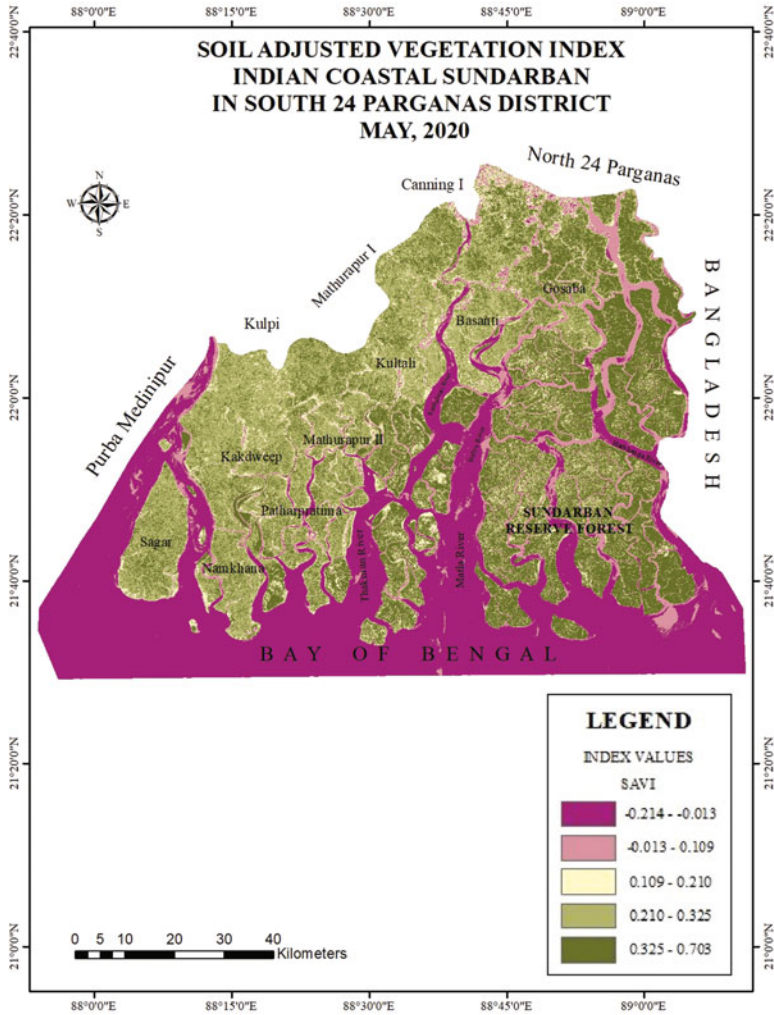
Map 2.9 SAVI map of the study area in May 2020
Source: Compiled from USGS Platform and Prepared by the Researchers

parts of the studied blocks signify high LSWI values for January, May and December 2020 (0.349, 0.371 and 0.365, respectively). Indicating dense vegetation concentration as this region falls under the Sundarban dense mangrove cover areas because the soil becomes full of moisture and solid tidal activities makes the land surface water index very high. The southern part, especially the Bay of Bengal, represents the medium LSWI values for the three maps (0.114, 0.149 and 0.129, respectively) as these regions fall under the deep seawater region. Here the coastal areas and riverbank areas of the study area reflect medium values. Part of Gosaba,
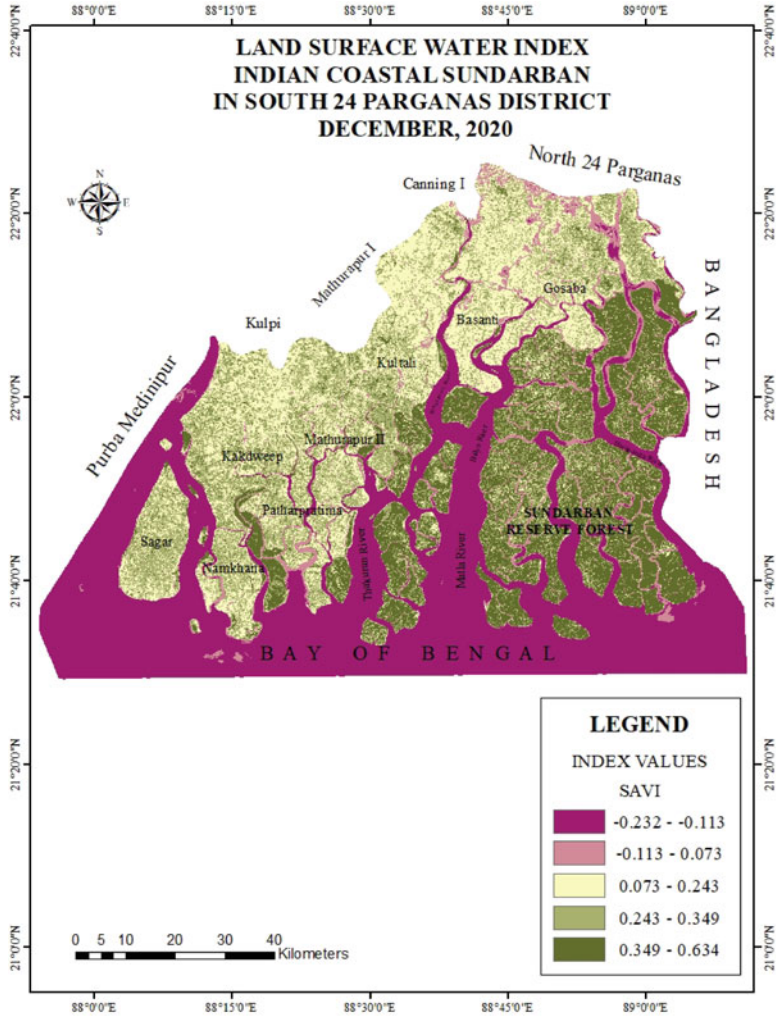
Map 2.10 SAVI map of the study area in December 2020
Source: Compiled from USGS Platform and Prepared by the Researchers

Basanti, Kkdwip, Sagar, Namkhana and Pathar Pratima blocks having very low LSWI values for the three maps (-0.146, -0.161 and -0.208, respectively) due to the relatively high concentration of non-vegetative areas.
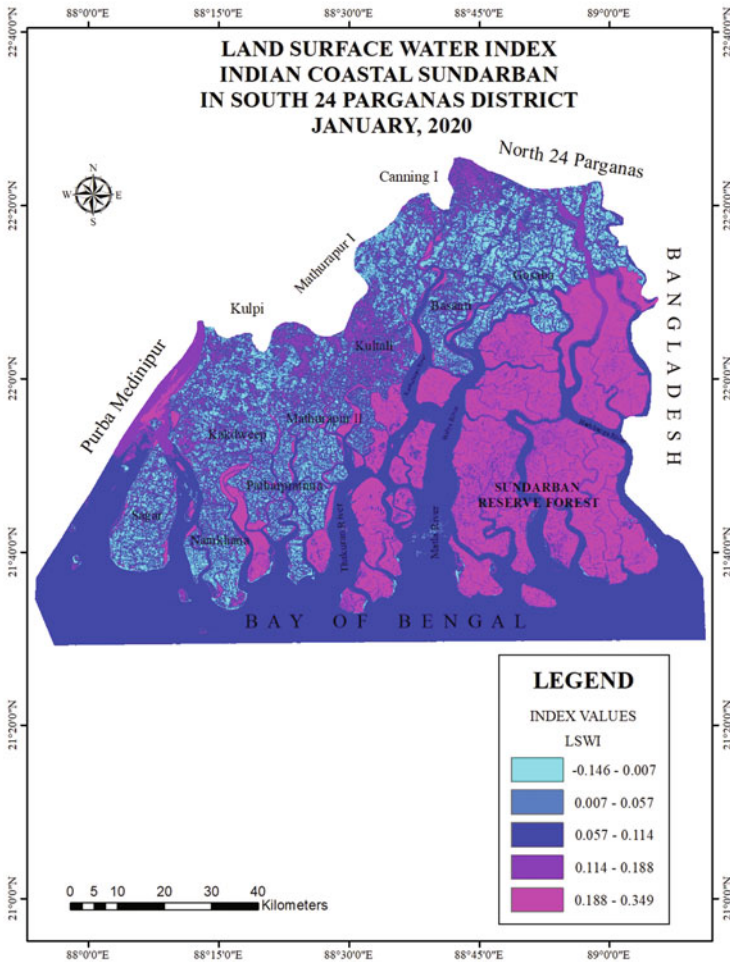
Map 2.11 LSWI map of the study area in January 2020
Source: Compiled from USGS Platform and Prepared by the Researchers

Comparative Analysis of Temporal Change Detection of Vegetation Health

In this research work, an attempt has been made to understand the temporal change detection analysis of vegetation health; the researchers calculated the rate of change (%) from January to May and May to December 2020 of each class of different indices, including NDVI, SAVI and LSWI. The chi-square technique (Rana and Singhal 2015) has been applied to determine if the rate of change is uniform or not. Chi-square has been calculated using the below formula:
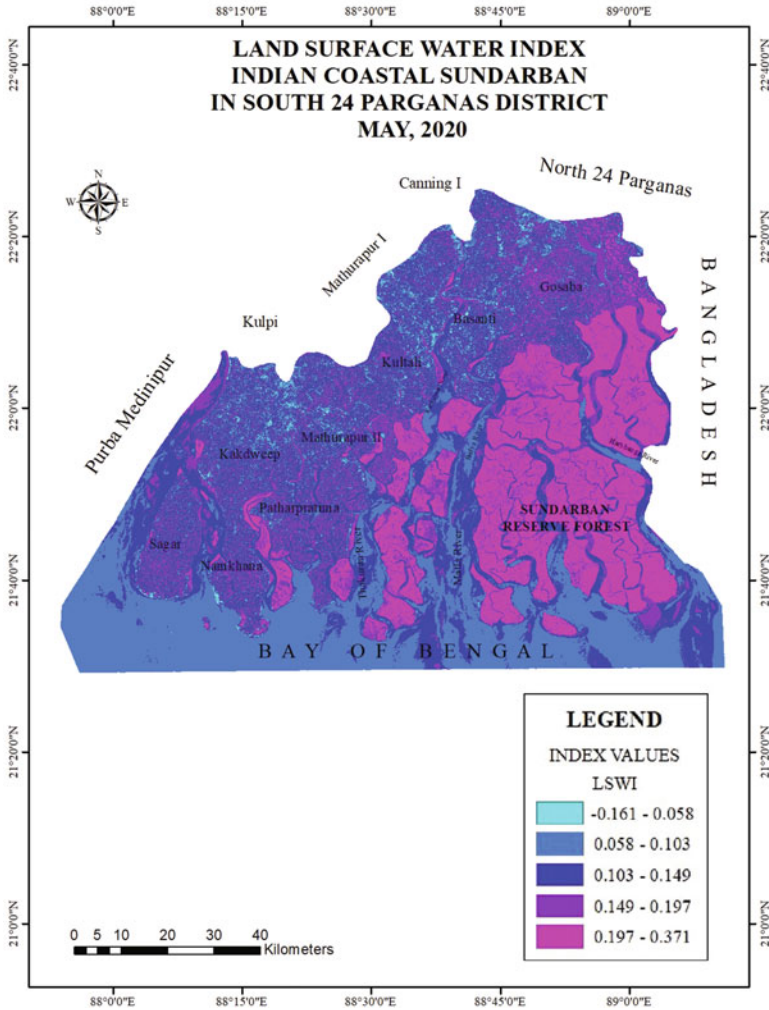
Map 2.12 LSWI map of the study area in May 2020
Source: Compiled from USGS Platform and Prepared by the Researchers

$$X^2 = \sum \frac{(o - e)^2}{e}$$

Where $X^2 = chi\text{-}square$
O = observed frequency
e = expected frequency

Expected frequency has been calculated using the below formula:
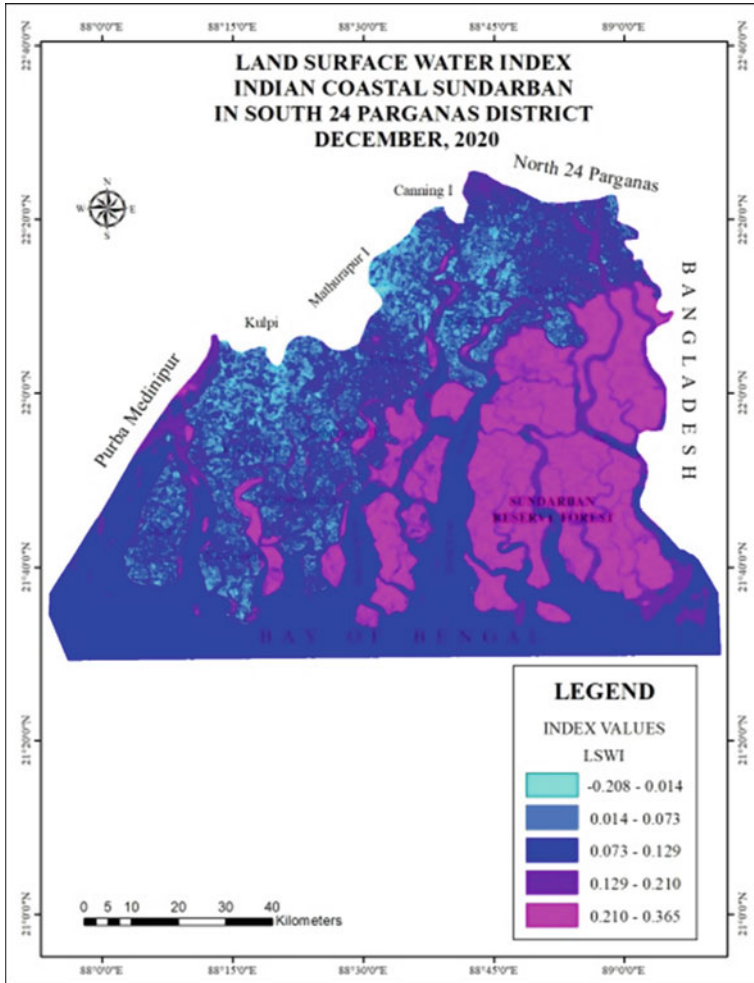
Map 2.13 LSWI map of the study area in December 2020
Source: Compiled from USGS Platform and Prepared by the Researchers

$$\textbf{Expected Frequency } (E) = \frac{\textbf{(Column Total* Row Total)}}{\textbf{Grand Total}}$$
$$\textbf{Degree of Freedom } (df) = \textbf{(Row} - \textbf{1)*(Column} - \textbf{1)}$$

Rate of Change of Vegetation Health from January

Table 2.16 shows the rate of change detection of different NDVI, SAVI and LSWI classes from January to May 2020. From this table, it can be stated that the very low

Table 2.16 Rate of change of vegetation health of selected three indices from January to May 2020

Classes	Rate of change between January and May 2020			Total
	NDVI	SAVI	LSWI	
Very low	41.32	7.64	82.67	131.63
Low	−29.48	87.59	175.70	233.81
Moderate	-29.04	10.25	−54.79	−73.58
High	12.90	−27.41	49.93	35.42
Very high	−18.77	−55.60	−28.64	−103.01
Total	−23.07	22.47	224.87	224.28

Pearson Chi-Square – 147.40, Degree of Freedom – 8, t Critical at the 0.05, i.e. 15.507. Hence there is a uniform change between January to May 2020 in all indices.

Source: Computed by the Researchers

(41.32%) and high class (12.90%) of NDVI represent positive change and low (−29.48%), moderate (−29.04%) and very high classes (−18.77%) represent negative change. Because of the rapidly increasing population, the built-up area also increased, and as a result, the vegetative area decreased. In addition, due to the immediate consequence of SuCS Amphan, the water level increased, so vegetation cover was affected. In the case of SAVI, a quite similar result can be identified. It is positive for very low (7.64%), low (87.59%) and moderate classes (10.25%) and negative for high (−27.41%) and very high classes (−55.60%). Owing to excessive rainfall and storm surges, the soil becomes moist and shows lower reflectance in this time frame. As a result, it indicates a low amount of non-vegetative area.

On the other hand, LSWI indicates a positive change for very low (82.67%), low (175.70%) and high classes (49.93%) and harmful for moderate (−54.79%) and very high classes (−28.64%). This is due to the concentration of dense mangrove cover in the study area. It indicates high LSWI values, but as an immediate result of Amphan, the forest cover area shows a decreasing trend. The result obtained from the chi-square test showed that there is a constant change between January to May 2020 in all indices.

Rate of Change of Vegetation Health from May to December 2020

Table 2.17 shows the rate of change detected of different NDVI, SAVI and LSWI classes from May to December 2020. From this table, it can be stated that moderate (37.83%) and very high (7.24%) classes of NDVI represent positive change and very low (−5.13%), low (−40.18%) and high classes (−2.22%) represent negative change. This indicates that within seven months after the incident of Amphan the vegetation cover of the study area started to grow positively. As a result, the positive change can be seen in the very high class of NDVI. In the case of SAVI, it is positive for very low (24.56%), high (52.10%) and very high classes (96.18%) and negative for low (−77.51%) and moderate classes (−11.29%). It means a rapid positive sign of the growth of vegetation can be seen in the study area; therefore, 96.18% change

Table 2.17 Rate of change of vegetation health of selected three indices from January to May 2020

Classes	Rate of change between May and December 2020			Total
	NDVI	SAVI	LSWI	
Very low	−5.13	24.56	−56.58	−37.15
Low	−40.18	−77.51	−62.63	−180.32
Moderate	37.83	−11.29	102.59	129.13
High	−2.22	52.10	−17.81	32.06
Very high	7.24	96.18	52.35	155.77
Total	−2.46	84.04	17.92	99.50

Pearson Chi−Square – −57.834, Degree of Freedom – 8, t Critical at the 0.05 i. e. 15.507. Hence no uniform changes occurred between May to December 2020 in all indices.

Source: Computed by the Researchers

can be observed in the very high class of SAVI. On the other hand, LSWI indicates a positive change for moderate (102.59%) and very high classes (52.35%) and negative for very low (−56.58%), low (−62.63%) and high classes (−17.81%). This is due to the concentration of dense mangrove cover in the study area. It indicates high LSWI values, which means the degraded health condition of the vegetation of the study area started to recover. The result obtained from the chi-square test showed that no uniform changes occur between May to December 2020 in all indices.

Correlation Analysis Among NDVI, SAVI and LSWI

We conducted several correlation analyses to understand the relationship between the percentage of area in different NDVI and SAVI classes in January 2020. From Fig. 2.8, it can be pointed out that a perfect positive relationship exists between different classes of NDVI and SAVI during January 2020. The square value of the correlation coefficient (R^2) is 1, which supports the strong positive relationship. That means during January, as the study region experienced the winter season when days are longer than the night due to plenty of sunshine and associated favourable environment, there is a high opportunity for the vegetation to grow. On the other hand, the relationship between the percentage of area in different SAVI and LSWI classes during January 2020 can be understood from the Fig. 2.9. Here it can be seen that there is a negative relationship between these two variables, and the value of R^2 (0.0072) also supports the statement. It is obviously because of less reflectance from the moist land surface of the study area. A significant difference can be observed from the scenario of May 2020.

Figure 2.10 points out that there is also a positive relationship between different NDVI and SAVI classes in May 2020. However, the degree of relationship is relatively lower ($R^2 = 0.146$) than in January. It is because of waterlogging in the low lying vegetative areas, storm surges, entry of saline water in the agricultural field, etc., caused by SuCS Amphan in the study area. As a result, some variation can be observed in the values of different classes of NDVI and SAVI during May 2020.

Fig. 2.8 Relationship
between percentage of area
in different NDVI and SAVI
classes (January 2020)
Source: Computed by the
Researchers

Relation Between Percentage of Area in Different NDVI and SAVI Classes, January, 2020

$y = 1x - 0.0004$
$R^2 = 1$

Fig. 2.9 Relationship
between percentage of area
in different SAVI and LSWI
classes (January 2020)
Source: Computed by the
Researchers

Relation Between Percentage of Area in Different SAVI and LSWI Classes, January, 2020

$y = -0.2527x + 25.054$
$R^2 = 0.0072$

Fig. 2.10 Relationship
between percentage of area
in different NDVI and SAVI
classes (May 2020)
Source: Computed by the
Researchers

Relation Between Percentage of Area in Different NDVI and SAVI Classes, May, 2020

$y = 0.295x + 14.1$
$R^2 = 0.1462$
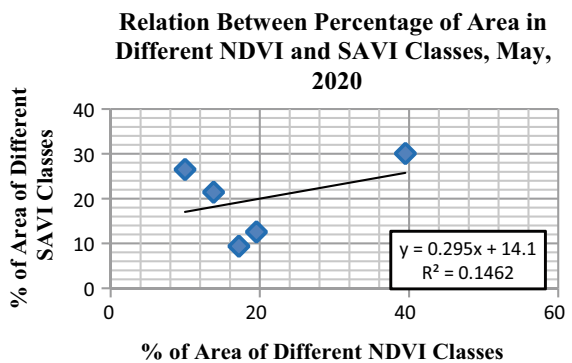
In the case of the relationship between the percentage of area in different SAVI and LSWI classes during May 2020, it can be seen in Fig. 2.11 that a very poor positive relationship exists between these two variables, where the R^2 value is 0.025 which is too poor to support the relationship.

Fig. 2.11 Relationship between percentage of area in different SAVI and LSWI classes (May 2020) Source: Computed by the Researchers
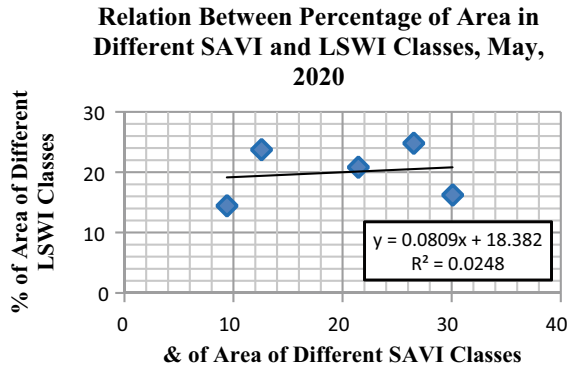
Fig. 2.12 Relationship between percentage of area in different NDVI and SAVI classes (December 2020) Source: Computed by the Researchers
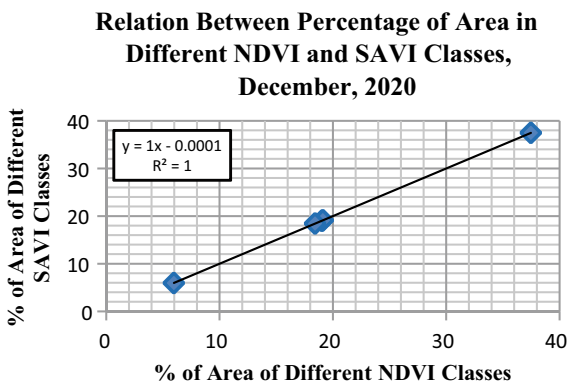
Fig. 2.13 Relationship between percentage of area in different SAVI and LSWI classes (December 2020) Source: Computed by the Researchers
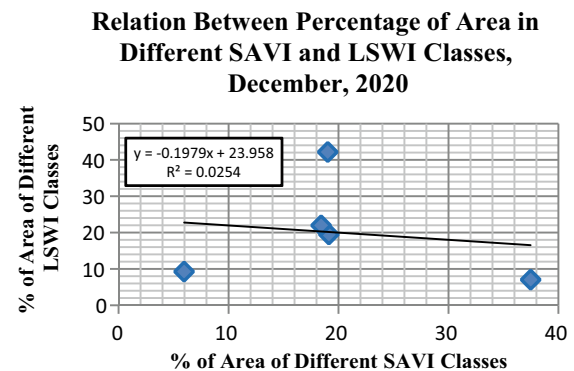
In the case of December 2020, a perfect positive relationship can be identified between different classes of NDVI and SAVI, which can be seen Fig. 2.12. The square value of the correlation coefficient (R^2) is 1, which supports the positive relationship very strongly. From this relationship, it can be understood that the post-Amphan phase is when the vegetative cover started to recover. Thus, both NDVI and SAVI represent very high values, especially in the southeastern part of the study area where the Sundarban Biosphere Reserve is located. Figure 2.13 shows the

relationship between the percentage of area in different SAVI and LSWI classes during December 2020. Here poor negative correlation can be found between the considered variables. The value of R^2 is 0.025, which indicated the relationship was very poorly supported. It is at that time when the effects of SuCS Amphan are gradually being recovered from, and there is an absence of rainfall which causes relatively low values of different classes of LSWI and high values of SAVI of the study area.

Findings of the Study

Significant findings of the study include:

1. The Super Cyclonic Storm (SuCS) "AMPHAN" was the second SuCS over the Bay of Bengal (BoB) after SuCS Odisha in 1999.
2. The highest percentage of area (43.73%) is occupied by the river during May among the studied months due to extreme cyclonic rainfall associated with Amphan in the study area.
3. Only 12.42%, i.e. the lowest percentage, of the area is occupied by agricultural land during May because of inundation of agricultural land due to flooding caused by the breakdown of the weak embankment.
4. A sharp decline of aerial coverage of mangrove forest can be seen during January to May because of uprooting of trees and destruction caused by SuCS Amphan.
5. Throughout the year, the built-up area represents a significantly increasing trend due to the increasing pressure of the study area population.
6. As an effect of SuCS Amphan, the maximum changes in LULC classes have occurred from May to December 2020.
7. The southeastern part and a few scattered southwestern parts of the studied blocks signify a high SAVI value (0.349–0.634), indicating dense vegetation concentration as this region falls under the Sundarban dense forest cover region dense mangrove cover areas.
8. Part of Gosaba, Basanti, Kkdwip, Sagar, Namkhana and Pathar Pratima blocks have very low LSWI values for the three maps (−0.146, −0.161 and −0.208, respectively) due to the relatively high concentration of non-vegetative areas.
9. The result obtained from the chi-square test indicated a uniform change between January and May 2020 in all indices, but it is not uniform in nature from May to December 2020.
10. There is a perfect positive relationship between different NDVI and SAVI classes during January 2020 and December 2020.

Problem Identified

Major problems that are identified in this study include:

1. The result of the aggregate rank score highlighted that maximum changes in land use and land cover classes had occurred from May to December 2020. In this time frame, a rapid population increase is noticed in the coastal blocks of the Indian Sundarban region, which is a threat to biological diversity.
2. Significant changes have been identified in the dense vegetation cover areas, which is the mangrove ecosystem of the study area. It is globally known that mangrove protects the coastal environment from any cyclonic harm. Still, from this research work, it has been evident that every year due to the frequent cyclonic storms, the mangrove ecosystem has gradually degraded, which is a matter of great concern.
3. The information extracted from Landsat 8 satellite imageries depicted the scenario of rapid loss of vegetative areas and loss of agricultural production due to the arrival of SuCS Amphan on the coast of the Indian Sundarban region.
4. Results obtained from the Land Surface Water Index (LSWI) indicated that, excluding the Sundarban area, the remaining part is capable of very low surface water. This region is now transforming into a non-vegetative human environment, which is a threat for the Sundarban.

Proposals

To eradicate the above mention problems, the following measures can be taken into consideration:

1. New mangrove species should be planted in the places where maximum vegetation damage occurred during SuCS Amphan.
2. Particular focus should be given to disaster management activities to handle the situation during the upcoming devastating cyclonic crisis efficiently.
3. Training activities should be encouraged for the coastal residents by which then can secure themselves during the violent cyclonic condition.
4. The government should be more careful about the construction of disaster shelter rooms, provision of grants, construction of new sustainable embankments, kind of activities, etc.
5. Nowadays, due to the advancement of modern technology, the Indian Meteorological Department (IMD) can project any climatic hazard very efficiently; therefore, robust network connectivity should be developed by which any kind of security alert related to coastal hazard projected by IMD can be spread the fastest way to the residents.
6. In Gosaba, Basanti and Sagar blocks, the jetty service was damaged due to the cyclone. Thus, special focus should be given to constructing new unbreakable eco-friendly jetty services of the study area.

7. A social forestry programme should be encouraged to increase attention regarding the significance of the mangrove ecosystem of the study area.

Conclusion

From this discussion, it can be concluded that Sundarban is worldwide famous because of its mangrove vegetation. Owing to the emergence of the frequent cyclonic storms, the mangrove ecosystem is degrading, which is one of the most severe issues in the present-day context. It is time for sustainable management of the Indian coastal Sundarban region occupied by the mangrove ecosystem. There is an urgent need to call for comprehensive interdisciplinary approaches for decision-making processes. As identified by this research work, the emerging geospatial technologies can offer the most accurate and cost-effective ways to protect the mangrove ecosystem from all kinds of adverse effects. The coastal region of Indian Sundarban is rapidly changing because frequent cyclonic storms have severe effects on land use and land cover condition, which is a matter of great concern. In this respect, the participation of local people with the governing body is a solid requirement to protect the future of the coastal environment from any meteorological harm.

Conflict of Interest   The authors declare no conflict of interest.

Ethical Considerations   Ethical issues (Including plagiarism, informed consent, misconduct, data fabrication and/or falsification, double publication and/or submission, redundancy, etc.) have been completely observed by the authors.

References

Print Media

Bhowmik AK, Cabral P (2013) Cyclone Sidr impacts on the Sundarbans floristic diversity. Earth Sci Res 2(2):62–79. https://doi.org/10.5539/esr.v2n2p62
Bid S (2016) Change detection of vegetation cover by NDVI technique on catchment area of the Panchet Hill Dam, India. Int J Res Geogr 2(3):11–20. https://doi.org/10.20431/2454-8685.0203002

Bofana J et al (2020) Comparison of different cropland classification methods under diversified agro-ecological conditions in the Zambezi River Basin. Remote Sens 12:1–23. https://doi.org/10.3390/rs12132096

Chandrasekar K et al (2010) Land Surface Water Index (LSWI) response to rainfall and NDVI using the MODIS Vegetation Index product. Int J Remote Sens 31(15):3987–4005. https://doi.org/10.1080/01431160802575653

Chaudhuri AB, Choudhury A (1994) Mangrove of the Sundarban, India, vol 1, no 1. IUCN- The World Conservation Union, Bangkok, pp 7–12

Datta D, Deb S (2012) Analysis of coastal land use and land cover changes in the Indian Sundarbans using remotely sensed data. Geo-spatial Inf Sci 15(4):241–250

Datta D, Guha P, Chattopadhyay RN (2010) Application of criteria and indicators in community based sustainable mangrove management in the Sundarban, India, pp 468–477

Debnath A (2018) Land use and land cover change detection of Gosaba island of the Indian Sundarban region by using multi-temporal satellite image. Pratidhwani Echo 7(1): 209–217. ISSN: 2278-5264

Demirel H, Ozcinar C, Anbarjafari G (2010) Satellite image contrast enhancement using discrete wavelet transform and singular value decomposition. IEEE Geosci Remote Sens Lett 7(2): 333–337

Epiphanio JCN, Huete AR (1995) Dependence of NDVI and SAVI on sun/sensor geometry and its effect on fAPAR relationships in Alfalfa. Remote Sens Environ 51(3):351–360. https://doi.org/10.1016/0034-4257(94)00110-9

Gandhi GM, Parthiban S, Thummalu N, Christy A (2015) Ndvi: vegetation change detection using remote sensing and GIS – a case study of Vellore District. Elsevier B V. https://doi.org/10.1016/j.procs.2015.07.415

Ganesh V, Kumar ST (2015) Impact assessment of Tropical Cyclone Hud Hud on coastal region of Visakhapatnam, Andhra Pradesh, India. ISPRS Ann Photogram Remote Sens Spat Inf Sci 2(2). https://doi.org/10.5194/isprsannals-II-2-W2-123-2015

Ghosh S, Mistri B (2020) Coastal agriculture and its challenges: a case study in Gosaba Island, Sundarban, India. Space Cult 8(2):140–154. https://doi.org/10.20896/saci.v8i2.747

Gupta S, Jain I, Johari P, Lal M (2018) Impact of climate change on tropical cyclones frequency and intensity on Indian Coasts. In: Proceedings, international conference on remote sensing for disaster risk management, Springer series in geomechanics and geo-engineering. https://doi.org/10.1007/978-3-319-77276-9_32

Haque A, Jahan S (2016) Regional impact of Cyclone Sidr in Bangladesh: a multi-sector analysis. Int J Disaster Risk Sci 7:312–327. https://doi.org/10.1007/s13753-016-0100-y

Hossain SM, Karlson M (2017) Assessment of land cover change in the sundarbans caused by Cyclone Roanu using Landsat imagery. In: Proceedings, international conference on disaster risk management, Dhaka, Bangladesh

Huete A (1988) A soil-adjusted vegetation index (SAVI). Remote Sens Environ 25(3):295–309. https://doi.org/10.1016/0034-4257(88)90106-X

Jensen JR (1996) Introductory digital image processing: a remote sensing perspective, 2nd edn. Prentice Hall, Inc, Upper Saddle River

Kar SN, Bondyopadhyay S (2015) Tropical Storm Aila in Gosaba Block of Indian Sundarban: remote sensing based assessment of impact and recovery. Geogr Rev India 77(1):40–54

Kumar S, Lal P, Kumar A (2020) Turbulence of tropical cyclone 'Fani' in the Bay of Bengal and Indian subcontinent. Nat Hazards 103:1613–1622. https://doi.org/10.1007/s11069-020-04033-5

Kunkel ML, Flores AN, Smith TJ, McNamara JP, Benner SG (2011) A simplified approach for estimating soil carbon and nitrogen stocks in semi-arid complex terrain. Geoderma 16(5):1–11

Liu B, Chen J, Zhang W (2018) Land cover change detection using multiple shape parameters of spectral and NDVI curves. Remote Sens:12–51. https://doi.org/10.3390/rs10081251

Malik S et al (2019) Intra-annual variations of vegetation status in a sub-tropical deciduous forest-dominated area using geospatial approach: a case study of Sali watershed, Bankura, West

Bengal, India. Geol Ecol Landsc 4(4):257–268. https://doi.org/10.1080/24749508.2019.1633219

Malo AR, Nicholson SE (1990) A study of Rainfall dynamics in African Sahel using Normalized Difference Vegetation Index. J Arid Environ 19:1–24

Mishra PS, Panigrahi R (2014) Storm impact on South Odisha Coast, India. Int J Adv Res Sci Eng 3(11):209–225

Morawitz DF, Blewett TM, Cohen A et al (2006) Using NDVI to assess vegetative land cover change in Central Puget Sound. Environ Monit Assess 114(3):85–106

Neogi S, Basu D, Mouri L, Kabir S, Masum M, Syed H, Kopprio G et al (2016) Sundarban mangroves: diversity, ecosystem services and climate change impacts, Bangladesh Agricultural University. Asian J Med Biol Res 2(4):488–507

Priyadarshini NK, Sivashankari V, Shekhar S (2019) An assessment of land cover change dynamics of Gaja Cyclone in Coastal Tamil Nadu, India Using Sentinel 1 SAR Dataset. Int Arch Photogram Remote Sens Spat Inf Sci XLII(3WB). https://doi.org/10.5194/isprs-archives-XLII-3-WB-323-2019

Rahman S, Rahman H, Shahid S, Khan UR, Jahan N, Ahmed UZ, Khanum R, Ahmed FM, Mohsenipour M (2017) The impact of Cyclone Aila on the Sundarban Forest ecosystem. Int J Ecol Dev 32(1):87–97

Rana R, Singhal R (2015) Chi-square test and its application in hypothesis testing. J Pract Cardiovasc Sci 1(1):69–71. https://doi.org/10.4103/2395-5414.157577

Richardson A, Everitt J (1992) Using spectral vegetation indices to estimate rangeland productivity. Geocarto Int 1:63–77

Ricotta C, Avena G, Palma AD (1999) Mapping and monitoring net primary productivity with AVHRRNDVI time-series: statistical equivalence of cumulative vegetation indices. ISPRS J Photogram Remote Sens 54:325–331

Rwanga SS et al (2017) Accuracy assessment of land use/land cover classification using remote sensing and GIS. Int J Geosci 8:611–622. https://doi.org/10.4236/ijg.2017.84033

Sarkhel P, Biswas D, Swin SS (2019) A review of cyclone and its impacts on the Coast Belt of Odisha. Int J Eng Res Technol 8(5):759–762

Scanlon TM, Albertson J, Caylor K, Williams C (2002) Determining land surface fractional cover from NDVI and rainfall time series for a savanna ecosystem. Remote Sens Environ 82:376–388

News Media

Adil A (2019) India: death toll from cyclone Fani climbs to 64, World, Asia-Pacific. Retrieved from https://www.aa.com.tr/en/asia-pacific

Ahmed M (2008) Fifteen killed in Bangladesh storm. Reuters. Retrieved from https://www.reuters.com/article/worldNews/idUSTRE49R0L920081028

Chowdhuri DR (2020) In pictures: Cyclone Amphan hits India and Bangladesh. Retrieved from https://edition.cnn.com

Khan F (2007) Cyclone kills hundreds in Bangladesh. Retrieved from https://www.nytimes.com/2007/11/17/world/asia/17bangladesh.html

Naeem R (2020) Fifty years of the cyclone that triggered a Civil War and created Bangladesh. Retrieved from https://thewire.in/history/cyclone-bhola-mujibur-rahman-bangladesh-liberation-yahya-khan-pakistan

Pal S (2017) Cyclone kills two in Malda, damages 6,000 houses, mango and litchi orchards. Retrieved from https://www.hindustantimes.com/kolkata

PTI (2013) 21 killed, over a lakh hit as cyclone Aila strikes, Business Standard. Retrieved from https://www.business-standard.com/article/economy-policy

Singh SS (2020) Cyclone Amphan kills 72 in West Bengal, brings life to a halt. Retrieved from https://www.thehindu.com/news/cities/kolkata

TOI (2019) Cyclone Bulbul kills 10 in West Bengal, 2.73 lakh families affected in the state. Retrieved from https://timesofindia.indiatimes.com

Yadav PB (2016). Deep Depression BOB 01 Warning Bulletin 5 issued on 18 May 2016. Retrieved from http://www.rsmcnewdelhi.imd.gov.in/images/cyclone_pdfs/indian_1463580122.pdf

Official Reports

India Meteorological Department (2015) Cyclonic Storm, KOMEN over the Bay of Bengal (26 July–02 August 2015): a report. Retrieved from http://rsmcnewdelhi.imd.gov.in/images/pdf/publications/preliminary-report/KOM.pdf

Indian Meteorological Department (2020) Super Cyclonic Storm "AMPHAN" over the southeast Bay of Bengal (16th–21st May 2020): summary. Retrived from https://reliefweb.int/report

International Federation of Red Cross and Red Crescent Societies (2013) Disaster relief emergency fund (DREF) Bangladesh: Tropical Cyclone Mahasen. Retrieved from https://reliefweb.int/sites/reliefweb.int/files/resources/MDRBD013dref.pdf

Needs Assessment Working Group (NAWG) Bangladesh (2020) Cyclone AMPHAN Joint Needs Assessment (JNA) Retrieved from https://reliefweb.int/report/bangladesh

UNICEF (2020) The impact of Cyclone Amphan across Kolkata. Retrieved from https://www.unicef.org/media/82101/file/India-West-Bengal-Cyclone-Amphan-SitRep-22-May-2020.pdf

Mr. Prosenjit Kayal is currently a PhD research scholar in the Department of Geography and Applied Geography, University of North Bengal. His current research interests include Application of Geoinformatics, Planning and Management, Geography of Rural development, Environmental Issues and Development related outlook.

Dr. Indrajit Roy Chowdhury is an Assistant Professor in the Department of Geography and Applied Geography, University of North Bengal. His current research interests are in the field of Remote Sensing & GIS, Social Geography, Cultural Geography, Geography of Rural development, Human Geography, Geography of Tourism, Regional Planning and Development.

Chapter 3
Flood Susceptibility Mapping Using the Frequency Ratio (FR) Model in the Mahananda River Basin, West Bengal, India

Arnab Ghosh ⬤, **Malabika Biswas Roy** ⬤, **and Pankaj Kumar Roy** ⬤

Abstract Floods are one of the most inevitable natural disasters that have occurred over time. Floods not only harm people but also livestock and property and, above all, generate the problem of land loss. Currently, the incidence of floods is increasing due to the variability of the weather and the variable nature and amount of rainfall. There are many rivers in the Duars and Barind region of West Bengal and its lowlands which cause severe flooding during the monsoon season. However, due to the changing and complex nature of this flood, it is not possible to measure and predict it. This chapter highlights flood susceptibility and vulnerability zones along the Mahananda River basin through the frequency ratio (FR) model. Flood-prone areas along the Mahananda River basin have been identified, using various parameters and machine learning algorithms. The flood susceptibility model has also been validated using the receiver operating characteristic curve (ROC). The flood vulnerable map constructed with the FR model is very accurate for this river basin with strong positive relation. The outcome of this chapter will help planners and decision makers take some probable measures to minimize vulnerability to floods in this region.

Keywords Flood susceptibility · Flood vulnerability · Mahananda River basin · Frequency ratio (FR) model · Receiver operating characteristic (ROC)

A. Ghosh · P. K. Roy
School of Water Resources Engineering, Jadavpur University, Kolkata, India
e-mail: pankaj.kroy@jadavpuruniversity.in

M. B. Roy (✉)
Department of Geography, Women's College, Calcutta, Kolkata, India

Introduction

Natural disasters such as earthquakes, landslides, floods, tsunamis, volcanic eruptions, etc. arbitrarily destroy the natural and cultural environment of a region. Floods are the most severe of these natural disasters and have inundated a vast area (Mallinis et al. 2011). Due to geomorphological reasons, the carrying capacity of the river decreases and the floodplain cannot carry excess water, causing floods in the area (Kazakis et al. 2015). At present, however, continuous population growth in the plains and encroachment on river flows have resulted in floods. Each year, 170 million people worldwide are affected by floods. However, in recent years, erratic weather has increased the amount of rainfall and caused floods (Demir and Kisi 2016). Floods not only inundate land, but also cause significant damage to people, livestock, and property (Phongsapan et al. 2019). The rivers of eastern India have been constantly flooded due to sedimentation. In addition, the states of Bihar, Uttar Pradesh, Assam, Odisha, and Jammu and Kashmir in India are prone to floods (Sahoo and Sreeja 2015; Patel et al. 2017). Not only sedimentation but also increased rainfall due to climate change and lack of scientific river planning are some of the reasons for these floods. Moreover, the floodplain region of eastern India has the highest population density, which in turn is a major obstacle to the creation of the River Regulation Zone (RRZ) and the cause of maximum flooding. In addition, increasing the amount of runoff in urban areas increases the amount of flooding, increasing the likelihood of flooding (Heidari 2014; Foudi et al. 2015). A region needs to have proper flood disaster management to control flooding. Flood disaster control requires proper assessment of the flood situation and proper management for flood mitigation. The exact and important result of this flood disaster management is the identification of flood-prone areas through the flood hazard index and the establishment of the necessary infrastructure for flood control (Hudson et al. 2014; Perera et al. 2015). However, not only in the plains, but also in the hilly areas, floods are often seen. Floods in mountainous areas are known as flash floods, which occur suddenly and in a short period of time and inundate large areas and cause extensive damage to people, property, and cattle. This type of flooding also occurs in desert or semi-arid regions. The foothills of the Himalayas are covered by steep plains, which are mainly fed by water carried by various mountain rivers (Das et al. 2015; Mandal and Chakrabarty 2016). As a result, these rivers come from the top of the hill and spread across the plains, creating a portion of floodplain in this area. Heavy rains during the monsoons cause the water level to rise in the mountain rivers, and this rising water descends into the floodplains at the bottom and floods the entire region.

Various models have been used by many researchers and government policymakers to understand the real causes, nature, and extent of floods (Kisi et al. 2012). However, various conventional hydrological models do not accurately comprehend the nature and extent of floods (Tehrany et al. 2014, 2015a, b, 2017). Currently, various hydrological model studies and spatial data analysis are being used to estimate the nature and outline of floods. A good example of a future flood control plan is the development of a flood hazard map, which helps identify

flood-inundated areas. However, this type of flood hazard map or flood zoning must take the help of several criteria (Jaafari et al. 2014). With the advent of Geographic Information System (GIS) and Remote Sensing (RS), it has become possible to easily create flood hazard maps by analysing natural disasters. Previously, considerable work has been done on flood hazard indexing, flood susceptibility mapping, and flood analysis with the help of GIS (Pradhan et al. 2014). However, a number of criteria must be used to identify flood-prone areas, which are essentially part of the multicriteria decision analysis (MCDA) (Malczewski 2006). The MCDA method is a significant tool that helps us to arrive at a definite conclusion by combining numerous inconsistent data. The MCDA method helps to arrive at solutions to any kind of practical, environmental, and socioeconomic problem (Ghanbarpour et al. 2013). By combining the MCDA method with GIS, any spatial modelling of natural disasters can be done and a conclusion can be reached. Among the models that are made using the MCDA method, the analytical hierarchy process (AHP) is popular for determining flood susceptibility in terms of quality and quantity (Sar et al. 2015; Dandapat and Panda 2017). Also, artificial neural networks (ANN) (Kia et al. 2012; Tiwari and Chaterjee 2010), adaptive neuro-fuzzy interface system (ANFIS) (Mukerji et al. 2009; Sezer et al. 2011), 1D water surface elevation/flood modelling (Kumar et al. 2017), Rainfall-Runoff-Inundation (RRI) model (Pakoksung and Takagi 2016), satellite-based discharge data and Gumbel's flood frequency analysis (Prasad and Pani 2017), weights of various models like evidence (WOE) (Rahmati et al. 2016a), logistic regression (LR) (Pradhan 2010), frequency ratio (FR) (Lee et al. 2012), HAZUS, HEC-FDA, etc. have been used to determine flood susceptibility and flood hazard in different areas around the world by many researchers. Although the ANN model is used to determine flood susceptibility, the long-range dataset cannot be properly aligned with this model, and the ANN model is not at all effective in determining the future location and nature of floods (Ghalkhani et al. 2013). Both ANN and ANFIS are based on incomplete and uncertain datasets, which do not give accurate results (Lohani et al. 2012). Again, the AHP model becomes more reliant on information from experts, giving a vague idea of the actual environmental data, which is a major problem for the AHP model (Chowdary et al. 2013). FR is the simplest and most understandable statistical method for determining flood susceptibility, which can be easily applied to any region and is used for flood risk analysis and mapping of that region (Samanta et al. 2018a, b; Sarkar and Mondal 2019). The FR model combines the LR and WOE models with flood risk mapping, flood susceptibility mapping, and analysis. Also, the FR model is basically a kind of bivariate statistical analysis (BSA), where each parameter is given importance according to their value, and the importance of each parameter in flood formation is examined (Jebur et al. 2014). The flood risk map based on the FR model plays an important role in determining the flood vulnerability of any region (Tehrany et al. 2015a, b; Samanta et al. 2018a, b). The FR model, with the help of various sophisticated software from RS and GIS, assembles with GIS to determine the susceptibility to floods of a region.

Mostly during the monsoon (June–September), floods occur in India. According to the National Flood Commission, about 40 million ha areas in India fall under flood

prone areas. About eight million ha of land is flooded in India every year, including 3.8 million ha of agricultural land. It is pertinent to mention that most floods (70%) in India are mainly due to overflowing river water. Forty-two per cent of West Bengal is prone to floods, confined to 111 blocks and 18 districts. West Bengal has the highest number of floods along the Gangetic floodplain, causing extensive damage to human life and property (Das and Bandyopadhyay 2015). However, the ecologically diverse and topographically distinct Himalayan foothills or the Tarai-Duars regions have completely different levels of flooding and in most cases are confined to flash floods. But when the mountain rivers in the region carry large amounts of water during the monsoon season in the flood-prone areas of the plains, floods occur. Also, extensive damage due to the pressure of overpopulation has been noticed. Mahananda River is one of the main rivers along the Tarai-Duars region of West Bengal, which originates from the Paglajhora falls in the Darjeeling Himalayas. Encompassing Siliguri, it flows through Katihar and Purnia district in Bihar and Uttar Dinajpur, Malda district, in West Bengal, and joins the Ganges at Godagiri in Nawabganj district of Bangladesh (Rana 2018; Shil and Singh 2019). The river is recognized as one of the lifelines of North Bengal and is rich in settlements, agriculture, and industry on both sides. But floods along the floodplain area of the river have become an obstacle to the normal life of the people in this area. Rivers along the foothills of the Himalayas in the Tarai-Duars region change their channel with the floods and cause a lot of damage. Earlier, flood susceptibility was discussed through FR model in Tarai-Duars region along Teesta, Kulik, etc. rivers, but little was done on Mahananda River. Much work has been done on the Mahananda River basin, with changes in its channel dynamics and its impact on the riparian population. But every time the Mahananda basin was severely damaged by the floods, it was not possible to identify the flood-prone areas properly. The main objective of this chapter based on the above points is to determine the flood susceptibility of the Mahananda basin based on ground observation and geospatial FR model, which will help in implementing improved flood management and strategy. Furthermore, flood-prone maps of the Mahananda basin can be identified through the FR model, and flood disaster maps can be constructed which will help local government officials, researchers, and planners in formulating flood mitigation plans.

Materials and Methods

Study Area

The entire catchment area of the Mahananda River basin is limited to India, Nepal, and Bangladesh (extended from 24° 58′ to 27° 10′N and 87° 6′ to 88° 31′E). After originating from Paglajhora falls near Chimli in eastern Kurseong, Darjeeling Himalaya, and flowing as a mountain stream up to 20 km, the Mahananda River enters the plain land near Siliguri city, West Bengal (Fig. 3.1). The downstream course of the Mahananda River flows south-west beyond the town of Siliguri and
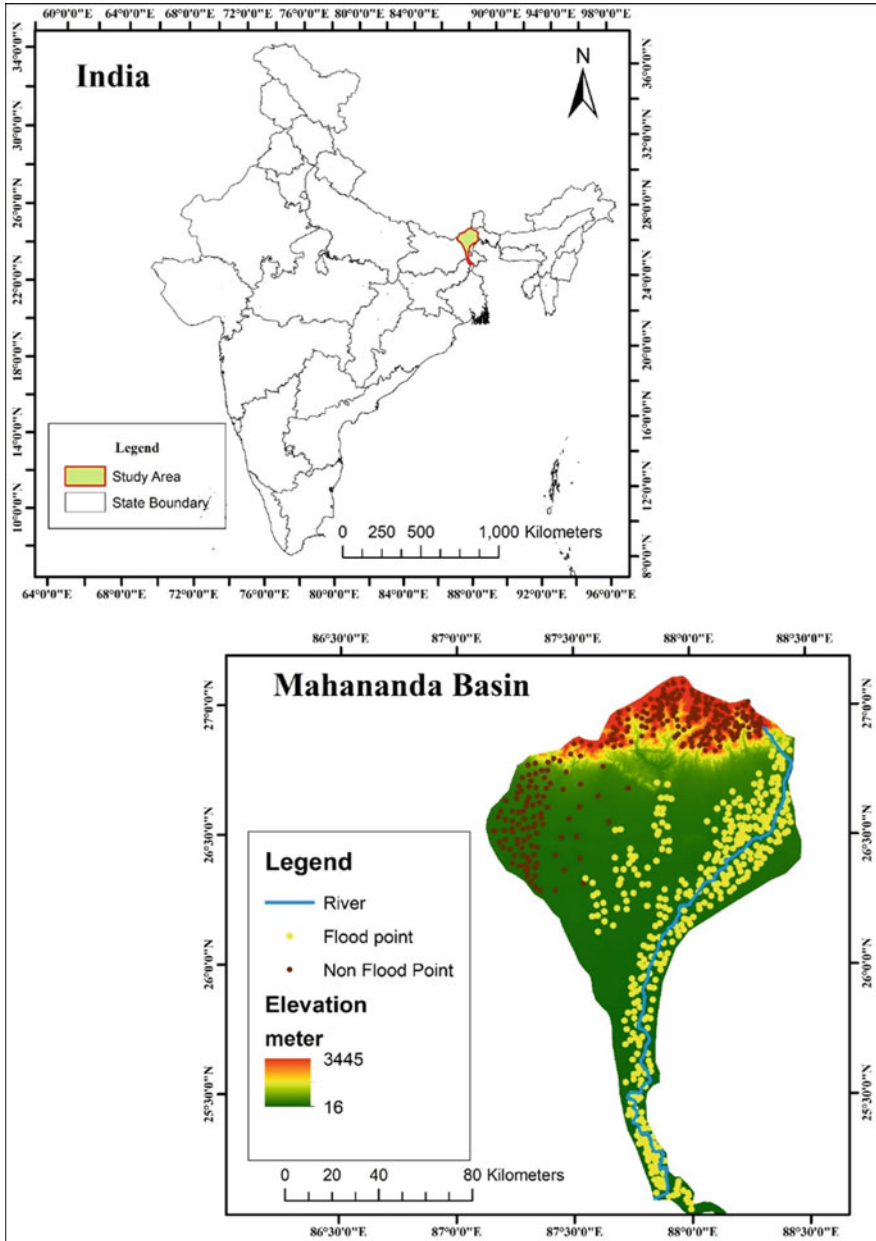
Fig. 3.1 Location of study area with training and prediction data set

joins the Ganges. After entering in Tentulia of Panchagarh District, Bangladesh, it re-emerges, crosses the north Dinajpur, Purnia, and Katihar districts, enters Bangladesh through Malda, and merges into the Ganges at Godagiri in Nawabganj

district. The Tangan, Douk, Nagar, Mechi, Kankai, Cheng, Balasan, and Kalindi rivers are the famous tributaries on the left and right banks of the Mahananda River (Rana 2018; Shil and Singh 2019). The 360-km-long Mahananda River flows 324 km in India and 36 km in Bangladesh, and the total catchment area is 20,600 sq. km, of which 11,530 sq. km are in India.

The Mahananda basin is based on the dendritic drainage pattern between Koshi Megafan in the west and Teesta Megafan in the east. The catchment area of the entire Mahananda basin is divided into two parts: the upper catchment (Sikkim Himalayas and Darjeeling Tarai-Duars region) and the lower catchment (the Barind plain formed between the Koshi–Mahananda corridors in the lower Gangetic southern plains with older alluvium). The entire basin region is composed of a hot and relatively humid monsoonal type of climate. The proximity of the Bay of Bengal to the southern part of the catchment, the location of the Himalayas and the Meghalaya Plateau to the north and north-east, controls the climate of the region (Rana 2018; Shil and Singh 2019). The coldest months in the region are January (17–21 °C), and after February, the temperature rises again. The monsoon prevails in the region in the first week of June, and the entire region experiences an uneven and spatial distribution of 120–400 cm of rainfall. The entire Mahananda basin region receives rainfall four times: during winter due to westerly winds, local cyclones in March–May, monsoon, and cyclonic rainfall. After leaving Siliguri at the upper catchment, the slope of the Mahananda River has decreased considerably, and it is safe to say that there is no continuous slope of the river in the Barind plain to the south. The existence of abundant oxbow lakes and abandoned palaeo channels in the lower catchment proves the dynamic behaviour of rivers in this region.

Data Used

Flood susceptibility mapping of the entire Mahananda basin has been developed based on the approval of six different types of thematic map layers (Table 3.1). Flood susceptibility is mapped by analysing and interpreting all data based on specific GIS platforms, consolidating data from all thematic map layers based on RS. Various weather and flood information from the IMD (Indian Meteorological Department), topographical map from the SOI (Survey of India), and soil information from NBSS-LUP (The National Bureau of Soil Survey and Land Use planning) have been collected to build flood susceptibility model of the basin area. Furthermore, field surveys were carried out during and after floods in the Mahananda basin in 2017 to obtain accurate flood information and identify accurate flood susceptibility areas. LANDSAT 8 OLI (Operational Land Images) of 2020 have been obtained from USGS Earth explorer for the survey and analysis of flood susceptibility mapping. The acquired Level 1 terrain corrected data (L1TC) has been carried through UTM 45 (Universal Transverse Mercator) north zone projection with WGS 84 (World Geodetic System) datum. The images have been retrieved from different sources and are not geo-corrected for accuracy. Geometric correction with a root-mean square

Table 3.1 Data sources used in this study

Sl. no.	Name of data	Data source	Character of data	Use of data
1	Satellite images	LANDSAT 8 OLI & Google earth	30 m & 0.5 m resolution	LULC, mapping flood-prone areas
2	Soil data	NBSS & LUP	1:50,000 scale	Soil types map
3	Rainfall data	IMD	Daily data	Rainfall distribution map
4	DEM & topo-graphical map	ALOS-PALSAR Grid & Hardcopy map	12.5 m resolution & 1: 50,000 scale	Slope, aspect, TWI, SPI, TRI, STI map
5	Field survey	Information about flood damaged area on 2017	GPS survey & image collection	Flooding areas of 2017
6	Published works	Paper, reports, Govt. office reports		

error (RMSE) of ± 0.5 pixels has been introduced to correct the image using the image registration technique. The Phased Array Type L-band Synthetic Aperture Radar (ALOS-PALSAR) data were acquired from the Japan Aerospace Exploration Agency (JAXA) and processed for the Digital Elevation Model (DEM) with 12.5 m resolution. All maps on susceptibility mapping were prepared with the help of Arc GIS v 10. 4.1.

Methodology

Flood Inventory Mapping

Past flood conditions must be scientifically verified to determine future flood conditions through flood susceptibility in a region (Manandhar 2010). To accurately explain the future flood situation, it is necessary to present the location and nature of past floods accurately (Merz et al. 2007). The flood inventory map of the Mahananda River basin has been compiled on the basis of field surveys and experimental observations of satellite images from the catastrophic flood situation of 2017. A total of 80 flood points have been randomly divided into two sections based on training and verification to calibrate and validate the results of flood susceptibility (Fig. 3.2). However, there are no specific rules for determining these points based on training and verification. But in the past literature as well as in present work, 70% of the flood points have been used for calibration, and 30% of the flood points have been used for validation (Pourghasemi and Beheshtirad 2014). On the basis of the discussions, it was found that most of the flood-prone areas are located on the river bank line or riparian zone of the floodplain area.
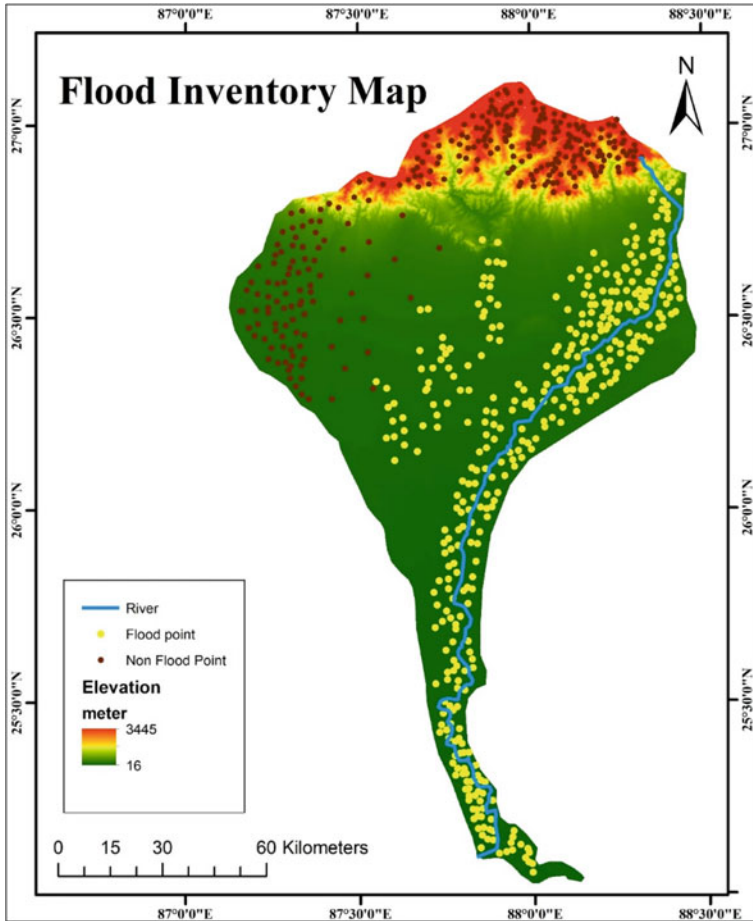
Fig. 3.2 Field observation point for flood inventory map of Mahananda basin

Flood Conditioning Factors

There are a number of geo-environmental and man-made factors behind the organization of floods in an area (Tehrany et al. 2015a). Therefore, in order to map the flood susceptibility of a region, appropriate factors have to be selected, as factors in one region may not be suitable for another region (Kia et al. 2012). However, for the current chapter, 12 factors have been identified (Table 3.2), namely: 1. slope, 2. aspect, 3. STI (sediment transport index), 4. TRI (topographic roughness index), 5. SPI (stream power index), 6. TWI (topographical wetness index), 7. rainfall, 8. distance from drainage, 9. LULC (land use and land cover), 10. soil type, 11. NDVI (normalized difference vegetation index), and 12. MNDWI (modification of normalized difference water index).

Table 3.2 Result of FR analysis on each factor

Factor	Class	Pixels number in class	% of pixel number class	Flood area in class	% of flood area class	FR value
Slope (^{0})	0–6.2	49,398	83.82	11,914,961	80.37	1.91
	6.21–15.5	2600	4.41	735,816	4.96	1.12
	15.51–24.24	1733	2.94	971,731	6.55	0.85
	24.25–33.26	2599	4.41	835,533	5.64	0.36
	33.27–71.89	2600	4.41	367,553	2.48	0.0
Aspect	Flat	12,133	20.59	1,893,844	12.78	1.36
	North	5200	8.82	809,218	5.46	0.48
	North-East	3466	5.88	1,384,370	9.34	0
	East	4333	7.35	1,649,764	11.13	0.52
	South-East	13,866	23.53	1,884,259	12.71	1.52
	South	4333	7.35	1,838,908	12.41	1.02
	South-West	5199	8.82	1,781,562	12.02	1.14
	West	6066	10.29	1,633,704	11.02	0.81
	North-West	2600	4.41	1,463,793	9.88	0
LULC	Agriculture	5199	8.83	1,652,616	11.09	0.87
	Build-up	7780	13.21	2,089,997	14.02	0.92
	Fallow	24,266	41.19	5,419,881	36.36	1.77
	Plantation	4333	7.36	721,437	4.84	0.35
	Sandbar	4333	7.36	1,516,575	10.17	0.78
	Vegetation	12,999	22.07	3,335,228	22.38	0.51
	Water body	0	0.00	170,231	1.14	0
Soil	Sandy loam	12,999	22.06	4,076,527	27.49	1.16
	Loam	11,266	19.12	1,898,694	12.81	1.04
	Silt loam	0	0.00	116,365	0.78	0.13
	Sandy clay	0	0.00	36,343	0.25	0.21
	Clay	1733	2.94	418,339	2.82	0.89
	Clay loam	32,932	55.88	8,280,943	55.85	2.45
NDVI	<−0.15	13,500	22.91	2,363,968	16.56	0.74
	−0.15–0.12	17,900	30.38	5,519,768	38.66	1.02
	>0.13	27,520	46.71	6,393,616	44.78	1.32
MNDWI	<−0.20	0	0.00	2	0.00	0
	−0.20–0	24,031	40.78	5,807,567	40.68	2.14
	0–0.20	27,700	47.00	6,255,862	43.82	2.66
	>0.20	7200	12.22	2,213,921	15.51	0.95
TWI	2.33–6.96	16,466	27.94	5,591,372	37.70	1.45
	6.97–9.7	23,399	39.71	5,166,381	34.84	1.12
	9.71–13.76	14,733	25.00	3,429,771	23.13	0.95
		4333	7.35	643,408	4.34	0

<div align="right">(continued)</div>

Table 3.2 (continued)

Factor	Class	Pixels number in class	% of pixel number class	Flood area in class	% of flood area class	FR value
	13.77–26.41					
TRI	0–20.75	58,918	99.998	14,818,898	99.9795	6.16
	20.76–55.03	1	0.002	1638	0.0111	0.23
	55.04–87.51	0	0	829	0.0056	0.11
	87.52–230.05	0	0	449	0.0030	0
SPI	0–7000.05	58,620	99.981	14,984,033	99.92865	5.21
	7000.06–14000.12	11	0.019	7718	0.05147	0.59
	14000.13–56000.24	0	0	2126	0.01418	0.21
	56000.25–123,000	0	0	777	0.00518	0
STI	0–2227.809	58,813	99.82	12,387,588	99.72	4.08
	2227.81–10470.701	56	0.10	27,412	0.22	0.62
	10470.702–30966.541	50	0.08	5478	0.04	0.21
	30966.542–56809.121	0	0	1308	0.01	0
Distance from drainage	400	1733	2.94	1,844,314	12.24	0.95
	800	1733	2.94	1,671,148	11.09	0.71
	1200	3466	5.88	1,506,651	10.00	0.25
	1600	5199	8.82	1,388,177	9.21	0
	>1600	46,799	79.41	8,662,553	57.47	2.37
Rainfall	1084.08–1694.62	12,132	20.59	1,949,335	13.14	0.52
	1694.63–2017.34	21,655	36.75	6,345,765	42.76	2.55
	2017.35–2296.45	15,599	26.48	3,802,649	25.62	1.13
	2296.46–2619.16	9533	16.18	2,641,538	17.80	0.91
	2619.17–3308.21	0	0	100,470	0.68	0

Since the Mahananda basin originates from hilly areas, slope is an important factor in determining flood susceptibility in this basin. After preparing the DEM based on Arc GIS, the slope can be understood from there. From the slope map, it can be inferred that if the slope of the land falls below 6.2^0, the amount of weightage

and also the flood will increase a lot. In the same way, DEM aspect maps are made to know the nature of river confluence and configuration on the slope of the land, and it is seen that most of the rivers are confined to the south and south-east section of the basin. STI (Moore and Burch 1986) is based on unit stream-power theory and length-slope factor in the revised universal soil loss equation (RUSLE) (where the slope of the land is less than 100 m and the slope is less than 14^0).

$$\text{STI} = (m + 1) * (A_S/22 \cdot 13)^m * \sin{(B + 0.0896)}^n \tag{3.1}$$

Where A_S is the specific catchment area estimated using one of the available flow accumulation algorithms in the Hydrology toolbox, B is the local slope gradient in degree, the value of contributing area exponent (m) is 0.4, and the value of slope exponent (n) is 1.4. Because the more the river flow is meandering or braided, the more flood situation will increase. The amount of STI in river floodplain flow is much higher. The TRI basically shows the undulation of the land, and it is intimately involved with the land slope (Riley et al. 1999).

$$\text{TRI}_m = \text{Log}\left[\frac{\alpha_n^d}{\tan{\beta}}\right] \tag{3.2}$$

Where α_n^d is the drained area/unit contour length, $\tan\beta$ is the local slope, and TRI_m is the roughness index comparing threshold shear value with flood inundation zone. Although roughness is higher in hilly areas, it decreases in the plains, and the impact of floods increases. The SPI is largely dependent on the erosion capacity of the river and the power of the water.

$$\text{SPI} = (\alpha * \tan{\beta}) \tag{3.3}$$

Where α is the flow accumulation of streams in an area and β is the slope. Like TRI, it is more on the tops of the hills, but much lower in the plains at the bottom. The land slope plays an important role in determining the SPI. TWI is an important technique to determine the likelihood of flooding. TWI also explores flood potential in the floodplain area (Rahmati et al. 2016a, b; Samanta et al. 2018a, b). The TWI map is created in Arc GIS with the help of a raster calculator based on DEM and the water flow equation (Ali et al. 2019).

$$\text{TWI} = \text{In}[A_S + \tan{(\beta)}] \tag{3.4}$$

Where A_S is the upstream contributing area and β is the slope gradient. The amount of rainfall in the entire Mahananda basin is determined using the arithmetic mean method based on the rainfall data obtained from the IMD. Topographic and satellite maps can be used to determine the distance from the river to any area of the floodplain. As the distance from the river increases, the chances of flooding decrease. According to the LULC, although the river floodplain area is overcrowded, the

meandering flow of the river and the presence of sandbars increase the likelihood of flooding. Soil maps are based on information provided by NBSS-LUP and show that most of the basin is composed of dense clay and clayey loam soils, which reduce water infiltration into the soil and increase the flood situation. Flood conditions are largely dependent on vegetation cover (NDVI) and water availability (MNDWI) of the basin area.

$$\text{NDVI} = \frac{\text{NIR band} - \text{R band}}{\text{NIR band} + \text{R band}} \tag{3.5}$$

$$\text{MNDWI} = \frac{\text{Green band} - \text{SWIR band}}{\text{Green Band} + \text{SWIR band}} \tag{3.6}$$

Where NIR is the near-infrared band, R is the red band, and SWIR is the short-wave infrared band in the satellite image sensor. In LANDSAT OLI, bands 4 and 5 were used to calculate NDVI, whereas bands 3 and 7 were used to calculate MNDWI. If the value of NDVI decreases and at the same time the value of MNDWI increases, there is the possibility of flood. However, judging from the weightage factor, it can be said that the flat floodplain area has a low slope, agricultural land, and fallow land, located farthest from the river, but is characterized as flood prone in the case of Mahananda basin.

Bivariate Statistical Analysis (Frequency Ratio Model)

Flood susceptibility mapping provides a comprehensive idea of the hydrology of a catchment. BSA (bivariate statistical analysis) has to be used to develop the frequency ratio (FR) model of flood arrival through different classified and independent components. The proportional probability of the presence and absence of each component of the probability of flooding is examined by the BSA factors. The dual potential of the independent variable of each component is measured based on the duration of the flood organization with the variable. When the dual or bivariate probability is greater than 1, a strong relationship develops between the flood organization and the flood control elements. Through various statistical calculations, it is possible to establish a relationship between the flood organization and the flood-supporting elements or variables. The spatial relationship that develops between flood organization and its control elements makes it possible to build a dual/bivariate probability model (FR model) through Arc GIS (Samanta et al. 2018a, b).

$$W_{ij} = \frac{\text{FL}_{ij}}{\text{FN}_{ij}} \tag{3.7}$$

Where W_{ij} is the frequency ratio of class i of parameter j, FL_{ij} is the frequency of observed flood in class i of parameter j in percent, and FN_{ij} is the frequency of the non-observed flood in class i of parameter j in percent. After all, each factor in the FR model is mapped together to create a flood susceptibility index (FSI). The FSI is measured through (Samanta et al. 2018a, b)

$$FSI = \sum_{j=1}^{n} W_{ij} \tag{3.8}$$

Where FSI is the flood susceptibility index, W_{ij} is the weight of class i in parameter j, and n is the number of parameters.

Results and Discussions

Spatial Variability of Flood Condition Factors

The flood susceptibility index for the entire Mahananda basin is also mapped based on the 12 independent flood occurrence factors described in the methodology. The highest land slope is seen in the entire basin region towards the northern highlands (33.28^0–61.89^0), and the lowest ($<6.2^0$) land slope is seen in the southern plains or floodplain areas. From this, it can be said that all the water carried by the river flows from north to south according to the slope of the land (Fig. 3.3a).

Aspect is also an important element that controls a flood with the slope of the land. The outline aspect of the river basin can be highlighted on the basis of the slope of the land. According to the aspect, all the rivers flow south and south-east following the slope of the land. As a result, it is safe to say that all rivers flow to the south (Fig. 3.3b).

The land use map of the entire basin is divided into agricultural land, built-up land, fallow land, plantation land, sand bar, vegetative land, and water bodies. Although there are more plantations and vegetative areas in the north of the basin, urban areas along the floodplain areas in the south, sand bars, and fallow lands have increased due to the meandering flow of the river. In the middle of the basin, there is an abundance of agricultural land (Fig. 3.3c).

The whole basin's soil can be divided into sandy loam, loam, silt loam, sandy clay, clay, and clay loam (Fig. 3.3d). Most of the basin is covered by clay and clayey loam, where excess water in the clay prevents infiltration and flooding. This type of soil is found mainly in the middle or southern part of the basin. However, hilly soils are more common in the northern hills.

The vegetative cover of the entire basin is inextricably linked with the organization of the flood through NDVI (Eq. 3.5) (Fig. 3.3e). The amount of vegetation in the middle of the basin is much higher (0.20). But as the size of the city increased to the south and south-east, the amount of vegetation decreased significantly (−0.54). As a
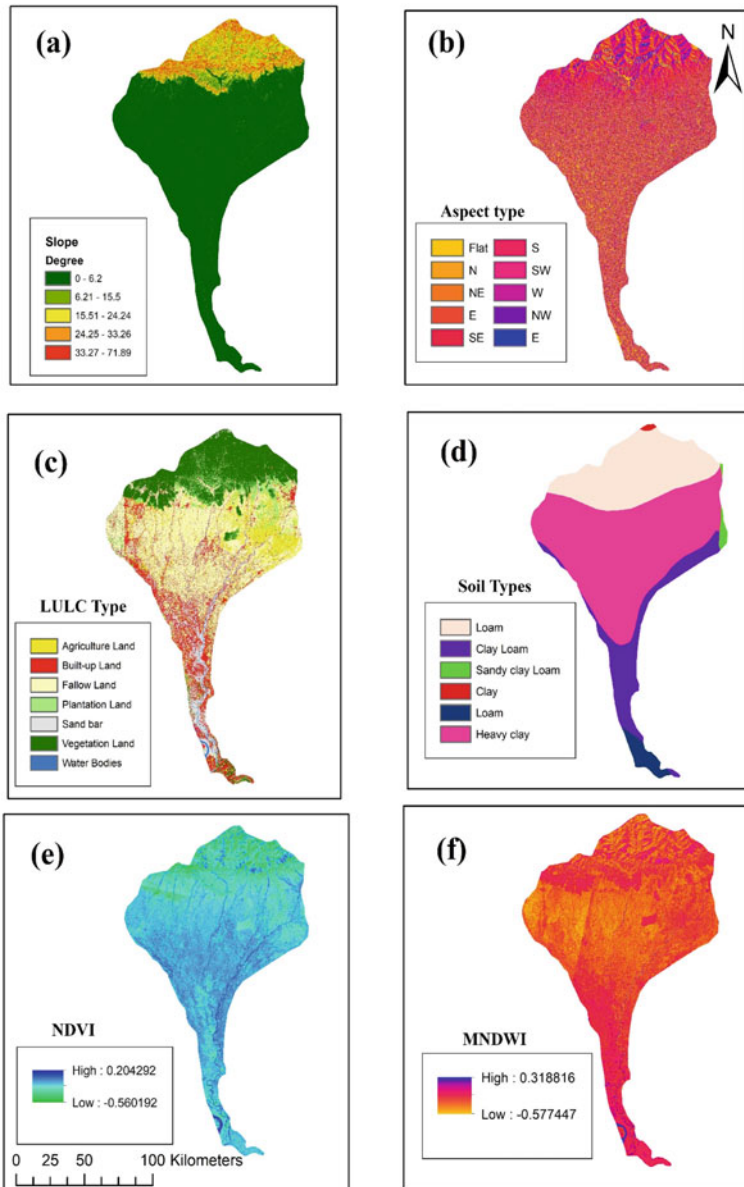
Fig. 3.3 Spatial variable layer used for preparing FR model: (**a**) slope; (**b**) aspect; (**c**) LULC; (**d**) soil type; (**e**) NDVI; f. MNDWI; (**g**) TWI; (**h**) TRI; (**i**) SPI; j. STI; (**k**) distance from drainage; (**l**) rainfall

result, the amount of flooding in all these areas has increased a lot. On the other hand, the amount and flow of water throughout the basin are determined by the MNDWI (Eq. 3.6) (Fig. 3.3f). Although the amount of water is much less in the middle of the
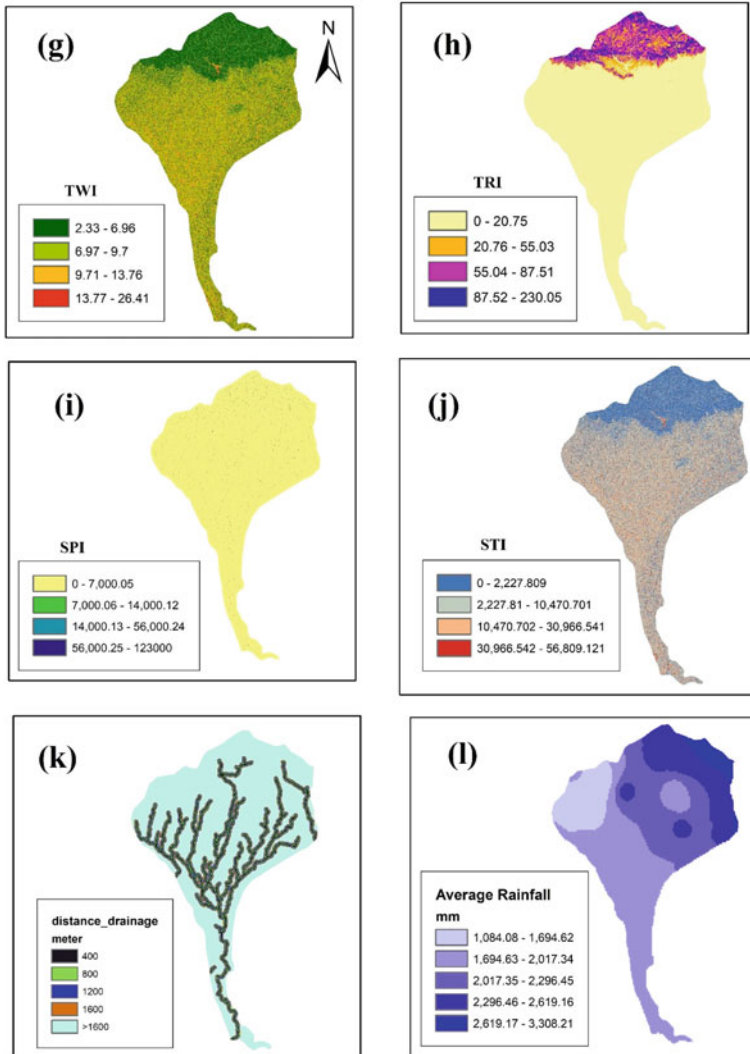
Fig. 3.3 (continued)

region (−0.58), the amount of water in the south and the south-east is much more (0.317). This shows that the incidence of floods in the region is much higher.

The TWI (Eq. 3.4) of the entire Mahananda basin is determined based on the information obtained from LANDSAT OLI satellite images through Arc GIS (Fig. 3.3g). The southern and south-eastern parts of the region have the highest TWI (6.98–13.8). Again, in some cases, this value is too high (13.6–28.41). As a result, the location of this type of TWI, which has the highest weight, greatly increases the risk of flooding in the region.

Land undulation across the basin is indicated by the TRI (Eq. 3.2) based on the measurement of land slope with the help of SRTM DEM (Fig. 3.3h). Land undulation is very low (<20.75) along the southern and central parts of the region, the river velocity is not very high, and the river water easily spreads around, making the possibility of flooding real. According to the TRI, as the velocity of the river decreases throughout the south and south-east, it affects later on the SPI (Eq. 3.3). Although the amount of SPI is higher in hilly rivers, it gradually decreases in the middle, south, and south-east section of the river basin (Fig. 3.3i). In fact, SPI has appropriate relationship with slope amount. Whenever river power decreases, the rate of river storage and the amount of sedimentation increases. River sedimentation is measured with the help of the STI (Fig. 3.3j). In the case of the STI (Eq. 3.1), the amount of sediment accumulation in the middle, south, and south-east of the basin continues to increase likewise in SPI. In some areas in the far south-east, the rate of STI is highest due to reduced meandering flow and land slope.

The greater the distance from the river, the less likely it is to flood (Fig. 3.3k). However, due to the inclusion of the southern and southern floodplain of the Mahananda basin, the distance from the river has increased, but the tendency to flood has increased. Rainfall plays an important role in flood management, and the spatial distribution of rainfall in this region is divided into six categories in total (Fig. 3.3l). The highest rainfall is seen in the north-eastern part of the entire basin, which is known as the source of the Mahananda River. As a result, during the rainy season, water comes down from the upper part of the mountain and organizes floods in the floodplain areas of the Mahananda River.

Applicability of FR Model

Determining the future flood situation of a particular region requires a thorough understanding of the nature and extent of current and past floods. Also, when mapping floods in a region, it is important to look not only at the floods in that region but also at the factors that contribute to the organization of the flood. Although elements that are potential for flood management have been discussed before, the relationship and role of various hierarchical elements in flood management are highlighted in the FR analysis. The relationship between the FR value and the flooded area depends on the applicability and relevance of the FR model in a basin. Judging by the relevance of the FR model in the Mahananda basin, it is seen that the FR value has a fairly close relationship with all independent variables except the aspect (Table 3.3).

The slope of the land forms a deep connection between the flood organization and the low-lying plain surface. If the FR ratio is more than 1, flooding occurs in almost flat areas with low slopes (land slope value less than 6.2^0). In view of this, it can be said that the higher the slope of the land in the hilly region, the greater the amount of flooding in the lower plains ($R^2 = 0.71$).

Table 3.3 Relation between flooded area and FR value

Factor	Linear regression	R^2 value
Slope	y = 1E-07x + 0.4893	0.71
Aspect	y = 1E-06x − 0.9181	0.53
LULC	y = 3E-07x + 0.1717	0.78
Soil	y = 2E-07x + 0.3731	0.89
NDVI	y = 1E-07x + 0.4119	0.89
MNDWI	y = 4E-07x + 0.0195	0.98
TWI	y = 3E-07x − 0.1241	0.95
TRI	y = 4E-07x + 0.1129	0.98
SPI	y = 3E-07x + 0.2655	0.97
STI	y = 3E-07x + 0.2729	0.98
Distance from drainage	y = 3E-07x + 0.0311	0.87
Rainfall	y = 4E-07x − 0.1846	0.97

In terms of aspect, it can be said that the higher the slope of the land, the less the river pattern is seen. The value of FR in flat areas is 1 or more, so the possibility of flood organization is much higher there ($R^2 = 0.53$). Again, all the rivers in the Mahananda basin flow south and south-east direction, and the amount of FR is higher in the south and south-east, depending on the slope of the land.

LULC plays an important role in flood assessment and organization. Where there is more vegetative cover, the land area is protected from flooding, and there is a negative relationship between the forest organization and the flood organization ($R^2 = 0.78$). Additionally, urban areas are more populated due to higher population density, resulting in increased runoff and flooding. The results of the FR model show that LULC has a close relationship with the flood organization. The FR ratio is much higher than 1 in agricultural fallow lands due to flooding and soil erosion and lack of vegetative cover.

Water cannot easily infiltrate in areas where the soil is rich in clay. As a result, the amount of runoff is higher. When the soil has more clay, the value of FR is more than 1 which is sufficient for flood organization ($R^2 = 0.89$). On the other hand, even if water does not enter the soil of hilly areas in that way, due to the steep slope of the land, the water flows downwards instead of flooding.

The rate of flood organization is very low where there is more vegetative cover. According to the NDVI, fallow lands without vegetative cover have a higher rate of flood organization and much higher FR value than 1 ($R^2 = 0.89$). According to the MNDWI, the higher the availability of water, the higher the rate of flood organization. Therefore, the value of FR in those regions is greater than 1. In hilly areas, on the other hand, since the water does not accumulate on the slopes, there is no flooding ($R^2 = 0.98$).

When the TWI value is between 13.6 and 28.41, the FR ratio is highest (1.45). It basically highlights the role of the topography required for runoff in the TWI basin and, of course, plays a special role in creating the saturation zone ($R^2 = 0.95$). There is a positive relationship of TWI with the value of FR, and the value of FR increases

with the value of TWI. In this case, soil moisture plays an important role in flood management.

The topographic roughness is highest in the hilly areas. So there the water goes down according to the slope of the land. The TRI value is quite low in hilly areas according to the FR value ($R^2 = 0.98$). But as the roughness in the plains decreased, the FR value increased a lot (more than about 6) and the floods were horribly organized. River power and visibility are based on TRI, which is measured by SPI. The amount of SPI is higher in hilly areas, and the value of FR is lower. But when the SPI value decreases in the plain region ($R^2 = 0.97$), the FR value increases too much (more than 5) and the flooding occurs. Similarly, STI also depends on TRI and SPI. Due to the steep slope of the land in hilly areas, sediment is not deposited if sediment is carried here. But as the land slope of the plains and the erosion capacity of the river decrease, sediment begins to accumulate in the river ($R^2 = 0.98$). As a result, the normal flow of the river is stopped, and floods occur, resulting in higher value of FR (more than 4).

Due to its location near the river, there is a high risk of flooding. However, this is not possible in mountainous areas ($R^2 = 0.87$). If the floodplain cannot carry its load in the area, the floodplain remembers the flood, and here, the FR value is always above 2. Rainfall is the most important means of organizing floods, and it is not possible to discuss floods without rain ($R^2 = 0.97$). The average rainfall in this region is highest in the north-east, with an FR value of more than 2.

Flood Susceptibility Index (FSI) Map

The flood susceptibility index (FSI) map (Eqs. 3.7 and 3.8) is obtained by sorting the important and collaborative elements of the flood organization according to their FR standards (Fig. 3.4). The FSI value of the entire Mahananda basin ranges from 0.98 to 38.51. Based on the quintile classifier method, we get four types of flood susceptibility zones. These are very high (>30), high (21–30), low (11–20), and very low (<10). These flood susceptibility values are completely relative to the flood organization. Flood susceptibility and flood organization continue to increase as the FR values increase. Most of the entire Mahananda basin falls within the very high (29% of the total basin or 5974 sq. km) and high susceptibility (37% of the total basin or 7622 sq. km) zones. Also, 21% (4326 sq. km) are in the low susceptibility zone, and the remaining 13% (2678 sq. km) are in the very low susceptibility zone. According to the flood susceptibility index, the southern and southern regions, including the entire Mahananda basin, are most prone to floods. Mainly, due to high rainfall in hilly areas, water accumulates in floodplains with low slopes in the south. Meandering flows and sedimentation of rivers, excess of clay soil, presence of agricultural fallow land use without vegetative cover, and increase in urban areas including densely populated region are the key characteristics of the high and very high flood susceptibility zone.
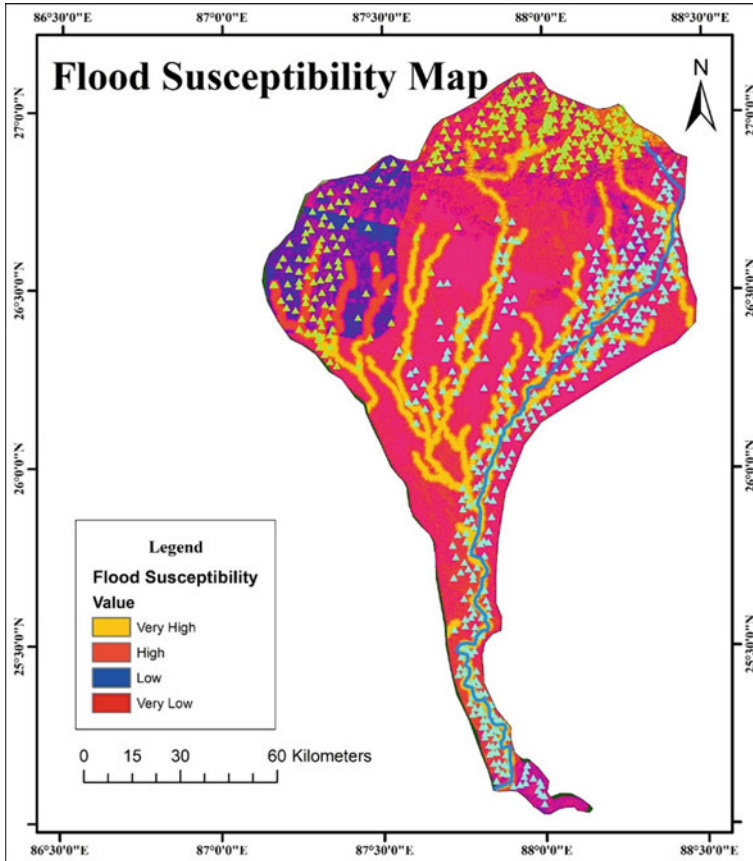
Fig. 3.4 Flood susceptibility map developed by FR model on the Mahananda basin

Validation of Flood Susceptibility Index (FSI) Map

The accuracy and quality of the flood susceptibility index (FSI) map forecast are tested using the area under the curve (AUC). The FR model is validated by comparing existing flood data with developed flood probability maps (Tien Bui et al. 2012; Youssef et al. 2016). Although the receiver operating characteristic (ROC) curve is used in this case to test the basis of the assessment through truth and falsehood (Chauhan et al. 2010). The flood susceptibility map obtained on the Mahananda basin is validated on the curve of success and prediction rates. Success rates are known using training datasets (50 points), which depend on flood locations in 63% of the region. On the other hand, the accuracy of the prediction depends on the rest of the dataset which was not used in the training (30 points) and guided the flood situation in 37% of the region. The graph shows the success curve in red and the prediction curve in blue. This curve basically measures goodness of fit and where
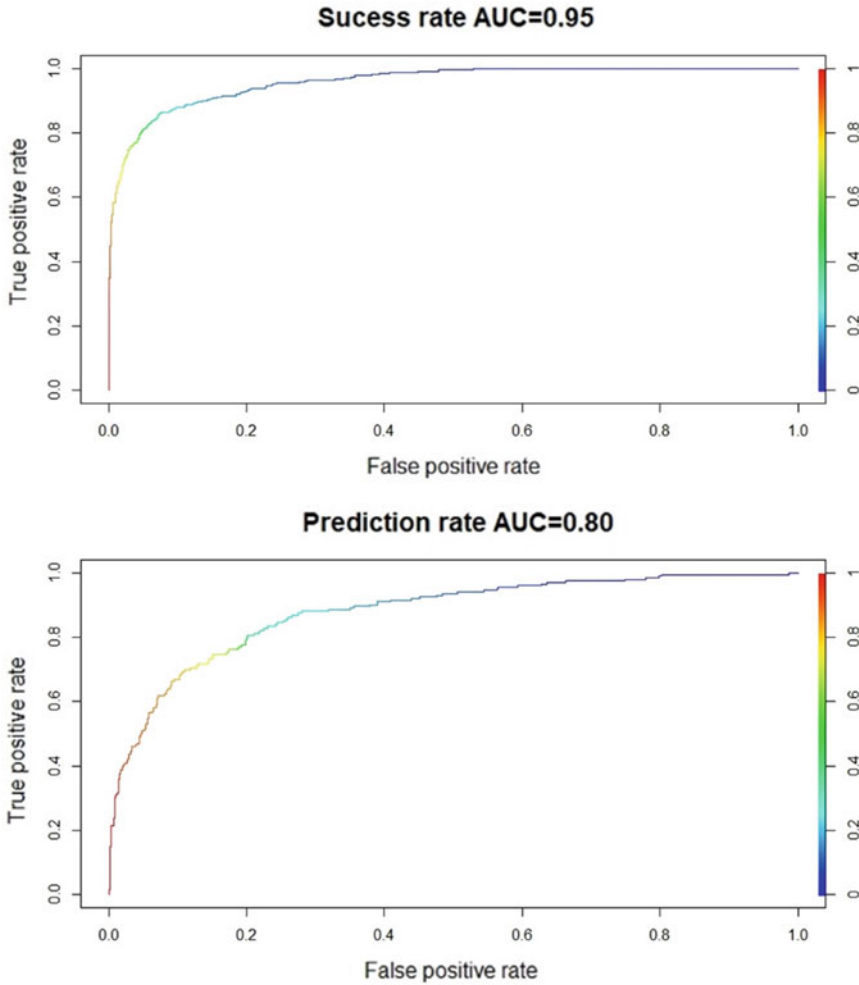
Fig. 3.5 ROC curve of success and prediction rate

a value greater than 1 indicates the best accuracy, proving that the model succeeds in accurately predicting flooding without any bias (Pradhan and Buchroithner 2010). Furthermore, the fact that the AUC value is close to 1 shows that the model is reliable. The success and prediction values of the AUC curve in this chapter are 0.95 and 0.80, respectively, which proves the accuracy of the model's prediction at 95% and 80%, respectively (Fig. 3.5).

Conclusion and Recommendations

Flood susceptibility mapping is important for urban hydrology, urban flood determination, and sustainable development in densely populated urban areas. With the help of GIS and BSA factors, the FR model shows the relationship between flood and flood-organizing factors. The FR model on independent variables has been replaced on the basis of the possibility of rearrangement and bifurcation over the entire Mahananda basin. Flood inventory maps have been prepared based on 50 flood locations (63%) based on the 2017 flood data in the region, and the data obtained have been used for statistical analysis. Data from the remaining 30 flood locations (37%) were used to validate the FR model. Throughout the model, 12 flood-organizing factors (slope, aspect, LULC, soil, NDVI, MNDWI, TWI, TRI, SPI, STI, distance from drainage, and rainfall) have been recognized as independent variables. Based on this, a flood susceptibility map is finally created, and these four flood susceptibility zones are divided into very high, high, low, and very low. The results obtained by BPA show that there are high flood susceptibility areas in the south and south-east of the entire basin. The ROC curve evaluates the validity and acceptability of the entire model. Measurement of the AUC value shows that the success and prediction levels of the model are 0.846 and 0.821, respectively.

- Needless to say, very few flood location points have been used compared to this huge basin. Also, many other factors responsible for floods such as river shifting/migration, water budget, river erosion, etc. are not taken into consideration in this discussion.
- However, predictions through flood susceptibility maps require more future flood data and calculations.
- Data from current research can help planners make decisions and allow governments to properly manage future flood management and planning. Additionally, its accuracy can improve results and enhance data quality for further research.

References

Ali SA, Khatun R, Ahmad A, Ahmad AN (2019) Application of GIS based analytic hierarchy process and frequency ratio model to food vulnerable mapping and risk area estimation at Sundarban region, India. Model Earth Sys Environ 5:1083–1102

Chauhan S, Sharma M, Arora MK (2010) Landslide susceptibility zonation of the Chamoli region, Garhwal Himalayas, using logistic regression model. Landslides 7:411–423. https://doi.org/10.1007/s10346-010-0202-3

Chowdary V, Chakraborthy D, Jeyaram A, Murthy YK, Sharma J, Dadhwal V (2013) Multi-riteria decision making approach for watershed prioritization using analytic hierarchy process technique and GIS. Water Resour Manag 27:1–1. https://doi.org/10.1007/s11269-013-0364-6

Dandapat K, Panda GK (2017) Flood vulnerability analysis and risk assessment using analytical hierarchy process. Model Earth Sys Environ. https://doi.org/10.1007/s40808-017-0388-7

Das B, Bandyopadhyay A (2015) Flood risk reduction of Rupnarayana River, towards disaster management? A case study at Bandar of Ghatal Block in Gangetic Delta. J Geogr Nat Disasters 5:135

Das S, Kar NS, Bandyopadhyay S (2015) Glacial lake outburst flood at Kedarnath, Indian Himalaya: a study using digital elevation models and satellite images. Nat Hazards 77:769–786. https://doi.org/10.1007/s11069-015-1629-6

Demir V, Kisi O (2016) Flood Hazard mapping by using geographic information system and hydraulic model: Mert River, Samsun, Turkey. Adv Meteorol 2016:4891015. https://doi.org/10.1155/2016/4891015

Foudi S, Osés-Eraso N, Tamayo I (2015) Integrated spatial flood risk assessment: the case of Zaragoza. Land Use Policy 42:278–292. https://doi.org/10.1016/j.landusepol.2014.08.002

Ghalkhani H, Golian S, Saghafian B, Farokhnia A, Shamseldin A (2013) Application of surrogate artificial intelligent models for real-time flood routing. Water Environ J 27:535–548. https://doi.org/10.1111/j.1747-6593.2012.00344.x

Ghanbarpour MR, Salimi S, Hipel KW (2013) A comparative evaluation of flood mitigation alternatives using GIS-Based River hydraulics modelling and multicriteria decision analysis. Flood Risk Manag 6:319–331. https://doi.org/10.1111/jfr3.12017

Heidari A (2014) Flood vulnerability of the Karun River system and short-term mitigation measures. Flood Risk Manag 7:65–80. https://doi.org/10.1111/jfr3.12032

Hudson P, Botzen W, Kreibich H, Bubeck P, Aerts J (2014) Evaluating the effectiveness of flood damage mitigation measures by the application of propensity score matching. Nat Hazards Earth Syst Sci 14:1731–1747. https://doi.org/10.5194/nhess-14-1731-2014

Jaafari A, Najaf A, Pourghasemi HR, Rezaeian J, Sattarian A (2014) GIS-based frequency ratio and index of entropy models for landslide susceptibility assessment in the Caspian forest, northern Iran. Int J Environ Sci Technol 11(4):909–926. https://doi.org/10.1007/s13762-013-0464-0

Jebur MN, Pradhan B, Tehrany MS (2014) Optimization of landslide conditioning factors using very high-resolution airborne laser scanning (LiDAR) data at catchment scale. Remote Sens Environ 152:150–165. https://doi.org/10.1016/j.rse.2014.05.013

Kazakis N, Kougias I, Patsialis T (2015) Assessment of flood hazard areas at a regional scale using an index-based approach and analytical hierarchy process: application in Rhodope–Evros region, Greece. Sci Total Environ 538:555–563. https://doi.org/10.1016/j.scitotenv.2015.08.055

Kia MB, Pirasteh S, Pradhan B, Mahmud AR, Sulaiman WNA, Moradi A (2012) An artificial neural network model for flood simulation using GIS: Johor River Basin Malaysia. Environ Earth Sci 67(1):251–264. https://doi.org/10.1007/s12665-011-1504-z

Kisi O, Nia AM, Gosheh MG, Tajabadi MRJ, Ahmadi A (2012) Intermittent streamflow forecasting by using several data driven techniques. Water Resour Manag 26(2):457–447. https://doi.org/10.1007/s11269-011-9926-7

Kumar N, Lal D, Sherring A, Issac RK (2017) Applicability of HEC-RAS & GFMS tool for 1D water surface elevation/flood modeling of the river: a Case Study of River Yamuna at Allahabad (Sangam), India. Model Earth Sys Environ 3:1463–1475. https://doi.org/10.1007/s40808-017-0390-0

Lee MJ, Kang JE, Jeon S (2012) Application of frequency ratio model and validation for predictive flooded area susceptibility mapping using GIS. In: Geoscience and remote sensing symposium (IGARSS), 2012. IEEE International, Munich, pp 895–898

Lohani A, Kumar R, Singh R (2012) Hydrological time series modeling: a comparison between adaptive neuro-fuzzy, neural network and autoregressive techniques. J Hydrol 442:23–35. https://doi.org/10.1016/j.jhydrol.2012.03.031

Malczewski J (2006) GIS-based multicriteria decision analysis: a survey of the literature. Int J Geogr Inf Sci 20:703–726. https://doi.org/10.1080/13658810600661508

Mallinis G, Gitas IZ, Giannakopoulos V, Maris F, Tsakiri-Strati M (2011) An object-based approach for flood area delineation in a transboundary area using ENVISAT ASAR and LANDSAT TM data. Int J Digital Earth 8947:1–13. https://doi.org/10.1080/17538947.2011.641601

Manandhar B (2010) Flood plain analysis and risk assessment of Lothar Khola, Nepal: Unpublished Ph.D. thesis, Tribhuvan University, Nepal

Mandal SP, Chakrabarty A (2016) Flash flood risk assessment for upper Teesta River basin: using the hydrological modelling system (HEC-HMS) software. Model Earth Sys Environ 2:59. https://doi.org/10.1007/s40808-016-0110-1

Merz B, Thieken AH, Gocht M (2007) Flood risk mapping at the local scale: concepts and challenges. In: Begum S, Stive MJF, Hall JW (eds) Flood risk management in Europe. Advances in natural and technological hazards research, vol 25. Springer, Dordrecht, pp 231–251

Moore ID, Burch GJ (1986) Physical basis of the length slope factor in the universal soil loss equation. Soil Sci Soc Am 50(5):1294–1298. https://doi.org/10.2136/sssaj1986.03615995005000050042x

Mukerji A, Chatterjee C, Raghuwanshi NS (2009) Flood forecasting using ANN, neuro-fuzzy, and neuro-GA models. J Hydrol Eng 14(6):647–652. https://doi.org/10.1061/(ASCE)HE.1943-5584.0000040

Pakoksung K, Takagi M (2016) Effect of satellite-based rainfall products on river basin responses of runoff simulation on flood event. Model Earth Sys Environ 2:143. https://doi.org/10.1007/s40808-016-0200-0

Patel DP, Ramirez JA, Srivastava PK, Bray M, Han D (2017) Assessment of flood inundation mapping of Surat city by coupled 1D/2D hydrodynamic modeling: a case application of the new HEC-RAS 5. Nat Hazards 89:93–130. https://doi.org/10.1007/s11069-017-2956-6

Perera E, Hiroe A, Shrestha D, Fukami K, Basnyat D, Gautam S, Hasegawa A, Uenoyama T, Tanaka S (2015) Community-based flood damage assessment approach for lower West Rapti River Basin in Nepal under the impact of climate change. Nat Hazards 75:669–699. https://doi.org/10.1007/s11069-014-1339-5

Phongsapan K, Chishtie F, Poortinga A, Bhandari B, Meechaiya C, Kunlamai T, Aung KS, Saah D, Anderson E, Markert K, Markert A, Towashiraporn P (2019) Operational flood risk index mapping for disaster risk reduction using earth observations and cloud computing technologies: a case study on Myanmar. Front Environ Sci 7:191. https://doi.org/10.3389/fenvs.2019.00191

Pourghasemi HR, Beheshtirad M (2014) Assessment of a data-driven evidential belief function model and GIS for groundwater potential mapping in the Koohrang Watershed, Iran. Geocarto Int 30:662–685. https://doi.org/10.1080/10106049.2014.966161

Pradhan B (2010) Flood susceptible mapping and risk area estimation using logistic regression, GIS andremote sensing. J Spat Hydrol 9(2):2–12

Pradhan B, Buchroithner MF (2010) Comparison and validation of landslide susceptibility maps using an artificial neural network model for three test areas in Malaysia. Environ Eng Geosci 16(2):107–126. https://doi.org/10.2113/gseegeosci.16.2.107

Pradhan B, Hagemann U, Tehrany MS, Prechtel N (2014) An easy to use ArcMap based texture analysis program for extraction of flooded areas from Terra SAR-X satellite image. Comput Geosci 63:34–43. https://doi.org/10.1016/j.cageo.2013.10.011

Prasad RN, Pani P (2017) Geo-hydrological analysis and sub watershed prioritization for flash flood risk using weighted sum model and Snyder's synthetic unit hydrograph. Model Earth Sys Environ 3:1491–1502. https://doi.org/10.1007/s40808-017-0354-4

Rahmati O, Pourghasemi HR, Zeinivand H (2016a) Flood susceptibility mapping using frequency ratio and weights-of-evidence models in the Golastan Province, Iran. Geocarto Int 31(1). https://doi.org/10.1080/10106049.2015.1041559

Rahmati O, Zeinivand H, Besharat M (2016b) Flood hazard zoning in Yasooj region, Iran, using GIS and multi-criteria decision analysis. Geomat Nat Haz Risk. https://doi.org/10.1080/19475705.2015.1045043

Rana NK (2018) Analysis of Mahananda River basin using geospatial data. In: Singh DS (ed) The Indian Rivers: scientific and socio-economic aspects. Springer Nature, Singapore

Riley SJ, DeGloria SD, Elliot R (1999) A terrain ruggedness index that quantifies topographic heterogeneity. Intermt J Sci 5(1-4):23–27

Sahoo SN, Sreeja P (2015) Development of flood inundation maps and quantification of flood risk in an urban catchment of Brahmaputra River. ASCE-ASME J Risk Uncertain Eng Syst Part A Civil Eng 3:A4015001. https://doi.org/10.1061/AJRUA6.0000822

Samanta RK, Bhunla GS, Shit PK, Pourghasemi HR (2018a) Flood susceptibility mapping using geospatial frequency ratio technique: a case study of Subarnarekha River Basin, India. Model Earth Sys Environ. https://doi.org/10.1007/s40808-018-0427-z

Samanta S, Pal DK, Palsamanta B (2018b) Flood susceptibility analysis through remote sensing, GIS and frequency ratio model. Appl Water Sci. https://doi.org/10.1007/s13201-018-0710-1

Sar N, Chatterjee S, Adhikari MD (2015) Integrated remote sensing and GIS based spatial modelling through analytical hierarchy process (AHP) for water logging hazard, vulnerability and risk assessment in Keleghai river basin, India. Model Earth Sys Environ 1:31. https://doi.org/10.1007/s40808-015-0039-9

Sarkar D, Mondal P (2019) Flood vulnerability mapping using frequency ratio (FR) model: a case study on Kulik river basin, Indo-Bangladesh Barind region. Appl Water Sci 10:17. https://doi.org/10.1007/s13201-019-1102-x

Sezer EA, Pradhan B, Gokceoglu C (2011) Manifestation of an adaptive neuro-fuzzy model on landslide susceptibility mapping: Klang Valley Malaysia. Expert Syst Appl 38(7):8208–8219. https://doi.org/10.1016/j.eswa.2010.12.167

Shil S, Singh UK (2019) Health risk assessment and spatial variations of dissolved heavy metals and metalloids in a tropical river basin system. Ecol Indic 106:105455. https://doi.org/10.1016/j.ecolind.2019.105455

Tehrany MS, Pradhan B, Jebur MN (2014) Flood susceptibility mapping using a novel ensemble weights-of-evidence and support vector machine models in GIS. J Hydrol 512:332–343. https://doi.org/10.1016/j.jhydrol.2014.03.008

Tehrany MS, Pradhan B, Jebur MN (2015a) Flood susceptibility analysis and its verification using a novel ensemble support vector machine and frequency ratio method. Stoch Environ Res Risk Assess 29(4):1149–1165. https://doi.org/10.1007/s00477-015-1021-9

Tehrany MS, Pradhan B, Mansor S, Ahmad N (2015b) Flood susceptibility assessment using GIS-based support vector machine model with different kernel types. Catena 125:91–101. https://doi.org/10.1016/j.catena.2014.10.017

Tehrany MS, Shabani F, Jebur MN, Hong H, Chen W, Xie X (2017) GIS-based spatial prediction of flood prone areas using standalone frequency ratio, logistic regression, weight of evidence and their ensemble techniques. Geomat Nat Hazards Risk 8(2):1538–1561. https://doi.org/10.1080/19475705.2017.1362038

Tien Bui D, Pradhan B, Lofman O, Revhaug I, Dick OB (2012) Landslide susceptibility mapping at Hoa Binh province (Vietnam) using an adaptive neuro-fuzzy inference system and GIS. Comput Geosci 45:199–211. https://doi.org/10.1016/j.cageo.2011.10.031

Tiwari MK, Chatterjee C (2010) Uncertainty assessment and ensemble flood forecasting using bootstrap based artificial neural networks (BANNs). J Hydrol 382(1):20–33. https://doi.org/10.1016/j.jhydrol.2009.12.013

Youssef AM, Pradhan B, Sefry SA (2016) Flash flood susceptibility assessment in Jeddah city (Kingdom of Saudi Arabia) using bivariate and multivariate statistical models. Environ Earth Sci 75:1–16. https://doi.org/10.1007/s12665-015-4830-8

Chapter 4
Climate Change Impact on Soil Salinity Dynamics at the Gosaba CD Block in India by Integrating Geospatial Indicators and Regression Techniques

Bijay Halder, Jatisankar Bandyopadhyay, and Md. Nazrul Islam

Abstract Saltwater intrusion into the coastal areas is a main concern nowadays. Owing to climate change, coastal areas are being affected by several natural hazards and suffering environmental vulnerability, with impacts on agricultural productivity, natural environment, food safety and massive economic loss. Salinity identification is the principal issue for coastal area conservation. Salinity variations on different time scales are also conducted and estimate the actual climate change effect on the coastal environment. Remote sensing techniques are used to identify different salinity indices in the Gosaba, South 24 Parganas district, West Bengal. After super cyclone "Aila," this area faced a huge amount of saltwater intrusion that directly affected agricultural productivity and the environment. Many coastal lands have been converted into inland fisheries due to saltwater intrusion. The land use and land cover were classified using the supervised classification technique and maximum likelihood algorithm. Agricultural land decreased by 13.73 sq.km and the inland fishery area increased by 13.45 sq.km in this study location. The relationship with land surface temperature (LST) and normalized difference salinity index (NDSI) showed a high negative correlation, the R^2 value was 0.45; $p < = 0.687$. The built-up land also increased by 8.3 sq.km in the Gosaba area. Basically, the southern, south-east and eastern parts of this area have been identified with extremely high soil salinity during field survey, which is also corroborated by the spectral indicators. This result will be helpful for administrators, local planers, and agricultural departments for the delineation of sustainable food security of this area.

B. Halder (✉) · J. Bandyopadhyay
Department of Remote Sensing and GIS, Vidyasagar University, Midnapore, India

Md. N. Islam
Department of Geography and Environment, Jahangirnagar University, Savar, Dhaka, Bangladesh
e-mail: nazrul_geo@juniv.edu

Introduction

Saltwater intrusion affects agricultural productivity in many parts of the world (Suarez 1989). Sea level rise due to climate change directly affects the coastal environment. Approximately two-thirds of the population depends directly or indirectly on agricultural activities and around 60% of the agricultural area under rainfed areas is affected by climate variation (World Bank Group 2018). Floods are on average the disasters that cause the highest yearly losses in India, estimated at $7 billion every year (UNISDR 2014). During the twentieth century, flood-related hazards increased across India. The insinuations of the overall tendency towards additional extreme precipitation events are indications for potential future flood levels. Soil salinization is a dynamic part, which can occur through natural processes such as sea-level rise and human activities such as urbanization or irrigation. The salinity of the soil depends on the level of solvable salt in soil. In irrigated areas, soil salinity is the most serious problem for agricultural productivity. Worldwide saline soil conditions have affected the value and productivity of considerable areas of land (Elhag 2016). Soil salinization is a foremost method of land degradation in agricultural zones, where information on the amount and magnitude of soil salinity is wanted for healthier planning and implementation of effective soil reclamation programs (Asfaw et al. 2018). Salinity affects the soil metabolism and reduces the production capacity of the land. At the next level, the salinity destroys all the plants and other living organisms in the soil.

Salinity affects the metabolism of soil organisms and reduces the productivity of the land area. The soil salinity is triggering land degradation and affecting land values, sustainable growth and causing a loss of economic benefit (Nguyen et al. 2020). The remote sensing techniques were widely used for mapping and monitoring the soil salinity of any area for economic activities, food production and food security (Dehni and Lounis 2012; Taghadosi et al. 2019). The Landsat Thematic Mapper (TM) and Operational Land Imager (OLI) are widely used for assessing soil salinity due to spectral indicators. Dry soil normally has a greater reflectance and no absorption in the red region has been used in developing the vegetation spectral indicator (Dehni and Lounis 2012). The numerous vegetation indicators such as Normalized Difference Vegetation Index (NDVI), Soil Adjusted Vegetation Index (SAVI), Normalized Difference Salinity Index (NDSI) and Vegetation Soil Salinity Index (VSSI) were used to characterize or monitor the crop growth condition influenced by the salinity. The soil salinity has affected the land use and land cover and resulted in different appearances such as colour, texture, shape and many other things (Verma et al. 1994). A detailed methodology has been used for identifying the soil salinity area and vulnerability over the Gosaba block of South 24 Parganas. The in situ techniques are used to validate the results and monitor the

proper development of this area. The NDVI indicator was less suitable for monitoring salinity but some factors dominated the NDVI values for delineating the salinity area over the Gosaba block.

Soil salinization is the main problem for agricultural productivity and increases the land transformation over an area because crop production is hampered by saltwater intrusion, as seen in the Gosaba block. Irrigation evaporation of moisture from the external or shallow depths within the shape and insufficient annual rainfall to wash the salt water intrusion from the plant rooting zone favor excessive accumulation of soluble salts in soils of arid and semi-arid regions, rendering such lands with only marginal success (Abdelfattah et al. 2009; Gorji et al. 2015; Asfaw et al. 2018). The arid and semi-arid regions are facing a huge amount of salinity and sodicity for irrigation purposes. The saline water increases the irrigation cost, technical complexity and requires more skilled management in the field. The saltwater intrusion affects the irrigation area and increases the water logging problem, high rate of water, reducing the productivity and soil fertility. The salinity area reduces the agricultural land, and several environmental hazards such as cyclone, drought and shoreline change have affected the productivity of the Gosaba block.

Several techniques and methods have been used to identify the soil salinity information derived from satellite remote sensing. The topographical condition, tidal effects and methodological condition have been affected by the saline water, and also the inland fishery has used the saline water for cultivation in this area. The Landsat TM and OLI/TIRS satellite imageries were used for this study. Also, field observation was required to validate the results. The method has been used to monitor the salinity condition over the Gosaba block, South 24 Parganas, West Bengal, India. The different spectral indicators were used for mapping the most affecting salinity area on the Gosaba block. LST was used to monitor the thermal condition and variation over 2000–2020. Also, correlation coefficients were used to identify the relationship between LST and different spectral indicators. This study is helpful for administrators, developers, planners, agricultural departments and other stakeholders for future planning and management toward sustainable rural development and food security of the Gosaba block and local area because West Bengal was the most paddy producing state of India. Also, some strategies are required for better development of this area. This area is not focused on by many researchers or scientists for development. This study may be helpful for general knowledge of the Gosaba block and indicates how much the saltwater inundation has affected the area and adaptation against that natural environment.

Study Area

The Ganga delta is the world's largest delta and is situated in the lower part of the Bengal Basin. These delta areas have two parts, one is Bhagirathi-Hoogli river area and the other is the Padma-Meghna estuary. The coastal region of the Ganga-Brahmaputra delta of India and Bangladesh are ecologically exceptional for

mangrove habitats known as the Sundarban Mangrove Forest. Those areas are situated approximately 1–2 m of mean sea level (Hait and Behling 2009). The Ganga delta is the most fertile and vegetated alluvial land, also called the "Green Delta". The total area of the Ganga delta is 105,000 sq.km and 60% of the area is in Bangladesh and 40% is in West Bengal, India. Alluvial soil is beneficial to people's lives because this area is suitable for growing forest, agricultural development, which helps builds a strong economy. Approximately two-thirds of the population depended on the agricultural field and other people work in the fisheries (Marian and Inland).

The total study area is 362.64 sq.km and situated at $88°40'$ E to $88°59'$ E and $22°3''$ N to $22°17'$ N. The annual average temperature is 29 °C and annual rainfall is 1200 mm. The total population of Gosaba area is 5369 (2011), according to the Census of India (https://censusindia.gov.in/). The elevation of this area is 6 m (20 ft.) and the nearest town is Canning, approximately 45 km away. The Gosaba CD blocks have 1 panchayat samity, 14 gram panchayats, 147 gram sansads, 51 mouzas and 50 inhabited villages (District Statistical Handbook).The major cultivations in this area include rice, jute, different types of vegetable, and many more. Low land value and agricultural sustainability are shown in the breakdown of the habitable suitability of the South 24 Parganas district. However, the inhabitants of this area face many challenges such as they are connected to each other only by water. They have to use boats to travel to the main part of the land. For some decades, sea surface change and increasing water level change accelerated habitation (Halder et al. 2021a). In 2009, tropical cyclone Aila hammered those areas (Fig. 4.1).

Materials and Method

Data Used

In the study area data, land use and land cover (LULC) alteration or dynamics were analyzed and monitored using Landsat TM and OLI/TIRS images. Different year images were used to identify the actual change scenario for the earth surface of the Gosaba block, South 24 Parganas, West Bengal, India (https://earthexplorer.usgs.gov/) with the least clouds and snow cover <10%. 2000, 2010, and 2020 year image was taken for LULC change detection and detects the salinity indicators and agricultural land over the Gosaba area. To better understand the agricultural land and inland fishery of this area, 2020 satellite image was deliberately included in this area despite a difference in the time interval. The selected satellite imageries information is shown in Table 4.1. The population data, administrative boundary and total Gosaba block of this study area were derived from the Census of India (https://censusindia.gov.in/). Supervised classification and maximum likelihood algorithm are used to classify the satellite images and delineation of the LULC change dynamics identified over the study area.
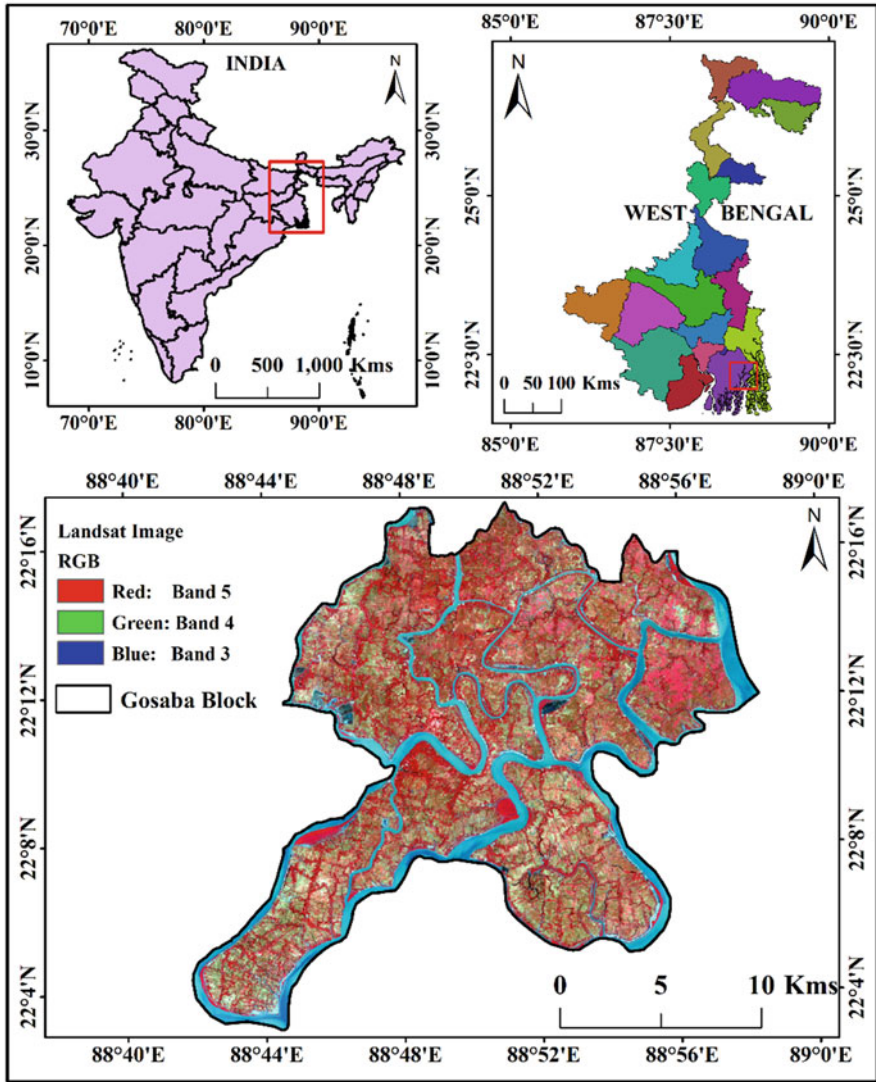
Fig. 4.1 Locational map of this study area

Table 4.1 Satellite data detail and data acquisition time

Satellite	Sensor	Date	Path & row	Data source
Landsat 5	TM	09-11-2000	138,44	https://earthexplorer.usgs.gov/
		06-02-2010	138,44	
Landsat 8	OLI/TIRS	18-12-2020	138,44	

Satellite Image Classification

The remote sensing satellite data were pre-processed to detect the LULC classification and extract the agricultural land and inland fishery of the study area for the years 2000, 2010 and 2020. With minimal alteration of the geometric accuracy, the satellite data were collected from different dates from 2000–2020. To improve the satellite data quality, images were enhanced using histogram equalization (Meshesha et al. 2016; Halder et al. 2020). Rectification is necessary to remove image distortion, and to achieve this, remote sensing satellite data were re-projected into World Geodetic System (WGS) 1984 Universal Transverse Mercator (UTM) zone 45 N. Satellite data were pre-processed in ERDAS IMAGINE version14 and ArcGIS version 10.5 and then notified software was used for geo-reference, atmospheric correction, radiometric correction and subsisting region of interest (ROI). A post-classification change detection technique was calculated in ERDAS IMAGINE version 14 software. Many researchers were used to detect the actual change of the rural environmental area or natural location and rate of change. The change detection was calculated on a pixel by pixel basis, and a new thematic layer was created using five class maps, containing different combination of 'from-to' change classes (Hassan et al. 2016) (Fig. 4.2).

Accuracy Assessment and Kappa Coefficient

Land cover (LC) is the natural earth surface topographies which grows naturally, such as vegetation coverage, water bodies, agricultural land, etc. The land use and land cover (LULC) change examination is additionally significant to classify the agricultural land or any land use and land cover along with the inland fishery area over the study area using different time periods (Ramachandra et al. 2013; Bharath et al. 2017). The rural fringe area, population pressure and industrialization greatly influence the natural land cover area and affect the vegetation cover, agricultural land, etc. The supervised classification method with the maximum likelihood algorithm was used to classifying the land use/land cover (LULC) dynamics investigation using different year Landsat TM and OLI/TIRS to conduct multitemporal LULC classification (Singh et al. 2017). The areas were classified into six classes: built-up area, vegetation, agricultural land, river, water body/pond and inland fishery.

The post-classification stage was used to increase the LULC classification accuracy (Cheruto et al. 2016). When using different years satellite remote sensing data, medium-spatial resolution of Landsat data (TM and OLI/TIRS) mixed pixels are a common problem (Lu and Weng 2005; Halder et al. 2021b). Remote sensing software (ERDAS IMAGINE v14 and ArcGIS v10.5) is used for the accuracy assessment, which is a technique that represents the correspondence between the aspect of earth surface and results of the classification. It is important to distinguish impeccable accuracy by the appropriate classification of different year satellite
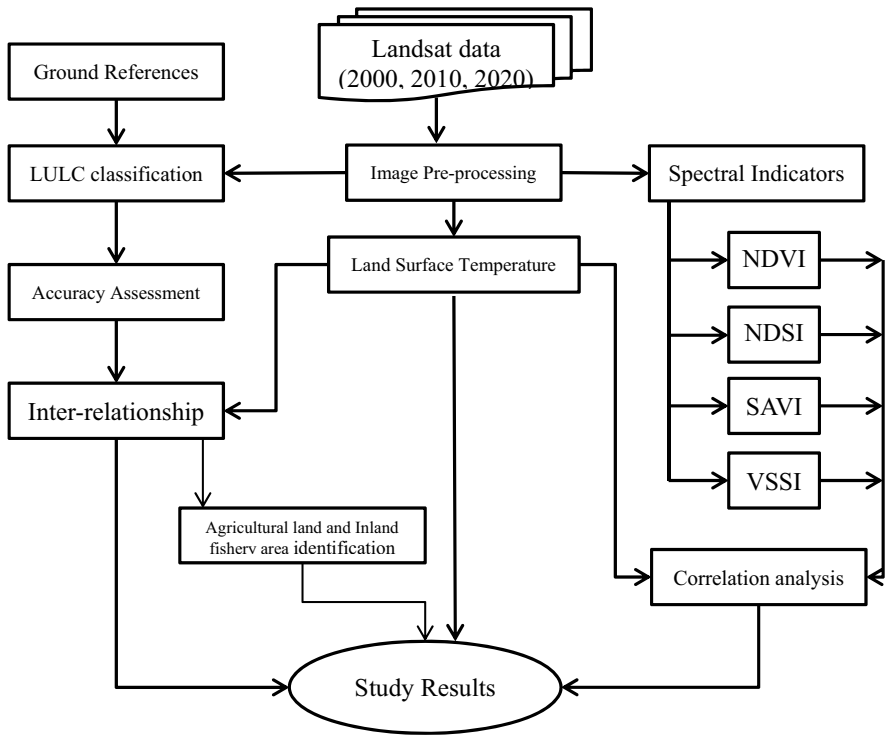
Fig. 4.2 Entire methodology of this study area

Table 4.2 Scale of kappa coefficient (Cohen 1968)

Sl No.	Value of K	Strength of agreement
1	<0.20	Poor
2	0.21–0.40	Fair
3	0.41–0.60	Moderate
4	0.61–0.80	Good
5	0.81–1.00	Very good

imageries to analyze the land use and land cover (LULC) changes (Owojori and Xie 2005). The accuracy assessment of the land use and land cover (LULC) maps were checked using the ground truth data and the results were interpreted using overall accuracy (OA) and kappa coefficient (k_i) (Table 4.2), which is shown in Eqs. 4.1 and 4.2.

$$OA = \left(\frac{\sum_{i=1}^{k} n_{ij}}{n} \right) \qquad (4.1)$$

$$K_i = \frac{(\text{Observed accuracy} - \text{Chance accuracy})}{(1 - \text{Chance accuracy})} \quad (4.2)$$

Where n_{ij} represents the diagonal elements in the error matrix, k is total number of classes in the LULC classification, n is total number of samples in the error matrix and K_i represents the kappa coefficient.

LST Calculation

LST for Landsat TM

The LST is calculated by an established formula. Ca et al. (2008) estimated brightness temperature using a two-stop process following from Landsat TM images. The equation is below.

1. Conversion of the digital number (DN) to spectral radiance (L) (USGS 2001) is calculated by Eq. 4.3.

$$L = \left(\frac{L_{\max} - L_{\min}}{\text{DN}_{\max}}\right) \times \text{Band} + L_{\min} \quad (4.3)$$

Where L is that the spectral radiance, $L_{\min}$ is 1.238 (spectral radiance of the DN value 1), $L_{\max}$ is 15.6000 (spectral radiance of DN value 255) and DN is the digital number.

2. Conversion of spectral radiance to temperature in kelvin (USGS 2001; Sobrino et al. 2001) is calculated by Eq. 4.4.

$$Tb = \frac{K2}{\left(\frac{K1}{L\lambda} + 1\right)} \quad (4.4)$$

Where $K1$ is the calibration constant 1 (607.76), $K2$ is the calibration constant 2 (1260.56) and Tb is the surface temperature (kelvin).

Calculation of NDVI

$$\text{NDVI} = \frac{(\text{NIR} - \text{R})}{(\text{NIR} + \text{R})} \quad (4.5)$$

Land surface emissivity (LSE) is calculated based on NDVI values. It used the NDVI Thresholds Method-

NDVITHM by applying Eq. 4.6 (Sabrino and Raissouni 2001).

$$LSE = (1.0094 + 0.047) \times In\ (NDVI) \tag{4.6}$$

The NDVI value ranges from 0.157 to 0.727. When the NDVI values are out of the range (0.157–0.727), the corresponding input LST constant values are used.

3. Conversion of kelvin to Celsius (Semenza et al. 1996) is estimated by Eq. 4.7.

$$LST = Tb - 273.15 \tag{4.7}$$

LST for Landsat OLI

1. Conversion of the Digital Number (DN) to spectral radiance (L) (Rasul et al. 2015; Scarano and Sobrino 2015) is calculated by Eq. 4.8.

$$L = \left(\frac{L_{max} - L_{min}}{DN_{max}}\right) \times Band + L_{min} \tag{4.8}$$

Where

L = Atmospheric spectral radiance (SR) in watts/(m^2*srad* μm), L$_{max}$ = maximum spectral radiance (SR) of the DN value, BandL$_{min=}$ minimum spectral radiance (SR) of band, DN$_{max}$ = Q $_{cal\ max}$ − Q $_{cal\ min}$ = maximum and minimum difference of sensor calibration

2. Using the thermal constants given in the metadata file, the TIRS band data converts from SR to BT once the DN values are converted to SR (Gutman et al. 2013, Halder et al. 2021b) (Eq. 4.9).

$$BT = \frac{K2}{Ln\left(\frac{K1}{L\lambda} + 1\right)} - 273.15 \tag{4.9}$$

Where

BT = brightness temperature in Celsius. K$_2$ and K$_1$ represent the band-specific thermal conversion constants,

3. Calculation of NDVI (Roy et al. 2014; Halder et al. 2021b) (Eq. 4.10):

$$NDVI = \frac{(NIR - R)}{(NIR + R)} \tag{4.10}$$

Where the range between: $-1 < NDVI < +1$.

4. Proportion of vegetation is calculated by minimum and maximum NDVI value (Yu et al. 2014) (Eq. 4.11).

$$Pv = \left(\frac{NDVI - NDVI_{min}}{NDVI_{max} - NDVI_{min}}\right)^2 \tag{4.11}$$

5. Land surface emissivity (LSE) is calculated based on P_v value. It uses the NDVI Thresholds Method- NDVITHM by applying Eq. 4.12 (Roy et al. 2014; Avdan and Jovanovska 2016).

$$LSE = 0.004 \times Pv + 0.986 \tag{4.12}$$

6. Conversion of kelvin to Celsius (Yu et al. 2014; Avdan and Jovanovska 2016; Halder et al. 2021c) is estimated by Eq. 4.13

$$LST = \frac{BT}{\left\{1 + \left[\frac{\lambda BT}{\rho}\right] In(LSE)\right.} \tag{4.13}$$

Where
λ = the wavelength of emitted radiance.

Spectral Indicators

Different spectral indicators were derived from satellite images in different years for delineating the soil condition of this study area. The spectral indicators have been calculated by the indicated formula. The spectral indicators were:

Normalized Difference Vegetation Index (NDVI)

Vegetation is an essential part of the land cover of the earth. A healthy vegetation area always helps to reduce soil erosion and flood problems. It also helps to balance

the carbon dioxide and oxygen cycle and the weather patterns are also affected by the vegetation. In India, 33% of the vegetation area is very essential for a healthy life. From the Normalized Difference Vegetation Index (NDVI) we can identify or measure the vegetation quality or quantity of any area. In the map of vegetation quality (NDVI), we identify the degradation or increase of vegetation in southern parts of the South 24 Parganas district. The NDVI is a multi-spectral remote sensing data technique for identifying the vegetation area, land cover classification, water bodies' identification, open area and many types of forest area (Halder et al. 2021b). The mathematical calculation of the NDVI is defined as the value -1.0 to $+1.0$ Water bodies are detected in NDVI values that are negative values (Eq. 4.14).

$$NDVI = \frac{(NIR - R)}{(NIR + R)} \tag{4.14}$$

Here NIR refers to the near infrared and R refers red band in the satellite imagery. For the vegetation damaged area calculation use Landsat OLI. In remote sensing, the change detection technique is the most powerful technique to identify the aerial changes in vegetation covered area and vegetation to the non-vegetation area or non-vegetation to vegetation area.

Normalized Difference Salinity Index (NDSI)

Normalized Difference Salinity Index (NDSI) was used to detect the salinity over the Gosaba block of the South 24 Parganas district, West Bengal, India. This technique was widely used for delineating the salinity index and salinity map of an area (Elhag 2016).

$$NDSI = \left(\frac{Red - NIR}{Red + NIR} \right) \tag{4.15}$$

The mathematical calculation of the NDSI is defined as the value -1.0 to $+1.0$. Vegetation areas are detected in negative NDSI values (Eq. 4.15).

Soil Adjusted Vegetation Index (SAVI)

Soil Adjusted Vegetation Index (SAVI) is the modified Normalized Difference Vegetation Index (NDVI) for the effect of soil brightness in the position where the vegetation protections is low (Congalton 1991). SAVI is calculated as a ratio between red and near infrared (NIR) values with the soil brightness improvement factor (L) defined as 0.5 to accommodate maximum land cover types of an area (https://www.usgs.gov/core-science-systems/nli/landsat/landsat-soil-adjusted-vegetation-index). SAVI Index is particularly problematic when evaluations are made

across different soil types that may reflect various amounts of light in the red and near infrared wavelengths (i.e., soils with different brightness values).

$$SAVI = \frac{NIR - RED}{(NIR + RED + L)} * (1 + L) \qquad (4.16)$$

Where NIR represents the reflectance value of the near infrared band, red denotes the reflectance value of the red band and L represents the soil brightness correction factor.

Vegetation Soil Salinity Index (VSSI)

Vegetation Soil Salinity Index (VSSI) was used for this study to monitor and map the vegetation and soil salinity condition over the Gosaba block. Green, red and near infrared bands of different years satellite data were used for the formula (Eq.4. 17).

$$VSSI = 2 \times Green - 5 \times (Red + NIR) \qquad (4.17)$$

The green, red and near infrared (NIR) bands of satellite data were used to calculate the Vegetation Soil Salinity Index (VSSI).

Other Salinity Index

Douaoui et al. (2006) used this salinity index for mapping and monitoring the salinity over an area. The equation used square root of green and red bands of satellite images.

$$Salinity\ Index\ (SI) = \sqrt{Green * Red} \qquad (4.18)$$

Result

Red, green and blue colour band combination of the five different year satellite imageries were used for classification using standard colour combination. Currently, there were food and residential problems due to up-scaling population pressure and rapid growth of infrastructural development in society. The land use and land cover change dynamics were calculated in the years 2000 to 2020 (Fig. 4.3).
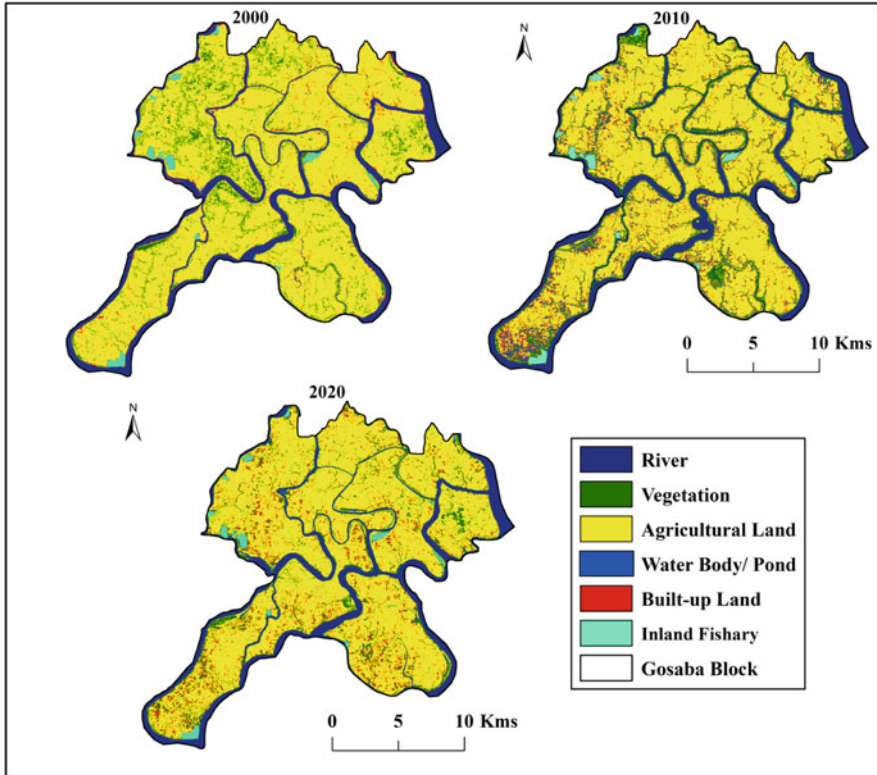
Fig. 4.3 LULC map of the Gosaba block in the years 2000–2020

LULC Dynamics

In the land use and land cover classification, supervised classification techniques with maximum likelihood algorithm have been used for the years 2000, 2010 and 2020. Six types of land classes were identified for three different years LULC maps, which are water bodies, river, inland fishery, vegetation, agricultural land and built-up land. Land transformation is the main reason for land use and land cover change. The overall area has seen a decrease in vegetation and agricultural land over the 20 years. Gradually, built-up land, water bodies and inland fishery were increased. Agriculture is the main occupation of this location but a huge amount of land transformation is affected by this natural phenomenon. This is the reason that primary economic activities are converted into secondary and tertiary economic activities because of residential land, recreational land and migration. The anthropogenic activities are much affected by the land use and land cover classes. Land values and quality of land change regularly.

Table 4.3 Area and percentage calculation of different LULC classes (2000–2020)

Class name	Area in sq.km			Area in percentage (%)		
	2000	2010	2020	2000	2010	2020
River	49.84	45.34	46.91	13.74	12.50	12.94
Vegetation	37.94	36.21	30.73	10.46	9.99	8.47
Agricultural land	225.57	221.49	211.84	62.20	61.08	58.42
Water body/pond	19.85	20.72	21.97	5.47	5.71	6.06
Inland fishery	15.28	17.96	28.73	4.21	4.95	7.92
Built-up land	14.16	20.92	22.46	3.90	5.77	6.19
Total	362.64	362.64	362.64	100	100	100

Table 4.4 Difference area calculation in different time scale

Class name	Difference in area (sq.km)		
	(2000–2010)	(2010–2020)	(2000–2020)
River	−4.50	1.57	−2.93
Vegetation	−1.73	−5.48	−7.21
Agricultural land	−4.08	−9.65	−13.73
Water body/pond	0.87	1.25	2.12
Inland fishery	2.68	10.77	13.45
Built-up land	6.76	1.54	8.3

The agricultural land decreased by 13.73 sq.km (2000–2020) and inland fishery increased by 13.45 sq.km (Table 4.4), which indicates that agricultural land was converted into inland fisheries and some area became built-up land. The agricultural land shown in the classification maps were 62.20% (2000), 61.08% (2010) and 58.42% (2020), which indicates that the agricultural land gradually increased due to salt water intrusion and saline land (Table 4.3). The vegetation area also decreased and converted into built-up land; the areas were 10.46% (2000), 9.99% (2010) and 8.47% (2020) and approximately 7.21 sq.km area has been decreased over the year 2000–2020. The inland fishery areas were 15.28 sq.km (2000), 17.96 sq.km (2010) and 28.73 sq.km (2020). The inland fishery area has increased during 2010–2020 because of cyclone Aila. Salt water intrusion damaged the soil fertility rate and influenced the crops production area. The built-up lands were increased gradually, which denote that amount of inhabited area increased; 14.16 sq.km (2000), 20.92 sq. km (2010) and 22.46 sq.km (2020) area were detected in LULC maps (Fig. 4.4). The accuracy assessment results were 96.25% (2000), 95% (2010) and 94.50% (2020), also the kappa coefficients were 0.95, 0.94 and 0.93 in the years 2000, 2010 and 2020, respectively (Tables 4.5, 4.6 and 4.7). Reducing salt water intrusion was a big problem, and the natural barrier mangroves were also damaged by the local people and natural extreme events. In this case, roads, bridges, and proper planning will be necessary for adopting new strategies.
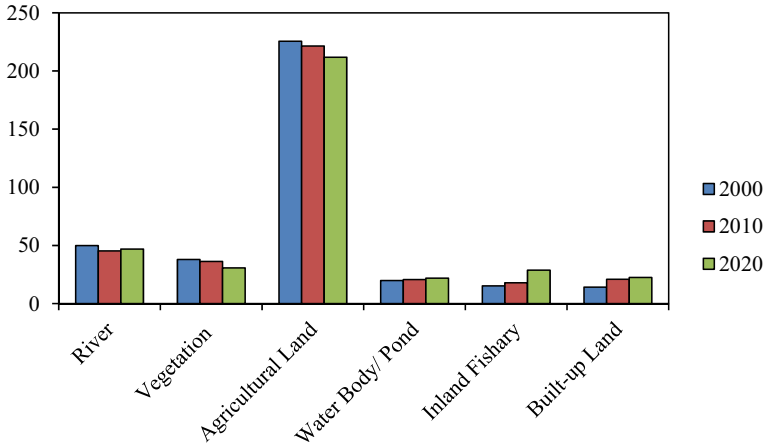
Fig. 4.4 Different LULC classes and area calculation

Topographical Distribution of LST

The land surface temperature (LST) maps were calculated by the given formulas. Vegetation is controlled by the temperature of an area. The spatio-temporal distributions of land surface temperature (LST) form the years 2000–2020 were derived from remote sensing (Landsat 5 TM and 8 OLI/TIRS) thermal bands using the provided equation. The red colour of this map is shows the highest temperature and simultaneously the blue colour denotes the lowest temperature in this region. The land surface temperature (LST) increased to around 4.22 °C during 2000–2020. The annual average LST was 0.14 °C (2000–2010), 0.28 °C (2010–2020), and 0.42 °C in the years 2000–2020 (Fig. 4.5). The highest temperature shows those southern parts in the year 2000, and the highest temperature was 26.25 °C and lowest 21.50 °C. The entire area was under low temperature in the year 2000, but after that, the temperature was increased due to anthropogenic activities, natural extreme events, etc. In 2010, most of the parts were located in high temperate zones. In 2020, central, southern and eastern parts were mostly temperate zones. The highest temperature was 30.47 °C and lowest 18.43 °C in 2020. Built-up land and many anthropogenic activities were the reason for temperature variation on the Gosaba block, South 24 Parganas, West Bengal, India.

Spectral Indicators

The remote sensing-based different spectral indicators are used to identify the urban heat island. Landsat 5 and Landsat 8 bands are used to calculate the Normalized Difference Vegetation Index (NDVI), and the Normalized Difference Salinity Index

Table 4.5 Accuracy assessment and kappa coefficient in 2000

Class name	Ground truth/reference						Row Total	Commission error	User accuracy
	Water body	Agricultural land	Vegetation	River	Inland fishery	Built-up land			
Water body	63	0	0	2	0	0	65	3.08%	96.92%
Agricultural land	0	125	1	2	0	1	129	3.10%	96.90%
Vegetation	0	0	39	1	0	1	41	4.88%	95.12%
River	1	0	1	51	0	0	53	3.77%	96.23%
Inland fishery	0	0	0	1	57	1	59	3.39%	96.61%
Built-up land	2	1	0	0	0	50	53	5.66%	94.34%
Column Total	66	126	41	57	57	53	400		
Omission error	4.55%	0.79%	4.88%	10.53%	0.00%	5.66%			
Produce accuracy	95.45%	99.21%	95.12%	89.47%	100.00%	94.34%			
Overall accuracy	**96.25%**				Kappa coefficient	**0.95**			

Table 4.6 Accuracy assessment and kappa coefficient in the year 2010

Class name	Ground Truth/Reference						Row total	Commission error	User accuracy
	Water body	Agricultural land	Vegetation	River	Inland fishery	Built-up land			
Water body	65	0	0	2	0	0	67	2.99%	97.01%
Agricultural land	0	134	2	2	0	1	139	3.60%	96.40%
Vegetation	0	0	49	0	1	1	51	3.92%	98.08%
River	2	0	0	33	0	0	35	5.71%	94.29%
Inland fishery	0	0	2	1	58	2	63	7.94%	92.06%
Built-up land	0	0	0	1	3	41	45	8.89%	91.11%
Column Total	67	134	53	39	62	45	400		
Omission error	2.99%	0.00%	7.55%	12.82%	6.45%	8.89%			
Produce accuracy	97.01%	100.00%	92.45%	87.18%	93.55%	91.11%			
Overall accuracy	95.00%				Kappa coefficient	0.94			

Table 4.7 Accuracy assessment and kappa coefficient in the year 2020

Class name	Ground Truth/Reference						Row total	Commission error	User accuracy
	water body	Agricultural land	Vegetation	River	Inland fishery	Built-up land			
Water body	62	1	0	1	1	0	65	4.62%	95.38%
Agricultural land	1	124	2	0	0	1	128	3.13%	96.88%
Vegetation	0	2	53	0	1	1	57	7.02%	92.98%
River	1	0	1	41	2	0	45	8.89%	91.11%
Inland fishery	2	0	0	2	30	0	34	11.76%	88.24%
Built-up land	0	2	1	0	0	68	71	4.23%	95.77%
Column Total	66	129	57	44	34	70	400		
Omission error	6.06%	3.88%	7.02%	6.82%	11.76%	2.86%			
Produce accuracy	93.94%	96.12%	92.98%	93.18%	88.24%	97.14%			
Overall accuracy	**94.50%**				Kappa coefficient	**0.93**			
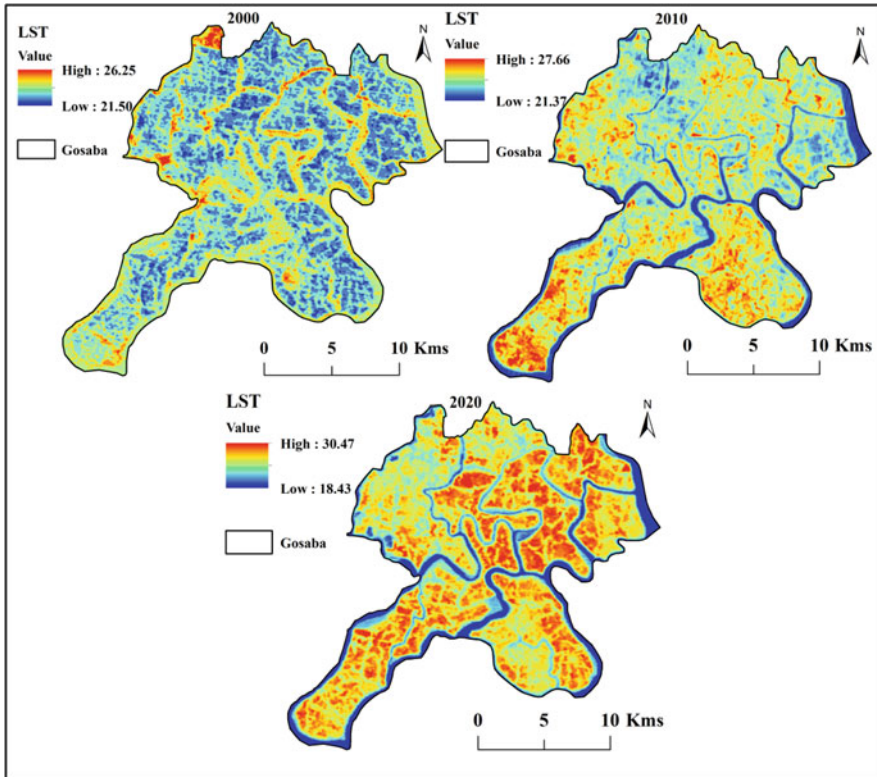
Fig. 4.5 Land Surface Temperature (LST) maps (2000–2020)

(NDSI), Vegetation Soil Salinity Index (VSSI) and Sail Adjacent Vegetation Index (SAVI) were used to estimate the salinity index. The NDVI was high in the year 2000 but after that the NDVI values decreased (Fig. 4.6). The highest NDVI value was 0.55 and lowest value was 0.39 between the years 2000 and 2020. The NDSI values fluctuated because of high salt water intrusion at the end of 2009. That is why the second NDSI value was high, which was 0.37 (Fig. 4.7). The high saline land located in 2010 in the central, east and south-eastern parts were mostly because of cyclone Aila. The Sail Adjacent Vegetation Index (SAVI) was used to monitor the vegetation soil variation over the Gosaba block. The maps show that the most affected year was 2010. The highest value of SAVI was 0.82, where vegetation was high in 2000, and lowest at 0.58, where the vegetation scenario was low in 2020 (Fig. 4.8). The Vegetation Soil Salinity Index (VSSI) was widely used for monitoring the soil salinity variation over the study area (Fig. 4.9). The salinity index was used to monitor the salinity variation over the study area (Fig. 4.10). The maps clearly show that 2010 was the most affected by saline water and the south to eastern parts were the most affected due to cyclone Aila. This natural condition has affected the local crop production and some land converted into inland fishery, thus decreasing agricultural land due to this extreme environmental condition.

Fig. 4.7 Normalized Difference Salinity Index (NDSI) maps (2000–2020)

Discussion

This study aimed to identify the LULC change, land surface temperature (LST) and soil salinity mapping and monitoring using different spectral indicators derived from different year's satellite imageries. The Landsat TM and OLI/TIRS remote sensing data were used because electric conductivities were used for mapping the salinity indices. Saltwater affected soils with salt encrustation at the surface area of the coastal area and high tidal zones are generally smoother than non-saline surfaces areas and cause high reflectance in the visible and near-infrared bands (Asfaw et al. 2018). Numerous studies have exposed that image enhancement techniques consisting of spectral indices (like NDVI, NDSI, SAVI and VSSI) have countless possibilities in improving and defining soil salinity details using the remote sensing satellite images (Noroozi et al. 2012). The results show that agricultural land decreased by 13.73 sq.km and the inland fishery area increased by 13.45 sq.km in this study location. The correlation with LST and NDSI showed a high negative
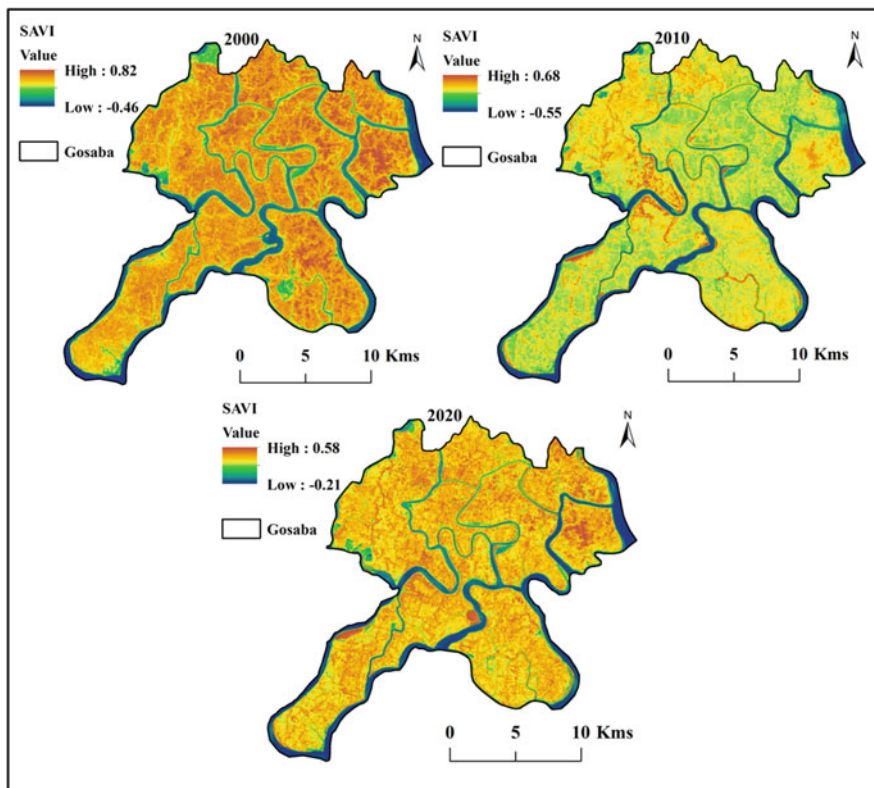
Fig. 4.8 Soil Adjacent Vegetation Index (SAVI) maps (2000–2020)

relationship in the year 2010 ($R^2 = 0.45$) because of the cyclone Aila. The land surface temperature (LST) increased to the highest around 4.22 °C during 2000–2020. The annual average LST was 0.14 °C (2000–2010), 0.28 °C (2010–2020) and 0.42 °C in the years 2000–2020. The built-up land increased by 8.3 sq.km area in the Gosaba block. The salinity was visible for near-infrared (NIR) bands using the electric conductivity of the bands. The Landsat bands characterized the pattern and features of soil salinity using a high rate of correlation.

Salt in land causes roughness of land, which induced variation of spectral reflectance of each land class (Goldshleger et al. 2013). Spectral reflectance was used for salt land identification and salt land also reduced the soil productivity and crop pattern in coastal, arid and semi-arid regions. Salted land has a high inception rate to infiltration of soil and spectral reflectance will be significantly higher (Metternicht and Zinck 1997). NIR bands shows a higher reflectance on saline land and that is why the spectral indicators identified the salt intrusion land over the Gosaba block, South 24 Parganas. Agricultural irrigation systems cannot absorb
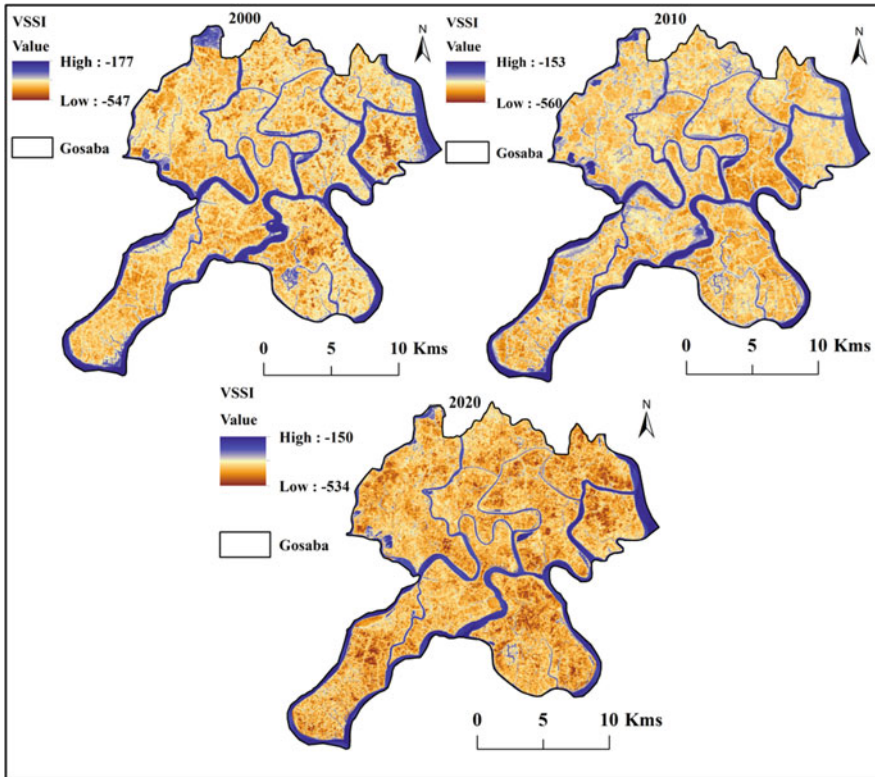
Fig. 4.9 Vegetation Soil Salinity Index (VSSI) maps (2000–2020)

the salt and accumulated in the land, which are cases of land transformation and strategy adaptation. Using remote sensing techniques, land salinity has been detected for planning purposes. The south, east and south-eastern parts of the Gosaba block has a high level of salinity due to saltwater intrusion during Aila and after that, deformation, tidal condition and shoreline stiffing are responsible for saline land. Those cases influenced the land transformation, crop production change and adopting new strategies for healthy livelihood. The area has experienced a huge amount of land transformation that mostly affected agricultural land and increased the inland fishery area due to saline water and natural disasters such as cyclones, hazards and environmental conditions. The LST has been increased due to built-up land, global climate change and methodological conditions.
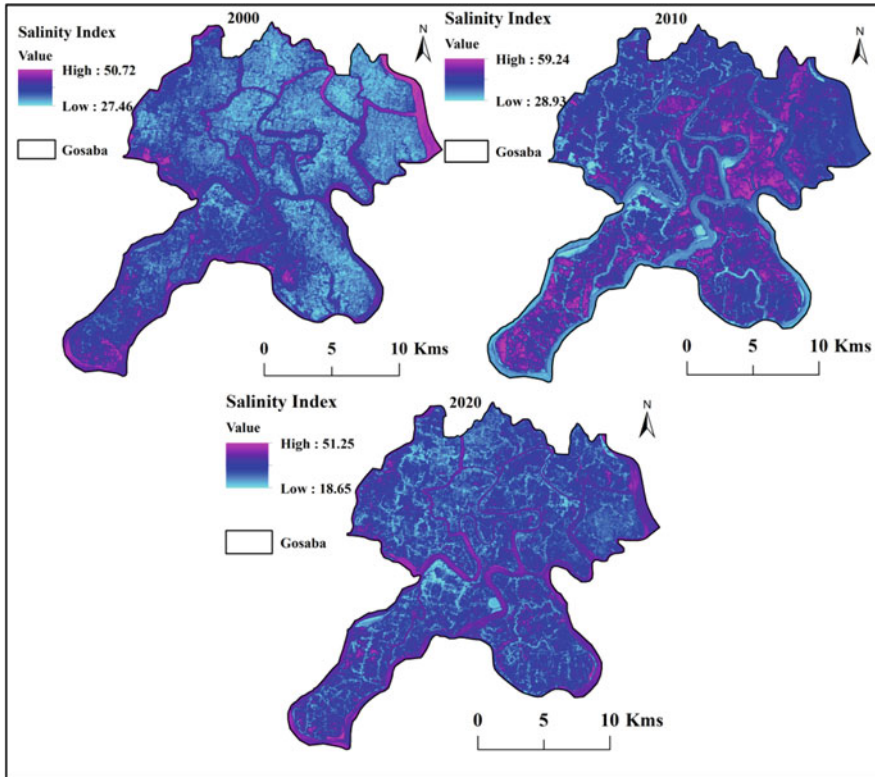
Fig. 4.10 Salinity Index (SI) maps (2000–2020)

Conclusion

The study investigated the saltwater intrusion effect on the natural environmental condition and crop productivities in the Gosaba block of South 24 Parganas, West Bengal, India. The study denoted that satellite remote sensing data with different dates were used to identify the LULC and spectral indicators for mapping and monitoring the salinity map over the Gosaba block. The NDVI, NDSI, VSSI and SAVI were used to map the salinity and validated using field data collection. Landsat TM and OLI/TIRS data were used to derive the indices. The thermal bands of satellite imageries were used to detect the land surface temperature over the study area during 2000–2020. The correlation with LST and NDSI showed a high negative relationship in the year 2010 ($R^2 = 0.45$) because of the cyclone Aila. Super cyclone Aila affected the southern parts of West Bengal and other reasons were because Gosaba is a riverine island, where tide and natural phenomenon are occurring gradually. That is why people can change crop production and adopt new strategies for a sustainable livelihood. Mangrove is a natural barrier, and the coastal area
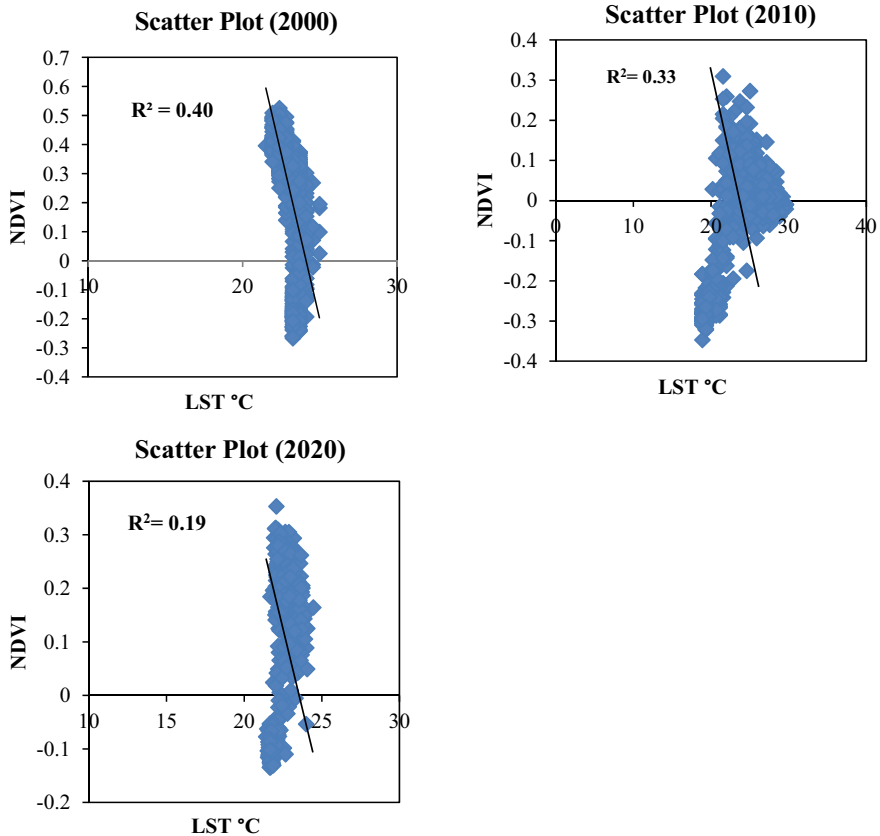
Fig. 4.11 Correlation with LST and NDVI maps (2000–2020)

Mangrove trees must be protected to prevent floods, hazards, environmental degradation and crop pattern changes. The coastal areas are struggling from the natural environmental condition.

The results show that agricultural land has decreased by 13.73 sq.km and the inland fishery area increased by 13.45 sq.km in this study location. Also, pond-based integrated fish farming, vegetable farming and shifting to inland fisheries will be better for future productivity on the Gosaba block; basically, the south, south-east and eastern parts of this study area. This result was also helpful for the administrators, local planners and others stakeholders for future planning over the Gosaba area. Future studies are necessary for this area such as site suitability for integrated fish farming, site suitability for agroforestry, site selection for the inland fishery and monitoring the effect of reduced agricultural land on their daily livelihood and socioeconomic condition change over the past decades due to natural extreme events. In addition, this methodology is suitable for others area with suitable modification of local condition.

Scatter Plot (2000)

Scatter Plot (2010)

Scatter Plot (2020)
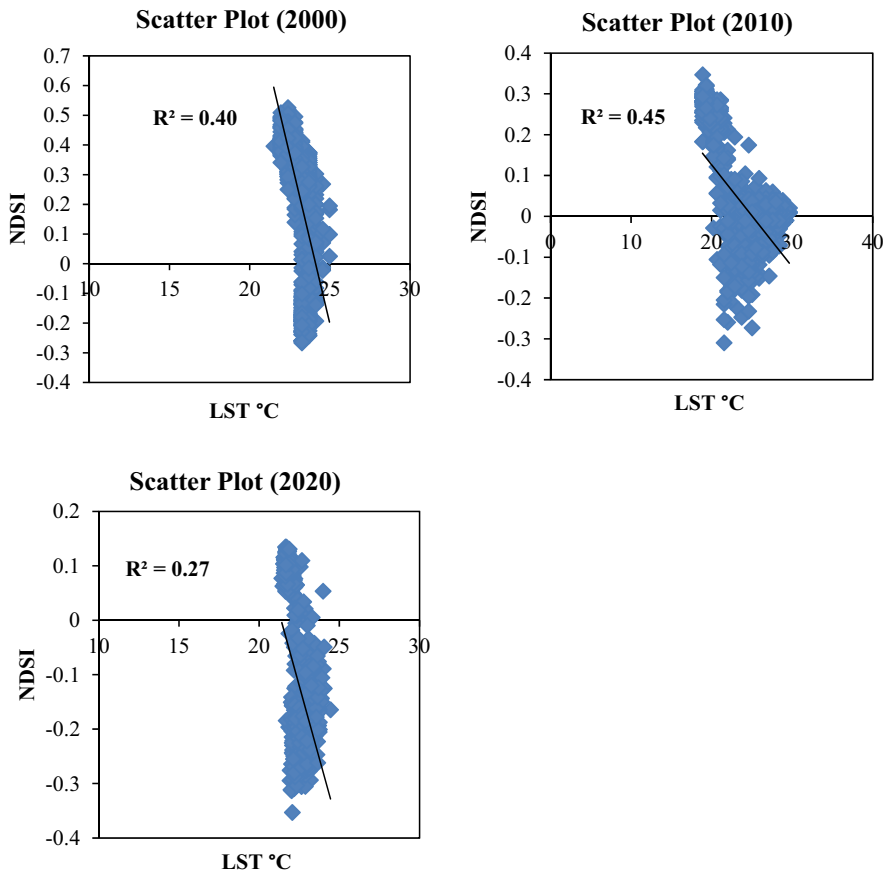
Fig. 4.12 Correlation with LST and NDSI maps (2000–2020)
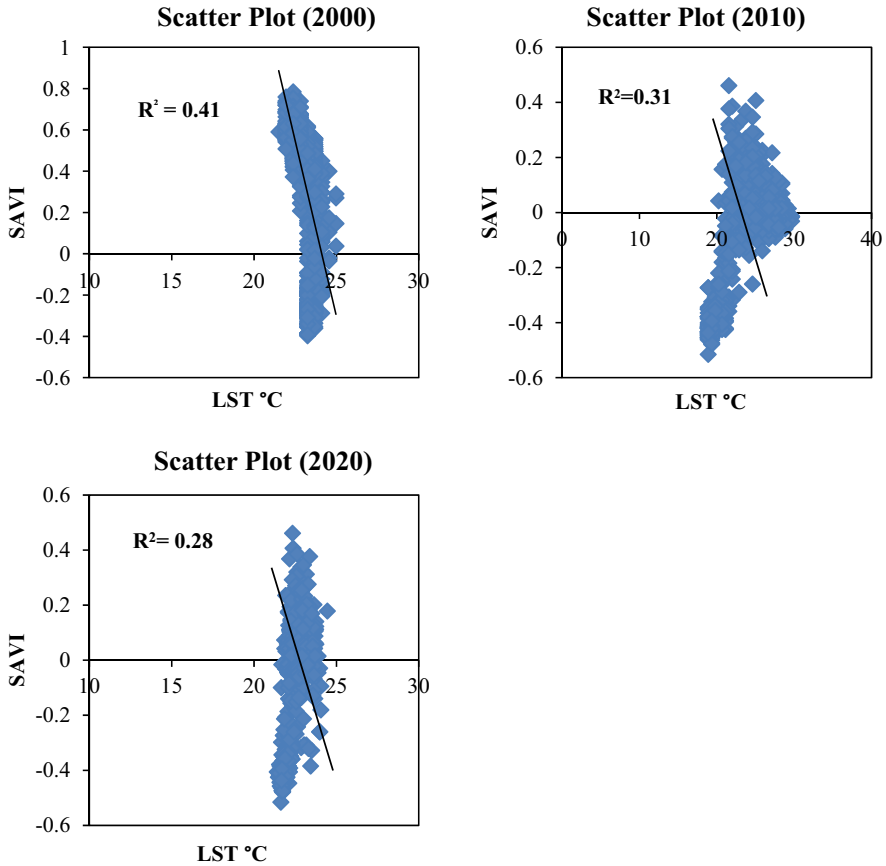
Fig. 4.13 Correlation with LST and SAVI maps (2000–2020)

References

Abdelfattah MA, Shahid SA, Othman YR (2009) Soil salinity mapping model developed using RS and GIS—a case study from Abu Dhabi, United Arab Emirates. Eur J Sci Res 26(3):342–351

Asfaw E, Suryabhagavan KV, Argaw M (2018) Soil salinity modeling and mapping using remote sensing and GIS: the case of Wonji sugar cane irrigation farm, Ethiopia. J Saudi Soc Agric Sci 17(3):250–258. https://doi.org/10.1016/j.jssas.2016.05.003

Avdan U, Jovanovska G (2016) Algorithm for automated mapping of land surface temperature using LANDSAT 8 satellite data. J Sens 2016. https://doi.org/10.1155/2016/1480307

Bharath HA, Chandan MC, Vinay S, Ramachandra TV (2017) Modelling the growth of two rapidly urbanizing Indian cities. J Geom 11(12):149–166

Ca L, Li P, Zhang L, Chen T (2008) Remote sensing image-based analysis of the relationship between urban heat island and vegetation fraction. Int Arch Photogramm Remote Sens Sp Inf Sci 37:1379–1383

Cheruto MC, Kauti MK, Kisangau DP, Kariuki PC (2016) Assessment of land use and land cover change using GIS and remote sensing techniques: a case study of Makueni County, Kenya, http://repository.seku.ac.ke/handle/123456789/3062

Cohen J (1968) Weighted kappa: nominal scale agreement provision for scaled disagreement or partial credit. Psychol Bull 70(4):213. https://psycnet.apa.org/doi/10.1037/h0026256

Congalton RG (1991) A review of assessing the accuracy of classifications of remotely sensed data. Remote Sens Environ 37(1):35–46

Dehni A, Lounis M (2012) Remote sensing techniques for salt affected soil mapping: application to the Oran region of Algeria. Procedia Eng 33:188–198. https://doi.org/10.1016/j.proeng.2012.01.1193

Douaoui AEK, Nicolas H, Walter C (2006) Detecting salinity hazards within a semiarid context by means of combining soil and remote sensing data. Geoderma 134:217–230

Elhag M (2016) Evaluation of different soil salinity mapping using remote sensing techniques in arid ecosystems, Saudi Arabia. J Sens 2016. https://doi.org/10.1155/2016/7596175

Goldshleger N, Chudnovsky A, Ben-Binyamin R (2013) Predicting salinity in tomato using soil reflectance spectral. Int J Remote Sens 34:6079–6093

Gorji T, Tanik A, Sertel E (2015) Soil salinity prediction, monitoring and mapping using modern technologies. Procedia Earth Planet Sci 15:507–512

Gutman G, Huang C, Chander G, Noojipady P, Masek JG (2013) Assessment of the NASA–USGS global land survey (GLS) datasets. Remote Sens Environ 134:249–265

Hait AK, Behling H (2009) Holocene mangrove and coastal environmental changes in the western Ganga–Brahmaputra Delta, India. Veg Hist Archaeobot 18(2):159–169. https://doi.org/10.1007/s00334-008-0203-5

Halder B, Bandyopadhyay J, Banik P (2020) Assessment of hospital sites' suitability by spatial information technologies using AHP and GIS-based multi-criteria approach of Rajpur–Sonarpur Municipality. Model Earth Syst Environ 6(4):2581–2596. https://doi.org/10.1007/s40808-020-00852-4

Halder B, Das S, Bandyopadhyay J, Banik P (2021a) The deadliest tropical cyclone 'Amphan': investigate the natural flood inundation over south 24 Parganas using google earth engine. Saf Extreme Environ 3:1–11. https://doi.org/10.1007/s42797-021-00035-z

Halder B, Banik P, Bandyopadhyay J (2021b) Mapping and monitoring land dynamic due to urban expansion using geospatial techniques on South Kolkata. Saf Extreme Environ 3:27–42. https://doi.org/10.1007/s42797-021-00032-2

Halder B, Bandyopadhyay J, Banik P (2021c) Evaluation of the climate change impact on urban Heat Island based on land surface temperature and geospatial indicators. Int J Environ Res 15:819–835. https://doi.org/10.1007/s41742-021-00356-8

Hassan Z, Shabbir R, Ahmad SS, Malik AH, Aziz N, Butt A, Erum S (2016) Dynamics of land use and land cover change (LULCC) using geospatial techniques: a case study of Islamabad Pakistan. Springer Plus 5(1):812. https://doi.org/10.1186/s40064-016-2414-z

Lu D, Weng Q (2005) Urban classification using full spectral information of Landsat ETM+ imagery in Marion County, Indiana. Photogramm Eng Remote Sens 71(11):1275–1284

Meshesha TW, Tripathi SK, Khare D (2016) Analyses of land use and land cover change dynamics using GIS and remote sensing during 1984 and 2015 in the Beressa watershed northern Central Highland of Ethiopia. Model Earth Syst Environ 2(4):1–12, https://link.springer.com/article/10.1007/s40808-016-0233-4

Metternicht G, Zinck JA (1997) Spatial discrimination of salt-and sodium-affected soil surfaces. Int J Remote Sens 18:2571–2586

Nguyen KA, Liou YA, Tran HP, Hoang PP, Nguyen TH (2020) Soil salinity assessment by using near-infrared channel and vegetation soil salinity index derived from Landsat 8 OLI data: a case study in the Tra Vinh Province, Mekong Delta, Vietnam. Prog Earth Planet Sci 7(1):1–16. https://doi.org/10.1186/s40645-019-0311-0

Noroozi AA, Homaee M, Farshad A (2012) Integrated application of remote sensing and spatial statistical models to the identification of soil salinity: a case study from Garmsar plain. Iran J Environ Sci 9:59–74

Owojori A, Xie H (2005, March) Landsat image-based LULC changes of San Antonio, Texas using advanced atmospheric correction and object-oriented image analysis approaches. In: 5th international symposium on remote sensing of urban areas, Tempe, AZ

Ramachandra TV, Bharath HA, Vinay S (2013) Land use land cover dynamics in a rapidly urbanising landscape. SCIT J 13:1–12

Rasul A, Balzter H, Smith C (2015) Spatial variation of the daytime surface urban cool island during the dry season in Erbil, Iraqi Kurdistan, from Landsat 8. Urban Clim 14:176–186

Roy DP, Wulder MA, Loveland TR, Woodcock CE, Allen RG, Anderson MC, Zhu Z (2014) Landsat-8: science and product vision for terrestrial global change research. Remote Sens Environ 145:154–172

Scarano M, Sobrino JA (2015) On the relationship between the sky view factor and the land surface temperature derived by Landsat-8 images in Bari, Italy. Int J Remote Sens 36(19–20): 4820–4835

Semenza JC, Rubin CH, Falter KH, Selanikio JD, Flanders WD, Howe HL, Wilhelm JL (1996) Heat-related deaths during the July 1995 heat wave in Chicago. N Engl J Med 335(2):84–90

Singh SK, Srivastava PK, Szabó S, Petropoulos GP, Gupta M, Islam T (2017) Landscape transform and spatial metrics for mapping spatiotemporal land cover dynamics using earth observation data-sets. Geocarto Int 32(2):113–127. https://doi.org/10.1080/10106049.2015.1130084

Sobrino JA, Raissouni N, Li ZL (2001) A comparative study of land surface emissivity retrieval from NOAA data. Remote Sens Environ 75(2):256–266

Suarez DL (1989) Impact of agricultural practices on groundwater salinity. Agric Ecosyst Environ 26(3–4):215–227. https://doi.org/10.1016/0167-8809(89)90014-5

Taghadosi MM, Hasanlou M, Eftekhari K (2019) Soil salinity mapping using dual-polarized SAR Sentinel-1 imagery. Int J Remote Sens 40(1):237–252. https://doi.org/10.1080/01431161.2018.1512767

UNISDR (2014) https://www.undrr.org/publication/unisdr-annual-report-2014

USGS (2001) Landsat science data user's handbooks, https://www.usgs.gov/land-resources/nli/landsat/landsat-8-data-users-handbook

Verma KS, Saxena RK, Barthwal AK, Deshmukh SN (1994) Remote sensing technique for mapping salt affected soils. Int J Remote Sens 15(9):1901–1914. https://doi.org/10.1080/01431169408954215

World Bank Group (2018) Climate change knowledge portal for development practitioners and policy makers. https://climateknowledgeportal.worldbank.org/country/india/impacts-agriculture

Yu X, Guo X, Wu Z (2014) Land surface temperature retrieval from Landsat 8 TIRS—comparison between radiative transfer equation-based method, split window algorithm and single channel method. Remote Sens 6(10):9829–9852

Chapter 5
Monitoring Retreat Rate of Glacier of Pindar Basin, Kumaun Himalaya Using Remote Sensing and GIS Techniques

Biswanath Das, Anoop K. Patel, Santosh Kumar, and Ismail Mondal

Abstract The Pindar Basin is situated at higher ranges of Kumaun Himalaya and is comparatively less studied from a climate change point of view. This basin's main glaciers are Pindari, Kafni, Bidalgwar, Mrigthuni, and Buriagal. The current trend of the surrounding basins shows that a majority of glaciers have sustained a decrease in this area at an accelerating rate. It is evident from the analysis that the average retreat rate of Pindar glacier was higher at 38.19 m/year from 2000–2010 but reduced to 55.41 m/year during 2010–2018. The average retreat increased to 45.84 m/year in 2000 and 2018. Annual observations of Mrigthuni snout retreated by 32.84 m/year between 2000 and 2010 and it continues to show a reducing trend – 50.90 m/year in 2010–2018 and the average retreat increased to 40.87 m/year between 2000 and 2018. Another glacier is Bidalgwar, with a similar decrease, its yearly observed snout retreated by 27.89 m/year in 2000–2010 and it continues to display a decreasing trend that is low corresponding to another glacier – 39.33 m/year in 2010–2018. The average retreat increased 32.97 m/year. The study of changes in the Himalayan glaciers with supporting help from RS& GIS techniques used LANDSAT-7, Sentinel-2A & DEM generated images to observe data from the different glaciers in the Pindar Basin.

Keywords Remote sensing · Climate change · Glacier retreat

B. Das
Madhya Pradesh Council of Science and Technology, Bhopal, India

A. K. Patel
Madhya Pradesh Agency for Promotion of Information Technology, Bhopal, India

S. Kumar
Mahatma Gandhi Chitrakoot Gramoday Vishwavidyalaya, Chitrakoot, India

I. Mondal (✉)
Department of Mining Engineering, Indian Institute of Engineering Science and Technology, Shibpur, India

Introduction

In the twenty-first century, humankind must focus on the socio-economic, advancement, and environmental problems that are occurring at the global scale (Kumar et al. 2009, 2017). The main worldwide environmental concerns are related to climate change. The threat of Global Warming is one of the most important issues challenging the planet (Kumar et al. 2009). The melting of ice mass and glaciers worldwide are the most well-known displays of a climate change. In previous decades, alteration in local weather conditions and climate have highly influenced the world's glaciers in cooperation with shape and features, reflected in the form of development or retreat of glacial snouts (Climate Change 2020). The alteration in the length, width, and area of the glaciers are the most prominent signs of global warming, and these alterations are the primary reasons glacial observations have been used for climate system monitoring for a long time, especially in the places where time series details on climate (mainly precipitation and temperature) is hard to obtain and where the signals of climate change remain unclear. The unusual rates of the glacial melting could have a major effect on the hydrology of the related water bodies and the people who rely on these water bodies and their ecosystems.

Scientifically, climate change is an alteration in the numerical distribution of weather conditions over the period that ranges from epochs to the millions of centuries (Climate Change 2009). It can be an alteration in the average weather or an alteration in the distribution of the weather conditions happening everywhere as usual. In recent years, especially in the context of environment systems, climate alterations are occurring to contemporary climate. It could be labeled as an anthropogenic climate phenomenon alteration, mostly known as "anthropogenic global warming" or "global warming."

Glacier as Thermometer of Climate Change

Nature's best thermometer, and perhaps most sensitive and unambiguous indicator of climate change, is ice. When ice becomes sufficiently warm, ice melts. Some glaciers, ice caps, and an ice shelf have disappeared altogether in this century. A glacier is a moving mass of ice that survives year to year, formed by compacting of snow into ice and set in motion by the gravitational force and the pressure of its assembled pile. Glaciers are generally found in high altitudes and latitudes (Polar Regions and Himalaya). Glaciers are subsequently vulnerable to the temperature variation that can accompany slight climate change and their regular monitoring may help understand the climate change. Late in the twentieth century, with a few anomalies, glaciers around the world were reported retreating at unprecedented rates.

Glacial Fluctuation in Himalaya

Himalaya is the earliest and one of the most fragile mountain structures in the world, originated their terms of a Sanskrit expression that means 'abode of snow'. The Himalayan mountain range extends approximately 2400 km in the direction of east-west in a curved figure laterally as the border of the northern side of India and it covers an area of approximately 500,000 km^2. The Himalayan Glaciers play a major role in upholding Asian ecosystem constancy because they act as barriers and regulate the excess water source from the high mountains zone into the plains throughout both dry and wet spells (Pandey et al. 2018). Here, the greater Himalayan glaciers account for approximately 70% of the globes non-polar glaciers and they affect the lives of people in many countries, i.e., India, China, Afghanistan, Pakistan, Bangladesh, and Nepal. The runoff of water bodies feeds two of the ancient rivers in the world, the Ganges and Indus, whose tributaries transport valuable water resources for the approximately 500 million people in the northeastern Indian regions. Many of the Himalayan glaciers are in the summer-accumulation category that has a major accumulation and ablation occurring concurrently during the summer time. The greater Himalayas contain approximately 33,000 km^2 of glaciered area (Kaul 1999; Dyurgerov and Meier 2004; Singh et al. 2010) and the source glaciers area in 10 of the major rivers in Asian sub-continent. Approximately 9575 large and small glaciers are in the greater Himalayas (Singh et al. 2009), standing as the biggest reserves of accessible water resource in the form of snow and ice outside of the Polar Regions (GSI 1999). Global warming has caused the snow line in the greater Himalayas to shift upward, signifying growth in the divergence area of the glaciers. Before the Tropic of Cancer regions, the greater Himalayan glaciers have received more warmth than the Arctic and moderate temperature mountain glaciers, and therefore they are very sensitive to the increasing temperature or climate change both at regional and worldwide levels. However, studies reveal that this change is more likely due to anthropogenic factors such as industrialization, green house effects, etc. The GSI records of the Himalayan glaciers show that the Bhagirathi catchment has the largest glaciated area of approximately 755 km^2 containing as many as 238 glaciers, including the Gangotri Glacier (26–30 km) (GSI 1999). The Himalayan glaciers have overall retreated as of 1850 and the recent literature review confirms that, for several, the average percentage of the retreat is accelerating. Jangpangi and Vohra (1962), Kurien and Munshi (1972), Srikanta and Pandhi (1972), Vohra (1981), and many other authors have done important studies on glacier snout oscillation of the greater Himalayan glaciers. However, this rate appears to have increased dramatically in the past three eras. Owen and Sharma, in 1998, studied the longitudinal profiles made by the river stretching in 1971 and 1996, and the Gangotri Glacier was shown to have retreated by approximately 850 m (Fig. 5.1). After 1971, average retreat rate was shown as 34 m every year. Between 1935 and 1996 of (61 years), time-series data of GSI has shown that the average retreat rate is approximately 28 m/year, and it indicates a clear rise in the rate since 1971 (Table 5.1) (GSI 1999).

Fig. 5.1 Retreat of Gangotri Glacier (1780–2001 Courtesy – Jeff Kargil, USGS)

Origin of the Problem

Almost a century ago, fears started to be revealed about the possible effect of the increase in atmospheric high temperature on the mountain glaciers. The uncertainties lead to the beginning of joint scientific attempts to recognize and inspect the variations along the front-snout of glaciers. The snow-pack divergence is highly vulnerable to the climatic differences. A rise in atmospheric temperature can intensify energy interchange among the atmosphere and with the snow-pack, and it could increase snow melting. Inspection suggested the climate sequence of a period, during the earlier ten million years or so, during that period, the world had alternative

Table 5.1 Recession of some glaciers in Uttarakhand

Glacier	Period of observation	Years retreat	Retreat (in meters)	Average (m/year)	Source
Milam	1848–1996	148	2472	16.70	Vohra (1981)
Pindari	1845–1966	121	2840	23.47	Strachey (1847) and Vohra (1981)
Gangotri	1935–1996	61	1147	18.80	Vohra (1981)
	1996–1999	3.5	76	22.24	Naithani et al. (2001)
Shanklup	1881–1957	76	518	6.82	Vohra (1981)
Poting	1906–1957	51	262	5.14	Vohra (1981)
Dunagiri	1992–1997	05	15	3.00	Swaroop et al. (1999)
Burphu	1966–1997	31	150	4.84	Srivastava and Swaroop (1996) and Srivastava (2001)
Chorabari	1992–1999	05	55	11	Swaroop et al. (1999)
Bhrigupanth	1962–1995	33	550	16.67	Srivastava and Swaroop (1996) and Srivastava (2001)
Tipra Bank	1960–1987	27	100	3.70	Vohra (1981)
Dokriani	1962–1991	29	480	16.5	Dobhal et al. (2008) and Dobhal and Mehta (2010)
	1991–2000	09	164	18.2	
Meru	1997–2008	32	395	17.17	Naithani et al. (2001)

rotations of cold and warm times. The global mean temperature variance in previous glacial extremes and the current warm days is approximately 5 °C. However, the rate of steady change is perhaps because of the rapid transformation in the twentieth century to industrialization. The large discharge of CO_2, aerosols, and other traces of gases have changed the atmosphere composition. This is transforming the worldwide radiation budget in the earth and atmosphere system. Inspection carried out through the Intergovernmental Panel on Climate Change (IPCC) has inferred that the average temperature of piles of the earth has increased by 0.6 ± 0.2 °C in the twentieth century (IPCC 1996). Earth's temperature can increase by 1.4–5.8 °C by the end of the century (Kulkarni et al. 2002, 2005; Kulkarni and Alex 2003). This rate of warming is predicted as much higher than what was observed during the twentieth century. Obviously, this will have an intense effect on snow amassing and divergence rate in the greater Himalaya, as glaciers and snow are vulnerable to change in the worldwide climate.

This temperature increase will continue in the present scenario (twenty-first century) and the average surface temperature of the earth will continuously transform the glaciers of the world, and changes have been recorded in glaciers in the Kumaon and Garhwal Himalayas along with the other portions of this greater Himalayan range (Kulkarni et al. 2002, 2005; Kulkarni and Alex 2003). Because Himalaya is a complex tectonic belt, glaciers and related landforms in the area are mostly situated in the remote regions, where access is generally tough and difficult and it takes several days to reach the area. This increases the difficultly of gathering data when regular and repetitive observations are required.

Remote sensing and GIS are best the techniques for data accessibility and proper spatial and temporal resolution, offering worldwide coverage and lower financial costs allowing for faster users, semi-automated, and cost-effective estimations of changes in the glacier parameters over the large regions. These methods allow for consistent observation of the properties of remotely situated glaciers, i.e., ice extent, terminus location, volume, and the surface elevation, from those glaciers in mass balance could also be inferred. These methods are mainly useful in remote areas with limited glaciological in situ measurements. The Pindar Basin in Kumaun Himalaya is comparatively less studied from the glacio-geomorphological point of view.

Finally, the main objectives are to attempt the study of glacial fluctuations using Landsat and Sentinel-2 Imageries, to understand landform evolution & style of deglaciation, and to determine limitations and challenges to the remote sensing application of glaciers mapping. Furthermore, an effort was made to study in the visible range to the infrared region using remote sensing datasets to estimate the glacier parameters, highlighting changes in the terminus position (lat-long and elevation) and area and to study how the DEM can be combined with satellite images to analyze the landform evolution. Second, a review of the present limitations and upcoming challenges for remote sensing application for mapping and modeling in various characteristics of the mountain glaciers has been discussed, exactly in the framework of the greater Himalaya.

Study Area

The Pindar Basin is a closed valley basin, situated at higher ranges of Kumaun Himalaya and comparatively less studied from a climate change point of view. The river basin consists of the five major glaciers, namely Pindari, Kafni, Bidalgwar, Mrigthuni, and Buriagal. Studies show that they have retreated rapidly during the past century (Jangpangi and Vohra 1962). These Glaciers are difficult to access as they are located in the upper most area of the basin, originating from Nanda Kot (5269 m), Nanda Khat (6545 m), Baljuri (5922 m), Changuch (6322 m), Panwali Doar (6663 m) peaks, and Nanda Bhanar Range, and are very difficult to track for regular observation. Owing to the remoteness of the, only a few studies have been done. The current trend of the surrounding basins shows that a majority of the glaciers have undergone a reduction in their area at an accelerating rate. The basin is named from the Pindar River that originates from the Pindari Glacier, which is a small valley type transverse glacier. Pindari's total length is approximately 3.231 km (GSI, 1999), and it extends from latitude $30°16'15''–30°19'10''$ N and longitude $79°59'00''–80°01'55''$ E (Fig. 5.2). The glacier arises from the southward neve fields as on the vertical slopes of the Nandakhat-Nandakot ridge at an altitude of approximately 5720 m. The stream emerging at the glacial portal is known as Pindar and has its confluence with the Alaknanda River at Karnprayag. The Pindari glaciated valley formed by linking into the ridges and peaks consisting of Nanda Khat
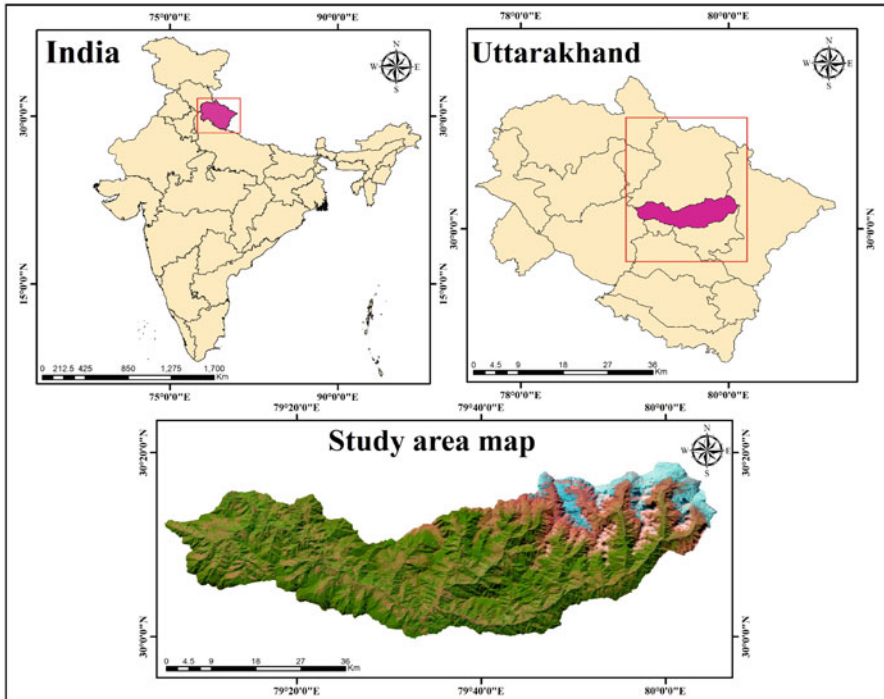
Fig. 5.2 Location map of the study area

(6545 m), Chhanguj peak (6322 m), Baljuri (5922 m), Panwali Doar (6663 m), and Pindari Kanda (Traill Pass: −5700 m).

Climate characteristics of the Pinder region include a long cold winter extending from October to March, during which considerable precipitation often occurs as snowfall, in association with western disturbances passing eastward across north India. The Himalaya region slopes are situated on the southern side, and receive most of their rainfall from the monsoon current, which penetrates the valley from June to September. The temperature in the winter season is below the freezing point, whereas the maximum temperature in summers is approximately 30 °C. Mostly overcast conditions exist during the monsoon months and for short spells when the region is affected by western disturbances; otherwise, it is generally clear with medium or high clouds (Figs. 5.3, 5.4, 5.5, and 5.6).

The north and southern ranges of the Kafni Glacier originate from the southern slope of Nanda Kot – top peak in the ranges. The Kafni Glacier is the main source of the stream that originates from the ice cavern it formed at the snout. This stream is a tributary of the Pindar River, meets near the tourist point Dwali, and then flows into the Alaknanda river system (Fig. 5.6). The Kafni Glacier formed from the two tributary glaciers that are no longer linked with the main stem. Now they exist in the form of the
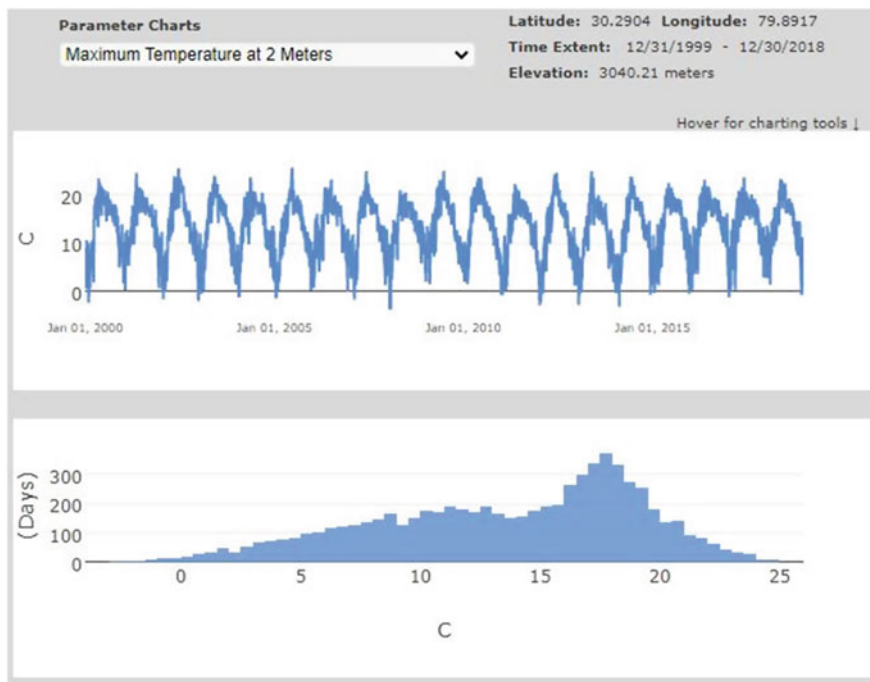
Fig. 5.3 Maximum temperature of the study area

hanging glaciers and its contribution to the riverine flow are through their melting. The drainage has been analyzed with the help of topographic sheets and Landsat imageries of the area. It is noticed that the drainage system is directly controlled by the lithology and structural configurations of the area. The characteristics of the drainage pattern are mostly dendritic and at places controlled by major fault zones.

Application of Remote Sensing and GIS in Glacier Study

Glaciers are usually situated in a remote area, where access is difficult and the topography takes several days to include the entire area. Therefore, it is very difficult to monitor the glaciers on a consistent basis, and in situ measurements are sometimes impossible. The field inventories and analysis of the glaciers used in conventional methods require extensive time and resources to obtain an accurate ground survey. Glacial geomorphologists, glaciologists, and the remote glaciers rely on the multi-spectral remotely sensed images to obtain the information about the glacier physical characteristics. The downstream monitoring and inventories of the glaciers could be done first and exactly using the multispectral satellite images and aerial photographs. Using all supplementary satellite images for the estimation of physical conditions in
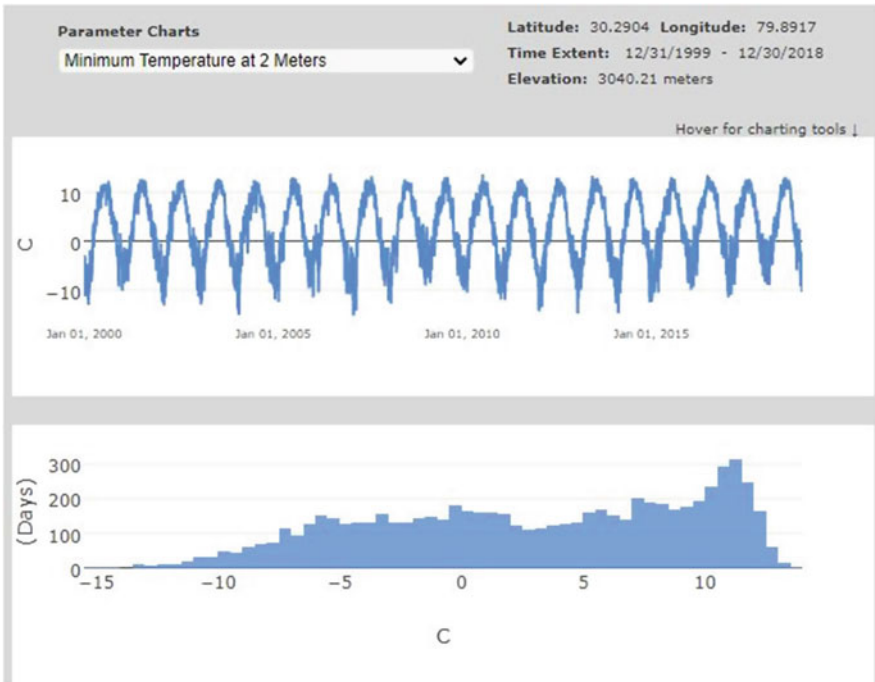
Fig. 5.4 Minimum temperature of the study area
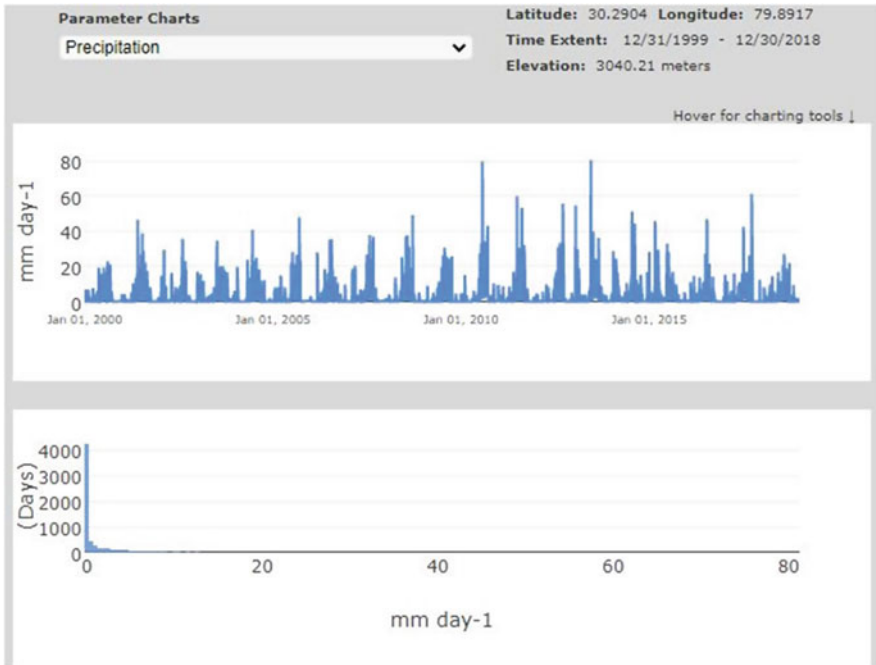
Fig. 5.5 Rainfall graph of the study area
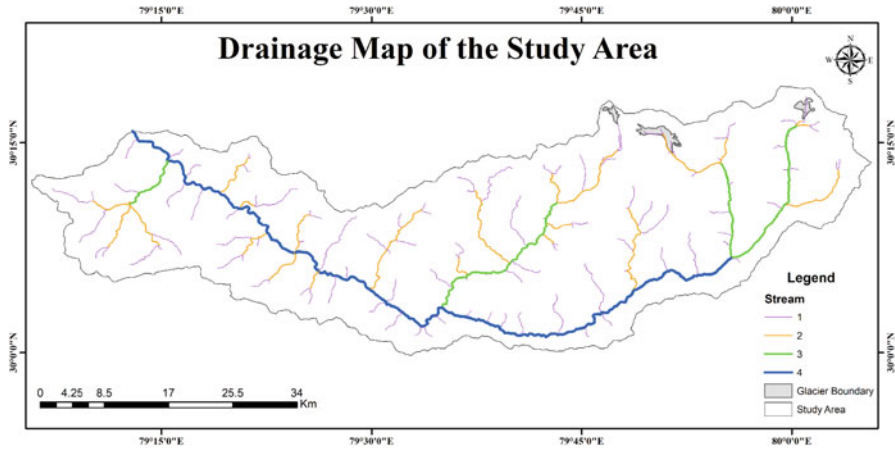
Fig. 5.6 Drainage map of Pindar Basin

the present study area has provided better accuracy. The multi-platform method has been used in remote sensing spectral data and in situ measurement to increase its ability and give better accuracy to the research work. The visual interpretation and digital image processing techniques integrated with the GIS platform are very useful for glacier studies.

A number of airborne and space-borne sensors have provided useful information for the glacial studies. A high-quality sensor is required for the spatial (in 2D and 3D), multi-temporal, and spectral reflectance information. The spatial resolution of detecting in the multi-sensor refers to the distance among the adjacent objects that could be determined and is assumed in components of length (i.e., meters). Normally, airborne sensors have a better resolution at the expense of a widespread image swath; however, the satellite-acquired imageries are inclined to provide a wider overview, but its information is less. The moderate (10–100 m) spatial resolution provided by the Sentinel (10 m), Landsat TM sensor (25 m), Landsat ETM+ (15 m), and SPOT HRV and HRVIR (10 m Pan, 20 m multispectral sensor) is normally used to monitor regional changes of the glacial level. The exquisite spatial resolution has to be provided through airborne multi-sensors or high-resolution multi-satellite sensors such as IKONOS, which are more suitable for comprehensive mapping of the glacier surfaces information and to sense the inconsistency in reflectance of characteristics over the glacier terminus. Most of the satellites orbit toward the earth, and their number has increased intensely in recent years and various commercially available imageries presently exist. All these images are used in different sensors, i.e., Landsat TM, ETM, ETM+, ESA-Sentinel-1, IKONOS, SPOT, ASTER, MODIS, and NOAA AVHRR scenes. All those satellites generate inventories of the mapping of sea ice, ice shelves, and glacier studies (Kumar et al. 2020). These

images are used to distinguish among the snow and ice for identification and accumulation of the ablation areas, assessing mass balance and the snowmelt runoff for glacier patterns and surface morphometric condition, glacier velocities, and for the distribution of the landforms structures and sediments.

For any glacial inventory, the basic materials that have been used in the collation of the database of the glaciers and glacial lakes are based on the topographic maps published by the Survey of India during the period from the 1950s to 1970s, but the current glacial fluctuations can be very well depicted on digital satellite image data sets. For this, the image data of Landsat and Sentinel series are widely used nowadays.

We know that snow and ice are the frozen state of the surface water bodies. Preliminary work with the satellite data has shown that mapping of snow and ice-capped areas should be carefully done as the comparison in spectral response among the clouds and snow cover due to limitations in the obtainable dataset. In the case of Kumaun and other glaciated regions of Himalaya, most of the ablation zones are debris-covered and the spectral signature of those areas has similar properties with the surrounding bedrock and loose deposits. Furthermore, improvement in spectral resolution in satellite data provides more spectral bands in the Sentinel-2 and Landsat series. Therefore, it has become easier to differentiate snow and cloud in the middle infrared (MIR) region of the spectrum, it particularly ranges in 1.55–1.75 μm (band 5) and 2.10–2.35 μm (band 7) wavelength in Landsat ETM+ sensor). The ranges of wavelengths, the cloud cover have much more reflectance and appear white on the satellite image, whereas the snow cover reflectance is very low and it appears in black color. In visible wavelength, near the infrared, and the thermal infrared region bands, with spectral unmixing between the snow and cloud covers, is not probable, whereas it is in the middle infrared.

The snow cover reflectance is generally too high in the visible ranges and it declines all over the reflective the infrared regions of the spectrum. The old snow and ice cover reflectance is always lower than that of fresh snow cover and also clean glacier in the visible range and reflective infrared regions of the color spectrum. To compare in clean snow and glacier, debris-covered of the glacier and its very old snow cover have much lower reflectance in the visible ranges of the color spectrum and higher in middle infrared regions of the spectrum. To classify the physical conditions of the distinct glaciers, dissimilar digital image processing techniques are very useful. However, it is complemented through the visual interpretation technique, with the proper knowledge and experience of the topography conditions. In false color composite (FCC), with different spectral bands, reflectance is highlighted in different landscape features using the information of visual image interpretation keys, i.e., image color, texture, pattern, shape, tone, association, and shadow. To composite of spectral ranges of the satellite images and tones in the separate band consequence of the reflectance DN values, the glaciers study appears white in separate bands in white to light blue scatter in color composite with the

variable sizes of regular and linear pattern shape shown in fine to medium texture, respectively; however, the thermal bands appear likely grey to black. The separate pattern associated with dendritic and linear with the slopes and valley bottoms of the high mountains region covered with diurnal snow can be illustrious in glaciers of the study area.

The digital image processing technique is used to analyze the image enhancement and spectral range wise classification of the land features and, therefore, it importantly helps in the present study of glacier mapping and retreat rate information. These techniques' regularly monitoring of the glaciers and lakes could be used for visual interpretation as well as the digital process. In both techniques, proper analysis and adequate in situ data investigation knowledge are very essential. Currently, the glaciers study data modeling, mapping, identification, and monitoring is done with the help of GIS remote sensing integrating these latest techniques. The digital elevation model (DEM) has been generated in the study area (Fig. 5.7), using the aerial photographs, stereo pair satellite images, and digitization of the topographic map, and it could play a big role in crucial rules for discrimination of land surface features as well as LULC maps in the GIS platform and for the better perspective of observing and presentation purposes. In the study area, DEM is used to create in different data sets, i.e., elevation, contour, slope, aspect, etc. For example, glacial lakes are covered by snow, the surfaces lake is flat, and snow, glaciers, and ice cover stretch roughly slope angle. However, in GIS integrated analysis decision rules could be assigned that, if the slope is not consequently prominent, then this area is documented as frozen glacial lakes. Here, DEM must be consistent with reliable quality features when it is likened with the other satellite data sets. The ortho-rectify photos or satellite images can be swathed over the DEM for explanation or presentation.
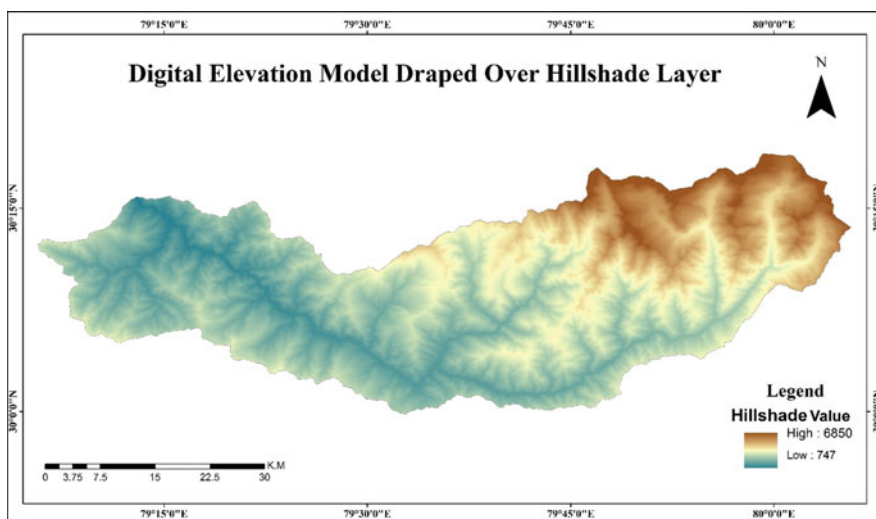
Fig. 5.7 Digital elevation model draped over hillshade layer. (Source – ASTER DEM)

Materials and Methods

Nowadays, researchers and scientists conducting glaciological studies are concentrating on observing changes of the glacier using remote sensing and GIS techniques in the mountain regions facing rapid changes to glaciers. The Himalayan glaciers monitoring is usually challenging using conventional techniques due to rocky terrain and its inaccessibility. Therefore, in situ measurement reports have been inadequate at the selected Himalayan glaciers. It could not provide a comprehensive and demonstrative scenario of the glacial monitoring retreat rate. The present study is carried out using time series data from a number of Landsat series of satellites, i.e., Multi-Spectral Scanner (MSS), Thematic Mapper (TM), Enhanced Thematic Mapper (ETM+), Sentinel 2A. Specifications of all datasets used are given in Table 5.2.

The previous and ancient information about the glacial extent is accessible on the US Army Map Series topographic maps due to the unavailability of Survey of India topo-sheets as the study area is highly classified as restricted. The topographic maps are based on a compilation of various topographic maps and vertical aerial photographs at different scales. Mapping of glacial extent is carried out using all Landsat images and the date of data acquisition is given in Table 5.2.

Glacier boundary is generated using toposheet map and digitized using GIS software. Glacier boundary is mapped using Satellite imagery (Standard FCC). The differences between the glacial and non-glacial extents were identified using the image enhancement technique. Snout positions of all three glaciers are marked through visual image interpretation and by comparing the absolute portion of snouts with the different geomorphologic features, i.e., moraines, its origin streams from the snouts and DEM (Figs. 5.7 and 5.8).

Glacier retreat is measured along the centerline. Repeated observations have provided the amount of glacier retreat during the 24 years. That will be a very important period toward providing an independent validation with the remote sensing and GIS-based methodology.

Results and Discussion

The Quaternary Time is popularly known for its repeated climatic changes. One of the most important characteristic of the Quaternary period is the periodic glacier activity during cold periods that have produced a rich track record of the glacial landforms. Therefore, by studying the glacier landforms, it is possible to rebuild, in considerable facts, the conditions of environment and actions responsible for making

Table 5.2 Satellite images and data acquisition date

S. No.	Satellite	Path	Row	Date
1.	Landsat – ETM	145	039	04-12-2000
2.	Landsat – ETM+	145	039	30-11-2010
3.	Sentinel 2A	T44RLU		24-10-2018
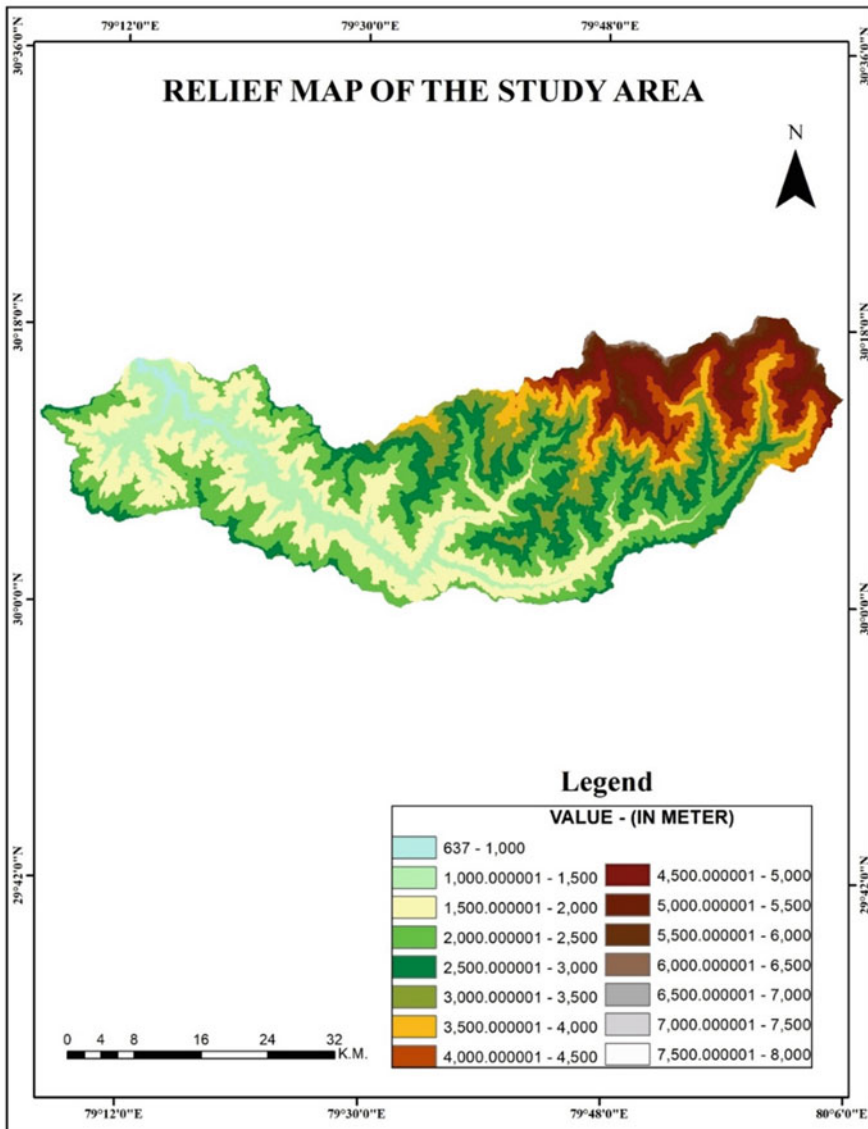
Fig. 5.8 Slope map in degree (0) derived from DEM. (Source – ASTER DEM)

the glacial topography. Such re-establishments are reasonable and also hold well, if the condition is ideal and no other activity affects and alters the landforms. However, many activities affect the existing landscape and change it. Rock falls, floods, debris flow, rock slides, mass movement, and small channels coming out from the tributary glaciers are significant processes that are not directly connected to the glacial activities but take place in a glaciated terrain and play a major role in affecting the

glacial activities. These activities are assembled together under a new title, paraglacial processes, which are the non-glacial processes in the glacial region.

The earliest glaciological studies in India date back to 1847, when Col. Strachey (1847) described the Pindari and Kafni Glaciers. His studies, though not very systematic, were remarkable at that time. The geological survey of India (GSI) took up systematic surveys of some of the glaciers in the Himalayas in 1906 (GSI 1999). The Pindari Glacier first plane table map was prepared by G. de P. Cotter in July (1906).

Pindari Glacier is a Cirque type transverse glacier that originates from Nandakhat Peaks and the present snout is marked at 4188 m elevation. The level stream of the glacier, beyond the tip of the median morain, steepens abruptly toward the Pindari–Kanda trail pass. The glacier has been actually located in the Survey of India topo-sheet maps (1:250,000) *62B* (SW part). The major accumulation area emerges from the névé field on the slopes of the Nandakhat–Nandakot ridge. A prominent medial moraine separates the two snow-melt streams (Fig. 5.4).

Janpangi (1962) reported two ice caves separated by the medial moraine. In comparison to the Kafni Glacier, the whole ablation surface is covered with a thin mantle of dust and debris, whereas the Kafni Glacier hosts high debris cover at the ablation zones.

The Kafni Glacier is another important glacier in the Pindar Basin and the existing snout location of that glacier lies at $30°13'12''$ N and $80°03'14''$ E. The Kafni Glacier extends from north to south and it originates from the southern slope of the Nanda Kot–it is a top peak in this region. It is the main source of the river Kafni and originates from the ice cave, and is formed at the snout, which is one of the glaciers. These rivers are the main tributaries of the River Pindar, which flows toward the Alaknanda river system.

The Kafni Glacier lies in the two tributary glaciers that have not been extended and it is attached to the main trunk. Now they exist to form the hanging glaciers and its subsidies as the river flows through their melt water.

Both the Pindari and Kafni valleys are U-shaped beyond Phurkiya and Baialigair, respectively (Figs. 5.9, 5.10, and 5.11). The downstream of Phurkiya is as far as Dwali, the Pindari valley is wide. The narrow gorge below Dwali (the confluence of the Pindari and Kafni rivers) is cut by the later river erosion, although the glacier had possibly moved downstream as far as Dwali during the late Pleistocene time. In the Pindar valley, the left moraine is wide and open though the right lateral moraine is imperfectly developed. Both lateral moraines have freshly exposed inner faces. Approximately two-thirds of the southern-upper portion of the left lateral moraine is grass covered, and the rest is freshly exposed.

It can be seen in the satellite imageries that the Sunderdunga Glacier is now almost resting on the southern slopes of Mactuli Peak though it can be evident by the lateral moraines that it used to be a moderate length glacier. In the current study, we attempt to map mainly three glaciers.

All the glacier boundaries including tributary glaciers are mapped using Landsat MSS, TM, ETM, and Sentinel satellite imageries. It is clearly evident that the warming of the surrounding environment has forced major changes on the glacial
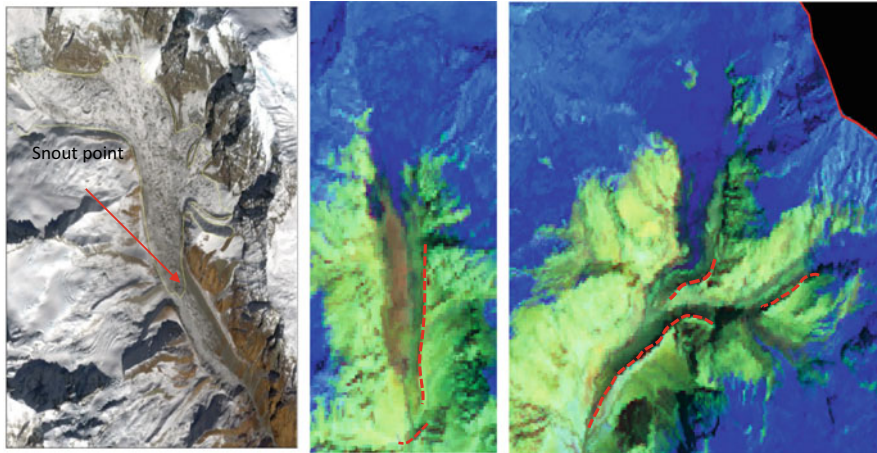
Fig. 5.9 Medial, Lateral and Terminal Moraines, Kafni & Pindari Glaciers
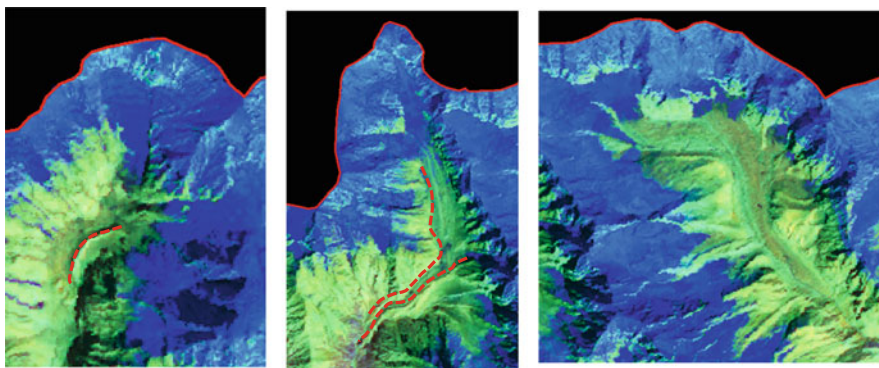
Fig. 5.10 Moraine distribution in Sunderdunga, Mrigtuni and Bidalgwar Valleys

set-up in parts of the Pinder Basin. Figure 5.12 shows that one of the major changes is seen in terms of "de-coupling" of the main trunk and tributary glaciers. The glaciers showing the same color are the detached parts of the major glacier system.

It is apparent from the data analysis that the average retreat rate of the Pindar Glacier was higher at 38.19 m/year from 2000–2010 but reduced to 55.41 m/year during 2010–2018. The average retreat increased to 45.84 m/year between 2000 and 2018. Annual observations show that the Mrigthuni snout retreated by 32.84 m/year from 2000 to 2010 and it is shown to have a reducing trend rate of 50.90 m/year between 2010–2018, and it increased the average retreat rate of 40.87 m/year between 2000 and 2018. A similar decrease was seen in Bidalgwar's yearly observed snout retreated of 27.89 m/year between 2000 and 2010 and it continues to show a reducing trend, which is low corresponding to another glacier–39.33 m/year in 2010–2018. The average retreat increased 32.97 m/year (Fig. 5.12; Table 5.3).
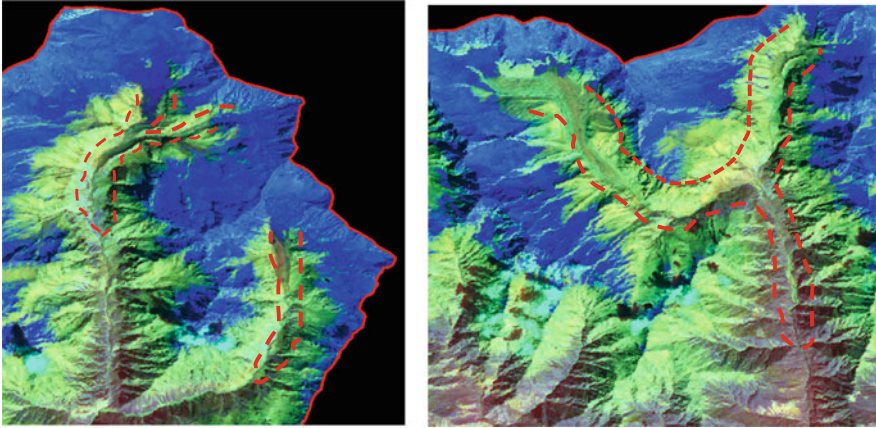
Fig. 5.11 U-shaped valleys in parts of Pinder Basin

Conclusion

In the study, we have made an attempt to present our understanding of the current changes in the Himalayan glaciers based on scientific evidence and analysis of observed data from different glaciers in the Pinder Basin. The climate change science is compounded, as it is not only about variations in temperature but also the effect of the local environmental issues; non-climate stressors play a correspondingly vital role.

The observations indicate that the glaciers' retreating rates are faster in this part of the Himalaya, and they are not only losing more glaciated parts but also in their tributary glaciers— a trend that has been perceived over the Himalaya for many others smaller glaciers.

Though glacial retreat is a natural phenomenon with the earth moving toward a warming phase, the accelerated rate of retreat forces us to think of the other factors having an impact on it at present. Based on our study and past scientific data, it is clear that climate change has a perceptible impact on the status and condition of some of the studied glaciers as is evident through the increase in the net loss of the mass year after year. It is worthwhile to note that the phenomenon of global warming and climate change will impact not only temperature but also other variables such as intensity and quantity of precipitation, cloud cover, wind, and radiation. These variables will respond in complex mode through their impacts on glacier fluctuations. Here, different glaciers in the same climatological system respond to different climatic alterations. Hence, to forecast the glacier retreat rate or present scenarios with confidence becomes very difficult.

The current observations in parts of the Pinder Basin strengthen the present observations particularly providing the image interpretation. Timely monitoring of the area may further help in precise assessments of the water flows and glacial melt
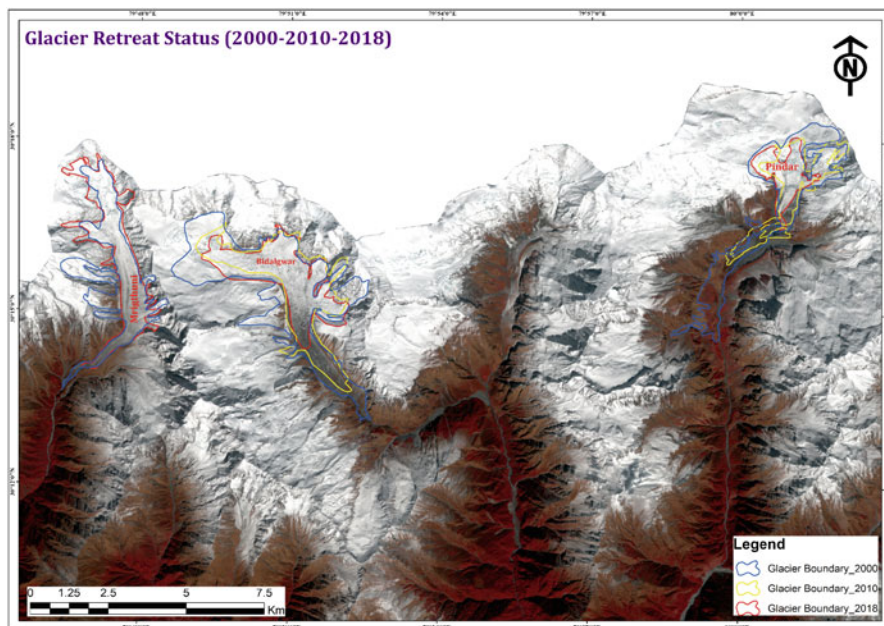
Fig. 5.12 Decoupling of main trunk and tributary glaciers

Table 5.3 Retreat of different glaciers in the Pindar Basin

Name of The glacier	Period of observation		Total retreat (in meter)	Average (m/year)	Speed of the glacier per year
	2000–2010	2010–2018			
Mrigthuni	328.42	407.27	735.69 m	40.87	41 meter approx.
Bidalgwar	278.93	314.68	593.61	32.97	33 meter approx.
Pindar	381.91	443.32	825.23	45.84	46 meter approx.

based on long-term data. Better use of these technologies could provide an efficient and scientifically sound method to study different patterns and changes in the glacier systems on various spatial and temporal scales.

References

Climate Change (2009) https://climatechange-jimmy.blogspot.com/
Climate Change and Himalayan Glaciers (2020) https://www.geographynotes.com/term-paper/himalayan-glaciers/climate-change-and-himalayan-glaciers-term-paper-geography/4501
Cotter G d P (1906) Notes on certain glaciers in Kumaon: rec. GeolSurv Ind 35(pt. 4):148–152

Dobhal DP, Mehta M (2010) Surface morphology, elevation changes and terminus retreat of Dokriani glacier, Garhwal Himalaya: implication of climate change. Himal Geol 31(1):71–78, Printed in India

Dobhal DP, Gergan JT, Thayyen RJ (2008) Mass balance studies of the Dokriani glacier from 1992 to 2000, Garhwal Himalaya, India. Bulletin of glaciological research. Jpn Soc Snow Ice 25:9–17

Dyurgerov M, Meier MF (2004) Glaciers and the study of climate and sea-level change. In: Bamber JL, Payne AJ (eds) Mass balance of the cryosphere: observations and modelling of contemporary and future changes. Cambridge University Press, Cambridge, pp 579–622

Geological Survey of India (1999) Inventory of the Himalayan Glaciers: A Contribution to the International Hydrological Programme, Special Publication No. 34, edited by M.K. Kaul

IPCC (1996) Climate Change 1995. The Science of Climate Change. Contribution of Working Group I to the Second Assessment Report of the Intergovernmental Panel on Climate Change. Cambridge University Press, Cambridge, United Kingdom and New York, NY, USA, 584 pp

Jangpangi BS, Vohra CP (1962) The retreat of the Skunkulpa (Ralam) Glacier in the Central Himalaya, Pithoragarh District, U.P., India, Inst. Assoc. Sci. Hydrol., Publ. No. 58, pp 234–238

Kaul MK (1999) Inventory of the Himalayan glaciers: A contribution to the international hydrological Programme, Spl pub. 34. GSI, Kolkata, p 165

Kulkarni AV, Alex S (2003) Estimation of recent glacial variations in Baspa Basin using remote sensing techniques. J Indian Soc Remote Sens 31:81–90. 13

Kulkarni AV, Mathur P, Rathore BP, Alex S, Thakur N, Kumar M (2002) Effect of global warming on snow ablation pattern in the Himalayas. Curr Sci 83:120–123

Kulkarni AV, Rathore BP, Mahajan S, Mathur P (2005) Alarming retreat of Parbati glacier, Beas basin, Himachal Pradesh. Curr Sci 88:1844–1850. 15

Kumar R, Areendran G, Rao P (2009) Witnessing change: glaciers in the Indian Himalayas. WWF-India & BIT, New Delhi

Kumar R, Rao P, Areendran G (2017) Understanding glacial retreat in the Indian Himalaya: historical trends and field studies from a large glacier, p 17. https://doi.org/10.4018/978-1-5225-1046-8.ch003

Kumar M, Al-Quraishi AMF, Mondal I (2020) Glacier changes monitoring in Bhutan high Himalaya using remote sensing technology. Environ Eng Res 6(1):190255. ISSN: 2005-968X. https://doi.org/10.4491/eer.2019.255

Kurien MN, Munshi MN (1972) A survey of Sonapani Glacier, Lahaul District, Punjab, Geol. Surv. India, Misc., Publ. No. 15. pp 83–88

Naithani AK, Nainwal HC, Sati KK, Prasad C (2001) Geomorphological evidences of retreat of Gangotri glacier and its characteristics. Curr Sci 80:87–94

Pandey A, Sarkar SM, Kumar M, Singh G, Lingwal S, Rawat SJ (2018) Retreat of Pindari glacier and detection of snout position using remote sensing technology. Remote Sens Appl Soc Environ 11(2018):64–69. https://doi.org/10.1016/j.rsase.2018.04.011

Singh P, Polglase L, Wilson D (2009) Role of snow and glacier melt runoff modeling in Hydropower projects in the Himalayan Region. In: (WEES-2009), International conference on water, environment, energy and society. New Delhi, 12–16 January 2009. Hydrologic and Hydraulic Modelling, 1, pp 366–371

Singh RD, Kumar R, Manohar A (2010) Snow/Glacier melt contribution to run-off in the Himalayan Rivers – Assessment of potential impact of climate change. National Convention of Global India Scientists and Technocrats. https://www.researchgate.net/publication/267271818

Srikanta SV, Pandhi RN (1972) Recession of the Bada Shigri Glacier. Geol. Surv. India, Misc., Publ. No. 15, pp 97–100

Srivastava D (2001) Glaciology of Indian Himalaya: A bilingual contribution in 150 year of geological survey of India, Special publication no. 63. Geological Survey of India, Kolkata, p 215

Srivastava D, Swaroop S (1996) Fluctuations of Dunagiri glacier, district Chamoli, U.P. Geol Surv India 21(2):153–156

Strachey R (1847) A description of the glaciers of the Pindari, and Kuphinee Rivers in the Kumaon Himalayas. J Asiatic Soc Bengal XVI, pt. 2:203

Swaroop S, Oberoi LK, Srivastava D, Gautam CK (1999) Recent fluctuation in snout front of Dunagiri and Chaurabari glaciers, Dhauliganga and Mandakini – Alaknanda basins, Chamoli district, Uttar Pradesh. In: Symposium on Snow, Ice and Glaciers – A Himalayan Perspective, Lucknow, 9–11 March 1999, 53:77–81

Vohra CP (1981) Himalayan glaciers. In: Lalland JS, Moddie AD (eds) The Himalayan aspect of change. Oxford University Press, New Delhi, pp 138–151

Chapter 6
Fractional Snow Cover Change in the Himalayan Region

Sanjib Mahata and Dibyendu Khalua

Abstract Snow cover fraction or fractional snow cover is the fraction of an area covered with snow for the total area. Today, climate change has become an issue throughout the world that proportionally affects the snow cover. To know about the quantity of water supply, we should study about fractional snow cover. If we study fractional snow cover, we can get huge information about the discharge of water, which may predict the future availability of water resources. We used a MODIS image with seven different bands to show the snow index for the Brahmaputra River catchment area. Based on the snow index, we calculated snow cover area change. This study has evaluated whether there is a signal in the NDSI that could be used to estimate the fraction of snow within a 500 m MODIS pixel and thereby enhance the use of the NDSI approach in monitoring snow cover. Snow is an important component of the cryosphere and an integral part of the global climate system; snow cover both affects and is affected by patterns of climate and climate change. Observation and monitoring of components of the cryosphere are necessary for an understanding of the cryospheric and terrestrial climate system. Predictions state of the environment, in particular the functioning of the climate system, cannot be attempted without a thorough analysis of cryospheric processes. The reason behind choosing the Himalayan belt as our study area is that there are very few papers that described the state-wise change in fractional snow cover on the Himalayan belt. Through the data analysis, we can understand the present as well as the future condition of snow cover of this region. The maximum snow cover for the time between 2001 and 2015 is observed in the eastern part of the Himalayas (Bhutan) and minimum snow cover is observed in the western part of the Himalayas. The same trend is also observed for

S. Mahata (✉)
Vidyasagar University, Seavantan Sikhan Mahavidyalaya, Midnapore, West Bengal, India

D. Khalua
Department of Geography, Vidyasagar University, Seavantan Sikhan Mahavidyalaya, Midnapore, West Bengal, India

the precipitation. It's because both fractional snow cover and precipitation are directly related to each other. This analysis shows that all three zones along with different states respond differently in terms of fractional snow cover and precipitation; however, more detailed investigation is required to support these observations.

Keyword Fractional Snow · Dynamics of Snow Cover · Climate Change · Geostatistics · Remote Sensing

Introduction

There are lots of geographers who have already calculated the snow cover fraction or the fractional snow cover change for the Himalayan ranges and its surroundings. In a research paper titled "Change in Snow Cover of Brahmaputra River Basin and Its Temperature Sensitivity" a Moderate Resolution Imaging Spectroradiometer (MODIS) image was used with seven different bands to show snow index for the Brahmaputra River catchment area (Swapnali and Bhattacharjya 2015). Based on the snow index, they calculated snow cover area change. Another group of geographers calculated snow cover and snow line altitude variation in the Alaknanda Basin, Uttarakhand, and Central Himalayas with the help of Moderate Resolution Imaging Spectroradiometer (MODIS) data for 12 years from 2000 to 2012 (Vivek and Asha 2015). They used multitemporal Landsat image with STRM data to estimate average snowline altitude, and they have also used shortwave infrared spectrum to estimate cloud from snow (dark). Mountainous areas exhibit a larger spatial variation in climate due to sharp differences in altitude, even over a small horizontal distance (McElory and Wilkinson 2005; Immerzeel et al. 2013). There are lots of techniques used for our research paper, and all of these are statistical techniques (Swapnali and Bhattacharjya 2015). Again, remote sensing is a promising alternative for mapping snow cover at higher elevations. The Moderate Resolution Imaging Spectroradiometer (MODIS) snow cover method can be used for mapping snow cover pixels by using Normalized Difference Snow Index (NDSI) and a threshold test (Hall et al. 1995). First, MIRRA and MODIS satellite photos from Giovanni. com, which is maintained by NASA, were taken. The data were collected for fractional snow cover as well as precipitation for 15 consecutive years from 2000 to 2015. After taking all those satellite photos from two different satellites, they were stacked in a single frame with the help of a GIS application. Then with the help of some basic statistical application, we analyzed all those stacked photos (Swapnali and Bhattacharjya 2015). After stacking all those photos in a single frame, they were plotted on Arc MAP 10.3 software above which prepared the shape file which contains India, Nepal, and Bhutan. For the better analysis of fractional snow cover change in the Himalayan belt, the whole Himalayan zone was divided into three different parts, Eastern Himalaya, Western Himalaya, and Central Himalaya.

In the very first step, I have used basic statistics in ArcGIS 10.3 to calculate the mean and standard deviation (SD) for selected states of India, Nepal, and Bhutan. These mean and standard deviations are the mean and standard deviation of fractional snow cover and precipitation. From these data, we concluded district-wise change of fractional snow cover in selected states of India, Nepal, and Bhutan.

In the second case, I used another basic statistical method to explain fractional snow cover change in India, Nepal, and Bhutan. To show this, I have divided the whole data for 15 different years based on selected categories (Mohammad et al. 2017). Mean fractional snow cover is shown through this as it changes from 2001 to 2015. In the third case, I have taken the calculated mean and standard deviation (SD), which is then calculated with the help of ArcGIS 10.3 software. In this portion, I have shown fractional snow cover of the Himalayan region with the help of mean and SD variation. To show this variation fast, I have divided the whole Himalayan belt into three different zones, which are Eastern Himalaya, Western Himalaya, and Central Himalaya.

Then I used previous oriented data of mean and SD from ArcGIS 10.3 software Last but not least, I used general linear regression to show the interrelationship between fractional snow cover and precipitation. The reason behind choosing the Himalayan belt as our study area is that there are very few papers that described the state-wise change in fractional snow cover on the Himalayan belt. Through the data analysis, the study can understand the present as well as the future condition of snow cover of this region. There are many research papers on the Himalayan region, but no one has explained the state-wise change of fraction snow cover on the Himalayan belt. One of the important objectives of our study was to know the present scenario of snow cover in the Himalayan belt and to predict what may happen in the future if climate change is continuing in the future at the same intensity as it happening today. Another objective of our study was to understand the amount of snowmelt discharge that happens due to the melting of snow cover.

Materials and Methods

The Himalayan mountain belt is the highest mountain chain on the Earth. The average elevation for the entire mountain belt is over 5000 meters. The Mount Everest is one of the peaks of the Himalayan Mountains at 8848 meters above sea level. We didn't choose the whole region of the Himalayan belt, and we have chosen the western part of the Himalayas toward the eastern portion up to Bhutan. There are lots of techniques which I have used for my research paper, and all of these are basically statistical techniques. First of all, I have taken MIRRA and MODIS satellite photos from Giovanni.com which is maintained by NASA. I have collected fractional snow cover as well as precipitation data for fifteen consecutive years from

2000 to 2015. Fractional snow cover data for research are collected from satellites on yearly basis from 2000 to 2015 for September. All these data have been collected from the MEERA satellite, and unit for fractional snow cover data is mm/day. Later, we used precipitation data from MODIS to correlate with fractional snow cover. All these precipitation data were taken for 16 consecutive years from 2000 to 2015. After taking all these satellite images from two different satellites, they were stacked in a single frame with the help of GIS application. Then with the help of some basic statistical application, we analyzed all those stacked photos.

After stacking all the photos in a single frame, I plotted them on Arc MAP 10.3 software above which I have plotted the shape file which contains India, Nepal, and Bhutan. For the better analysis of fractional snow cover change in Himalayan belt, I have divided the whole Himalayan zone into three different parts:

- Eastern Himalaya
- Western Himalaya
- Central Himalaya

In the very first step, I have used basis statistics In ArcGIS 10.3 to calculate mean and standard deviation for selected states of India, Nepal, and Bhutan. These mean and standard deviations are the mean and standard deviation of fractional snow cover and precipitation.

Results and Discussions

The maximum snow cover for the time between 2001 and 2015 has been observed in the eastern part of the Himalayas (Bhutan), and minimum fractional snow cover is observed in the western part of the Himalayas. The same trend is also observed for the precipitation. It's because both fractional snow cover and precipitation are directly related to each other. This analysis shows that all three zones along with different states respond differently in terms of fractional snow cover and precipitation. From these data, we came to a conclusion on district-wise change of fractional snow cover in selected states of India, Nepal, and Bhutan. In the second case, I have used another basic statistical method to explain fractional snow cover change in India, Nepal as well as Bhutan. To show this, I have divided data for 15 different years on the basis of selected categories. Mean fractional snow cover is shown through this as it changed from 2001 to 2015. In the third case, I have taken calculated mean and standard deviation, which have been calculated with the help of ArcGIS 10.3 software. In this portion, I have shown fractional snow cover of the Himalayan region with the help of mean and SD variation. To show this variation fast, I have divided the whole Himalayan belt into three different zones as follows:

- Eastern Himalaya
- Western Himalaya
- Central Himalaya

Then, I used previously oriented data of mean and SD from ArcGIS 10.3 software.

Eastern Himalaya

Name	Mean	STD
Bumthang	0.1199	0.0061
Chhukha	0.2326	0.0744
Dagana	0.2502	0.0780
Gasa	0.0726	0.0162
Haa	0.1482	0.0340
Lhuentse	0.1183	0.0064
Monggar	0.1584	0.0173
Paro	0.1027	0.0000
Pemagatshel	0.2189	0.0296
Punakha	0.0960	0.0064
Samdrup Jongkhar	0.1999	0.0253
Samtse	0.3554	0.0000
Sarpang	0.2746	0.0524
Thimphu	0.1047	0.0155
Trashigang	0.1590	0.0139
Trongsa	0.1399	0.0130
Tsirang	0.1950	0.0000
Wangdue Phodrang	0.1215	0.0148
Yangtse	0.1307	0.0000
Zhemgang	0.2037	0.0521

Central Himalaya

Name	Mean	STD
Central	0.1918	0.0351
East	0.1953	0.0355
Far-western	0.1678	0.0408
Mid-western	0.1229	0.0480
West	0.1700	0.0540

Western Himalaya (Tables 6.1 and 6.2; Fig. 6.1)

Table 6.1 Zone-wise fractional snow cover distribution in the Himalayan region

Name	Mean	STD
Himachal Pradesh	0.1270	0.0369
Jammu and Kashmir	0.0715	0.0452
Sikkim	0.2220	0.0392
Uttarakhand	0.1602	0.0196

Table 6.2 Zonal variations of fractional snow cover map (standard deviation)

Zones of Himalaya	Mean	Standard deviation
Western Himalaya	0.0146	0.0374
Central Himalaya	0.0039	0.0163
Eastern Himalaya	0.0035	0.0129
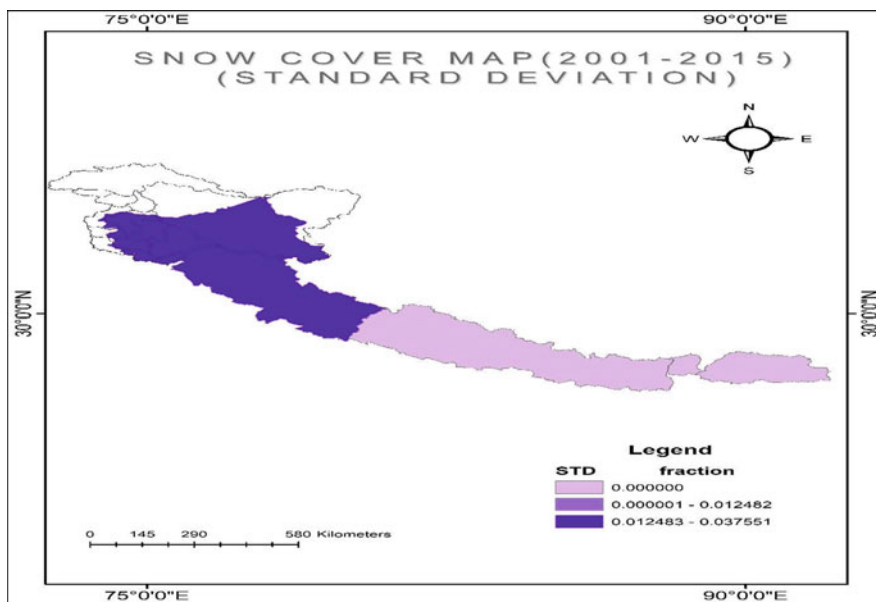
Fig. 6.1 Fractional snow cover map (standard deviation)

Figure 6.2 was prepared to show the fractional snow cover variation of the different regions of the Himalayas (west, middle, and east). As we can see that there is no such region that has a medium range of fractional snow cover, we have divided the whole region into three different parts to show regional variation. We can see that the western part of the Himalayas has a high amount of fractional snow cover (STD). The remaining middle and the eastern Himalayas have a low amount of fractional snow cover.

Figure 6.3 was prepared to show the mean fractional snow cover variation of the different regions of the Himalayas (west, middle, and east). As we can see that there is no such region that has a medium range of fractional snow cover, we have divided the whole region into three different parts to show regional variation. As we can see that western part of the Himalayas has a high amount of fractional snow cover, spatial patterns of snow cover are complicated which are subject to change due to
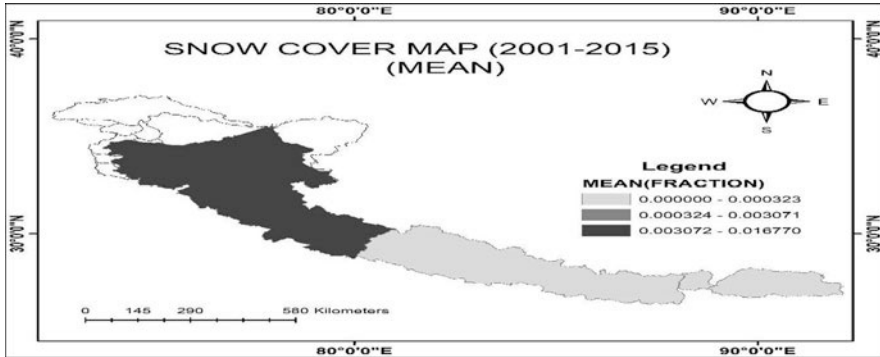
Fig. 6.2 Fractional snow cover map (mean)
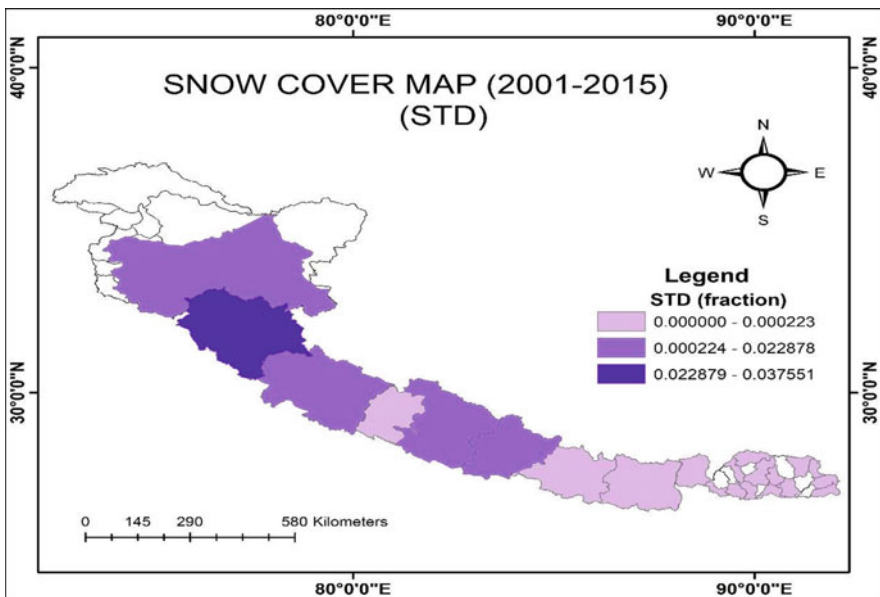
Fig. 6.3 State-wise variations of fractional snow cover map (standard deviation)

interaction between climate and other physical as well as cultural objects. Figure 6.4 represents the snow cover of the Himalayan and its adjacent area. From the west toward the eastern part of the map, the fractional snow cover is significantly changed. The western part of the map has a median range of fractional snow cover (0.000224–0.022878). As it moves toward Himachal Pradesh, it became very high in terms of fractional snow cover change. Due to climatic change Himachal Pradesh is
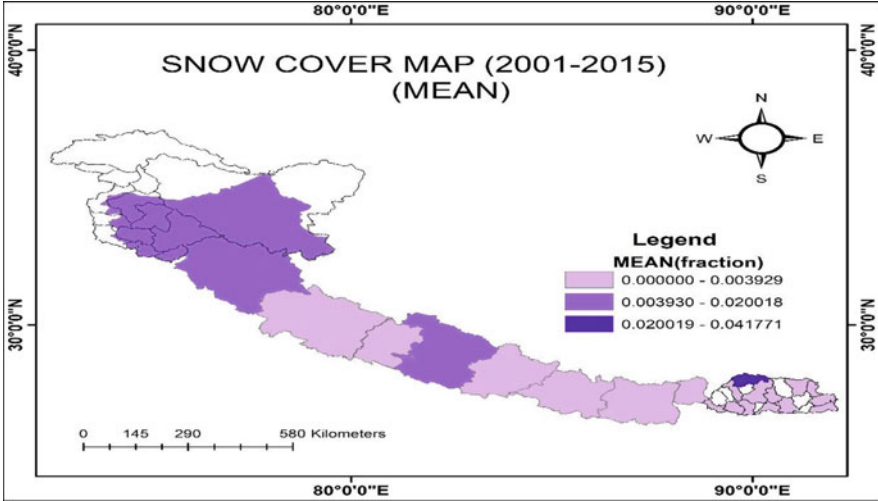
Fig. 6.4 State-wise variations of fractional snow cover map (mean)
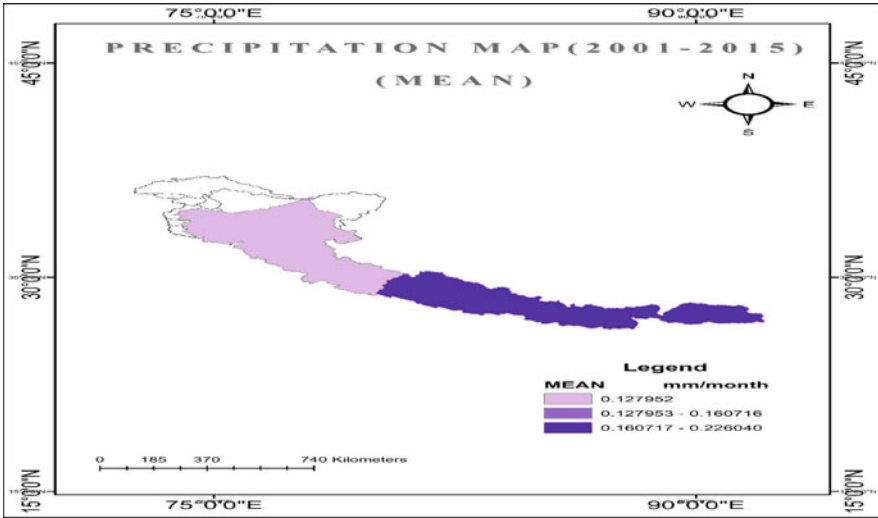
Fig. 6.5 Zonal variations of precipitation from 2001 to 2015 precipitation (mean)

directly affected which the main reason behind the fraction. Further, if we look forward from the western part, we can see that the eastern part of the map has a very low level of fractional snow change which is in between 0 and 0.000223. Figure 6.5 shows the spatial variations of snow cover based on mean fraction for the Himalayan
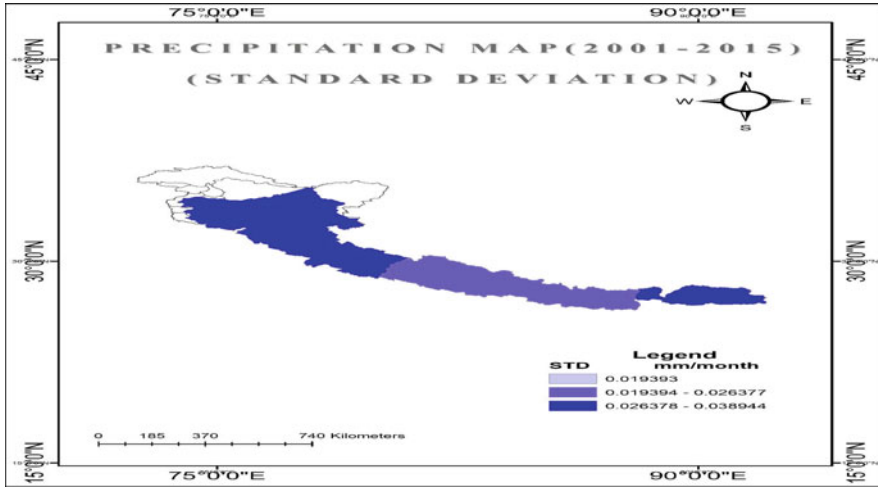
Fig. 6.6 Precipitation map (2001–2015) standard deviation

region. As we move from the west toward the eastern part of the Himalayas, we can see that with the change of area, snow cover is significantly changed. The western part of the Himalayas has a medium range of mean snow cover change that is in between 0.003930 and 0.020018, and except the western part of Nepal, all the area comes under low-range mean fractional snow cover change. The state of Bhutan has the highest amount of fractional snow cover that is between 0.020019 and 0.041771.

Figure 6.6 shows the precipitation variation of the Himalayan region with the help of state-wise mean data, collected from 2000 to 2015 for the specific region.

Three different classes have been made to show the variations. The maximum state of this region belongs to the area having a moderate to low amount of precipitation rate. Some parts of western Bhutan have a high amount of mean precipitation rate, that is, 0.2076–0.3424 mm. Precipitation (Standard Deviation) map shows the change of precipitation for the different states of India, Nepal as well as Bhutan. These maps are generated with the help of standard deviation. A map was generated showing the change of precipitation for the different states of India, Nepal, as well as Bhutan. These maps are generated with help of standard deviation data from 2000 to 2015 (Fig. 6.7).

As we move from the western part toward the eastern part, we can see that the western part of India and both the eastern and western parts of Nepal have a very high-level precipitation that lies between 0.0294 and 0.7804 mm. Except for a few states of Bhutan, all the remaining regions have medium level of precipitation, that is, 0.0139–0.0294 mm.
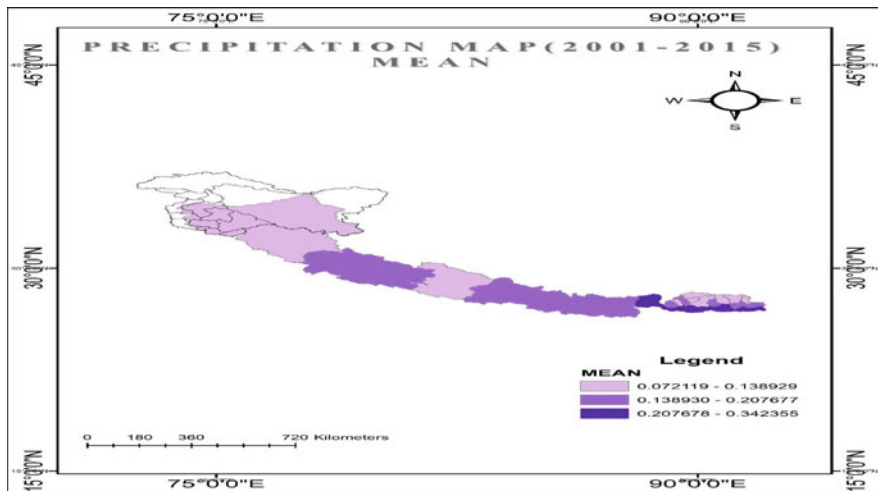
Fig. 6.7 State-wise variations of precipitation (mean)

Figure 6.8 shows the precipitation variation of the Himalayan region with the help of state-wise mean data which are been collected from 2000 to 2015 for the specific region. Three different classes were made to show the variations. The maximum state of this region belongs to the area having a moderate to low amount precipitation rate. Some parts of western Bhutan have a high amount of mean precipitation rate, which is 0.2071–0.3426 mm.

A map was generated showing the change of precipitation for the different states of India, Nepal as well as Bhutan. These maps were generated with help of standard deviation data from 2000 to 2015. As we move from the western part toward the eastern part, we can see that the western part of India and both the eastern and western parts of Nepal have a very high-level precipitation that lies in between 0.0294 and 0.0780 mm. Except for a few states of Bhutan, all the remaining regions have a medium level of precipitation, which is 0.013994–0.029498 mm (Fig. 6.9).

Table for Fractional Snow Cover (2001–2015)

A contour map was drawn to show the zonal variations of fractional snow cover for the Himalayan region, and in this map, selected areas of the Himalayan belt are divided into five different zones based on fractional snow cover value. Above that, 5 different contours were drawn, which are 0 to 0.02, 0.02 to 0.05, 0.05 to 0.08, 0.08 to 0.11, and 0.11 to 0.16. In the map, we can see that the central part of the Himalayas has the highest concentration of fractional snow cover change, as it moves from central toward west and east, variations of fractional snow cover decrease as compared to the central part (Fig. 6.10).
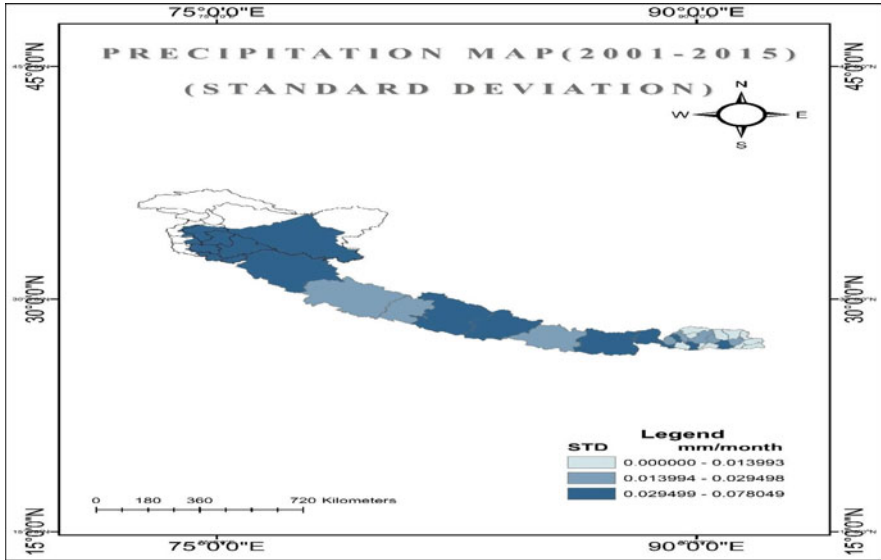
Fig. 6.8   State-wise variations of precipitation (standard deviation)
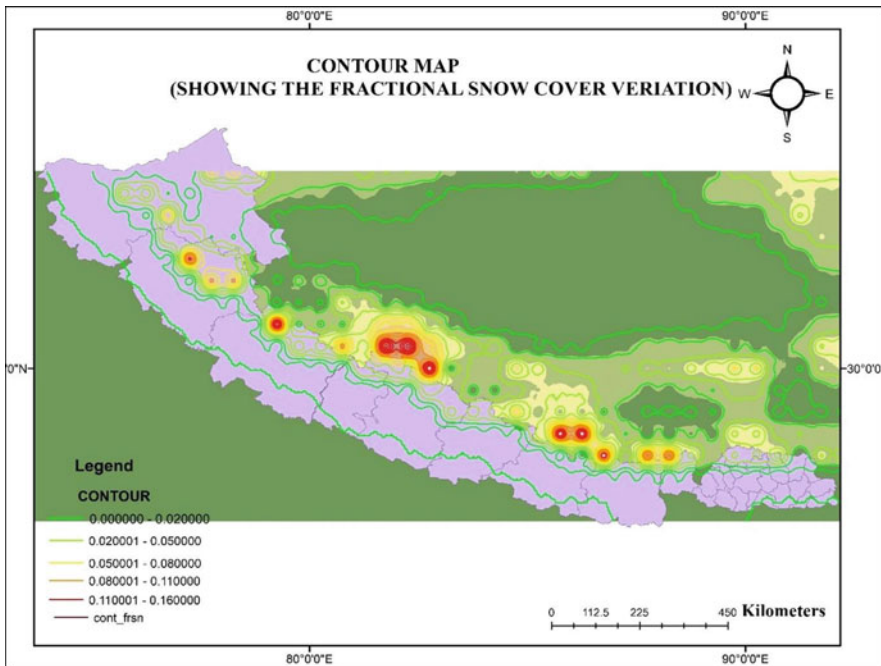
Fig. 6.9   Contour variations of fractional snow cover from 2001 to 2015
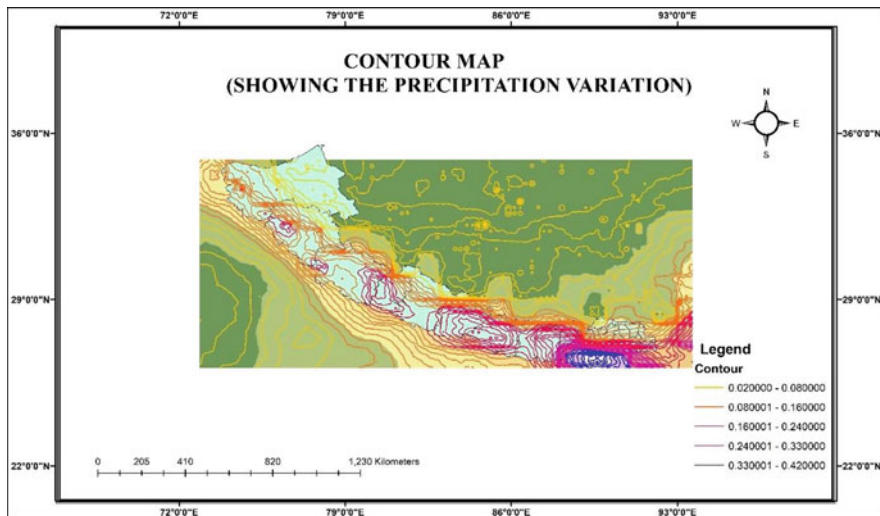
Fig. 6.10 Contour variations of precipitation from 2001 to 2015

A contour map was drawn to show the zonal variations of precipitation for the Himalayan region, in which selected areas of the Himalayan belt are divided into five different zones based on precipitation value. Above that, five different contours were drawn, which are 0.02 to 0.08, 0.08 to 0.16, 0.16 to 0.24, 0.24 to 0.33, and 0.33 to 0.41. In the map, we can see that the eastern part of the map has the highest rate of precipitation, and as it moves from the western part, the concentration of precipitation gradually decreases (Figs. 6.11, 6.12 and 6.13).

Figure 6.14 shows a line graph to show year-wise mean precipitation concentrations of different states of India, Nepal as well as Bhutan. From the above graph, it is clear that with comparisons to India and Nepal, Bhutan has the highest concentrations of precipitation. Where mean precipitations of India and Nepal lie between 0.1 and 0.2 mm/month, that of Bhutan lie between 0.2 and 0.3 mm/month mean precipitation. It is because both precipitation and fractional snow cover have direct relations; changes in one affects the other.

Figure 6.15 shows a line graph to show the mean fractional snow cover distributions over the Himalayan belt. All the data are prepared from the general statistics, as it clear from the above diagram. Maximum of these states have very low fracitinal Snow cover variations but in the case of Gasa (Bhutan), fractional Snow Cover Data is slightly higher in the years 2002 and 2006.

Figure 6.16 shows a relation between fractional snow cover and precipitation, as we all know that these both have direct relation in between them. In the above diagram from the data, it is clear that both precipitation and fractional snow cover have positive relationships (R = 0.01883) (Figs. 6.17, 6.18 and 6.19).

Name	2001	2002	2003	2004	2005	2006	2007	2008	2009	2010	2011	2012	2013	2014	2015
Himachal Pradesh	0.003487	0.020842	0.003191	0.009173	0.004479	0.014258	0.022907	0.066797	0.013369	0.029966	0.003189	0.012445594	0.001749	0.014542	0.04138
Jammu and Kashmir	0.007262	0.018704	0.009648	0.00719	0.005351	0.024179	0.022208	0.057311	0.011949	0.019362	0.01033	0.020766215	0.003767	0.016265	0.063664
Sikkim	0	0	0	0	0	0.005167	0	0	0	0	0	0	0	0	0
Uttarakhand	0.000168	0.003296	0.000668	0.007337	0.003891	0.001917	0.008543	0.010902	0.004095	0.004896	8.11×10^{-6}	6.01036×10^{-5}	0.000273	0.000567	0.001744
Central	0	0	0	0	0	0	0	0	0	0	0	0	0	0	0
East	0					0.000	0					0	0	0	0
Far-western				6.62×10^{-5}		47	0.00132								
Mid-westren	0.001298	0.01793	0.012026	0.010508	0.011322	0.003888	0.025928	0.050731	0.00072	0.014241	0.004484	0.007304737	0.004717	0.00341	0.000506

(continued)

Name	2001	2002	2003	2004	2005	2006	2007	2008	2009	2010	2011	2012	2013	2014	2015
West	0.0 0133	0.0 0622 1	0.0 0116 1	0.0 0210 3	0.0 0357 9	0.0 0106 6	0.0 0550 1	0.0 1563	0.0 0333 4	0.0 0296 5	0.0 0389 9	0.00 6611 515	0.0 0210 5	0.0 0210 2	0.0 0056 6
Chhukha	0	0	0	0	0	0	0	0	0	0	0	0	0	0	0
Dagana	0	0	0	0	0	0	0	0	0	0	0	0	0	0	0
Gasa	0.0 2015 5	0.1 3066 9	0.0 1049 1	0.0 0908 4	0.0 1233 8	0.2 0863 7	0.0 1329 3	0.0 2722 9	0.0 1321 2	0.0 1172 7	0.0 0792 5	0.01 6837 036	0.0 1886 9	0.0 5617 8	0.0 0927 1
Lhuentse	0	0	0	0	0	0	0	0	0	0	0	0	0	0	0
Samdrup Jongkhar	0	0	0	0	0	0	0	0	0	0	0	0	0	0	0
Samtse	0	0	0	0	0	0	0	0	0	0	0	0	0	0	0
Sarpang	0	0	0	0	0	0	0	0	0	0	0	0	0	0	0
Thimphu						0.0 1019						0.00 4925			
	0	0	0	0	0	4	0	0	0	0	0	126	0	0	0
Trashigang	0	0	0	0	0	0	0	0	0	0	0	0	0	0	0
Trongsa	0	0	0	0	0	0	0	0	0	0	0	0	0	0	0
Wangdue Phodrang	0	0	0	0	0	0	0	0	0	0	0	0	0	0	0
Yangtse	0	0	0	0	0	0	0	0	0	0	0	0	0	0	0
Zhemgang	0	0	0	0	0	0	0	0	0	0	0	0	0	0	0

Source- MODIS data
https://giovanni.gsfc.nasa.gov/giovanni/
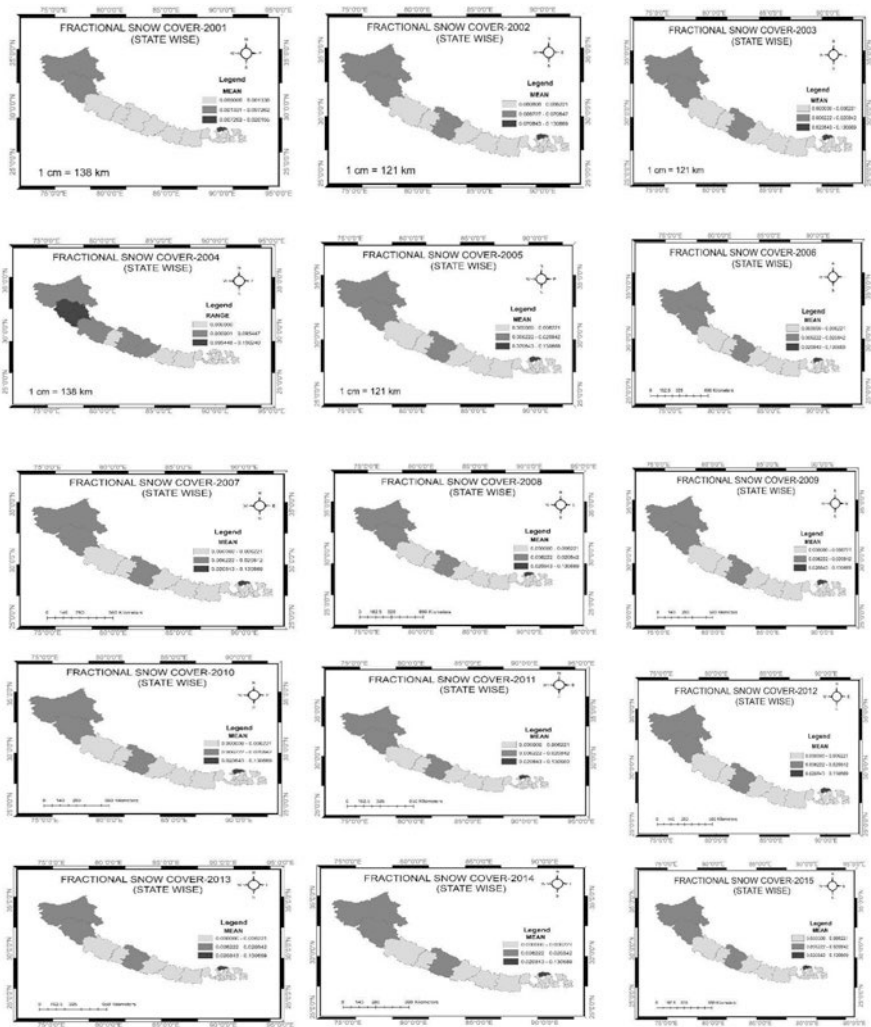
Fig. 6.11 Fractional snow cover variations (2001–2015) state wise
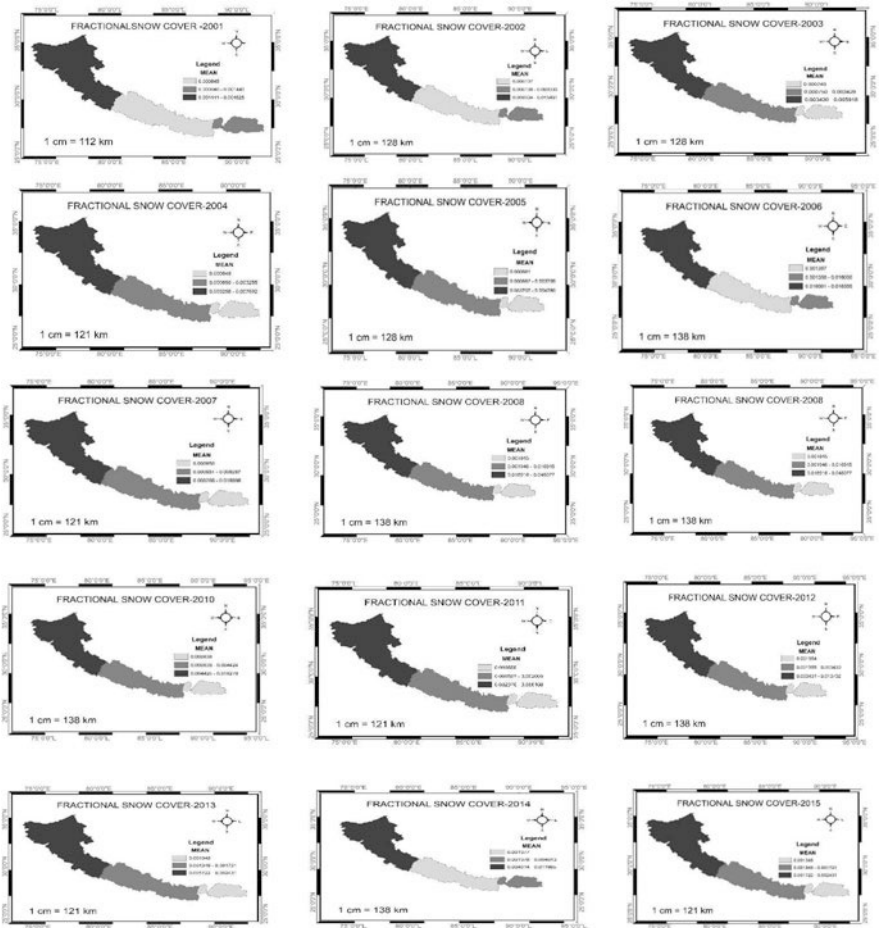
Fig. 6.12 Fractional Snow Cover Variations (2001–2015) zone
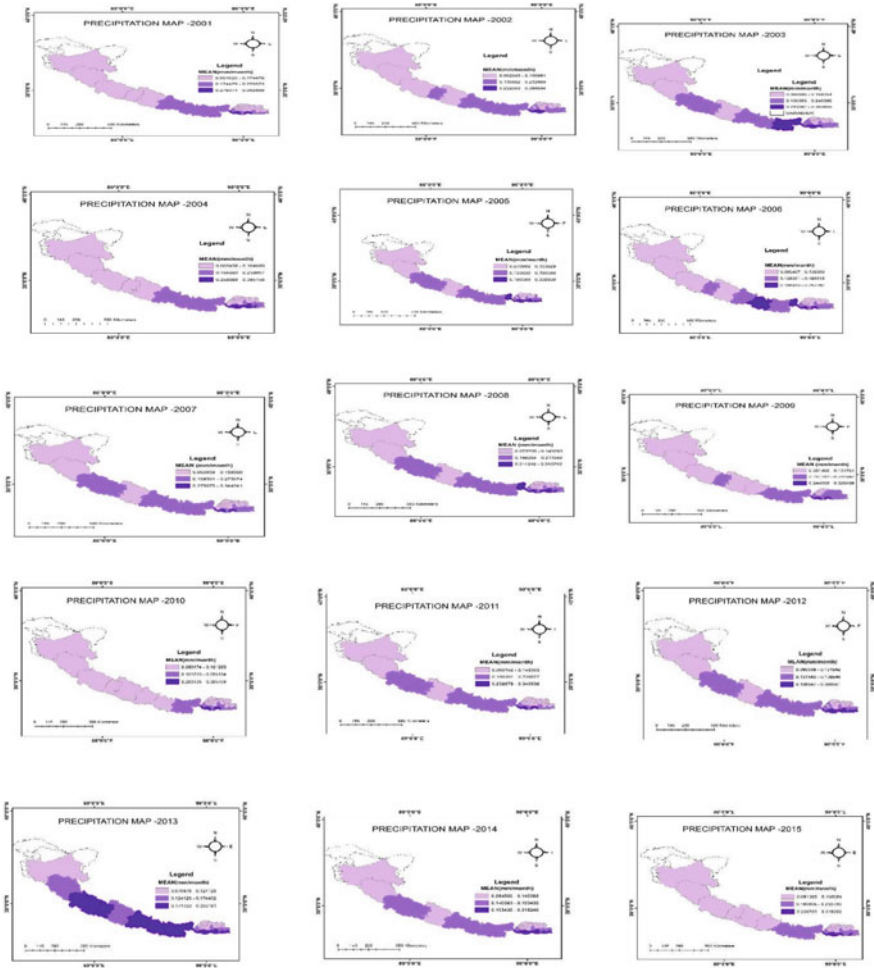
Fig. 6.13 Precipitation variations (2001–2015) state wise

Yearly Change of Precipitation (2001-2015)
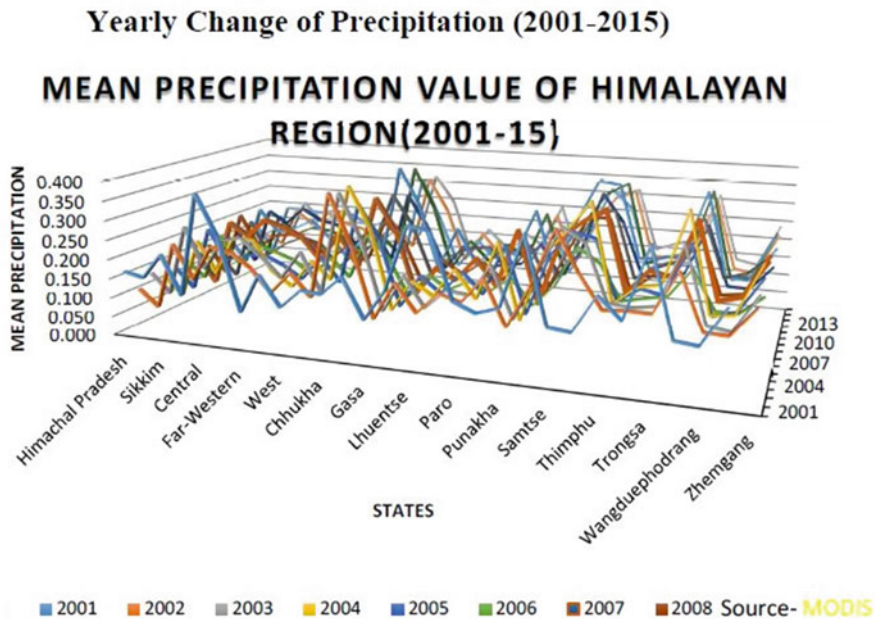
Fig. 6.14 Yearly change of precipitation (2001–2015)
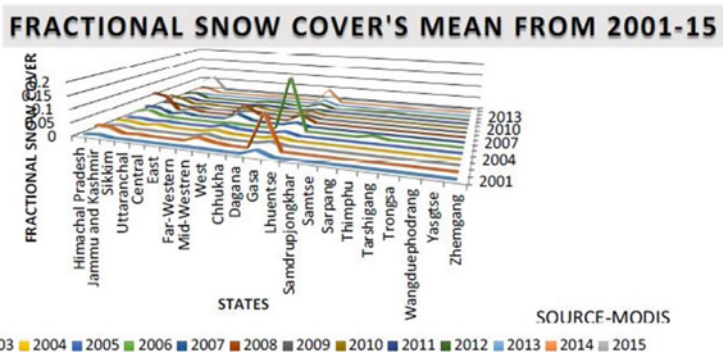
Fig. 6.15 Yearly change of fractional snow cover (2001–2015)
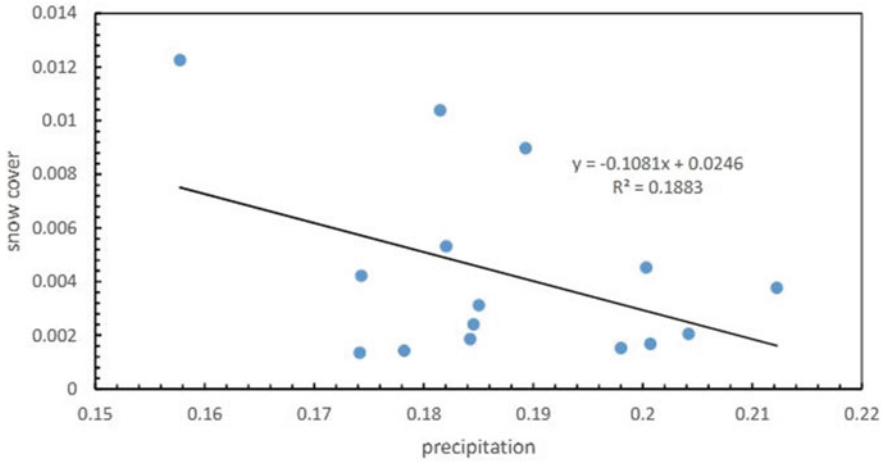
Fig. 6.16 Relation between fraction snow cover and precipitation
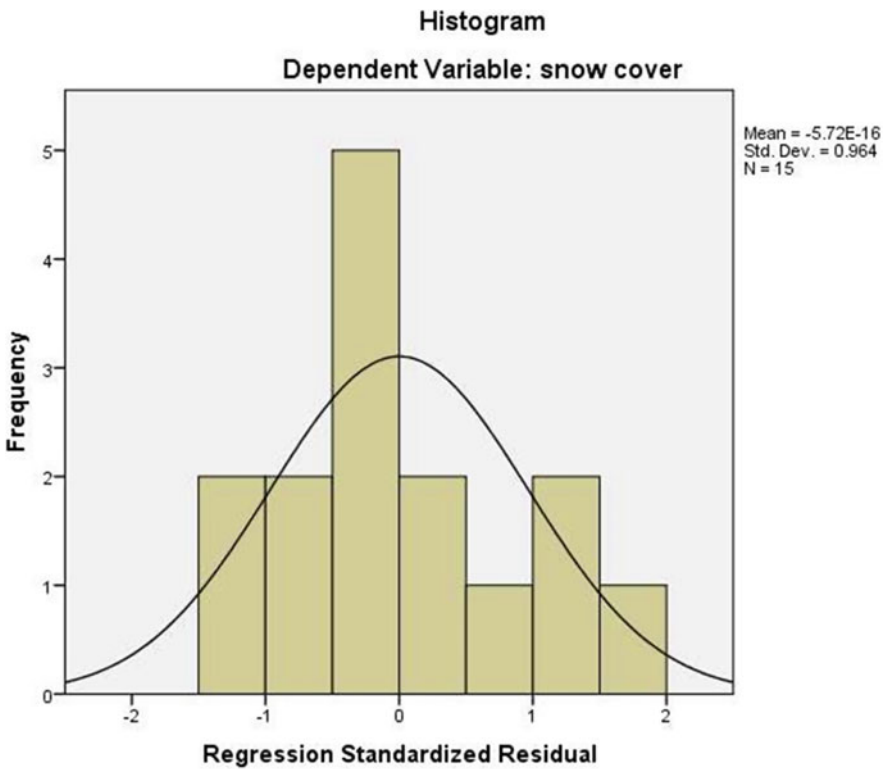
Fig. 6.17 Regression standardized residual
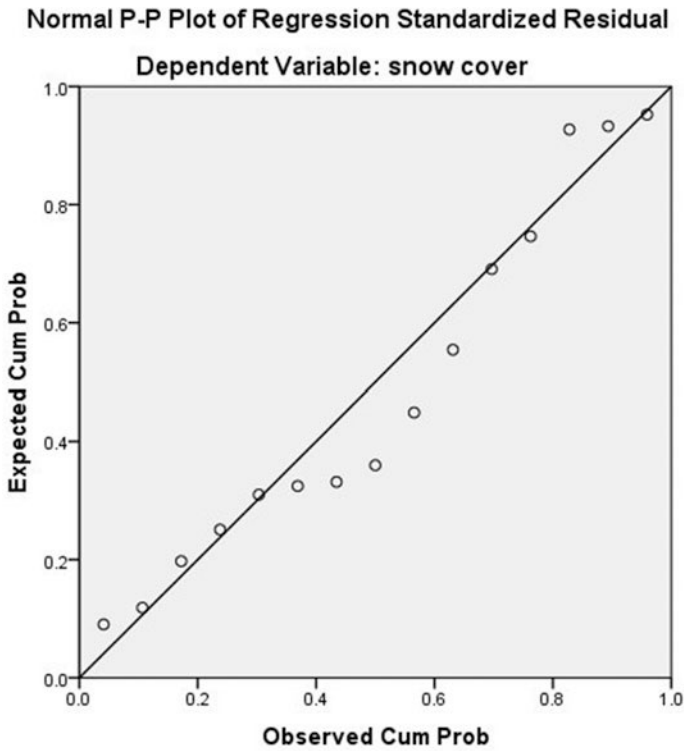
Fig. 6.18 Scatterplot-dependent variable snow cover
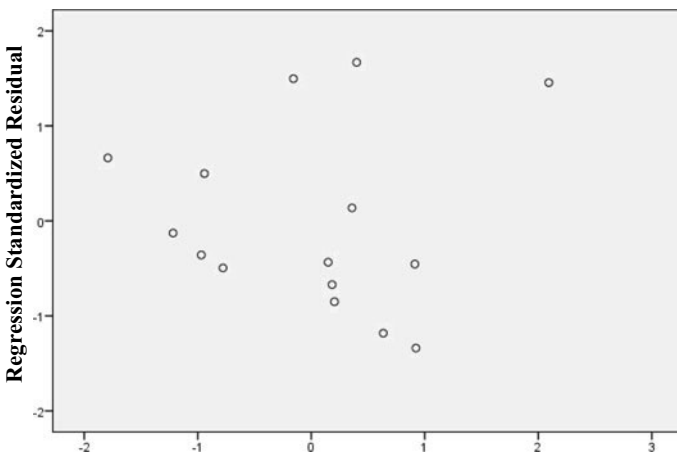
Fig. 6.19 Regression-standardized predicted value

Conclusions

Fractional snow cover and precipitations for three major regions of the Himalayas are Western Himalayas, Eastern Himalayas, and Central Himalayas. The maximum snow cover for the time between 2001 and 2015 is observed in the eastern part of the Himalayas (Bhutan), and minimum fractional snow cover is observed in the western part of the Himalayas. The same trend is also observed for the precipitation. It's because both fractional snow cover and precipitation are directly related to each other. This analysis shows that all three zones along with different states respond differently in terms of fractional snow cover and precipitation; however, a more detailed investigation is required to support these observations.

References

Hall DK, Riggs GA, Salomonson VV (1995) Development of methodsfor mapping global snow cover using moderate resolution imagespectroradiometer data. Remote Sens Environ 54(6): 127–140

Immerzeel WW, Droogers P, de Jong SM, Bierkens M (2013) Large-scale monitoring of snow cover and runoff simulation in Himalayan river basins using remote sensing. Remote Sens Environ 113:40–49

McElroy B, Wilkinson B (2005) Climatic control of continental phys-iography. J Geol 113:47–58

Mohammad S, Keikhosravi K, Seyed MA, Robert BC, Bohumil SM (2017) Spatial and temporal variations of snow cover in the Karoon River Basin, Iran, 2003–2015. Water 9(965):3–16. https://doi.org/10.3390/w9120965

Swapnali B, Bhattacharjya KR (2015) Change in snow cover area of Brahmaputra river basin and its sensitivity to temperature. Environ Syst Res 1–10. https://doi.org/10.1186/s40068-015-0043-0

Vivek D, Asha (2015) Snow cover and snowline altitude variations in Alaknanda Basin, Uttarakhand, Central Himalayas. Int J Sci Res (IJSR) 4(2):546–551. https://www.ijsr.net/archive/v4i2/SUB151126.pdf

Chapter 7
Watershed Delineation and Land Use Land Cover (LULC) Study of Purna River in India

Darshan Mehta, Keyur Prajapati, and Md. Nazrul Islam

Abstract Surface water and ground water are used for agricultural, industrial, and domestic purposes. Rainfall and the corresponding runoff generated are important hydrological processes which depend on the local physiographic, climatic, and biotic factors. Remotely sensed data provide valuable and real-time spatial information on natural resources and physical parameter. Due to climate changes and human interference to the river systems, flood risks have also increased. Flood losses can be reduced by proper floodplain management. Watershed means a naturally occurring hydrologic unit that contributes storm runoff to a single waterway classified on the basis of its geographical area. The aim of the study is to throw some light on the importance of watershed management using geospatial techniques. In this analysis, studies of the slope, contour, and terrain profile of study area and behavior of stream segments, drainage direction, flow accumulation, Land Use Land Cover (LULC), drainage map, etc. were carried out using QGIS-ArcMap 10.1. There are two river basins in upper Tapi region—one is Tapi River and the other is Purna River. Results show the depletion of both ground and surface water in the watershed. Green cover is considerably reduced in the region, and hence, the watershed is less humid and dry. Study also reveals that due to change in land use and land cover, there are more wastelands in the watershed. The study also provides an indication to restore the vegetation cover and will be able to help policy and decision-makers to understand the importance of watershed and need for its characteristics analysis.

D. Mehta (✉)
Civil Engineering Department, Dr. S. & S. S. Ghandhy Government Engineering College, Surat, Gujarat, India

K. Prajapati
Department of Environmental & Water Resources Engineering, University of Western Ontario, London, ON, Canada

Md. N. Islam
Department of Geography and Environment, Jahangirnagar University, Savar, Dhaka, Bangladesh
e-mail: nazrul_geo@juniv.edu

Keywords Watersheds · Watershed delineation · Basin characteristics · Geospatial technology · Tapi River Basin · India

Introduction

The environment has been influenced by human beings for centuries. However, it is only since the beginning of the industrial revolution that the impact of human activities has begun to extend to a global scale (Natarajan and Radhakrishnan 2019; Nimkar et al. 1992). Today, environmental issues have become the biggest concern for mankind as a consequence of scientific evidence about the increasing concentration of greenhouse gases in the atmosphere and the changing climate of the Earth. Globally, temperature is increasing and the amount and distribution of rainfall are being altered (Rathore et al. 2018; Samanta et al. 2018). A watershed means a naturally occurring hydrologic unit that contributes storm runoff to a single water-way classified on the basis of its geographical area (Azam et al. 2017). In spite of extensive research on specific impacts of climate change, research and information on the impacts of climate change to watershed systems remain in its infancy. Evaluation of climate change on the watershed system is important to develop alternative strategies and policies to mitigate the impacts of global warming (Martin et al. 2012). Analysis of large watersheds is quite tedious and time-consuming. Remote sensing data provide a fast and economic way to analyze large watersheds by virtue of synoptic and repetitive coverage (Basarudin et al. 2014; Bose et al. 2014). Geographic information system (GIS) is an effective tool in watershed modeling as remote sensing-derived information can be well integrated with the conventional database for estimating runoff, which can help in planning suitable soil and water conservation measures (Belayneh et al. 2020; Ben Khélifa and Mosbahi 2021). Since the modeling of runoff is essential for sustainable development, it is desirable that some suitable methods are used for quantifying the hydrological parameter from all parts of the watershed (Cahyano and Adidarma 2019; Choudhari et al. 2014). The present study aims at the delineation of watersheds by considering different variables, e.g., DEM, land use/land cover, hydro geomorphology, elevation, and slope in the watershed of the Purna river basin in Maharashtra by integration of remote sensing and GIS. A larger drainage basin or a large watershed consists of several subwatersheds (Darji et al. 2019; Derdour et al. 2018). Each subwatershed then drains to a single outlet on a stream which is a part of the basin's drainage network and is hydrologically connected to the other subwatersheds of the basin through this network (Giuli et al. 1994; Gumindoga et al. 2017). Geographic information systems or GIS, when integrated with hydrologic process models, provides the basis for the development of such a framework (Haibo et al. 2018; Khaleghi et al. 2015). The GIS layers include the watershed boundary, streams, contours, habitations, soils, land use, and geology. Erosion and sediment transport processes are also influenced by climate change, with the highest soil loss rates occurring in regions that have high variability in precipitation and runoff (Masseroni et al. 2017; Meresa 2019). Terrestrial and aquatic ecosystems are sensitive to climate

change on a variety of temporal and spatial scales (Mistry et al. 2017; Mokhtari et al. 2016). A digital elevation model of the area was also generated in ArcMap 10.4 (Halwatura and Najim 2013; Haque et al. 2017). The usual procedures involving the prediction of runoff require more time and money to gather different data and produce erroneous results (Ibrahim-Bathis and Ahmed 2016; Joo et al. 2014). Hence, the recent advanced techniques—remote sensing and geographic information system (GIS)—were used in the collection, storing, and analysis of the data with respect to spatial and temporal distribution (Latif 2018; Mandal and Chakrabarty 2016). This chapter aims to study basin area by using LULC and drainage map, so if the capacity of the stream is known, it helps optimize the usage of water, thereby increasing the water table in a particular area (Komolafe 2021; Kumar et al. 2021).

The scope of this project is to identify various physical characteristics of the watershed that are involved in the hydrological process. The creation of watershed using GIS techniques is based on the profile of the area like slope, contour, drainage line, soil properties, LULC, etc. Thus, generated watershed will be useful in the application of hydrological studies like rainfall-runoff model generation and flood warning systems.

Problem Definition of Purna Basin

Rainwater is the only source to replenish and recharge surface and groundwater, respectively. Most of the rainwater collected in the tributaries is short-lived and drains out as runoff due to high slopes. Flash flood is a regular phenomenon of the Purna river basin. Large areas of cultivated land get devastated and eroded by flash floods, causing damage to houses and cattle, and eroding the soil. The magnitude of the problem is so high that in some of the area it is directly affecting the socioeconomic setup, i.e., desertification or over flooding of villages, reduction of crop yield, and infertility of soil. Inland groundwater salinity is high, so the groundwater of the area is unsuitable for both drinking and agricultural purposes. More than 400 villages falling in the saline areas are continuously facing severe problems of drinking water. In September 1959, due to heavy rains, a hazardous flood occurred, which affected 179 villages in the Amravati district. An area of about 74 km^2 with standing crops was also completely swept away by floods. In October 1988, August 2006, and September 2008, flood caused major damage too.

Background Environment and Livelihood of the Study Area

The main alluvium area of the Purna Valley covers a large stretch of low-lying land between Paturda and the confluence of the river Purna with that of Tapi–Jalgaon district. In the river valleys and where superficial rain-wash has accumulated, a mixture of black cotton soil associated with light brown laterite material is noticeable

at places; otherwise, there is little variation in the nature and extent of soil or any variety of geological interest. The alluvium of the plains is usually of considerable depth. Much of the alluvium produces effervescence of sodium salts. Majority of the wells sunk in the area have brackish water. The soil in the Purna basin can be broadly classified into three groups: coarse shallow soils: their depth is generally between 25 and 50 cm and seldom more, and their texture from surface to subsurface varies from silty loam to clay; medium black soils: their depth is generally between 50 cm and 1 m. These soils are fair in their contents of phosphates and potash but low in organic matter and nitrogen; and deep black soils: These soils are more found along the Purna River. The depth of this soil varies from 1 to 6 m. The soil has very high clay content of montmorillonite predominating and not easily workable during monsoon.

Study Area

The Purna is the principal tributary of the Tapi River. It rises in the eastern Satpura Range of southern Madhya Pradesh and flows westward, draining Maharashtra's Marathwada and Vidarbha regions before merging with the Tapi River. The Purna drains a total area of 18,929 km^2. The length of the Purna River is 379 km (Bose et al. 2014). There are three stream gauging stations, namely, Gopalkheda, Lakhpuri, and Yerli gauging sites located at 229 km, 226.7 km, and 299 km, respectively, from the origin of the Purna River. Purna basin is a part of the upper Tapi basin is covered by rocks of the Deccan volcanic of Creteceo-Eocene age, and a few alluvium patches of the Purna and Penganga basin, respectively. The Purna catchment is characterized by more of a flatter topography with most of the land area used for agriculture purpose. The trap rocks are usually fine to coarse grained, dark gray to greenish-black basalts of vesicular and massive types. The vesicular and nonvesicular flows are at places separated by thin beds of ash or scoriae, but typical intertrappean sedimentary rocks have not been recognized in the area. No dykes have been found associated with the trap flows in the district where a lava pile of approximately 800 m is preserved. Both shallow and deep aquifers experience low to high levels of salinity creating major socio-economic problem in the area. Agriculture is the main land use in the Purna river basin area. Cotton is a major crop in Kharif season, followed by jowar, mung, tur, and soybean, whereas some farmers also crop the gram, wheat, and groundnut in Rabi season. In the saline tract area, the well water is moderately to highly saline and unsuitable for irrigation; therefore, the agriculture is mainly rain-fed. Majority of farmers in the village of the basin own the land that indicates the higher percentage of marginal farmers. The basin covers Amravati, Buldhana, and Akola districts. There are 18 rain gauge stations in the basin (Fig. 7.1).
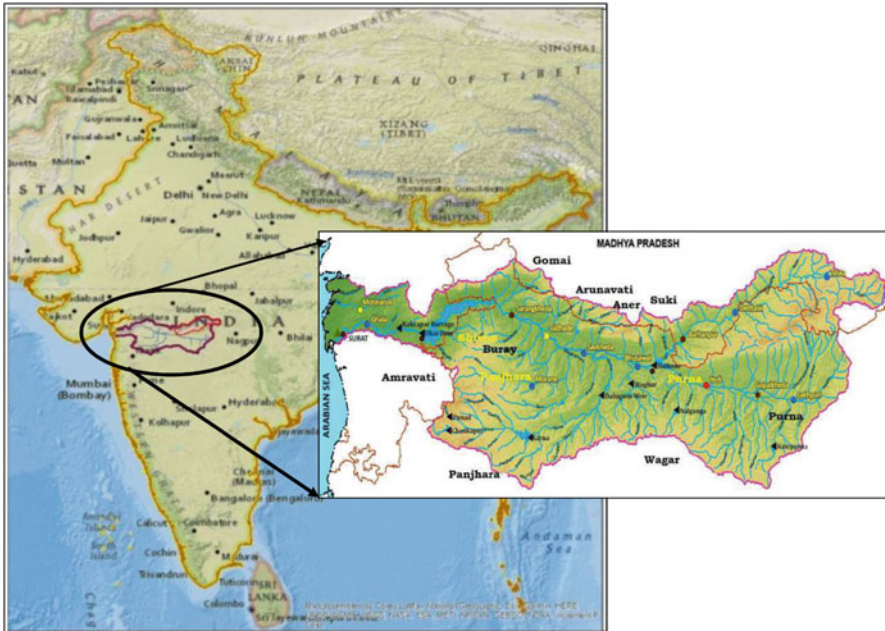
Fig. 7.1 Boundary map

Data Collection

DEM was downloaded from https://bhuvan.nrsc.gov.in/ of year 2015. The Centre Water Commission, Surat, provided the discharge data and rainfall data for the Purna river station of Gopalkheda, Lakhpuri, and Yerli from 1974 to 2017. The following data were collected to enhance the study of rainfall runoff modeling. There are 18 rain gauge stations available in Purna Basin: Amravati, Raver, Burhanpur, Edalabad, Jamner, Bhainsdehi, Murtajpur, Buldana, Nandura, Shegaon, Ratur, Athner, Telhar, Akol, Akola, Dharni, Multai, Chilkhalda, Anjangaon, Daryapur, Murtajpur, Achalpur, and Lakhpuri.

There are three gauging sites, Lakhpuri, Gopalkheda, and Yerli, of CWC department available in the Purna River Basin. Line diagram of the Purna River basin is as below.

- The distance between Lakhpuri and Gopalkheda is 55.5 km.
- Distance between Gopalkheda and Yerli is 77.7 km.
- Distance between Yerli and Hatnur dam is 77.4 km.
- From the water level data, travel time between two sites is found to be 6 hours for peak flood.

Digital Elevation Model (DEM)

The first step is to download the DEM from https://bhuvan.nrsc.gov.in/. This tile is used in Arc-GIS to obtain the topography of the basin area. A DEM is a digital image of terrains surface, commonly for a planet, and it can be either in 2D or 3D. Determination of the hydrologically correct DEM and its derivatives, particularly flow direction and flow accumulation grids, often requires some iteration of the measurement of the drainage path in order to accurately depict the flow of water through the catchment area. The hydrologically accurate DEM must have adequate resolution to capture the specifics of the surface flow (Fig. 7.2).

The steps for DEM creation are as below (Makkena 2016).

Watershed delineation process starts with the generation of a digital terrain model. In the present study, the terrain model is available and downloaded from www.bhuvan.nrsc.gov.in.

Thus, the downloaded terrain model is imported in ArcMap for further watershed processing. Before initiating the process, all titles which involve the study reach were merged and a mosaic raster was created with WGS 1984 UTM Zone 43 N (This reference varies with co-ordinate system).

After creating a mosaic raster with relevant co-ordinate system, it is necessary to complete the raster layer with cell information. Hence, the fill tool in ArcMap was used. By using the fill tool, the value of sink is raised to the lowest value of its surrounding cell. The elevation of pit cells is increased until a down-slope path to a cell becomes available, under the constraint that flow may not return to a pit cell (Fig. 7.3). This tool helps to create a raster layer with no empty cell value in the digital terrain model.

It is very necessary to determine the flow direction after creating a fill raster. In ArcMap for watershed processing and to identify the direction of flow for each cell, there is a tool named "Flow direction." This function assigns a value of flow

Fig. 7.2 Digital elevation model
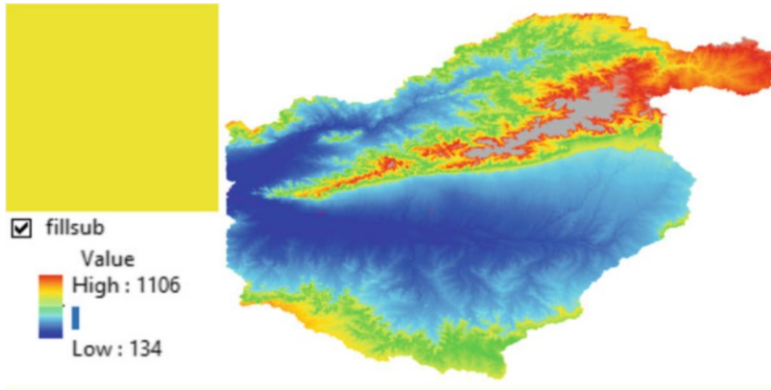
Fig. 7.3 Fill raster

Fig. 7.4 Flow direction raster

direction to every cell in grid according to the eight-direction pour point method (Fig. 7.4).

Now, we have a flow direction raster that shows the direction of flow into the watershed. As most of the cells which reflect the tributary, stream, or water body, i.e., lake or river, have the same value, the tool "Flow accumulation" records the number of cells that drain into an individual cell in the grid. The flow accumulation grid is essentially the area of drainage to a specific cell measured in grid units. (Select flow accumulation, then give value >15,000) (Fig. 7.5).

In the natural system, small streams merge and form the tributary and many tributaries drain to from a river or a channel. Hence, to identify the flow network in watershed in the form of stream, tributary, or river, Stream Link tool is used. Here, the stream flow path is defined by a number of cells that accumulate in an area before they are recognized. It assigns unique values to sections of a raster linear network

Fig. 7.5 Flow
accumulation raster
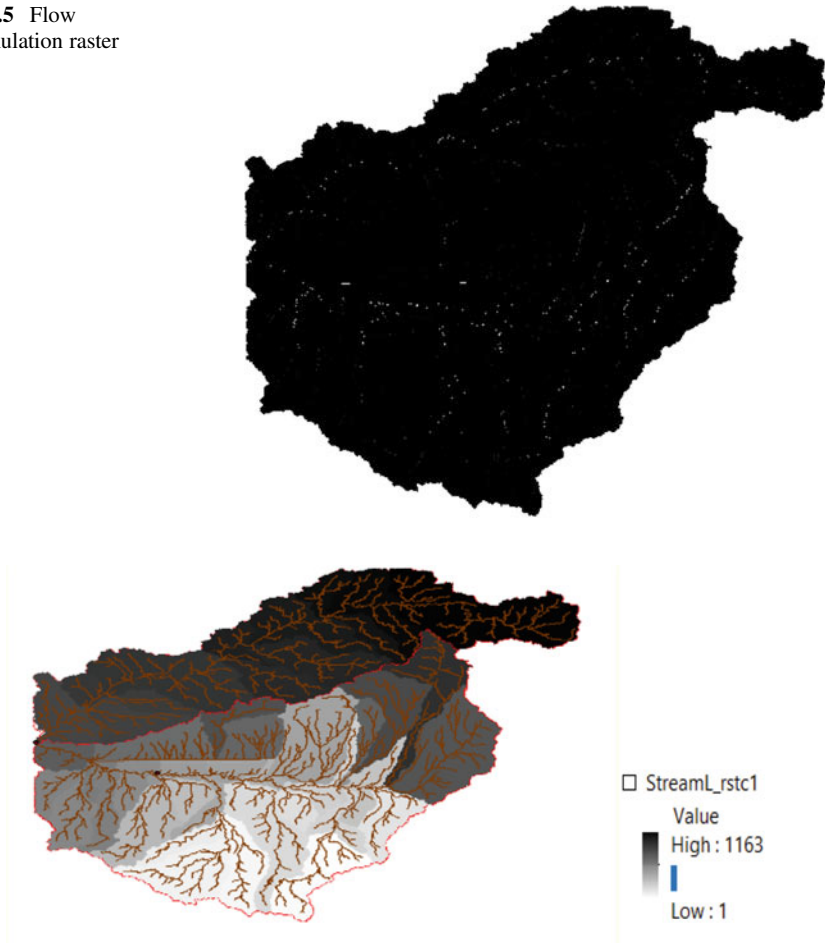
Fig. 7.6 Stream link raster

between intersections (Fig. 7.6). It then identifies and connects stream, tributary, and
river into the raster layer.

Now, it is important to identify the stream order. Stream order is a process to
assigning a number of links in a stream network, so it is easy to identify the stream of
the catchment area. Lower number is assigned to the flow generating small streams,
and higher number is given when two or more streams having same order number
merge and form a tributary. Streams, including those that don't flow all of the time,
make up much of the country's waters. They could be a drizzle of snowmelt that runs
down a mountainside crease, a small spring-fed pond, or a depression in the ground
that fills with water after every rain and overflows into the creek below. They protect
against floods, filter pollutants, recycle potentially harmful nutrients, and provide
food and habitat for many types of fish (Fig. 7.7).

Fig. 7.7 Stream order raster

Fig. 7.8 Watershed raster
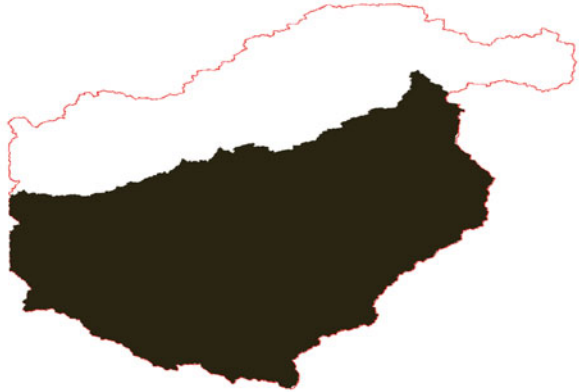
Now after generating stream network and assigning stream order, it is clear in the raster layer that there are two higher-order streams. First is the upper part of the catchment, which is draining out in different regions and not contributing any runoff into the Purna River. Second is the lower part of the catchment, which drains off all water into the Purna River. Hence, the lower portion of the raster layer showed in dark in Fig. 7.8 is clipped, and a new clip raster image (Fig. 7.9) is created.

In any watershed, all water drains out from one outlet point in most of the cases in river. In watershed delineation process, an outlet point or pour point is identified based on the steam network or stream order which is a point at the end of watershed. It flows out the water from the catchment area (Fig. 7.9).

Thus, Purna River watershed is created.

Results

Watershed Delineation of Tapi River Basin

Upper Tapi river basin, which is draining into the Purna River, is a flood-prone area mainly due to its topography and mixed land use. It is necessary to understand the
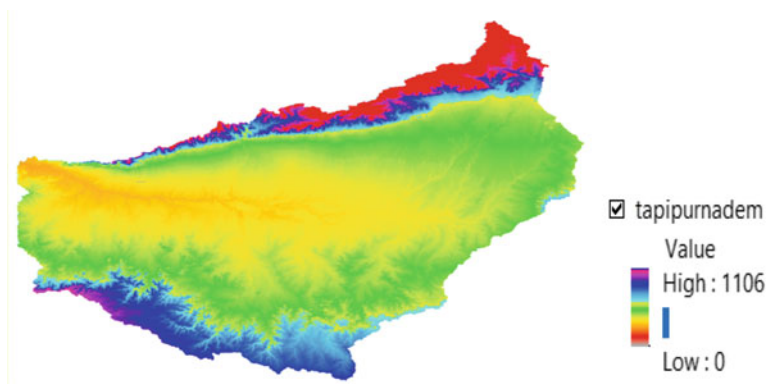
Fig. 7.9 Subwatershed raster

river network, topography of basin, and land use and land cover. Land use and land cover plays an important role in a watershed planning and management. Upper Tapi river basin mainly consists of crop land which means most of the soil is clay. Clay has low permissible rate than other soils, which contributes to less infiltration of water and more surface runoff in the watershed. Hence, to identify such land mass in the study area is crucial. Watershed delineation helps to understand the water interaction, flow pattern, and outlet points across the study area along with changing land use and land cover pattern. Watershed delineation is also beneficial to develop a floodplain map identifying the flood-prone area for design floods. Planning and implementation of new flood mitigation strategies can be done by identifying the potential ways to divert the flood discharge or convey it safely from a region which may cause more social and economic loss.

Land Use and Land Cover (LULC) Change

Land use land cover (LULC) map is used to identify the basic change in the study area. LULC map classifies areas covered by water, vegetation, forest, urbanization, etc. in different categories. LULC maps are usually created by satellite images and compared with historic data to help understand the growth and situation of land use land cover across the study area.

The process given below shows the steps for creating land use and land cover map.

To identify the change in the LULC, decadal land use and land cover classification data across India for the years 1985, 1995, and 2005 were downloaded. From these data, information corresponding to the study area was extracted and imported into Arc-GIS. Now to identify the change in the LULC, the symbology was changed so that variation in all classes of the LULC categories can be easily visible and distinct. The same process was repeated for all files to identify each land use and land

Fig. 7.10 Land use land cover (LULC) map

cover distinctively. Now, after preparing all LULC data with distinct symbology, the LULC data were extracted for the study area using "Mask Tool" in the Arc-GIS. Thus, a new raster file is generated with LULC data. This raster file was converted into a shape file. The newly generated shape file consists of grid code and corresponding color. It is advisable to change the grid codes in the attribute table that refers to the land cover classification codes as mentioned in the downloaded data. A new color scheme and name of grid code are set according to classification in the present study area (Fig. 7.10).

Land use detail of Purna river basin shows that area covered by crop land is 42.30%, forest land is 25.01%, mixed forest is 2.62%, shrub land is 8.81%, water bodies is 6.76%, fallow land is 4.74%, built up land is 1.90%, watershed is 5.99%, and plantation is 1.87%. Land use map of the basin was prepared using LULC map of India of years 1985, 1995, and 2005 in ArcMap 10.1. Land use cover is defined as observed physical features on the earth's surface. A major part of the basin is covered with agriculture. The major crops cultivated in this basin are wheat, sugarcane, rice, gram, etc.

Conclusion

Watershed delineation using geographic information system (GIS) will provide more and clear vision of basin characteristics that help to identify areas prone to flash flood. Land use and land cover (LULC) map helps us to identify the critical areas that are being deforested in basin and either converted to crop land or in land use. It is evident from the LULC map that in the given basin, a large area covered by cropland compared to forest land gives rise to soil erosion, less water retention, high salinity in the soil, and low groundwater table. From watershed delineation and

LULC map, it is suggested to take steps for watershed management which includes the forestation of land, construction of weirs, or check dams.

References

Azam M, Kim HS, Maeng SJ (2017) Development of flood alert application in Mushim stream watershed Korea. Int J Disaster Risk Reduc 21:11–26. https://doi.org/10.1016/j.ijdrr.2016.11.008

Basarudin Z, Adnan NA, Latif ARA, Tahir W, Syafiqah N (2014) Event-based rainfall-runoff modelling of the Kelantan River Basin. In: IOP conference series: earth and environmental science, vol 18, no 1. IOP Publishing, p 012084

Belayneh A, Sintayehu G, Gedam K (2020) Evaluation of satellite precipitation products using HEC-HMS model. Model Earth Syst Environ 6:2015–2032. https://doi.org/10.1007/s40808-020-00792-z

Ben Khélifa W, Mosbahi M (2021) Modeling of rainfall-runoff process using HEC-HMS model for an urban ungauged watershed in Tunisia. Model Earth Syst Environ. https://doi.org/10.1007/s40808-021-01177-6

Bose AC, Sridhar P, Giridhar MVSS, Viswanadh GK (2014) Watershed delineation and stream network analysis using GIS. Int J Watershed Eng Hyderabad 1(1):1–13

Cahyono C, Adidarma WK (2019) Influence analysis of peak rate factor in the flood events' calibration process using HEC–HMS. Model Earth Syst Environ 5:1705–1722. https://doi.org/10.1007/s40808-019-00625-8

Choudhari K, Panigrahi B, Paul JC (2014) Simulation of rainfall-runoff process using HEC-HMS model for Balijore Nala watershed, Odisha, India. Int J Geomatics Geosci 5(2):253

Darji K, Khokhani V, Prakash I, Mehmood K, Pham BT, Final ME (2019) Rainfall-runoff modelling using HECHMS model: an application of regression analysis. J Emerg Technol Innov Res JETIR 6:10

Derdour A, Bouanani A, Babahamed K (2018) Modelling rainfall runoff relations using HEC-HMS in a semi-arid region: case study in Ain Sefra watershed, Ksour Mountains (SW Algeria). J Water Land Dev 36(1):45–55. https://doi.org/10.2478/jwld-2018-0005

Giuli D, Baldini L, Facheris L (1994) Simulation and modeling of rainfall radar measurements for hydrological applications. In: Recent studies in geophysical hazards. Springer, Dordrecht, pp 109–122

Gumindoga W, Rwasoka DT, Nhapi I, Dube T (2017) Ungauged runoff simulation in Upper Manyame Catchment, Zimbabwe: Application of the HEC-HMS model. Phys Chem Earth A/B/C 100:371–382

Haibo M, Xin D, Wenjuan C (2018) Application of synthetic unit hydrograph on HEC-HMS model for flood forecasting. In: MATEC web of conferences, vol 246. EDP Sciences, p 01076

Halwatura D, Najim MMM (2013) Application of the HEC-HMS model for runoff simulation in a tropical catchment. Environ Model Softw 46:155–162

Haque S, Islam AKMS, Islam GT, Salehin M, Khan MJU (2017) Event based flash flood simulation at Sunamganj using HEC-HMS. In: 6th international conference on water & flood management (ICWFM-2017)

Ibrahim-Bathis K, Ahmed SA (2016) Rainfall-runoff modelling of Doddahalla watershed—an application of HEC-HMS and SCN-CN in ungauged agricultural watershed. Arab J Geosci 9(3):170

Joo J, Kjeldsen T, Kim HJ, Lee H (2014) A comparison of two event-based flood models (ReFH-rainfall runoff model and HEC-HMS) at two Korean catchments, Bukil and Jeungpyeong. KSCE J Civ Eng 18(1):330–343. https://doi.org/10.1007/s12205-013-0348-3

Khaleghi S, Mahmoodi M, Karimzadeh S (2015) Integrated application of HEC-RAS and GIS and RS for flood risk assessment in Lighvan Chai River. Int J Eng Sci Invent 4(4):38–45

Komolafe AA (2021) Integrated methodology for urban flood inundation modeling: a case study of Ichinomiya River Basin, Japan. Model Earth Syst Environ. https://doi.org/10.1007/s40808-021-01204-6

Kumar V, Sen S, Chauhan P (2021) Geo-morphometric prioritization of Aglar micro watershed in Lesser Himalaya using GIS approach. Model Earth Syst Environ 7:1269–1279. https://doi.org/10.1007/s40808-020-01000-8

Latif MZA (2018) Simulation of flood event in Kelantan on December 2014 as revealed by the HEC-HMS. J Civil Eng Forum 4(3):215–222. https://doi.org/10.22146/jcef.34020

Makkena J (2016) Modelling the hydrology of watershed by using HEC-HMS. Doctoral dissertation, Kelappaji College of Agricultural Engineering and Technology, Tavanur

Mandal SP, Chakrabarty A (2016) Flash flood risk assessment for upper Teesta River basin: using the hydrological modeling system (HEC-HMS) software. Model Earth Syst Environ 2(2):59

Martin O, Rugumayo A, Ovcharovichova J (2012) Application of HEC HMS/RAS and GIS tools in flood modeling: a case study for river Sironko–Uganda. Global J Eng Design Technol 1(2):19–31

Masseroni D, Cislaghi A, Camici S, Massari C, Brocca L (2017) A reliable rainfall–runoff model for flood forecasting: review and application to a semi-urbanized watershed at high flood risk in Italy. Hydrol Res 48(3):726–740

Meresa H (2019) Modelling of river flow in ungauged catchment using remote sensing data: application of the empirical (SCS-CN), Artificial Neural Network (ANN) and Hydrological Model (HEC-HMS). Model Earth Syst Environ 5:257–273. https://doi.org/10.1007/s40808-018-0532-z

Mistry A, Lodha PP, Prakash I, Mehmood K (2017) Estimation of direct runoff for purna river sub-basin, using SCS-CN method, Dangs District, Gujarat. Development 4(4)

Mokhtari EH, Remini B, Hamoudi SA (2016) Modelling of the rain–flow by hydrological modelling software system HEC-HMS–watershed's case of wadi Cheliff-Ghrib, Algeria. J Water Land Dev 30(1):87–100

Natarajan S, Radhakrishnan N (2019) Simulation of extreme event-based rainfall–runoff process of an urban catchment area using HEC-HMS. Model Earth Syst Environ 5:1867–1881. https://doi.org/10.1007/s40808-019-00644-5

Nimkar AM, Deshpande SB, Babrekar PG (1992) Evaluation of salinity problem in swell-shrink soils of a part of the Purna Valley, Maharashtra. Agropedology 2:59–65

Rathore R, Kumar V, Ranjan A, Tiwari S, Goswami A, Agwan M (2018) Extraction of watershed characteristics using GIS and digital elevation model. IJRESM 1:62–65

Samanta RK, Bhunia GS, Shit PK, Pourghasemi HR (2018) Flood susceptibility mapping using geospatial frequency ratio technique: a case study of Subarnarekha River Basin, India. Model Earth Syst Environ 4(1):395–408

Chapter 8
Anthropogenic Factors Change the Ecological Condition of Wetlands in the Southern Kerala Districts in India

P. S. Amritha and K. Varunprasath

Abstract The Indian subcontinent has a vast mix of freshwater, saline, and marine wetlands. Wetlands in the Southern Kerala district (SKD) have a great natural wetlands ecosystem, but it is not well detailed. The present study investigates the anthropogenic factors that shift the ecological status (ES) of wetlands in the SKD because few surveys have been carried out. Seventy-five chosen wetlands were surveyed by a range of methods at five different districts, namely Alappuzha, Ernakulam, Kottayam, Thrissur, and Palakkad districts. Results revealed that most were hydrologically isolated wetlands, and a few were semi-parched in the summer. Dominant forms of wetlands were five acres in size. The human disturbance scores (HDS) showed that the Alappuzha district wetlands was high impacted (HI), the Palakkad district wetlands was mid impacted (MI), and the rest of the district wetlands were in the least impacted (LI) category. Overall, the population around the wetland habitat indicated 500 individuals were common in all wetlands. The Pearson correlation results revealed a statistically significant, positive interaction between the wetland habitat population and the HDS scores noted in riverine wetlands ($n = 48$), ($r = 0.058$, $p <= 0.687$) and palustrine wetlands ($n = 13$), ($r = 0.817$, $p > 0.000$). Also, the correlation test was not significant in Lacustrine wetlands ($n = 8$), ($r = -0.21$, $p < .954$). However, anthropogenic activities caused the all the wetland degradation. The factor-wise degradation of wetlands differs among the districts. The results propose fundamental details on the anthropogenic factors that impact the ecological status of wetlands in SKD, which will aid the extent of regional strategies for wetlands management.

Keywords Ecosystem service · Biodiversity · RAMSAR · Southern Kerala · Wetlands · Fish farming

P. S. Amritha · K. Varunprasath (✉)
Department of Zoology, PSG College of Arts and Science, Coimbatore, Tamil Nadu, India
e-mail: varunprasath@psgcas.ac.in

Introduction

Wetlands are vital for human survival. Wetlands cover 12.1 million km^2 of total area and account for 40.6% of the overall global ecosystem services rate (Costanza et al. 2014; Ramsar Convention on Wetlands 2018). In the past 150 years, over half of the global wetlands have been modified or degraded due to human activities (Sica et al. 2016), more than 50% of the world's wetlands have been lost (Davidson 2018). In general, 1052 sites in Europe, 289 sites in Asia, 359 sites in Africa, 175 sites in South America, 211 sites in North America, and 79 sites in the Oceania sites are identified as Ramsar sites or wetlands of International importance (RAMSAR 2013). The wetlands are also extremely prime areas throughout the world for wildlife protection, recreation, sediment control, and flood prevention (Nitin Bassi et al. 2014). Despite their importance to human societies, wetlands are rapidly being degraded and destroyed (Zedler and Kercher 2005). Wetlands are acknowledged as equally crucial for ES release (Mitsch and Gossilink 2000; Rebelo et al. 2017; Zhang et al. 2017; Sieben et al. 2018) and notably affected by a range of human actions (Ramsar Convention Secretariat 2006; Zhang et al. 2017; Tong et al. 2017; Best 2019; Sieben et al. 2018). Despite the ecosystem functions and supplies of human livelihoods, 30–90% of the wetlands of the world are strongly customized or have vanished (Reis et al. 2017), and several remain threatened and ruined because of high population pressure and urbanization (Bassi et al. 2014). Anthropogenic influences, such as agricultural and industrial activities, urbanization, and over-exploitation of water resources, have had a negative impact on wetlands (Sajinkumar et al. 2017). Ecosystem functions refer varyingly to the habitat, physical and biological benefits, and ecosystem processes (Costanza and Folke 1997). India has a diversified wetland ecosystem that maintains distinct habitats.

The wetlands provide various ecological supplies and services, but they are exposed to immense pressure because of human actions and the shrinkage of their original extent and decline in the hydrological, economic, and ecological functions they perform (Nitin Bassi et al. 2014). In India, initial attempts to prepare a wetland inventory were made between the 1980s and early 1990s. The largest area of Wetlands exists in Kerala State (Nayar and Nayar 1997). Kerala state contains 35,892 private ponds, 6820 Panchayat ponds, 3357 public ponds, 2634 holy ponds and streams, 904 quarry ponds, and 838 irrigation tanks (Pan Fish Book 2002). Also in Kerala state, a few wetlands of International and National importance exist, including Vembanad Kole, Ashtamudi, and Sasthamkotta Lake, which are Ramsar sites (Kokkal et al. 2007). In addition, Kotpuli and Kadalundi in Kozhikode and Malappuram districts were approved by the Ministry of Environment and Forests, Government of India, under National Wetland Conservation Programme. In Kerala state, various authors have recorded wetlands studies (Michael Sinclair et al. 2019, 2020).

The outcomes of ecosystem service estimation has been used to deal with environmental issues and guide decision-making (Burkhard et al. 2012). The present

study aims to evaluate the anthropogenic factors that shift the ecological status (ES) of wetlands in the five districts of SKD. The Specific objectives include:

1. To review the ecological condition of wetlands in association with anthropogenic disturbance.
2. To determine the correlation of wetland habitat population status with the degradation factors derived from the five districts of wetlands in SKD.

Study Area

Kerala state is on the southern Malabar Coast of India, also known as God's own country. Kerala state is also bordered by Karnataka state to the north, east and south by Tamil Nadu, and western by the Lakshadweep Sea. Our study area mainly focuses on the five southern districts of Kerala, namely Alappuzha, Kottayam, Ernakulam, Thrissur, and Palakkad. The Alappuzha district is in the southern state and bounded on the northeast by Ernakulam and Kottayam districts, on the east by Pathanamthitta, the southeast by Kollam, and west by the Arabian Sea. The Kottayam district is in central Kerala state, bordered on the north by Ernakulam, east by Idukki, to the south of Alappuzha and Pathanamthitta districts. In addition, the Ernakulam district includes the biggest metropolitan area of the Kerala state. Ernakulam is bordered by Thrissur in the north, the Idukki district in the east, the Arabian Sea in the west, and Alappuzha and Kottayam districts in the south. Also, the central region of Kerala State is the Thrissur district, which is bounded on the north by Malappuram and Palakkad districts, south by Idukki and Ernakulam districts, east by the Palakkad district and the Coimbatore district of Tamil Nadu state, on the west by Lakshadweep Sea. In addition, Palakkad is usually called the Gateway of Kerala, which is surrounded in the north by the Malappuram district, east by the Coimbatore district of Tamil Nadu, south by the Thrissur district, and in the west are Thrissur and Malappuram districts (Fig. 8.1). We used the Mapitute Version 2020 software to create Landsat satellite images of study areas. The images were collected based on quality and clarity (less than 20% of cloud cover) during the period of 18/11/2020, and also used India Vavteq2012 for their image type. The mapping ratio is 1:1,313,972.

Data Sources and Methods

The wetland survey and the questionnaire interviews were conducted from June 2019 to April 2020 in the society existing within a 1 km radius of each wetland. Collected water samples from all wetlands were kept inside polythene bottles until water quality analysis was performed in the laboratory using the standard method (APHA 1985).

(a)
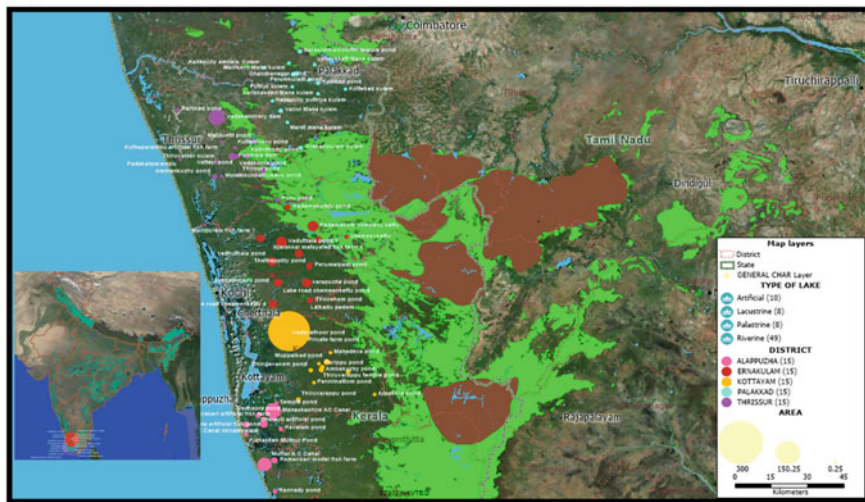
(b)
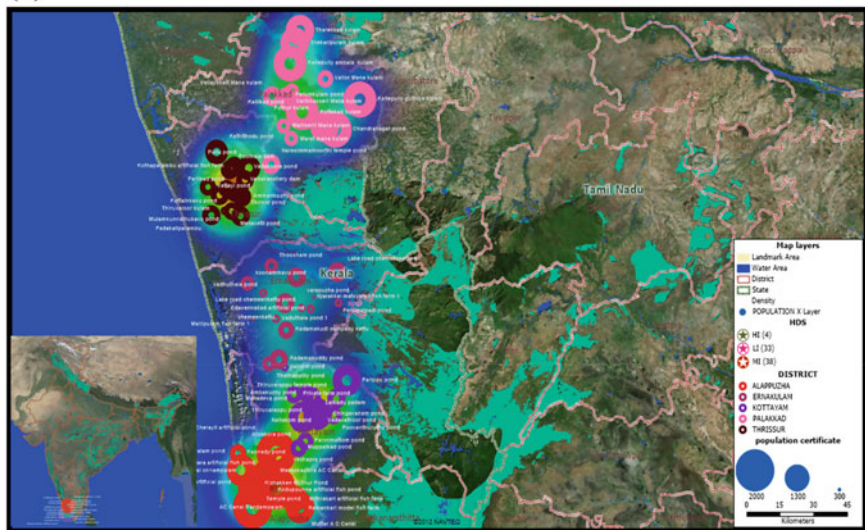
Fig. 8.1 (**a**) Satellite image of surveyed wetlands in SKD. (**b**) Wetlands habitat population density image of surveyed wetlands in SKD

Human Disturbance Score

Wetlands ecological and biological conditions were calculated by a variety of techniques (interviews, ecosystem services (ES), human disturbance (HD), and physical characteristics). Wetlands were further graded and categorized into low,

middle, and high impact for the human disturbance. The physical characteristics of water are determined by measuring the water standard and the ecological status of the wetlands. The extent of human disturbance to the wetlands had been considered using the human disturbance score (HDS) protocol method (Gernes and Helgen 2002). Ecosystem services (ES) or benefits gained from each wetland were accredited and evaluated using data from the original cluster interviews. A field study was conducted to determine the interference of wetlands from the ground, ecosystem services, and physical status of the wetlands. The gathered data brought together various quantifiable factors to compute the human disturbance factor.

Factor 1: Crucial zone—Disturbance inside 50 from the margin of wetlands 0–18 points
Factor 2: Buffer zone—Disturbance inside 500 from the margin of wetlands 0–18 points
Factor 3: Habitat alteration—Disturbance within 50 from the edge of wetlands 0–18 points
Factor 4: Hydrological alteration—Disturbance within 50 from the edge of wetlands 0–21 points
Factor 5: Chemical pollution—Disturbance within 50 from the edge of wetlands 0–21 points
Factor 6: Presence or absence of fish yield 0–4 points

Full enumeration was used to gather data on wetland kind, hydrological conditions, land use patterns, ecological state, and habitat assessment. Finally, each factor was valued and classified (scored) in one of four categories ranging from best to poor as stated previously. All scored values from each factor concluded for each study wetland to gain their human disturbance gradient score (HD) out of 100%. If the categorical range of HD of a wetland value falls within the ranges of 0–33, 33–67, and 67–100 (Gernes and Helgen 2002), it can be ranked as least impacted, mid impacted, and most or highly impacted, accordingly. The respondents were requested to value the ES quoted for each wetland using terms of relative importance, particularly socioeconomic characteristics, wetland importance, and management aspects.

Wetlands Ecosystem Services

Key Informant Interviews

Representatives of the government agencies, NGOs, research institutes, and researchers exchanged views for an inventory of ecosystem services of the wetlands before the survey. The vital points asked during interviews concentrated on subsistence strategies and drivers of modification in the wetland ecosystem. A sum of 15 representatives from diverse organizations consulted as vital informants during the study to help us realize the patterns of change and the drivers. Criteria used to

choose the crucial informants was their acquaintance with the wetland resources and people's reliance and commitment in the wetland's operation.

Data Analysis

The quantitative statistics were evaluated using frequency analysis from the Statistical Package for Social Sciences (SPSS) 25th Version computer software program, and bird diversity was measured by the Shannon index method. To determine regional individuals' reliance and the impacts of various drivers on the wetland ecosystem, qualitative statistics derived from interviews were first coded and classified into themes under the research points, and the same coded themes were grouped. The ecosystem service grading executed participatory tools. Participants in focus group discussions had sought to detect critical ecosystems available from the wetlands. After listed key ecosystem services, the participants were asked to grade the listed ecosystem services on a scale of 1 to 10 (1 with the least preference and 10 with the highest). The overall ranking was based on the total marks for each ecosystem service separated by the number of respondents. Likewise, drivers of ecosystem alteration defined via both qualitative analyses (focus group discussion) were also obtained from household questionnaires.

Results

The questionnaire survey was completed by 375 respondents. The mean respondent's age was 46 years for males and 44 years for females. The respondent's occupations included farming (45%), daily laborers (37%), and others (18%), and the average mean of respondents' age, total number, and occupations are reported (Table 8.1).

In SKD, out of 75 wetlands, each district had 15 wetlands selected for this study (Attached with Supplementary file). The selected wetlands were chosen because of easy accessibility and availability; maximum wetlands in the different districts, an altitude range below 100 feet, except for the Palakkad district. In the Alappuzha district alone, four wetlands, such as Manackachira AC Canal and Muttar AC Canal, were the biggest, and the rest of the wetlands were less than 50 acres in size.

Physical Characteristics of Wetlands in the SKD

The analyzed wetlands were grouped by physical characteristics into seven parameters for a better understanding of wetlands in SKD. In all the districts, the temperature ranged from 23 to 29 °C. In SKD, physically, there are differences among the

Table 8.1 Description of survey respondents in the southern Kerala districts

	Alappuzha district N = 75	Ernakulam district N = 75	Kottayam district N = 75	Palakkad district N = 75	Thrissur district N = 75	Total respondents N = 375 (%)
Male age	41 years	44 years	42 years	54 years	50 years	46%
Female age	35 years	37 years	38 years	50 years	55 years	44%
Female respondent	43	40	39	48	45	57%
Male respondent	32	35	36	27	30	43%
Occupation						
Farming	31	30	36	37	33	45%
Daily laborers	26	31	28	29	27	37%
Others	18	14	11	9	15	18%

wetland structures that were noted. Overall, n = 65 (86.7%) wetlands were colorless and n = 10 (13.3%) were green. The largest size of wetlands were in the Alappuzha district (Manackachira AC Canal, Muttar AC Canal, AC Canal Randampalam, and AC Canal Onnampalam wetlands) and the average mean values of size and depth of each district wetland is mentioned in Table 8.2. According to the RAMSAR category, the wetlands in the SKD were divided into five major types: marine, estuarine, lacustrine, palustrine, and riverine. In addition, many artificial wetlands seed to culturing species (shrimp/fish/prawn farms). In SKD, the riverine wetlands were common, which comprises 50 wetlands (67%), 15 (20%) palustrine types, and ten wetlands (13%) are lacustrine type, which were present in the Ernakulam district. Man-made (artificial) wetlands mostly in the Palakkad district became famous for the fish and prawn culture in this area. According to the area size, wetlands were classified into three types. Forty-one wetlands (55%) were less than 5 acres in size and 30 wetlands (40%) were 6–50 acres. The remaining wetlands were more than 51 acres, comprises four wetlands (5%), namely Manackachira AC Canal, Muttar AC Canal, AC Canal Randampalam, and AC Canal Onnampalam, Laikadupadam, and Pullutchemeenkettu wetlands. Of the wetlands, 56% have a depth of less than 5 feet, 43% were 6–20 feet depth, and 1% were more than 20 feet such as a Kotharaparambu fish farm, which was an artificial wetland. The chief origins of the water to the wetlands were rainfall, river water, and drainage or the canal system. In the SKD, 68% of wetlands received water from rivers, 21% of the wetlands depend on precipitation, and 11% of wetlands received water from the drain or the canals. In Kerala wetlands, (99%) of the wetlands were seldom dried out because of they always filled with water either as rainfall or the canal water supply, except for one wetland (LaikaduPadam) that dried out occasionally during the summer.

Table 8.2 Average mean water quality parameters of wetlands in SKD

District	Alappuzha	Ernakulam	Kottayam	Palakkad	Thrissur
Temperature (C°)	27.13 ± 1.72	27.49 ± 0.933	27.27 ± 1.83	24.07 ± 4.02	29.91 ± 0.758
Turbidity (NTU)	7.69 ± 2.71	10.79 ± 0.307	74.838 ± 63.47	100.30 ± 10.0	8.10 ± 0.27
Ph (Ph meter)	6.79 ± 0.57	7.46 ± 0.324	8.35 ± 12.07	7.13 ± 0.29	5.97 ± 0.34
Electrical conductivity (μS/cm)	288.20 ± 19.14	263.20 ± 167.03	239.40 ± 110.06	487.03 ± 11.4	786.40 ± 33.74
Total solids (Mg/l)	1868.66 ± 73.97	2181.93 ± 47.40	156.06 ± 54.97	605.16 ± 18.5	696.60 ± 31.64
BOD ((Mg/l)	24.41 ± 13.32	6.53 ± 1.68	1.15 ± 0.94	1.47 ± 0.33	17.33 ± 1.29
DO (Mg/l)	3.63 ± 0.163	5.53 ± 1.125	3.38 ± 0.20	16.55 ± 9.37	4.02 ± 0.39
Average area (Acres)	16.3 ± 27.3	25.8 ± 15.2	19.1 ± 72.2	25 ± 3.9	11.3 ± 22.9
Average depth (feet)	2.3 ± 1.0	2.4 ± 0.4	1.8 ± 0.3	2.2 ± 1.6	2.4 ± 2.7
Altitude (meter)	35.7 ± 0.5	10.3 ± 0.3	88.9 ± 0.3	255.3 ± 1.7	67.3 ± 1.9

Water Quality of Wetlands in SKD

There was minimal difference in temperature, and pH between the different wetlands was recorded. Their respective district average values of the wetlands is mentioned in Table 8.2. The turbidity of water was more or less the same, but in Palakkad and Kottayam district, the values were slightly higher. The electrical conductivity (EC) in Thrissur and Palakkad districts was much higher but within the permissible limit. Total solids (TS) were in different parameters in each district wetland. The biological oxygen demand (BOD) and dissolved oxygen (DO) in the wetlands was within the control limits of the World Health Organization (WHO) or the American Public Health Association (APHA) standard level. The total solids were the highest in the Ernakulam district, followed by Alappuzha, and least in the Kottayam district (Table 8.2).

Ecological Status of Wetlands in the SKD

Buffer landscape was degraded the highest in the Alappuzha district, specifically damaging the wildlife habitat ($n = 10$, AM: 4.0, SD: 2.92). Most of the wetlands were under protection by either fencing or shoreline protection methods; highest in the Palakkad district ($n = 12$, AM: 4.8, SD: 2.48). Infrastructure development and sewage mixing into the wetland habitat was observed in the Alappuzha district (4=4, AM: 1.60, SD: 2.74). Around the wetland habitat, tree cutting in the SKD was not noted.

Figure 8.2 represents the comparison of the buffer zone and the landscape alteration of the SKD, and the results show that the disturbance score in the buffer
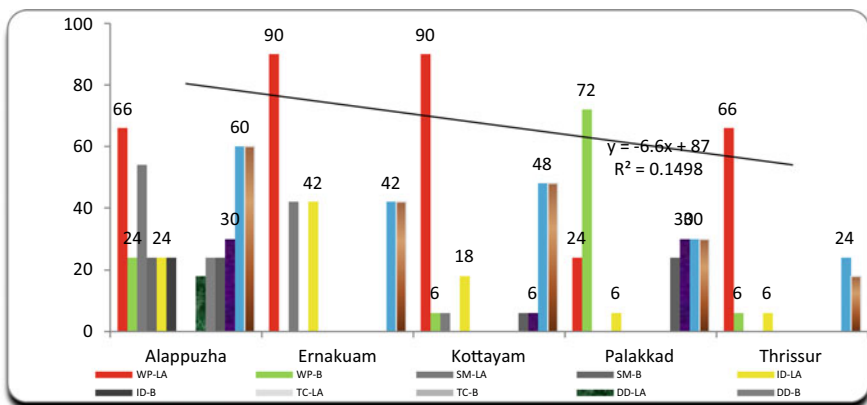
Fig. 8.2 Average mean buffer zone and landscape disturbance of wetlands in SKD
Abbreviations used: *WP* wetland protection, *SM* sewage mixing, *ID* infrastructure development, *DD* dumping debris, *CG* cattle grazing, *WH* wildlife habitat, *LA* landscape, *B* buffer zone

zone was high when compared to landscape degradation. Landscape disturbance was the highest in the Alappuzha district and wildlife habitat alteration ($n = 10$, AM: 4.0, SD: 2.92). Except for Thrissur wetlands, the infrastructure development, including constructing a commercial or residential building or road construction, was present in the remaining SKD wetlands and the maximum quantity was recorded in the Ernakulam ($n = 7$, AM: 2.8, SD: 3.09) district. Wetlands were protected by fence lines around the border, but in the landscape zone, almost all SKD wetlands were out of wetland protection, with the highest noted in the Ernakulam district ($n = 15$, AM: 6.0, SD: 0.0). Dumping of debris and sewage mixing was a major type of degradation of the wetlands in SKD. Tree cutting around the wetland habitats was not observed in the entire SKD, even in the landscape habitat. Habitat alteration was highest in the Palakkad district ($n = 13$, AM: 5.2, SD: 2.1) brought about by the developmental activities such as offices for either private or government buildings occupied in and around the wetland areas. Transportation by boat is causing the second-highest alteration of habitat recorded in the Alappuzha, Ernakulam, and Thrissur districts.

Development of roads nearby the wetland habitat was present throughout the entire SKD. The hydrology disturbances, such as water channelization, were recorded and highest in the Alappuzha district ($n = 14$, AM: 6.5, SD: 1.80). Except for the Palakkad district, there was water flooding recorded in the remaining wetlands and the highest in the Alappuzha and Ernakulam district ($N = 15$, AM: 7.0, SD.1.20). The wetlands water withdrawals were observed in the Palakkad district. The sewage and drainage discharge ($n = 4$, AM1.87, SD; 3.20) was the highest in the Alappuzha district. Infrastructural activities and municipal waste were a vital concern in most of the wetlands in the SKD, specifically in the Alappuzha district. Overall the chemical pollutant disturbance was highest in the Alappuzha district. Household, municipal waste discharge, demolition of debris, and sewage outflow were the simple mode of pollution into the wetlands in the SKD. Except for the Kottayam district, few wetlands had odors in nature. Watercolor changes were highest recorded in (5.1) the Palakkad district. Waterbirds are a vital component of most of the wetland ecosystems as they occupy several tropic levels in the food web of wetlands. The present study recorded 22 bird species in and around the wetland habitat. In SKD, according to the Shannon Weiner index (H) results, the highest number were observed in the Ernakulam district (1.7427) followed by Palakkad (1.6923), Kottayam (1.6751), Alappuzha (1.6686), and Thrissur (1.5040) during the study period.

All the HDS results (Fig. 8.3) were within the Potential range of (0–100). The wetlands impact score was significantly different among the districts in the SKD. Overall, high impact (HI) on human disturbance scores registered in the Alappuzha district (72) were due to buffer zone disturbance and the hydrology alteration. The one-way ANOVA results in the Alappuzha district showed that (df (2, 2), F = 1.386, $P < .419$) the impact score of the district wetlands was not significant . In the Palakkad district, HDS scores (40) fell under the mid impact (MI) category mainly
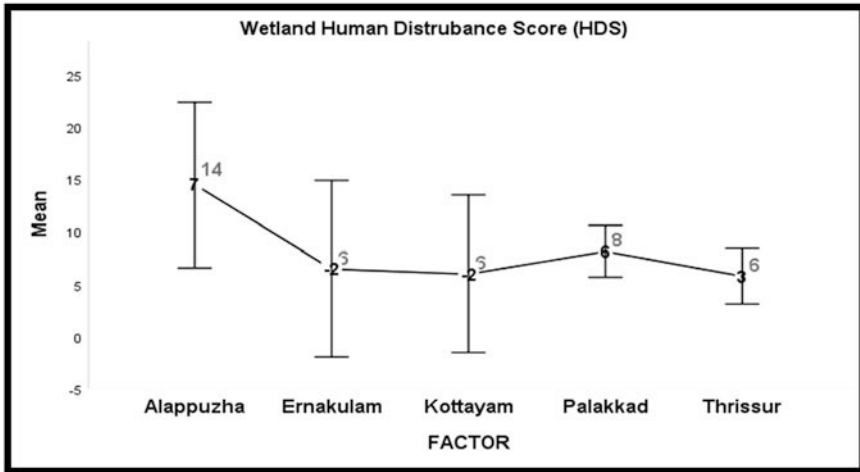
Fig. 8.3 Human distribution value the wetlands of SKD

because of habitat and hydrology alterations, and statistically (df (2,2), $F = 0.459$, $P < .685$) the impact score of the wetlands was not significant. The remaining districts, namely Ernakulam, Kottayam, and Thrissur districts, were in the least impacted (LI) category of wetlands. In the Ernakulam district, the HDS score (24) was caused by the alteration of landscape and hydrology, and the statistical results were not significant (df (212), $F = 0.261$, $P < .811$) with impact score. In the Thrissur district, the HDS score (26.2) was because of hydrology alteration and chemical pollutant and was statistically not significant (df (2,2), $F = 6.585$, $P < 132$). In the Kottayam district (df (2,2), $F = 0.941$, $P < .515$) wetlands were not statistically significant with the impact score.

We give the overall wetlands HDS scores in Fig. 8.4a. Among the different wetlands, the Pearson correlation results showed a statistically significant, positive correlation between the population around the wetlands habitat, and the riverine wetlands Human Disturbance Scores were $n = 48$, $r = 0.058$, $p <= 0.687$. Also, population status around the wetlands explained 0.3% of the variation in the riverine wetlands HDS scores observed (Fig. 8.4b). The Pearson correlation results were statistically significant, showing a strong positive correlation between the population around the wetlands habitat, and the HDS scores of palustrine wetlands were $n = 13$, $r = 0.817$, $p > 0.000$. The population status explains 66% of the variation in the palustrine wetlands HDS scores (Fig. 8.4c). The Pearson correlation results were statistically not significant, showing a strong negative relation between the population around the wetlands habitat, and the HDS scores of lacustrine wetlands were $n = 8$, $r = -0.021$, $p < .954$. The population status around the wetland habitat explains 91% of the variation in the lacustrine wetlands HDS scores (Fig. 8.4d).
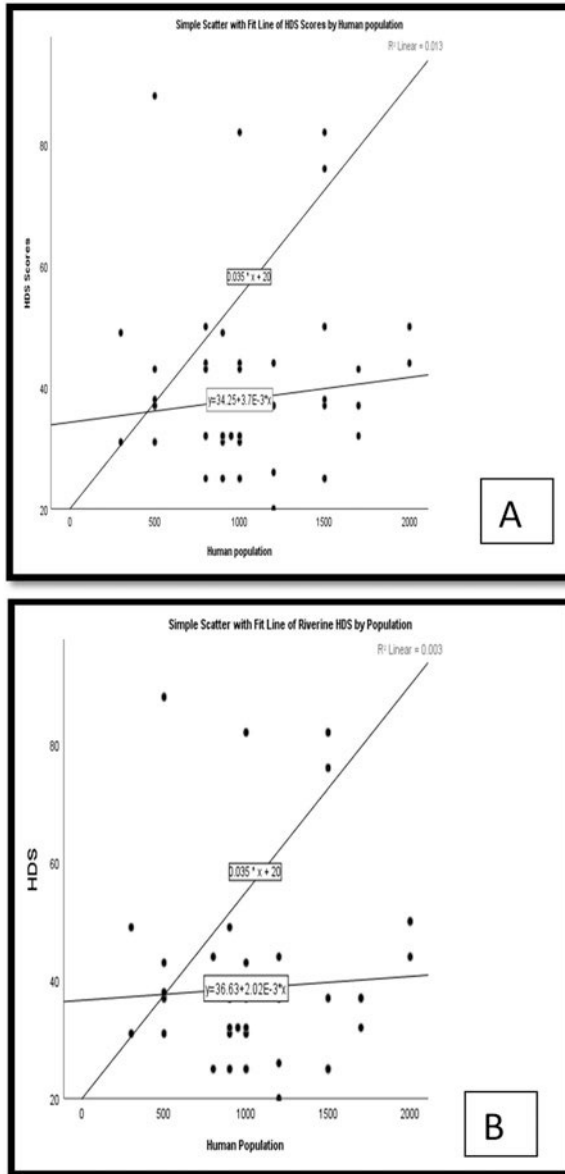
Fig. 8.4 Human disturbance scores (HDS) of wetlands in SKD
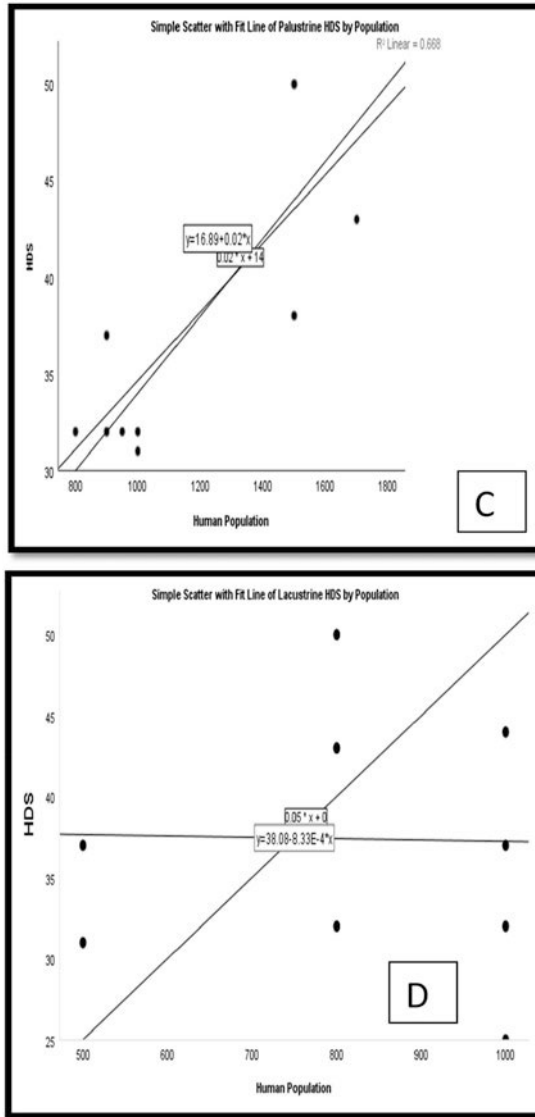
A. Overall HDS of wetlands   B. Riverine wetlands
C. Palustrine wetlands   D. Lacustrine wetlands

Fig. 8.4 (continued)

Discussion

Water temperature is an important water quality parameter, and wetlands will naturally show temperature changes seasonally. The temperature variations in the wetlands had been noticed as 23–29 °C during summer because of the open nature of the wetland site and hot summer climate. In SKD, 10 wetlands were green because of water-rich phytoplankton, algal growth; organic pollution and erosion usually appear green. In SKD, 65% of wetlands are riverine in nature because the Western Ghats (WG) receives rainfall from southwest monsoon and northeast monsoon resulting in almost water-logged surroundings in approximately 20% of the entire geographic area of the state. The artificial wetlands or man-made wetlands occur mostly in the Palakkad district, and they are famous because of the fish and prawn culture in this district. Small wetlands can deliver the service of water purification (Blackwell and Maltby 2003), and our study indicated that 65% of the wetlands of smaller size provided water purification. The wetland depth was based on wetland types, locations, and hydrology. We recorded that 77% of the wetlands were 6–20 feet deep in SKD. Our study supported that 99% of the wetlands had water stagnant throughout the year because wetlands had filled with water from rainfall or the canal water supply. Suspended matter such as clay, silt, organic and inorganic matter, plankton, and other microorganisms also contributes to the turbidity of water, and our results showed that turbidity of water was more or less the same in SKD districts. The EC in Thrissur and Palakkad districts was higher but within the permissible limit. Total solids (TS) were different in each area. The Ph, BOD, and DO in wetlands were shown within the control limits by World Health Organization (WHO) or the American Public Health Association (APHA) standard level.

Wetlands buffer landscape was degraded in the Alappuzha district chiefly wildlife habitat because of agricultural activities, cattle rearing, building infrastructure, and alteration of natural habitat. In SKD, cattle grazing on wetlands is related to vegetation alteration, affects nesting sites for birds, and changes the water quality, as noted in the Palakkad and Alappuzha districts. Fencing around the wetlands reduces the anthropogenic activities both as protection for wildlife habitat or nesting sites for birds, and avoiding cattle grazing will reduce the water quality alteration. In SKD, except for the Ernakulam district, the remaining wetlands had either fencing or shoreline protection even up to the wetland core zone level, but the impact of anthropogenic activities gradually increases from the core area due to the lack of fencing. Our study noticed that debris dumping around the wetland habitat recorded in the Alappuzha district affects the overall health of the wetland ecosystem. Except for coastline manipulation in the Alappuzha district, almost all human development such as shopping centers, highways, suburban developments, and coastline manipulation, causes a loss of wetlands. The landscape disturbance degraded the wildlife habitat for the entire SKD, but the highest disturbances were noted in the Alappuzha district because of infrastructure development despite that constructing commercial buildings or residential buildings and roads were present in the entire district, except for Thrissur district. The absence of wetland protection in the landscape zone was

observed in all districts because of a lack of management activities. Also, in the landscape zone, cattle grazing was common in most of the SKD. Anthropogenic litter represents another significant threat to urban ecosystems, especially with growing consumption patterns of a larger middle class (Hoellein et al. 2014), and this resulted in dumping of debris and sewage mixing noted in some wetlands in the SKD.

Habitat alteration of the wetlands was highest in the Palakkad district because of developmental activities such as offices in either private or government buildings occupied in or around the wetlands areas. Tourism and recreational activities can also affect wetlands. Our study showed that boating and tourism are famous in Kerala, and they impacted wetlands habitat alteration noted the highest in the Alappuzha and Ernakulam districts. Buildings and roads near wetlands weaken the connectivity of urban wetlands (Hassall 2014) and our study supported that developments of roads near the wetland habitat showed that all SKD districts cause an increase in the anthropogenic activities around the wetland habitat. Also, except for the Ernakulam district, the remaining SKD districts were the educational institutions near the wetlands because of the urbanization development. Livestock grazing was common in all the districts because wetlands' adjacent areas provide excellent dry season foraging opportunities for grazers and irrigation. Nowadays, it is widely recognized that many of the world's wetlands have been placed under considerable stress through anthropogenic disturbance such as dumping debris in wetlands habitat, as recorded in the Alappuzha districts.

Except for the Palakkad district, the hydrology alteration was highest in the Alappuzha district (19.6) caused by the recorded water channelization. Wetland water withdrawals were noted in a few wetlands of the Palakkad district during the summer because of irrigation and household purposes. Also, sewage discharges were highest in the Alappuzha district, and even low-level pollution of these ecosystems can cause adverse effects to the ecology. Infrastructural activities and municipal waste were a vital concern in most of the wetlands, specifically the Alappuzha district. The chemical pollutants and sewage disposal were highest in the Alappuzha district and cause excessive macrophytic growth. In addition, in the Alappuzha district, waste debris had been dumped into the nearby wetlands habitat because of the lack of strict law and management. In the Palakkad district, water discoloration was most observed. Color is a vital factor for aquatic life for making food from sunrays and photosynthetic activity had reduced because of discoloration resulting from pollution in the water. The odor of water is caused by gases produced from the anaerobic decomposition of organic matter, and this was recorded the most in the Palakkad district. The Alappuzha district showed the highest impact of human disturbance score recorded, due to buffer zone alteration, landscape disturbance, habitat alteration, hydrology, and pollution aspects.

A mid impact was recorded in the Palakkad district, and the remaining districts were in least impacted wetlands category. Our study showed that the local communities living nearby wetlands have a high dependence on the ES supplied by wetlands. The vital sources of income as per the survey noted that fish rearing was the dominant source of income, followed by rearing prawns, tourism, spiritual

activity, farming, fruit cultivation, livestock rearing, seedling and vegetable cultivation, and wetland products. Currently, the number of livestock populations decreased because of the intensive practice of rice agriculture, and the amount of grazing land is reducing over time, and it influences forage cattle. Wetland water is used for irrigation and cultivation of crops during the summer because of the shortage of water supply from the dam. The wetlands were used for drinking purpose used in a few incidents because of the scarcity of water in the summer. Our study shows that the vegetables produced around wetland habitat are increasing due to demand–supply in the Kerala district. In very few areas, wetlands water for domestic usage was recorded. Wetlands play a significant role in the hydrological cycle, influencing groundwater, evaporation, water retention, and flood control and protection. The wetlands are becoming ever more significant as tourism destinations, educational, and research activities that will help to promote awareness of wetland conservation and management for future use. Spiritual activities are the highest in the Ernakulam district because of the many temples and are related to a pond. It is widely acknowledged that wetlands are vital for water storage and purification, carbon sequestration, and wildlife habitats, including for the 23 bird species were recorded.

Conclusion

For the first time we surveyed the 100 wetlands in five different districts of SKD by using the questionnaire method along with field visits. The wetlands were assessed by various ecological parameters. The scientific consideration of wetland services has exploded, but few studies have been conducted on wetland ES and ES for conservation and management. The ecological status of the Alappuzha district had the highest HDS score under the (HI) category, whereas Ernakulam district (MI) category. The wetland buffer zone alteration is the primary reason for wetland degradation all over the SKD. Wetlands provide 12 provisional services. Fish and prawn rearing was the vital source of livelihood income, and farmers used to rear within five acres in size. Most of the farmers are interested in the wetland conservation program. Wetland types and locations will be necessary to strengthen the basis for decision-making for conservation and management aspects. Apart from government regulation, an improved monitoring method is required to raise the awareness of the physical, chemical, and biological characteristics of the wetland assets. Also creating, awareness about wetlands will create a better understanding and management of wetlands. These characteristics are valuable and significant in preparing an inventory to reflect the present condition of the wetlands. The climate change effects show the need for a broad wetland study that could be used to build proper executive strategies. Research on status, distribution, number of wetlands, area size, landscape position, and the influence of neighboring anthropogenic activities provided fundamental knowledge of the wetlands. With this combined

information obtained on wetland operation, the vulnerability of wetlands can also be precisely assessed.

References

APHA (1985) Standard method for the examination of water and wastewater, 16th edn. American Public Health Association, Washington, DC

Bassi N, Kumar MD, Sharma A, Pardha-Saradhi P (2014) Status of wetlands in India: a review of extent, ecosystem benefits, threats and management. J Hydrol Reg Stud 2:1–19. https://doi.org/10.1016/j.ejrh.2014.07.001

Best J (2019) Anthropogenic stress on the world's big river. Nat Geosci 12:7–21

Blackwell M, Maltby E (2003) Environmental and economic assessment of the location of wetland buffers in the landscape for nutrient removal from agricultural runoff. In: Turner KE, van den Bergh JCJM, Brouwer R (eds) Managing wetlands: an ecological economics approach. Cheltenham

Burkhard B, Kroll F, Nedkov S, Müller F (2012) Mapping supply, demand and budgets of ecosystem services. Ecol Indic 21:17–29. https://doi.org/10.1016/j.ecolind.2011.06.019

Costanza R, Folke C (1997) Nature's services: societal dependence on natural ecosystems (Daily G, ed). pp 49–70

Costanza R, de Groot R, Sutton P, Ploeg S, Anderson SJ, Kubiszewski I, Farber S, Turner RK (2014) Changes in the global value of ecosystem services. Glob Environ Chang 26:152e158

Davidson N (2018) Wetland losses and the status of wetland-dependent species. In: The wetland book: II: distribution, description, and conservation, pp 369–381

Gernes MC, Helgen JC (2002) Indexes of Biological Integrity (IBI) for large depressional wetlands in Minnesota. Minnesota Pollution Control Agency, St. Paul

Hassall C (2014) The ecology and biodiversity of urban ponds. Wiley Interdiscip Rev 1:187–206

Hoellein T, Rojas M, Pink A, Gasior J, Kelly J (2014) Anthropogenic litter in urban freshwater ecosystems: distribution and microbial interactions. PLoS ONE 9(6):e98485. https://doi.org/10.1371/journal.pone.009848

Kokkal K, Harinarayanan P, Sabu KK (2007) Wetlands of Kerala. Proc Taal:1889–1893

Mitsch WJ, Gosselink JG (2000) The value of wetlands: importance of scale and landscape setting. Ecol Econ 35(1):25–33

Nayar S, Nayar NM (1997) Wetlands. In: Thampi KB, Nayar NM, Nayar CS (eds) The natural resources of Kerala. WWF State Office, Trivandrum

Panfish Book Master Panfish Book (2002) Department of Fisheries, Vikas Bhavan, Thiruvananthapuram

Ramsar Convention on Wetlands (2018) Global wetland outlook: state of the world's wetlands and their services to people. Ramsar Convention Secretariat, Gland

Ramsar Convention Secretariat (2006) The Ramsar Convention manual: a guide to the convention on wetlands, 4th edn. Ramsar Convention Secretariat, Gland

Ramsar Convention Secretariat (2013) The Ramsar Convention manual: a guide to the convention on wetlands (Ramsar, Iran, 1971), 6th edn. Gland

Rebelo AJ, Scheunders P, Esler KJ, Meire P (2017) Detecting mapping and classifying wetland fragments at a landscape scale. Rem Sens Appl Soc Environ 8:212e223

Reis V, Hermoso V, Hamilton SK, Ward D, Fluet-Chouinard E, Lehner B et al (2017) A global assessment of inland wetland conservation status. Bioscience 67:523–533. https://doi.org/10.1093/biosci/bix045

Sajinkumar KS, Revathy A, Rani VR (2017) Hydrogeochemistry and spatio-temporal changes of a tropical coastal wetland system: Veli-Akkulam Lake, Thiruvananthapuram, India. Appl Water Sci 7(3):1521–1534. https://doi.org/10.1007/s13201-015-0333-8

Sica YV, Quintana RD, Radeloff VC, Gavier-Pizarro GI (2016) Wetland loss due to land use change in the Lower Paraná River Delta, Argentina. Sci Total Environ 568:967–978

Sieben EJJ, Khubeka SP, Sithole S, Job NM, Kotze DC (2018) The classification of wetlands: integration of top-down and bottom-up approaches and their significance for ecosystem service determination. Wetl Ecol Manag 26:441–458

Sinclair M, Ghermandi A, Moses SA, Joseph S (2019) Recreation and environmental quality of tropical wetlands: a social media based spatial analysis. Tour Manag 71:179–186

Sinclair M, Ghermandi A, Moses SA, Joseph S (2020) Ecosystem service assessment and mapping for sustainable management of wetlands in Kerala, India. In: Environmental assessments. Edward Elgar Publishing

Tong Y et al (2017) Decline in Chinese lake phosphorus concentration accompanied by shift in sources since 2006. Nat Geosci 10:507–511

Zedler JB, Kercher S (2005) Wetland resources: status, trends, ecosystem services and restorability. Annu Rev Environ Resour 30:39–74. https://doi.org/10.1146/annurev.energy.30.050504.144248

Zhang Y et al (2017) Global loss of aquatic vegetation in lakes. Earth Sci Rev 173:259–265

Chapter 9
Design of Hydrologic Condition for Urban Storm Water Drainage Under Climate Change Impact

A. S. Pathan, A. P. Nilawar, M. L. Waikar, G. R. Gandhe, and S. D. Shinde

Abstract Strom water management under climatic vulnerability is becoming a significant concern in urban areas of the world. The analysis and design of an urban storm water drainage/channel/stream/nallah system under non-stationary extreme rainfall intensity is a challenging task in any area. Apart from this, more attention is required to develop possible methods and techniques for alternate design of storm drains in fast growing urbanization. This research describes a hydrological and hydraulic comparison between the Strom Water Management Model (SWMM) and Modified Rational Method (MRM) for design peak discharge and forecast peak flow estimation in a Mega Industrial Park (MIP) in Bidkin, Aurangabad, India. The Intergovernmental Panel on Climate Change (IPCC) CMIP5 models of Representative Concentration Pathways (RCP 2.6, RCP 4.5, RCP 6 and RCP 8.5) are used for the future climate change scenarios. Furthermore, the study is carried out over a 100 years return period in which period (1970–2015) is considered as a historical period and (2016–2057) and (2058–2100) as future periods. The results of this research indicate that the estimated highest annual peak discharge of the stream at catchment for historical time period and for two future time periods by the SWMM model are higher as compared with the MRM method. Overall results show that non-stationary extreme rainfall intensity and design peak discharge indicated an increasing scenario in the future periods, it will lead to challenges for simulation of peak flow and hydrologic design of urban drainage/channel/stream in the study area catchment.

Keywords Climate change impact · Extreme rainfall intensity · Hydrologic simulation · Mega industrial park · EPA- SWMM · MRM

A. S. Pathan (✉) · G. R. Gandhe · S. D. Shinde
Department of Civil Engineering, Deogiri Institute of Engineering and Management Studies, Aurangabad, Maharashtra, India

A. P. Nilawar · M. L. Waikar
Department of Civil Engineering, Shri Guru Gobind Shingji Institute of Engineering & Technology, Nanded, Maharashtra, India

Introduction

Climate change and urbanization are converging to challenge urban drainage infrastructure due to their adverse impacts on precipitation extremes and the environment of urban areas (Zhou 2014). More importantly, future drainage design needs to take the increased frequency and intensity of precipitation into account in order to design the system properly (Miller and Hess 2017). Urbanization leads to serious effects on the quantity and quality of urban runoff. In urban areas, natural streams have changed in the artificial drainage network (Antrop 2004; Haase 2014; Agilan and Umamahesh 2015) and the natural and rural area has changed to impervious surfaces. Moreover, the volume and peak flow/discharge of channel/stream water should increase. The increased volume and peak flow of storm water discharges may cause problems, such as flooding and erosion (Dietz and Clausen 2008; Schoonover et al. 2006; Wang 2005). Determination of peak flow and volume of runoff is of prime importance in order to estimate the flood magnitude, and thus design urban runoff management systems in urban watersheds (Walega et al. 2020). The SWMM is widely used in simulating stream flow, peak flow, and base flow from an urban watershed because it is capable of simulating conveyance systems (NayebYazdi et al. 2019). The SWMM is an effective tool for urban flood estimation in a semi-arid area (Rabori and Ghazavi 2018; Alam et al. 2014; Barco et al. 2008).The SWMM (Huber and Dickinson 1988) is one of the urban watershed models that is effective in simulating the rainfall–runoff process for urban storm water. (Vallecillo et al. 2019).

The main challenge in the assessment of climate change impacts on the estimation of extreme rainfalls (ERs) for urban drainage systems design is how to establish the linkages between the climate projections given by Global Climate Models (GCMs) at global scales and the observed extreme rainfalls at a given local site (Nguyen and Nguyen 2020).The present approach of design standards of urban drainage/channel/stream/nallah systems which are based on the historic climate information only, but under changing climate and non-stationary extreme rainfall intensity hydrologic engineers, planners and various stakeholders need to understand the possible effects for developing suitable management decisions for the future. Possible changes may demand new regulations, guidelines for storm water management studies, revision and update of design practices and standards of current infrastructure or even developing additional ones (Nirupama and Simonovic 2007).

Still analysis and design of an urban storm water drainage/channel/stream/nallah system under stationary, non-stationary extreme rainfall intensity, impact of climate change on rainfall IDF curves are great challenges facing hydrologic engineers, planners and designers of drainage systems, consultants and various stakeholders across the world (Mamo 2015). Apart from this, more attention is required to develop possible methods and techniques for alternate design of storm drains in fast growing urbanization (Yazdanfar and Sharma 2015). If the system is designed without considering these effects, there is a possibility that design of drainage systems is either over-designing or under-designing or fails more frequently, then such a system will cause economy losses (Wang et al. 2011).Therefore, storm water

drainage/channel/stream/nallah systems are required to be planned and designed by considering various design principles, operation, maintenance and economics (Mailhot and Duchesne 2010a, b). Also, continuously developing urban area, which have significantly changed the catchment hydrological and hydraulic characteristics, will present challenges for simulation of peak flow and hydrologic design of urban drainage/channel/stream (Hasan et al. 2019).

In view of the above challenges and issues, the main approach of the research that deals with the maximum daily rainfall values are abstracted for different durations and the rainfall IDF curves are developed for the catchment by using the stationary, non-stationary, and 16 GCM models under various RCPs scenarios (RCP2.6, RCP4.5, RCP6 and RCP8.5) which are designed for a 100 year return period design inflow flood by considering the intensity of rainfall from these IDF curves. The IDF curves are therefore recommended for the prediction of rainfall intensities and design in the catchment (Burian and Shepherd 2005). This research integrated the modified rational method and EPA-SMMM is used to simulate the response of a catchment to storm events, which is used to obtain peak flow hydrographs of streams in the catchment (Clifton et al. 2018; Guan et al. 2015a, b).

Materials and Methods

Study Area

The study area is the mega industrial park at Bidkin, District Aurangabad (Maharashtra), India, covering an area of 3179.1 (hectares). The area slopes towards the south-southeast as the drainage of the area is guided through various small streams and seasonal channels. The annual rainfall over the study area varies from approximately 500 to 840 mm. The climate of the area is characterized by a hot summer with dry conditions throughout the year except during the south-west monsoon season. The maximum and minimum temperature in the study area is 42.50 °C and 28.50 °C.

A major part of the district constitutes a sequence of basaltic lava flows (Deccan trap). The area extends within 19°45′41.12″ N – 75°21′25.01″ E Latitude and 19°45′06.90″ N – 75°22′50.17″ E Longitude. High drainage density in the study area enables the region to be developed as a hub for future storm water management systems subjected to the same average climatic and geologic conditions. The area is covered by survey of India toposheet map no. 47 M/5 on scale 15′ latitude x 15′ longitude (1:50,000). Six land-use cover classes for Bidkin (MIP) are used to define a range of total watershed percent impervious conditions: three land-use classification scenarios for 2016–2020, 2021–2025, and 2026–2030, and four hypothetical cases were derived from the year 2030 land-use classification to provide extreme cases (Fig. 9.1).

In study catchment Bidkin, Aurangabad (Maharashtra) India, future IDF curves are developed using 16 GCM outputs and KNN weather generator based on the
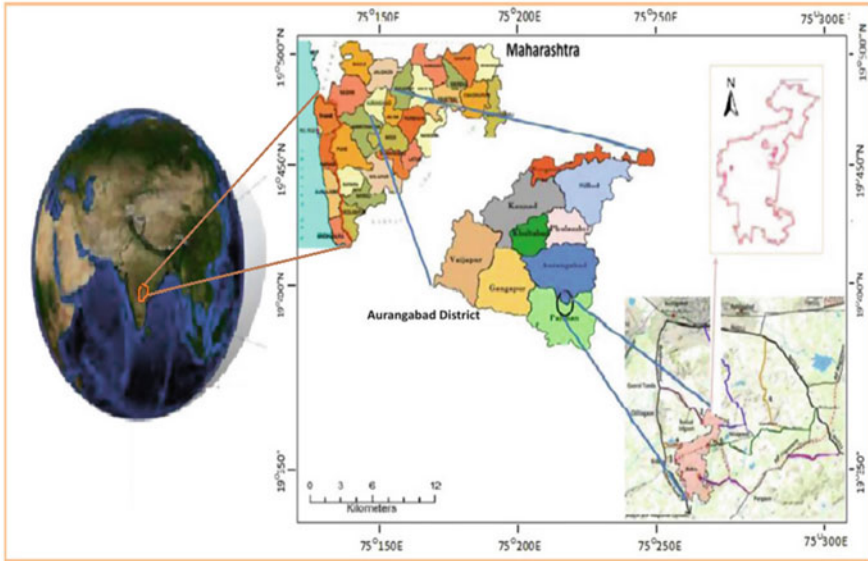
Fig. 9.1 Location map of study area

downscaling method (Boe et al. 2007). The 16 General Circulation Models (GCMs) precipitation flux outputs for historical and future periods are downloaded from the CMIP5 website http://www.ipccdata.org/sim/gcm_monthly/AR5/Reference-Archive.html (accessed during September and October 2017). Also, the appropriate data wherever required in this study are downloaded from NOAA Earth System Research Laboratory (ESRL), Earth System Grid Federation (ESGF), DAI, and Canadian Climate Impacts Scenarios (CCIS).

Methodology

The main approach of this research is hydrologic simulation of storm water peak flow discharge and design of a drainage/channel/stream system passing through the study area catchment under climate change impact. The methodologies applied to achieve the objective of this research are:

1. Future IDF curve developed with the help of GCM simulations and using best covariates for various return periods under different RCP scenarios.
2. The SWMM is selected to simulate and evaluate urban hydrological response to rainfall events and MRM is used to determine the peak flow discharge and Manning's equation for design of a drainage/channel/stream system in the study area catchment under climate change impact.

3. Comparison of peak flow discharge by the SWMM model and MRM method for historic time (1970–2015) period and for two future times (2016–2057) and (2058–2100) period of the study area MIP catchment stream outlet.

Model Descriptions and Application

The SWMM is selected to simulate and evaluate urban hydrological response to rainfall events in the study catchment. The model has hydrological components, including catchment characteristics such as imperviousness, depression storage, infiltration, slope and Manning's 'n' and hydraulic components, including drainage volume, slope, size and elevation are required for simulation (NayebYazdi et al. 2019).

The EPA-SWMM model uses historical and projected rainfall events or design storm water events for simulation (Jiang et al. 2015), and it is also capable of hydraulic simulation, including drainage/channel/stream flow routing (Diya et al. 2018) (Fig. 9.2).

MRM to Estimate Peak Discharge (Q_p)

The modified rational unit hydrograph method is used to develop a unit hydrograph to estimate the runoff hydrograph for all storm events from each watershed (Dhakal et al. 2011). The rainfall–runoff model that can be developed by using MRM is a modern method as compared to rational method by developing the flood hydrograph, which is related to rainfall–runoff events in a specific catchment/basin (Freire Diogo and Antunes do Carmo 2019). Worldwide, the MRM is used to calculate 140 rainfall–runoff events at 80 catchment basins in Texas by a developed hydrograph (Sillanpaa and Koivusalo 2015; Dhakal et al. 2014). The MRM is also used in hydrological procedure No.16 (HP 16): Flood estimation of urban areas in Peninsular Malaysia By Urban Drainage Unit of the Drainage and Irrigation Department, Malaysia (2012). The MRM method is described in Eq. (9.1):

$$Q_P = \widehat{C}_s \times C \times I \times A \qquad (9.1)$$

Where Q_P is peak discharge (m³/sec.), $\widehat{C}_s$ is storage coefficient, C is runoff coefficient, which depends on soil type, topography, and vegetation cover of the catchment basin value shown in Table (9.1), 'I' is rainfall intensity (mm/h) and 'A' is drainage area (m²).

In order to estimate the sub-catchment average runoff coefficient, the entire catchment is divided into different land use land cover, which is denoted by j = 1,
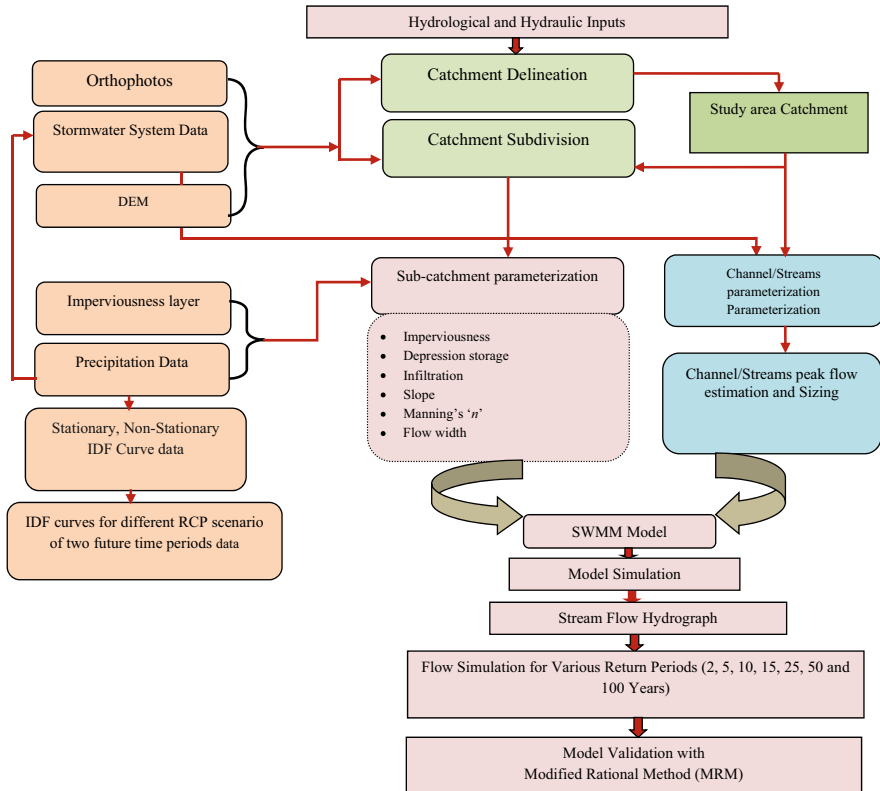
Fig. 9.2 Flowchart of methodology for peak discharge simulation using EPA-SWMM and MRM in the study area (MIP) catchment

2... m and is calculated by Eq. (9.2) and parameter '$\widehat{C}_s$' is calculated by using Eq. (9.3).

$$C_{avg} = \frac{\sum_{j=1}^{m} C_j A_j}{\sum_{j=1}^{m} A_j} \tag{9.2}$$

Where C_{avg} is average coefficient, C_j is runoff coefficient of segment i, A_j is area of segment j and m is total number of segments of sub-catchment.

$$\widehat{C}_s = \frac{2t_c}{2t_c + t_{d'}} \tag{9.3}$$

Where $\widehat{C}_s$ is storage coefficient, t_c is time of concentration in (min) and $t_{d'}$ is time of flow in drainage/channel/stream (min).

Table 9.1 Typical values for runoff coefficient 'C' in urban areas: Source–Pilgrim (1978)

Description of land use	Runoff coefficient "C"
A] Business	
Down town areas	0.70–0.95
Neighborhood areas	0.50–0.70
B] Residential	
Single family areas	0.30–0.5 0
Multiunit detached	0.40–0.60
Multiunit attached	0.60–0.75
C] Residential (suburban)	0.25–0.40
D] Apartment dwelling area	0.5–0.70
E] Industrial	
Light areas	0.5–0.80
Heavy areas	0.60–0.90
F] Parks, cemeteries	0.25–0.3 5
G] Play ground	0.25–0.35
H] Rail road yard areas	0.30–0.40
I] Unimproved areas	0.20–0.40
J] Streets	
Asphalt	0.7–0.95
Concrete	0.80–0.95
Brick	0.70–0.85
K] Drivers and walks	0.75–0. 85
L] Roofs	0.75–0.85
M] Lawns: Sandy soil	
Flat 2%	0.05–0.010
Average 2–7%	0.10–0.15
Steep 7%	0.1.5–0.20
O] Lawns: Heavy soils	
Flat 2%	0.13–0.17
Average 2–7%	0.18–0.22
Steep 7%	0.25–0.35

Time of concentration is the sum of time of travel from farthest point into the drainage network and time of travel through the drainage network to the outlet is calculated by following Kirpich Eq. (9.4)

$$T_c = 0.0078 \ L^{0.77} S^{-0.385} \tag{9.4}$$

Non-stationary Future Intensity Duration Frequency (IDF) Curve for Various Return Periods

The design storm intensity (I_{ds}) correlated with return period (T-year) is estimated using the following equation (Coles and Tawn 1996)

$$I_{ds} = \begin{cases} \mu - \dfrac{\sigma}{\xi}\left[1 - \{-\text{In}(1-p)\}^{\xi}\right], \forall \xi \neq 0 \\ \mu - \sigma \log\{-\log(1-p)\}, \forall \xi \to 0 \end{cases} \tag{9.5}$$

Where p is the exceedance probability.

In the case of the non-stationary GEV model, once parameters are calculated, the rainfall intensity with various return periods is estimated by using Eq. (9.6) (Chen et al. 2017; Coles 2001; Cheng and AghaKouchak 2014).

$$I_{ds} = \begin{cases} \acute{\mu} - \dfrac{\acute{\sigma}}{\acute{\xi}}\left[1 - \{-\text{In}(1-p)\}^{\acute{\xi}}\right], \forall \acute{\xi} \neq 0 \\ \acute{\mu} - \sigma \log\{-\log(1-p)\}, \forall \acute{\xi} \to 0 \end{cases} \tag{9.6}$$

$$\mu(t) = \mu_0 + \mu_1 c; \sigma(t) = \exp(\sigma_0 + \sigma_1 c) \text{ and } \xi(t) = \xi \tag{9.7}$$

Where c is any covariate (i.e. ENSO cycle (E), Urbanization (U), IOD cycle (D), Global warming (G), Local temperature changes (L) and Time (T).

The 95 percentile of the location variable value allow the actual return period (Cheng and AghaKouchak 2014).

$$\acute{\mu}_{95} = Q_{95}(\acute{\mu}_{t1}, \acute{\mu}_{t2}, \ldots, \acute{\mu}_{tm}) \text{ and } \acute{\sigma}_{95} = Q_{95}(\acute{\sigma}_{t1}, \acute{\sigma}_{t2}, \ldots, \acute{\sigma}_{tm}) \tag{9.8}$$

The location and scale variable are calculated with Eq. (9.8) and by substituting in Eq. (9.6) to estimate non-stationary rainfall intensity of different return periods.

In this study, K-NN (nearest neighbor) non-parametric weather generator is used to generate future rainfall values for any duration, return period and any RCPs scenarios (RCP2.6, RCP4.5, RCP6 and RCP8.5) (Fig. 9.3).

These change factors are then applied to the observed for-the-day maximum rainfall time series of different rainfall durations (Rossman 2010). Towards developing future rainfall IDF curves, the annual maximum rainfall series is extracted from the REA techniques resample datasets and these annual maximum rainfall series are fitted (Balistrocchi and Grossi 2020). Furthermore, return levels are calculated for different return periods with REV distribution parameters which are obtained from the future extreme rainfall time series of different RCP scenarios. The return levels calculated with future downscaled rainfall data for different durations and return periods are given in Table 9.2 for both 2016–2057 and 2058–2100 time periods.
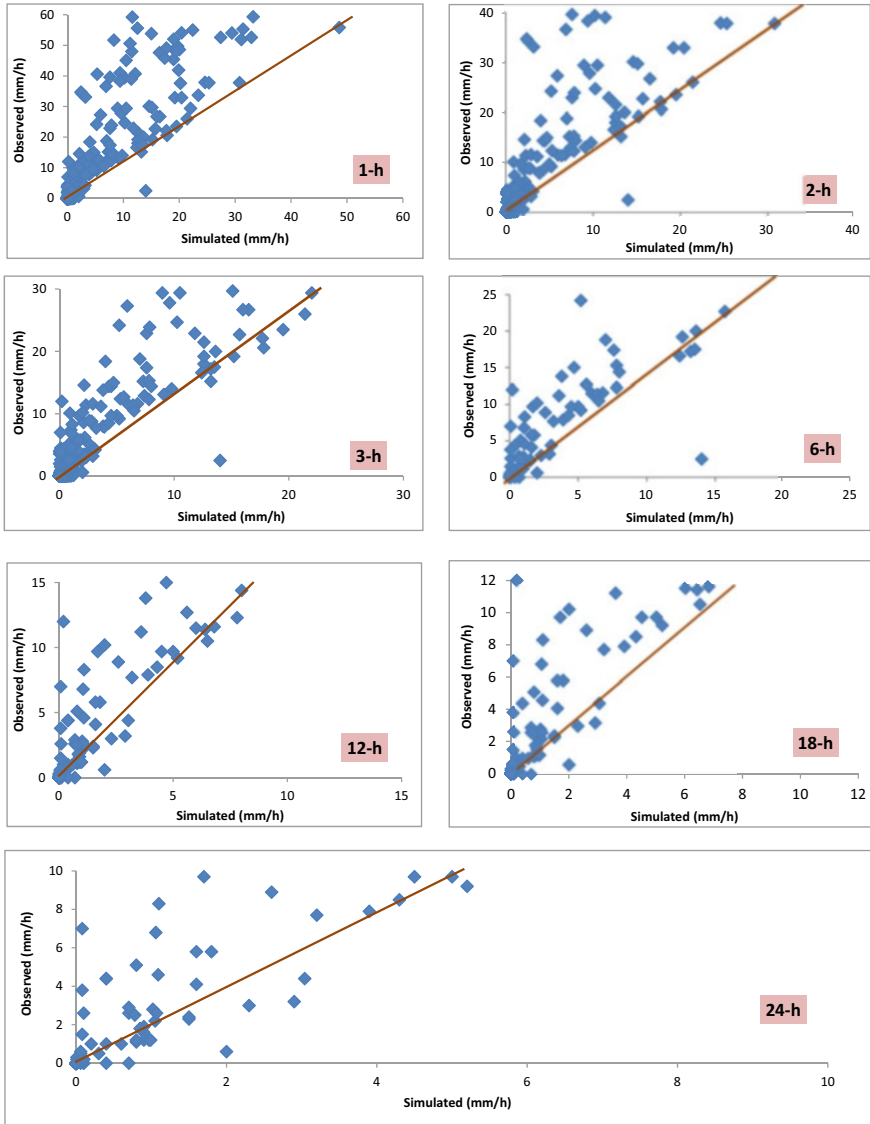
Fig. 9.3 Scatter plot between observed maximum rainfall (from day) of different durations and K-nearest neighbor (K-NN) simulation

Model Setup

The core process in SWMM includes the delineation of the targeted catchment into a collection of sub-catchments that receive rainfall and generate runoff, and the

Table 9.2 The rainfall intensity (mm/h) for different rainfall duration and return period of the study area for two future time periods (2016–2057 and 2058–2100)

Duration and return period	Observed stationary (S)	Observed non-stationary (NS)	2016–2057				2058–2100			
			RCP2.6	RCP4.5	RCP6.0	RCP8.5	RCP2.6	RCP4.5	RCP6.0	RCP8.5
2-year										
1-h	43.86	49.9	44.14	41.61	42.04	43.61	40.28	49.21	47.86	49.28
2-h	27.63	31.6	29.26	26.01	27.54	28.44	27.57	30.89	30.39	31.42
3-h	20.15	22.15	21.43	18.83	18.97	20.67	20.87	22.42	22.75	22.67
6-h	11.60	13.06	12.21	10.84	11.34	11.69	11.15	12.60	12.94	12.58
12-h	5.27	7.90	5.32	6.12	6.67	7.01	6.25	7.14	7.07	7.22
18-h	5.12	6.32	5.98	4.87	4.80	4.66	4.61	4.98	4.48	5.62
24-h	3.50	4.98	3.72	3.92	3.75	3.89	3.87	3.28	3.96	4.28
5-year										
1-h	52.27	56.68	53.87	50.55	52.33	54.31	52.59	60.76	63.48	59.64
2-h	32.89	35.97	34.86	31.45	32.99	34.81	33.51	39.15	40.65	39.31
3-h	24.29	26.49	25.59	23.70	24.89	24.88	24.94	28.57	30.15	28.63
6-h	14.03	15.06	14.72	14.00	14.51	15.10	14.60	16.76	17.62	16.59
12-h	8.44	10.10	8.72	8.16	8.65	9.01	8.33	9.98	9.93	10.02
18-h	6.38	7.88	6.84	6.23	6.55	6.57	6.42	7.23	6.85	7.59
24-h	5.21	6.67	5.34	5.12	5.26	5.41	5.38	5.74	6.04	5.90
10-year										
1-h	54.26	58.66	54.52	51.24	53.25	54.64	53.60	61.28	64.49	61.32
2-h	33.15	37.42	35.05	32.54	33.62	34.95	33.53	40.18	41.64	40.25
3-h	23.36	27.16	26.63	25.41	26.25	24.76	24.95	29.36	32.16	28.39
6-h	15.10	16.04	15.03	16.01	16.09	15.18	14.68	17.81	18.67	17.85
12-h	9.27	10.13	9.86	8.16	9.41	10.58	8.74	10.27	10.87	11.15
18-h	7.82	8.17	6.84	7.20	7.52	7.82	6.78	7.29	7.15	8.15
24-h	6.31	7.81	6.32	6.21	6.29	6.14	5.47	5.98	7.52	6.25

25-year										
1-h	59.64	64.03	62.83	58.34	62.60	64.96	62.47	77.88	86.30	70.39
2-h	39.01	41.20	41.74	36.51	37.64	41.12	40.50	48.76	55.50	46.94
3-h	31.68	33.96	33.35	30.46	32.10	32.79	31.96	37.15	41.14	36.49
6-h	19.37	20.10	20.30	18.95	19.12	20.22	20.37	23.33	25.03	22.98
12-h	12.16	13.05	12.55	12.27	11.03	11.43	12.41	15.35	15.77	14.78
18-h	9.59	11.55	9.74	8.67	9.06	10.19	9.75	11.88	13.38	10.24
24-h	8.30	10.40	8.00	7.36	8.30	7.94	8.34	10.48	12.26	9.46
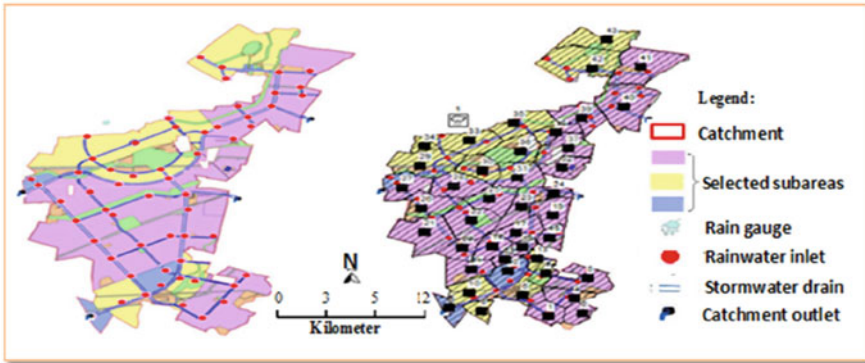
Fig. 9.4 Seven catchment assigned to the four outlets and sub catchments in study area
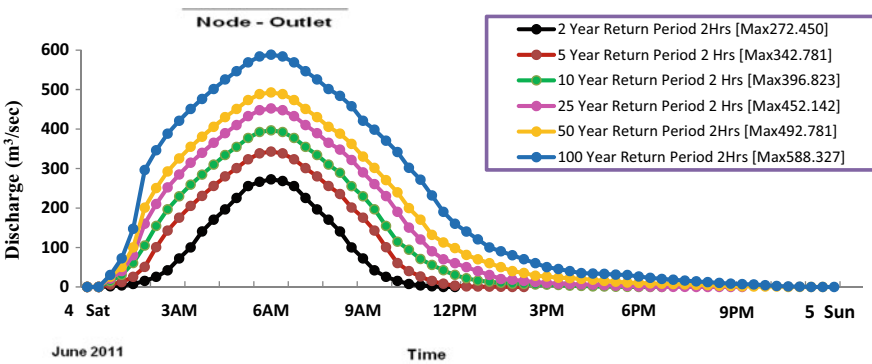
Fig. 9.5 Streams/Nallah network in the study area catchment

tracking of excess rainwater from sub-catchments to catchment outlets through stormwater networks. In this research, study area MIP is first divided into seven catchments assigned to the four outlets. Each catchment surface in study area MIP is categorized into several sub-catchments using different land cover types. Further subdivision is based on the characteristics of pervious or impervious. Several high-resolution sub-catchments are obtained, each of which are enhanced with homogenous land cover and imperviousness properties. The catchment is divided into 42 sub catchments, with an average area of 75.69 ha. The catchment is drained through the stormwater network, consisting of 7 drainage zones with 56 rainwater inlets. Each sub catchment is treated as a nonlinear reservoir, which receives inflows from precipitation and generates outflows and losses based on the assigned catchment parameters such as area, average slope, flow width, imperviousness, depression storage and Manning's roughness. Overland flow is routed between sub-areas, between sub catchments or between entry points of a drainage system. The drained flow is transported through the stormwater network system of links and nodes. The detailed summary and Q_p catchment are given in Appendix A (Fig. 9.4).

The study area has an overall slope towards the south-west and is drained by a network of small and large, gently-flowing six major natural stream/nallahs are crossing the study area and one stream is passing in close proximity to the project boundary on the eastern side (Lee and Liao (2021) (Fig. 9.5).

Model Run

The historical and future rainfall intensities of stationary, non-stationary and 16-GCM under various RCPs scenarios estimated in Table 9.2 are used as input parameters in the SWMM model. In this study, hydrological modelling is used in order to obtain flow hydrographs of each sub-catchment and stream flow hydrograph at various recurrence intervals (Onosakponome 2009; Titmarsh et al. 1978). Also, to estimate the performance and efficiency of drainage network and streams, hydrological and hydraulic simulation is carried out in the study area MIP catchment (Singh and Bardossy 2012). At the end, the peak flow discharge from SWMM is validated with an MRM to compare the estimated peak flow discharge with the simulated peak flow discharge (Zongxue and Gang 2016).

Rainfall Time Series and Intensity Duration Frequency (IDF) Values

The daily recorded rainfall data from the year 1970 to 2016 are collected from IMD Department, Pune. The highest daily seven rainfall storm events recorded occurred on 1 September 1983, 11 October 1990, 9 June 199, 3 September 1992, 6 August 2006, 2 June 2011 and 4 June 2011, with a 127 (mm), 158 (mm), 157 (mm), 186 (mm), 124 (mm), 137 (mm) and 536(mm) rainfall depth. The Gamble's distribution type-I in terms of 2, 5, 10 and 25, 50- and 100-year return levels, the 100-year return period extreme rainfall of 24-h duration is 100.13 mm/h (Pathan and Waikar 2019). Similarly, the future rainfall intensity using the 16-GCM model under various RCPs scenario as per Table 9.2 for two future time periods, for 2016–2057 under various RCPs scenarios, the 25-year return period future extreme rainfall intensities of 1-hr duration are 62.83, 58.34, 62.60 and 64.96 mm/h. For the period of 2058–2100 under various RCPs scenario, the 25-year return period future extreme rainfall intensities of 1-hr duration are 62.47, 77.88, 86.30 and 70.39 mm/h. The design average rainfall intensities under various RCPs scenario are found to be increased for two future time scenarios in comparison to that calculated with respect to observed data (for 1970–2016). Projected peak discharge flow (Q_p) for two future time periods (2016–2057) and (2058–2100) at study area (MIP) sub-catchment for 1-h 25-year return period under RCP8.5 scenario are given in Appendix B.
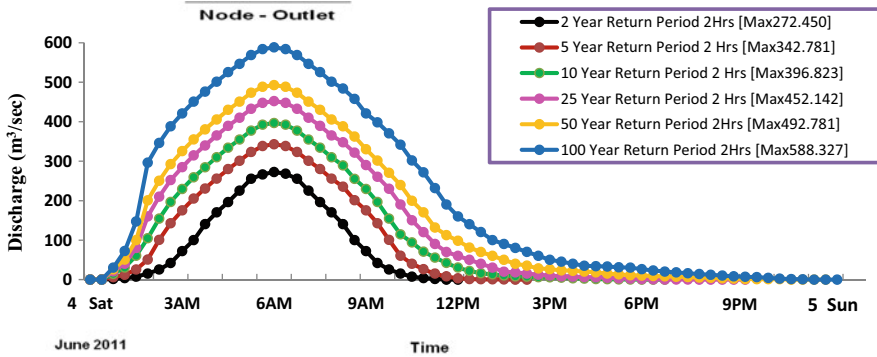
Fig. 9.6 Design peak flow discharge hydrograph at outlet of stream for different durations and return periods by SWMM model
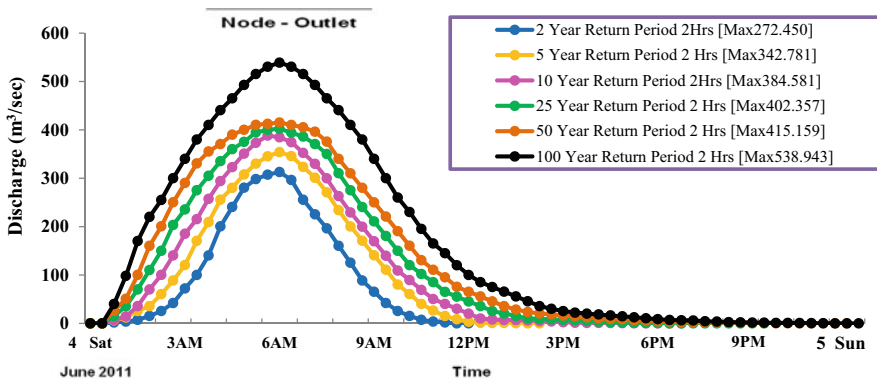
Fig. 9.7 Design peak flow discharge hydrograph at outlet of stream for different durations and return periods by MRM method

Results and Discussion

Design Flow Hydrograph at Outlet of Stream

The simulated flow hydrographs are developed for different return periods, particularly on maximum peak discharge at 2 h. Duration for the study area stream outlet. Figures 9.6 and 9.7 show the total design flow hydrographs developed from each sub-catchment for the study area catchment outlet with the SWWM model and MRM method (Mailhot and Duchesne 2010a, b) (Tables 9.3 and 9.4).

Table 9.3 Flow discharge of the study area stream outlet for different durations and return periods by SWMM model

Storm duration	Return period T (Year)					
	2 -Year	5 -Year	10 -Year	25 -Year	50 -Year	100 -Year
5 min	88.367	97.678	105.962	113.971	124.189	131.922
10 min	125.745	144.851	161.583	177.767	198.614	214.249
15 min	168.961	203.543	231.337	257.770	292.104	317.992
30 min	191.678	269.093	323.635	375.876	443.306	494.170
1-h	230.546	305.460	372.454	412.480	473.198	532.832
2-h	272.450	342.781	396.823	452.142	492.781	588.327
6-h	192.956	231.382	253.055	312.489	334.787	416.350
12-h	100.732	173.165	196.563	236.731	260.168	377.833
24-h	70.125	101.457	112.360	167.450	199.022	208.164

Table 9.4 Flow discharge of the study area stream outlet for different durations and return periods by MRM method

Storm duration	Return period T (Year)					
	2 -Year	5 -Year	10 -Year	25 -Year	50 -Year	100 -Year
5 min	41.642	52.138	64.159	76.369	96.385	108.36
10 min	67.891	88.587	98.125	112.587	120.992	164.865
15 min	145.369	165.876	188.573	207.985	214.482	268.608
30 min	191.678	269.093	311.393	326.091	365.684	444.786
1-h	230.546	305.460	360.212	388.695	395.576	483.448
2-h	312.835	353.895	384.581	402.357	415.159	538.943
6-h	214.125	231.382	240.813	262.704	284.165	366.966
12-h	155.357	173.165	184.321	186.946	196.546	328.449
24-h	72.369	96.258	100.118	117.665	121.442	158.78

Model Calibration and Validation

The study area catchment stream has no stream flow gauging station available for calibration of data. In order to validate the SWMM model output, the comparison of design peak discharge is done with MRM. The temporal comparison between the SWMM model and MRM method is shown in Table 9.5. In the study area (MIP) catchment, the values of peak discharge by the MRM method is higher in 2- and 5-year return periods while in the case of the SWMM model, the peak discharge is higher in 10, 25, 50 and 100 return periods. The peak discharge hydrograph obtained for the EPA-SWMM model in the case of 2, 5, 10, 25, 50 and 100 years return periods are 272.45, 342.781, 396.823, 452.142, 492.781 and 588.327 m^3/s, respectively. The peak discharge hydrograph obtained by MRM method in the case of 2, 5, 10, 25, 50 and 100 years return periods are 312.835, 353.895, 384.581, 402.357, 415.159 and 538.943 m^3/s, respectively. Similarly, the peak discharge hydrograph calculated for two future time periods (2016–2057) and (2058–2100) by the SWMM

Table 9.5 Comparison of peak flow discharge for historic time (1970–2015) period and for two future time (2016–2057) and (2058–2100) periods of the study area (MIP) catchment stream outlet

Method	EPA-SWMM			Modified rational method (MRM)		
Return period T (year)	Peak discharge (Q_p) (m^3/sec.)					
	1970– 2015	2016– 2057	2058– 2100	1970– 2015	2016– 2057	2058– 2100
		RCP8.5	RCP8.5		RCP8.5	RCP8.5
2	272.45	280.457	305.672	312.835	325.628	337.943
5	342.781	354.127	375.621	353.895	366.228	387.341
10	396.823	403.427	425.972	384.581	398.357	416.825
25	452.142	466.918	488.693	402.357	426.316	451.346
50	492.781	501.657	535.872	415.159	474.628	493.271
100	588.327	596.351	662.724	538.943	584.134	610.425

model and MRM method are presented in Tables 9.5 and 100-year return period peak discharge hydrograph under RCP8.5 are plotted in Fig. 9.8(a–f).

According to the above results, it is found that with increasing return period, the total designed peak discharge is increased. In particular, during 2016–2057 and under the RCP 8.5 scenario, the 100-year return period future extreme designed peak discharge of 2-h duration is 596.351 m^3/s. Also, during 2058–2100 and under the RCP 8.5 scenario, the 100-year return period future extreme designed peak discharge of 2-h duration is 662.724 m^3/s (from the SWMM model) (Peterson and Wicks 2006). Similarly, during 2016–2057 and under the RCP 8.5 scenario, the 100-year return period future extreme designed peak discharge of 2-h duration is 584.134 m^3/s. Also, during 2058–2100 and under the RCP 8.5 scenario, the 100-year return period future extreme designed peak discharge of 2-h duration is 610.425 m^3/s (from the MRM method). After accurately calculating the designed peak discharge for historical and two future time periods using the SWMM model and MRM method, the 40 min design storm for 2, 5, 10, 25, 50 and 100-year return periods is considered to design a drainage/stream system in the study area (Rjeily et al. 2018).

Peak Discharge Estimation

In the study area, the peak discharge in all streams is calculated by considering the various sub-catchments. The peak discharge calculated by the SWMM model simulation and MRM method are summarized in Table 9.5 and shown in Fig. 9.8. The 100 years return period designed peak discharges for historical time period (1970–2015) estimated by SWMM model in channel/stream 1, 2, 3, 4, 5 and 6 are 588.327, 485.156, 385.698, 272.347, 196.485, and 161.028 m^3/s, respectively. Similarly, 100 years return period designed peak discharges for historical time period (1970–2015) estimated by the MRM method in channel/stream 1, 2, 3, 4,
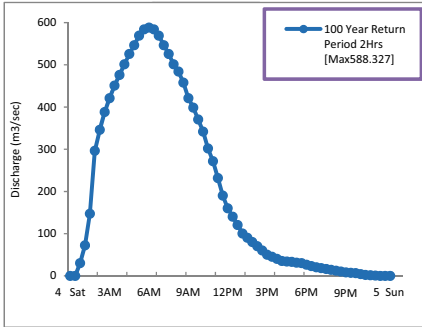
[a] Q$_p$ by SWMM on 4th June 2011 Storm Event
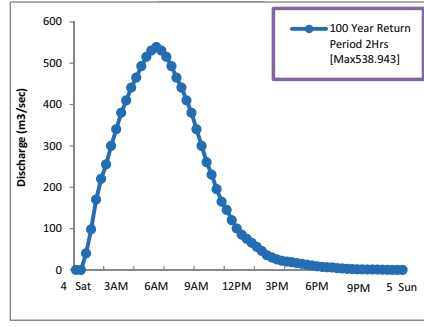
[b] Q$_p$ by MRM on 4th June 2011 Storm Event
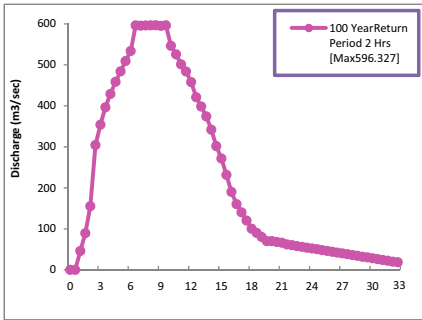
[c] Q$_p$ By SWMM on 8th July 2038 Storm Under RCP8.5
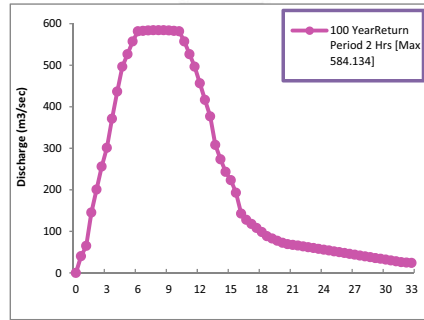
[d] Q$_p$ By MRM 8th July 2038 Storm Under RCP8.5
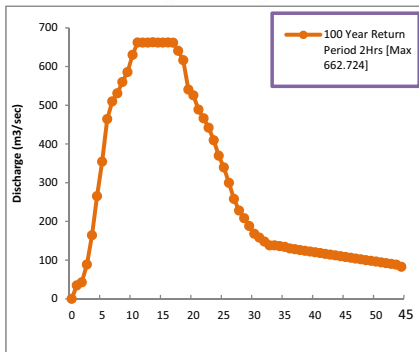
[e] Q$_p$ By SWMM on 24th July 2088 Storm Under RCP8.5
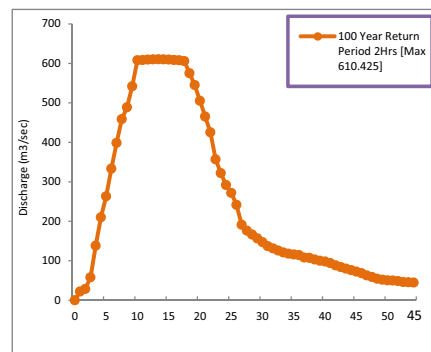
[f] Q$_p$ By MRM on 24th July 2088 Storm Under RCP8.5

Fig. 9.8 Comparison between the SWMM model and MRM method design discharge (m^3/s) hydrograph at outlet of stream for 100 years return period for historical time period (1970–2015) and for two future time periods (2016–2057) and (2058–2100) under the RCP8.5 scenario

5 and 6 are 538.943, 390.610, 296.879, 242.571, 151.302, and 115.415 m^3/s, respectively and all the streams designed for 100 years return period peak discharge are summarized in Tables 9.6 and 9.7. Also, peak discharges estimated for future time period (2058–210) are summarized in Tables 9.8 and 9.9.

Table 9.6 Estimated peak flow discharge and sizes of all channels for historic time (1970–2015) period by SWMM model

Channel no./ return periods	Length of channel within boundary	Design discharge SWMM (1970–2015) Periods	Channel slope	Manning's coefficient	Depth of channel	Left and right-side slope	Bottom width	Top width	Velocity
	(m)	(Cumecs)	(m/m)		(m)	(m/m; H: V)	(m)	(m)	(m/s)
1	1903	588.327	0.01452	0.035	2.50	4.00	33.12	53.14	5.47
2	3632	485.156	0.01396	0.035	2.50	4.00	26.98	46.98	5.26
3	5136	388.698	0.01326	0.035	2.50	4.00	21.20	41.21	4.99
4	4904	272.347	0.01240	0.035	2.50	4.00	13.76	33.75	4.58
5	1662	196.485	0.01483	0.035	2.50	4.00	6.98	26.99	4.64
6	959	161.028	0.01353	0.035	2.50	4.00	5.08	25.06	4.29

Table 9.7 Estimated peak flow discharge and sizes of all channels for historic time (1970–2015) period by MRM method

Channel no./ return periods	Length of channel within boundary	Design discharge MRM (1970–2015) Periods	Channel slope	Manning's coefficient	Depth of channel	Left and right-side slope	Bottom width	Top width	Velocity
	(m)	(Cumecs)	(m/m)		(m)	(m/m; H: V)	(m)	(m)	(m/s)
1	1903	538.943	0.01452	0.035	2.50	4.00	29.75	49.74	5.42
2	3632	390.610	0.01396	0.035	2.50	4.00	20.60	40.61	5.10
3	5136	296.879	0.01326	0.035	2.50	4.00	14.86	34.80	4.78
4	4904	242.571	0.01240	0.035	2.50	4.00	11.63	31.60	4.49
5	1662	151.302	0.01483	0.035	2.50	4.00	3.82	23.80	4.38
6	959	115.415	0.01353	0.035	2.50	4.00	2.90	20.12	3.93

Table 9.8 Estimated peak flow discharge and sizes of all channels for future time (2058–2100) period by SWMM model under RCP8.5 scenario

Channel no./ return periods	Length of channel within boundary	Design discharge SWMM (2058–2100) Periods under RCP8.5	Channel slope	Manning's coefficient	Depth of channel	Left and right-side slope	Bottom width	Top width	Velocity
	(m)	(Cumecs)	(m/m)		(m)	(m/m; H: V)	(m)	(m)	(m/s)
1	1903	662.724	0.01452	0.035	2.50	4.00	37.75	57.72	5.55
2	3632	612.432	0.01396	0.035	2.50	4.00	35.31	55.29	5.40
3	5136	564.892	0.01326	0.035	2.50	4.00	33.16	53.11	5.23
4	4904	486.715	0.01240	0.035	2.50	4.00	29.01	49.00	4.99
5	1662	365.392	0.01483	0.035	2.50	4.00	18.21	38.18	5.18
6	959	252.874	0.01353	0.035	2.50	4.00	11.57	31.30	4.69

Table 9.9 Estimated peak flow discharge and sizes of all channels for future time (2058–2100) period by MRM method under RCP8.5 scenario

Channel no./ return periods	Length of channel within boundary	Design Discharge MRM (2058–2100) Periods under RCP8.5	Channel slope	Manning's coefficient	Depth of channel	Left and right-side slope	Bottom width	Top width	Velocity
	(m)	(Cumecs)	(m/m)		(m)	(m/m; H: V)	(m)	(m)	(m/s)
1	1903	610.425	0.01452	0.035	2.50	4.00	34.41	54.38	5.50
2	3632	567.872	0.01396	0.035	2.50	4.00	32.39	52.38	5.36
3	5136	488.904	0.01326	0.035	2.50	4.00	28.02	48.00	5.14
4	4904	376.451	0.01240	0.035	2.50	4.00	21.20	41.18	4.82
5	1662	289.326	0.01483	0.035	2.50	4.00	13.22	32.88	4.77
6	959	178.495	0.01353	0.035	2.50	4.00	6.31	25.41	4.38

Sizing of the Drainage/Channel/Stream in Study Area Catchment

In the study area catchment, there are six major streams/nallah. The surface runoff (storm water) originating from each sub-catchment is to be drained at various locations into streams/nallah. The peak discharge (Q_p) from each sub-catchment is estimated by using MRM using Eq. (7.1) and EPA-SWMM simulation and the design of all streams using Manning's equation in the model to determine the width, depth and velocity of flow as per Eq. (9.5);

$$V = \frac{1}{N} \times R^{2/3} \times S^{1/2} \tag{9.5}$$

$$Q_p = A \times \frac{1}{N} \times R^{2/3} \times S^{1/2} \tag{9.6}$$

$$R = A \div P = bd \div b + 2d \tag{7.6a}$$

$$Q = bd \div n \, (bd \div b + 2d)^{2/3} S^{1/2} \tag{7.6b}$$

Where 'Q_p' is peak discharge (m^3/s.), 'V' is velocity of flow in drain/stream/nallah, 'N' is Manning's constant, 'R' is hydraulic mean depth (m) and 'P' wetted perimeter (m).

Considering the topography, slope and nature of soil in the study area the value of 'C' is assessed and found to be in between 0.7 and 0.9.

Summary and Conclusion

This chapter described a hydrological and hydraulic comparison between the SWMM model and MRM method for design peak discharge (Cumecs) estimation in all streams for a 100 years return period for historical time period (1970–2015) and for future time period (2058–2100) under the RCP8.5 scenario. The design of all streams used Manning's equation in the model to determine the width, depth and velocity of flow in the study area catchment. The 100 years return period designed peak discharges for historical time period (1970–2015) estimated by the SWMM model in channel/stream 1, 2, 3, 4, 5 and 6 are 588.327, 485.156, 385.698, 272.347, 196.485 and 161.028 Cumecs, respectively. Similarly, the100 years return period designed peak discharges for historical time period (1970–2015) estimated by the MRM method in channel/stream 1, 2, 3, 4, 5 and 6 are 38.943, 390.610, 296.879, 242.571, 151.302, and 115.415 Cumecs, respectively. Also, the100 years return period designed peak discharges for future time period (2058–2100) estimated by the SWMM model in channel/stream 1, 2, 3, 4, 5 and 6 are 662.724, 612.432,

564.892, 486.715, 365.392, and 252.874 Cumecs, respectively. Similarly, by the MRM method in channel/stream 1, 2, 3, 4, 5 and 6 they are 610.425, 567.872, 488.94, 376.451, 289.326, and 178.495 Cumecs, respectively.

The estimated highest annual peak discharge of the stream at catchment for historical time (2070–2015) period by the SWMM model is 588.327 Cumecs and for future time (2058–2100) period under RCP8.5 it is 662.724 Cumecs (in the case of stream one). Similarly, the estimated highest annual peak discharge of the stream at catchment for historical time (2070–2015) period using the MRM method is 538.943 Cumecs and for future time (2058–2100) period under RCP8.5 it is 610.425 Cumecs (in the case of stream one). The estimated average velocity of the stream at catchment for historical time (2070–2015) period by the SWMM model is 4.87 m/s and for future time (2058–2100) period under RCP8.5 it is 5.17 m/s and the width/depth ratio is 11.01. The estimated average velocity of the stream at catchment for historical time (2070–2015) period using the MRM method is 4.68 m/s and for future time (2058–2100) period under RCP8.5 it is 4.99 m/s and the width/depth ratio is 9.03.

Appendixes

Appendix A:

Table 9.10 Estimated detailed summary of study area (MIP) sub-catchment

Sub-catchment ID	Sub-catchment area (Ai)	Sub-catchment Dch (m)	Sub-catchment length L (m)	Sub-catchment slope (S)	Time of concentration Tc (min)
MIP01	60.25	5	477.14	0.01048	5.21
MIP02	55.32	5	439.22	0.01138	4.73
MIP03	65.87	5	430.65	0.01161	4.63
MIP04	78.69	5	588.33	0.00850	6.64
MIP05	54.67	5	508.00	0.00984	5.60
MIP06	40.28	1	279.65	0.00358	5.22
MIP07	35.42	2	288.32	0.00694	4.14
MIP08	24.36	2	219.67	0.00910	3.03
MIP09	76.84	6	535.13	0.01121	5.54
MIP 10	77.53	6	573.95	0.01045	6.01
MIP 11	71.87	5	498.66	0.01003	5.48
MIP12	28.36	2	285.00	0.00702	4.09
MIP13	58.25	5	536.00	0.00933	5.96

(continued)

Table 9.10 (continued)

Sub-catchment ID	Sub-catchment area (Ai)	Sub-catchment Dch (m)	Sub-catchment length L (m)	Sub-catchment slope (S)	Time of concentration Tc (min)
MIP14	22.56	2	304.36	0.00657	4.41
MIP15	29.36	2	347.41	0.00576	5.14
MIP16	68.69	5	538.42	0.00929	5.99
MIP17	41.34	2	392.46	0.00510	5.92
MIP18	82.84	4	624.78	0.00640	7.75
MIP19	76.94	3	513.27	0.00584	6.90
MIP20	98.36	5	1058.1	0.00473	13.07
MIP21	92.18	4	833.07	0.00480	10.81
MIP22	88.36	2	365.53	0.00547	5.45
MIP23	36.69	1	223.53	0.00447	4.03
MIP24	91.85	3	636.031	0.00472	8.84
MIP25	88.96	4	711.37	0.00562	9.00
MIP26	78.69	4	777.71	0.00514	9.98
MIP27	92.87	4	814.38	0.00491	10.53
MIP 28	101.25	4	810.00	0.00494	10.46
MIP 29	97.36	3	549.11	0.00546	7.46
MIP 30	97.36	3	648.94	0.00462	9.05
MIP 31	94.58	3	465.14	0.00645	6.16
MIP 32	105.36	5	812.79	0.00615	9.64
MIP 33	48.36	3	386.90	0.00775	4.98
MIP 34	103.36	3	511.79	0.00586	6.88
MIP 35	100.28	4	695.26	0.00575	8.77
MIP 36	102.8	4	595.27	0.00672	7.33
MIP 37	87.96	3	347.35	0.00864	4.40
MIP 38	103.87	4	687.71	0.00582	8.66
MIP 39	109.26	4	777.44	0.00515	9.98
MIP 40	104.45	4	773.04	0.00517	9.91
MIP 41	107.45	5	919.48	0.00544	11.11
MIP 42	98	3	408.77	0.00734	5.30

Dch Difference in contour height (m), *L* Horizontal length along the flow direction passing through the measured area

Table 9.11 Estimated peak discharge flow (Q_p) for historical time period (1970–2016) at study area (MIP) Sub-catchment for 24 h 100-yearreturn period

Sub-catchment ID	Sub-catchment area (Ai) (ha)	Time of concentration (Tc) (min)	Runoff coefficient (C)	Catchment intensity (i) (mm/h)	Sub-catchment flow by (MRM) method (m^3/s)
MIP01	60.25	5.21	0.95	100.13	16.05
MIP02	55.32	4.73	0.95	100.13	14.73
MIP03	65.87	4.63	0.95	100.13	17.54
MIP04	78.69	6.64	0.95	100.13	20.96
MIP05	54.67	5.60	0.7	100.13	10.73
MIP06	40.28	5.22	0.7	100.13	7.91
MIP07	35.42	4.14	0.7	100.13	6.95
MIP08	24.36	3.03	0.7	100.13	4.78
MIP09	76.84	5.54	0.7	100.13	15.08
MIP 10	77.53	6.01	0.7	100.13	15.22
MIP 11	71.87	5.48	0.7	100.13	14.10
MIP12	28.36	4.09	0.7	100.13	5.57
MIP13	58.25	5.96	0.7	100.13	11.43
MIP14	22.56	4.41	0.7	100.13	4.43
MIP15	29.36	5.14	0.7	100.13	5.76
MIP16	68.69	5.99	0.7	100.13	13.48
MIP17	41.34	5.92	0.7	100.13	8.11
MIP18	82.84	7.75	0.7	100.13	16.26
MIP19	76.94	6.90	0.7	100.13	15.10
MIP20	98.36	13.07	0.7	100.13	19.30
MIP21	92.18	10.81	0.7	100.13	18.09
MIP22	88.36	5.45	0.7	100.13	17.34
MIP23	36.69	4.03	0.7	100.13	7.20
MIP24	91.85	8.84	0.7	100.13	18.03
MIP25	88.96	9.00	0.7	100.13	17.46
MIP26	78.69	9.98	0.7	100.13	15.44
MIP27	92.87	10.53	0.6	100.13	15.62
MIP 28	101.25	10.46	0.6	100.13	17.03
MIP 29	97.36	7.46	0.6	100.13	16.38
MIP 30	97.36	9.05	0.6	100.13	16.38
MIP 31	94.58	6.16	0.6	100.13	15.91
MIP 32	105.36	9.64	0.6	100.13	17.72
MIP 33	48.36	4.98	0.6	100.13	8.14
MIP 34	103.36	6.88	0.6	100.13	17.39
MIP 35	100.28	8.77	0.6	100.13	16.87
MIP 36	102.8	7.33	0.6	100.13	17.29
MIP 37	87.96	4.40	0.6	100.13	14.80

(continued)

Table 9.11 (continued)

Sub-catchment ID	Sub-catchment area (Ai) (ha)	Time of concentration (Tc) (min)	Runoff coefficient (C)	Catchment intensity (i) (mm/h)	Sub-catchment flow by (MRM) method (m^3/s)
MIP 38	103.87	8.66	0.9	100.13	26.21
MIP 39	109.26	9.98	0.9	100.13	27.57
MIP 40	104.45	9.91	0.9	100.13	26.36
MIP 41	107.45	11.11	0.9	100.13	27.11
MIP 42	98	5.30	0.9	100.13	24.73

Appendix B:

Table 9.12 Projected peak discharge flow (Q_p) for future time period (2016–2057) at study area (MIP) sub-catchment for 1 h 25-year return period under RCP8.5 scenario

Sub-catchment ID	Sub-catchment Area (Ai) (ha)	Time of concentration (Tc) (min)	Runoff coefficient (C)	Catchment intensity (i) (mm/h)	Catchment flow by (MRM) method (m^3/s)
MIP01	60.25	5.21	0.95	64.96	10.41
MIP02	55.32	4.73	0.95	64.96	9.56
MIP03	65.87	4.63	0.95	64.96	11.38
MIP04	78.69	6.64	0.95	64.96	13.60
MIP05	54.67	5.60	0.7	64.96	6.96
MIP06	40.28	5.22	0.7	64.96	5.13
MIP07	35.42	4.14	0.7	64.96	4.51
MIP08	24.36	3.03	0.7	64.96	3.10
MIP09	76.84	5.54	0.7	64.96	9.78
MIP 10	77.53	6.01	0.7	64.96	9.87
MIP 11	71.87	5.48	0.7	64.96	9.15
MIP12	28.36	4.09	0.7	64.96	3.61
MIP13	58.25	5.96	0.7	64.96	7.42
MIP14	22.56	4.41	0.7	64.96	2.87
MIP15	29.36	5.14	0.7	64.96	3.74
MIP16	68.69	5.99	0.7	64.96	8.75
MIP17	41.34	5.92	0.7	64.96	5.26
MIP18	82.84	7.75	0.7	64.96	10.55
MIP19	76.94	6.90	0.7	64.96	9.80
MIP20	98.36	13.07	0.7	64.96	12.52
MIP21	92.18	10.81	0.7	64.96	11.74
MIP22	88.36	5.45	0.7	64.96	11.25

(continued)

Table 9.12 (continued)

Sub-catchment ID	Sub-catchment Area (Ai) (ha)	Time of concentration (Tc) (min)	Runoff coefficient (C)	Catchment intensity (i) (mm/h)	Catchment flow by (MRM) method (m³/s)
MIP23	36.69	4.03	0.7	64.96	4.67
MIP24	91.85	8.84	0.7	64.96	11.69
MIP25	88.96	9.00	0.7	64.96	11.33
MIP26	78.69	9.98	0.7	64.96	10.02
MIP27	92.87	10.53	0.6	64.96	10.14
MIP 28	101.25	10.46	0.6	64.96	11.05
MIP 29	97.36	7.46	0.6	64.96	10.63
MIP 30	97.36	9.05	0.6	64.96	10.63
MIP 31	94.58	6.16	0.6	64.96	10.32
MIP 32	105.36	9.64	0.6	64.96	11.50
MIP 33	48.36	4.98	0.6	64.96	5.28
MIP 34	103.36	6.88	0.6	64.96	11.28
MIP 35	100.28	8.77	0.6	64.96	10.94
MIP 36	102.8	7.33	0.6	64.96	11.22
MIP 37	87.96	4.40	0.6	64.96	9.60
MIP 38	103.87	8.66	0.9	64.96	17.00
MIP 39	109.26	9.98	0.9	64.96	17.89
MIP 40	104.45	9.91	0.9	64.96	17.10
MIP 41	107.45	11.11	0.9	64.96	17.59
MIP 42	98	5.30	0.9	64.96	16.04

Table 9.13 Projected peak discharge flow (Q_p) for future time period (2058–2100) at study area (MIP) Sub-catchment for 1 h 25 year return period under RCP8.5 scenario

Sub-catchment ID	Sub-catchment area (Ai) (ha)	Time of concentration (Tc) (min)	Runoff coefficient (C)	Catchment intensity (i) (mm/h)	Catchment flow by (MRM) method (m³/s)
MIP01	60.25	5.21	0.95	70.39	11.28
MIP02	55.32	4.73	0.95	70.39	10.36
MIP03	65.87	4.63	0.95	70.39	12.33
MIP04	78.69	6.64	0.95	70.39	14.73
MIP05	54.67	5.60	0.7	70.39	7.54
MIP06	40.28	5.22	0.7	70.39	5.56
MIP07	35.42	4.14	0.7	70.39	4.89
MIP08	24.36	3.03	0.7	70.39	3.36

Table 9.13 (continued)

Sub-catchment ID	Sub-catchment area (Ai) (ha)	Time of concentration (Tc) (min)	Runoff coefficient (C)	Catchment intensity (i) (mm/h)	Catchment flow by (MRM) method (m³/s)
MIP09	76.84	5.54	0.7	70.39	10.60
MIP 10	77.53	6.01	0.7	70.39	10.70
MIP 11	71.87	5.48	0.7	70.39	9.92
MIP12	28.36	4.09	0.7	70.39	3.91
MIP13	58.25	5.96	0.7	70.39	8.04
MIP14	22.56	4.41	0.7	70.39	3.11
MIP15	29.36	5.14	0.7	70.39	4.05
MIP16	68.69	5.99	0.7	70.39	9.48
MIP17	41.34	5.92	0.7	70.39	5.70
MIP18	82.84	7.75	0.7	70.39	11.43
MIP19	76.94	6.90	0.7	70.39	10.61
MIP20	98.36	13.07	0.7	70.39	13.57
MIP21	92.18	10.81	0.7	70.39	12.72
MIP22	88.36	5.45	0.7	70.39	12.19
MIP23	36.69	4.03	0.7	70.39	5.06
MIP24	91.85	8.84	0.7	70.39	12.67
MIP25	88.96	9.00	0.7	70.39	12.27
MIP26	78.69	9.98	0.7	70.39	10.86
MIP27	92.87	10.53	0.6	70.39	10.98
MIP 28	101.25	10.46	0.6	70.39	11.97
MIP 29	97.36	7.46	0.6	70.39	11.51
MIP 30	97.36	9.05	0.6	70.39	11.51
MIP 31	94.58	6.16	0.6	70.39	11.18
MIP 32	105.36	9.64	0.6	70.39	12.46
MIP 33	48.36	4.98	0.6	70.39	5.72
MIP 34	103.36	6.88	0.6	70.39	12.22
MIP 35	100.28	8.77	0.6	70.39	11.86
MIP 36	102.8	7.33	0.6	70.39	12.16
MIP 37	87.96	4.40	0.6	70.39	10.40
MIP 38	103.87	8.66	0.9	70.39	18.42
MIP 39	109.26	9.98	0.9	70.39	19.38
MIP 40	104.45	9.91	0.9	70.39	18.53
MIP 41	107.45	11.11	0.9	70.39	19.06
MIP 42	98	5.30	0.9	70.39	17.38

References

Agilan V, Umamahesh NV (2015) Detection and attribution of non-stationarity in intensity and frequency of daily and 4-h extreme rainfall of Hyderabad. India J Hydrol 530:677–697

Alam S et al (2014) Comparative assessment of urban flood risks due to urbanization and climate change in the turnhout valley of Belgium. ABC J Adv Res 3(1):14–23. oaji.net/pdf.html?n=2015/814-1431431574.pdf

Antrop M (2004) Landscape change and the urbanization process in Europe. Landsc Urban Plan 67:9–26. https://doi.org/10.1016/S0169-2046(03)00026-4

Balistrocchi M, Grossi G (2020) Predicting the impact of climate change on urban drainage systems in northwestern Italy by a copula-based approach. J Hydrol Reg Stud 28:100670. https://doi.org/10.1016/j.ejrh.2020.100670

Barco J, Wong K, Stenstrom M (2008) Automatic calibration of the U.S. EPA SWMM model for a large urban catchment. J Hydraul Eng 134:466–474. https://doi.org/10.1061/(ASCE)0733-9429, 134:4 (466)

Boe J, Terray L, Habets F, Martin E (2007) Statistical and dynamical downscaling of the seine basin climate for hydro-meteorological studies. Int J Climatol 27(12):1643–1655

Burian SJ, Shepherd JM (2005) Effect of urbanization on the diurnal rainfall pattern in Houston. Hydrol Process 19:1089–1103

Chen J, Theller L, Gitau MW, Engel BA, Harbor JM (2017) Urbanization impacts on surface runoff of the contiguous United States. J Environ Manag 187:470–481. https://doi.org/10.1016/j.jenvman.2016.11.017

Cheng L, AghaKouchak A (2014) Non-stationary precipitation intensity-duration frequency curves for infrastructure design in a changing climate. Nat Sci Rep 4:7093

Clifton CF, Day KT, Luce CH, Grant GE, Safeeq M, Halofsky JE, Staab BP (2018) Effects of climate change on hydrology and water resources in the Blue Mountains, Oregon, USA. Climate Serv 10:9–19. https://doi.org/10.1016/j.cliser.2018.03.001

Coles S (2001) An introduction to statistical modeling of extreme values. Springer, London

Coles SG, Tawn JA (1996) A Bayesian analysis of extreme rainfall data. J R Stat Soc. Series C (Applied Statistics) 45(4):463–478. https://doi.org/10.2307/2986068

Dhakal N, Fang X, Cleveland TG, Thompson DB (2011) Revisiting modified rational method. World Environ Water Res Congr 2011. https://doi.org/10.1061/41173(414)77

Dhakal N, Fang X, Thompson DB, Cleveland TG (2014) Modified rational unit hydrograph method and applications. Proc Inst Civ Eng Water Manag 167:381–393

Dietz ME, Clausen JC (2008) Stormwater runoff and export changes with development in a traditional and low impact subdivision. J Environ Manag 87:560–566. https://doi.org/10.1016/j.jenvman.2007.03.026

Diya SZ et al (2018) Developing an intelligent waste sorting system with robotic arm: A step towards green environment. In 2018 International Conference on Innovation in Engineering and Technology (ICIET), pp 1–6. IEEE

Freire Diogo A, Antunes do Carmo J (2019) Peak flows and Stormwater networks design current and future Management of Urban Surface Watersheds. Water 11(4):759. https://doi.org/10.3390/w11040759

Guan M, Sillanpaa N, Koivusalo H (2015a) Storm runoff response to rainfall pat-tern, magnitude and urbanization in a developing urban catchment. Hydrol Process. https://doi.org/10.1002/hyp.10624

Guan M, Sillanpaa N, Koivusalo H (2015b) Modelling and assessment of hydrological changes in a developing urban catchment. Hydrol Process 29:2880–2894. https://doi.org/10.1002/hyp.10410

Hasan HH, Mohd Razali SF, Ahmad Zaki AZI, Mohamad Hamzah F (2019) Integrated hydrological-hydraulic model for flood simulation in tropical urban catchment. Sustainability 11(23):6700. https://doi.org/10.3390/su11236700

Haase D et al (2014) A quantitative review of urban ecosystem service assessments: concepts, models, and implementation. Ambio 43(4):413–433. https://doi.org/10.1007/s13280-014-0504-0

Huber WC, Dickinson RE (1988) Storm water management model, user's manual, version 4.0, EPA-600/3-88-001a. U.S. Environmental Protection Agency, Athens, GA, www.dynsystem.com/netstorm/docs/swmm4manuals.pdf

Jiang L, Chen Y, Wang H (2015) Urban flood simulation based on the SWMM model. Proc IAHS 368:186–191. https://doi.org/10.5194/piahs-368-186-2015

Lee Y-C, Liao P-T (2021) The effect of tourism on teleconnected ecosystem services and urban sustainability: an emergy approach. Ecol Model 439:109343. https://doi.org/10.1016/j.ecolmodel.2020.109343

Mailhot A, Duchesne S (2010a) Design criteria of urban drainage infrastructures under climate change. J Water Resour Plan Manag 136(2):201–208. https://doi.org/10.1061/(asce)wr.1943-452.0000023

Mailhot A, Duchesne S (2010b) Design criteria of urban drainage infrastructures under climate change. J Water Resour Plan Manag 136(2):201–208. https://doi.org/10.1061/(asce)wr.1943-5452.0000023

Mamo TG (2015) Evaluation of the potential impact of rainfall intensity variation due to climate change on existing drainage infrastructure. J Irrig Drain Eng 141(10):05015002. https://doi.org/10.1061/(asce)ir.1943-4774.0000887

Miller JD, Hess T (2017) Urbanization impacts on storm runoff along a rural-urban gradient. J Hydrol 552:474–489. https://doi.org/10.1016/j.jhydrol.2017.06.025

NayebYazdi M, Ketabchy M, Sample DJ, Scott D, Liao H (2019) An evaluation of HSPF and SWMM for simulating stream flow regimes in an urban watershed. Environ Model Softw 118:211–225. https://doi.org/10.1016/j.envsoft.2019.05.008

Nguyen T-H, Nguyen V-T-V (2020) Linking climate change to urban storm drainage system design: an innovative approach to modeling of extreme rainfall processes over different spatial and temporal scales. J Hydro Environ Res 29:80–95. https://doi.org/10.1016/j.jher.2020.01.006

Nirupama N, Simonovic SP (2007) Increase of flood risk due to urbanization: a canadian example. Nat Hazards 40(1):25–41. https://doi.org/10.1007/s11069-006-0003-0

Onosakponome OR (2009) Comparative study of different methods of runoff discharge estimation for drainage design. Published doctoral thesis, University of Nigeria, Nsukka

Pathan AS, Waikar ML (2019) Precipitation intensity-duration-frequency curves under changing climate on developing urban catchment – Aurangabad (Ms), India. Springer, Cham, pp 851–867. https://doi.org/10.1007/978-3-030-16848-3_77

Peterson EW, Wicks CM (2006) Assessing the importance of conduit geometry and physical parameters in karst systems using the storm water management model (SWMM). J Hydrol 329(1–2):294–305. https://doi.org/10.1016/j.jhydrol.2006.02.017

Rabori AM, Ghazavi R (2018) Urban flood estimation and evaluation of the performance of an urban drainage system in a semi-arid urban area using SWMM. Water Environ Res 90(12):2075–2082. https://doi.org/10.2175/106143017x15131012188213

Rjeily YA, Abbas O, Sadek M, Shahrour I, Chehade FH (2018) Model predictive control for optimizing the operation of urban drainage systems. J Hydrol. https://doi.org/10.1016/j.jhydrol.2018.09.044

Rossman LA (2010) Storm water management model user's manual, version5.0. Water supply and water resource division, national risk management research laboratory, office of research and development, US Environmental Protection Agency

Schoonover JE, Lockaby BG, Helms BS (2006) Impacts of land cover on stream hydrology in the West Georgia Piedmont, USA. J Environ Qual 35(6):2123–2131

Sillanpaa N, Koivusalo H (2015) Impacts of urban development on runoff event characteristics and unit hydrographs across warm and cold seasons in high latitudes. J Hydrol 521:328–340. https://doi.org/10.1016/j.jhydrol.2014.12.008

Singh SK, Bardossy A (2012) Calibration of hydrological models on hydrologically unusual events. Adv Water Resour 38(2012):81–91. https://doi.org/10.1016/j.advwatres.2011.12.006

Titmarsh GW, Cordery I, Pilgrim DH (1978) Calibration procedures for the rational and USSCS design flood methods. J Hydr Eng 121(1):61–70

Vallecillo S, La Notte A, Zulian G, Ferrini S, Maes J (2019) Ecosystem services accounts: valuing the actual flow of nature-based recreation from ecosystems to people. Ecol Model 392:196–211. https://doi.org/10.1016/j.ecolmodel.2018.09.023

Walega A, Amatya DM, Caldwell P, Marion D, Panda S (2020) Assessment of storm direct runoff and peak flow rates using improved SCS-CN models for selected forested watersheds in the Southeastern United States. J Hydrol Reg Stud 27:100645. https://doi.org/10.1016/j.ejrh.2019.100645

Wang B (2005) Fundamental challenge in simulation and prediction of summer monsoon rainfall. Geophys Res Lett 32(15):L15711. https://doi.org/10.1029/2005gl022734

Wang Q, Zhang X, Wei M, Zhou Y, Li P, Bai G (2011) Research summary of planning and design standards for storm water system in Beijing City. Water Wastewater Eng 37:34–39

Yazdanfar Z, Sharma A (2015) Urban drainage system planning and design – challenges with climate change and urbanization: a review. Water Sci Technol 72(2):165–179. https://doi.org/10.2166/wst.2015.207

Zhou Q (2014) A review of sustainable urban drainage systems considering the climate change and urbanization impacts. Water 6(4):976–992. https://doi.org/10.3390/w6040976

Zongxue X, Gang Z (2016) Impact of urbanization on rainfall-runoff processes: case study in the Liangshui river basin in Beijing, China. In: 7th International water resources management conference of ICWRS, Bochum, Germany, IWRM2016-9-2, pp 1–6. https://doi.org/10.5194/piahs-373-7-2016

Chapter 10
Modeling the Impact of Surface Water Dynamics on the LULC and LST Alteration at the North 24 Parganas in India

Bijay Halder, Jatisankar Bandyopadhyay, and Md. Nazrul Islam

Abstract Surface water area change is the most essential indicator of environmental condition, climate change, availability of water, water planning, and anthropogenic activities. Water resources management is one of the critical evidence for sustainable development and water availability for the future. After cyclone "Aila," North 24 Parganas underwent a huge amount of spatial change. According to the Development Research Communication and Services Centre, a total of 55,600 ha cropland area has been affected in this district due to "Aila." Cropland was transformed into aquacultural pond due to saltwater intrusion in this area. Water intrusion has changed the agricultural practices, livelihood, and also land degradation. Remote sensing data is used for land use and land cover types like water and vegetation area detection. Land surface temperature (LST) is an essential aspect in global climate change studies used in calculating radiation budgets, heat balance studies, and also estimating the climate change scenario in a particular area. Landsat multitemporal imageries during the period of 2000–2020 data are used to identify the water area change detection in the southern parts of North 24 Parganas district, West Bengal. Thick vegetation area was changed by 460.4306 (25.999%), and water bodies were increased by 305.548 sq. km (17.253%) over the study region. Water area change is directly affected by land use and land cover, land surface temperature and also increased sustainable livelihood. This study is helpful for planners, policymakers, and administrators for sustainable development of this area.

Keywords Remote sensing · Multi-temporal satellite image · Water area change · Effects on land · North 24 Parganas

B. Halder (✉) · J. Bandyopadhyay
Department of Remote Sensing and GIS, Vidyasagar University, Midnapore, India

Md. N. Islam
Department of Geography and Environment, Jahangirnagar University, Savar, Dhaka, Bangladesh
e-mail: nazrul_geo@juniv.edu

Introduction

Water is a very important part of worldwide natural resource management that is critical to human survival. The huge amount of population pressure and effective level of human intervention like industrialization, urbanization, and effluent disposal into the surface and groundwater resources needing suitable water resource management have become the complex assignment throughout the world. Managing, assessing, and planning of water resources for suitable use have become the most important challenge in public health, particularly in the region of low rainfall and unpredictable and very high groundwater depth. Investigation, management, and research of the surface and groundwater resources have always been a hot topic since they are key to social, anthropological, ecological, health, and economic development (Sun et al. 2012). Water quality evaluation and water environment have become more important in the current era (Meng et al. 2015; An et al. 2014). Water management strategies not only reveal the water pollution or other situations but also predict the scientific and sustainable water management, decision-making for water pollution control, water scarcity-related education, and appropriate daily water control practice.

Surface water quality or information extraction is the main criterion for investigating water resource management and any environmental condition monitoring (Perrin et al. 2014). Field-based data acquisition takes more time rather than the remotely sensed data collection. Scientists and researchers have been using remote sensing data for estimating the water resource management of an area with the advantages of a large areal observation range, high acquisition, proper information, precise measurement, and low costs (McFeeters 2013). Water quality assessment, water area change, and many other essential techniques are used for water resource management. Numerous satellite imageries are used for surface water extraction and information. Landsat image is used to estimate water resources management like moderate spectral resolution and sensitive response to the surface water. Satellite remote sensing data is an important part of observing, monitoring, detecting, quantifying, and mapping land use and land cover patterns and their changes because satellite covers large spatial coverage, repetitive data acquisition, the digital format available for computer processing, and proper georeferencing application (Loveland and Dwyer 2012). Different spectral indices are used for detecting the water area change.

Land surface temperature is the crust temperature of the earth's surface occurrences. It is reflected in how much hot the earth's surface is and also depends on the different categories of LULC categories (Kayet et al. 2016; Halder et al. 2021b). Many scientists and researchers are worried about the global LST change and its impact on environmental issues. Rural–urban surface temperature variation in a large-scale study has been comprehensively documented since the 1970s (Chandler and TJ 1976; Oke 1982; Quattrochi and Pelletier 1991). North 24 Parganas is one of the districts of West Bengal with a combination of urban and rural parts. The southern part is a dense forest, and the west and northwestern parts are located in an urban area.

The area has mostly agricultural land. Due to rapid urbanization process and increasing construction area, vegetation areas are affected and cause climate change and growing global greenhouse gases. Nowadays, it has become a serious environmental issue. Rajarhat-Newtown, Barasat, Madhyamgram, and Dum Dum areas are a peripheral part of Kolkata, and it increases their urbanization process rapidly. Due to urbanizing process, this area is facing a huge amount of vegetation damage that is affecting this areal evapotranspiration. For those types of environmental cases, this area has been facing a huge climate change since the past decades.

LST is used for calculating and estimating earth's surface temperature diversity depending on different land use and land cover patterns. Vegetation monitoring, built-up area change, and global climate change monitoring are the essential parts, and LST is used for calculating these worldwide difficulties. Due to worldwide climate change, land surface temperature calculation is the most essential factor for surface heat energy balance. Landsat series data is used to identify the land surface temperature of an area using thermal band. The land surface temperature and vegetation have been collected in a scatter plot to get temperature–vegetation space, which reveals the chronological trajectory of pixels ranging from low-temperature high vegetation conditions of urbanization methods (Amiri et al. 2009). Using satellite remote sensing and ground meteorological data, Kato and Yamaguchi (2005) have developed a new method to isolate the anthropogenically settled heat and natural heat radiation from the sensible heat flux, based on their heat balance model. LST is influenced by short-wave surface reflectivity, and it is an important factor of surface component (Ishola et al. 2016; Halder et al. 2021c). Temperature vegetation index is used to estimate the land use and land cover monitoring of an urban area using multitemporal and multispatial satellite remote sensing data. Surface urban heat island includes an assessment of areal land surface temperature that is not the direct capacity of surface radiation, upwelling thermal radiance, and surface emissivity using thermal remote sensing techniques (Voogt and Oke 2003). Satellites do not measure temperature. They measure radiances in various wavelength bands, which mathematically calculate the inference of temperature.

Water is an important part of every ecosystem and people. Climate change is hammering the environment along with the earth's surface change. After "Aila," the North 24 Parganas district has faced a huge amount of water area changes. Not only the water area but also the water quality has changed due to these types of cyclones. Saltwater intrusion can change the surface water area and lifestyle of people. The agricultural area has been changed into a water body. According to the Development Research Communication and Services Centre (DRCSC), a total of 55,600 ha cropland area has been affected in this district due to "Aila." Water body extraction using remote sensing has been the most important method for investigating the water area changes, water quality assessment, and water planning and effect in environmental conditions. Recently, remote sensing techniques have been used to measure the water quality and water body area. Different types of multitemporal imageries in the periods of 2000–2020 data were used for the water area change. Landsat TM and Landsat OLI data were used to identify different types of satellite-derived indexes, such as Normalized Difference Water Index (NDWI), Modified Normalized Difference Water Index (MNDWI), Normalized Difference Vegetation Index (NDVI), and

Water Ratio Index (WRI), for surface water extraction and the total changes of southern parts of North 24 Parganas district. These types of water indices and NDVI were calculated to identify the total water area change in some decades and estimate the most suitable water index model. ERDAS IMAGINE v14 software was used to calculate supervised classification and change detection for total areal changes. The entire water index model was estimated using ArcGIS software. For the result between 2000 and 2020, a huge water body has increased in this district. Barasat-II, Basirhat-II, Sandeshkali-I, some parts of Rajarhat, Haroa, Manikhan, and Hasnabad blocks were changed into a water body in some parts. In some decades, inland fisheries and water bodies were increased in this area.

Study Area

North 24 Parganas is a district of southern West Bengal and the eastern part of India. This area extends in the topical zone from 22°11′ 6″ to 23°15′ 2″ north latitude and 88°20′ to 89°5′ east longitude (Fig. 10.1). In the northern part is located Nadia district, and Bangladesh (Khulna division) is situated in the northern and eastern parts. South 24 Parganas and Kolkata are located in the southern part and Kolkata, Howrah, and Hoogly in the western part. Barasat is the district headquarter of North 24 Parganas. The total area is 141,000 per km^2, and the total population is 1.098 billion (District Handbook 2011, http://wbpspm.gov.in/publications/District%20Statistical%20 Handbook). The average annual precipitation was 1579 mm. North 24 Parganas is situated in lower Ganga, basically located in the Bhagirathi–Hoogly River. In this
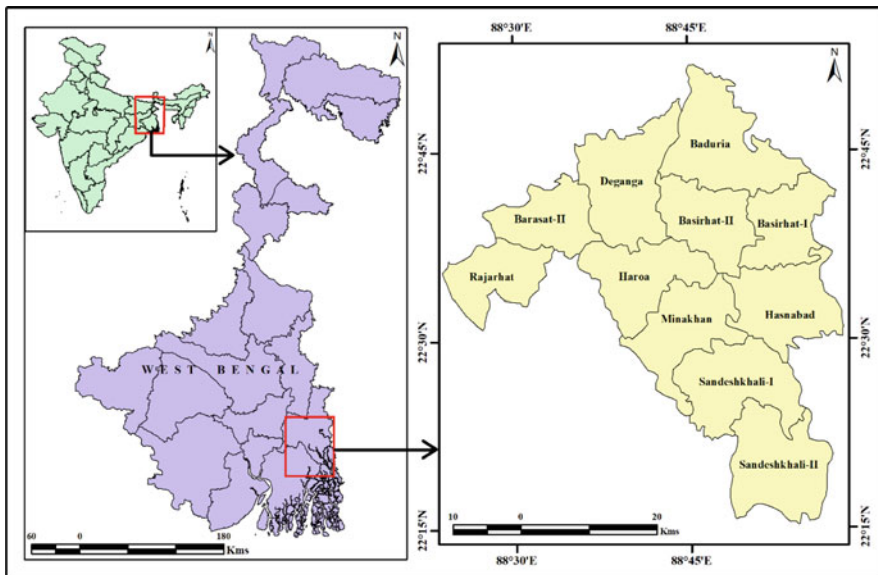
Fig. 10.1 Location map of the study area

area, soil varies widely from alluvial to clay loam. The average temperature is 41 °C in May and 10 °C in January, whereas relative humidity ranges between 50% in March and 90% in July (Methodological Department, India, https://mausam.imd. gov.in/). The main study area, southern parts of North 24 Parganas, covers 1771 sq. km area, and this area has faced huge amount of water change in recent years (Fig. 10.1).

Materials and Methods

Data Sources

The satellite imageries were collected from the USGS website (https://earthexplorer. usgs.gov/). ArcGIS v10.5 and ERDAS IMAGINE v14 software were used for classification and map layout (Fig. 10.2). First, the images were pre-processed and enhanced and then classified with the help of ERDAS IMAGINE. Pixel-wise different types of area were identified, and then changes of the resulting images
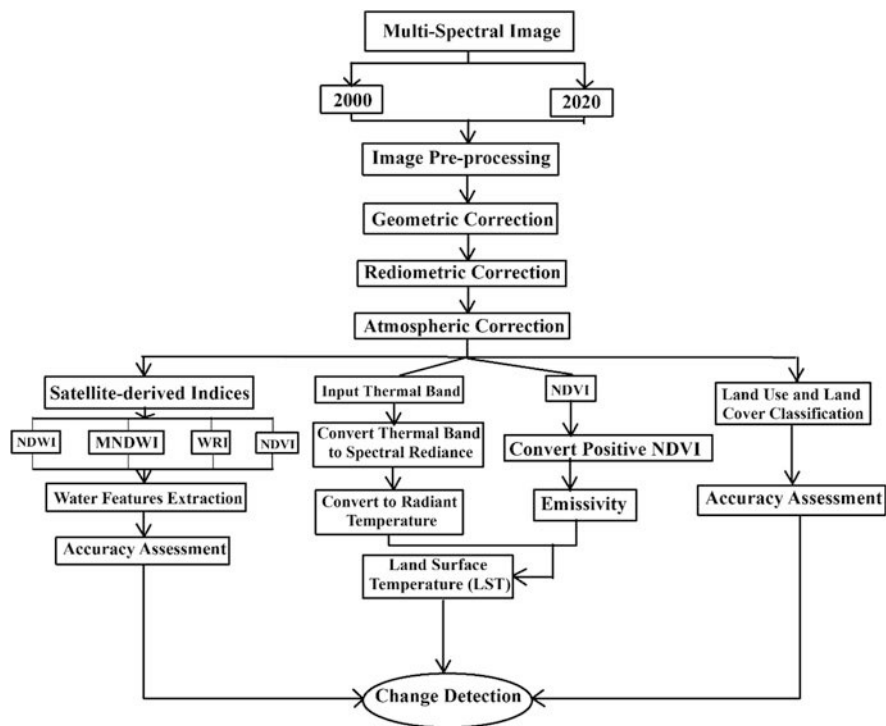
Fig. 10.2 Methodology details of the study

Table 10.1 Information about the Landsat satellite imageries

Sl. no.	Satellite	Sensor	Path and row	Data source
1	Landsat 4–5	TM	138, 44	USGS website
2	Landsat 8	OLI	138, 44	USGS website

were calculated. Satellite data of two different years were used in this study. Multitemporal imageries of two different years (Landsat TM and OLI image 2000–2020) were used to prepare the water area changes (Table 10.1).

Image Processing

The image preprocessing, including geometric, atmospheric, and topographic corrections, was carried out by the Geographical Information System (GIS) indicating spatial and temporal comparability of datasets. Before starting the image classification of satellite data, there was an essential part of preprocessing. This is the procedure to more accurately detect the biophysical phenomena on the bottom, and therefore, the actual data. Data were preprocessed in ERDAS IMAGINE for layer stacking, georeferencing, masking, and subsetting using areas of interest (AOIs). The main objective of satellite image classification was that the per-pixel overlaying in LULC change detection of different years calculated the actual thematic observations.

Image Classification

Satellite image classification was established by acquiring different types of spectral signature of Landsat images. After acquiring the imageries, band color composite selection was the most essential part for different land classes. It can easily detect the different land observations. Near-infrared color composite NIR (band 4), SWIR (band 5), and red (band 3) were applied for different types of vegetation identification. Other color composites like short-wave infrared (7), near-infrared (4), and red (2) band combination were very sensitive in moisture content identification, which was build-up area and bare soil (https://www.usgs.gov/faqs/). Each spectral signature was created using polygon in respective satellite images (Table 10.2). A satisfactory signature is the one ensuring that there is "minimal confusion" among the land use and land cover to be mapped (Halder et al. 2020). In the supervised classification, maximum likelihood method was used. A maximum likelihood classification method is a useful method for classification in remote sensing. It is a pixel-based classification of corresponding classes. The likelihood Lk is defined as the posterior probability of a pixel belonging to class k.

Table 10.2 Descriptive parts of each classified factor of this area

Sl. no.	LULC classes	Description
1	Built-up area	Residential area, commercial, industrial, transportations, roads, and construction area
2	Thick vegetation	Areas having plantation or natural growing forest, including many types of trees
3	Open space	These types of classes are mainly playground, open area, and many others
4	Water bodies	Rivers, ponds, lakes, and open water areas
5	Agricultural land	Cropland and fallow land of this area
6	Open vegetation/grassland	Grass area, open vegetated area

$$Lk = P\,(k/X) = P\,(k) * P(X/k)/\Sigma P\,(i) * P(X/i) \qquad (10.1)$$

where $P(k)$ is the prior probability to observe X from class k or probability density function.

Usually, $P(k)$ is assumed to be equal to each other, and $\Sigma P\,(i)*P(x/i)$ is also common to all classes. Therefore, Lk depends on $P(X/k)$ or the probability density function (http://sar.kangwon.ac.kr/etc).

Post-classification

The post-classification step is used to improve classification accuracy (Cheruto et al. 2016). Using different types of satellite data, medium-spatial resolution of Landsat data mixed pixels is a common problem (Lu and Weng 2005), and mainly the urban areas are heterogeneous mixtures including residential areas, roads, railways, soil, trees, water, and grassland (Jensen et al. 2007). Visual interpretation is an important part of LULC change analysis. After image classification, the geographical area for each land use land cover classes was calculated for change in land use type within two different years. Also, the total percentages were calculated using ERDAS IMAGINE v14 software.

Accuracy Assessment

Remote sensing software is used for accuracy assessment. Accuracy assessment is a technique that represents the correspondence between the aspects of the earth's surface and the results of the classification. It is very important to detect perfect accuracy by proper classification of satellite imageries of different years to analyze the land use changes (Owojori and Xie 2005). Accuracy assessment is an essential

part of any kind of satellite data classification. This method is used to compare the accurate or ground truth data and the classified one. The ground truth data were collected by field or survey. The accuracy was calculated by a classified map using random points from the ground truth data. Nonparametric kappa test was also used for classification accuracy.

Kappa Statistic

Kappa coefficient is not only the diagonal element, it's also used for estimating the confusion matrix of the satellite image clasification. The kappa values are a matric that can compare observed accuracy and expected accuracy or random change (Table 10.2). This value is not only the calculating factor of a single classifier but also the evaluating classifier. The kappa does not take in the degree of disagreement between observers, and all disagreements are treated equally as total disagreement (Cohen 1968; Altman 1991). The kappa statistic is calculated by Eq 10.2 (Table 10.3):

$$K = \frac{(\text{Observed accuracy} - \text{Chance accuracy})}{(1 - \text{Chance accuracy})} \qquad (10.2)$$

Land Surface Temperate Calculation

LST for Landsat TM

The LST is calculated by an established formula. Supported by Cao et al. (2008), to estimate brightness temperature, a two-stop process is followed from Landsat TM images. The equation is calculated as follows:

1. Conversion of the digital number (DN) to spectral radiance (L) (USGS 2001; Halder et al. 2021b) is calculated by Eq. 10.3:

Table 10.3 Scale of kappa coefficient

Sl. no.	Value of K	Strength of agreement
1	<0.20	Poor
2	0.21–0.40	Fair
3	0.41–0.60	Moderate
4	0.61–0.80	Good
5	0.81–1.00	Very good

$$L = \left(\frac{L_{\max} - L_{\min}}{DN_{\max}}\right) \times \text{Band} + L_{\min} \tag{10.3}$$

where L is the spectral radiance, Lmin is 1.238 (spectral radiance of the DN value 1), Lmax is 15.6000 (spectral radiance of DN value 255), and DN is the digital number.

2. Conversion of spectral radiance to temperature in Kelvin (USGS 2001) is calculated by Eq. 10.4:

$$Tb = \frac{K2}{\left(\frac{K1}{L\lambda} + 1\right)} \tag{10.4}$$

where $K1$ is the calibration constant 1 (607.76), $K2$ is the calibration constant 2 (1260.56), and Tb is the surface temperature (Kelvin).

3. Calculation of NDVI:

$$NDVI = \frac{(NIR - R)}{(NIR + R)} \tag{10.5}$$

Land surface emissivity (LSE) is calculated based on NDVI values. It uses the NDVI thresholds method
NDVITHM by applying Eq. 10.5 (Sobrino et al. 2001; Halder et al. 2021c):

$$LSE = (1.0094 + 0.047) \times \text{In}\,(NDVI) \tag{10.6}$$

The NDVI value ranges from 0.157 to 0.727. When the NDVI value is out of range (0.157–0.727), the corresponding input LST constant values are used.

4. Conversion of Kelvin to Celsius (Semenza et al. 1996) is estimated by Eq 10.7:

$$LST = Tb - 273.15 \tag{10.7}$$

LST for Landsat OLI

1. Conversion of the digital number (DN) to spectral radiance (L) (Rasul et al. 2015; Scarano and Sobrino 2015; Halder et al. 2021b) is calculated by Eq. 10.8:

$$L = \left(\frac{L_{\max} - L_{\min}}{DN_{\max}}\right) \times \text{Band} + L_{\min} \tag{10.8}$$

where L is the atmospheric spectral radiance (SR) in Watts/(m^2*srad* μm), L_{max} is the maximum spectral radiance (SR) of the DN value, $BandL_{min}$ is the minimum spectral radiance (SR) of band, and $DN_{max} = Q_{cal\,max} - Q_{cal\,min}$ is the maximum and minimum difference of sensor calibration.

2. Using the thermal constants given in the metadata file, the TIRS band data is converted from SR to BT, once the DN value is converted to SR (Gutman et al. 2013; Halder et al. 2021c) (Eq. 10.9):

$$BT = \frac{K2}{Ln\left(\frac{K1}{L\lambda} + 1\right)} - 273.15 \tag{10.9}$$

where K_2 and K_1 represent the band-specific thermal conversion constants, and BT is the brightness temperature in Celsius.

3. Calculation of NDVI (Roy et al. 2014) (Eq. 10.10):

$$NDVI = \frac{(NIR - R)}{(NIR + R)} \tag{10.10}$$

where the range is between $-1 < NDVI < +1$.

4. Proportion of vegetation is calculated by minimum and maximum NDVI values (Yu et al. 2014). The equation is (Eq. 10.11)

$$Pv = \left(\frac{NDVI - NDVI_{min}}{NDVI_{max} - NDVI_{min}}\right) \tag{10.11}$$

5. Land surface emissivity (LSE) is calculated based on the P_v value. It uses the NDVI thresholds method- NDVITHM by applying Eq. 10.5 (Avdan and Jovanovska 2016; Roy et al. 2014) (Eq. 10.12):

$$LSE = 0.004 \times Pv + 0.986 \tag{10.12}$$

6. Conversion of Kelvin to Celsius (Avdan and Jovanovska 2016; Roy et al. 2014; Yu et al. 2014) is estimated by Eq. 10.13:

$$LST = \frac{BT}{\left\{1 + \left[\frac{\lambda BT}{\rho}\right] In(LSE)\right\}} \tag{10.13}$$

where λ is the wavelength of emitted radiance.

Different Water Extraction Indices

Surface water area extraction in North 24 Parganas from each image for three different time periods is a principal assignment for the water area change detection. In this case, water area is extracted using different water extraction index-based methods to identify the actual changes of this area.

Normalized Difference Vegetation Index (NDVI)

Vegetation is one of the essential parts of the land cover of earth. A healthy vegetation area always helps to reduce soil erosion and floods. It also helps to balance carbon dioxide and oxygen cycle, and the weather change is also affected by the vegetation. In India, 33% of vegetation area is very essential for a healthy life. From the Normalized Difference Vegetation Index (NDVI), we can identify or measure the vegetation quality or quantity of any area. In the map of vegetation quality (NDVI), we identify the degradation or increase of vegetation in southern parts of North 24 Parganas district. Landsat surface reflectance resulted in the Normalized Difference Vegetation Index (NDVI) calculated from the Landsat TM, Landsat ETM+, and Landsat OLI (USGS, NDVI). The NDVI is a multispectral remote sensing data technique used to identify the vegetation area, land cover classification, water body identification, open area, and many types of forest areas. The mathematical calculation of NDVI is defined as the value −1.0 to +1.0. Water bodies are detected in NDVI values to the negative values (Fig. 10.3):

$$NDVI = \frac{NIR - R}{NIR + R} \tag{10.14}$$

where NIR refers to the near-infrared and R refers to red band in the satellite imagery. For the vegetation damaged area calculation, Landsat TM and Landsat OLI are used. In remote sensing, the change detection technique is the most powerful technique to identify the aerial changes in vegetation-covered area and vegetation to the nonvegetation area or nonvegetation to vegetation area.

Normalized Difference Water Index (NDWI)

The Normalized Difference Water Index (NDWI) was first developed by McFeeters in 1996 to detect the surface water areas in the wetland, lake, or water body environment and to allow for the measurement of surface water body extension (McFeeters 2013). The index was created to be used with Landsat multispectral imageries, and it has been successfully used with other sensors in presentation where the measurement of the extended version of the water is desirable (McFeeters 2013; Chowdary et al. 2009). The NDWI is calculated using Eq. (10.15):
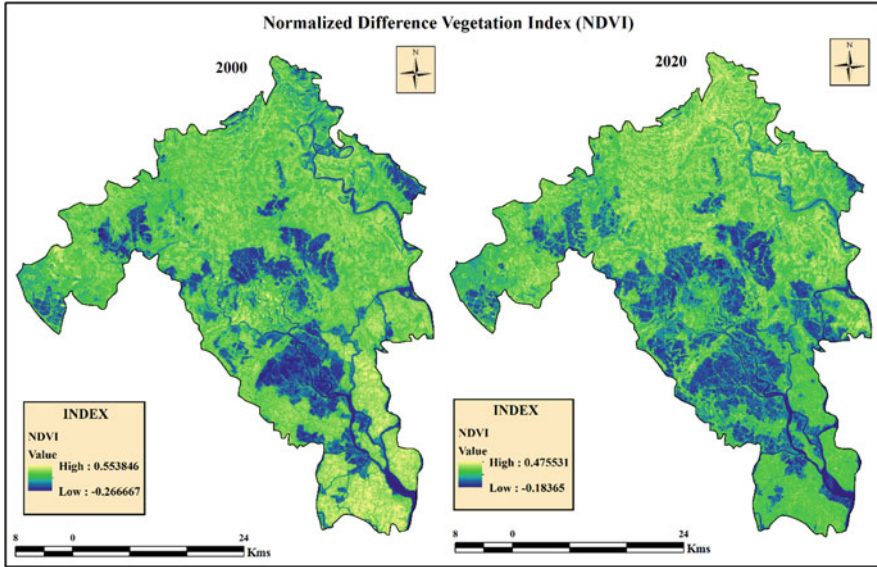
Fig. 10.3 NDVI map of the area between 2000 and 2020

$$NDWI = \frac{Green - NIR}{Green + NIR} \qquad (10.15)$$

This equation represents the green band of the Landsat image, and NIR represents the near-infrared band of the Landsat image (Fig. 10.4). NDWI values greater than zero assume that this area represents the actual water surfaces, whereas values less than or equal to zero show the nonwater body area or surfaces in the particular region. NDWI values are calculated using ArcGIS software and analysis.

Modified Normalized Difference Water Index (MNDWI)

The dynamic thresholds are directly affected by the overall accuracy of surface water area extraction. MNDWI is a formula proposed by Xu (2006) to identify the water area, which is as follows:

$$MNDWI = \frac{Green - SWIR1}{Green + SWIR1} \qquad (10.16)$$

The proposed water extraction technique applied the Modified Normalized Difference Water Index (MNDWI) method in combination with the adaptive dynamic threshold (Fig. 10.5). The MNDWI is used for investigating the water senarioes in the earht surface, which is the modified version of NDWI. The background values are calculated for estimaitng the MNDWI using satellite images.
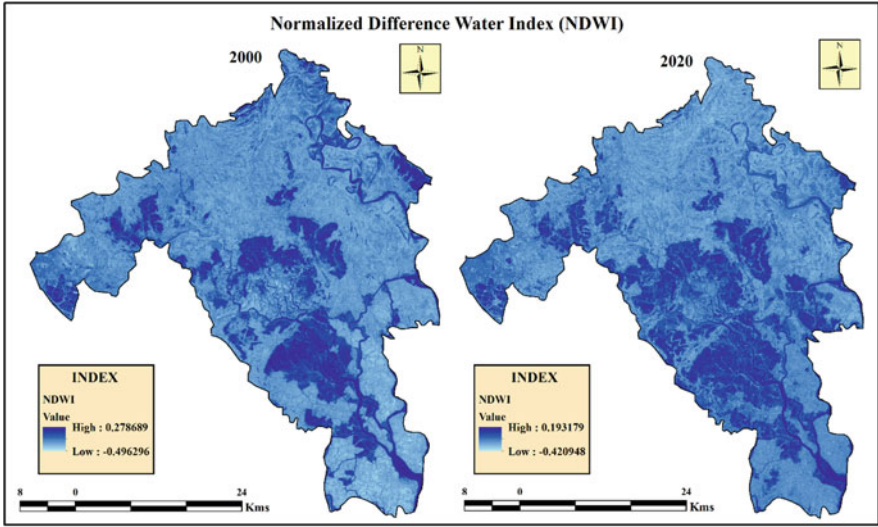
Fig. 10.4 NDWI map of the area between 2000 and 2020
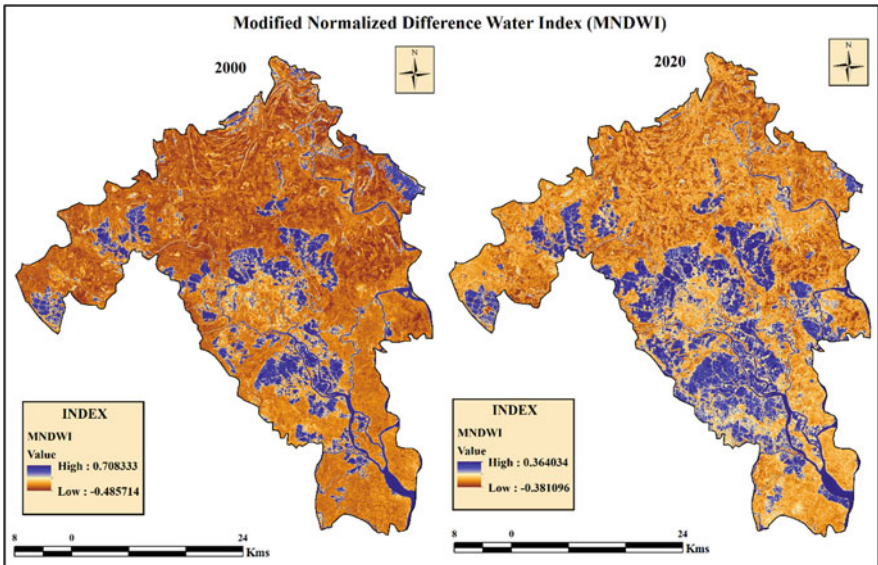
Fig. 10.5 MNDWI map of the area between 2000 and 2020

Water Ratio Index (WRI)

Water Ratio Index dominates spectral reflectance of water bodies in green and red bands as compared to near-infrared and medium infrared (Fig. 10.6). WRI shows the resulting value in general to be greater than 1 for the water body area (Shen and Li 2010):

$$\text{WRI} = \frac{\text{Green} + \text{Red}}{\text{NIR} + \text{SWIR1}} \tag{10.17}$$

Results

After the preprocessing and subsetting areas of interest (AOIs), two satellite images were processed for the derivation of water bodies using different water area extraction equations. The notified water indices were then converted into water area and nonwater features. Different satellite images were classified and validated using accuracy assessment and kappa coefficient. Land surface temperature (LST) was estimated using the notified formula, and the results or changes in this region were inspected.
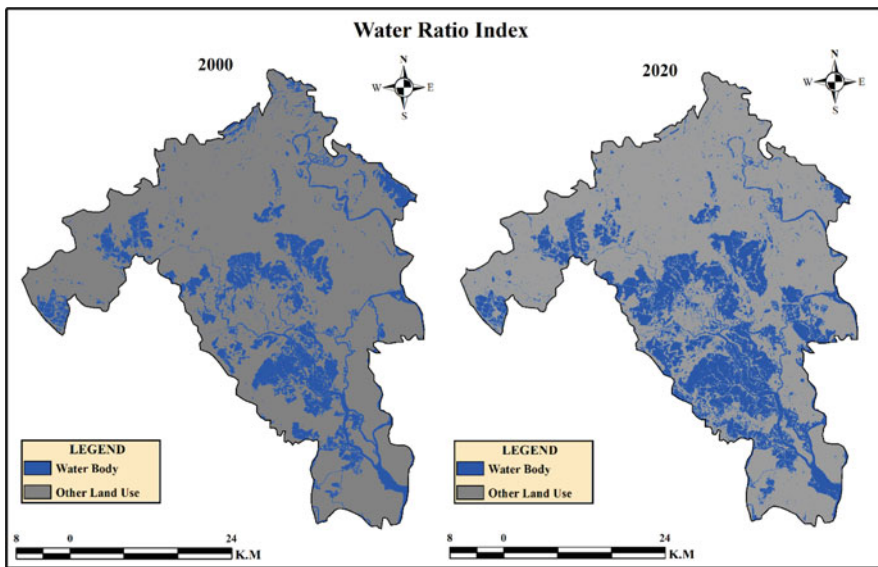
Fig. 10.6 WRI map of the area between 2000 and 2020

Changing Aspects of Surface Water

Due to the diversity, environmental condition, and anthropogenic activities, the local surface water has changed in the past years (2000–2020). The MNDWI variation shows the highest value 0.708333 and lowest value −0.485714 in the year 2000 and 0.364034 and −0.381096, respectively, in the year 2020 (Fig. 10.5). NDWI shows the highest value 0.278689 and lowest value −0.496296 in the year 2000 and 0.193179 and −0.420948, respectively, in the year 2020 (Fig. 10.4). The same changing condition was developing on WRI (Fig. 10.6) and NDVI (Fig. 10.3). Surface water area change is directly affected by population, income condition, and land use and land cover change detection. Most of the areas face a huge amount of water area changes.

Land Use and Land Cover Change

In this study, six types of features were acknowledged for the land use and land cover map: water bodies, built-up area, open space, agricultural lands, thick vegetation area, and open vegetation or grassland areas. The rapid growth of population due to many factors and water area changes caused changes in land use pattern over the region. Also, these blocks acknowledge the rapid growth of water area and decrease in vegetation area (Fig. 10.7).
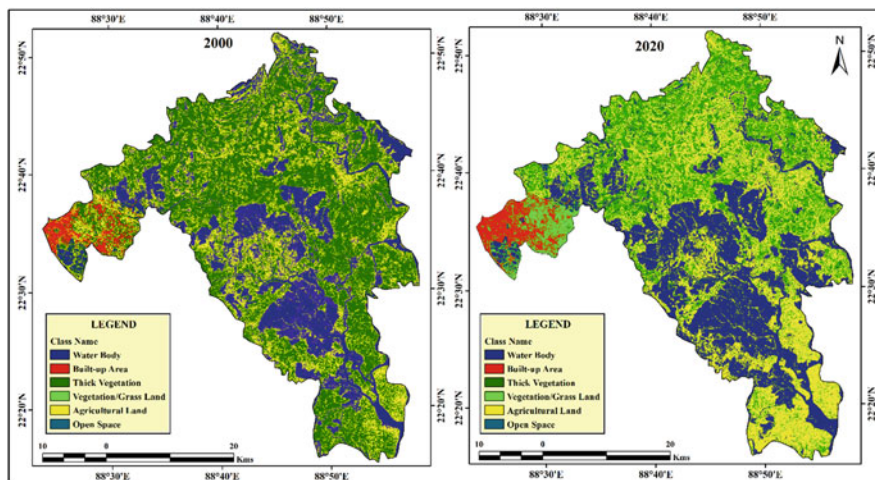
Fig. 10.7 Land use and land cover map in the years 2000 and 2020

Water Bodies

Water bodies are the most controlling factor in the environment. Water is an essential part of people's daily life. The increasing urbanization process can reduce the water bodies in a particular region, but due to the saltwater intrusion during "Aila," the water area increased rapidly in some past decade. In this study area, water bodies increased by around 305.548 sq. km (17.253%) (Fig. 10.8).

Built-up Area

Residential area is mostly affected by land use change. In this region, due to upselling population, built-up area was capturing other areas such as open space, some vegetation cover area, and agricultural land. In this change of 2 years (the years 2000–2020), built-up area increased by about 26.1147 sq. km (1.474%).
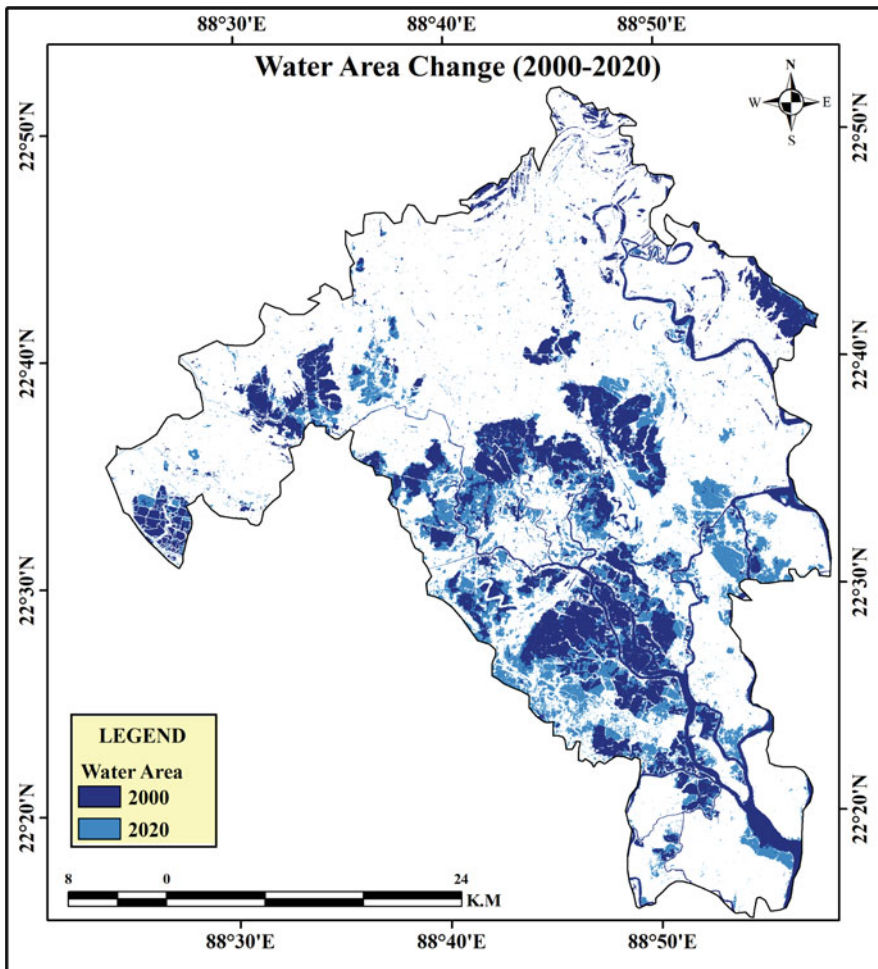
Fig. 10.8 Water area changes during 2000–2020

Table 10.4 Land use and land cover changes analysis

Sl. no.	Class name	Area (sq. km)		Percentage		Increase/decrease	
		2000	2020	2000	2020	Area (sq. km)	Percentage
1	Water body	387.315	692.8625	21.870	39.123	305.5475	17.253
2	Built-up area	63.59541	89.70978	3.591	5.065	26.1147	1.474
3	Open space	25.32684	37.51005	1.430	2.118	12.18321	0.688
4	Agricultural land	334.3774	538.2819	18.881	30.394	203.9045	11.513
5	Thick vegetation	813.1644	352.7338	45.916	19.917	460.4306	25.999
6	Open vegetation/ grassland	147.2214	59.90193	8.313	3.382	93.3201	4.931
	Total area	1771	1771	100	100		

Open Space

Another important land class was open space; it increased to 12.1832 (0.688%). Open space is a better solution to build a residential area or industries. In this study area, the northern part of this entire region was a very good open space location. But in the 2020 census, open space had increased (Table 10.4).

Agricultural Land

The economic stability in rural–urban fringe or rural area is mostly dependent on agricultural land. Man is habited to change his productivity, including agricultural area and other things, in technology. But in this area, they lost their land because in urban regions it is better sustainable rather than in rural regions. So in this case, this region has now grown to become more urbanized and the economy has increased, which is the reason for agricultural land being converted into residential areas. The agricultural land has increased by 203.9045 (11.513%).

Thick Vegetation

When urbanization process was moving forward, the pressure was increased in open space, agricultural land, and vegetation. In this area, due to metro expansion and other facilities, the vegetation-covered area has rapidly decreased. A total of 460.4306 (25.999%) areas were decreased between 2009 and 2019.

Open Vegetation/Grass Land

Grassland is an open vegetation area. Thick vegetation was cut down during anthropogenic activities and scattered some vegetation. Over the 20 years, 93.3201 (4.931%) sq. km grassland area has decreased (Table 10.4).

The accuracy assessment and kappa coefficient were 96% and 0.95 in the year 2000 and 92.80% and 0.91 in the year 2020 (Tables 10.5 and 10.6).

Table 10.5 Accuracy assessment and kappa coefficient in the year 2000

Class name	Ground truth/reference						Row total	Commission error	User accuracy
	Water body	Build-up area	Thick vegetation	Open vegetation/ grassland	Agricultural land	Open space			
Water body	85	0	0	2	0	0	87	2.30%	97.70%
Built-up area	0	34	0	0	0	1	35	2.86%	97.14%
Thick vegetation	0	0	135	3	2	1	141	4.26%	95.74%
Open vegetation/ grassland	0	0	1	112	0	0	113	0.88%	99.12%
Agricultural land	0	0	3	3	64	1	71	9.86%	90.14%
Open space	2	1	0	0	0	50	53	5.66%	94.34%
Column total	87	35	139	120	66	53	500		
Omission error	2.30%	2.86%	2.88%	6.67%	3.03%	5.66%			
Producer accuracy	97.70%	97.14%	97.12%	93.33%	96.97%	94.34%			
Overall accuracy	96.00%								
Kappa coefficient	0.95								

Table 10.6 Accuracy assessment and kappa coefficient in the year 2020

Class name	Ground truth/reference						Row total	Commission error	User accuracy
	Water body	Build-up area	Thick vegetation	Open vegetation/ grassland	Agricultural land	Open space			
Water body	91	0	0	5	0	2	98	7.14%	92.86%
Built-up area	0	58	0	0	0	1	59	1.69%	98.31%
Thick vegetation	0	3	119	5	1	0	128	7.03%	92.97%
Open vegetation/ grassland	0	4	1	97	4	1	107	9.35%	90.65%
Agricultural land	0	0	4	1	58	0	63	7.94%	92.06%
Open space	0	0	0	1	3	41	45	8.89%	91.11%
Column total	91	65	124	109	66	45	500		
Omission error	0.00%	10.77%	4.03%	11.01%	12.12%	8.89%			
Producer accuracy	100.00%	89.23%	95.97%	88.99%	87.88%	91.11%			
Overall accuracy	92.80%			Kappa coefficient	0.91				

4.3. Land Surface Temperature Change Analysis

During 2000–2020, the entire region was facing a huge amount of temperature variation. Some parts of this area were converted from thick forest to water bodies and thick forest to agricultural land. The spatiotemporal distributions of LST from the years 2000–2020 were derived from Landsat thermal bands using the same formula. The red color shows the lowest temperature and green shows the highest temperature in this region. The LST variation of the year 2000 is 20.6194–29.1833 °C and for the year 2020 is 22.0007–31.12714 °C (Fig. 10.9). The average temperatures are 24.90135 °C and 26.5639 °C in the years 2000 and 2020, respectively (Table 10.7). The urban areas, such as Newtown and Bidhannagar, are facing a huge amount of temperature variation, and in other parts of this area such as Haroa, Basirhat, Chantal, Nazat, and Sandeshkhali areas changes in LST due to deforestation, water area change during "Aila," and anthropogenic activities can be seen (Table 10.8). In the year 2000, south and southeastern parts faced the lowest amount of temperature, but due (1) to deforestation and (2) aquacultural activities, the normal temperature has changed in this area. Urbanization, population pressure, and climate change directly affect the LST, and this change is clearly shown in Fig. 10.9.
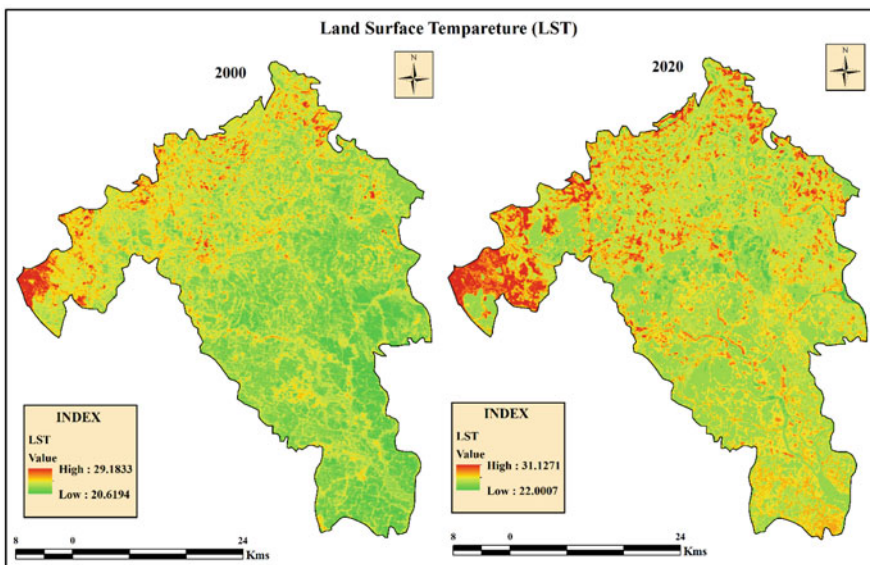
Fig. 10.9 Land surface temperature during 2000–2020

Table 10.7 Maximum and minimum temperature variation in between 2000 and 2020

Data used	Min temperature (°C)	Max temperature (°C)	Average temperature (°C)
Landsat TM	20.6194	29.1833	24.90135
Landsat OLI	22.0007	31.1271	26.5639

Table 10.8 Temperature variation in different areas

Important area	Temperature (°C) in 2000	Temperature (°C) in 2020
Newtown	28.72	31.07
Bidhannagar	29.9	31.1
Hasnabad	23.5	28.3
Haroa	22.4	28.9
Basirhat	27.6	29.8
Gagramari	23.25	23.02
Chaital	22.37	23.45
Minakhan	23.69	23.25
Nazat	22.81	23.06
Sandeshkhali	22.8	24.02

Discussion

Assessment of Water Indices with LULC and LST

According to the DRCSC, a total of 55,600 ha/556 sq.km cropland area was affected in this district due to "Aila." The southern parts of this area faced a huge change in the water area. Not only the cropland area but also the vegetation parts were changed due to this environmental hazard. South and southeastern parts of the study area were changing all aspects of LULC class and LST. Water indices like MNDWI, NDWI, WRI, and NDVI showed water bodies developing more during the years 2000–2020. Also, the middle parts were also facing the same condition. Saltwater intrusion affected the cropland area and land lost its productive energy. Population pressure and lower-income families converted their agricultural land into water areas. Due to the total LST in the years 2000–2020, a huge amount of change was observed. The correlation with different water indices and LST shows variation of water bodies (Fig. 10.10).

Impact Factor of Surface Water Area Changes

The surface water area change dynamics are related to climate change and human factors. The influencing factors are increasing temperature, precipitation, and also the super cyclone Aila. After this hazard, saltwater intrusion has changed the local people's lives and has led them to be economically strong, and side-by-side they are cutting down the forest or vegetation area and converting them into aquacultural ponds. Only the northern parts have been changed into built-up areas. But the middle, south, and southeastern parts of this area have been changed into water bodies. Sustainable fish cultivation and marketing is good for this area due to government policies. Awareness, training, and other essential criteria were being filled up by the concerned authorities. This has contributed more to fish production and has increased their better livelihood after water area changes.
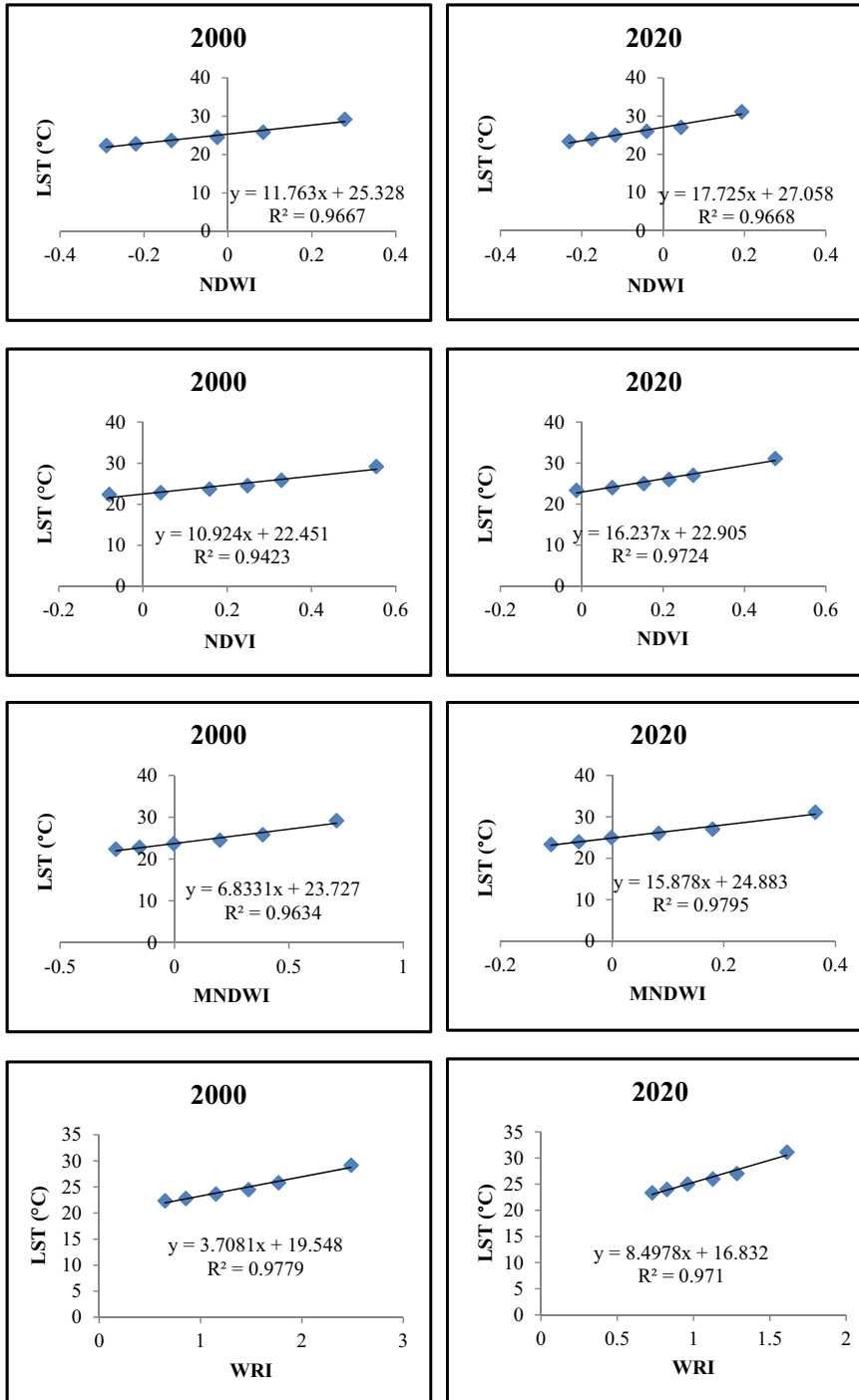
Fig. 10.10 Relationship between different water indices and LST

Conclusion

This study has evaluated water area change and over LULC change during the periods of 2000–2020 and its impact of LST over the southern parts of North 24 Parganas district region of southeast India. In this study estimate, the total water area increased by approximately 18% (305.5475 sq. km) since the year 2000; simultaneously, the thick vegetation decreased by over 26% since the year 2000. The LST increased by around 2 °C over the area because this area is facing a huge amount of water body changes, but urban areas like Rajarhat-Newtown and Bidhannagar have witnessed a huge amount of land surface temperature increase. Sundarban areas are most affected due to natural hazards and climate changes. After Aila, the entire region is facing a massive amount of water area changes due to saltwater intrusion. Many areas have adopted the change and are transforming agricultural land into water areas. The anthropogenic activities like urban area expansion, deforestation, and daily needs also affect the LULC change, but after the land area was converted into water area, the local people have become economically stronger. The local name "Bheri" is used for fish cultivation. The middle part of this area evaluated a huge amount of water area changes. Between 2000 and 2020, anthropogenic activities and natural hazards affected the entire region. LULC is also changed its effect on LST. West Bengal is a cultivated state of India, and basically, rice is the major crop production in this state. Currently, fish production is the leading cultivation in West Bengal, and this region contributes their best.

Further investigative studies are essential to precisely explain the environmental condition and climate change effects in this region. River dynamics and the water area changes clearly show the change in water bodies in this area. River area conservation, land dynamics, flood monitoring, and water intrusion are the major future research topics in this region. The LST mapping provides the necessary information that will help the environmental management in this area and control the climate change effect. The administrative authorities can improve the more required essential things to better sustainable cultivation in this region. Also, control the land transformation and build an environmentally strong region. The anthropogenic activities are more harmful to the natural conserved area. The mangrove region protects humans from natural hazards like floods, cyclones, or coastal vulnerabilities. The administrative authorities are focusing on this region and have given them a sustainable livelihood for the future. This methodology is also further used in another area with their suitable areal modification. Water quality, fish production, land transformation, LULC prediction, and socioeconomic conditions are the furthermore investigative studies essential to this region.

References

Altman DG (1991) Mathematics for kappa. Pract Stat Med Res 1991:406–407

Amiri R, Weng Q, Alimohammadi A, Alavipanah SK (2009) Spatial–temporal dynamics of land surface temperature in relation to fractional vegetation cover and land use/cover in the Tabriz urban area, Iran. Remote Sens Environ 113(12):2606–2617

An Y, Zou Z, Li R (2014) Water quality assessment in the Harbin reach of the Songhuajiang River (China) based on a fuzzy rough set and an attribute recognition theoretical model. Int J Environ Res Public Health 11(4):3507–3520. https://doi.org/10.3390/ijerph110403507

Avdan U, Jovanovska G (2016) Algorithm for automated mapping of land surface temperature using LANDSAT 8 satellite data. J Sens 2016

Cohen J (1968) Weighted kappa: nominal scale agreement provision for scaled disagreement or partial credit. Psychol Bull 70(4):213. https://psycnet.apa.org/doi/10.1037/h0026256

Chandler TJ, TJ C (1976) Urban climatology and its relevance to urban design. Chowdary VM, Chandran RV, Neeti N, Bothale RV, Srivastava YK, Ingle P, . . . & Singh R. (2008). Assessment of surface and sub-surface waterlogged areas in irrigation command areas of Bihar state using remote sensing and GIS. Agric Water Manag 95(7):754–766

Ca L, Li P, Zhang L, Chen T (2008) Remote sensing image-based analysis of the relationship between urban heat island and vegetation fraction. Int Arch Photogramm Remote Sens Spat Inform Sci 37

Cheruto MC, Kauti MK, Kisangau DP, Kariuki PC (2016) Assessment of land use and land cover change using GIS and remote sensing techniques: a case study of Makueni County, Kenya. http://repository.seku.ac.ke/handle/123456789/3062

Chowdary VM, Ramakrishnan D, Srivastava YK, Chandran V, Jeyaram, A (2009) Integrated water resource development plan for sustainable management of Mayurakshi watershed, India using remote sensing and GIS. Water resources management 23(8): 1581–1602.

Gutman G, Huang C, Chander G, Noojipady P, Masek JG (2013) Assessment of the NASA–USGS global land survey (GLS) datasets. Remote Sens Environ 134:249–265

Halder B, Bandyopadhyay J, Banik P (2020) Assessment of hospital sites' suitability by spatial information technologies using AHP and GIS-based multi-criteria approach of Rajpur–Sonarpur municipality. Model Earth Syst Environ 6(4):2581–2596. https://doi.org/10.1007/s40808-020-00852-4

Halder B, Das S, Bandyopadhyay J, Banik P (2021a) The deadliest tropical cyclone 'Amphan': investigate the natural flood inundation over south 24 Parganas using google earth engine. Safety Extreme Environ:1–11. https://doi.org/10.1007/s42797-021-00035-z

Halder B, Banik P, Bandyopadhyay J (2021b) Mapping and monitoring land dynamic due to urban expansion using geospatial techniques on South Kolkata. Saf Extreme Environ. https://doi.org/10.1007/s42797-021-00032-2

Halder B, Bandyopadhyay J, Banik P (2021c) Evaluation of the climate change impact on urban heat Island based on land surface temperature and geospatial indicators. Int J Environ Res. https://doi.org/10.1007/s41742-021-00356-8

Ishola KA, Okogbue EC, Adeyeri OE (2016) Dynamics of surface urban biophysical compositions and its impact on land surface thermal field. Model Earth Syst Environ 2(4):1–20

Jensen R, Mausel P, Dias N, Gonser R, Yang C, Everitt J, Fletcher R (2007) Spectral analysis of coastal vegetation and land cover using AISA+ hyperspectral data. Geocarto Int 22(1):17–28. https://doi.org/10.1080/10106040701204354

Kato S, Yamaguchi Y (2005) Analysis of urban heat-island effect using ASTER and ETM+ data: separation of anthropogenic heat discharge and natural heat radiation from sensible heat flux. Remote Sens Environ 99(1–2):44–54. https://doi.org/10.1016/j.rse.2005.04.026

Kayet N, Pathak K, Chakrabarty A, Sahoo S (2016) Spatial impact of land use/land cover change on surface temperature distribution in Saranda Forest, Jharkhand. Model Earth Syst Environ 2(3): 127. https://doi.org/10.1007/s40808-016-0159-x

Lu D, Weng Q (2005) Urban classification using full spectral information of Landsat ETM+ imagery in Marion County, Indiana. Photogramm Eng Remote Sens 71(11):1275–1284. https://doi.org/10.14358/PERS.71.11.1275

Loveland TR, Dwyer JL (2012) Landsat: building a strong future. Remote Sens Environ 122(22–21):29

McFeeters SK (2013) Using the normalized difference water index (NDWI) within a geographic information system to detect swimming pools for mosquito abatement: a practical approach. Remote Sens 5(7):3544–3561. https://doi.org/10.3390/rs5073544

Meng X, Zhang Y, Yu X, Zhan J, Chai Y, Critto A et al (2015) Analysis of the temporal and spatial distribution of lake and reservoir water quality in China and changes in its relationship with GDP from 2005 to 2010. Sustainability 7(2):2000–2027. https://doi.org/10.3390/su7022000

Oke TR (1982) The energetic basis of the urban heat island. Q J R Meteorol Soc 108(455):1–24

Owojori A, Xie H (2005) Landsat image-based LULC changes of San Antonio, Texas using advanced atmospheric correction and object-oriented image analysis approaches. In 5th international symposium on remote sensing of urban areas, Tempe, AZ

Perrin JL, Raïs N, Chahinian N, Moulin P, Ijjaali M (2014) Water quality assessment of highly polluted rivers in a semi-arid Mediterranean zone Oued Fez and Sebou River (Morocco). J Hydrol 10:26–34. https://doi.org/10.1016/j.jhydrol.2013.12.002

Quattrochi DA, Pelletier RE (1991) Remote sensing for analysis of landscapes: an introduction. Ecol Stud 82:51–76

Rosenfield GH, Fitzpatrick-Lins K (1986) A coefficient of agreement as a measure of thematic classification accuracy. Photogramm Eng Remote Sens 52(2):223–227. https://pubs.er.usgs.gov/publication/70014667

Roy DP, Wulder MA, Loveland TR, Woodcock CE, Allen RG, Anderson MC et al (2014) Landsat-8: science and product vision for terrestrial global change research. Remote Sens Environ 145: 154–172

Rasul A, Balzter H, Smith C (2015) Spatial variation of the daytime Surface Urban Cool Island during the dry season in Erbil, Iraqi Kurdistan, from Landsat 8. Urban Clim 14:176–186

Semenza JC, Rubin CH, Falter KH, Selanikio JD, Flanders WD, Howe HL, Wilhelm JL (1996) Heat-related deaths during the July 1995 heat wave in Chicago. N Engl J Med 335(2):84–90

Sobrino JA, Raissouni N, Li ZL (2001) A comparative study of land surface emissivity retrieval from NOAA data. Remote Sens Environ 75(2):256–266. https://doi.org/10.1016/S0034-4257(00)00171-1

Shen L, Li C (2010) Water body extraction from Landsat ETM+ imagery using adaboost algorithm. In 2010 18th International Conference on Geoinformatics, IEEE, pp 1–4

Sun F, Sun W, Chen J, Gong P (2012) Comparison and improvement of methods for identifying waterbodies in remotely sensed imagery. Int J Remote Sens 33(21):6854–6875. https://doi.org/10.1080/01431161.2012.692829

Scarano M, Sobrino JA (2015) On the relationship between the sky view factor and the land surface temperature derived by Landsat-8 images in Bari, Italy. Int J Remote Sens 36(19–20): 4820–4835

USGS, NDVI: https://www.usgs.gov/land-resources/nli/landsat/landsat-normalized-difference-vegetationindex?Qt-science_support_page_related_con=0#qt-science_support_page_related_con

USGS (2001) Landsat Science Data User's handbooks https://www.usgs.gov/land-resources/nli/landsat/landsat-8-data-users-handbook

Voogt JA, Oke TR (2003) Thermal remote sensing of urban climates. Remote Sens Environ 86(3):370–384. https://doi.org/10.1016/S0034-4257(03)00079-8

Xu H (2006) Modification of normalised difference water index (NDWI) to enhance open water features in remotely sensed imagery. Int J Remote Sens 27(14):3025–3033

Yu X, Guo X, Wu Z (2014) Land surface temperature retrieval from Landsat 8 TIRS—comparison between radiative transfer equation-based method, split window algorithm and single channel method. Remote Sens 6(10):9829–9852

Chapter 11
Role of Natural Gas in Energy Security and Climate Change Mitigation: Indian Context

Anirbid Sircar, Kriti Yadav, Namrata Bist, Hemangi Oza, and Kamakshi Rayavarapu

Abstract India is the third largest economy in the world. India's energy mix has only 6% natural gas contribution. Key drivers for natural gas production and utilization in India depend on urbanization and industrialization. Natural gas is a clean fuel that emits minimum particulate matter. Natural gas will play an important role in energy security and climate change in India. The Ministry of Petroleum and Natural Gas is committed to improving the percentage of natural gas in the energy mix of India up to 15% by 2030. This will help to fulfil the commitment of India to the Paris Climate Agreement (COP21) ratified on 2 October 2016. The chapter discusses natural gas resources and reserves of India, natural gas demand in India, gas pipeline infrastructure, liquefied natural gas (LNG) infrastructure, city gas distribution (CGD) and compressed natural gas (CNG) infrastructure of India. The chapter discussed the strategies for the increasing role of natural gas in the energy basket of India. Finally, the chapter summarizes the role of natural gas in the transition to a lower-carbon economy.

Keywords Energy security · Climate change · CGD · CNG · LNG

Introduction

Natural gas is a colourless, odourless clean gas. It is lighter than air and is harmless to the human body. The gas may cause asphyxiation in a confined place and can kill if it displaces air. It has a high calorific value. Gas distribution companies face both opportunities and challenges in helping their communities take advantage of newly

A. Sircar (✉) · K. Yadav · N. Bist · H. Oza · K. Rayavarapu
School of Petroleum Technology, Pandit Deendayal Petroleum University, Gandhinagar, Gujarat, India
e-mail: anirbid.sircar@spt.pdpu.ac.in; Yadav-kriti.yphd15@spt.pdpu.ac.in;
namrata.bist@spt.pdpu.ac.in; hemangi.oza@spt.pdpu.ac.in;
kamakshi.rayavarapu@spt.pdpu.ac.in

abundant supplies of natural gas. Technology advancement of natural gas extraction has opened opportunities to unlock recoverable resources that can last the next 100 years. In recent years, unconventional energy extraction in the oil and natural gas industry allows access to gas that has not been thought to be economical in the oil and gas industry. Natural gas has been produced from low permeability source rock using a combination of hydraulic fracturing and horizontal drilling. Confidence has been seen in the gas market across the world. Power generators are planning more investment in power plants. Transportation companies are adding compressed natural gas (CNG) and liquefied natural gas (LNG)-based automobiles, vans and trucks to their fleets and are considering the use of LNG in locomotives, barges and ships over the past five years. It has become evident that unconventional technologies have made a vast new natural gas resource accessible to development. In recent years, estimates of technically recoverable resource base have ranged from 2300 to 3800 TCF, enough to supply current consumption for 88–154 years (IHS CERA 2014). According to recent technology development, biogas can also be upgraded to produce biomethane of good quality to inject into the existing gas grid. The process requires the separation of CO_2 using physical absorption, chemical absorption, cryogenic separation, membrane separation or pressure swing adsorption processes. Processing leaves a gas stream with greater than 97% methane content, which can be injected into the existing gas grid. The advantage of biomethane is that it has a high calorific value than biogas. It can be used more flexibly because it is virtually indistinguishable from natural gas. The other source of natural gas is methane hydrate which consists of methane molecules within a cage of ice crystals. Methane hydrate has an enormous potential global gas resource, but development is still years away. On the other hand, hydrates may accelerate global warming. There is a lot of speculation whether hydrates could be the 'next shale gas'.

India has relied on coal to power its electricity sector. Coal is abundantly available in India, and the country holds 7% of the world's proven coal reserves. Currently, India primarily depends upon coal to meet its energy needs. Going forward, a contribution from natural gas (being a cleaner fuel) is expected to increase significantly, displacing oil products, while coal may still dominate the energy basket. By 2025, India's energy basket will have 20% of natural gas. The gas price of domestic natural gas for the period 1 April 2015 to 30 September 2015 was $4.66/MMBTU. From 1 October 2015 till 31 March 2016, it will be of the order of US $3.82/MMBTU on gross calorific value (GCV) basis. The gross production of natural gas for November 2015 was 2716 MMSCM which was lower by 3.9% compared with the corresponding month of the previous year (2827 MMSCM).

Natural Gas: Properties and Security

Natural gas is a gaseous fossil fuel consisting primarily of methane. It may also contain other gaseous heavier hydrocarbons, namely, ethane, propane, butane, etc. Sometimes nitrogen, helium, carbon dioxide, traces of hydrogen sulphide and water

Table 11.1 Composition of natural gas

Sr. no.	Name of the constituent	Chemical formula	Percentage
1	Methane	CH_4	70–90
2	Ethane	C_2H_6	0–20
3	Propane	C_3H_8	0–20
4	Butane	C_4H_{10}	0–20
5	Carbon dioxide	CO_2	0–8
6	Oxygen	O_2	0–0.2
7	Nitrogen	N_2	0–5
8	Hydrogen sulphide	H_2S	0–5
9	Rare gases	A, He, Ne, Xe	Traces

are also associated with natural gas. Mercury may also be present in natural gas in small amounts in some fields. The exact composition of natural gas varies between gas fields. The typical composition of natural gas is shown in Table 11.1.

Natural gas is a colourless, odourless and tasteless non-toxic gas. It burns with a blue flame. Natural gas is about 40% lighter than air. Being so, it tends to dissipate in the air if it ever leaks. Natural gas has a density of 0.717 kg/m^3 and a boiling point of $-161.60\,^{\circ}$C. It has a high auto-ignition temperature and narrow flammability range, which means it will auto-ignite at 580 $^{\circ}$C and burn at 5–15% mixture in air. Natural gas has a high calorific value of about 950–1150 Btu/lb, which varies depending upon the composition. Natural gas properties vary to some extent with the composition of the gas. Processed natural gas is harmless to the human body, but it may lead to asphyxiation in confined space.

Natural Gas: India and World

In India global consumption growth was weaker then production. The present trend in oil consumption and its discouraging prospects make natural gas a viable replacement for oil in near future. Natural gas is one of the most important energy sources for the future and the cleanest fuel with less carbon dioxide than oil. Natural gas demand has increased significantly in recent years due to the increase in the availability of gas, competitive pricing and the development of transmission and distribution infrastructure.

Indian Scenario

Indian economy is expected to achieve average GDP growth of 6.4% during 2008–2035 (Vision 2030, PNGRB 2013). The natural gas sector in India is on the threshold of rapid growth due to an increase in demand for clean and sustainable

energy sources, greater exploration activities under New Exploration Licensing Policy (NELP) and commissioning of new LNG terminals and gas pipelines across India (GAIL Voice 2014). Natural gas industries in the country started in the 1960s with the gas discoveries in Gujarat and Assam field. Exploration activities in India were carried out by National Oil Companies (NOCs) such as ONGC and OIL under nomination regimes (MoPNG, Annual Report 2014–2015). The discovery of natural gas in KG D-6 fields was expected to have a big change in the oil and gas market, but due to geological challenges in the field, there was a decline in production of about 55 MMSCMD in 2010 to 13 MMSCMD in 2013 (Sah 2013).

According to BP statistics review 2014, India is the fourth largest consumer of energy in the world. Domestic gas production during 2014–2015 was around 91.77 MMSCMD and supply was 74.79 MMSCMD. Consumption of natural gas is 119.34 MMSCMD for domestic gas and 44.55 MMSCMD for imported R-LNG (MoPNG, Annual Report 2014–2015). The power demand, CGD and the industrial user have been raised and increased the import and investment in supporting infrastructure. The growth in natural gas demand offers huge opportunities in the Indian natural gas industry.

The graph (in Fig. 11.1) indicates the gap between supply and demand for natural gas in the country. To decrease the deficit of natural gas, India has increased the import of natural gas in recent years.

World Scenario

According to BP Statistical Review, natural gas accounted for 23.7% of primary energy consumption in the world in 2014. As per the International Energy Outlook
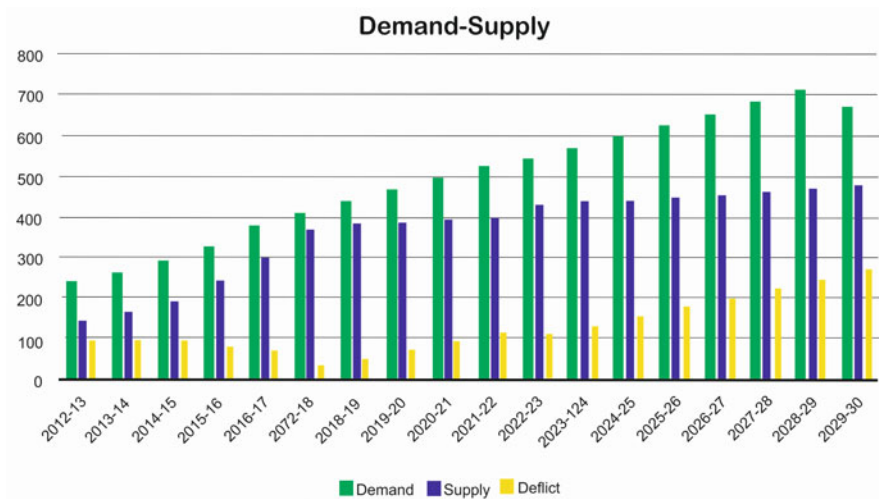
Fig. 11.1 Demand supply of natural gas. (In million metric standard cubic metre per day, MMSCMD; Vision 2030, PNGRB 2013)

World Energy Consumption by Source, 1990-2040
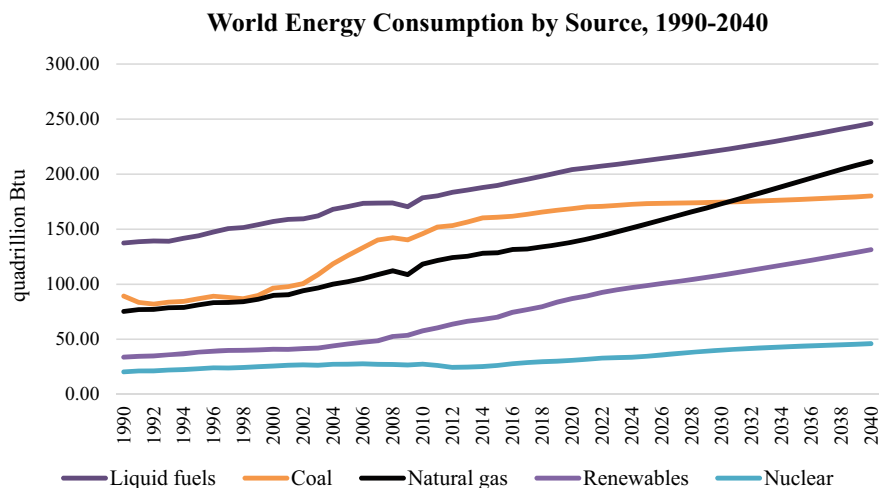
Fig. 11.2 World energy consumption from 1990 to 2040. (International Energy Outlook, EIA, 2016)

2016 released by EIA, natural gas may grow fastest among fossil fuels, and by 2030 natural gas may surpass coal as the world's second largest energy source after oil (Fig. 11.2).

As per the International Energy Outlook 2016, the world's total natural gas consumption may increase by 1.9% per year on average. The increase is projected from 120 trillion cubic feet (TCF) in 2012 to 133 TCF in 2020 and 2030 TCF in 2040. The driving force for such rapid growth in the consumption of natural gas is the exploitation of abundant natural gas resources, particularly from shale formations. Robust production procedures due to advances in horizontal drilling and hydraulic fracturing technologies have also played a role in the growth of the natural gas industry. From 2015 to 2040, natural gas demand is expected to increase in all end-user sectors, with the largest increment in the electric power sector and the industrial sector. In the power sector, natural gas is an attractive choice for new power-generating plants because of its fuel efficiency and environmental friendliness due to low carbon dioxide (CO_2) and carbon monoxide (CO) emissions.

In 2014, New Policies Scenario, the International Energy Agency (IEA) forecasts that non-OECD demand will continue to constitute the majority of world gas demand, growing from 53% (1806 billion cubic metres) in 2012 to 61% (3035 BCM) in 2035 (Sen 2015). Consumption of all the fuels has increased, and global consumption growth of oil and natural gas was weaker than production in 2014 (BP Statistical Review of World Energy, 2015).

The Organisation for Economic Co-operation and Development's (OECD) consumption is larger than average decline, whereas EU and Japan have above-average growth than in the United States. Due to the fall in oil and gas prices, energy price development is generally weak. Global primary energy consumption had increased by 0.9% in 2014 (BP Statistical Review of World Energy, 2015).

Global natural gas production is increased by 1.6% (BP Statistical Review of World Energy, 2015), and its growth was below average in all regions except North America. EU production fell sharply, and the United States was recorded to have the world's largest production accounting for 77% of net global growth. Russia and the Netherlands had the largest volumetric decline. Global natural gas trade registered a fall of 3.4%, a rare contraction in 2014.

World natural consumption increased by 0.4%, and growth was below average in both OECD and emerging countries. Europe and Eurasia had volumetric decline in the world, that is, Germany, Italy, Ukraine, France and the United Kingdom.

Natural Gas Sources and Gas Discoveries

Natural gas is mined from drilled wells of depth between 1000 m to 1500 m approximately (pre- and post-tertiary). This gas can be either thermogenic or biogenic. Depending on the calorific value of the gas, the gas is utilized for CGD sectors as a source after processing and transportation of the same. India imports nearly a quarter of its natural gas needs but fails to meet demand. This may be attributed to insufficient domestic gas production and full utilization of existing import capacity. Power and fertilizer consume the major share of gas available in the country. The gas demand has also significantly increased attributing to demand in other growing sectors such as CGD, refining and petrochemicals. Due to this reason, India's dependence on LNG has increased. According to the BP Statistical Review of World Energy 2015, India is the world's third largest importer of LNG with an import of 18.9 billion cubic metres. The supply of natural gas from gas-producing wells is erratic and has also led to a demand–supply gap. Due to this reason, it is prudent to explore alternate gas sources for the sector.

Natural Gas Sourcing and Allocation

Natural gas available in India can be categorized into domestic natural gas and imported natural gas. LNG, gas from hydrates, coal-bed methane (CBM), and shale are some of the gas sources for the CGD industry. Domestic gas can be further divided into subcategories, viz., Administrative Price Mechanism (APM) and non-APM gas available from nominated blocks of National Oil Companies (NOCs); pre-NELP gas and NELP gas. Domestic gas is allocated to various sectors, such as power, fertilizer, gas distribution, petrochemical sector, etc., based on government guidelines. Imported gas is freely available for marketers to purchase/ sell the same.

Till 2010, gas produced from existing fields of the nominated blocks of NOCs, like OIL and ONGC, was being supplied predominantly to fertilizer plants, and power plants at APM rates. These gas-producing blocks were allotted to NOCs on a

nomination basis under the tax royalty regime. NOCs, like ONGC and OIL, are free to charge a market-determined price for gas produced from new fields in their existing nominated blocks. But the government has issued a pricing schedule and guidelines for commercial utilization of non-APM gas produced by NOCs from their nominated blocks.

To overcome funding constraints, NOCs made discoveries and auctioned the pre-NELP blocks to private sector E&P companies. In pre-NELP production sharing contracts (PSCs), the government can appoint a nominee for purchasing and marketing the gas. Under the New Exploration Licensing Policy (NELP), the government auctioned blocks to private investors and NOCs to ensure level playing. The government extended the same fiscal and contract terms, and accordingly, several gas discoveries have been made under the IX rounds of NELP conducted so far. Under NELP contracts, freedom has been given to the contractor to market gas subject to the allocation made by the government under its policy on utilization of natural gas.

Till 2013, the fertilizer sector, power sector and LPG plants were given priority over the CGD sector for allocation of APM gas. The policy of gas allocation to various sectors changed in late 2014, giving first preference to CGD sector, second preference to plants providing inputs to strategic sectors of atomic energy and space research, third preference to LPG plants, fourth preference to fertilizer plants and fifth preference to power plants.

LNG in India

As far as gas sourcing is concerned, liquefied natural gas (LNG) is the milestone step in the direction of supply security. In addition to domestic sources of natural gas, re-gasified liquefied natural gas (R-LNG) is emerging as the preferred source for assured gas supply for India in future. In future, R-LNG will be the preferred source for city gas distribution. India is building a strong R-LNG infrastructure with a planned capacity of around 35 MMTPA till 2016. More than 40% of the current natural gas supply is met through LNG imports, and the share is expected to increase around 50% by 2016.

LNG is composed of predominantly methane and is converted into liquid form for storage and transportation. It is odourless, colourless, non-toxic and non-corrosive. LNG is cooled to −259 °F through a process known as liquefaction. Certain concentrations of hydrocarbons, water, carbon dioxide, oxygen and some other sulphur compounds are either reduced or removed. LNG floats if spilt on water. LNG is transported in ships specifically designed to handle the low temperature of LNG. When LNG is received at most terminals, it is transferred to insulated storage tanks specially designed to hold LNG. It is a viable alternative to compressed natural gas and is useful for heavy-duty vehicle applications. These vehicles are typically classified as 'class 8' (33,000–80,000 pounds, gross vehicle weight).

Given the scope of India's expected demand growth and the likely long lead times and other problems in pipeline options, India has settled on a comprehensive
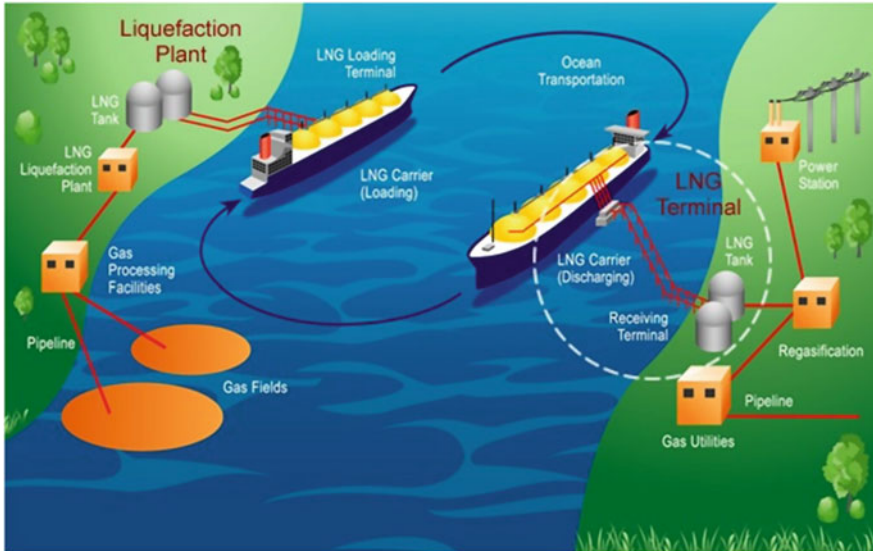
Fig. 11.3 LNG value chain. (http://www.pttlng.com/)

programme of establishing LNG terminals around the country and expanding its domestic gas pipeline infrastructure to deliver that re-gasified LNG to market as shown in Fig. 11.3. In the case of imported gas, the marketers are free to import LNG and sell the R-LNG to customers.

- *Hazira LNG Terminal:* In this terminal, LNG cargo is unloaded to the cryogenic tanks. The main components of the terminal are an LNG jetty with cryogenic unloading arms, cryogenic tanks to store LNG at –160 °C. LNG pumps to boost pressure to 80–100 barg. LNG vaporizes, and send-out pipelines carry the gas to the delivery point, which is located at a distance of 12.5 km from the terminal. The LNG jetty has two liquid unloading arms both of which are cryogenic and are designed to unload LNG at −160 °C. Unloading of LNG can be done at a maximum rate of 11,000 m^3/hour. The LNG unloaded is carried in cold condition by a 1.6 km pipeline to the LNG tankers. The terminal has two LNG tanks with a capacity of 16,000 m^3 each. These tanks have pre-stressed concrete outer and 9% nickel inner tank to hold the LNG at −160 °C. LNG cryogenic pumps are installed inside the tanks, which pump out LNG from the tanks at an intermediate pressure. Finally, the pressure is boosted to 100 barg before being sent to the regasification section. LNG is re-gasified in open rack vaporizers, using seawater as the heating medium. The terminal has three open rack vaporizers which are used to vaporize LNG.
- *Kochi LNG Terminal:* Kochi LNG terminal was set up by LNG Petronet. It is south India's first LNG receiving, regasification and reloading terminal with a capacity of 5 MMTPA. The terminal is at the Special Economic Zone (SEZ) of

Puthuvypeen near the entrance to Cochin port. The jetty is designed to receive LNG tankers between 65,000 to 2, 16,000 cubic metres. The terminal has two full containment above-ground LNG storage tanks of a net capacity of 1,55,000 cubic metres each. The terminal was commissioned in August 2013, and the reloading operation of South Asia was carried out in January 2015. The first supply of LNG as a bunker to small ships was carried out successfully in February 2015.

- *Dahej LNG Terminal:* LNG Petronet has set up South East Asia's first LNG Receiving and Regasification Terminal with a capacity of 5 MMTPA at Dahej, Gujarat. The capacity of the terminal has been expanded to 10 MMTPA, and the same was commissioned in June 2009. The expansion involved the construction of two additional LNG storage tanks and other vaporization facilities. The terminal is meeting around 20% of the total gas demand of the country. The company has completed and commissioned the second LNG jetty at Dahej.
- *Dabhol LNG Terminal:* GAIL has owned the LNG terminal associated with the 1967 megawatt Dabhol Power station, operated by the Ratnagiri Gas and Power Pvt Ltd for about Rs. 2400 crore. GAIL plans to boost up 5 million tons per annum regasification terminal by 2018. India has four regasification terminals, including the one at Dabhol, with a total capacity of 25 MTPA.

Gas from Gas Hydrate

Gas hydrates are known as 'Fire Ice'. The gas hydrate technology in this area tries to free gas using depressurization or injecting CO_2 which replaces gas in the ice. ONGC, the flagship explorer, explored four times bigger gas reserves than KG D6. The discovery was made in August last year by the second exploratory expedition under the government's gas hydrate programme in collaboration with scientists from the United States and Japan. The potential resources are to the tune of 134 TCF. The recoverable resource at 30% recovery is 40.2 TCF and that at 10% recovery is 13.4 TCF. Reliance's recoverable resource at KG D6 is 9 TCF. India's annual gas consumption (domestic production + imports) is 0.73 TCF, and 80% of India's energy demand is met through imports. The hydrate discovery reiterates the government's initiative in finding an alternate source of energy and attracts investments in such type of exploration business. The discoveries have been made in blocks 98/2, D3, D6 and D9 in the Krishna Godavari basin, off Andhra coast. These blocks are 30 km southwest of Reliance Industries Ltd natural gas block KG D6.

Shale Gas

Shale gas is a natural gas produced from shale formations. Newer technologies of horizontal drilling and hydraulic fracturing have allowed access to large volumes of shale gas that were previously uneconomical to produce. Shale gas has been increasingly popular in countries like the United States, Canada, the United Kingdom, Poland, Australia, etc. to become an unconventional gas source. The

government of India has issued a Policy Guidelines for Exploration and Exploitation of Shale Gas by National Oil Companies (ONGC and OIL) as India has large resources of shale gas, which upon production in near future can be directed to be used in CGD business.

Coal-Bed Methane (CBM)

Coal-bed methane (CBM) is a form of natural gas extracted from coal beds. It occurs within coal beds as free gas in fractures or dissolved form in water. In recent years, it has become an important source of energy in the United States, Canada, Australia, and other countries. India has the fifth largest coal reserve in the world. CBM, upon exploitation, has the potential to become an important unconventional gas resource, which can be used to meet the growing demand in CGD business in India.

Indian Gas Discoveries and Infrastructure

In comparison with some developed countries, India has a relatively underdeveloped gas pipeline infrastructure. Currently, India has a network of about 13,000 km of transmission pipelines for natural gas with a capacity of around 337 MMSCMD. The largest network for the infrastructure of the natural gas transmission present in the country is owned by GAIL India. Currently, the company is operating high-pressure natural gas pipelines of about 9000 km with more than 160 MMSCMD transmission capacities. Hazira–Vijaipur–Jagdishpur (HVJ) pipeline is the longest natural gas pipeline network in India. This network has been unable to meet the increase in domestic natural gas supplies stemming from the commencement of production at the KG D6 field and the increase in India's all over RLNG capacity. Gujarat State Petronet Limited (GSPL) and Reliance Gas Transportation Infrastructure Limited (RGTIL) have owned the rest of the country's natural gas trunk pipeline network and also a small network owned by Gujarat Gas Company Limited (GGCL) and Assam Gas Company Limited (AGCL).

Krishna Godavari KG D6 Field

The major development of the upstream has begun in the past few years with the start of the deepwater Krishna Godavari KG D6 (Block DWN-98/3) field operated by RIL (Reliance). This field was discovered in 2002 and began producing in 2009 with its estimated potential of about 337 BCM (11.9 TCF) (DGH). According to the Indian gas policy which is reflecting the recent decisions on volumes and end consumers,

the gas has to be sold. The gas produced during phase l (40 MCM/d) would therefore be allocated with the following priority and volumes (IEA Report, 2010).

- Existing gas-fired power plants and plants to be commissioned before April 2010: 18 MCM/d
- Fertilizer companies: 15 MCM/d
- City gas distribution: 5 MCM/d
- LPG and petrochemical plants: 3 MCM/d

Reliance initially had contracts to sell gas to 19 power plants, 15 fertilizer manufacturers and 3 steel companies for the first 40 MCM/d. A sale and purchase agreement had been signed by Reliance for its LPG plant with GAIL and its city gas with Indraprasth Gas for 0.3 MCM/d. RIL had been forced to cap out as close to one-fourth of the initial allocations were not taken during the first month of production in 2009. The customers for State Power Utility like GAIL, Essar Power, National Thermal Power Corporation (NTPC) and Ratnagiri Gas and Power were not taking their allocated quantities or were taking very irregular quantities which could threaten the field's operations.

Deendayal-GSPC Field

In February 2003, GSPC had discovered KG-OSN-2001/3 offshore block under a production sharing contract with the government of India. A total of 18 exploratory/appraisal wells have been drilled in this field. Some of these wells were drilled up to the depth of 6000 m, which are among the deepest HPHT wells globally. The reservoir temperature and pressure are 460 °F and 14,000 psi, respectively.

A detailed geological and geophysical study had been carried out by GSPC internationally renowned technical consultants, that is, Schlumberger, Fugro Robertson, PetroTel LLC and Blade Energy were deployed. A better understanding had developed for geological fault systems and reservoir heterogeneity after these technical studies.

With the first offshore high-pressure high–temperature (HPHT) field development in India, the company is fully geared up and committed to proceed ahead with the successful implementation of the Deendayal West (DDW) Field Development project. The prognosticated resource of DDW is 0.8 TCF over an area of 8 km^2. An additional mining lease area of 20.5 km^2 was granted by the government of India in January 2012. Both the initial area and the new area are accordingly being used as the first phase of development (GSPC, 34th Annual Report, 2012–2013).

The Deendayal Field Development plan consists of four major segments:

1. Well head platform (WHP)
2. An offshore process-cum-living quarter platform (PLQP)
3. Sub-sea pipeline
4. Onshore gas terminal (OGT)

Indian Gas Reserves

India does not have to remain this dependent on foreign energy commodities. An estimated 75% of India's sedimentary basins have yet to be adequately explored. Of the 26 known sedimentary basins in the country, only 7 are currently producing oil and gas. According to BP Statistical report 2015, India had a total proved reserve of 50.4 TCF by the end of 2014. But a more recent report by GE indicates that since 1950 roughly 69 TCF of proven and probable recoverable gas reserves have been discovered in India. However, only 42 TCF have been developed and are currently under production. That leaves 18 TCF of reserves yet to be produced and 27 trillion cubic feet of reserves yet to be developed. According to an analysis of 12 basins across India, approximately 64 TCF of risked recoverable resources are yet to be found. Thus, India holds at least 91 trillion cubic feet of recoverable gas reserves. On top of conventional gas reserves, India also holds an estimated 63 trillion cubic feet of recoverable shale gas. While these reserves are considered to be a secondary energy option, Indian agencies are encouraging exploration, and leading companies, such as ONGC and OIL, have implemented pilot projects to assess the shale opportunity (GE Bulletin 2015).

City Gas Distribution

According to T4S Standards, 'City or local natural gas distribution network (CGD) means an interconnected network of gas pipelines and the associated equipment used for transporting natural gas from a bulk supply high-pressure transmission main to the medium pressure distribution grid and subsequently to the service pipes supplying natural gas to domestic, industrial or commercial premises and CNG stations situated in a specified geographical area' (reproduced from PNGRB T4S).

Natural gas is converted to compressed natural gas (CNG) and piped natural gas (PNG), which cater to various sectors of society. CNG is used in the transportation sector, where it acts as a fuel for vehicles, while PNG is used as a fuel by domestic consumers (households), commercial consumers (hotels, offices, canteens, etc.) and industrial consumers (dryers, boilers, furnace, etc.) in the country.

Figure 11.4 pictorially describes the entire CGD value chain from production to transmission to distribution.

According to a recently published report by TechSci Research (2015), the CGD network in India increased exponentially at a compound annual growth rate (CAGR) of around 21% during 2010–2014. The ease of availability and competitive cost of natural gas in comparison to other fuels is one of the major contributors to the growth of the CGD sector. Due to the rise in population, an increasing number of vehicles and urbanization in the country, the CGD sector is anticipated to grow rapidly during 2016–2030. Based on the recent decisions taken by the government of India, the
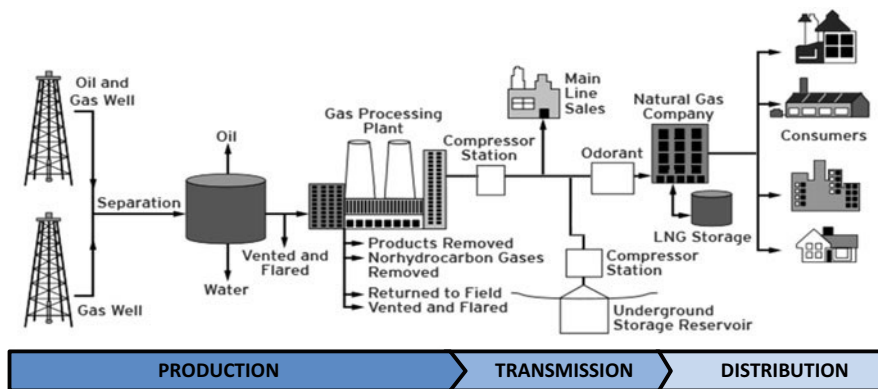
Fig. 11.4 CGD value chain of non-hydrocarbon gases. (https://www2.dteenergy.com/)

CGD sector has been given priority as far as gas allocation is concerned. This has opened new doors for expanding the CGD business in India.

City Gas Distribution: Indian Scenario

CNG in India

CNG is made by compressing natural gas (which is mainly composed of methane, CH_4) to less than 1% of the volume, it occupies at standard atmospheric pressure. It is stored and distributed in hard containers at a pressure of 20–25 MPa (2900–3600 psi), usually in cylindrical and spherical shapes. Natural gas vehicles are increasingly used in the Indian capital of Delhi, and other large cities like Ahmedabad, Mumbai and Kolkata – as well as cities such as Lucknow, Kanpur, etc. Its use is also increasing in South America, Europe and North America because of rising gasoline prices. CNG is starting to be used also in tuk-tuks, pickup trucks, transit and school buses and trains. CNG kits have appeared as a cost-saving measure to manage expenses for the fuel. Any vehicle with a spark-ignited engine could run with CNG. The CNG kit helps convert the engine. The CNG could get filled up through a slow-filling method within 5–8 h and could get filled up by a fast-filling method within 3–5 min. The likely potential CNG requirement is 74.34 MMSCMD.

CNG vehicle numbers have increased due to regulatory dictates for conversion like buses, three-wheelers, taxis and light commercial vehicles. In the automobile sector the growth is sluggish. Nearly the entire CNG bus market has been catered to by the two majors – Ashok Leyland and Tata Motors. In the last few years, players like Eicher Motors, Swaraj Mazda, Volvo, etc., have entered the market. Tata Motors and Ashok Leyland have begun to produce low-floor specially designed urban CNG buses. Car models are produced by Tata and Maruti Udyog Limited. So far CNG

programme has not been extended to the large highway trucks. Over a while, two broad technology approaches have evolved for heavy-duty internal combustion natural gas engines that have bearing on emissions, fuel economy and power of the vehicles. These are stoichiometric engines and lean-burn engines. In India, the bus industry had started with the conventional stoichiometric engines with three-way catalytic converters, but while moving to Euro III they moved to lean-burn CNG engines that the United States used in the 1990s. The recent innovation is towards advanced stoichiometric engines with advanced three-way cat convertors that are more effective in lowering NO_X emissions.

PNG in India

'Under its ambitious smart city scheme, the government has set the target to launch a plan to replace LPG connections with Piped Natural Gas (PNG) in the identified areas which will be developed as modern localities' – *The Times of India, Nov 2015* (Dash 2015).

Piped natural gas (PNG) is a more efficient system than cylinders as PNG ensures a continuous uninterrupted supply of gas, whereas an LPG cylinder has to be replaced once it is empty. There is no subsidy on PNG, which is cheaper than subsidized liquefied petroleum gas. It is used for domestic, commercial and industrial consumption. PNG has several distinctions to its credit of being a pollution-free fuel, economical and safer fuel. PNG is supplied through pipe 24×7. There is no storage space required. In the case of commercial and industrial consumption, the customer is relieved from storage space for the fuel. Table 11.2 captures the PNG status of India.

Current Status and Future Outlook of CGD Business In India

The CGD sector is a growing business sector in India. An increase in accessibility, and infrastructure development, and priority in gas allocation are some of the factors contributing to the growth of CGD in India. In September 2014, there were about 981 CNG stations, and 23,29,256 vehicles in India, which depicts that CNG demand is increasing rapidly. In the case of PNG, there were about 26,98,027 consumers in September 2014, which includes domestic, commercial and industrial consumers.

Till January 2016, 6 rounds of bidding were completed, and 64 geographical areas of India have been allocated, out of which only 22 geographical areas got authorization. If we combine all the authorization, which includes authorization through bidding procedure by PNGRB, non-bidding procedure by PNGRB and by the central government, then the total geographical areas authorized till now is 47, which includes regulation 18(1).

In the coming years, the implementation of the CGD network will grow steadily due to the expansion of CGD in new cities on the account of less price of CNG

Table 11.2 PNG status in India, March 2015

State	City covered	Company	Domestic PNG	Comm. PNG	Ind. PNG
Delhi	Delhi, Noida, Greater Noida, Ghaziabad	IGL	560,752	1560	726
Maharashtra	Mumbai, Pune, Thane, Kalyan, Ambernath, Panvel, Mira-Bhayandar, Bhiwandi	MGL, MNGL	817,468	2654	154
Gujarat	Ahmedabad, Baroda, Surat, Ankleshwar	GSPC, Sabarmati Gas, Gujarat Gas, HPCL, VMSS, Adani Gas	1,392,657	16496	3869
Uttar Pradesh	Agra, Kanpur, Bareilly, Lucknow	Green Gas Ltd (Lucknow), CUGL (Kanpur)	22,559	187	464
Tripura	Agartala	TNGCL	17,996	294	47
Madhya Pradesh	Dewas, Indore, Ujjain, Gwalior	GAIL Gas, AGL	3278	34	75
Rajasthan	Kota	GAIL Gas	189	1	18
Assam	Tinsukia, Dibrugarh, Sivasagar, Jorhat	Assam Gas Co. Ltd	28,050	991	377
Andhra Pradesh	Kakinada, Hyderabad, Vijayawada, Rajahmundry	BGL	3163	46	3
Haryana	Sonipat, Gurgaon, Faridabad	GAIL Gas, Adani Gas, Haryana City Gas	23,236	93	185
Total			2,869,348	22,356	5918

Source: http://petroleum.nic.in/

coupled with increasing application of PNG in domestic, industrial and commercial sectors. Moreover, the environmental factor is pushing it further especially in the automotive and industrial sectors as it acts as a coal replacement fuel in industries.

CGD: A Consumer-Friendly Business

In an attempt to make CGD a user-friendly business, in 2014, MoPNG decided to maximize the allocation of domestic gas (as far as possible) to meet the requirement of CNG and PNG. CGD entities have also been directed to pass the entire benefit coming out of increased domestic gas supply to domestic consumers. To ensure transparency in gas pricing, the government holds a right to ask for a break-up of CNG and PNG pricing. CGD entities have been mandated to display a break-up of CNG price at CNG stations and a break-up of PNG price in the gas bill to the domestic consumers. To be open to the customers, CGD entities are required to provide details of the cost of gas to the CGD entity; supply and distribution cost of the CGD entity; entity's margin; excise; VAT and any other tax. Non-compliance with the above guidelines by CGD entities can also lead to the cancellation of their domestic gas allocation (ref no.L-16013/3/2012-GP-II, MoPNG, 2014).

Convergence of CGD Network Development with the Smart City Mission
The government of India has launched a Smart City Mission intending to promote sustainable and inclusive development of cities by addressing the issue of infrastructure, land use planning, transport, urban design and architecture in a holistic manner. One of the core features of smart cities is to have efficient and cleaner energy management, which requires the substitution of coal and petroleum liquids usage with environment-friendly natural gas. The development of city or local natural gas distribution (CGD) is therefore essential in Smart Cities.

Out of 98 cities approved under the Smart City Plan, 35 cities are either covered or approved for CGD networks, 3 cities are proposed to be covered in the sixth round of CGD bidding. According to the Ministry of Petroleum and Natural Gas, the remaining potential Smart Cities will be considered for the development of CGD networks in synchronization with the development of the envisaged National Gas Grid.

According to MoPNG, the potential features for convergence of CGD and Smart Cities development are the following:

- Common utility corridor for a gas pipeline along with underground utilities such as water line, drainage line, OFC cables, electric cables, etc.
- Common Geographic Information System for all utilities. Any pit-opening permission granted to any utility for maintenance or other work shall automatically be intimated to all utility operators in the region. Other utility operators may also like to take the prerequisite maintenance work at the same time.
- Mandatory PNG network in upcoming/new residential colonies/apartments like water, sewerage and electricity lines.
- Earmarking open plots for setting up CNG Stations in Smart Cities for ensuring equitable availability of CNG to all parts of the city.
- Implementation of a Smart Metering System for electric, water and gas utilities and hiring of a single agency for metering/billing purposes.

Natural Gas as an Environment-Friendly Fuel

Natural gas and its constituents, as well as the methods of extraction, have an impact on our ecosystem. It is the cleanest and most efficient power source among fossil fuels (Likhanov and Lopatin 2017). Natural gas and oil have different greenhouse gas (GHG) implications when utilized for combustion or as a feedstock (Kapsalyamova and Paltsev 2020). Life cycle analysis (LCA) is a technique for assessing the environmental impacts of all stages of a product's life, from cradle to grave (Shrivastava and Unnikrishnan 2019). To fully assess the GHG and AQ impacts of gas generation, emissions from additional life cycle stages associated with natural gas production and distribution must be considered. Pre-production, gas production, transmission, distribution and storage, as well as production end of well life, are the life cycle stages of natural gas (Khan et al. 2015). All parts of site

exploration, clearance and road construction, as well as drilling, hydraulic fracturing and well completion, are included in pre-production. Compressors, pumps, heaters, leaks, venting and flare activities, and other maintenance processes all contribute to the production stage, which involves the recovery, compression and processing of gas to ensure pipeline quality criteria are fulfilled. The transfer of processed gas to end users, including long-distance pipelines and local distribution networks, is part of natural gas transmission, storage and distribution. Pre-production can last weeks to months, whereas production can last years or decades, necessitating consideration of the implications throughout time (Balcombe et al. 2017). Drilling and extracting natural gas from wells, as well as transporting it through pipelines, results in the leakage of methane, a key component of natural gas that traps heat 34 times better than CO_2 over 100 years and 86 times better over 20 years (Myhre et al. 2013).

According to preliminary studies and field observations, these 'fugitive' methane emissions account for 1–9% of overall life cycle emissions (Tollefson 2013). Upstream methane emissions have been characterized using a range of methodologies and methods, including engineering analysis and quantification, using both bottom-up and top-down approaches. The anticipated leakage rate, the global warming potential of methane over different periods, the energy conversion efficiency and other factors all contribute to natural gas having lower life cycle greenhouse gas emissions than coal and oil. Even if higher GHG intensity liquefied natural gas (LNG) is used as a fuel, available life cycle studies generally show a benefit over coal. Depending on plant efficiencies and natural gas emissions variability, life cycle GHG emissions from Marcellus shale natural gas production increased by 3% over traditional gas and also increased to 11% GHG emissions compared to ordinary domestic gas (without combustion) (Jiang et al. 2011). If methane leakage rates do not exceed 3.2% of total system production, natural gas electrical generation may cut GHG emissions on all time scales relative to coal (Ener 2015).

Understanding the AQ consequences of conventional and unconventional gas production is challenging since emissions from these activities vary in composition, amount and duration, and are dependent on a variety of parameters such as raw gas composition, extraction technology and handling approach. Unconventional gas resources (e.g. shale gas, gas hydrates) have been predicted to have 30–50% higher leakage rates than conventional gas, with GHG emissions that might equal coal over 20 years. Furthermore, unconventional gas has been claimed to have a lower GHG impact per megajoule (MJ) than conventional gas. The extraction and production of natural gas have been related to significant ozone precursor emissions, such as NOx and VOC (Kargbo et al. 2010). The release of NOx, methane, CO_2 and other VOC from processing plants and diesel truck exhaust has been linked to ozone and other AQ problems in areas of gas extraction in Texas, Utah, Wyoming and Colorado. In the perspective of this, a regional analysis of increased natural gas use in the Texas power industry found net reductions in NOx and SO_2, as well as net increases in VOC emissions, resulting in minor ozone (0.2–0.7 ppb) and PM2.5 (0.1–0.7 mg/m^3) reductions (Mac Kinnon et al. 2018). Total NOx emissions in countries that support high levels of gas production can be 20–40 times greater than permissible values for a single, minor source. Compressor engine and flare emissions have been shown to

considerably enhance ambient ozone (610 ppb) downwind of a hypothetical gas processing complex. As a result, in addition to improvements from power generation sites, a comprehensive view of AQ consequences from transitions to natural gas must account for the potential worsening of AQ in locations supporting gas growth (Mac Kinnon et al. 2018). The study found that direct plant emission reductions could offset increases in emissions at gas production facilities.

Conclusion

This chapter summarizes the economic value of natural gas for India in satisfying its expanding energy needs while minimizing environmental impacts. The utilization of natural gas on a wide scale will help India to achieve its commitment to the Paris Climate Agreement (COP21). In power plants, natural gas has been considered an ideal fuel due to its high fuel efficiency. In India, there is a gap between demand and supply of natural gas, and thus India is importing a quarter of its natural gas needs to fulfil this gap. In India, the growing demand for natural gas in the CGD business is being fulfilled by exploitation of the most potential unconventional gas resource, that is, coal-bed methane. Considering life cycle assessment of the fuels from production to final consumption, environmental benefits of natural gas are more than other fuels. The unconventional sources of natural gas like shale gas, gas hydrates, etc. are having high methane emissions compared to the conventional sources.

References

Balcombe P, Anderson K, Speirs J, Brandon N, Hawkes A (2017) The natural gas supply chain: the importance of methane and carbon dioxide emissions. ACS Sustain Chem & Eng 5(1):3–20

BP Statistical Review of World Energy, June, 2015, 64th Edition

Dash D K (2015) Govt. wants to replace LPG with PNG in smart cities, The Times of India, 13 November, 2015

Ener DG (2015) Study on actual GHG data for diesel, petrol, kerosene and natural gas. European Commission, Directorate-General for Energy

GAIL Voice (2014) Natural gas: demand-supply dynamics in India, 29 December, 2014

GE Bulletin (2015) India's massive untapped natural gas reserves could help free up $306 million a day on imported oil, http://qz.com/461424/indias-massive-untapped-natural-gas-reserves-could-help-free-up-306-million-a-day-on-imported-oil-2/, July 22, 2015

http://petroleum.nic.in/docs/pngstat.pdf

http://www.pttlng.com/en/mr_chain.aspx

http://www.referenceforbusiness.com/

http://www2.dteenergy.com/

IHS CERA, Fueling the Future with Natural Gas: Bringing It Home, January 2014

International Energy Agency (IEA), Natural gas in India, Report 2010

Jiang M, Griffin WM, Hendrickson C, Jaramillo P, VanBriesen J, Venkatesh A (2011) Life cycle greenhouse gas emissions of Marcellus shale gas. Environ Res Lett 6(3):034014

Kapsalyamova Z, Paltsev S (2020) Use of natural gas and oil as a source of feedstocks. Energy Econ 92:104984

Kargbo DM, Wilhelm RG, Campbell DJ (2010) Natural gas plays in the Marcellus shale: Challenges and potential opportunities

Khan MI, Yasmin T, Shakoor A (2015) International experience with compressed natural gas (CNG) as environmental friendly fuel. Energy Syst 6(4):507–531

Likhanov VA, Lopatin OP (2017) Use of natural gas, methanol, and ethanol fuel emulsions as environmentally friendly energy carriers for mobile heat power plants. Therm Eng 64(12): 935–944

Mac Kinnon MA, Brouwer J, Samuelsen S (2018) The role of natural gas and its infrastructure in mitigating greenhouse gas emissions, improving regional air quality, and renewable resource integration. Prog Energy & Combust Sci 64:62–92

Ministry of Petroleum and Natural Gas (MoPNG), Annual Report 2014–2015

Ministry of Petroleum and Natural Gas (MoPNG), Annual Report, 2014–2015

Myhre G, Shindell D, Bréon FM, Collins W, Fuglestvedt J, Huang J, Koch D, Lamarque JF, Lee D, Mendoza B, Nakajima T, Robock A, Stephens G, Takemura T, Zhang H (2013) Anthropogenic and natural radiative forcing. In: Climate change

No. L-12011/10/2011-GP, Guidelines on Swapping of Natural Gas, Government of India, Ministry of Petroleum & Natural Gas, Shastri Bhawan, New Delhi, Dated the March 15, 2012

PNGRB T4S, Technical Standards and Specifications including Safety Standards for City or Local Natural Gas Distribution Networks

"Presentation on Pakistan Gas Industry Demand Supply Constraints & Sustainable Solutions" by Shahzad Iqbal, Executive Director (Gas) Oil & Gas Regulatory Authority Pakistan

Sah S (2013) Overview of gas scenario in India, moneycontrol.com, 13 Nov 2013

Sen A (2015) Gas Pricing Reform in India: Implications for the Indian gas landscape, The Oxford Institute for Energy Studies, OIES PAPER-NG 96, April 2015

Shrivastava S, Unnikrishnan S (2019) Review of Life Cycle Assessment and Environmental Impacts from The Oil & Gas Sector. Int J Oil, Gas Coal Tech 27(1):95–110

Sui Northern Gas Pipelines Ltd. Available at: www.sngpl.com.pk/

Sui Southern Gas Company Ltd. Available at: www.ssgc.com.pk/

TechSci Research (2015) India City Gas Distribution Market Forecast & Opportunities, 2030

Tollefson J (2013) Methane leaks erode green credentials of natural gas. Nature News 493(7430):12

USA. American Gas Association. Available from: https://www.aga.org/

USA. Energy Information Administration. Available from: https://www.eia.gov/

USA. EIA (Energy Information Administration). Available at: http://www.eia.gov/

Vision 2030: Natural Gas Infrastructure in India (2013) Report by Industry Group, Petroleum & Natural Gas Regulatory Board, 2013

Chapter 12
Farmer's Perception on Impact of Climate Change and Adaptive Strategies in Sikkim Himalaya

Aakash Upadhyay and S. C. Rai

Abstract The impact of climate change has become very evident in the Himalayan region. Sikkim Himalaya is not an exception where climate change is adversely affecting agriculture and associated ecosystems. At the local level, studies suggest that the impact is evident and has contributed to unpredictable and erratic precipitation, shifts in the seasonal pattern of sowing and harvesting period of crops, drying up of local water sources, species migrating to higher elevations, and increased incidence of diseases and pests in crops as well as in fodder species. This research has been carried out on the *Reshi Khola* watershed in the west district of Sikkim Himalaya. The study examines how farmers perceive climate change concerning temperature and rainfall. This work tries to identify the primary challenges of local farmers for ensuing adaptive capacity and water security in the rural agrarian system. The results from the field are based on 50 household surveys, where farmers above 40 years were selected based on purposive random sampling. Focused group discussions were also held with a group of age-old farmers apart from the interview schedule. The data collected was later validated with the meteorological data available from the regional center to see how scientific the local's perception was. The results from the study highlight that people perceive climate change as a real threat to agriculture based on their experience and local knowledge. The study aims to document and develop a model for building an adaptive system to climate change that combines local tradition and indigenous knowledge with modern scientific research and government policies.

Keywords Climate change · Sikkim Himalayan traditional agriculture · Perception · Adaptive capacity · Sustainable agriculture

A. Upadhyay · S. C. Rai (✉)
Department of Geography, Delhi School of Economics, University of Delhi, Delhi, India

Introduction

Climate change has become an explicit phenomenon across the globe, often labeled as a "wicked problem," characterized by many underlying strata of nested, intractable, and unforeseen predicaments. Climate change influences, and will continue to influence, natural resources, the environment, and regional economies. Agricultural ecosystems are sensitive to differences in climate, and climate changes have inevitable and significant effects on agricultural production (Sharma et al. 2009). Recent studies have shown that averaged globally combined land and ocean temperature has increased to 0.85 °C over the period 1880–2012 (IPCC 2014). Over the Himalayan region, the temperature has been experiencing an increase in mean temperature by 0.6–1.3 °C between 1975 and 2006 (Dimri and Dash 2011). Rupa et al. (1992) reported a significant decreasing trend in rainfall. Studies have reported that the Hindu-Kush Himalayan region is prone to ongoing climate change. In Hindu-Kush Himalaya, there are around 54,000 glaciers, covering an area of approximately 60,000 km^2 with almost 6000 km^2 of ice volume reserves (Bajracharya and Shrestha 2011; Sharma and Shrestha 2016). The glacier retreat in terms of change in area and volume is evident in the Himalaya (Bolch et al. 2012; Gardelle et al. 2013; Rai and Mukherjee 2021).

It is reported that increasing temperature has impacted flora and fauna. Changes in temperature and precipitation directly affect crop growth, grain yield, and food quality (Xu et al. 2009; Mishra and Rai 2019). The mid-to-high-latitude regions show an increase in crop and pasture yields with a moderate increase in temperature, whereas in low-latitude and seasonally dry regions, slight warming would lead to decreasing yields (IPCC 2007). Therefore, farmers need to have a good understanding of the negative impacts of climate change on the agricultural system to adapt and develop mitigation strategies. Scientific database of the region is the recent phenomenon while the person living within the region and their knowledge and their experience has been since the time they started living there. The local farming communities are directly dependent on the services of nature, livelihood sources, ecosystem services, and various biodiversity services like water sources for irrigation that are often the first to accurately perceive changes change. Hence, the local practices are crucial for the agricultural ecosystem and livelihood sustainability. Keeping this in mind, a study was conducted in Reshi Khola watershed of West Sikkim in Sikkim Himalaya, which is known for its traditional agriculture. A perception-based study on various climatic factors and associated events like rainfall, productivity, temperature, water scarcity, and extreme events was conducted in 2019–2020, with the following broad objectives, that is, (i) farmers' perception of climate change and their precision, (ii) identify local practices as an adaptive strategy, and (iii) suggest measures for successful adaption to climate change impacts.

The Study Area

Reshi Khola watershed is located between 27° 11′ to 27° 14′ N and 88°10′ to 88° 20′ E, covering an area of 4391.94 ha (Fig. 12.1). Elevation in the study area ranges from 1500 m near the river basin to the valley up to 1750 m above msl on the outer edges of the watershed. The region remains cool with gradually sloping topography. The economy is mainly agrarian, where the majority of people are engaged in agriculture. Reshi Khola is a major tributary of Rangit Khola, which fetches its water from Chisung Khola, Pareng Khola, and Thaplel Khola. The average annual temperature for most of Sikkim is around 18 °C (64 °F), and the average rainfall is about 85 inches annually. The region has many power projects and enjoys almost uninterrupted electricity. Roads are in poor condition owing to the frequent landslide and mudslides.

Methodology

The study is based on both primary and secondary databases that have been analyzed for perception and adaptive strategy adopted by the local farming community to cope with climate change. Secondary sources of data like the IMD, IPCC reports on policy and planning, programs and activities regarding climate-related risk management, and adaptation practices were also consulted for the analysis. Studies on
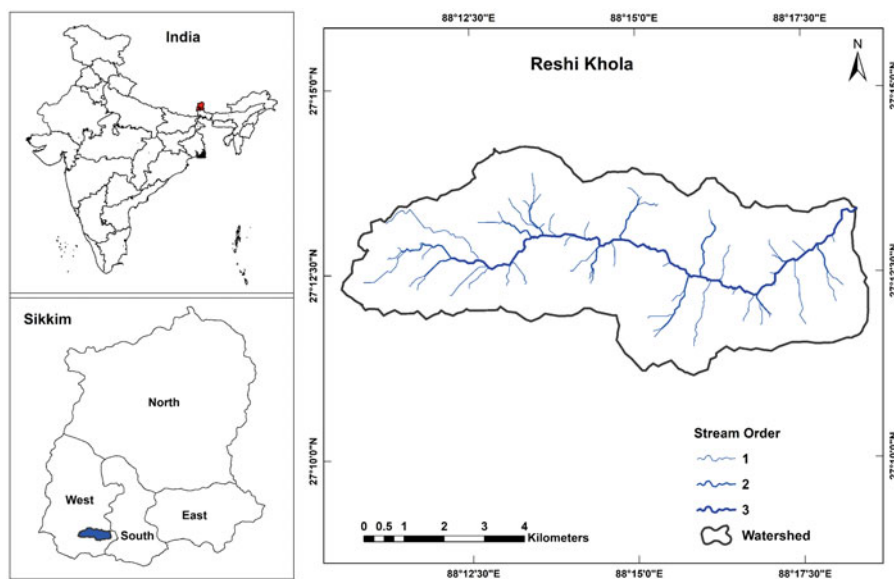
Fig. 12.1 Location map of Reshi Khola watershed in Sikkim Himalaya

Table 12.1 Demographic information of the respondents

Category	Items/elements	Percentage
Gender	Male	64
	Female	36
Age	Below 35	20
	Above 35	80
Education	Illiterate	30
	Primary	50
	Middle and above	20
No. of family members	Below 3	20
	3–5	55
	5 and above	25
First source of income	Agriculture	66
	Off-farm	16
	Others	18

perceptions, responses, and local knowledge of climate variability, impact on farming and adaptive strategies at the household and community levels were gathered through field observations, personal interviews, key informant interviews, as well as consultation with institutions and community-based organizations like forest protection committee and self-help groups. Semi-structured questionnaires were used to ask the farmers whether they have noticed long-term changes in mean temperature, mean precipitation, extreme climatic events, and change in natural resources over the past 25–30 years and how are they coping with the changes over the years. A primary survey was conducted in 2019–2020 where purposive random sampling was used to select the interviewee using several indicators of climate change frequently used in other similar studies (Chaudhary and Bawa 2011). The interviewees selected for the interview were all above the age of 40 or more as they are the ones who have seen the climate changing over the past three decades (Table 12.1).

The basic nature of the study demanded both qualitative and quantitative methods, and they have been used effectively to analyze the result. The data collected during the interview was later complied with and quantified for analysis. Different statistical tools from MS Office like MS Excel (bar and column diagram), tabulation, and simple regression have been used to represent the findings in the best possible way.

Results and Discussion

Climate Change in the Himalaya

A recent study in the Himalaya showed that Himalaya has been experiencing an increase in mean temperature by 0.6–1.3 °C between 1975 and 2006 (Dimri and

Dash 2011; Kumar et al. 2020). However, the major emphasis revolves around snowmelt, glacier retreat, and its impact on future water supplies river flows, groundwater, natural hazards, biodiversity, and livelihoods of the entire region as a whole (Xu et al. 2009). The local communities who are directly dependent on natural resources for various ecosystem and biodiversity services and water sources can perceive changes in the environment much precisely. The scientific database developed over the years is a recent phenomenon, while the person living within the region, their knowledge, and experience has been with them since the time they started living there. It would therefore be appropriate to refer to them as metaphoric "miners' canaries" concerning the effects of climate change (Ingty and Bawa 2012). The existing traditional ecological knowledge can be utilized as a base for long-term data set development and future planning. A case from the Arctic can be cited where Berkes 2002 shows that it is possible for scientists and local people to work together and profit from various knowledge systems. It has been found that perception study of the local community can be an effective tool of complementing scientific data with indigenous knowledge to improve climate change mitigation and adaptation strategies. The study area also showed the common trend in both scientific records and the perception of the local community. The role of the community's age-old knowledge and experience would be an important source of combating climate change. However, the perception about the change varied based on the location of a place, age, gender, socioeconomic status, and educational qualification. The study will highlight some of those important aspects and local practices and their relevance in combating and adapting to the influence of climate change.

Climate Change in Reshi Khola Watershed

Locals' Perception on Climate Change

Locals perceive that climate is changing in the study area with the response varying from place to place, ethnicity, culture, age, gender, educational qualification, and socioeconomic background. There was a clear idea among respondents of the agreed changes in the climate and environment. About more than 90% (Fig. 12.2) of the respondents responded about a clear-cut change in the climatic phenomena and weather patterns, over the years in the area, 5% said that there was no climate change while 5% had no idea about the climate change. About 85% responded that they are observing an increasing trend in temperature, while 10% said it was constant, and the remaining 5% had no idea about it (Fig. 12.3). They are of the opinion that the climate in both seasons turns out to be extreme with summer getting warmer and winter getting colder. As per the respondents, active winter is not more than 90 days as per 65% of the respondents while summer extends for more than 6 months. This indicates that the region is getting warmer slowly.

Fig. 12.2 People's
perception on climate
change
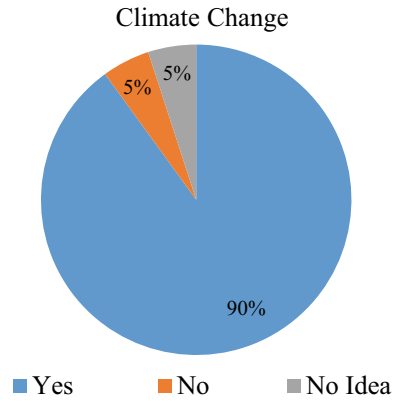
Fig. 12.3 People's
response to temperature
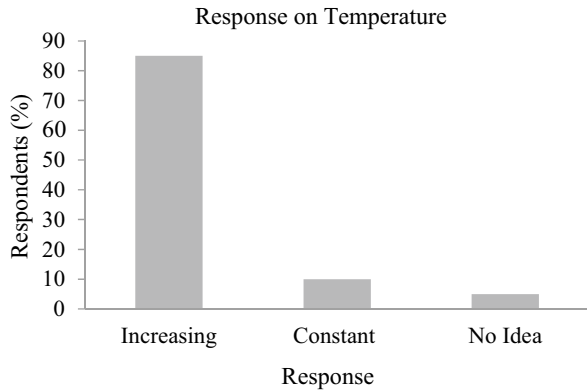
The locals cited increasing temperature, decreasing rainfall, changing seasonal, water sources, and decreasing productivity as the major reason for their perception. Some of them can be seen as follows.

Decreasing Water Availability

The respondents were informed about the increasing scarcity of water in the region. About 50% of the respondents informed reduction in water availability, while 40% said there are no changes over the past decades (Table 12.2). In the present time, they have been seeing a continuous decrease in water availability for various purposes. Small springs, a common attribute of Himalayan geohydrology, and major domestic and drinking water sources to the hill folks have started drying up. They are also important indicators of groundwater status and water table across the elevated land systems, which are prominent during the monsoon season due to abundant surface

Table 12.2   People's perception of various aspects of climate and its related element

Impact	Yes (%)	No (%)	Don't know (%)
Temperature has been increasing	85	10	5
Erratic/unpredicted rainfall	65	20	15
Seasons changing	85	5	10
Reduction in annual yield and productivity	70	25	5
Shift in agricultural zone	75	10	15
Availability of water	50	40	10
Extreme events like hail/flood/drought	70	15	15
Disappearing springs	50	30	20
Change in fruit ripening timing/early ripening	70	20	10
New disease and problem of pest	85	5	10

water. Villages like Samdong and Deythang were facing such problems owing to geomorphic factors and the rock composition, and decreasing rain.

Erratic Monsoon and Unpredictable Rainfall

The local people had a similar perception as the temperature, about the precipitation, and its trend over the years. More than 65% of the respondents reported erratic monsoon, rainfall variability with untimely, late monsoon start, no winter rain, and high-intensity pattern with short periods, while 20% said it was normal (Table 12.2). It was mainly the female respondents who agreed about the changing pattern of monsoon. About 75% believed that the drought-like situation has been increasing, while 20% thought just the opposite (Fig. 12.4). This condition of untimely and unusual rainfall patterns over the past few years was cited as the reason behind their perception. As mentioned earlier, they made a special mention of drier and wetlands (Pakho bari area and Bagarey Dara) with special reference to crops like paddy and wheat, which are showing a declining trend in their production due to the inadequate moisture content in the soil of the region. A paddy sowing festival called *Aashar Mahautsav* (Aashar is a month in Nepali) is observed, which means the time for monsoon has arrived and rain would follow is delayed.

Increasing Pests and Diseases

Farmers are informed about the increasing incidence of existing pests, insect attacks, and diseases. It is becoming common with about 85% of the respondents complaining about the increasing influence of insects and pests (Table 12.2). These pests infect the leaves and stems of the tree that restricts the food production process called photosynthesis of trees and plants, thus reducing the productivity as
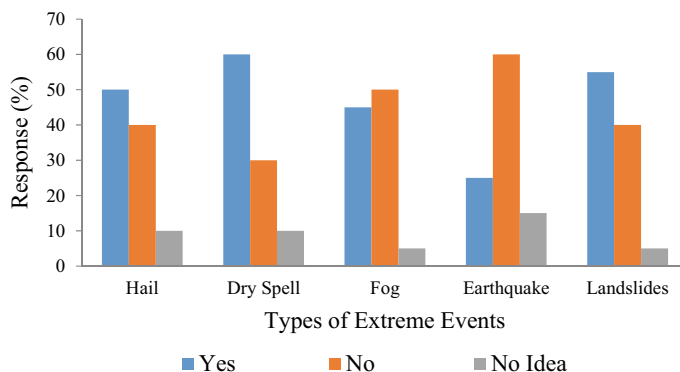
Fig. 12.4 People's perception on incidences of extreme events over the years

well as the biomass. Fruits are falling prematurely, changing shape and size in crops like Pear (*nashpati*) Mashyam and Bhotmas (*Glycine max*). Popular crops like ginger are badly affected by pests and other diseases that are heavily bringing down their annual productivity. The oil content in the ginger has been reducing continuously, making it an inferior product over the years.

Decreasing Yield and Productivity

An important determinant of agricultural richness and climate change, the yield and productivity of various crops over the years have been continuously reducing over the years. About 70% of the respondents responded about the decreasing trend in productivity in some of the specific crops like wheat and ginger (Table 12.2). They further reported the vanishing of cultivation of traditional crops like ginger (*Zingiber officinale Roscoe*), paddy (*Oryza sativa*), buckwheat (*Fagopyrum esculentum*), and oranges (*Citrus sinensis*) as they were becoming increasingly uneconomic and severely affected by increasing temperature and decreasing moisture content.

Seasonal Change

Respondents intervened about the seasonal changes taking place over the years. Although there is no major shift in the seasonal pattern, smaller shifts could be recollected based on their experience. About 85% of respondents were informed about the seasonal changes, while 5% said there is no change (Table 12.2). Early fruiting, falling up of fruits before time, and stunted growth do signify that normal seasonal pattern is changing. During the survey, an example of pear (*nashpati*) was cited as an example for the perceived opinion signifying that the climatic condition

that was to arrive after some days arrived earlier, leading to falling of fruits with reduced size.

Incidences of Extreme Events

Global warming is attributed to promoting extreme climatic events like heat waves, monsoons, droughts, landslides, mudslides, etc. across the globe. Hailstorms, fog, and dry spells in the study area are becoming a common phenomenon (Fig. 12.4). People informed variation in annual and diurnal rainfall post-2011 Mangan earthquake. Strong hail does a great deal of damage to vegetables like cabbage and other small vegetables. Even a small temporal and spatial shift in hailstorm would lead to negative consequences in maize productivity through the minimum change in average temperature.

Fog causes a lot of physiological damage to post-Kharif affect photosynthetic activities (Mildenbergera et al. 2009). A similar trend was noticed in the study area. Incidents of drought, landslide, and mudslide have become recurring phenomena in the region and could also be attributed to human-induced developmental activities like road cutting, which damages the nearby fields during monsoon. Further, the installation of some major hydropower projects has considerably reduced the water flow in the river, which has reduced the water available for irrigation and river, which tend to be dry during the lean season.

The general notion of people believing in climate change was a reduction in crop yield, productivity, pests, and diseases, but some of the people came up with a counterargument that "this soil has become used to urea (or other fertilizing agents), and now if you suddenly boycott it and come back to natural manuring soil will take its time to adjust to change, regain its lost fertility and start yielding the natural production. The region is in the transformation phase of agricultural productivity so it will take its time to adjust and productivity will become normal."

Climate Change

Temperature Trend

The temperature has increased gradually in the study area over the past 25 years. The primary survey also revealed a similar trend of increasing temperature over the region. The area has shown an upward trend in temperature with temperature increasing by about 1.5 °C from 1990 till 2015. While in the case of the mean annual temperature of the area, it has increased by about 2.5–3 °C over the past 25 years (from January 1990 to December 2015), thus showing an upward trend. It implies that the average increase in temperature is 0.085 °C/year over the past 25 years. The summer temperatures have gone up (Fig. 12.5).
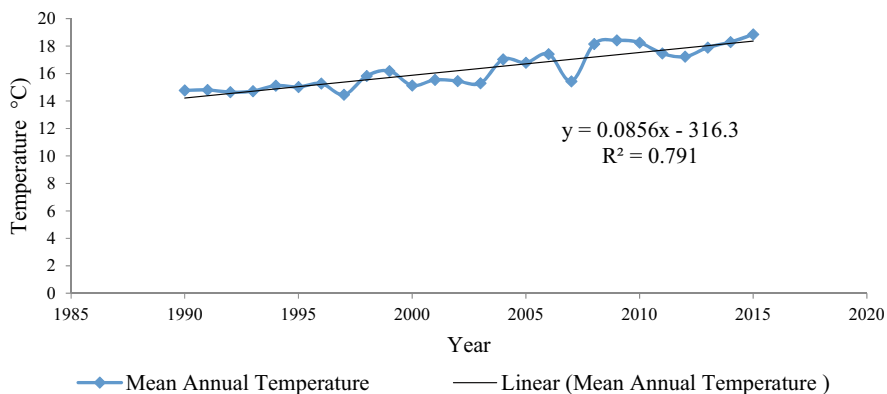
Fig. 12.5 Mean annual temperature (1990–2015)

Summer Trend

The maximum temperature for July ranged from 21 °C (1990) to 27 °C (2014), which implies that the range varied by 5–6 °C in the past 25 years, although this is not a normal trend and was seen on a very few occasions. On the other hand, the minimum annual temperature range varied from 16.70 °C (1993) to 19.57 °C (2014), showing an increase of about 2–2.5 °C. The mean monthly maximum temperature for July showed a gradually increasing trend throughout, except in July 2014, when the average maximum observed temperature increased from 25.04 °C (2013) to 27.11 °C (2014). A sudden increase of about 2 °C in one year could be linked with 2014 being one of the hottest years in recent history. While the average minimum July temperature also showed a steady rise except in 2007, when it fell nearly by about 5 °C from 17.79 °C (2006) to 11.43 °C (2007), which again increased to 19.15 (2008), meaning on an average the minimum temperature is increasing by about 0.080°C/year.

Winter Trends

Winter is gradually warming up but fluctuating every year, with two maximum average fluctuations in 1993 (9.03 °C) (lowest) to 2010 (18.08 °C) (highest), which means the temperature fluctuated to almost double in one instance. However, it was not the normal trend. The average maximum temperature increased from 13.15 °C in 1990 to 16.01 °C in 2015. The average maximum winter temperature has increased by about 3 °C. The minimum temperature recorded in January 1990 was 3.10 °C (lowest), which has increased to 5 °C in 2015 with the range of 1.5 °C. Respondents stated about warmer winter as the number of active winter days is reduced and frost-free winter could be co-related with increasing temperature. But there were also

Fig. 12.6 Average July temperature

$$y = 0.291x - 559.19$$
$$R^2 = 0.7643$$

$$y = 0.0801x - 142.51$$
$$R^2 = 0.1322$$
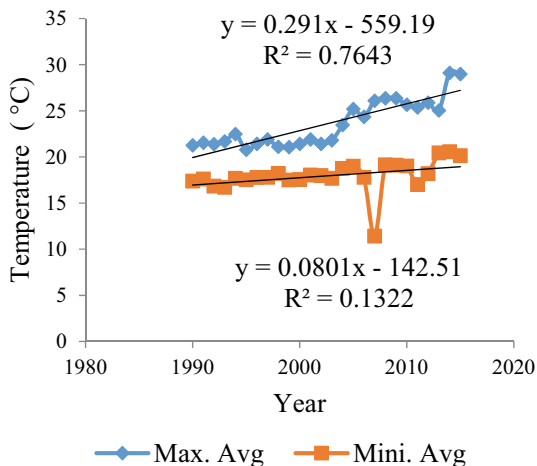
Fig. 12.7 Average January temperature
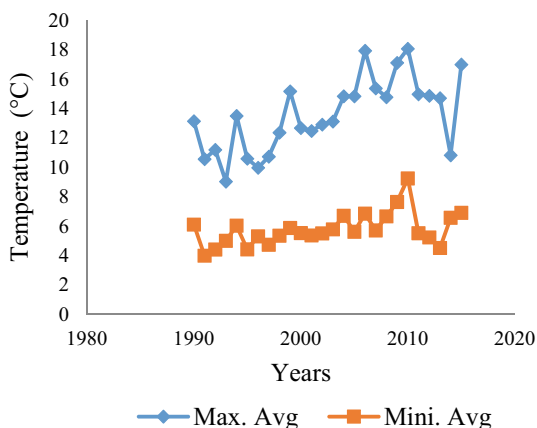
various incidents of severe winters when temperature even dipped below 2°C. There were incidents of January mean temperature going below 2 °C as in 1991(0.50), followed by 2013 (0.90), 2007 (1.10), 1999 (1.10), and 2011 (2.0). During these years, winters were severe where fog cover was common, which could damage post-Kharif or pre-rabi crops like maize and buckwheat (Figs. 12.6 and 12.7).

Precipitation Trend

The trend of continuous rainfall is changing, and incidences of the heavy short shower are increasing. The time of onset and withdrawal of the monsoon is changing, showing erratic and discontinuous rainfall with fluctuating number of rainy
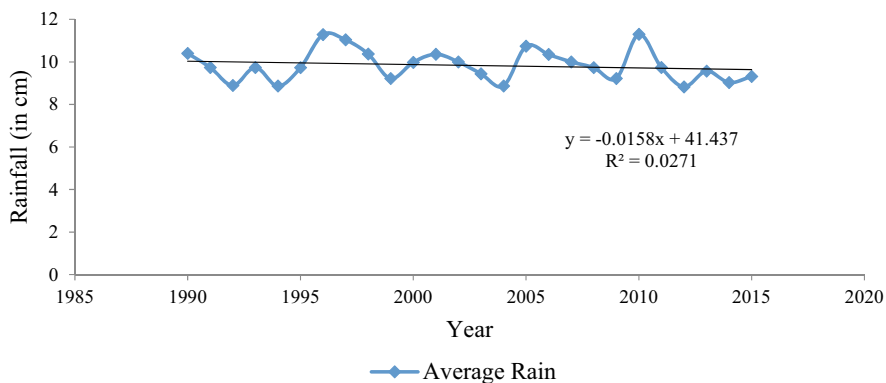
Fig. 12.8 Average annual rainfall

days. There is a decline in the annual rainfall over the years, although very minimal from 10.40 cm in 1990, which reduced to about 9.32 in 2015. The number of rainy days showed a fluctuating, moreover decreasing trend over the study period except in 1999, which reduced from 220 to 200 days. It reduced from 232 in 1990 to 217 days in 2015. Although rainy days are reducing and rainfall showing a declining trend, the maximum annual rainfall is the same; moreover, it is increasing from 503.90 cm in 1990 to 567.32 cm in 2015. It proves the point that steady and continuous rainfall pattern is changing into small and heavy spells as stated by the local farmers. On the other hand, there is no clear trend in terms of minimum rainfall, except an abnormal increase in 1995 (17.90) from 1994 (4.30), whereas it was 5.8 in 1990 to 4.98 in 2015. Data shows July (16.88 cm) as the wettest month while minimum rainfall was recorded in November (0.41), followed by January (0.95). While June (14.24), July (16.88), August (16.06), and September (14.75) gave most of the rain to the region from the monsoon (Fig. 12.8).

Perception vis-à-vis Observed Meteorological Data

It can be concluded that local farmers demonstrated a clear understanding of climate change, and most of their perceptions about climate change were consistent with the trends in the climate data. Temperature showed a gradual upward trend and both minimum and maximum observed temperature showing an increasing trend. The mean annual temperature in the study area has increased by about 2–3 °C over the past 25 years. This could be related to changing agricultural patterns of the farmers, and as some of the traditional crops are no more an integral part of the cropping pattern, the area under crops like paddy (rice), *bhatmas* (soyabean), buckwheat, and oranges are reducing in the region. This could be co-related with secondary data obtained from the agricultural department, which show areas under different crops

have reduced over the years that could be attributed to people's perception that paddy cultivation is no more useful or profitable (Table 12.3). Agriculture is directly dependent on climatic factors, which would limit the farmers in the coming years.

However, there were some farmers who were not attributing to climate change and did not see any clear changes in precipitation or temperature. Although they could correlate with increasing temperature in the case of precipitation, they could not identify clear changes in the normal trend. This could be mainly due to variation in rainfall during the study period, which could have made annual changes more difficult to identify specifically. Furthermore, the analysis of the meteorological data showed no obvious increases in precipitation, but a similar trend continued over 25 years. Moreover, if we compare the annual rainfall of 1990–2015, we see a marked reduction in the rainfall pattern.

In the case of winter trend, observed data showed a gradually increasing trend, with more than half of the respondents reporting that winter had become increasingly severe (although for short spells), which was not consistent with the trends in the meteorological data except in 2013, where the mercury dipped below 1 °C (0.9 °C). It could be possibly due to farmers' inability to identify significant fluctuations in temperature over a considerable period as they lack proper scientific equipment to precisely judge the change and the assumptions are based on their past experiences. Also on a few occasions when the mercury dipped, it could be that those severe incidents be still fresh in their memory, which determined their perception. While on another occasion, normal heating trend could be traced.

Local Practices for Fertility Management of Agricultural Field

Local practices will play an important role in combating different issues of climate change. Fertility management plays an important role in maintaining the yield, productivity, and keeping away pests and insect attacks. Apart from this, local farmers manage soil erosion and landslide, which becomes vital from the food security aspect, as soil erosion leads to removal of the top fertile layer of the soil that directly influences the production process. Some of the mechanical or the local fertility management can be seen as follows.

Natural Manuring

This is the most commonly used agricultural fertilization technique, whose importance has increased after the ban on the use of urea. It is available at a zero cost from the animal excreta; only the transportation charges (labor) are needed. Almost 100% of the farmers practiced it, where villages like Shreebadam even sell it at some cost to the nearby villages as it had an abundance of cow dung due to their daily practices. It enhances soil fertility and has no negative impact on the environment. The advent

Table 12.3 Impact analysis of climate on the area under cultivation for west district (1990 and 2013)

Crops	District	1990–1991			2012–2013			Changes		
		Area in 000' hectares	Production in 000' tons	Productivity in kg/Ha	Area in 000' hectares	Production in 000' tons	Productivity in kg/Ha	Area in 000' hectares	Production in 000' tons	Productivity in kg/Ha
Paddy	West	5.51	7.11	1290.38	3.95	7.18	1818	−1.56	0.07	527.62
	State	16.05	22.04	1373.21	12.07	20.88	1729.91	−3.98	−1.16	356.7
Wheat	West	2.37	3.79	1599.16	0.37	0.41	1120.1	−2	−3.38	−479.06
	State	7.82	13.08	1672.63	0.79	0.71	900.5	−7.03	−12.37	−772.13
Soyabean	West	1.24	1.04	846.77	1.19	1.04	875.5	−0.05	0	28.73
	State	3.62	3.01	834.25	3.87	3.47	896.64	0.25	0.46	62.39

of chemical fertilizer, reducing cattle size, and vanishing labor system had reduced its importance, but it is again gaining ground after the complete ban on urea.

Cowsheds in the Field (Goth)

An age-old practice, where the cattle are tied in the agricultural fields, enables farmers to naturally manure (cowdung) the field with the natural manure, which saves time and labor cost. It is a very effective means of fertilization, but changing social behavior and crimes like cattle theft, frequent attacks by the wilds, and reducing cattle size discourage farmers from practicing it (thunderstorm in 2014). However, about 15% practiced it, and villages like Mangbir (40%) and Chucen (40%) practice it the most, whereby they tie their cattle's fields near to their home.

Burning of Dried Leaves/Weeds in the Field

This is a common fertilization method practiced in drier fields post-crop harvest in summer, where farmers collect the remaining leftover of different crops and burn them in the field. It is generally done during cloudy and rain-like situations to prevent fire from spreading and also equitable mixing of the burnt ash, which improves the phosphate content for the next crop. To expose the harmful insects (consumed by birds), effective mixing and pulverization of the field is ploughed, which enables rich nutrients derived from the soil to get back to the soil. About 45% of the farmers in the area practice controlled burning as a fertility enhancer but also as a weed and waste management. The farmers from the Deythang (65%) and Samdung (60%) villages practiced it the most.

Crop Rotation

This is a commonly practiced cropping method, where legumes with cereals are cultivated in sequence to take advantage of different feeding zones. It not only maintains nutrient and water moisture, but also the ill-effects of mono-cropping like pests, diseases, and other insects. Almost everyone (100%) practiced it. In the study area, the basic crop combination that was observed was ginger–maize–paddy–millet (few patches); potatoes were also grown in a few patches (Shreebadam and Samdung). The system also sees a fallow patch of a few weeks to months during the dry spells.

Mulching

Mulching is a common agricultural practice where immediately after planting beds are covered with mulches consisting of forest litters, straw, grasses, and another

plant residue up to 6–8 cm thickness [Neem, Chilauney (*Schima Wallichii*), Kalijhar, Titeypati, fodder grass are used]. The majority of the local farmers practice it, mainly the ginger (about 85%)-growing village in the watershed. Almost (100%) farmers from Zeel, Shongri, Chuchen, and lower Hathidhunga villages practice it.

Water/Moisture Control Measures

Terraces or Bench Terraces

They are strips of flatbeds constructed across the hill slopes used for the cultivation of various crops like maize, wheat, paddy, and other local pulses by almost (100%) all households. Generally, terraces (benched) have a height of 2–5 m width, 2–5 m height, and length between 20 and 35 m, outward-facing slope, for quick drainage of excess water that used to be stored of terrace risers. They act as effective speed controllers during excess water in monsoon when there is heavy rain, reducing water velocity, preventing soil erosion, and preventing crops from being drowned. Zeel, Samdung (Bada Samdung precisely), and Mangbir villages practice it as they are also among the rice-growing villages within the watershed.

Water-Harvesting Pits (Tanks Now)

Almost every household (100%) in the villages surveyed had small pits for storing water for the nondrinking purposes like feeding cattle and watering vegetables and flowers. Slowly converting into rainwater-harvesting tanks with high capital investment is constructed village-wise based on the requirements. Almost every village has these except Shreebadam, Reshi, and Samdung, which are under construction. These water-harvesting tanks are used as an irrigation source during the lean and dry period, which can be used to grow vegetables to supplement the farming income. The entire community (CDGs) is responsible for the maintenance of such harvesting tanks and is actively working in the maintenance and management of different small waterways and water sources. This is also called source management, where plants like *dhokrey* and *banana* are planted above the water source to revive water.

Waterways/Irrigation/Kholchas or Kulhos

Both Kharif and rabi crops are practiced in combination, and locals have evolved with efficient water management systems through the use of kulhos (mud way), jhoras, and kholchas. Another sign of traditional water transportation from the source to the house is by using local bamboo (known as boom baans or filengey). It forms an important aspect of private forestry, which fetches them a good economic return, forms a vegetative barrier, and is an important fodder to the cattle. About 80%

of the farmers maintain and manage the waterways regularly mainly during the pre-monsoon and monsoon season. Muddy irrigation channel serves as a natural boundary to the fields, but over time they have started becoming dry, weeds covering them and shrinking area symbolizing uneven rainfall. MNREGA can be effectively used in reviving such water channels and promote employment.

Agroforestry

It is the integration of tree species with crops and pastures on the same land unit, which results in the integration of economic and ecological interactions. A favored land management system in the area aimed to curtail the problem of soil fertility, fuelwood, food security, fodder, and land degradation. However, it could also play an important role in climate change adaptation. Major agroforestry practices in the area include fodder grasses, boundary planting, fertility-enhancing trees/plants (nitrogen-fixing trees), and cardamom plantation promoting the coping capacity of local farmers to climate change risks. With dwindling signs for crops like paddy, maize, buckwheat, and oranges in changing climatic conditions, traditional large cardamom (*Amomum subulatum*)-based agroforestry could be a suitable alternative. This has been adopted in recent times as it accelerates nutrient cycling, increases soil productivity and soil fertility, soil erosion, conserve biodiversity, conserves water and soil, serves as a carbon sink, and improves farming income. As per reports, it can store 3.5 times more carbon than rain-fed agriculture, showing potential mitigation possibilities of agroforestry by sequestration of the atmospheric carbon. Almost 90–95% of the household surveyed cropped cardamom, but the intensity varied from place to place.

Suggestive Measures

Diversification of Livelihood Options

As is evident, the traditional agricultural practices are giving diminishing returns, hence paddy is slowly phasing out mainly due to water stress and uneconomic returns, which is replaced by ginger, cardamom, and seasonal vegetables. Promoting and adapting nonfarming activities like mushroom cultivation, poultry, piggery, goat rearing livestock, and hydel power projects would be a viable alternative to the nonperforming agricultural sector. Over the years, off-farm activities like seasonal vegetables and other products like chilies are increasing. Dalle Khurasni (*bell pepper*) thrives well and is yielding a great result. An estimate of about 10–15 quintals of Dalle chili (khursani) is produced and sold approximately in one season. But they practice it intensively and are a major source of income and practice using the guideline provided by the state agricultural board (water tanks for off-season vegetables). Government initiatives like NREGA provide 100 days of paid labor

within the village, but only 14 days are assured, which is also an alternative option; hence, people look to migrate to capital for seasonal employment opportunities in construction sites and other developmental activities, making it a climate change-induced displacement.

Bamboo Cultivation as an Important Livelihood Diversifying Options

Promotion of non-timber forest products (NTFPs) like bamboo (*Bambusoideae*) would be vital in diversifying livelihood options in the study area that houses species like common bamboo or Filengey, Bhalu baans (*Dendrocalamus sikkimensis*), Lahure bans (*Melocanna baccifera*), and Mal baans. Its multiple and wide range of uses make it a suitable alternative to timber products and food to rural poor and tribals. It is very useful in the construction of houses, agricultural activities, boundary barriers, storing fodder, and shelter for animals. Apart from the environmental impact, it also has a high economic value; if developed, it could make the community resilient to the economic vulnerabilities of climate change. This can be achieved by mutual cooperation between the authorities and the rural poor participatory management like Joint Forest Management (JFM), Forest Development Agency (FDA), and Eco-Development Community (EDC).

Crop Diversification

Crop diversification would be a viable adaptive option as it gives a wider choice in the production, which is adopted to expand production activities of various crops and also to lessen the risk of failure of one crop. The creation of the national-level Technology Mission on Oilseeds (TMO) to give thrust on oilseeds production as a national need to reduce import could be taken up as an example. Crop diversification would be a lucrative option for reducing the loss from another crop. The Lepcha community uses their traditional knowledge for crop diversifying through agroforestry, intercropping, and other new improved varieties to combat climate change challenges on agriculture and livelihood options. Though crop diversification is related to cereals and oilseeds, in the present context, it can be replaced by cropping of soyabeans and bhatmas along with maize and buckwheat. Paddy is becoming less economic and dryness is increasing, so dry crops like millets, other cereals like urd, and oilseeds like soyabean and bhatmas can be promoted in the study area. Although they existed once but are ceasing to exist slowly, this can be conserved and promoted in the future. In dry conditions, shift from wet to dry can help in diversifying the local agriculture and cropping pattern, which can be a suitable alternative in the present scenario. Also, adjusting the timing of the cropping and harvesting period could yield better results.

Conservation and Management of Water Resource

Initiatives like various plantation drives could be carried out to check erosion and increase infiltration by promoting traditional means of the water system and maintain small streams. Apart from these, locals should be educated and made aware of increasing water stress and resulting threats by involving them in the planning process. Government should promote rejuvenation and revival of traditional springs across the region, which is underway. Further strict laws should be in place against the expansion of human habitation in river basins and rampant construction activities.

Role of Institutions at Various Levels

Local community-based, governmental, and nongovernmental institutions like SHGs, CDGs, along with NERLP can play a vital role in making locals resilient to socioeconomic stress and environmental challenges in the era of climate change. Initiatives like small cash credits from SHGs, crop insurance from the government, and effective dissemination of information through Panchayati raj institutions could play a vital role. Here, the new means of dissemination of information like community radio (in local language) could be effective in disseminating information and make locals aware of the various aspects and challenges of climate change. Other institutions like the Northeast Rural Livelihood Program (NERLP), Horticulture/Agriculture Departments, Integrated Pest Control and Management (IPCM), Soil and Water Conservation Departments, and National Rural Employment Guarantee Act (NREGA) could play an important role in assisting the local community, generating employment, and in long-term agricultural development.

Implementation of Innovative Technical Practices

Modern agriculture signified by the use of machines, HYV seeds, and other fertilizer has no or little relevance in the context of Sikkim Himalaya. Innovations and modernization of agriculture to the local communities mean modernizing their traditional practices and promoting economic and sustainable farming practices. Researchers and policymakers have suggested and come up with various such techniques and means. NERLP has been working constantly in promoting sustainable rural livelihood through various means. Some of the techniques that could be implemented and promoted in the area can be listed as

- Bio-composting
- Promoting azolla
- Greenhouse/poly house
- Drip and sprinkler irrigation
- Economic household or community tanks

Conclusion

Here, it can be concluded that the Reshi Khola watershed of Sikkim Himalaya is consequently responding to the global climatic trend. Locals had a clear understanding of climate change, and their perceptions were consistent with the meteorological trend. The region showed a clear warning sign with an increase of 1.52 in average surface temperature representing an increase of .50/9 years. While in terms of precipitation there was no clear trend of increase or decrease was noticed, but it has become unpredictable and erratic. Over the years, the number of rainy days has reduced from 232 in 1990 to 215 in 2015, but the annual rainfall is constant or moreover has been a marginal decrease from 10.40 mm in 1990 to 9.32 mm in 2015.

The changing climatic trend is leading to various environmental and ecological problems like water shortage, low productivity, declining agricultural land, erratic monsoon, and the problem of pests and disease. To keep up with the mounting pressure, locals have stuck to their traditional local practices of mixed cropping, mulching, natural manuring, agroforestry, vegetative barriers, adjusting the timing, and organic farming as adaptive measures that could turn out to be important in the future. Though this has been practiced for ages, post-urea ban and mounting challenge from climate change are increasing their importance. Some respondents believed that there is no climate change and perspective varied from person to person, age, sex, and education, terming it a natural change. The majority of the response and local practices were based on their local experience and traditional knowledge and not completely attributed to climate change, which is a recent development. Here, the local practices become an important adaptive means to cope up with climate change. Apart from them, an initiative like crop diversification, livelihood diversification, and implementation of different innovative techniques would help overcome the climate change challenges. Documentation of local knowledge and incorporation of modern scientific research would help both policymakers to frame better policies and farmers to better adapt to climate change challenges.

References

Bajracharya SR, Shrestha B (2011) The status of glaciers in the Hindu Kush Himalayan region. International Centre for Integrated Mountain Development (ICIMOD), Kathmandu

Berkes F (2002) Epilogue: making sense of Arctic environmental change. In: Krupnik I, Jolly D (eds) The earth is faster now: indigenous observation of Arctic environmental change. Arctic Research Consortium of the United States, Fairbanks, pp 334–349

Bolch T, Kulkarni AV, Kaab A, Huggel C, Paul F, Cogley JG, Frey H, Kargel JS, Fujita K, Scheel M, Bajracharya S, Stoffel M (2012) The state and fate of Himalayan glaciers. Science. https://doi.org/10.1126/science.1215828

Chaudhary P, Bawa KS (2011) Local perceptions of climate change validated by scientific evidence in the Himalayas. Biol Lett. https://doi.org/10.1098/rsbl.2011.0269

Dimri AP, Dash SK (2011) Wintertime climate trends in the Western Himalayas. Clim Chang. https://doi.org/10.1007/A10584011-0201-y

Gardelle J, Berthier E, Amaud Y, Kaab A (2013) Region-wide glacier mass balance over the Pamir-Karakoram-Himalaya during 1999–2011. Cryosphere. https://doi.org/10.5194/tc-7-1263-2013

Ingty T, Bawa KS (2012) Climate change and indigenous people in Sikkim Himalaya. In: Arrawatia ML, Tambe S (eds) Climate change in Sikkim: patterns, impacts and initiatives. Government of Sikkim, Gangtok, pp 275–291

IPCC (2007) Summary for policymakers. In: Climate Change 2007: climate change impacts, adaptation and vulnerability, working group II contribution to the intergovernmental panel on climate change fourth assessment report

IPCC (2014) In core writing team. In: Pachauri RK, Meyer LA (eds) Climate change 2014: synthesis report., the contribution of working groups, I, II and III to the fifth assessment report of the intergovernmental panel on climate change. IPCC, Geneva, 151pp

Kumar P, Sharma MC, Saini R, Singh GK (2020) Climate variability at Gangtok and Tadong weather observatories in Sikkim, India, during 1961–2017. Sci Rep 10:15177. https://doi.org/10.1038/s41598-020-71163-y

Mildenbergera K, Beiderwiedena E, Hsiac YJ, Klemma O (2009) CO_2 and water vapour fluxes above a subtropical mountain cloud forest-the effect of light conditions and fog. Agric Forest Meteorol 149(10):1730–1736

Mishra AK, Rai SC (2019) Assessment of spatio-temporal variability of temperature using geostatistical techniques: a case study of Upper Teesta River basin, India. Environ Sustain. https://doi.org/10.1007/s42398-019-00049-1

Rai SC, Mukherjee NR (2021) Spatio-temporal change delineation and forecasting of snow/ice-covered area of Sikkim Himalaya using multispectral and thermal band combinations of Landsat imagery. Environ Chall. https://doi.org/10.1016/j.envc.2021.100163

Rupa K, Pant GB, Parthasarathy B, Sontakke NA (1992) Spatial and sub-seasonal patterns of the long-term trends of Indian summer monsoon rainfall. Int J Climatol 12:257–268

Sharma RK, Shrestha DG (2016) Climate perceptions of local communities validated through scientific signals in Sikkim Himalaya, India. Environ Monit Assess 188:578. https://doi.org/10.1007/s10661-016-5582-y

Sharma E, Chettri N, Tse-ring K, Shrestha AB, Jing F, Mool P, Eriksson M (2009) Climate change impacts and vulnerability in the eastern Himalayas. ICIMOD, Kathmandu, pp 5–6

Xu J, Grumbine RE, Shrestha A, Erikksson M, Yang X, Wang Y, Wilkes A (2009) The melting Himalayas: cascading effects of climate change on water, biodiversity, and livelihoods. Conserv Biol 23(3):520–530

Chapter 13
Land Use Change and Ecological Implications in Uttar Pradesh in India: A Sectoral Perspective

Shahab Fazal, S. K. Azharuddin, and Salma Sultana

Abstract Land is a resource of utmost importance on account of its use for diverse functions. However, this finite resource has been experiencing threat due to it being utilized. The way it is being used and modifications made by humans greatly affect the ability of natural systems to support life over the earth. This present study was carried out in Uttar Pradesh, one of the states of India. It is the fourth largest in area and interestingly has the largest rural population in the country. Moreover, this state has been going through large-scale land use transformations, particularly after economic reforms. Thus, this study made an attempt to understand the dynamics of land use in Uttar Pradesh as it is directly or indirectly associated with their living. This study largely focused on three sectors, namely, ecological, agricultural, and nonagricultural sectors, for analyzing this status. It primarily focused on secondary sources of data incorporating various government publications from 2000 to 2015. The findings of this research reveal that the growth rate of different categories of land use has witnessed declining trends, except the area under nonagricultural land use. Whereas ecological sector is passing through a critical phase of land transformation as the area under forest is declining along with pastures and miscellaneous trees. It also points out considerable decrease in net sown area in the agricultural sector but increase in the current fallow land.

Keywords Land use · Dynamics · Ecological · Agricultural and nonagricultural sectors

Introduction

Humans are the major force of change around the globe, transforming land to provide food, shelter, and products for use. Changes in the cover, use, and management of the land have occurred throughout history in most parts of the world as

S. Fazal (✉) · S. K. Azharuddin · S. Sultana
Department of Geography, Aligarh Muslim University, Aligarh, Uttar Pradesh, India

population has changed and human civilizations have risen and fallen (Turner II et al. 1990). Land transformation is perhaps the most profound result of human actions because it affects many of the planet's physical and biological systems (Kates et al. 1990).

Land is an important resource. Humans require land for all kinds of activities. Natural scientists define land use in terms of complexes of human activities such as agriculture, forestry, and building construction that alter land surface processes. Land use and land cover change (LU/LCC), also known as land use change, is a general term for the human alteration of Earth's terrestrial surface. Land use is the product of interactions between culture and physical requirements of the society with the natural potential of land (Karwariya and Goyal 2011). Change in land use/land cover (LU/LCC) is one of the most profound human-induced alterations of the Earth's system (Vitousek et al. 1997). Land use/land cover change is one of those major challenges that also change the natural landscape. It is one of the main driving forces of global environmental change and central to the sustainable development debate (Lambin et al. 2000). These include its impact on water quality, land and air resources, ecosystem processes, and function and climate (Lambin et al. 2000); biodiversity (Liu and Ashton 1998); soil degradation (Trimble and Crosson 2000); and the ability of natural systems to support life (Vitousek et al. 1997).

The changes in land use affect the ecosystem of an area in terms of vegetation, local weather effects, land quality itself, and the quality of life that can be sustained (Pandey and Tewari 1987). On the other hand, rapid pace of economic development along with population growth, urbanization, and industrialization exerts tremendous pressure on the limited finite natural resource base of any geographical space (Bardhan and Tewari 2010).

In modern times, population growth, economic transformation, and environmental change are being witnessed in every part of the earth. The world population has crossed seven billion. Moreover, more and more people are concentrated in urban areas, and the process of urbanization is being witnessed as very dominant. This process of urbanization started since the mid-eighteenth century along with industrialization. But during the last century, the process of urbanization accelerated and projections suggest that it would continue, especially among India and other developing countries. Presently about 55% of the world's population live in urban area and expected to be 68% by 2050. This will certainly exert more stress on land resource.

India is predominantly a rural and agrarian country and depends directly or indirectly heavily on the land resource for sustenance of its large population. The population in rural areas is also increasing rapidly, and its results may have effects on the dynamics of land use and other related resources. India is the second largest populated country in the world after China, but if land-man ratio is taken into consideration, its land area is relatively much smaller. India's population reached about 12,110 million in 2011, which shares about 17% of the world population while land share is only about 2.4%.

In the state of Uttar Pradesh, one of the most populated and resource-rich states in India, land is going through significant transformations because of changes in land use due to increasing population, industrialization, and urbanization. In 2011, the population of Uttar Pradesh was roughly 201.1 millions, which accounts for about 16.16% of the Indian population while the per capita availability of land is only about 0.13 hectares, which is much less than the national average.

Several studies have highlighted the characteristics of land use dynamics in India. Maitima et al. (2009) noted that the land cover changes have transferred to farm-lands, grazing lands, human settlements, and urban centers at the expansion of natural vegetation. These changes also show linkages with biodiversity loss and land degradation, which indicates that as native vegetation is lost, indigenous plant and animal biodiversity and plant cover are also lost. Pushpa and Akashraj (2014) attempted to analyze intra- and intersectoral land use dynamics in Karnataka from ecological perspective for the period from 1980–1981 to 2008–2009 by using multiple linear regression equation and indicated that small and marginal farmers have a negative impact on area under desirable ecological sector and urbanization has influenced the land shift toward nonagriculture, whereas the land shift toward undesirable ecological sector has been shown stagnant in most of the districts during the study period.

Malik et al. (2013) used geospatial techniques for combining geospatial themes to analyze the urban sprawl mapping and detect changes in urban land use/land cover through different years in Jammu city. They observed that the built-up area has been on constant increase, while agricultural land is the prime victim of this land transformation. Dale et al. (2000) showed that the management and use of land are made with meager attention to ecological impacts; five ecological principles for land use with particular implications can assure that fundamental processes of Earth's ecosystems are sustained. These deal with time, species, place, disturbance, and the landscape.

Land use is an important parameter for a number of agricultural and ecological models, which organize significant tools for development, plan, and management of the natural resources in the region. Better land management involves identifying ecological benefits and costs that arise from land use practices, as well as finding the best alternatives for each area (Wu et al. 2001). There are broad differences in the distribution and utilization of land resources over different districts of the state, based on topographic, geographical, political, and other factors. Therefore, an understanding of the land use dynamics and their ecological implications in Uttar Pradesh would be of immense help. This present pattern of sector-wise land uses, their growth rate, and the trends of changes helped to determine such problems related to it. Also, the various determinant parameters with sectoral land use will help in understanding the future trends and adaptation for the proper utilization of land.

Data and Methodology

The present study is based on the analysis of secondary sources of data on land use pattern for a ninefold classification collected over the districts and state level for four time periods, that is, 2000, 2004–2005, 2010–2011, and 2015, in Uttar Pradesh. The study uses secondary datasets that have been collected from the Directorate of Economics and Statistics, Department of Agriculture, Lucknow, Government of Uttar Pradesh.

The first accounting identity summed up area under all land use classes that were equal to the total reporting area, given by Equation (R):

$$R = Fr + P + M + N + U + W + Fe + Fo + C \qquad (13.1)$$

where $\mathbf{R} =$ is the reporting area, $\mathbf{Fr} =$ area under forests, $\mathbf{P} =$ permanent pastures, $\mathbf{M} =$ miscellaneous trees, $\mathbf{B} =$ barren land, $\mathbf{W} =$ culturable wastelands, $\mathbf{Fc} =$ current fallows land, $\mathbf{Fo} =$ other fallows, $\mathbf{C} =$ net sown area, and $\mathbf{N} =$ nonagricultural uses.

The dynamics of land use shift is examined with the help of a simple identity of linearly additive land use changes. The accounting identity for land use changes over time is expressed as

$$\Delta R = \Delta F_r + \Delta P + \Delta M + \Delta B + \Delta W + \Delta F_c + \Delta F_o + \Delta C + \Delta N \qquad (13.2)$$

where Δ represents change for different time periods.

In this present study, total land endowment (reporting area) of ninefold land use classes is categorized into three broad sectors, that is, ecological sector (E), agricultural sector (A), and nonagricultural sector (N):

$$\Delta R = \Delta E + \Delta A + \Delta N$$

1. The net changes in the *ecological sector* (ΔE) (Eq. 13.3):

   The ecological sector is further divided into two subsectors, viz.,

$$\Delta E = \textbf{enviable ecology } (\Delta EE) + \textbf{unenviable ecology } (\Delta UE) \qquad (13.3)$$

(a) *Enviable ecological sector:* ΔEE = *area under forests* (ΔFr) + *permanent pastures* (ΔP) + *miscellaneous tree* (ΔM)

   The changes in enviable ecological sector consist of changes in the area under forest, permanent pasture, and miscellaneous trees and groves.

(b) *Unenviable ecological sector: – ΔUE = barren lands* (ΔB)

However, changes in unenviable ecological sector represent changes in land under barren and unculturable area. The study assumes that land use shifts have ecological implications. Thus, if the land transformation takes place from unenviable to enviable ecology, then it would have favorable ecological effects, but if the land of enviable ecology shifts to unenviable ecology, then it may result in adverse impacts on ecology. Even land use dynamics within enviable ecology may also have ecological implications. If land shifts from permanent pasture and miscellaneous tree and groves of forest, this change is considered to have positive ecological implications. On the contrary, negative ecological implications would be inflicted if the forest land turns into permanent pastures.

2. The net changes in *the agricultural sector* (ΔA) (Eq. 13.4):

$$\Delta A = \text{Culturable wastelands } (\Delta W) + \text{Current fallows } (\Delta F_c) \\ + \text{Other fallow land } (\Delta Fo) + \text{Net sown area } (\Delta C) \tag{13.4}$$

The second category is agricultural sector. It comprises four "sub-land use classes." These are culturable waste land, current fallow land, other fallow, and net sown area.

The net change in the agricultural sector, if positive ($+\Delta A$), will be at the cost of the ecological sector, which means that it draws land from forest, permanent pastures, and land under miscellaneous trees. When the net change in the agricultural sector is negative ($-\Delta A$), the land use shift may occur to either the ecological sector (enviable/unenviable ecological sector) or nonagricultural sector or both. The shift of land from agricultural sector to the unenviable ecological sector would have an adverse impact on the agricultural sector.

Land transformations within the agricultural sector have important implications depending upon the dynamics of change among the classes. If there is a positive change to the agricultural sector ($+\Delta A$), and also an increase in the net sown area ($+\Delta C$), this situation would be in favor of the agricultural sector and considered as desirable change. Even there is a negative net change ($-\Delta A$), but positive change in the net sown area ($+\Delta C$), the dynamics are considered favorable for the agricultural sector and assumed as desirable land use dynamics as the cropped area is increasing. But a decrease in the net sown area by a shift of cultivated land toward fallow land and culturable waste land has a negative impact on the agricultural sector. Further, this situation would require larger investments and efforts to reclaim such waste land.

3. The net changes in the *nonagricultural sector* (ΔN) (Eq. 13.5):

$$\Delta N = \textbf{Area under non} - \textbf{agricultural } (\Delta N) \tag{13.5}$$

The third category is the nonagricultural sector consisting of land under nonagricultural land uses. This sector is another critical sector of land use change. The increment in land under nonagricultural sector can be in three ways; it may occur at the cost of ecological sector or agricultural sector and even drawing land from both. If the land under enviable ecological sector gets transformed into nonagricultural sector, this will have adverse effects on the ecology. Thus, better utilization is assumed to be when nonagricultural sector draws land from unenviable ecological sector. While increase in the nonagricultural sector gaining land from agricultural sector is considered detrimental as this may result in food shortage.

The overall intersectoral land use transfers can be budgeted as

$$\Delta \mathbf{R} = \Delta \mathbf{E} \, (\Delta \mathrm{EE} + \Delta \mathrm{UE}) + \Delta \mathbf{A} + \Delta \mathbf{N}$$

To quantify the determinants of ecological, agricultural, and nonagricultural sector land use in Uttar Pradesh, multiple linear regression model was fitted. Dependent variables included in the model are population density, urban population, rural population, average size availability of land, GDP in industry, irrigated area, GDP in agriculture, and road length in districts of Uttar Pradesh.

Study Area

Uttar Pradesh is one of the important and most populous states of India. It is also largely an agriculture-dependent state. It lies between 23°52′ N to 30°28′ N latitudes and 77°03′ to 84°39′ E longitudes and covers an area of 243,290 km^2 (93,933 sq. mi), equal to 7.33% of the total area of this country, and is the fourth largest Indian state by area. The state contributes 16.16% to India's total population. Uttar Pradesh is divided into 75 districts under the 18 divisions. In the national context, it enjoys a strategic location lying at the intersection of the Himalayan Region in the north and the Peninsular Region in the south, encompassing the extremely fertile plains of River Ganga and Yamuna. It has a humid subtropical climate and experiences four seasons. Uttar Pradesh is the third largest Indian state by economy, with a GDP of ₹9763 billion (US$150 billion) and the fourth largest contributor to India's net domestic product. Agriculture and service industries are the largest parts of the state's economy. The service sector comprises travel and tourism, hotel industry, real estate, insurance, and financial consultancies (Fig. 13.1).

Trends in Different Land Use Classes in Uttar Pradesh

This study includes nine different land use classes in Uttar Pradesh. To find the trends for these land use classes, both growth rate and percentage changes were calculated (Table 13.1).
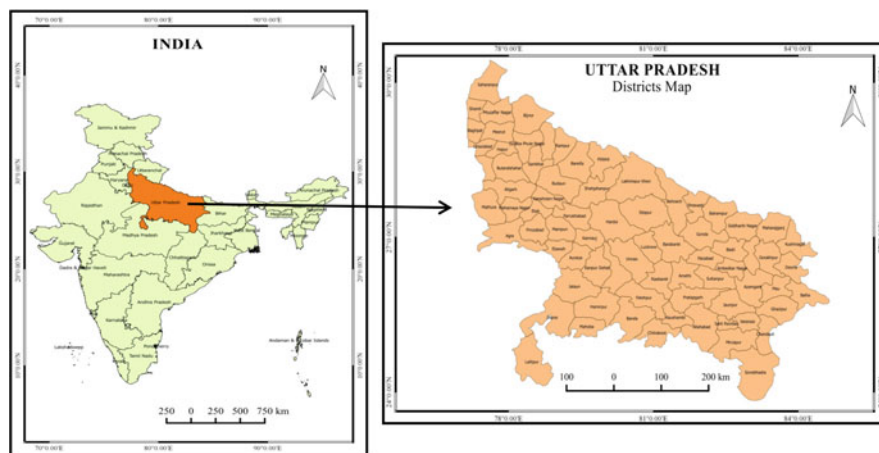
Fig. 13.1 Study area map

Table 13.1 Trends in different land use classes in Uttar Pradesh (2000–2015)

Land use classes	Area in hectares			
	2000	2015	2000–2015	2000–2015
Total reported area	24210209	24174524	−35685 **−0.15**	−0.011*** **−0.004**
Area under forests	1691128 **6.99**	1659461 **6.86**	−31667 **−1.87**	−0.135 **0.102**
Permanent pastures land	70077 **0.29**	66571 **0.28**	−3506 **−5.00**	−0.366 **0.42**
Land under misc. tree crops	337631 **1.39**	325441 **1.35**	−12190 **−3.61**	−0.262 **0.656**
Barren and unculturable land	623232 **2.57**	464492 **1.92**	−158740 **−25.47**	−0.163* **0.054**
Culturable waste land	536858 **2.22**	410072 **1.70**	−126786 **−23.62**	−1.906 **0.114**
Fallow lands other than current fallows	644228 **2.66**	538656 **2.23**	−105572 **−16.39**	−1.367 **0.128**
Current fallows	1055154 **4.36**	1135309 **4.70**	80155 **7.60**	0.524 **0.738**
Net area sown	16809542 **69.43**	16548823 **68.46**	−260719 **−1.55**	−0.112** **0.05**
Area nonagricultural use	2442327 **10.09**	3025699 **12.52**	583340 **23.89**	1.542*** **0.008**

Source: Based on Directorate of Agriculture, Lucknow, Uttar Pradesh
In area, bold indicates the percentages
In CAGR, bold indicates the rate of significance where *** significant at 1% level, **significant at 5% level, and *significant at 10% level

This table shows a marginal decline in total reporting area by about 35,685 hectares (0.15%) from 2421 thousand hectares in 2000–2417 thousand hectares in 2015. Here, the first land use class is area under forest. It was 1,691,128 hectares in 2000, which was 6.99% of the total reporting area. However, it decreased by about 31,667 hectares (1.87%) during the study period of the 15 year to 1,659,380 hectares, which was 6.86% in 2015. This decline could be attributed to reckless felling of trees and a wide gap between rates of deforestation.

Permanent pastures and grazing land constitute second land use class, which are an important source of livelihood for pastoralists and other marginalized communities. This category has also shown a decline by about 3506 hectares (5.00%) from 70,077 hectares in 2000, which was 0.29% to 66,571 hectares, which reduced to 0.28% to the total reporting area in 2015.

The third land use class is area under miscellaneous tree crops. It was reported as 337,631 hectares in 2000, which was 1.39%. However, it decreased by 12,190 hectares (3.61%) to 32,544 hectares, which was 1.35% of the total reporting area in 2015. These trends of land use changes are likely to generate severe ecological imbalances.

The barren and unculturable land is the fourth land use class, which also revealed a highly declining trend by about 158,740 hectares (25.47%). The area under this land use class has significantly dropped at an annual compound growth rate of about 0.163%. The share of barren and unculturable land has reduced from 2.57% of the total reporting area in 2000 to 1.92% in 2015.

It is also evident from the table that during the study period the area under culturable wasteland, which is the fifth land use class, has declined by 5484 hectares (1.27%) and the land share decreased from 536,858 hectares (2.22%) to the total reporting area in 2000 to 410,072 hectares (1.70%) in 2015.

The area under fallow land other than current fallow land was 644,228 hectares in 2000, which was 2.66% of the total reporting area. It makes sixth land use class and revealed a decrease by 105,571 (16.39%) during the study period from 538,656 hectares, which was 2.23% in 2015. Interestingly, the area under this land use class witnessed a decline for the three time period blocks, that is, 2000 and 2015.

Uttar Pradesh is an agriculturally dominated state. However, net sown area constituting eighth land use class has shown decreasing trend during the study period at the growth rate of about 260,719 hectares (1.55%) from 16,809,542 hectares (69.43%) in 2000 to 1,654,8823 hectares (68.46%) to the total reporting area in 2015. The compound growth rate (0.112%) has also revealed a significant declining trend, which is really a serious concern to a state like Uttar Pradesh, where a large share of population depends on agricultural activities for gaining their livelihoods.

The last land use class is area under nonagricultural use. There has been a significant shift in the land use in favor of nonagricultural activities throughout the period, but at varying rates over time. It has shown a substantial increase at about 583,340 hectares (23.89%) from 2,442,327 hectares (10.09%) in 2000 to 3,035,699 hectares (12.52%) to the total reporting area in 2015. The compound growth rate of (1.542%) has also revealed significant increasing trends. Infrastructural

development, urbanization, industrialization, etc. have resulted in the expansion of area under nonagricultural uses. This trend may have serious implications in the long run.

Sectoral Land Use Pattern in Uttar Pradesh

This study focuses on three main sectors of land use in the state: (1) ecological sector including both enviable and unenviable; (2) agricultural sector; and (3) nonagricultural sector. The district-wise pattern of different land use classes for these three sectors is analyzed utilizing the data of two time periods, viz., 2000 and 2015. The study of different land use ranking is very useful in understanding the distributional pattern in any region because it provides an idea of relative dominance of different land in order of importance. Thus, to achieve the same objective, district-wise sectoral land use pattern in Uttar Pradesh is as follows.

Within the ecological sector, forest accounts for the highest share at around 7% while permanent pastures and grazing land and miscellaneous trees and groves together account for (1.63%) of the total reporting area (enviable ecological subsector). On the other hand, barren and unculturable land has shown a relatively large share with 1.92% of the total reporting area (unenviable ecological subsector). The district-wise analysis revealed that the area under forest as a percentage of the total reporting area was recorded relatively high in the southeastern and northern districts like Sonebhadra, Chandauli, Mirzapur, Lakhimpur Kheri, and Pilibhit. Northwestern and southern districts like Maharajganj, Etawah, Balrampur, and Shravasti also showed increase in this land use class. However, the districts that reported lower forest land share were Varanasi, Moradabad, Ballia, Azamgarh, and Sambhal.

The area under permanent pasture as a percentage of total reporting area was highest in Lucknow followed by Kanpur Nagar, Kannauj, Raebareli, Amethi, and Faizabad district, while the area under miscellaneous crops recorded highest in Sonebhadra followed by Chitrakoot, Pratapgarh, Mirzapur, and Raebareli district. The districts with lower percentage of pasture land share were Varanasi, Shravasti, Chitrakoot, Chandauli, and Rampur, while in miscellaneous crops, districts like Aligarh, Maharajganj, Meerut, Bulandshahar, and Baghpat had a lower percentage share during the study period.

The share of barren land to the total reporting area was found highest in Jhansi followed by Chitrakoot, Mainpuri, Kanpur Dehat, Kanpur Nagar, and Kaushambi, while districts like Maharajganj, Shravasti, Saharanpur, and Sambhal recorded lower share of barren land. Moreover, Mirzapur and other central districts also registered declining share of land area under barren land. However, the share had increased in Sonebhadra and northwestern districts for the same category.

The second sector is the agricultural sector. In this sector, net sown area accounts for the largest share (68.46%) of the total reporting area in the state. Moradabad (83.22%) recorded the highest share of land under net sown area followed by Budaun (82.13%). Whereas Gautam Budh Nagar, Mirzapur, and Sonebhadra constituted a

comparatively smaller proportion of land area under the same category with 42.37%, 42.19%, and 21.46%, respectively. Additionally, Farrukhabad, Varanasi, Allahabad, Pratapgarh, and Gautam Budh Nagar district also registered a noticeable decline in the proportion of net sown area during the period of 2000–2015.

The districts like Gautam Budh Nagar, Pratapgarh, Raebareli, and Allahabad had shown larger proportion (23–18%) of area lying under fallow land to the total reporting area. While Bulandshahar, Saharanpur, Rampur, and Shravasti recorded a relatively smaller proportion (from 1% to 2%) of other fallow and current fallow land. However, the share of culturable wasteland was found highest in Lalitpur followed by Kanshiram Nagar, Etah, and Raebareli district. In contrast, districts like Maharajganj, Saharanpur, Shravasti, and Rampur outlined very low share of wasteland (less than 1%) (Figs. 13.2 and 13.3).

The third is nonagricultural sector. Ghaziabad, Gautam Budh Nagar, Lucknow, Pratapgarh, and Varanasi revealed higher shares (18–30%) of area under nonagricultural uses to the total reporting area. This shift is largely attributed to the increasing pace of urbanization and industrialization. On the other hand, districts like Jalaun, Hamirpur, Jyotiba Phule Nagar, and Lalitpur recorded relatively lower proportion (less than 8%) of land area under the same category.

Budgeting of Intersectoral Land Use Shifts

The budgeting of intersectoral analysis was carried out to find the pattern and extent of land use shifts in Uttar Pradesh. The results of this dynamics are presented in Table 13.2. It is evident from the table that land use shifts have been occurring from the desirable ecology, undesirable ecology, and agricultural sector toward nonagricultural sector during the study period for all the four blocks. The compound growth rate figures also indicate significant changes among all the sectoral land use classes during the period of 2000–2015 in this state.

The agricultural and ecological sectors have shown negative growth rate of 0.16% and 0.56% per annum, respectively, whereas the nonagricultural sector has recorded a significant positive growth rate (1.54% per annum). The shifts of land from these favorable sectors to the nonagricultural sector have serious implications and require an immediate check. The unfavorable trends of desirable ecological and agricultural sector land use dynamics lead to the degeneration of this important natural resource and cultivable land, which needs priority to management (Fig. 13.4).

The budgeting of intersectoral estimates for undesirable ecology sector has shown a significant decline, indicating that the land has been shifted toward the nonagricultural sector. This association of land use shift clearly demonstrates that this land is being consumed under urbanization, industrialization, infrastructural support of rural roads, irrigation development, market area, etc. However, agricultural growth and development of enviable ecological sector are largely required to maintain the balance of favorable land uses.
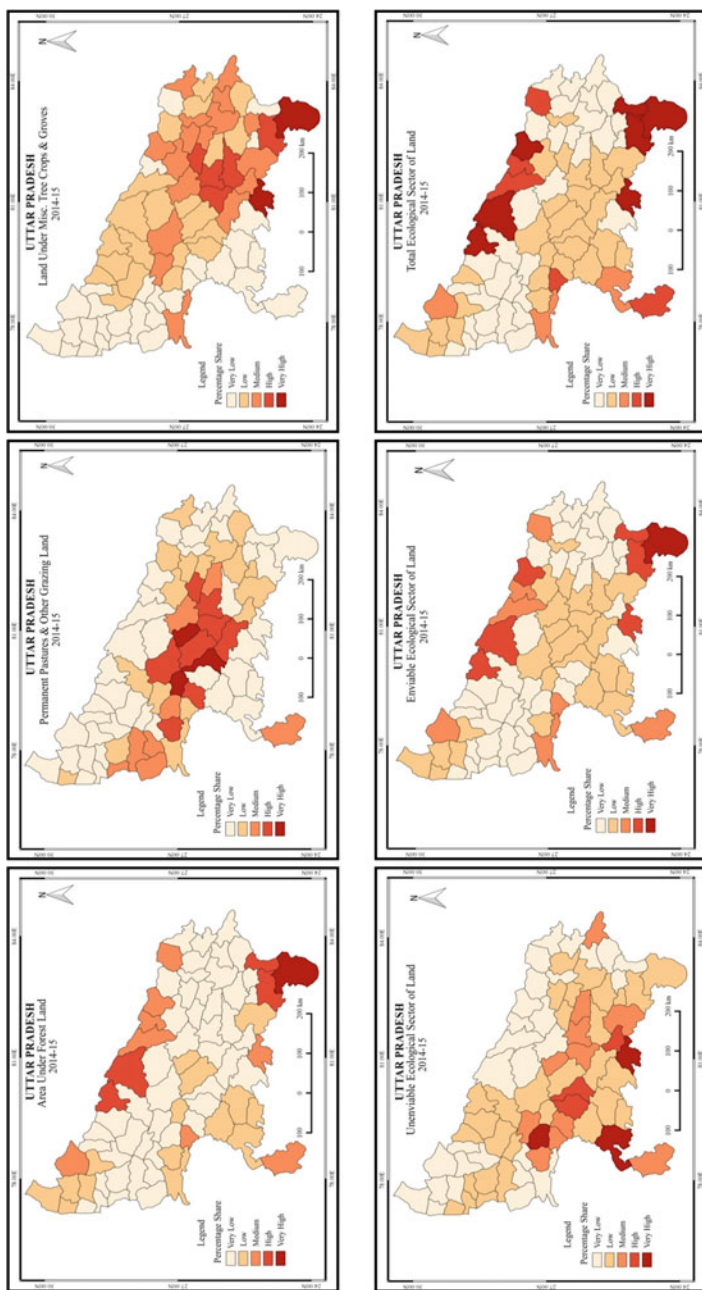
Source: Based on Directorate of Agriculture, Lucknow, Uttar Pradesh.

Fig. 13.2 Land use pattern in the ecological sector (2015) (in percentage). (Source: Based on Directorate of Agriculture, Lucknow, Uttar Pradesh)
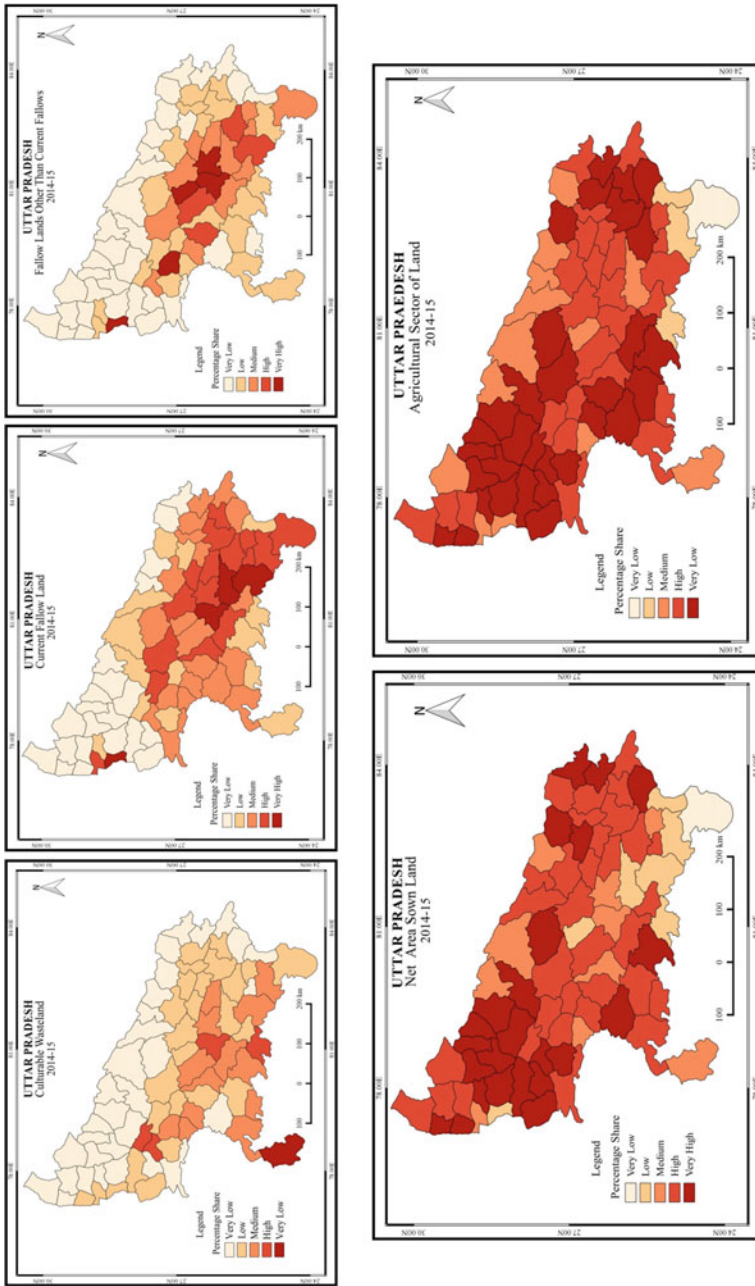
Fig. 13.3 Land use pattern in the agricultural sector (2015) (in percentage). (Source: Based on Directorate of Agriculture, Uttar Pradesh, Lucknow)

Table 13.2 Budgeting of intersectoral land use shifts in Uttar Pradesh 2000–2015

Land use class	Area in hectares		Change in growth rate 2000–2015	CAGR in % 2000–2015
	2000	2015		
Total land under enviable ecological sector ΔEE ($\Delta F_r+\Delta P+\Delta M$)	2098836 (**8.67**)	2051473 (**8.49**)	−47363 (**−2.26**)	−2.078* (**0.057**)
Total land under unenviable ecological sector ΔUE (ΔB)	623232 (**2.57**)	464492 (**1.92**)	−158740 (**−25.47**)	−0.163* (**0.054**)
Total land under ecological sector ΔE ($\Delta UE+\Delta EE$)	2722068 (**11.24**)	2515965 (**10.41**)	−206103 (**−7.57**)	−0.561** (**0.014**)
Total land under agricultural sector ΔA ($\Delta W+\Delta F_c+\Delta F_o+\Delta C$)	19045782 (**78.67**)	18632860 (**77.08**)	−412922 (**−2.17**)	−0.156*** (**0.005**)
Total land under nonagricultural sector ΔN	2442327 (**10.09**)	3025699 (**12.52**)	583340 (**23.88**)	1.542*** (**0.008**)
Net sectoral changes (ΔR) ($\Delta E+\Delta A+\Delta N$)	24210209	24174524	−35685 (**−0.15**)	−0.011*** (**0.004**)

Source: Based on Directorate of Agriculture, Uttar Pradesh, Lucknow

In area, bold indicates the percentages

In growth rate of changes, bold indicates annual growth rate of changes

In CAGR, bold indicates the rate of significance where ***significant at 1% level, ** significant at 5% level, and *significant at 10% level
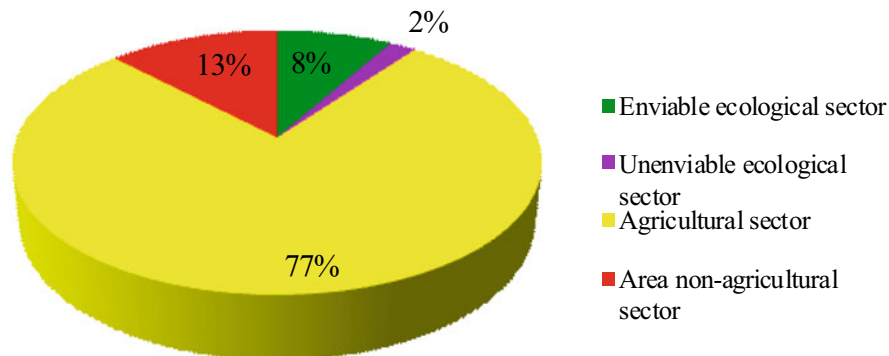
Source: Based on Directorate of Agriculture, Lucknow, Uttar Pradesh.

Fig. 13.4 Sector-wise land use pattern in Uttar Pradesh (2015). (Source: Based on Directorate of Agriculture, Lucknow, Uttar Pradesh)

Land Use Dynamics

Figures 13.5, 13.6, and 13.7 depict district-wise estimation of growth rate of land use changes for various land use classes, while Table 13.2 shows different sectoral growth rate changes. So, firstly, dynamics of different land use classes is explained, followed by sectoral changes.
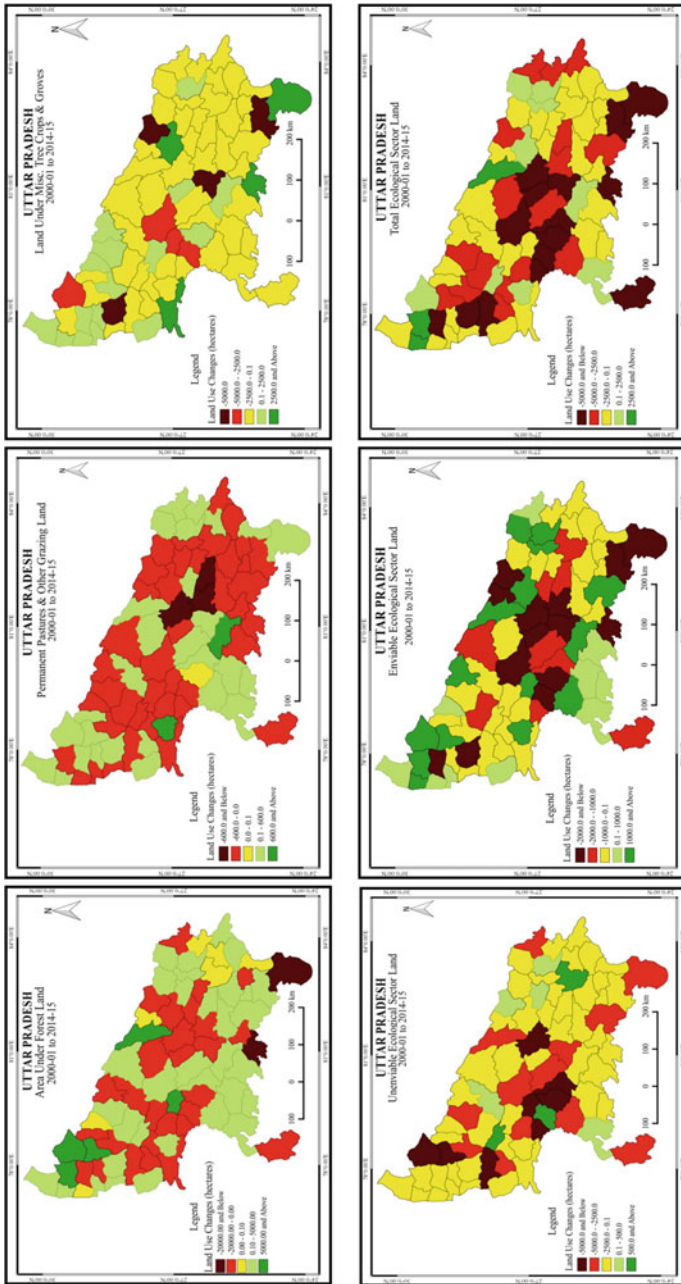
Source: Based on Directorate of Agriculture, Lucknow, Uttar Pradesh.

Fig. 13.5 Land use dynamics in the ecological sector. (Source: Based on Directorate of Agriculture, Lucknow, Uttar Pradesh)
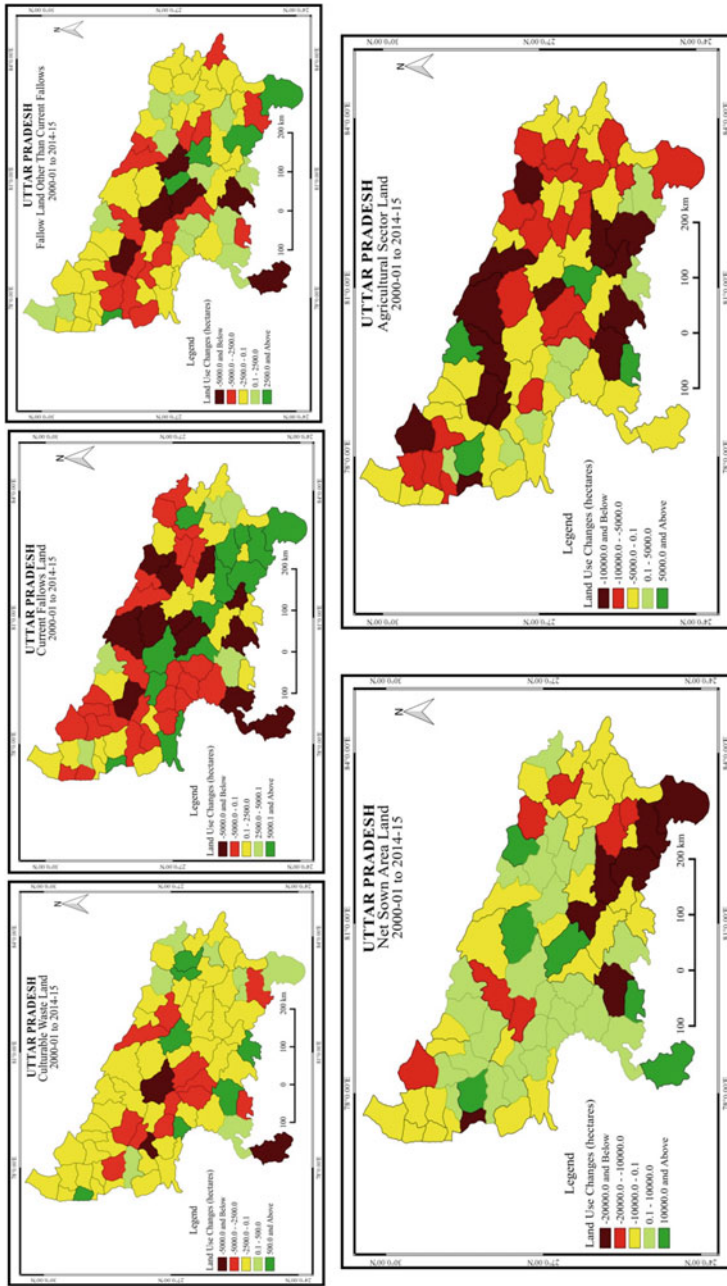
Source: Based on Directorate of Agriculture, Lucknow, Uttar Pradesh.

Fig. 13.6 Land use dynamics in the agricultural sector. (Source: Based on Directorate of Agriculture, Lucknow, Uttar Pradesh)

UTTAR PRADESH
Area Under Non-Agricultural Sector Land
2000-01 to 2014-15

Legend

Land Use Changes (hectares)

-1176.0 - 0.1

0.1 - 5000.0

5000.0 - 10000.0

10000.0 and Above
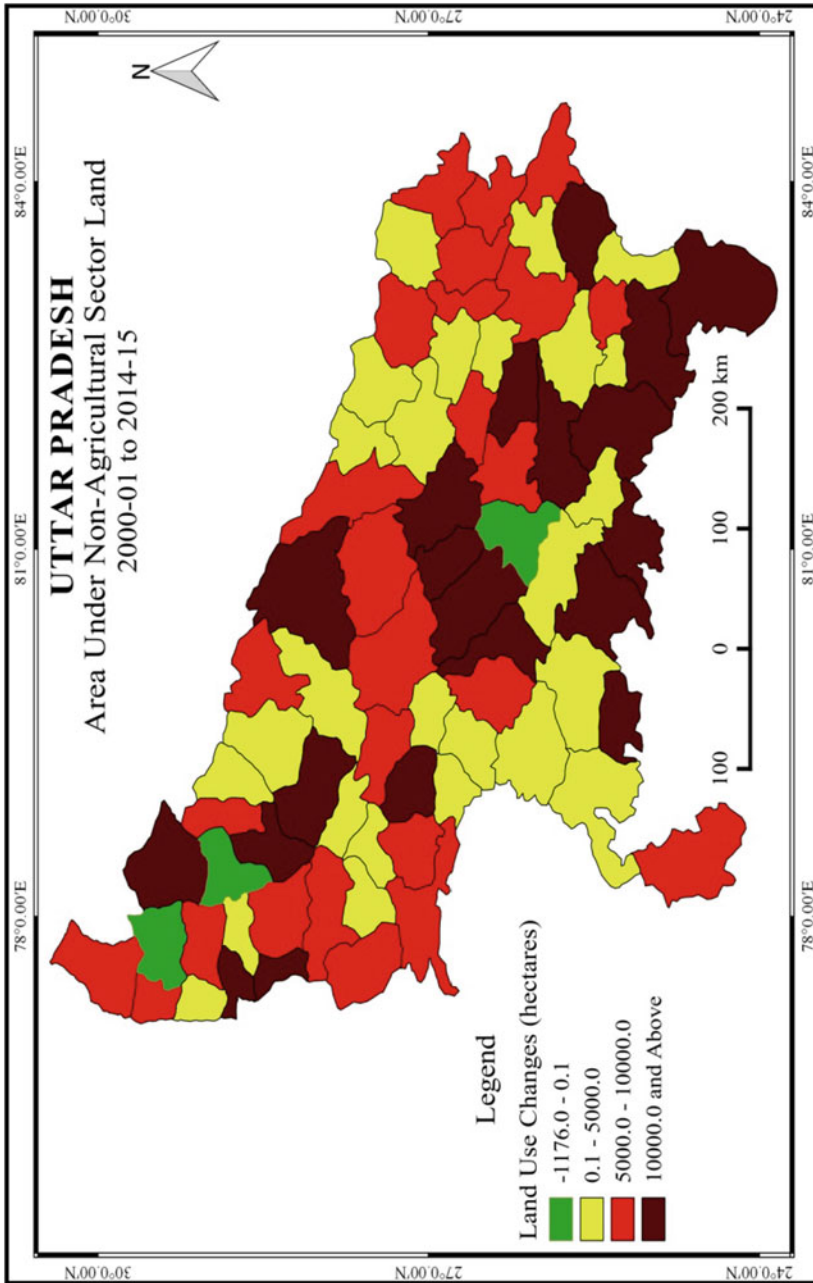
Source: Based on Directorate of Agriculture, Lucknow, Uttar Pradesh.

Fig. 13.7 Land use dynamics in the nonagricultural sector. (Source: Based on Direcotrate of Agriculture, Lucknow, Uttar Pradesh)

The first sector is ecological sector comprising three broad land use classes: (1) forest land use, (2) pasture and grazing land use, and (3) miscellaneous trees and groves land use.

The changes in area under forest land use varied among different districts. For example, the district of Sonebhadra recorded the highest negative growth rate (37,712 hectares) in area under forest land use between 2000 and 2015. Other districts that recorded negative growth rate for the same class included Chitrakoot, Agra, Lucknow, Meerut, Kanpur Dehat, Auraiya, etc. This will require massive tree plantation and vigorous restrictions on the rampant felling of trees. However, Bijnor (10,479 hectares) reported the highest increment in the area under forest land use, followed by Jyotiba Phule Nagar, Behraich, Kannauj, Muzaffar Nagar, Maharajganj, Shamli, etc. The districts like Azamgarh, Chandauli, Deoria, Mau, Rampur, and Shravasti recorded no change in this category. Nonetheless, declined area has to be recovered and brought back under forests to save the land from the adverse effects of deforestation.

The dynamics of area under pasture and grazing land use was observed for 2000–2015. Amethi (1178 hectares) registered the highest decline, followed by Sultanpur, Barabanki, Lalitpur, Hardoi, Bareilly, Mirzapur, Gonda, Shravasti, etc. However, Firozabad recorded highest increase of 1231 hectares followed by Fatehpur, Kushinagar, Raebareli, Hamirpur, Mathura, Mahoba, etc. The decline in this land use class is largely ascribed to free grazing practices, lack of management, and natural constraints like extremes of temperature, steepness of slopes, varying precipitation, and scarcity of moisture.

The changes in area under miscellaneous trees and groves land use were also varied among different districts, for example, Mirzapur recorded highest decline. Other districts that witnessed a significant decline in area under this land use included Bulandshahar, Raebareli, Balrampur, Auraiya, Bijnor, Hardoi, etc.

As the population has been shifting from rural to urban areas, therefore, gradual increase in the proportion of people living in urban areas develops pressure and demands for agricultural raw materials, and hence, the area under miscellaneous tree crops and groves has been declining consistently. While, during the same period, Sonebhadra (33,586 hectares) recorded the highest increase in area under this land use followed by Chitrakoot, Agra, Gonda, Pilibhit, Gorakhpur, Lucknow, etc.

The sectoral land use dynamics reveals that the area under the unenviable ecological sector has declined in most of the districts during the study period. Jyotiba Phule Nagar recorded the highest decline (12,526 hectares) in area under this land use in 2015 from the base year 2000. Other districts that also showed a significant decline in area under the unenviable ecological sector land use included Kanpur Dehat, Kanpur Nagar, Kannauj, Barabanki, Etawah, Bijnor, Aligarh, etc. In contrast, Auraiya recorded the highest increase (1066 hectares) in this sectoral land use. Other districts that witnessed a marginal increment in the same category included Azamgarh, Kanshiram Nagar, Balrampur, Gorakhpur, Jhansi, Basti, and Shahjahanpur.

In area under enviable ecological sector land use, Mirzapur recorded the highest decline (13,945 hectares) for the same study period. Other districts that also noticed a

decline in this land use included Chitrakoot, Auraiya, Bulandshahar, Lucknow, Raebareli, Meerut, Balrampur, etc. This sectoral land use is reporting disturbances involving both natural as well as human-induced actions such as clearing forest, building roads, urbanization, floods, etc. However, Muzaffar Nagar recorded a great increase (8194 hectares) in area under the enviable ecological sector land use followed by Jyotiba Phule Nagar, Behraich, Bijnor, Kannauj, Shamli, Gonda, and Fatehpur.

In total ecological sector land use, Mirzapur (14,818 hectares) reported a highly declining growth rate, followed by Kanpur Dehat, Raebareli, Chitrakoot, Lucknow, Kanpur Nagar, Bulandshahar, Barabanki, etc. While Muzaffar Nagar (6215 hectares) recorded high positive growth rate in the same sectoral land use followed by Behraich, Shamli, Gorakhpur, Gonda, Fatehpur, Maharajganj, Sant Kabir Nagar, etc. These land use changes in the ecological sector component are also affecting global environmental change.

The second is the agricultural sector consisting of four land use classes: (1) culturable waste land, (2) current fallow land, (3) fallow land other than current fallows, and (4) net sown area.

The dynamics of culturable waste land use reveals that Lalitpur district recorded the highest declining trend of 36,563 hectares in this category from 2000 to 2015. Other districts that also witnessed a significant decline in area under culturable waste land use included Hardoi, Etah, Bulandshahar, Kannauj, Unnao, Behraich, etc. Whereas Gorakhpur registered a high increasing trend of 1667 hectares followed by Chitrakoot, Hamirpur, Sant Kabir Nagar, Etawah, Barabanki, Baghpat, etc.

In the area under current fallow land use for the same study period of 2000–2015, Banda district showed the highest decline followed by Lucknow, Sitapur, Balrampur, Lakhimpur Kheri, Jhansi, Unnao, etc. On the other hand, Allahabad recorded highest increase in the area under current fallow land use followed by Mirzapur, Sonebhadra, Raebareli, Gautam Budh Nagar, Farrukhabad, Varanasi, etc.

The analysis explains that the area under fallow land other than current fallows has reduced due to proper utilization of fertilizers, improved irrigation facilities, crop rotation and combination, and several other similar farm techniques that help to increase agricultural production. Lalitpur followed by Hardoi, Unnao, Budaun, Barabanki, Banda, Etah, Mathura, etc., recorded a declining trend for this land use. However, Sonebhadra reported the highest increment, followed by Amethi, Allahabad, Lucknow, Gautam Budh Nagar, Raebareli, Hamirpur, etc.

The dynamics of land use change in net sown area discloses that Allahabad recorded the highest decline followed by Sonebhadra, Gautam Budh Nagar, Pratapgarh, Hamirpur, Mirzapur, Raebareli, etc. It clearly indicates that the area under net sown land use is contracting day by day. Lalitpur district recorded the highest increase in this land use adding 51,760 hectares more net sown area. Other districts with a significant increase in this same land use included Mahoba, Unnao, Sitapur, Bulandshahar, Balrampur, etc., during the periods from 2000 to 2015.

The sectoral land use dynamics reveals that the rate of land expansion in agricultural sector also varied among different districts. For example, Pratapgarh

recorded the highest decline (30,151 hectares) in area under agricultural sector land use. Other districts that also noticed a significant decline in this category included Hamirpur followed by Banda, Shahjahanpur, Lucknow, Gautam Budh Nagar, Lakhimpur Kheri, Kanshiram Nagar, etc. It is interesting to note that some of the districts have been able to bring additional land under agricultural sector. For example, in Mahoba, total agricultural land increased by about 15,516 hectares. Other districts that recorded an increase included Pilibhit followed by Raebareli, Bulandshahar, Kanpur Dehat, Auraiya, Firozabad, Mirzapur, Chitrakoo, Mahamaya Nagar, Sant Ravidas, and Hapur.

The third sector is the nonagricultural land use. The dynamics of this land use reveals that the highly productive agricultural land and villages are being absorbed due to raising demands for nonagricultural activities. Lucknow recorded the highest increase (31,225 hectares) in area under nonagricultural land use, followed by Pratapgarh, Allahabad, Unnao, Sonebhadra, Lakhimpur Kheri, Budaun, Chitrakoot, etc. It is worth noting that only three districts, Raebareli, Muzaffar Nagar, and Jyotiba Phule Nagar have shown a marginal decline for the same land use during the study period of 2000–2015. These results of changes in area under nonagricultural land use indicate that there has been a continuous increase in area in this land use in Uttar Pradesh.

It is evident from Fig. 13.8 that land use shifts have been occurring from the desirable ecological, unenviable ecological, and agricultural sector toward the nonagricultural sector during all the study periods of four blocks. The shift of land
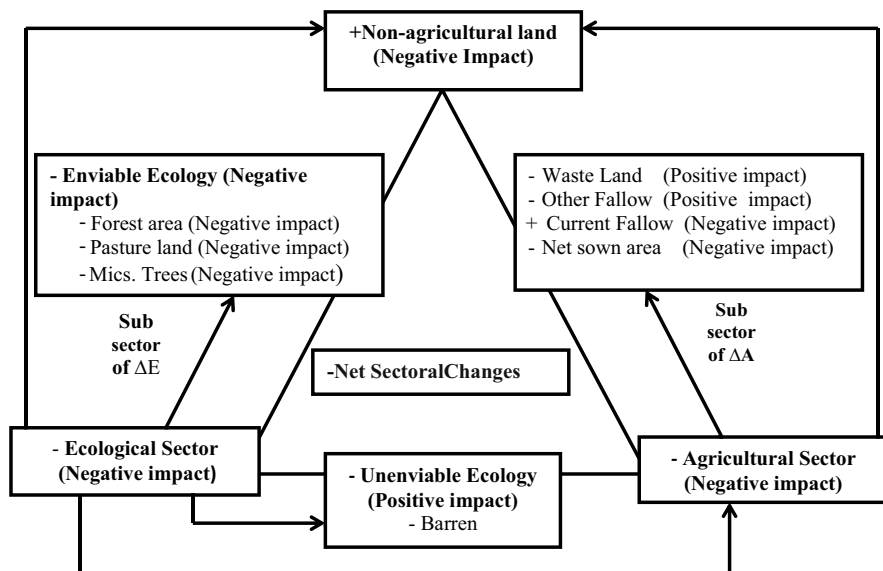
Source: Based on Directorate of Agriculture, Lucknow, Uttar Pradesh.

Fig. 13.8 Impact of land use changes of inter- and intrasector. (Source: Based on Directorate of Agriculture, Lucknow, Uttar Pradesh)

from these favorable sectors to nonagricultural sector would have serious implications. In particular, the land shifted from the ecological sector to nonagricultural sector needs immediate attention in a state like Uttar Pradesh where only 10.41% of the total area is covered under the ecological sector of land use. This study also indicates that the decline in the area under waste land, other fallow land, and barren land is the positive indicator if the land shifts toward the ecological or agricultural favorable land uses, but this land is shifting toward the nonagricultural sector land use.

Land Use Sustainability and Human Well-Being

Land and its use are critical to human activities and for the functioning of the ecosystem. Land resource requirement (demand) and intensity of utilization has increased substantially in the last few decades. This increase is attributed to an increase in population but also more due to economic transformations. In recent times, claims on land and transformations in its use have posed serious challenges to development paradigms. There is an increasing credence that land use change is a threat to sustainable development (Jingan et al. 2005). In India, land resource was always integral to socioeconomic development. But these developments have also changed the perspective for land resource. Land use change is largely a socioecological system that is driven by human needs, their activities, and its drivers. Land resource and its use require attention with sustainability perspective for current and future population, livelihoods, well-being, and sustain the larger environment. This requires harmonious links between biophysical processes, functions, services, values, and benefits. Changing patterns of land use also impact the ability of ecosystem, resulting in degradation of natural resources with potential consequences on livelihood and well-being (Groffmanet et al. 2014)

The use of land reflects our efforts to achieve sustainability to land resource. The present study observes that judicious use of land in India is urgently required. The use of land and transformations is increasingly going on in an unsustainable manner. There is a significant increase in nonagricultural uses, which in some way are necessary for economic and infrastructural development. But the pace and spatial spread is a serious concern. Especially, drawing more land from enviable ecological sector, instead of unenviable ecological sector, has severely jeopardized the efforts to sustainable development. Another critical transformation trend is observed in the agricultural sector. The study area being a predominantly agrarian state, agricultural activity and farming lands are vital for the livelihood and well-being of its population. The study suggests that there is increasing loss of farming lands and substantial increases in fallow lands (loss of productive gains leading to unsustainability). This trend again needs to be contained with urgent restrictive policy intervention. Similarly, enviable ecological sector also requires protection as decreases are detrimental not only in realizing sustainable development goals but also cascading impacts on biodiversity, larger environment, and human population.

Conclusion

Land is an important and finite natural resource of the earth. The pressure exerted by Uttar Pradesh's growing economy on land and other natural resources has intensified in the post-liberalization phase and will further intensify in the future in the face of the burgeoning population and the demand for the conversion of agricultural land to nonagricultural uses. The trends of land utilization are critical in this state because of changes in the economic sector.

The overall picture regarding land use pattern in Uttar Pradesh shows a divergent situation in regard to land use changes across different districts. It is an agriculturally dependent and ecologically scared state. The growth rate of different categories of land use has shown that all the land uses have witnessed declining trends except the area under nonagricultural land use. It has revealed significant increasing trends as it reflects the development processes that the state is carrying out and land being transferred for the other land use classes.

The study also finds that the land in the enviable ecological sector in Uttar Pradesh is passing through a critical phase of land transformation. The area under forest is decreasing along with the land under pasture and miscellaneous trees. The districts like Sonebhadra, Mirzapur, Chandauli, Chitrakoot, Pilibhit, and Lakhimpur Kheri have reported notable declining trends in the state. This makes the state ecologically fragile and poses severe threats on the local rural ecology. Likewise, most of the districts recorded similar trends in Uttar Pradesh such as Bijnor, Jyotiba Phule Nagar, Shamli, Behraich, etc., except northwestern districts, which are relatively having a prosperous agricultural background.

The areas under wasteland, fallow land, and net sown are equally important in the agricultural sector. This study points out that there is a considerable decrease in the wasteland and net sown area but increase in current fallow lands. It indicates that the efforts to improve this poor land are not really effective and also the heavy investment has not been able to transform these infertile land to productive agricultural land and thus the share of the current fallow land is increasing constantly. These trends have been shown among agriculturally poor and highly populated districts like Allahabad, Mirzapur, Sonebhadra, Raebareli, Gautam Budh Nagar, Farrukhabad, Varanasi, etc. In a nutshell, the pressure will be immense on the net sown area if the land from the agricultural sector would continue to be utilized for nonagricultural purposes.

The land is a finite natural resource and should be properly and judiciously utilized for the overall development, which is a serious matter of concern. The study emphasizes formulating a long-term sustainable land use planning on the type of land to be assigned for urbanization and industrialization in various regions of the state like Uttar Pradesh. This also points to the idea of forming special agricultural zones (SAZ) to protect the diversion of agricultural land to nonagricultural uses.

References

Bardhan D, Tewari SK (2010) An investigation into land use dynamics in India and land under-utilisation. Indian J Agri Econ 65(4):14–18

Dale VH, Brown S, Haeuber RA, Hobbs NT, Hunty N, Naiman RJ, Valone TJ (2000) Ecological principles and guidelines for managing the use of land. Ecol Appl 10(3):639–670

Groffmanet PM et al (2014) Ecosystems, biodiversity, and ecosystem services. In: Melillo JM et al (eds) Climate change impacts in the United States: the third National Climate Assessment. U.S. Global Change Research Program. https://doi.org/10.7930/J0TD9V7H

Jingan S et al (2005) Land use change and its corresponding ecological response: a review. J Geogr Sci 15(3):305–328

Karwariya S, Goyal S (2011) Land use and land cover mapping using digital classification technique in Tikamgarh District, Madhya Pradesh, India using remote sensing. Int J Geomat Geosci 2:519–529

Kates RW, Clark WC, Norberg-Bohm V, Turner BL, II (1990) Human sources of global change: a report on priority research initiatives for 1990–1995. Discussion paper G-90-08,Global Environmental Policy Project, John F. Kennedy School of Government, Harvard University, Cambridge, Massachusetts, USA

Lambin EF, Rounsevell MDA, Geist HJ (2000) Are agricultural land-use models able to predict changes in land-use intensity? Elsevier Agri Ecosyst Environ 82:321–331

Liu J, Ashton PS (1998) FORMOSAIC: an individual-based spatially explicit model for simulating forest dynamics in landscape mosaics. Ecol Model 106:177–200

Maitima JM, Mugatha SM, Reid RS, Gachimbi LN, Majule A, Lyaruu H, Mugisha S (2009) The linkages between land use change, land degradation and biodiversity across East Africa. Afr J Environ Sci Technol 3(10):310–325

Malik T, Manzoor MA, Arshad A (2013) Urban land use dynamics and its future prospectus (a case study of Jammu City). Int J Eng Res Dev 9(6):50–55

Pandey VK, Tewari SK (1987) Some ecological implications of land use dynamics in Uttar Pradesh. Indian J Agri Econ 42(3):388–394. (An Investigation into Land Use Dynamics in India and Land Under-Utilisation/journal)

Pushpa CO, Akashraj DP (2014) An investigation into land use dynamics in Karnataka – an ecological perspective. Merit Res J Agri Sci Soil Sci 2(3):047–052

Trimble SW, Crosson P (2000) Land use: U.S. soil erosion rates. Myth and reality. Science 289:248–250

Turner BL II, Clark WC, Kates RW, Richards IF, Mathews JT, Meye WB (1990) The earth as transformed by human action. Cambridge University Press, Cambridge

Vitousek PM, Mooney HA, Lubchenco J, Melillo JM (1997) Human domination of Earth's ecosystems. Science 277:494–499

Wu J, Ransom MD, Kluitenberg GJ, Nellis MD, Seyler HL (2001) Land use management using a soil survey geographic database for Finney County, Kansas. Am J Soil Sci 65:169–177

Chapter 14
Study and Analysis of Precipitation Trends and Variability for Karnataka State in India

Shashwata Chatterjee and Sathyanathan Rangarajan

Abstract In this study, the precipitation data for the period 1901–2015 was analyzed for the state of Karnataka enclosing 66 grid points spread throughout the state. Gridded rainfall data of 0.50×0.50 resolution has been investigated to draw a conclusion regarding long-term dimensional and temporal trends on an annual and seasonal scale in the state located in Southern India. The various statistical methods such as Mann–Kendall trend test and Theil–Sen's slope test were adopted in analyzing the data besides departure analysis being performed to determine the extent of precipitation deficit and to ascertain the drought years. The change point year has been ascertained to be 1956 by homogeneity test for the state. The annual mean precipitation was estimated to be 1069 mm. The yearly rainfall received in the state of Karnataka is contributed by four seasons, viz., southwest monsoon, post-monsoon, winter, and summer. Also, 70% of the annual rainfall (751.28 mm) is contributed by southwest monsoon following which 18% (186.81 mm) is contributed by post-monsoon. The mean precipitations for summer and winter seasons are 128 mm and 3 mm, respectively, and the corresponding contributions are 12% and 0.29%, which corroborates the fact that winter season has negligible contribution to annual precipitation.

Keywords Precipitation · Statistical analysis · Trend · Mann–Kendall test · Sen's slope estimator · Karnataka state · India

S. Chatterjee
Graduate Civil Engineer, Department of Civil Engineering, SRM Institute of Science and Technology, Kattankulathur, Chennai, Tamil Nadu, India

S. Rangarajan (✉)
Department of Civil Engineering, SRM Institute of Science and Technology, Kattankulathur, Chennai, Tamil Nadu, India
e-mail: sathyanr5@srmist.edu.in

Introduction

Precipitation is an important component of the hydrological cycle that affects the availability of water globally. Due to global warming and other anthropogenic issues, the earth is facing varying trends in precipitation. Concerning experimental data, it has been observed that over a hundred years climate and temperature have tuned to alter globally beyond normal averages, which result in variation of precipitation trend.

The analysis of seasonal trend is used to find out the dimensional pattern of precipitation in a region. Arun Kumar Taxak et al. (2014) studied the change in rainfall trends in the Wainganga basin of the Godavari river and reported that the annual series were prepared for each grid and scale trend analysis was carried out. Mann–Kendall test was employed to detect the presence of annual and seasonal precipitation trends. The magnitude of the trend was estimated by Theil–Sen's slope estimator test. Sheikh Hefzul Bari et al. (2016) aimed to study and examine 50 years (1964–2013) of seasonal and annual trends of rainfall and their variation over time in northern Bangladesh. Trends were detected with the use of nonparametric test such as Mann–Kendall test. Theil–Sen's slope test was performed to establish trend magnitude over a while. It was found that southwest monsoon and post-monsoon rainfall exhibited an upsurge in trend in most of the rainfall stations, whereas a decrease in seasonal rainfall trend was found after the early 1990s for most of the stations. Duhan and Pandey (2013) investigated the spatial and temporal investigation of rainfall at 45 districts of the Madhya Pradesh state in India for the period 1901–2002 on a seasonal and annual basis. Sen's slope test and Mann–Kendall estimator test were employed to investigate the trend direction and magnitude of change over a time array on a seasonal and annual basis. The significant decreasing trend was found in annual precipitation series at some stations, whereas in summer season significant increasing trend was found in other stations of Madhya Pradesh. Vijay Kumar et al. (2010) predicted that there is a decreasing trend in annual and monsoon rainfall and a rising trend in pre-monsoon and post-monsoon rainfall between the years 1871 and 2005. The statistical significance of the trend in monthly, seasonal, and annual series was analyzed using the nonparametric Mann–Kendall test, and the magnitude of the trend in the time series was determined using Sen's estimator. Jain SK and Kumar V (2012) carried out temperature data and trend analysis of rainfall for India and reported that there was a rising trend in the south, central, and western parts of India and a falling trend in the north and northeastern parts of India. In the study on basin-wise trend analysis, 15 basins were found to follow a downfall trend in annual rainfall; only one basin showed a significant down surge in trend. During rainy days at the annual and seasonal scale, most of the basin had a similar direction and trend of rainfall, but the mean minimum temperature has shown a rise as well as significant decreasing trend. Goyal MK (2014) studied an analysis of rainfall variation in Assam, India, for a period of 102 years from 1901 to 2002. Precipitation values from 21 stations were collected and analyzed for both seasonal and annual variation. No significant changes or trend

in annual rainfall were observed over the entire state in 102 years. From the study, it was predicted that the southwest monsoon season had the strongest correlation with seasonal and annual rainfall. Kundu S et al. (2014) concluded that there is a decline in trends of precipitation in the region of Maharashtra and Madhya Pradesh border region in India, Central Northeast India, and in the zones of homogeneous India in pre-monsoon and post-monsoon season. There were only two regions (northwest and peninsular India) which showed positive rainfall trends. The Sen's slope and Mann–Kendall test were applied in the study. Archana Nair et al. (2014) found that there was maximum average rainfall during pre-monsoon, winter, and post-monsoon over the southern part of Kerala. In contrast, in the monsoon season, maximum rainfall regime shifted to the northern districts of Kerala during 1901–2000. The study showed that there was a significant decreasing trend in the trend of rainfall in most of the 18 regions of Kerala, especially in the 3 months, viz., January, July, and November. Rajeevan M et al. (2008) analyzed rainfall data for 104 years from 1901 to 2004 to test variability and trends of extreme precipitation in central India. The probability of rainfall event exhibits enormous interannual and interdecadal variations along with a statistically significant trend for a more extended period. Detailed analysis showed that interannual, interdecadal extreme rainfall events were influenced by the sea surface temperature variations over the tropical Indian ocean.

Though many studies have been furnished to study the long-term temporal and spatial precipitation trends over many states in India, no papers have been found to analyze similar kinds of precipitation data over the gross state of Karnataka, and this chapter focuses on doing the same. Also, the runoff coefficient for the Cauvery river basin has been found to be low relative to the other major river basins such as Brahmaputra, Narmada, and Mahanadi river basins prevailing in India according to Mohan Z et al. (2005). So, the results of the analysis of precipitation data in the state of Karnataka may be helpful to elicit the reason for such lower runoff coefficient. Also, the study of variability will assist in framing the water management practices throughout the state.

Materials and Methods

Study Area

The study of the precipitation trends has been carried out for the entire Indian state of Karnataka, which is located 11°30′ north and 18°30′ north latitudes and 74° east and 78°30′ east longitude. Karnataka lies on a mesa where the Western and Eastern Ghat ranges converge into the complex, in the western part of the Deccan Peninsular region of India. The various river basin systems prevailing in the state of Karnataka are Godavari, Krishna, Cauvery, North Pennar, South Pennar, and Palar. The catchment area of the Godavari river system for the state of Karnataka is 4406 sq. km. The drainage area for the river Krishna in the state of Karnataka is 1,13,271 sq. km, whereas for Cauvery it is 34,273 sq.km. Harangi, Hemavathy,
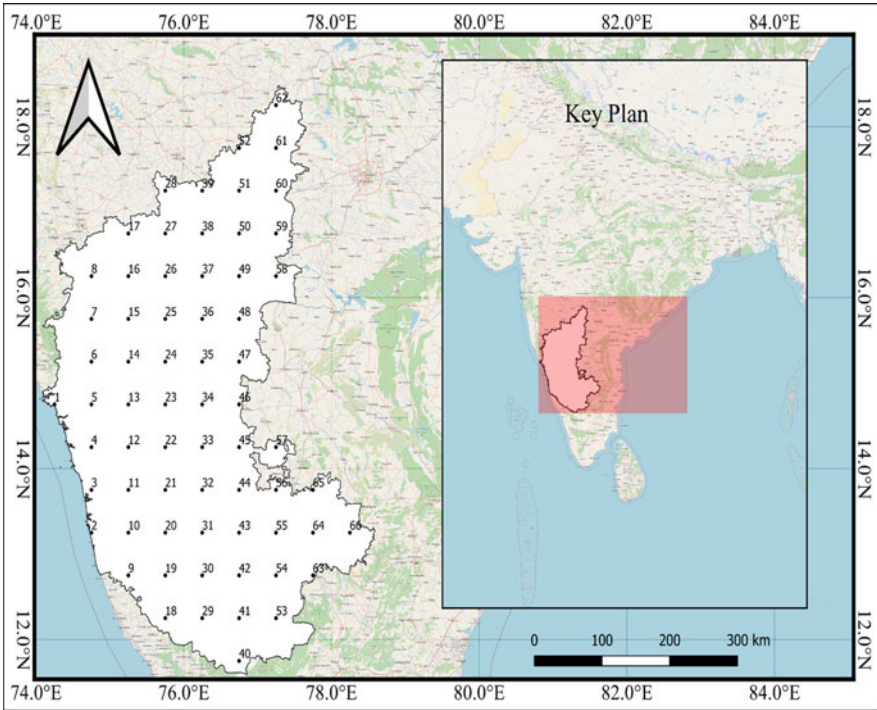
Fig. 14.1 Map for the study area (Karnataka state in the present study) enclosing 66 grid points

Lakshmanathirtha, Kabini, Shimsha, Arkavathi, and Suvarnavathy are the principal tributaries of Cauvery in Karnataka. All these rivers, except Kabini, Arkavathy, and Suvarnavathy, rise and flow fully in Karnataka (Fig. 14.1).

Data and Methodology

In our study, the precipitation data for the period 1901–2015 at $0.5° \times 0.5°$ resolution was downloaded from the "Centre of Environmental Data Archival (http://badc.merc.ac.uk)" for the whole Karnataka state enclosing 62 grid points. The precipitation data was then processed by using MATLAB and MINITAB software. A detailed statistical analysis was carried out using MINITAB 2017 and XLSTAT 2018 software.

The statistical analysis of the precipitation data includes Mann–Kendall trend test and Theil–Sen's slope test. A similar kind of analysis has been done by Rangarajan S et al. (2018).

Mann–Kendall Trend Test

This test is applied to detect the presence of trend in annual and seasonal rainfall. This is the rank-based nonparametric test used to detect trends in precipitation data. Test statistic "S" is defined as

$$S = \sum_{x=i}^{n-1} \sum_{j=i+1}^{n} \text{sgn}\left(x_j - x_i\right)$$

where x_j are the sequential data values, and "n" has been taken as the length of the dataset and

$$\text{sgn}(y) = \begin{cases} 1.....\text{if } (y > 0) \\ 0.....\text{if}(y = 0) \\ -1.....(y < 0) \end{cases}$$

It has been documented that when $n \geq 8$ the statistic S is approximately normally distributed with the mean $(S) = 0$ and variance as

$$V(s) = \left[n(n-1)(2n+5) - \sum_{i=1}^{m} t_i^2 - t_i\right)(2t_i+5)],$$

where m has been taken as the number of tied groups and t_i is the size of the ith tied group. The standardized test statistic "Z" is

$$Z_{\text{MK}} = \begin{cases} \dfrac{S-1}{\sqrt{\text{Var}(S)}}.....\text{when } S > 0 \\ 0......\text{when } S = 0 \\ \dfrac{S-1}{\sqrt{\text{Var}(S)}}.....\text{when } S < 0. \end{cases}$$

Theil–Sen's Slope Estimator Test

The magnitude of a precipitation trend is estimated by Sen's slope test. Theil–Sen's estimator has been used to estimate slope of "n" pairs of data points by

$$Q_i = \frac{x_j - x_k}{j - k} \text{ for } i = 1....N$$

where x_j and x_k are data values at time j and k, respectively, where $j > k$.

The median of these N values of Q is Sen's slope estimator of slope. If there is only one data in each period, then

$$N = \frac{n(n-1)}{2}$$

where "n" is the number of periods.

The median of the N estimated slopes is obtained in the usual way:

$$\text{Sen's Slope estimator} = \begin{cases} Q_{\frac{N+1}{2}} \ldots\ldots \text{if } N \text{ is odd} \\ 0.5\left(Q_{N/2} + Q_{(N+2)/2}\right) \ldots\ldots\text{if } N \text{ is even} \end{cases}$$

Results and Discussion

Precipitation Characteristics for Karnataka State

It was observed that the southwest monsoon season has maximum mean precipitation of 751.28 mm, which contributes to 70% of annual rainfall. This is followed by post-monsoon with mean precipitation of 186.81 mm with a contribution of 18% of annual rainfall. The mean precipitation for the summer and winter seasons was 128 mm and 3 mm, respectively, and corresponding contributions are 12% and 0.29%. So, it can be concluded that winter season was having a negligible contribution to annual precipitation.

The coefficient of variation of precipitation for the winter season over the state of Karnataka was computed to be 86%, while for the summer, southwest monsoon, and post-monsoon seasons, the coefficient of variation was found to be 40%, 82%, and 25%, respectively. This underlines the fact that, over the state of Karnataka, the coefficient of variation is maximum for the winter season followed by the southwest monsoon, summer, and post-monsoon seasons successively. For annual rainfall, the coefficient of variation was found to be 63%.

The elaborate statistics of the seasonal contribution of precipitation data for the entire state of Karnataka during the period of 1901–2015 is depicted in Fig. 14.2.

Departure Analysis of Rainfall

From the results obtained from departure analysis for Karnataka state, which is shown in Fig. 14.3, it is inferred that from 1901 to 2015, that is, in 115 years, normal, excess, deficient, and scanty rainfall was recorded for 79, 11, 23, and 2 years, respectively.

CONTRIBUTION OF SEASONS TO ANNUAL RAINFALL

■ S-W Monsoon   ■ Post Monsoon   ■ Winter   ■ Summer

12%

0%

18%

70%
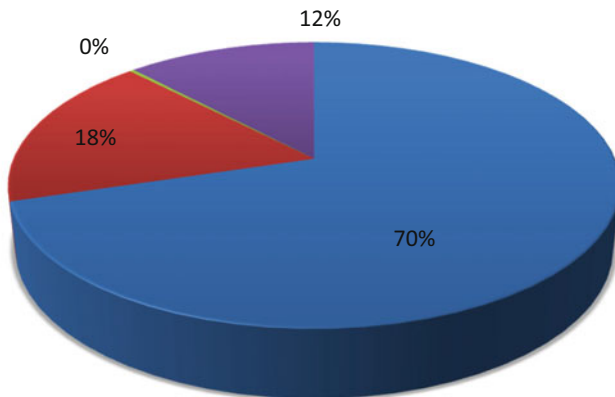
Fig. 14.2 Contribution of seasons to annual rainfall

RESULTS OF PERCENTAGE DEPARTURE ANALYSIS FOR KARNATAKA

■ Normal ■ Excess ■ Deficit ■ Scanty ■ No Rain

2%   0%

20%

10%

68%
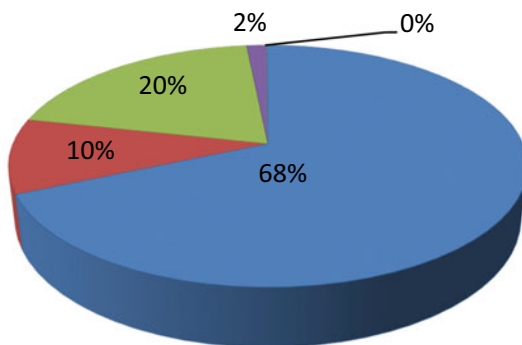
Fig. 14.3 Percentage departure analysis for Karnataka
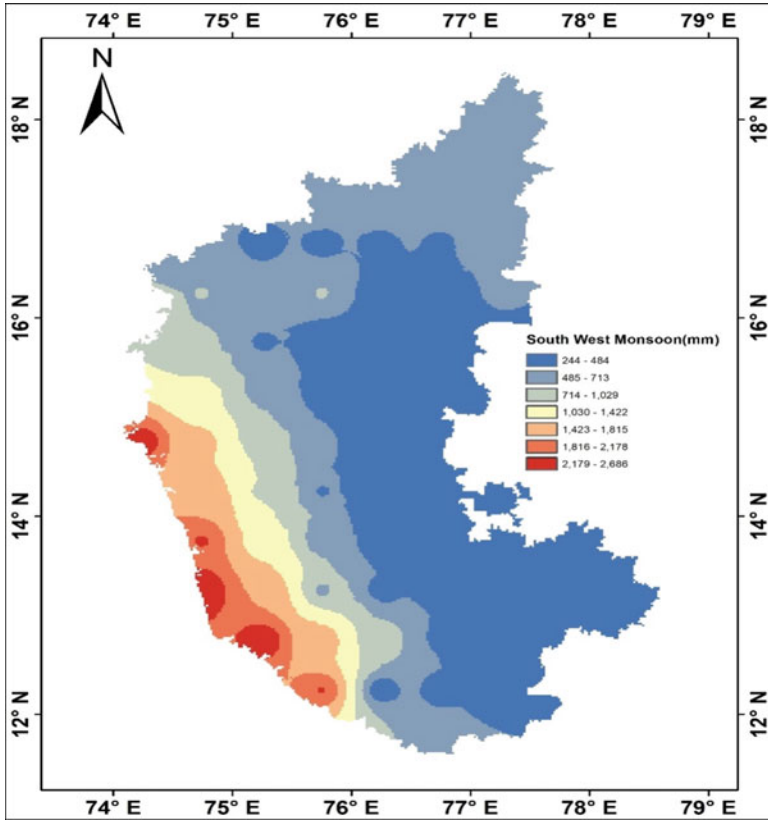
Fig. 14.4 Variation of southwest monsoon over the Karnataka state

Variation of Annual Precipitation, Southwest Monsoon, and Post-monsoon over the Karnataka State

The variations of the southwest monsoon, post-monsoon, and annual precipitation over the state of Karnataka are depicted in Figs. 14.4, 14.5 and 14.6, respectively.

In Fig. 14.4, it can be noticed that the southwest monsoon has a descending trend on moving from the extreme western part of the state, which comprises the Western Ghats to the eastern part of the state. The southwest monsoon contributes maximum rainfall in the range of 2179–2686 mm in the regions represented by dark red color. The western districts of Karnataka, which are neighboring to states of Telangana and Andhra Pradesh, receive the least precipitation due to southwest monsoon, and the rainfall varies between 244 mm and 484 mm. The northern districts, which share border with Maharashtra state, receive average southwest precipitation of 600 mm.
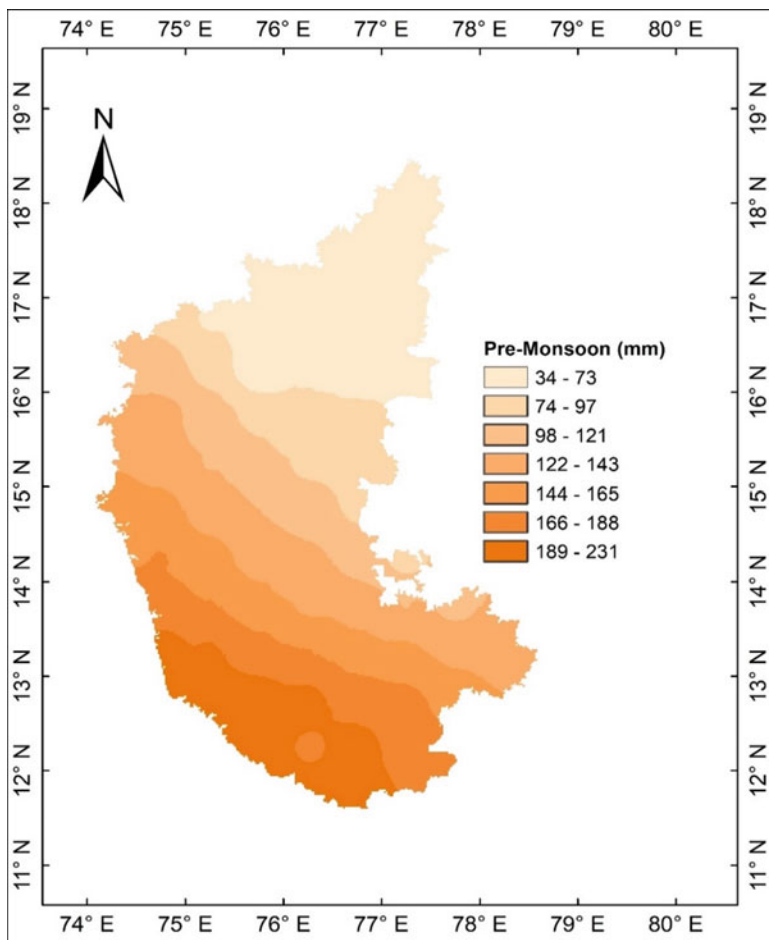
Fig. 14.5 Variation of pre-monsoon over Karnataka state

Figure 14.5 throws light on the fact that the pre-monsoon exhibits a decreasing trend from the southern to the northern part of the state with maximum precipitation ranging between 189 mm and 231 mm over the extreme southern districts. The precipitation goes on depressing as it moved to the northern districts through the central districts with the minimum in the range of 34–73 mm. The central districts receive precipitation of varied ranges, which has been shown in the figure.

From Fig. 14.6, it can be noticed that the precipitation received by Karnataka from post-monsoon season exhibits a decreasing trend as we move from southern districts to northern districts. The precipitation over the extreme southern region ranges from 257 mm to 296 mm and 232 mm to 256 mm, respectively. Central Karnataka receives precipitation over a wide range, which has been depicted in the figure. The ranges between which these precipitation values lie are 207–231 mm,
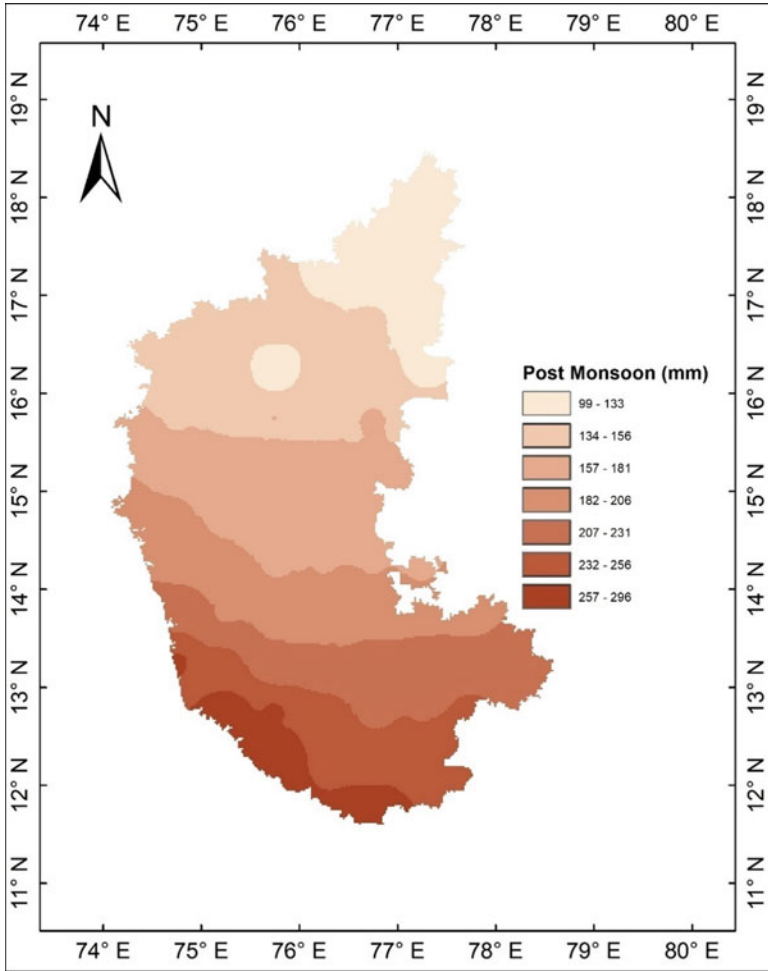
Fig. 14.6 Variation of precipitation due to post-monsoon over Karnataka state

182–208 mm, 157–181 mm, and 134–156 mm. The northern districts receive post-monsoon contributed precipitation of 99–133 mm.

Figure 14.7 depicts the variation of annual precipitation over the state of Karnataka. It is observed that the annual precipitation exhibits a decreasing nature as it moved from the Western Ghats comprising extreme western districts to the eastern districts through the central districts. The western districts of the coastal belt receive annual precipitation in varied ranges of 2387–3155 mm, 1950–2386 mm, and 1556–1949 mm, respectively. The annual precipitations in the central districts show values in the range of 1202 mm to 921 mm. A major portion of central Karnataka receives annual precipitation in the later range of lowest ambit of 505–713 mm. The annual precipitation over the northern districts sharing borders with Maharashtra ranges between 714 mm and 921 mm.
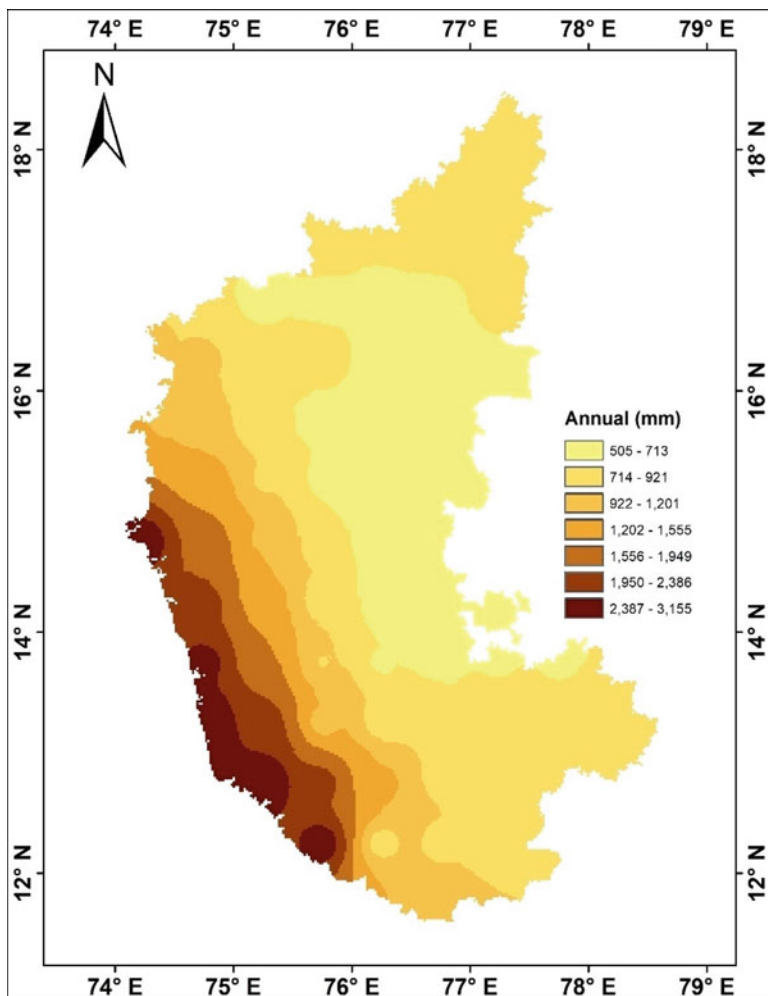
Fig. 14.7 Variation of annual precipitation over Karnataka state

Results of Mann–Kendall's Test (1901–2015)

For Mann–Kendall's test statistic, a positive value of Z indicates an increasing trend and a negative value of Z indicates a declining trend. When the Z value is greater than 1.96, it confirms a significant rising trend, while if Z is less than -1.96, it establishes a significant falling trend at 5% level of significance.

It can be observed that in the annual array of precipitation all the grid points spread over the Karnataka state exhibited an increasing trend in precipitation except grids 4–8 and 12–14, which showed a nonsignificant decreasing trend in

precipitation. Among the remaining grid points, which show an increasing trend of precipitation, grids 26–28, 37–39, 49–52, 54–56, and 58–62 show a significant increasing trend, which constitutes 33% of the total 66 grid points spread over the state of Karnataka.

For the southwest monsoon array of Table 14.1, grids 1, 4–8, and 12–14 showed nonsignificant decreasing trends in precipitation. All other grids establish an increasing trend in which grids 26, 38, 53–55, 58, and 63–66 show a significant increasing trend constituting 15% of the total 66 grid points. No grids indicated significant decreasing trends.

For the post-monsoon array, grids 1–6, 9–14, 18–24, 29–34, and 40–44 indicate a nonsignificant decreasing trend in rainfall and no grid points establish significant decreasing trend. Hence, 45% of the total 66 grid points establish a declining trend in rainfall. The grid points 27, 28, 38, 39, 49–52, and 58–62 constituting 14% of the total 66 grids show a significantly increasing trend.

And for the summer array, 10 grids establish a nonsignificant decreasing trend and for the winter nearly 58 grids showed decreasing trends with most of them falling under a significant range.

Results of Theil–Sen's Slope Test (1901–2015)

The Sen's slope estimator test was done for obtaining the true slope for the precipitation data. Percentage deviation is median slope (β) times the period length divided by the corresponding mean expressed as a percentage.

For the annual array shown in Table 14.1, the grid points 17, 26–28, 36–39, and 46–66 establish an increase in precipitation of magnitude greater than 10% to the mean of the array. These grid points constitute about 44% of the total grid points. The grid points 4–8 and 12–14 showed negative percentages. The remaining grid points indicated a positive value of less than 10%. From Fig. 14.8, it is observed that the annual precipitation has increased by a magnitude of 18–24% in the northeastern and southeastern regions of the state, whereas in the western region encompassing the Western Ghats, the precipitation has dipped by 0.3–5%. Central Karnataka has experienced increasing precipitation in the range of 4–9%.

For the southwest monsoon, grid points 17, 26–28, 37–39, 41–44, and 49–66 establish more than 10% increase in precipitation, and these constitute 48% of the total number of grid points. Grids 4–8 and 12–14 indicated negative percentages as that of annual array. The remaining grid points indicated a positive value in slope. When interpreted spatially as depicted in Fig. 14.8, the precipitation received during the southwest monsoon almost has a similar trend like annual rainfall. This proves the fact that the southwest monsoon has a dominant impact on annual precipitation being the major contributor.

For the post-monsoon season, 33% of the total grid points 16, 17, 26–28, 37–39, 49–52, and 57–66 undergo an increase in precipitation of more than 10% in magnitude, and some of the grids show a decline in precipitation with a magnitude

Table 14.1 Results of Mann–Kendall test and Sen's slope test (1901–2015)

Grid point	Grids	Annual		Winter		Summer		S-W monsoon		Post-monsoon	
	LONG_LAT	Z	% change	Z	% change	Z	% change	Z	% change	Z	% change
1	74.25_14.75	0.174	1.472	-1.767	0.000	-0.563	-5.474	-0.130	1.298	-0.228	3.149
2	74.75_13.25	0.865	5.582	-0.008	0.000	0.198	2.785	0.986	7.214	-1.300	-14.914
3	74.75_13.75	0.372	2.690	0.488	0.000	-0.198	-3.082	0.585	4.947	-0.955	-11.099
4	74.75_14.25	-0.302	-1.885	-2.389	0.000	-0.317	-5.156	-0.017	-0.275	-0.341	-5.216
5	74.75_14.75	-0.938	-5.709	-1.226	0.000	-0.537	-6.243	-1.068	-7.761	-0.155	-2.468
6	74.75_15.25	-0.534	-3.097	0.182	0.000	-0.350	-4.065	-0.981	-6.172	-0.005	0.394
7	74.75_15.75	-0.624	-3.858	-0.580	0.000	0.150	2.399	-1.051	-7.319	0.145	1.623
8	74.75_16.25	-0.143	-0.935	0.134	0.000	-0.160	-2.407	-0.215	-1.809	0.459	6.094
9	75.25_12.75	0.638	3.934	-1.611	-25.213	0.164	2.928	0.911	6.824	-1.537	-17.313
10	75.25_13.25	0.614	3.983	-1.609	-22.352	0.331	4.372	0.894	6.717	-1.477	-17.200
11	75.25_13.75	0.372	2.203	-1.901	-17.578	0.123	1.463	0.595	4.807	-1.027	-12.268
12	75.25_14.25	-0.529	-3.074	-1.698	-12.028	-0.222	-2.103	-0.493	-3.330	-0.800	-8.907
13	75.25_14.75	-0.856	-4.645	-1.536	0.000	0.000	0.000	-1.051	-7.689	-0.425	-4.925
14	75.25_15.25	-0.382	-2.407	0.171	0.000	0.288	2.876	-0.819	-5.616	-0.348	-3.653
15	75.25_15.75	0.566	3.434	0.071	0.000	0.080	1.314	0.276	1.864	0.457	5.242
16	75.25_16.25	1.093	6.838	0.588	0.000	0.068	1.051	0.715	5.263	1.102	15.071
17	75.25_16.75	1.726	10.717	0.183	0.000	-0.242	-3.524	1.421	11.393	1.363	20.958
18	75.75_12.25	0.798	4.471	-2.034	-41.872	0.012	0.052	0.834	6.130	-0.962	-10.646
19	75.75_12.75	0.875	5.364	-1.831	-33.043	0.094	1.092	1.233	8.669	-1.107	-11.793
20	75.75_13.25	0.365	2.480	-2.362	-44.152	0.263	2.790	0.914	7.690	-1.252	-13.917
21	75.75_13.75	0.488	3.149	-2.430	-43.604	0.894	9.354	0.522	4.295	-0.718	-8.673
22	75.75_14.25	0.111	0.738	-2.659	-43.070	0.331	3.416	0.331	2.752	-0.967	-10.745
23	75.75_14.75	0.498	3.052	-2.206	0.000	0.439	6.319	0.416	3.467	-0.503	-5.921
24	75.75_15.25	0.713	4.196	-1.932	0.000	0.916	10.865	0.300	2.412	-0.070	-0.941

(continued)

Table 14.1 (continued)

Grid point	Grids LONG_LAT	Annual Z	% change	Winter Z	% change	Summer Z	% change	S-W monsoon Z	% change	Post-monsoon Z	% change
25	75.75_15.75	1.073	6.692	−1.464	0.000	1.095	13.918	0.534	4.125	0.300	3.964
26	75.75_16.25	2.006	16.063	−2.350	−36.939	−1.112	−19.85	2.069	16.714	1.250	24.293
27	75.75_16.75	2.560	17.936	−0.632	0.000	0.517	6.504	1.392	11.837	1.958	27.888
28	75.75_17.25	2.864	19.650	0.227	0.000	0.114	1.495	1.929	14.717	2.071	38.092
29	76.25_12.25	0.343	1.677	−2.417	−55.758	−0.529	−5.758	0.326	2.541	−0.802	−8.010
30	76.25_12.75	1.008	5.356	−0.292	0.000	0.224	4.819	0.808	8.368	−1.226	−8.320
31	76.25_13.25	0.771	4.107	−0.002	0.000	0.945	8.194	0.875	7.775	−0.848	−9.358
32	76.25_13.75	0.863	4.807	−2.879	−63.889	1.298	11.816	0.686	5.765	−0.653	−7.497
33	76.25_14.25	0.486	3.054	−2.774	−55.779	0.950	9.059	0.541	4.518	−0.425	−5.473
34	76.25_14.75	0.672	4.222	−2.695	0.000	0.508	4.675	0.616	5.236	−0.549	−7.072
35	76.25_15.25	1.477	9.511	−2.083	0.000	1.397	14.282	0.638	6.505	0.198	2.452
36	76.25_15.75	1.719	11.349	−2.309	−29.745	1.777	20.821	0.735	6.330	0.551	7.464
37	76.25_16.25	2.453	16.271	−1.286	0.000	1.564	19.555	1.300	10.313	1.603	22.261
38	76.25_16.75	3.304	23.945	−1.057	−8.016	1.129	17.573	1.975	17.550	2.930	44.811
39	76.25_17.25	2.879	20.295	−0.812	−5.164	0.701	11.029	1.678	15.102	2.758	45.939
40	76.75_11.75	0.621	3.046	−2.954	−74.223	0.000	0.000	0.464	3.104	−0.051	−0.486
41	76.75_12.25	1.322	8.106	−2.778	−67.958	0.256	2.404	1.673	12.197	−0.036	−0.272
42	76.75_12.75	1.537	9.336	−2.502	−54.181	0.703	6.734	1.516	13.479	−0.285	−3.559
43	76.75_13.25	1.419	8.845	−0.176	0.000	0.817	7.499	1.450	12.495	−0.372	−4.157
44	76.75_13.75	1.400	8.471	−0.224	0.000	1.199	12.617	1.165	10.564	−0.227	−3.409
45	76.75_14.25	1.247	8.371	−0.190	0.000	1.281	12.475	1.056	8.794	0.048	0.583
46	76.75_14.75	1.482	10.369	−2.694	−59.899	1.726	16.865	0.969	8.710	0.430	5.805
47	76.75_15.25	1.885	12.632	−2.501	−45.654	1.750	19.888	1.134	9.551	0.752	9.184
48	76.75_15.75	1.719	11.349	−2.309	−29.744	1.777	20.822	0.735	6.330	0.551	7.464

49	76.75_16.25	3.121	23.032	−2.175	−34.865	2.101	28.981	1.946	17.107	2.013	32.208
50	76.75_16.75	2.840	21.319	−1.484	−18.153	1.866	25.949	1.697	15.383	2.497	40.571
51	76.75_17.25	2.586	18.815	−1.140	−6.935	1.453	21.363	1.484	13.350	2.432	41.880
52	76.75_17.75	2.676	19.096	−0.989	−7.131	1.201	17.561	1.379	13.715	2.495	42.118
53	77.25_12.25	1.859	11.505	−2.556	−55.314	0.022	0.452	2.001	16.524	0.737	7.042
54	77.25_12.75	2.446	15.779	−2.379	−54.447	0.769	7.001	2.349	21.698	0.604	8.182
55	77.25_13.25	2.301	15.660	−2.059	−40.528	0.776	8.885	2.045	19.768	0.181	2.479
56	77.25_13.75	2.040	13.540	−0.149	0.000	1.158	11.458	1.641	15.923	0.384	5.125
57	77.25_14.25	1.919	13.343	−0.030	0.000	1.218	12.439	1.424	13.409	1.049	10.847
58	77.25_16.25	3.070	22.884	−1.496	−18.657	2.432	31.719	1.960	16.653	2.146	33.319
59	77.25_16.75	2.905	21.408	−1.487	−18.904	2.028	30.324	1.868	15.045	2.316	37.771
60	77.25_17.25	2.562	18.178	−1.015	−9.293	1.448	20.290	1.576	12.694	2.296	38.536
61	77.25_17.75	2.608	18.696	−1.048	−7.786	1.367	19.738	1.480	13.253	2.408	40.845
62	77.25_18.25	2.642	18.896	−1.019	−7.459	1.284	18.650	1.430	13.484	2.452	41.482
63	77.75_12.75	2.843	18.438	−2.649	−60.653	1.027	11.635	2.538	23.145	1.143	13.673
64	77.75_13.25	2.780	18.796	−2.343	−57.547	1.105	12.525	2.582	23.046	1.071	11.956
65	77.75_13.75	2.594	18.506	−2.292	−57.164	1.842	19.031	1.965	18.190	1.281	14.296
66	78.25_13.25	2.852	18.969	−1.776	−34.107	1.832	22.770	2.611	21.861	1.390	14.343
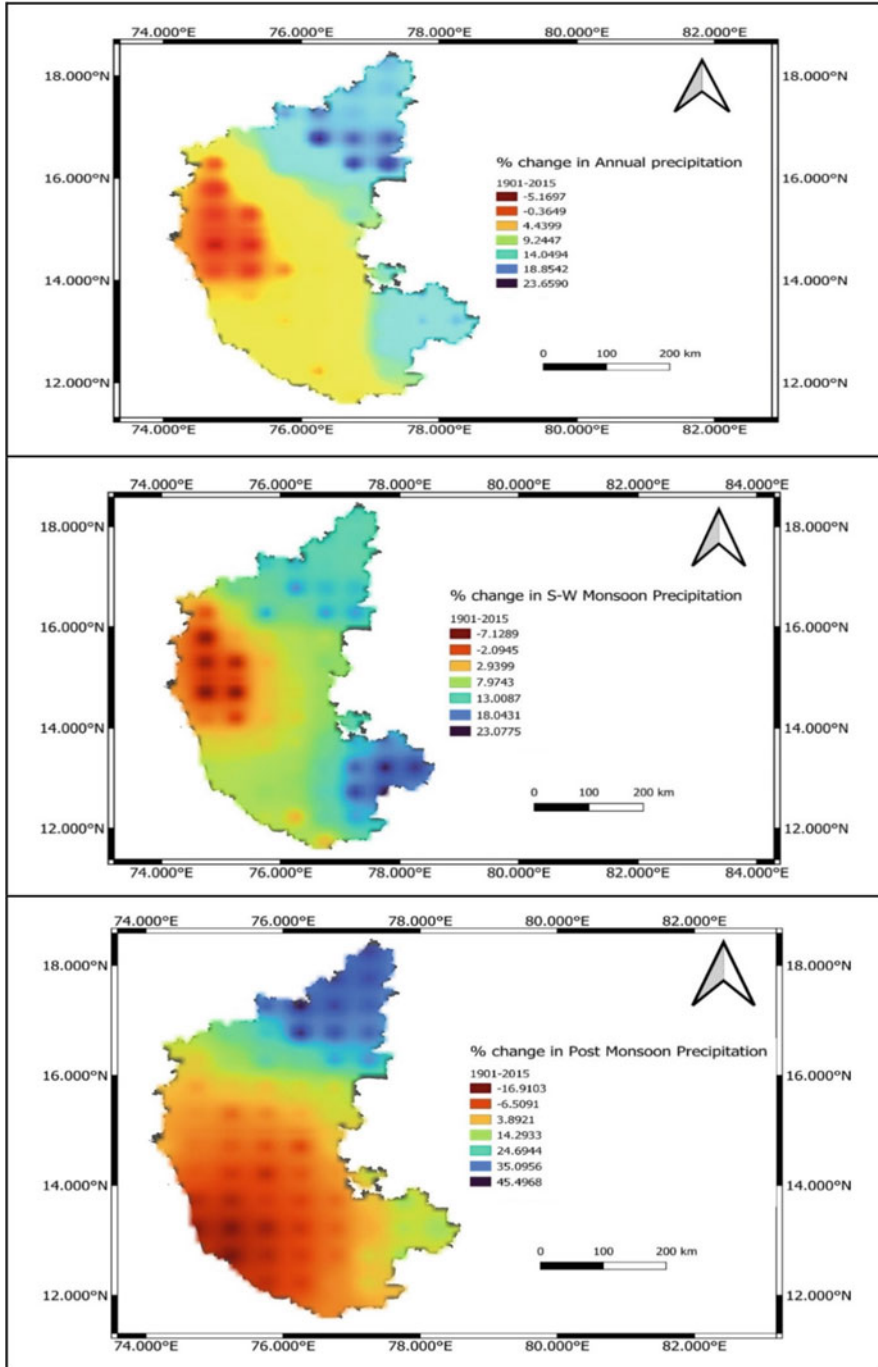
Fig. 14.8 Spatial representation of percentage change in precipitation for time array 1901–2015

greater than 10%. Southern Karnataka indicates a dip in post-monsoon precipitation throughout the period 1901–2015, but the scenario alters as it moved toward the northern districts. The magnitude of dips and increments with respect to spatial distribution over the state is shown in Fig. 14.8.

Grids 24, 25, 32, 35–39, 44–52, and 56–66 indicate a greater than 10% increase in precipitation for the summer season. Other grids undergo less than 10% increase or decrease in precipitation except grid 26, which records a decline of greater than 10% in precipitation.

Homogeneity Test

Homogeneity tests have been conducted to ascertain whether a series may be considered homogeneous over time or whether there is a time at which a change occurs. The variety of the tests comes from the fact that there are many possible alternative hypotheses: changes in distribution, changes in average (one or more times), or presence of trend. Pettit's test and Buishand's test were employed to test the homogeneity of a precipitation series. Pettit's test is based on rank and is a nonparametric test that does not require any assumption of normality. Buishand's test is based on cumulative deviations from the mean or partial sums. The test is carried out for monsoon, post-monsoon, and annual time series.

Homogeneity Results for Annual Precipitation Series

The ultimate change point year for Karnataka turns out to be 1956 for both Pettit's test and Buishand's test.

Homogeneity Results for Southwest Monsoon Series

The year 1956 is the change point for the southwest monsoon array by both Pettit's test and Buishand's test.

It is to be noted that from the result of the seasonal contribution of rainfall it has been observed that 70% of the annual rainfall is contributed by the southwest monsoon. So, it was expected that the change point year for the annual rainfall series and southwest monsoon series will not vary to a considerable extent. Being coherent with the expectation, the homogeneity analysis results indicate the change point year to be the same for both annual series and southwest monsoon series. Also, it shows the precision of estimation.

Homogeneity Test Results for Post-monsoon Series

The change point year was found to be 1952 from Pettit's test and 1951 from Buishand's test for the post-monsoon array.

Mann–Kendall Test and Theil–Sen's Slope Test Results for Two Successive Time Series

After performing the homogeneity analysis, the change point year was determined to be 1956 for Karnataka state. As the change point year was fixed, Mann–Kendall test and Theil–Sen's slope test were performed for the precipitation values of all the 62 grid points in two phases for determining the trends in precipitation in two successive time series. In the first phase of analysis, time series was taken from 1901 to 1956, and for the second phase of analysis, time series was taken from 1957 to 2015 (Tables 14.2 and 14.3).

Trend Analysis

For annual array, Mann–Kendall standardized test statistic Z-value indicates that 32 grid points that constitute 48% of the total 66 grid points undergo a change in the phase of precipitation between the series. The grid points undergoing change in the phase were 1–17, 21–25, 27, 35–37, 39, 48, 50–52, and 60. Only four grid points, namely, 7, 8, 15, and 16, exhibit a significant increase ($Z > 1.96$) of precipitation in the first time series and only two grid points 7 and 8 exhibit a significant decrease ($Z < -1.96$) of precipitation in the second time series. Of the 32 grid points that exhibit a phase change, 28 grids have a change in phase from positive to negative. This implies that these 28 grid points exhibit an increasing trend in precipitation from 1901 to 1956, but the precipitation trend decreases in the next time series from 1957 to 2015. These 28 grid points comprise grids 1, 4–8, 11–17, 21–25, 27, 35–37, 39, 48, 50, 51, 52, and 60. The remaining four grid points out of the 30 grids establish a change in phase from negative to positive, that is, the precipitation increases in the second time interval from 1957 to 2015. These grid points include grids 2, 3, 9, and 10.

For annual array, from Sen's slope test, the grid points 1, 5–8, 13–17, 24, and 25 (12 out of 66 grid points), which had a significant boom in magnitude of precipitation (greater than 10%) in the first time interval, exhibit an abrupt alteration in the second time interval, where there has been a significant decline in precipitation showing negative magnitude in the range of -5 to -25%. Grid points 27, 35–37, 39, 48, 50–52, and 60 (10 out of 66 grid points) exhibit an increase in the magnitude of 10–20% in rainfall for the first time series but exhibit a decrease in precipitation

Table 14.2 Man–Kendall test and Theil–Sen's slope test results during the period 1901–1956

Grid points	Grids LONG_LAT	Annual Z-value	% change	S-W monsoon Z-value	% change	Post-monsoon Z-value	% change
1	74.25_14.75	1.322	12.442	0.629	7.021	2.226	44.481
2	74.75_13.25	−0.177	−2.244	−0.770	−7.456	0.092	0.663
3	74.75_13.75	−0.233	−2.413	−0.516	−5.628	0.820	9.957
4	74.75_14.25	0.191	1.514	−0.205	−2.396	1.520	31.086
5	74.75_14.75	1.011	8.567	−0.021	−0.537	2.127	42.757
6	74.75_15.25	1.746	12.772	0.968	8.698	1.986	45.694
7	74.75_15.75	2.361	17.393	1.392	12.746	1.922	42.275
8	74.75_16.25	2.184	14.942	1.293	11.827	1.618	38.923
9	75.25_12.75	−0.247	−1.894	−0.502	−6.963	−0.580	−8.741
10	75.25_13.25	−0.219	−2.564	−0.629	−7.141	−0.254	−6.622
11	75.25_13.75	0.219	1.877	−0.445	−5.387	0.403	6.794
12	75.25_14.25	0.671	4.989	−0.375	−3.785	1.046	18.771
13	75.25_14.75	1.166	9.470	0.049	0.224	1.830	33.843
14	75.25_15.25	1.618	14.220	0.714	6.228	1.604	32.232
15	75.25_15.75	1.965	17.627	1.138	11.605	1.725	34.182
16	75.25_16.25	2.000	16.987	1.237	11.519	1.576	33.802
17	75.25_16.75	1.746	16.349	1.124	10.869	1.244	33.060
18	75.75_12.25	1.279	7.417	0.452	5.375	−0.163	−2.229
19	75.75_12.75	0.403	3.448	0.134	1.260	−0.113	−1.509
20	75.75_13.25	0.686	5.546	0.007	0.305	−0.191	−2.842
21	75.75_13.75	0.912	5.947	−0.021	−0.840	0.155	2.434
22	75.75_14.25	0.841	7.556	0.000	0.024	0.247	6.109
23	75.75_14.75	1.159	9.952	0.168	1.771	0.921	18.04
24	75.75_15.25	1.675	13.787	0.601	6.475	1.315	24.500
25	75.75_15.75	1.505	15.635	1.088	11.864	1.152	25.736
26	75.75_16.25	1.477	16.380	1.067	10.545	1.965	47.610
27	75.75_16.75	1.668	16.517	0.855	9.191	1.124	27.971
28	75.75_17.25	1.336	13.544	1.152	12.392	0.728	22.228
29	76.25_12.25	1.039	7.459	0.431	4.020	0.219	5.037
30	76.25_12.75	1.004	6.887	0.459	5.208	0.318	5.160
31	76.25_13.25	1.025	9.540	−0.007	−0.253	0.318	5.963
32	76.25_13.75	1.194	10.781	−0.028	−0.612	0.474	10.643
33	76.25_14.25	0.940	8.751	−0.120	−1.053	0.481	9.596
34	76.25_14.75	0.954	8.996	0.021	0.360	0.290	7.708
35	76.25_15.25	1.237	11.479	0.431	4.506	0.735	17.124
36	76.25_15.75	1.746	17.219	1.053	11.970	1.145	26.088
37	76.25_16.25	1.618	13.377	1.138	13.956	0.954	22.002
38	76.25_16.75	1.774	18.524	1.223	17.809	1.209	28.371
39	76.25_17.25	1.760	19.549	1.180	15.849	0.954	26.194
40	76.75_11.75	0.770	5.851	−0.134	−0.732	0.353	4.557
41	76.75_12.25	0.919	7.573	0.254	1.901	0.891	12.622

(continued)

Table 14.2 (continued)

Grid points	Grids	Annual		S-W monsoon		Post-monsoon	
	LONG_LAT	Z-value	% change	Z-value	% change	Z-value	% change
42	76.75_12.75	1.315	10.586	0.544	4.840	0.827	16.701
43	76.75_13.25	1.166	10.059	0.219	2.144	0.587	12.568
44	76.75_13.75	1.067	10.742	0.092	1.489	0.671	15.045
45	76.75_14.25	0.912	9.211	−0.049	−1.047	0.601	13.989
46	76.75_14.75	0.997	12.499	0.148	2.270	0.636	12.003
47	76.75_15.25	1.124	12.155	0.290	4.341	0.671	12.578
48	76.75_15.75	1.746	17.219	1.053	11.970	1.145	26.088
49	76.75_16.25	1.703	20.843	1.336	17.432	0.954	25.683
50	76.75_16.75	1.675	19.626	1.293	20.502	1.039	29.640
51	76.75_17.25	1.583	19.316	1.307	17.853	0.841	25.767
52	76.75_17.75	1.626	18.384	1.180	16.115	0.841	23.507
53	77.25_12.25	0.770	7.494	−0.155	−1.723	0.855	17.772
54	77.25_12.75	1.053	8.880	0.353	4.541	1.053	21.682
55	77.25_13.25	1.293	10.320	0.141	1.767	0.848	17.708
56	77.25_13.75	1.329	12.704	0.035	1.102	0.876	14.651
57	77.25_14.25	0.813	9.231	−0.021	−0.650	0.594	9.990
58	77.25_16.25	1.703	19.672	1.187	16.507	1.279	33.956
59	77.25_16.75	1.647	17.214	1.124	15.629	1.053	29.633
60	77.25_17.25	1.534	16.286	1.053	14.644	0.728	18.561
61	77.25_17.75	1.581	17.995	1.180	16.204	0.803	22.612
62	77.25_18.25	1.604	18.190	1.180	16.160	0.822	23.060
63	77.75_12.75	1.025	9.722	0.148	3.208	0.855	16.301
64	77.75_13.25	1.230	11.176	0.247	3.691	1.018	15.822
65	77.75_13.75	1.088	12.232	0.120	1.279	0.834	16.914
66	78.25_13.25	0.558	5.392	−0.233	−1.959	0.368	7.615

magnitude of −0.656% to −5.402% in the successive time series. The grid points 28, 32, 38, 42–44, 46, 47, 49, 58, 59, and 62 (12 out of 66 grids) exhibit a change in magnitude from greater than 10% increase in the range of 10.059% to 20.843% to less than 10% increase in the magnitude of range 0.414–5.433% as it moved from the first time series to the second time series.

From Figs. 14.9 and 14.10, it can be observed that in the gross northern Karnataka state the annual precipitation has declined to a considerable extent. Throughout the first time array, where there is an increase in precipitation magnitude of 16–20% in these regions, after the change point year, change in magnitude of precipitation is recorded to be −25% to −4%. The phase change in precipitation, that is, from 15% to −22%, has specially been underscored in the northwestern ghats. The southern districts exhibit an average percentage increase in precipitation from 7.5% to 10% as it moved from the first to the second time series.

Table 14.3 Mann–Kendall and Theil–Sen's slope test results during the period 1957–2015

Grid points	Grids LONG_LAT	Annual Z-value	% change	S-W monsoon Z-value	% change	Post-monsoon Z-value	% change
1	74.25_14.75	−0.916	−9.508	−0.889	−9.812	−0.281	−8.334
2	74.75_13.25	0.314	2.566	0.249	2.210	0.216	3.729
3	74.75_13.75	0.013	0.049	0.092	1.306	0.222	3.256
4	74.75_14.25	−0.438	−5.292	−0.347	−4.205	0.118	2.256
5	74.75_14.75	−1.256	−12.899	−1.112	−12.673	−0.275	−5.120
6	74.75_15.25	−1.785	−17.436	−1.615	−17.286	−0.347	−8.224
7	74.75_15.75	−2.629	−25.963	−1.877	−21.539	−0.425	−8.538
8	74.75_16.25	−2.485	−25.564	−1.602	−17.219	−0.033	−0.442
9	75.25_12.75	0.000	0.151	0.183	2.590	0.575	10.278
10	75.25_13.25	0.327	3.507	0.458	5.339	0.366	7.524
11	75.25_13.75	−0.026	−0.431	0.353	3.354	0.314	5.483
12	75.25_14.25	−0.556	−5.217	−0.262	−3.215	0.229	4.643
13	75.25_14.75	−1.177	−11.454	−0.772	−8.810	−0.085	−2.205
14	75.25_15.25	−1.537	−14.627	−1.092	−13.529	−0.183	−4.787
15	75.25_15.75	−1.779	−17.983	−0.850	−10.409	−0.183	−2.411
16	75.25_16.25	−1.713	−16.666	−0.680	−7.735	0.150	2.139
17	75.25_16.75	−1.491	−14.737	−0.275	−3.717	0.163	3.269
18	75.75_12.25	0.340	2.477	0.432	5.383	0.987	14.947
19	75.75_12.75	0.641	5.858	0.889	9.811	0.700	9.033
20	75.75_13.25	0.307	3.606	0.837	10.133	0.510	6.150
21	75.75_13.75	−0.249	−3.084	0.419	5.456	0.405	6.617
22	75.75_14.25	−0.379	−4.471	0.157	1.728	0.242	3.808
23	75.75_14.75	−0.641	−8.06	−0.167	−1.666	0.113	4.104
24	75.75_15.25	−1.046	−8.256	−0.327	−2.809	−0.157	−2.670
25	75.75_15.75	−1.033	−9.948	−0.170	−2.525	−0.007	−0.103
26	75.75_16.25	0.419	5.887	0.811	12.860	0.719	19.754
27	75.75_16.75	−0.497	−5.402	0.183	2.720	0.209	2.800
28	75.75_17.25	0.549	5.146	−0.183	−2.122	0.994	26.250
29	76.25_12.25	0.327	3.586	0.602	6.695	0.785	12.510
30	76.25_12.75	0.549	4.810	1.046	12.701	0.680	9.936
31	76.25_13.25	0.451	2.813	1.040	15.108	0.347	5.950
32	76.25_13.75	0.334	1.959	0.530	8.043	0.386	5.815
33	76.25_14.25	0.092	0.817	0.517	5.407	0.543	7.060
34	76.25_14.75	0.039	0.389	0.275	3.228	0.451	4.400
35	76.25_15.25	−0.157	−0.656	0.000	0.000	0.046	0.782
36	76.25_15.75	−0.340	−3.642	−0.092	−1.581	−0.183	−3.169
37	76.25_16.25	−0.157	−0.900	0.353	3.834	0.294	3.899
38	76.25_16.75	0.078	1.771	0.523	6.138	0.536	11.000
39	76.25_17.25	−0.013	−0.174	0.294	3.214	0.569	9.848
40	76.75_11.75	0.255	2.081	0.778	7.755	0.497	5.112
41	76.75_12.25	0.405	4.768	1.046	11.465	0.641	8.611

(continued)

Table 14.3 (continued)

Grid points	Grids	Annual		S-W monsoon		Post-monsoon	
	LONG_LAT	Z-value	% change	Z-value	% change	Z-value	% change
42	76.75_12.75	0.523	5.372	0.909	11.760	0.235	4.585
43	76.75_13.25	0.634	5.433	0.987	11.589	0.229	4.979
44	76.75_13.75	0.602	4.673	0.706	8.986	0.105	2.287
45	76.75_14.25	0.883	7.363	0.693	8.817	0.693	7.910
46	76.75_14.75	0.804	7.810	0.523	6.068	0.831	12.147
47	76.75_15.25	0.111	1.022	0.379	5.655	0.360	4.802
48	76.75_15.75	−0.340	−3.642	−0.092	−1.581	−0.183	−3.169
49	76.75_16.25	0.366	3.307	0.301	3.883	0.628	11.573
50	76.75_16.75	−0.065	−0.861	0.275	2.570	0.458	10.088
51	76.75_17.25	−0.137	−1.284	0.039	0.317	0.347	7.615
52	76.75_17.75	−0.059	−0.718	0.167	1.766	0.569	11.894
53	77.25_12.25	1.007	8.190	0.994	11.690	0.438	6.800
54	77.25_12.75	1.072	9.562	1.138	13.402	0.157	4.346
55	77.25_13.25	1.269	14.159	1.216	14.981	0.327	4.905
56	77.25_13.75	1.275	11.600	0.844	10.573	0.785	10.620
57	77.25_14.25	1.334	11.386	0.667	7.996	1.347	16.301
58	77.25_16.25	0.288	3.645	−0.052	−0.638	0.706	13.523
59	77.25_16.75	0.039	0.414	−0.209	−1.372	0.791	14.761
60	77.25_17.25	−0.026	−0.755	−0.196	−1.841	0.791	18.218
61	77.25_17.75	1.559	17.801	1.180	16.249	0.713	18.741
62	77.25_18.25	0.750	8.532	0.674	9.008	0.641	15.318
63	77.75_12.75	1.713	14.947	1.177	15.148	0.510	8.333
64	77.75_13.25	1.746	15.891	1.079	14.059	0.765	10.924
65	77.75_13.75	1.556	13.172	0.772	9.074	1.059	12.572
66	78.25_13.25	1.648	12.791	0.929	12.291	0.994	11.457

For the southwest monsoon series, from the Z-value of Mann–Kendall test, 33 grid points indicate a change in phase of precipitation between the series. Also, 19 grid points exhibit a transition from positive phase to negative phase between the series and 14 grid points exhibit a transition from negative phase to positive phase between the series. No significant increase or decrease in precipitation is established in any of the grids constituting both the arrays for S-W monsoon. Three grid points 7, 8, and 15 have greater than 10% increase in precipitation for the early time series but undergoes greater than 10% decrease in precipitation for the successive time series. Nine grid points 16, 17, 25, 28, 36, 48, and 58–60, which has greater than 10% increase in magnitude of precipitation in the first half, show a negative magnitude of less than 10% in the second half of time array. Finally, grid points 37–39 and 49–52 and 62, that is, 8 grid points, exhibit greater than 10% increase in precipitation from 1901 to 1956 but less than 10% increase in precipitation from 1957 to 2015.
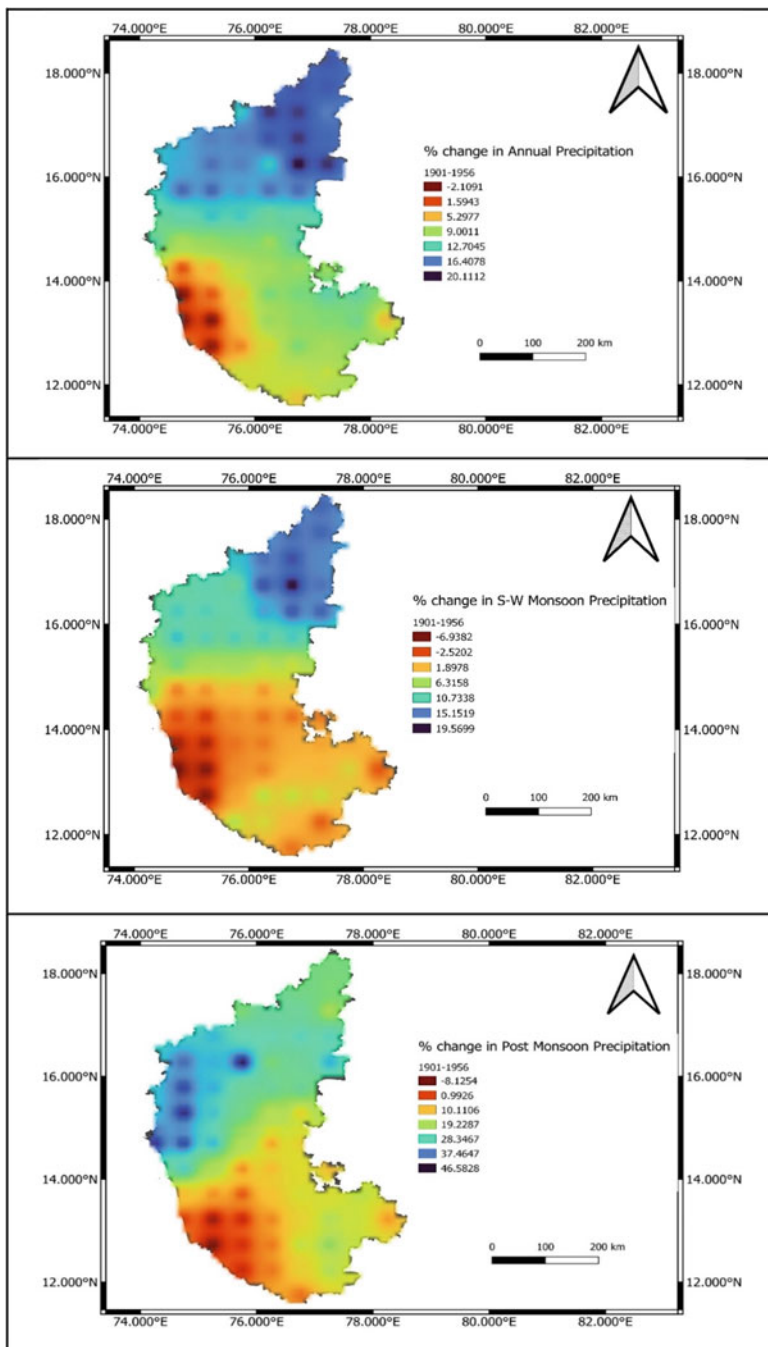
Fig. 14.9 Spatial representation of percentage change in precipitation for time array 1901–1956
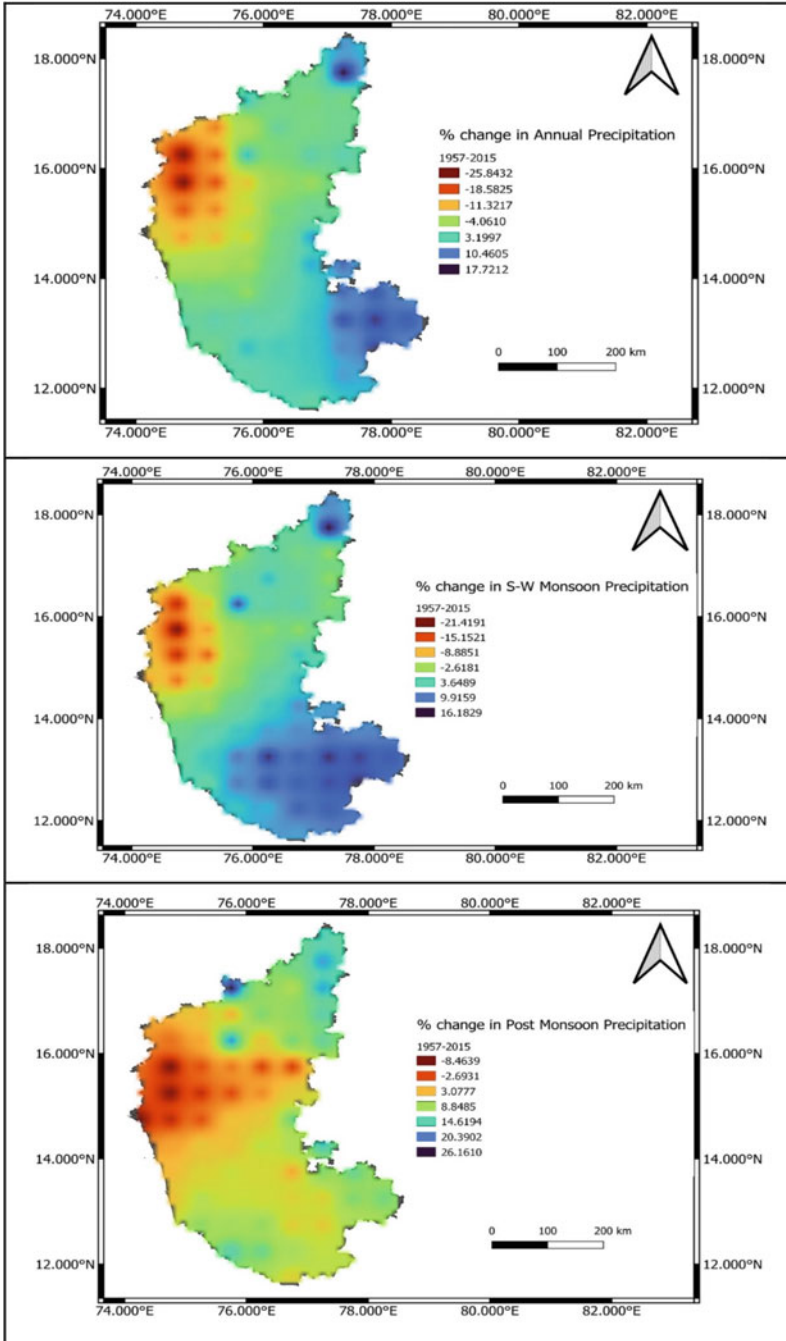
Fig. 14.10 Spatial representation of percentage change in precipitation for time array 1957–2015

Table 14.4 Mann–Kendall test and Sen's slope estimator test results for the basin of Karnataka

Year range	Annual			S-W monsoon			Post-monsoon		
	Z-value	β-value	% change	Z-value	β-value	% change	Z-value	β-value	% change
1901–2015	1.344	0.635	6.834	0.904	0.495	5.715	0.232	0.054	3.298
1901–1956	1.095	1.464	7.788	0.318	0.498	2.848	0.841	0.546	16.264
1957–2015	0.013	0.027	0.150	0.288	0.453	2.643	0.628	0.249	7.922

When the percentage change in precipitation received in southwest monsoon is projected spatially over the map of Karnataka state, it is noted that a sharp boom in precipitation becomes pervasive over the southern districts of the state in between the two successive time series under study. Throughout the period 1901–1956 in the southwestern region, the southwest monsoon precipitation has an average decline of 4%. But in the southeastern districts, the average increase in precipitation throughout the same time array is found to be 4%. In the successive time series (1957–2015), the entire southern domain of the state establishes boom in precipitation, the magnitude of boom ranging from 3% to 16%. The northwestern ghat districts experienced a pathetic decrease in precipitation throughout the successive time series. In this regard, the former time array in which a 6–10% increase in southwest monsoon precipitation is recorded witnesses a pathetic decline in the range of 8–21% in the later time array. The extreme north districts also witness a dip in precipitation increment magnitude but no decline is recorded.

For post-monsoon array, 17 grid points exhibit a change in phase of precipitation between the series, and 12 grid points undergo alteration from a positive phase to a negative phase. Five points undergo a transition from a negative phase to a positive phase. Grid points 1, 5, 6, 7, 8, 13–15, 24, 25, 36, and 48, which have a greater than 10% increase in magnitude of precipitation in the first half, show a negative magnitude of less than 10% in the second half of the time array.

When analyzed spatially, the post-monsoon precipitation has shown changes in southern districts as it moved from the first time series to the second time series, but the changes vary both with respect to phase and magnitude. In the first half, the precipitation change is ascertained to be −8% to 1% in the southwest region, which transforms to 8–14% in the second half. Again in the northern districts, the post-monsoon precipitation increases by 20–46% throughout the time array of 1901–1956, but the magnitude of increment reduces to 3–20% throughout the period 1957–2015. Also, some of the regions in northwestern Karnataka register a dip in precipitation as compared to the boom on moving from the first to second time array (Table 14.4).

For annual precipitation, the trend suggests that the increase in the magnitude of precipitation dips from 7.788% to 0.15% when it moved from the first time series to the second. Southwest monsoon exhibits a nonsignificant increase in trend. However, the percentage change remains almost identical for both the time series. Post-monsoon exhibits a decrease in the percentage increase of rainfall from 16.264% in the first time series to 7.922% in the second time series.

Conclusion

The present study analyzes the precipitation trends over the entire state of Karnataka from 1901 to 2015 by employing CRU $0.5° \times 0.5°$ gridded rainfall data. Karnataka receives a mean annual precipitation of 1073 mm with southwest monsoon contributing 70% of it, followed by the post-monsoon season, which contributes about 18%. The summer and winter seasons have negligible contribution to annual precipitation. The coefficient of variation for annual precipitation is 68%. The departure analysis for 115 years of precipitation data underlines the fact that 79 years received normal precipitation, 11 years received excess precipitation, 23 years received deficient precipitation, and only 2 years had scanty precipitation.

The results obtained from the analysis of spatial distribution of precipitation throughout the south Indian state under study reveal that the southwest monsoon has a descending trend on moving from the extreme western part of the state, which comprises the Western Ghats, to the eastern part of the state, whereas the pre-monsoon exhibits a decreasing trend from the southern to the northern part of the state. The precipitation received by Karnataka from the post-monsoon season exhibits a decreasing trend as we move from the southern districts to the northern districts. It is observed that the annual precipitation exhibits a decreasing nature as it moved from the Western Ghats comprising extreme western districts to the eastern districts through the central districts.

From the trend analysis results, it is observed that the precipitation in the western region of Karnataka comprising the Western Ghats and its adjoining areas has decreased over the period under consideration. Of the 32 grid points spread throughout the state, which exhibit a phase change, 28 grids have a change in phase from positive to negative. This implies that these 28 grid points exhibit an increasing trend in precipitation from 1901 to 1956, but the precipitation trend decreases in the next time series from 1957 to 2015. The precipitation in this region establishes increasing precipitation in the first time series, and the trend reverses in the second time series. The change point year is estimated to be 1956. Also, the annual precipitation over the entire state of Karnataka increases by 7.78% in the first time array (1901–1956) and the increasing trend dips too much, reduced 0.15% in the second time array (1957–2015). The southwest monsoon and post-monsoon seasons being the influential contributors to the annual rainfall also echo the same trend over the successive time series. Also, the central and eastern parts of the state experience a decreasing trend of rainfall, but the extent of decrease in the trend is less as compared to the Western Ghats and adjoining areas.

References

Archana Nair, K. Ajith Joseph, K.S. Nair (2014) Spatio-temporal analysis of rainfall trends over a maritime state Kerala of India during the last 100 years. Atmos Environ 88:123–132. Elsevier

Arun Kumar Taxak, A.R. Murukumar, D.S. Arya (2014) Long term spatial and temporal rainfall trends and homogeneity analysis in Wainganga basin, Central India. Weather Clim Extremes 4:50–61. Elsevier

Duhan D, Pandey A (2013) Statistical analysis of long term spatial and temporal trends of precipitation during 1901–2002 at Madhya Pradesh, India. Atmos Res 122:136–149. Elsevier

Goyal MK (2014) Statistical analysis of a trend of rainfall during 1901–2002 at Assam, India. Water Resour Manag 28:1501–1515

Jain SK and Kumar V (2012) Trend analysis of rainfall and temperature data for India. Curr Sci (Bangalore) 102(1):37–49

Khare D, Kundu S, Mondal A (2014) Spatial and temporal analysis of rainfall and temperature trend of India. Theor Appl Climatol 122(1):143–158

Kundu S, Khare D, Mondal A and Mishra P (2014) Long term rainfall trend analysis (1871–2011) for whole India. Climate Change Biodiver 1:45–60

Mohan Z, Ray SS, Dutta S, Panigrahy S (2005) Analysis of runoff pattern for all major basins of India derived using remote sensing data. Curr Sci Assoc 88(8):1301–1305

Rajeevan M, Jaswal AK, Bhate J (2008) Analysis of variability and trends of extreme rainfall events over India using 104 years of gridded daily rainfall data. Geophys Res Lett 35:1–6

Rangarajan S, Ritwik S, Thattai D, Yellasiri R (2018) Detecting changes in annual and seasonal rainfall patterns for Chennai, India. J Hydrol Eng 23(04). https://doi.org/10.1061/(ASCE)HE.1943-5584.0001630

Reference for study area: Website 'http://waterresources.kar.nic.in/river_systems.htm'

Sheikh Hefzul Bari, Md. Tauhid Ur Rahman Hoque, Muhammad Azizul Hoque, Md. Manjurul Hussain (2016) Analysis of seasonal and annual rainfall trends in the northern region of Bangladesh. Atmos Res 176–177:148–158. Elsevier

Vijay Kumar, Sharad K. Jain, Yatveer Singh (2010) Analysis of long-term rainfall trends in India. Hydrol Sci J 55:484–496

Chapter 15
Trend Analysis of Precipitation (1901–2015) over Telangana State, India

Aravind Murali [ID]**, Sathyanathan Rangarajan, Deeptha Thattai** [ID]**, Manikandan Kamaraj, Divyashri Varadharajan, Sangay Yangzom Bhutia, and Md. Nazrul Islam**

Abstract Precipitation is an essential component of the hydrological cycle, and its variability is the principal determinant of irrigation practices and other water developmental works. In the present study, gridded rainfall values of $0.5° \times 0.5°$ resolution spanning 115 years (1901–2015) were taken for the recently formed Telangana state in India for analysis of annual and seasonal variability. The average annual precipitation varied between 691.64 mm and 1141.01 mm. The north and northeastern regions of Telangana were the most fed regions during the monsoon season, contributing 79% of the annual rainfall. Further, the departure analysis of rainfall revealed 14 excess years, 77 normal years, 22 deficient years, and 2 scanty years for the state. Mann–Kendall test and Sen's slope test revealed an overall significant positive trend in most grid points, and the slope of the trend was lower in the northern regions for the annual rainfall series. Monsoon (89%) and post-monsoon

A. Murali
MASc Civil Engineering, Carleton University, Ottawa, ON, Canada

S. Rangarajan (✉)
Department of Civil Engineering, SRM Institute of Science and Technology, Kattankulathur, Chennai, Tamil Nadu, India
e-mail: sathyanr5@srmist.edu.in

D. Thattai
Independent Researcher, Chennai, Tamil Nadu, India

M. Kamaraj
Research Scholar, SRM Institute of Science and Technology, Chennai, Tamil Nadu, India

D. Varadharajan
Research Intern, Indian Institute of Science (IISc), Bengaluru, Karnataka, India

S. Y. Bhutia
M.Eng. Civil Engineering, University of British Columbia, Vancouver, BC, Canada

Md. N. Islam
Department of Geography and Environment, Jahangirnagar University, Savar, Dhaka, Bangladesh
e-mail: nazrul_geo@juniv.edu

series (59%) depicted a significantly positive trend. From the homogeneity analysis, the most probable change point year was found to be 1952. An increase of 11% and 10% in the annual and monsoon rainfall, respectively, was found after the shift for the entire region.

Keywords Telangana · Mann–Kendall test · Sen's slope test · Precipitation · Departure analysis · Rainfall trend

Introduction

Water is one of the most valuable and in-demand natural resources for livelihood, whose availability is temporally and spatially affected by the amount of precipitation occurring in the respective watersheds (Kumar et al. 2017; Taxak et al. 2014). With the constant increase in water demand due to exponential growth in agricultural and hydropower industries, any change in the magnitude and the timely arrival of precipitation could adversely affect a country's economy (Murari et al. 2016). According to World Population Prospects 2019, India's population would surpass China's by 2027 with a projected population increase of about 27%. Moreover, India's population may cross 1.67 billion by 2050; this is an alarm bell for India's existing natural water resources (https://population.un.org/wpp/; Rangarajan et al. 2018). This growth will for sure result in more encroachment of water bodies, resulting in an imbalance in the demand–supply chain of water. At the same time, the rising heatwaves around the globe, rampant wildfires, and chaotic weather system further worsen the natural water cycle (Mondal et al. 2015). This unevenness in the water circulation leads to excessive exploitation of water, and this, combined with the economic diversity of the population, will cause disparity among water users (Mishra and Singh 2011). The most affected sections of people will be the poor, marginalized people, immigrants, and women.

Rainfall is a significant variable that determines the availability of water to meet the requirements of various energy and food sectors and the domestic and industrial water supply systems (Rohan et al. 2017). A majority of the densely populated states in India are highly dependent on the monsoon, which is utilized after being captured by temporary storage systems such as reservoirs and tanks through natural or artificial drainages. The storage varies proportionally based on the quantum of rainfall received at that time, which unfortunately becomes challenging to predict in this sensitive weather system. This is because even small disturbances in the system can massively impact the atmospheric conditions, making it impossible to predict weather reliably for beyond 2 weeks. On the other hand, recent studies have indicated a significant surge in extreme climatic events such as severe droughts, hazardous floods, and devastating cyclones in the past 40 years (Nico et al. 2010).

Furthermore, the increasing temperatures around the globe have also influenced the weather extrema, resulting in recurring uncertainties in precipitation (Kishtawal and Krishnamurti 2001). This considerable variation in the hydro-meteorological parameters could severely affect the adaptability of the organisms to the environment, thereby leading to the extinction of rare species (Mawdsley et al. 2009;

Schwartz et al. 2006; Root et al. 2003; Gitay et al. 2002; Stenseth et al. 2002; Root and Schneider 2002; Inkley et al. 2004; Fischlin et al. 2007). As end users of water, we are witnessing unforeseen changes in our demand and supply. Hence, it becomes essential to quantify the long-term trends in the annual and seasonal rainfall patterns to have a better insight into the effects of drastic changes.

Several parametric and nonstatistical methodologies were adopted by researchers to predict the existing trend and explore the variability in the rainfall pattern (Praveen et al. 2020; Yang et al. 2017b; Chatterjee et al. 2016; Tian et al. 2017; Xia et al. 2012; Rao et al. 2014; Talaee 2014; Hamed 2008; Yue and Hashino 2003; Goyal 2014). Most of the precipitation trend analysis incorporates methodologies such as regression analysis (Piao et al. 2010), Kendall rank correlation test (Kendall 1975), Sen's slope estimation (Sen 1968; Pingale et al. 2014), Mann–Kendall test (MK) (Rangarajan et al. 2019; Jain et al. 2013; Sathyanathan et al. 2020), Spearman rank correlation test, and other graphical methods (Maragatham 2012). The trend analysis also includes change detection methods such as the Standard Normal Homogeneity Test (SNHT) (Alexandersson and Moberg 1997), Buishand range test (Buishand 1982), and Pettitt's test (Pettitt 1979) to determine the possible year of trend shift over the entire time series under consideration. In addition, based on the approximate shift point identification, researchers have analyzed the trends, pre- and post-shift point, to understand the variations for the given period (Villarini et al. 2009; Mondal et al. 2015; Buishand 1982).

Precipitation trend analysis facilitates a more efficient management of available water resources (Chatterjee et al. 2009). In the Indian context, substantial economic development is mainly through agriculture practices, which in turn rely on the monsoon contributions. In recent years, due to unexpected frequent droughts in India, there have been considerable losses to native crops, and as a result, suicide among the farming communities (Meshram et al. 2017; Praveen et al. 2020). Also, a lot of the rivers in southern India are nonperennial, whose water source is governed by the monsoon showers. So, it is significant to evaluate the precipitation for the Indian scenario to identify any variable shifts in their pattern and distribution.

Many studies investigate the seasonal, annual, and spatial variability of rainfall, which has been documented by the Intergovernmental Panel on Climate Change (IPCC 2007) across Asia. In recent times, many studies have focused on studying and determining the precipitation trends in India at varying spatial scales (Kumar 2013; Kumar et al. 2010; Goswami et al. 2006; Praveen et al. 2020; Mohammad and Goswami 2019; Guhathakurta and Rajeevan 2008; Joshi and Pandey 2011; Parthasarathy and Dhar 1974; Sarkar and Kafatos 2004; Rangarajan et al. 2019). A regional-scale study is vital in governing the aspects of the water resource and its risk management than continental-scale research (Chandra et al. 2018).

Rangarajan et al. (2018) have identified an insignificant increasing trend in Chennai district's annual rainfall pattern and concluded that if the southwest monsoon provides excess rainfall, the northeast monsoon gets subdued and vice versa. Patra et al. (2012) attempted a discrete trend analysis on Orissa's monthly, seasonal, and annual rainfall data. They found a long-term insignificant negative trend in the annual and monsoonal rainfall series, and a positive trend in the post-monsoon

season. Goutam Kumar Ghosh and Kapil Ghosh (2019) focused on analyzing rainfall variation between 1986 and 2018 in North Sikkim and concluded that the monsoon season's variability was higher when compared to the annual variability of rainfall. Similarly, Raji Reddy et al. (2007) and Reddy and Sreenivas (2016) reported a decreasing trend in the annual rainfall of the northern districts of Telangana state.

Following similar investigations, the present study attempts to detect the temporal trends in annual and seasonal rainfall series for Telangana state. The nonparametric tests seem to be versatile in identifying minor outliers by incorporating independent time-series data; this analysis relies on this methodology to accurately assess the trend over the region under consideration. The percentage contribution of the seasonal rainfall to the annual rainfall, the rainfall departure analysis, and the detection of change points in the rainfall trend were conducted for the rainfall series. To make the analysis more decisive, the (MK) and Sen's slope estimator tests were performed to bring out the variation in trends before and after the shift point.

Area of Study

Positioned between 17.366 °N latitude and 78.475 °E longitude in the Deccan Plateaus, Telangana state was created in 2014 with a total land cover of 112,077 km^2 (Fig. 15.1a). The state is situated on the eastern part of the Indian Peninsula with the elevation ranging from 14 to 1355 m (Fig. 15.1b) and bounded by the states of Andhra Pradesh in the south and east, Karnataka to the west, Maharashtra to the north, and Chhattisgarh to the east. The state's landscape consists of moderately steep mountain ranges, fertile valleys, barren lands, and dense forests. Rivers Krishna and Godavari from the northern and southern tips, respectively, are the two primary sources of storage and water supply to meet the requirements of the growing population. It has a semi-arid climate with hot, dry weather and is covered mainly by the dry deciduous forests of the Central Deccan Plateau in the northern regions, while the moist deciduous forests of the Eastern Highlands cover the eastern part. The state experiences an average maximum daily temperature between 40 and 43 °C during May and a mean lowest daily temperature in the range of 13–17 °C in December and January (https://www.telangana.gov.in/). Telangana climate can be divided into winter (January–February), pre-monsoon (March–May), monsoon (June–September), and post-monsoon (October–December) (https://imdhyderabad.gov.in/). The state receives a majority of its rainfall in both monsoon and post-monsoon periods. Rice is cultivated in irrigated regions, and other crops such as cotton, pulses, jowar, and maize are grown in rainfed regions. The usual practice incorporated by the populace of Telangana to conserve water is rooftop rainwater harvesting systems since drought is a recurring phenomenon in the state.
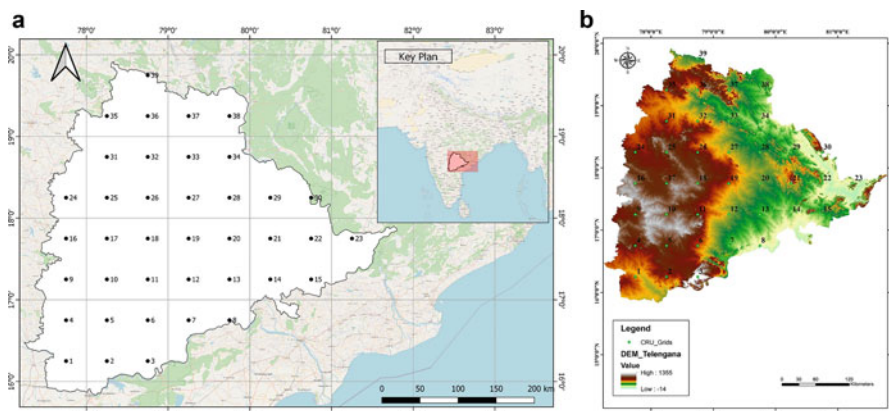
Fig. 15.1 (**a**) Location of Telangana and (**b**) grid points with DEM

Data Source

Rainfall data were downloaded from the Climatic Research Unit (University of East Anglia) and NCAS web portal (https://crudata.uea.ac.uk/cru/data/hrg/) (Harris et al. 2020). Also, 39 grid points at an interval of $0.5° \times 0.5°$ resolution falling within the region of Telangana were extracted for the period of 115 years (1901–2015) (Fig. 15.1a).

Methodology

Rainfall Analysis

The annual and monthly data series were prepared for each grid, and the monthly rainfall data were grouped into four seasonal series, viz., winter, pre-monsoon, monsoon, and post-monsoon. Basic descriptive statistical parameters such as average, standard deviation, and coefficient of variation of the annual and seasonal rainfall series were determined to evaluate the proximity of each series to its overall mean. The percentage contribution of seasonal precipitation to the mean annual series was calculated for each grid point to determine the influential season(s). The departure analysis was done for the annual rainfall series to categorize the precipitation of each year as described in Table 15.1 (IMD 2017; Nicholls et al. 2014; Nicholls and Cazenave 2010; Rangarajan et al. 2018; Kant et al. 2014). This was followed by estimating the magnitude of the rainfall trend for annual and seasonal series using (MK) and Sen's slope estimator tests. Homogeneity tests were carried out using Pettitt's, Buishand's, and SNHT tests to verify the predicted trend, which detects the break of homogeneity in the middle or at the beginning of the trend, in

Table 15.1 Trend classification

Limits of Z_{MK}	Trend classification
$Z_{MK} \leq -1.96$	Significantly decreasing
$-1.96 < Z_{MK} < 0$	Insignificantly decreasing
$0 < Z_{MK} < 1.96$	Insignificantly increasing
$Z_{MK} \geq 1.96$	Significantly increasing

turn delivering the breakpoint of the rainfall trend shift. Based on the shift point year, the whole set was divided into two sets and the trend before and after the shift point year was drawn using the (MK) and Sen's slope estimator tests to provide additional insights. The spatial distribution of rainfall trends over the state was interpolated based on the inverse distance-weighted interpolation technique using ArcGIS.

Trend Detection

Mann–Kendall (MK) Test

Mann–Kendall (MK) test is a nonparametric rank-based test that determines the monotonic change in the trend of a time series. For this test, the null hypothesis is that there is no trend identified in the time series, and the alternative hypothesis is that the two-sided test has a trend or that the one-sided test has an upward trend or a downward trend. The test statistic used to predict the trend for the time series of x_1, x_2, ..., x_n is given by Eq. 15.1 (Kendall 1975):

$$S = \sum_{i=1}^{n-1} \sum_{j=i+1}^{n} \text{sgn} \left[x_j - x_i \right] \tag{15.1}$$

where S is the test statistic, x_j is the sequential data values, n is the length of the data set, and sgn is given by Eq. 15.2:

$$\text{sgn}(y) = \left\{ \begin{array}{c} 1 \dots \text{if}(y > 0) \\ 0 \cdots \text{if}(y = 0) \\ -1 \cdots \text{if}(y = 0) \end{array} \right\} \tag{15.2}$$

It has been authenticated that when $n \geq 8$ the statistic S is approximately said to follow a normal distribution with its mean $E(S) = 0$ and variance as given in Eq. 15.3:

$$V(S) = \frac{n(n-1)(2n+5) - \sum_{i=1}^{m} t_i(t_i - 1)(2t_i + 5)}{18} \tag{15.3}$$

where m is the number of tied groups, and t_i is the size of the ith tied group.

Table 15.2 Classification of regional rainfall distribution based on percentage departure of realized rainfall from normal rainfall

Terminology	Definition
Excess	+20% or more
Normal	−19% to +19%
Deficit	−20% to −59%
Scanty	−60% to −99%
No rain	−100%

Finally, the standardized test statistic Z from the MK iterations are computed using Eq. 15.4:

$$Z_{MK} = \begin{cases} \dfrac{s-1}{\sqrt{var(S)}} \text{ when } S > 0 \\ 0 \cdots \text{when } S = 0 \\ \dfrac{S+1}{\sqrt{var(S)}} \text{ when } S < 0 \end{cases}$$ (15.4)

where Z_{MK} is the MK trend value.

The classification of the rainfall distribution is based on the standard threshold markings (Bari et al. 2016) as presented in Table 15.2.

Sen's Slope Estimator

The magnitude of the univariate time series trend was calculated using Sen's slope estimator (Theil 1950; Sen 1968). This approach involves computing slopes for every pair of ordinal time instant and then using the medians of these slopes to estimate the overall slope.

The slope of n pairs of data points was estimated using Theil–Sen's estimator (Eq. 15.5):

$$Q_i = \frac{x_j - x_k}{j - k} \text{ for } i = 1, \cdots N$$ (15.5)

where x_j and x_k are the data values at times j and k ($j > k$), respectively. The median of these N values of Q_i is termed Sen's estimator of the slope. If there is only one data in each period, then N is given by Eq. 15.6:

$$N = \frac{n(n-1)}{2}$$ (15.6)

where n is the number of time periods.

The medians of the N number of estimated slopes are obtained in the usual way, that is, the N values of Q_i are ranked by $Q_1 \leq Q_2 \leq \cdots \leq Q_{N-1} \leq Q_N$. Moreover, Sen's estimator (β) is given by Eq. 15.7:

$$\beta = \begin{cases} Q_{\frac{N+1}{2}} & \text{if } N \text{ is odd} \\ \left(\frac{1}{2}\right)\left(Q_{N/2} + Q_{(N+2)/2}\right)_{\text{if } N \text{ is even}} \end{cases} \qquad (15.7)$$

The percentage change in trend was calculated by multiplying the Sen's slope value with the number of years (115) and further dividing by the mean annual rainfall for each of the 39 grid points (Kundu et al. 2014).

Homogeneity Test and Change Point Analysis

The homogeneity analysis was carried out in the present study to accurately predict the change point year of the overall trend shift using XLSTAT 2020.1.3. The p-values were obtained from three different statistical checks, namely, Pettitt's test, Standard Normal Homogeneity Test (SNHT), and Buishand's test, to precisely conclude a shift between two segments of the time series when the null hypothesis gets rejected (Kocsis et al. 2020). Pettitt's test is a replica of the rank-based Mann–Whitney test, which requires no assumption about the dissemination of data to predict the time at which the shift occurs (Pettitt 1979; Liu et al. 2012). The SNHT usually correlates the annotations of the time series with its average, thus concluding that there exists a shift in the time series. This outcome confirms the result obtained in Pettitt's test. Buishand's test (1982) is a versatile tool to note the existence of a point from which the variables following any distribution change their mean. The most likely occurring year is chosen as the shift year of the time series to further analyze the rainfall's variability before and after the change point. The MK test and Sen's slope estimator were applied to the two different uneven time series to assess the pre- and post-shift point trend using the same methodology discussed in the previous sections. These checks could deliver a macro-level view of the overall rainfall pattern existing around each grid point.

Results

Preliminary Findings

The various statistical parameters for the annual and seasonal series are listed in Table 15.3. The annual average precipitation was maximum in grid #23 (1141 mm), which was centered in the eastern end of Telangana. On the other hand, minimum rainfall was observed in grid #3 (691.64 mm), falling in the southern part of the state. The standard deviation varied between 144.10 and 219.09 mm. With an annual average coefficient of variation of 20 over the Telangana region, the peak and nadir were between 21.87 and 16.74 in grid #11 and grid #30, respectively. The annual

average precipitation in the Telangana region showed a gradually increasing pattern toward north and northeast directions, resulting in maximum precipitation in the eastern periphery (Fig. 15.2). A more or less similar pattern was observed in the case of monsoon rainfall, which is the most significant contributor to the annual series (Fig. 15.3a).

Grid #39, located in the extreme northern end, recorded the highest average monsoon rainfall of 946.62 mm, while grid #6, located on the southern side, registered the lowest at 458.48 mm. In the post-monsoon season, the pattern was reversed, and the higher rainfall magnitudes (144–180 mm) were observed in the southeastern regions compared to the northern belts (Fig. 15.3b). The winter season (Fig. 15.3c) contributed an abysmal amount of rainfall in the range of 3–18 mm, while the pre-monsoon rainfall (Fig. 15.3d) contributed 17–97 mm across the grids. Grid #21, falling on the mountainous leeward side, received lower rainfall in all the seasons.

Percentage Contribution Analysis

Figure 15.4 represents the percentage contribution of seasonal series to the overall annual rainfall magnitude. The monsoon season contributed the maximum of 79.3%, while the winter, pre-monsoon, and post-monsoon seasons contributed 1.2%, 6.5%, and 13.1%, respectively.

Trend Prediction in Annual and Seasonal Precipitation

The Z statistic from the MK test is employed to evaluate the annual and seasonal trends in rainfall for 1901–2015 for all the 39 grid points. The positive and negative signs of the Z-values indicate the nature of the trend as increasing and decreasing, respectively. As we gradually move from the east toward the western parts of the region, it could be observed that the tendency of insignificancy decreasing trend nullifies due to the increasing elevation of the ground surface. From Table 15.4, it is evident that in the annual series, most of the grid points indicated a significantly increasing trend barring grids #21, #36, #38, and #39 showing an insignificantly increasing rainfall trend. The lowest (0.69%) and highest (22.25%) percentage changes in annual rainfall were found in grid #39 and grid #6, respectively, over 105 years. The annual rainfall trend was lower in the northern regions when compared to other zones, and the respective z statistic value ranged between 0.07 mm/year and 1.91 mm/year (Fig. 15.5a).

Most similarly to the annual trend, monsoon rainfall depicted a positive trend in 38 out of 39 grids, with 21 grids being significant (Table 15.4). Also, the percentage change in monsoon rainfall for 33 grid points was more than 10%, and the northwestern regions experienced higher slope values in the order of 0.99–1.43 mm/year,

Table 15.3 Mean and SD of the annual and seasonal precipitation series, Telangana state, 1901–2015

Grid	Latitude	Longitude	Annual (mm)		Seasonal (mm)								
					Winter		Pre-monsoon		Monsoon		Post-monsoon	
			Mean	SD	Mean	SD	Mean	SD	Mean	SD	Mean	SD
1	16.25	77.75	754.20	157.51	2.95	3.31	61.77	31.41	568.61	132.42	120.87	64.59
2	16.25	78.25	742.86	154.28	5.07	5.58	64.25	34.05	544.05	125.20	129.49	68.85
3	16.25	78.75	691.64	149.63	8.06	9.12	63.93	34.71	458.48	108.39	161.16	81.00
4	16.75	77.75	840.08	181.25	3.86	4.77	57.72	31.33	665.67	156.22	112.83	65.43
5	16.75	78.25	806.59	175.44	5.07	5.75	59.31	33.16	625.59	146.70	116.63	69.18
6	16.75	78.75	748.21	162.60	10.26	11.08	58.77	31.92	539.11	123.67	140.08	79.19
7	16.75	79.25	775.95	165.35	11.11	11.46	58.26	30.84	540.20	123.57	166.38	86.24
8	16.75	79.75	872.32	183.35	11.23	11.94	70.19	41.26	611.18	139.66	179.73	90.23
9	17.25	77.75	863.01	182.00	5.94	6.78	61.01	32.40	682.39	157.49	113.67	66.87
10	17.25	78.25	816.41	176.05	9.24	10.86	61.01	33.29	632.11	147.00	114.05	68.95
11	17.25	78.75	762.13	166.71	12.10	13.02	60.98	32.94	565.72	129.87	123.34	75.09
12	17.25	79.25	808.00	174.52	12.86	13.60	54.95	28.70	600.69	135.78	139.50	81.55
13	17.25	79.75	906.12	183.81	11.29	12.16	68.62	37.62	678.57	147.22	147.64	79.27
14	17.25	80.25	1028.2	204.38	9.00	10.11	87.70	52.47	776.24	172.13	155.21	79.27
15	17.25	80.75	1039.1	219.09	10.22	12.49	91.28	60.48	769.73	179.44	167.85	86.15
16	17.75	77.75	916.28	190.66	10.19	11.10	59.54	31.37	733.09	166.45	113.45	68.86
17	17.75	78.25	916.77	192.82	11.02	11.56	56.85	30.57	743.39	166.86	105.51	67.60
18	17.75	78.75	852.39	180.21	13.16	13.60	56.18	29.88	674.43	150.38	108.62	68.03
19	17.75	79.25	874.72	180.19	14.48	14.80	53.86	27.81	684.28	148.34	122.10	71.09
20	17.75	79.75	938.43	187.86	13.44	14.59	62.35	31.94	731.60	155.79	131.03	71.65
21	17.75	80.25	745.21	144.10	9.41	9.21	16.69	14.70	652.22	134.30	66.90	44.57
22	17.75	80.75	1084.6	204.90	10.09	10.86	90.56	50.68	833.14	177.37	150.80	73.98
23	17.75	81.25	1141	199.78	11.21	12.10	97.24	52.68	853.11	166.52	179.46	85.48
24	18.25	77.75	1011.5	208.20	10.68	10.91	50.77	27.38	850.29	187.47	99.72	61.56

25	18.25	78.25	1042.56	217.98	11.27	12.38	50.10	27.70	888.68	195.70	92.51	60.73
26	18.25	78.75	964.26	193.84	15.15	16.17	49.17	26.58	804.00	171.14	95.94	60.95
27	18.25	79.25	935.06	188.24	15.50	15.63	46.95	25.60	765.03	160.77	107.58	65.60
28	18.25	79.75	971.16	186.75	15.03	14.12	55.93	28.59	784.63	159.66	115.57	66.02
29	18.25	80.25	1052.04	195.09	12.78	12.27	70.54	34.98	849.36	168.13	119.36	65.72
30	18.25	80.75	1137.59	190.47	12.45	11.47	86.27	40.33	906.58	161.89	132.29	67.29
31	18.75	78.25	1038.63	205.46	16.47	16.81	48.29	27.12	890.10	187.53	83.78	52.77
32	18.75	78.75	988.04	187.31	14.10	15.01	45.20	24.57	840.16	167.65	88.58	55.93
33	18.75	79.25	974.51	182.40	11.57	11.46	47.27	25.59	818.53	160.23	97.14	60.59
34	18.75	79.75	1014.14	185.52	11.57	10.15	52.90	26.71	848.57	163.19	101.10	61.58
35	19.25	78.25	1002.40	190.55	16.93	15.65	45.70	25.23	860.49	171.65	79.28	50.30
36	19.25	78.75	1014.45	183.01	14.14	12.75	46.38	25.29	869.92	164.75	84.01	54.95
37	19.25	79.25	966.89	178.07	10.56	9.57	50.56	26.52	817.17	158.50	88.61	57.91
38	19.25	79.75	1059.75	188.22	12.90	11.12	52.97	27.28	903.47	166.71	90.41	59.17
39	19.75	78.75	1089.71	188.55	18.28	15.65	46.55	26.44	946.62	169.77	78.26	54.70

Fig. 15.2 Mean annual precipitation
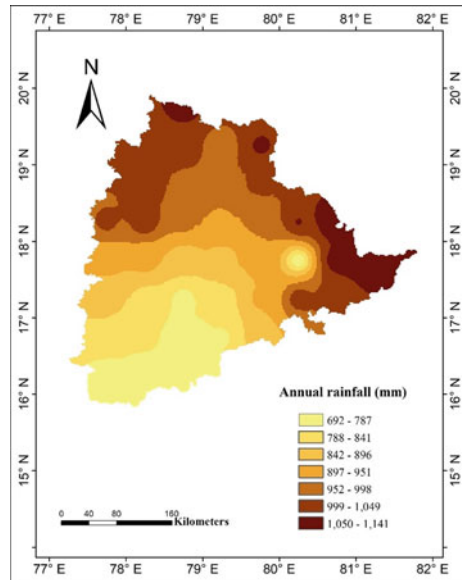
portraying a pattern similar to that of the annual rainfall trend (Fig. 15.5b). Since monsoon is a substantial contributor to the cumulative annual rainfall, the higher slope values in most stations reveal an aggregating futuristic trend.

In the winter, all the grid points depicted an insignificant trend, with more than half being a decreasing trend. The extreme percentage changes in winter rainfall were identified at grid #1 (-14.43%) and grid #8 (15.29%). The Sen's slope ranges between -0.01 and 0.01, representing a nearly flat slope, reflecting minimal variations in the rainfall pattern along the period considered.

However, an insignificant increasing trend was witnessed in most grids for the pre-monsoon season, whose rainfall trend increased from southeast to northwest, as seen in Fig. 15.6a. Out of 39 locations, grid #7, #8, #12, #14, #15, and #20 showed an insignificant declining trend in the pre-monsoon rainfall, but the level of insignificancy was low (between $-0.0.1$ and -0.81), as seen in Table 15.4.

A peculiar reversed pattern of increasing rainfall trend was observed in the post-monsoon season in contrast to the pre-monsoon season, with its slope increasing from northwest to southeast regions of Telangana, as seen in Fig. 15.6b. The post-monsoon rainfall trend for grids #4, #9, #12, #13, #14, #16, #18, #19, #20, #24–#29, and #34 continued to show an increasing trend as from the monsoon season. Except grid #21 falling in the east–central region, all other grids exhibited an increasing trend, insignificantly. A similar pattern at grid #21 was also observed in the monsoon and the annual rainfall trend, where the slope tends to flatten.
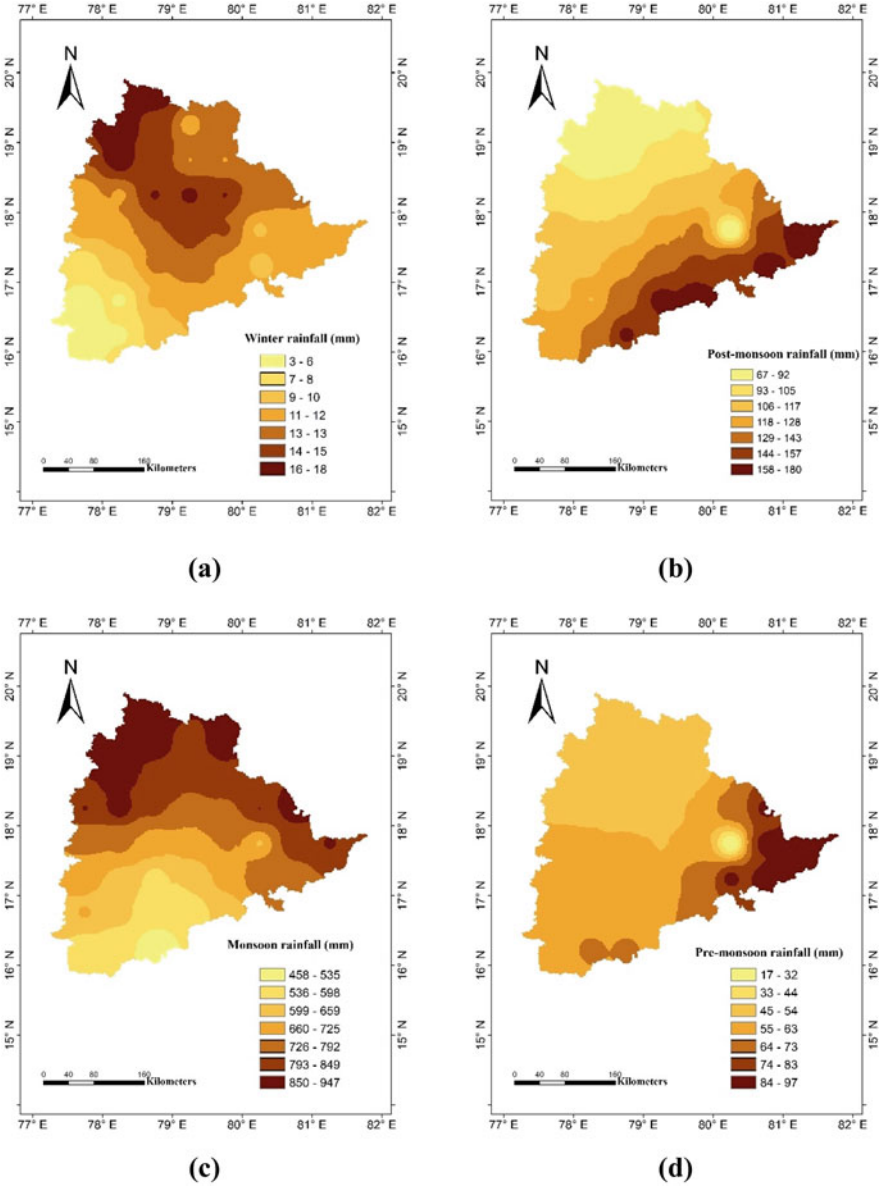
Fig. 15.3   Average rainfall: (**a**) monsoon, (**b**) post-monsoon, (**c**) winter, and (**d**) pre-monsoon

Fig. 15.4 Percentage
contribution of seasons
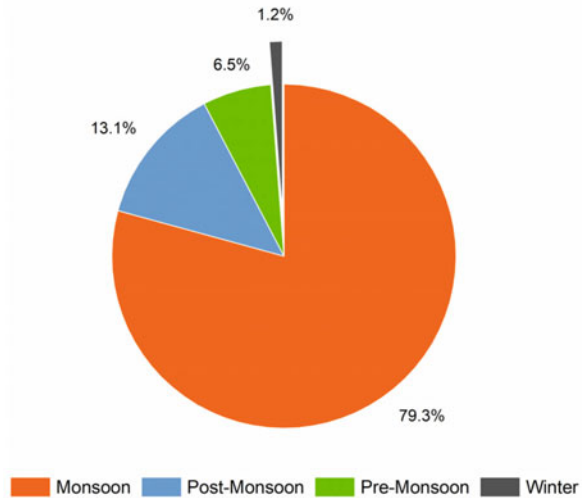
Precipitation Departure Analysis

Departure analysis was carried out to critically introspect the drought years from 1901 to 2015 (Table 15.5). The grids falling in the northern belts (#33, #35, #36, #37, #38, and #39) exhibited no rain scenario for a year. In contrast, the southern regions displayed more extreme rainfall years (14–20) than the northern regions. The maximum excess rainfall of 20 years was noticed in grid #10, and a minimum number of 10 years was recorded in grid #39. The grid points falling in the eastern and northeastern parts showed a higher number of normal rainfall years ranging between 80 and 88 years. Altogether, the number of normal years outweighed the other categories in all the grid points. To summarize, Telangana state had, in 1901–2015, 14 excess years, 77 normal years, 22 deficient years, 2 scanty years, and 0 no rain category.

Homogeneity Test: Check for Shift Point of the Trend

The MK and Sen's slope tests depicted a notable rising trend in the annual and monsoon rainfall series. Further, to detect the exact trend shift point, homogeneity tests, namely, the Pettitt's, SNHT, and Buishand's tests, were performed.

As evident from Table 15.6, grid lying on the state's northern tip, including grids #39, #38, #37, #36, and #35, exhibited a shift in annual rainfall from 1930. Contradictorily, grids located at the southern extremity (grids #1, #2, #4, #5, #6, #9, and #10) displayed a change in rainfall trend from 1946. This proves that the precipitation series does not have any monotonous trend over the period under

Table 15.4 Trend analysis results for the entire series (1901–2015)

Grid	Annual			Winter			Pre-monsoon			Monsoon			Post-monsoon		
	Z	β	% Change	Z	β	% Change	Z	β	% Change	Z	β	% Change	Z	β	% Change
1	2.97	1.40	21.35	−1.32	0.00	−14.43	1.99	0.15	27.93	1.97	0.80	16.23	1.69	0.28	26.37
2	3.03	1.41	21.79	−1.00	0.00	−9.86	1.70	0.14	24.41	2.05	0.80	16.97	1.58	0.28	25.16
3	3.16	1.33	22.14	−0.30	0.00	3.10	1.06	0.07	13.36	2.19	0.67	16.75	1.70	0.38	27.14
4	2.91	1.53	20.96	−1.22	0.00	−11.24	1.73	0.13	26.57	2.17	0.93	16.00	2.06	0.33	33.19
5	3.17	1.55	22.11	−1.11	−0.01	−12.27	1.29	0.10	19.75	2.25	0.97	17.88	1.90	0.30	29.91
6	3.33	1.45	22.25	−0.53	−0.01	−6.29	1.20	0.09	18.16	2.56	0.87	18.49	1.80	0.38	31.45
7	2.97	1.43	21.14	0.41	0.00	3.98	−0.39	−0.03	−5.05	2.23	0.79	16.89	1.86	0.44	30.32
8	2.95	1.57	20.75	0.87	0.01	15.29	−0.81	−0.07	−11.31	2.13	0.76	14.38	1.83	0.48	30.88
9	2.64	1.45	19.37	−0.94	0.00	−9.22	1.11	0.08	15.71	1.87	0.87	14.72	2.09	0.34	34.65
10	2.66	1.35	19.06	−0.97	−0.01	−11.03	1.09	0.09	16.13	2.00	0.88	15.94	1.72	0.28	28.57
11	2.70	1.26	19.03	−0.54	−0.01	−5.34	0.67	0.05	10.24	1.98	0.73	14.88	1.87	0.36	33.15
12	2.86	1.38	19.65	0.23	0.00	0.00	0.11	0.01	1.49	1.93	0.77	14.72	2.07	0.46	38.09
13	2.98	1.50	19.04	0.39	0.00	4.25	−0.31	−0.03	−4.57	1.85	0.80	13.56	2.33	0.51	39.92
14	2.76	1.63	18.23	1.09	0.01	14.19	−0.56	−0.07	−9.39	2.06	0.95	14.04	2.09	0.49	36.27
15	2.55	1.47	16.32	0.91	0.01	11.85	−0.36	−0.05	−6.30	1.80	0.87	13.05	1.53	0.39	26.90
16	2.70	1.48	18.59	−1.05	−0.01	−12.09	1.48	0.12	23.84	1.83	0.90	14.05	2.22	0.39	39.13
17	2.85	1.56	19.55	−0.89	−0.01	−10.10	1.08	0.08	16.59	2.23	1.07	16.60	1.87	0.31	34.15
18	2.74	1.36	18.35	−0.60	−0.01	−6.83	0.70	0.05	10.92	2.03	0.90	15.43	2.00	0.34	35.76
19	2.81	1.41	18.59	−0.10	0.00	0.00	0.23	0.02	4.40	1.98	0.91	15.31	2.28	0.42	39.16
20	2.97	1.54	18.86	0.26	0.00	2.85	−0.10	−0.01	−1.00	2.12	0.99	15.58	2.38	0.49	43.27
21	0.51	0.25	3.83	−0.27	0.00	−4.22	1.60	0.04	30.62	0.63	0.30	5.37	−0.43	−0.05	−8.36
22	2.53	1.53	16.19	0.98	0.01	14.25	0.05	0.01	0.89	1.76	0.92	12.63	1.75	0.37	28.37
23	2.03	1.23	12.39	0.78	0.01	12.36	0.05	0.01	0.70	1.45	0.74	9.95	1.12	0.31	19.89

(continued)

Table 15.4 (continued)

Grid	Annual			Winter			Pre-monsoon			Monsoon			Post-monsoon		
	Z	β	% Change	Z	β	% Change	Z	β	% Change	Z	β	% Change	Z	β	% Change
24	2.72	1.60	18.15	−0.68	−0.01	−6.60	1.63	0.12	27.39	2.02	1.09	14.77	2.12	0.36	41.91
25	3.13	1.91	21.05	−0.26	0.00	−2.96	1.32	0.10	22.96	2.42	1.43	18.45	2.04	0.33	41.44
26	2.69	1.59	18.92	−0.35	−0.01	−4.22	0.95	0.06	14.62	2.26	1.19	16.96	2.00	0.34	40.70
27	2.33	1.31	16.14	−0.01	0.00	0.00	0.78	0.05	12.36	1.90	0.91	13.74	2.16	0.41	43.32
28	2.60	1.41	16.69	0.01	0.00	0.00	0.57	0.05	9.95	1.91	0.93	13.61	2.37	0.45	44.78
29	2.80	1.59	17.42	0.37	0.00	0.00	0.75	0.07	10.80	2.07	0.99	13.46	2.39	0.46	44.27
30	2.37	1.29	13.01	0.46	0.01	7.92	0.76	0.09	11.43	1.38	0.74	9.38	1.75	0.34	29.84
31	2.77	1.62	17.92	−0.18	0.00	−1.60	1.64	0.11	27.32	2.28	1.25	16.10	1.75	0.27	37.19
32	2.54	1.43	16.64	0.08	0.00	0.00	1.39	0.09	22.59	2.16	1.11	15.15	1.70	0.25	31.97
33	2.17	1.25	14.73	0.15	0.00	2.69	1.57	0.10	24.33	1.77	0.79	11.12	1.85	0.30	35.08
34	2.31	1.34	15.19	0.04	0.00	0.00	1.38	0.09	18.84	1.69	0.81	10.98	2.08	0.36	40.78
35	2.11	1.17	13.41	−0.48	−0.01	−8.20	2.16	0.13	32.82	1.80	0.88	11.78	1.27	0.16	23.26
36	1.85	1.02	11.52	−0.15	0.00	−1.89	2.13	0.12	30.89	1.59	0.70	9.29	1.22	0.16	21.79
37	1.97	1.00	11.89	−0.16	0.00	−2.18	1.63	0.11	25.33	1.63	0.73	10.32	1.46	0.23	29.43
38	1.66	0.77	8.39	−0.22	0.00	−4.05	1.74	0.12	24.98	1.14	0.55	7.03	1.29	0.21	26.48
39	0.10	0.07	0.69	−0.28	−0.01	−5.55	1.93	0.12	29.77	−0.16	−0.09	−1.06	0.30	0.04	6.57

Note: Bold text represents a significantly increasing trend, nonbold normal text represents an insignificantly increasing trend, bold italic text represents a significantly decreasing trend, and nonbold italic text represents an insignificantly decreasing trend
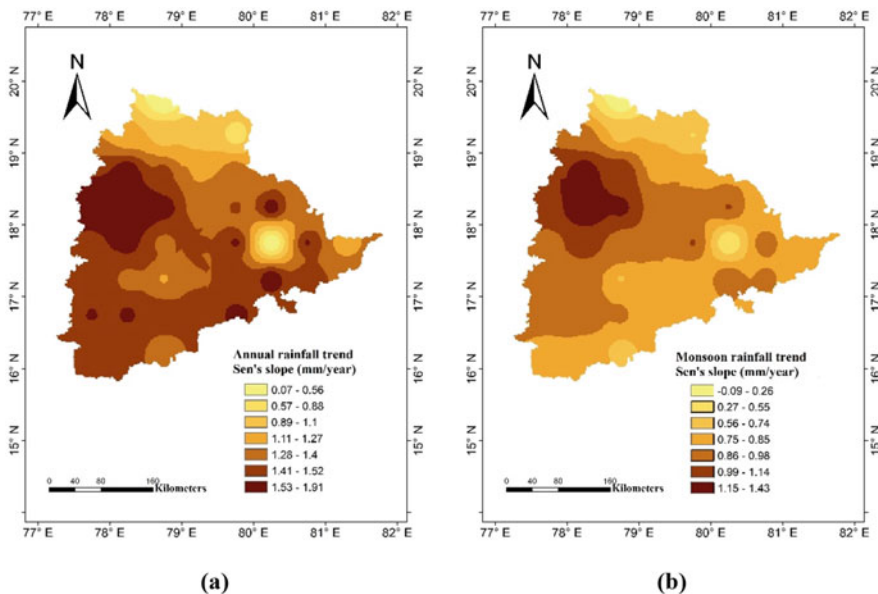
Fig. 15.5 Rainfall trend: (**a**) annual and (**b**) monsoon
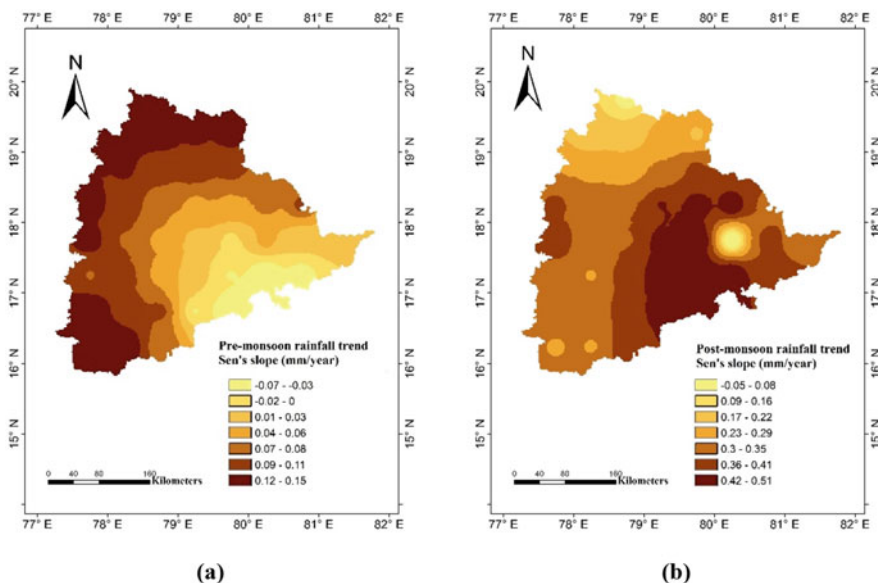
Fig. 15.6 Rainfall trend: (**a**) pre-monsoon and (**b**) post-monsoon

consideration. Since most grid points revealed 1952 as the transition year, the pre- and post-series trends were investigated based on this year. Several climatological researchers adopted a similar consideration to conclude their tentative change point (Duhan and Pandey 2013).

Pre- and Post-change Point Trend Analysis for Annual and Seasonal Rainfall Series

The MK and Sen's estimator tests were performed for the two split annual and seasonal series, whose outcomes are displayed in Tables 15.7 and 15.8, respectively. It could be noticed that no grid point showed a significant positive or negative trend in any seasonal or annual series before and after shift point year though the overall trend for the majority of grids in annual and monsoon season was significantly positive. The combined contribution of pre- and post-shift precipitation resulted in the overall significant increasing trend in the majority of stations in annual and monsoon seasons.

All the grid locations depicted an insignificantly increasing trend for the first part of the annual series (1901–1952). In contrast, the second part (1953–2015) depicted an insignificantly decreasing trend in most stations, with only five stations (#6, #7, #8, #13, and #20) depicting an insignificantly increasing trend in the annual series. On the other hand, grids #14 and #19 did not represent any positive or negative trend in the second half of the split series. Interestingly, the slope values of annual rainfall for the first half (Fig. 15.7a) increased from the south toward the north and north-eastern belts, while the pattern got reversed for the second half of the series (Fig. 15.7b). A similar pattern was observed for the monsoon season, which revealed an insignificantly decreasing rainfall trend in the second part of the series, even though the overall trend was significantly increasing. As a result, the northern regions in the first part of the series had higher slope rates (0.97–1.46 mm/year) when compared to other regions (Fig. 15.8a), and the values of the slopes reached the range of −1.4 to −0.39 mm/year in the second period as depicted in Fig. 15.8b.

Though the annual and monsoon rainfall trend increased for the overall series (1901–2015), a decreasing trend in the second part of the series is attributed to the following reasons. The annual average of the first half of the series was lower (876.34 mm) than the second half (970.40 mm) due to the presence of a maximum number of lower rainfall extrema (18 numbers) whose intensity got enhanced in the second half of the series. Also, the percentage change between the mean rainfalls of both the split series was determined with respect to the average of the first part, as shown in Table 15.9. It was found that the percentage variation was negative for all the annual and monsoon rainfall series. These negative percentages clearly show that the average rainfall of all the grid points in the second part of the series was higher than the first part of the series, which may be attributed to the significantly increasing trend in the overall rainfall series. Moreover, an increase in annual and monsoonal precipitation by 11% and 10%, respectively, was found for the entire region after the shift point. These findings will be helpful for the water managers and agricultural

Table 15.5 Departure analysis

Grid	Normal	Scanty	Deficient	No rain	Excess	Grid	Normal	Scanty	Deficient	No rain	Excess
1	74	4	22	0	15	21	80	3	20	0	12
2	75	4	19	0	17	22	76	0	25	0	14
3	77	3	21	0	14	23	84	0	21	0	10
4	72	4	22	0	17	24	74	3	23	0	15
5	74	3	20	0	18	25	71	3	25	0	16
6	74	3	22	0	16	26	76	2	22	0	15
7	75	0	26	0	14	27	78	2	23	0	12
8	72	0	27	0	16	28	81	1	22	0	11
9	75	3	22	0	15	29	83	1	21	0	10
10	69	3	23	0	20	30	87	1	17	0	10
11	71	2	24	0	18	31	79	2	20	0	14
12	72	1	26	0	16	32	82	2	18	0	13
13	71	0	29	0	15	33	83	1	19	1	11
14	74	0	26	0	15	34	86	1	17	0	11
15	79	0	23	0	13	35	80	1	20	1	13
16	74	3	23	0	15	36	85	1	16	1	12
17	72	3	23	0	17	37	85	0	17	1	12
18	73	3	23	0	16	38	88	0	15	1	11
19	74	1	26	0	14	39	88	2	15	0	10
20	73	1	25	0	16						

Table 15.6 Change point detection

Grid points	Pettitt's test	SNHT	Buishand's test	Grid points	Pettitt's test	SNHT	Buishand's test
1	1946	1946	1946	21	1930	1930	1930
2	1946	1946	1946	22	1952	1952	1952
3	1943	1973	1973	23	1923	1923	1953
4	1942	1942	1946	24	1946	1946	1946
5	1946	1946	1946	25	1952	1952	1952
6	1946	1952	1952	26	1952	1952	1952
7	1952	1974	1952	27	1952	1952	1952
8	1952	1987	1974	28	1952	1952	1952
9	1946	1946	1946	29	1952	1952	1952
10	1946	1946	1946	30	1923	1923	1924
11	1952	1952	1952	31	1952	1952	1952
12	1952	1952	1952	32	1952	1952	1952
13	1952	1952	1952	33	1952	1930	1952
14	1952	1952	1952	34	1952	1930	1952
15	1952	1953	1953	35	1930	1930	1930
16	1946	1946	1946	36	1930	1930	1930
17	1946	1946	1952	37	1930	1930	1930
18	1952	1952	1952	38	1930	1930	1930
19	1952	1952	1952	39	1930	1930	1930
20	1952	1952	1952				

scientists to plan for water management and the best cropping practices to be adopted in the Telangana region.

The winter season showed a flattened decreasing trend in 1901–1952, which shifted to a nearly significantly increasing trend in 1953–2015. However, these findings may not help plan water management goals since the winter season's annual contribution is insignificant. Also, the slope values in the second split half series were very low, which may not greatly affect the overall rainfall accumulation.

Between 1901 and 1952, post-monsoon had an insignificantly increasing trend that continued in the second part of the shift (1953–2015), except in grids #21, #23, #35, and #39, which showed an insignificantly decreasing trend. Although the change in the MK values that incurred between the split seasons were lower, there were severe divergences in the percentage variation of rainfall between the series. Between 1901 and 1952, the slopes for the post-monsoon were higher in the eastern region (Fig. 15.9a), which shifted to the southeast region in the second part of the series (Fig. 15.9b).

In the pre-monsoon season, most grid locations had an insignificantly increasing rainfall trend before and after the shift point year, with only nine grid points depicting an insignificantly decreasing trend in the second half. As a result, a gradual increase in the slope value was observed toward the northeast regions (Fig. 15.10a)

Table 15.7 Trend before and after the change point

	Annual						Seasonal						Pre-monsoon					
	1901–1952			1953–2015			Winter						1901–1952			1953–2015		
							1901–1952			1953–2015								
Grid	Z	B	% Change	Z	B	% Change	Z	B	% Change	Z	B	% Change	Z	B	% Change	Z	B	% Change
1	0.62	1.01	7.49	−0.27	−0.32	−2.56	−0.57	0.00	−5.86	1.73	0.01	28.20	0.46	0.11	12.63	0.29	0.07	6.35
2	0.72	1.16	8.71	−0.17	−0.18	−1.47	−0.83	−0.02	−14.50	1.94	0.02	26.48	0.61	0.20	21.77	0.30	0.08	7.25
3	0.95	1.12	8.97	−0.50	0.51	4.39	−0.75	−0.03	−16.82	1.83	0.05	40.25	0.38	0.08	8.44	0.78	0.15	14.39
4	0.62	1.07	7.14	−0.49	−0.46	−3.23	0.05	0.00	0.00	1.47	0.01	19.02	0.45	0.13	15.84	0.12	0.03	3.01
5	0.80	0.94	6.53	−0.31	−0.34	−2.53	−0.41	−0.01	−9.30	1.63	0.02	20.40	0.44	0.09	10.45	0.24	0.06	5.95
6	0.60	0.94	7.03	0.27	0.42	3.35	−0.92	−0.04	−20.96	1.76	0.04	24.86	0.58	0.14	16.19	0.38	0.07	7.48
7	0.56	0.68	4.85	0.46	0.62	4.77	−0.10	−0.05	−27.16	1.48	0.05	26.12	0.28	0.07	7.60	0.27	0.06	6.47
8	0.75	1.06	6.71	0.58	0.73	5.04	−0.64	−0.03	−16.51	1.66	0.09	47.63	0.46	0.07	6.19	0.31	0.09	8.18
9	0.24	0.60	3.87	−0.59	−0.72	−4.97	0.11	0.00	0.00	1.49	0.02	24.19	0.47	0.13	14.51	−0.14	−0.03	−2.92
10	0.50	0.77	5.23	−0.50	−0.66	−4.84	−0.01	0.00	0.00	1.66	0.03	23.14	0.45	0.13	14.50	−0.07	−0.02	−1.95
11	0.30	0.33	2.40	−0.32	−0.33	−2.58	−0.47	−0.02	−8.48	1.55	0.04	21.07	0.57	0.12	13.07	−0.04	−0.01	−0.59
12	0.32	0.57	3.91	−0.05	−0.04	−0.33	−1.06	−0.06	−25.48	1.39	0.05	22.98	0.03	0.00	0.00	0.22	0.03	3.36
13	0.69	1.20	7.33	0.27	0.34	2.23	−0.48	−0.02	−7.43	1.42	0.05	26.39	0.62	0.18	16.40	0.15	0.04	3.70
14	1.00	1.86	10.01	0.00	−0.01	−0.04	−0.09	0.00	0.00	1.37	0.05	31.92	1.03	0.41	28.39	0.52	0.17	12.60
15	1.18	1.83	9.67	−0.05	−0.05	−0.31	−0.06	0.00	0.00	1.24	0.05	28.30	0.73	0.36	24.04	1.03	0.31	22.00
16	0.70	1.15	6.97	−0.69	−0.90	−5.90	0.19	0.01	3.95	1.53	0.05	32.14	0.92	0.21	24.30	−0.02	−0.02	−1.98
17	0.56	0.76	4.62	−0.43	−0.70	−4.56	−0.60	−0.02	−8.18	1.75	0.05	31.08	0.74	0.18	21.25	0.01	0.00	0.32
18	0.36	0.50	3.25	−0.21	−0.29	−2.01	−0.37	−0.02	−5.69	1.55	0.06	29.75	0.73	0.20	23.38	−0.12	−0.01	−1.09
19	0.47	0.95	6.02	0.00	−0.01	−0.04	0.00	0.00	0.00	1.61	0.08	35.75	0.62	0.16	19.02	−0.02	0.00	−0.23
20	0.60	1.11	6.56	0.07	0.12	0.76	0.12	0.01	1.92	1.57	0.08	37.76	0.64	0.22	22.02	0.08	0.02	2.04
21	1.22	1.88	13.44	−1.36	−1.22	−10.11	0.27	0.02	7.56	1.50	0.07	50.97	0.00	0.00	0.00	−0.03	0.00	0.00

(continued)

Table 15.7 (continued)

Grid	Annual						Seasonal Winter						Pre-monsoon					
	1901–1952			1953–2015			1901–1952			1953–2015			1901–1952			1953–2015		
	Z	B	% Change	Z	B	% Change	Z	B	% Change	Z	B	% Change	Z	B	% Change	Z	B	% Change
22	1.13	1.88	9.49	−0.24	−0.39	−2.18	0.24	0.01	3.27	1.41	0.05	29.87	0.95	0.43	28.98	1.20	0.40	28.80
23	1.48	2.62	12.39	−0.34	−0.39	−2.09	0.52	0.04	16.62	1.26	0.05	27.58	0.95	0.51	32.19	1.19	0.48	31.80
24	0.77	1.54	8.47	−0.65	−1.00	−5.91	0.00	0.00	0.00	1.80	0.08	51.78	0.86	0.22	29.70	0.20	0.03	3.49
25	0.95	1.70	9.16	−0.43	−0.70	−4.01	−0.11	0.00	−1.39	1.69	0.07	39.05	0.95	0.23	30.82	0.08	0.01	1.20
26	0.47	1.22	7.04	−0.18	−0.35	−2.19	−0.46	−0.02	−7.37	1.64	0.09	36.78	1.05	0.26	34.81	−0.02	−0.01	−1.24
27	0.21	0.50	2.95	−0.19	−0.34	−2.18	−0.51	−0.04	−12.89	1.55	0.09	35.50	0.96	0.27	37.18	0.20	0.04	4.60
28	0.97	1.67	9.47	−0.07	−0.13	−0.82	0.93	0.10	32.36	1.52	0.09	40.01	1.22	0.31	35.17	−0.03	0.00	0.00
29	0.99	1.91	10.02	−0.11	−0.19	−1.09	0.88	0.06	21.54	1.49	0.08	38.81	0.77	0.31	28.05	0.52	0.10	9.19
30	1.55	2.48	11.79	−0.20	−0.30	−1.58	1.06	0.09	36.41	1.09	0.06	30.89	1.16	0.45	33.07	0.72	0.21	15.25
31	1.11	2.02	10.82	−0.73	−0.92	−5.29	0.49	0.05	13.82	1.82	0.14	55.88	1.27	0.31	43.70	0.01	0.01	0.61
32	0.83	1.59	8.89	−0.38	−0.64	−3.92	0.00	0.00	0.00	1.68	0.10	43.55	1.25	0.23	33.86	0.16	0.03	4.27
33	0.68	1.44	8.09	−0.28	−0.41	−2.55	0.15	0.01	5.96	1.76	0.09	48.22	1.52	0.27	37.91	0.27	0.05	6.40
34	0.97	2.00	10.78	−0.25	−0.31	−1.86	0.81	0.06	25.58	1.51	0.08	45.59	1.52	0.29	35.52	0.18	0.02	2.68
35	1.10	2.21	12.09	−0.83	−1.21	−7.29	0.47	0.08	21.37	1.86	0.14	57.11	1.32	0.27	41.20	0.23	0.03	3.83
36	1.40	2.36	12.60	−0.61	−0.72	−4.33	0.61	0.06	21.92	1.78	0.13	59.31	1.60	0.33	48.78	0.33	0.05	6.37
37	1.32	2.75	15.43	−0.45	−0.68	−4.30	1.04	0.08	35.47	1.86	0.09	59.12	1.85	0.41	53.45	0.24	0.03	3.61
38	1.21	2.57	13.02	−0.36	−0.42	−2.43	1.09	0.11	37.65	1.78	0.10	54.41	1.47	0.34	42.28	0.35	0.06	6.89
39	1.13	1.87	8.99	−0.84	−1.10	−6.32	1.11	0.14	36.11	1.54	0.14	53.45	1.27	0.23	33.98	0.41	0.07	8.86

Note: Bold text represents a significantly increasing trend, nonbold normal text represents an insignificantly increasing trend, bold italic text represents a significantly decreasing trend, and nonbold italic text represents an insignificantly decreasing trend

Table 15.8 Trend before and after change point – Cont

	Seasonal											
	Monsoon						Post-monsoon					
	1901–1952			1953–2015			1901–1952			1953–2015		
Grid	Z	B	% Change	Z	B	% Change	Z	B	% Change	Z	B	% Change
1	*-0.01*	-0.01	-0.10	*-0.98*	-1.01	-10.60	1.08	0.48	22.17	0.68	0.28	13.72
2	0.02	0.01	0.10	*-1.02*	-1.06	-11.62	0.80	0.42	17.86	0.88	0.39	18.33
3	0.09	0.11	1.34	*-0.91*	-0.74	-9.63	0.54	0.46	15.56	1.15	0.58	21.84
4	0.04	0.10	0.84	*-0.77*	-0.87	-7.80	1.03	0.46	23.40	0.58	0.24	12.44
5	0.10	0.24	2.15	*-0.93*	-0.92	-8.75	0.91	0.42	20.38	0.78	0.31	15.69
6	0.10	0.08	0.83	*-0.57*	-0.55	-6.07	0.58	0.37	14.83	0.88	0.55	23.32
7	*-0.07*	-0.10	-1.03	*-0.47*	-0.54	-5.99	0.70	0.57	19.16	0.98	0.62	22.19
8	*-0.13*	-0.16	-1.45	*-0.37*	-0.39	-3.83	0.86	0.66	20.63	1.00	0.71	23.44
9	*-0.40*	-0.08	-0.65	*-0.74*	-1.03	-9.07	0.80	0.32	16.41	0.53	0.24	12.21
10	0.02	0.04	0.35	*-0.82*	-0.96	-9.12	0.36	0.21	10.55	0.57	0.21	10.78
11	0.18	0.30	2.92	*-0.87*	-0.93	-9.91	0.25	0.20	9.38	0.62	0.29	13.68
12	0.01	0.04	0.37	*-0.98*	-0.96	-9.63	0.40	0.36	14.99	0.84	0.51	21.20
13	*-0.24*	-0.30	-2.44	*-0.82*	-0.68	-6.03	0.82	0.71	28.05	0.90	0.53	20.76
14	0.10	0.12	0.86	*-0.91*	-1.00	-7.71	0.13	0.92	34.14	0.68	0.35	13.15
15	0.06	0.12	0.86	*-0.73*	-0.94	-7.34	1.20	0.97	32.37	0.12	0.12	4.25
16	0.23	0.46	3.45	*-0.83*	-0.93	-7.65	0.10	0.03	1.60	0.71	0.26	12.96
17	0.39	0.60	4.48	*-0.83*	-1.00	-8.06	0.07	0.05	2.83	0.47	0.22	11.87
18	0.50	0.60	4.89	*-0.73*	-0.89	-7.96	0.06	0.02	1.10	0.34	0.12	6.28
19	0.31	0.36	2.90	*-0.69*	-0.80	-7.05	0.45	0.26	12.68	0.74	0.32	14.95
20	0.06	0.08	0.60	*-0.60*	-0.64	-5.26	0.46	0.30	13.67	0.75	0.41	17.81
21	0.79	1.40	11.47	*-1.07*	-1.05	-9.92	0.09	0.43	33.11	*-1.58*	-0.39	-37.02
22	0.09	0.13	0.86	*-0.76*	-0.99	-7.17	1.32	0.90	33.67	0.15	0.11	4.16

(continued)

Table 15.8 (continued)

Grid	Seasonal											
	Monsoon						Post-monsoon					
	1901–1952			1953–2015			1901–1952			1953–2015		
	Z	B	% Change	Z	B	% Change	Z	B	% Change	Z	B	% Change
23	0.36	0.61	3.88	-0.73	-0.82	-5.85	1.48	0.10	3.03	-0.23	-0.15	-4.91
24	0.53	0.91	5.89	-0.72	-1.25	-8.86	0.13	0.06	3.72	0.37	0.19	10.62
25	0.70	1.27	7.96	-0.82	-1.14	-7.66	0.30	0.17	11.38	0.14	0.08	4.81
26	0.73	1.19	8.17	-0.65	-0.71	-5.31	0.39	0.20	12.65	0.27	0.10	5.87
27	0.23	0.37	2.65	-0.56	-0.74	-5.85	0.50	0.29	16.21	0.33	0.15	7.90
28	0.20	0.49	3.42	-0.41	-0.58	-4.47	0.73	0.47	24.39	0.49	0.26	12.77
29	0.21	0.38	2.46	-0.57	-0.85	-6.04	1.18	0.68	34.10	0.44	0.24	11.43
30	0.53	0.92	5.47	-0.66	-0.69	-4.66	1.63	0.99	42.55	0.10	0.05	2.22
31	0.60	1.24	7.71	-0.69	-0.98	-6.60	0.50	0.22	15.77	0.13	0.05	3.39
32	0.72	1.34	8.76	-0.62	-0.95	-6.82	0.87	0.39	25.70	0.26	0.11	7.18
33	0.60	0.92	6.12	-0.67	-0.75	-5.57	1.05	0.53	31.69	0.39	0.14	8.36
34	0.39	0.68	4.36	-0.73	-0.87	-6.24	1.28	0.81	46.91	0.45	0.22	12.55
35	0.72	0.98	6.23	-1.13	-1.38	-9.71	0.95	0.42	30.04	-0.19	-0.09	-6.69
36	0.78	1.43	8.88	-0.80	-0.98	-6.88	0.92	0.42	27.71	0.12	0.07	4.99
37	0.90	1.46	9.66	-0.53	-0.68	-5.08	1.07	0.59	37.99	0.08	0.03	1.99
38	0.73	1.28	7.59	-0.68	-0.83	-5.62	1.03	0.62	38.17	0.11	0.06	3.97
39	0.58	0.93	5.14	-0.97	-1.20	-7.94	0.10	0.52	34.47	-0.27	-0.12	-9.68

Note: Bold text represents a significantly increasing trend, nonbold normal text represents an insignificantly increasing trend, bold italic text represents a significantly decreasing trend, and nonbold italic text represents an insignificantly decreasing trend
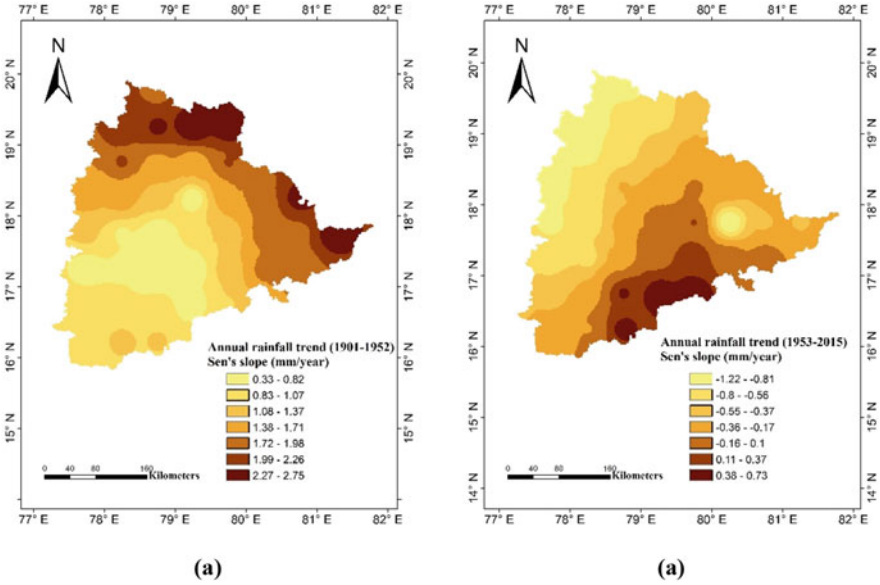
Fig. 15.7 Annual rainfall trend: (**a**) 1901–1952 and (**b**) 1953–2015
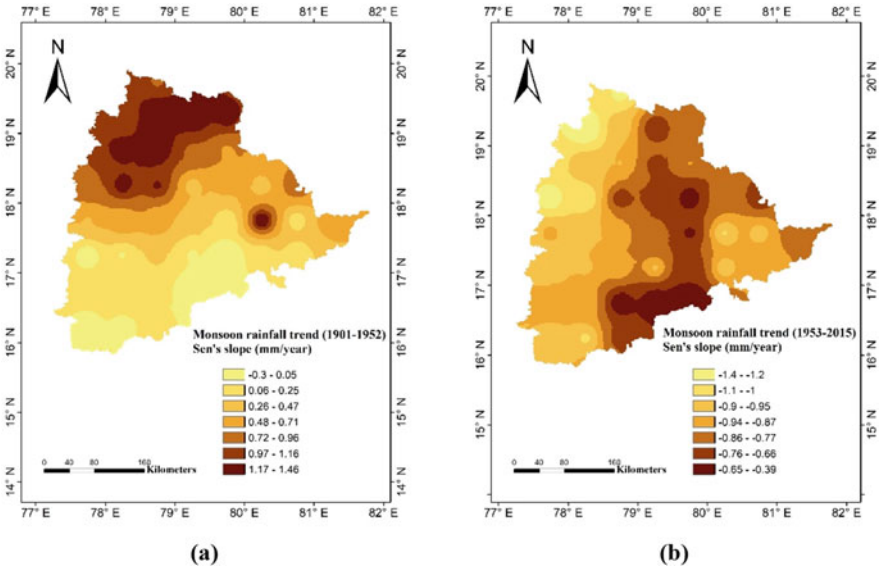
Fig. 15.8 Monsoon rainfall trend: (**a**) 1901–1952 and (**b**) 1953–2015

in the first part, and in the second part, an increase in the slope value was noticed in the eastern regions (Fig. 15.10b).

Table 15.9 Percentage variation before and after the change point year

Grid	Percentage change		Grid	Percentage change		Grid	Percentage change		Grid	Percentage change	
	Annual	Monsoon		Annual	Monsoon		Annual	Monsoon		Annual	Monsoon
1	−0.14	−0.13	11	−0.12	−0.11	21	−0.04	−0.05	31	−0.13	−0.12
2	−0.13	−0.13	12	−0.12	−0.11	22	−0.10	−0.10	32	−0.11	−0.10
3	−0.12	−0.13	13	−0.12	−0.11	23	−0.07	−0.08	33	−0.10	−0.08
4	−0.14	−0.13	14	−0.12	−0.12	24	−0.13	−0.11	34	−0.09	−0.08
5	−0.14	−0.14	15	−0.10	−0.11	25	−0.15	−0.13	35	−0.10	−0.09
6	−0.14	−0.14	16	−0.13	−0.10	26	−0.13	−0.11	36	−0.08	−0.07
7	−0.12	−0.12	17	−0.13	−0.12	27	−0.11	−0.10	37	−0.08	−0.07
8	−0.11	−0.12	18	−0.12	−0.11	28	−0.11	−0.10	38	−0.06	−0.06
9	−0.13	−0.11	19	−0.12	−0.11	29	−0.11	−0.10	39	−0.01	−0.01
10	−0.12	−0.12	20	−0.12	−0.11	30	−0.07	−0.07			
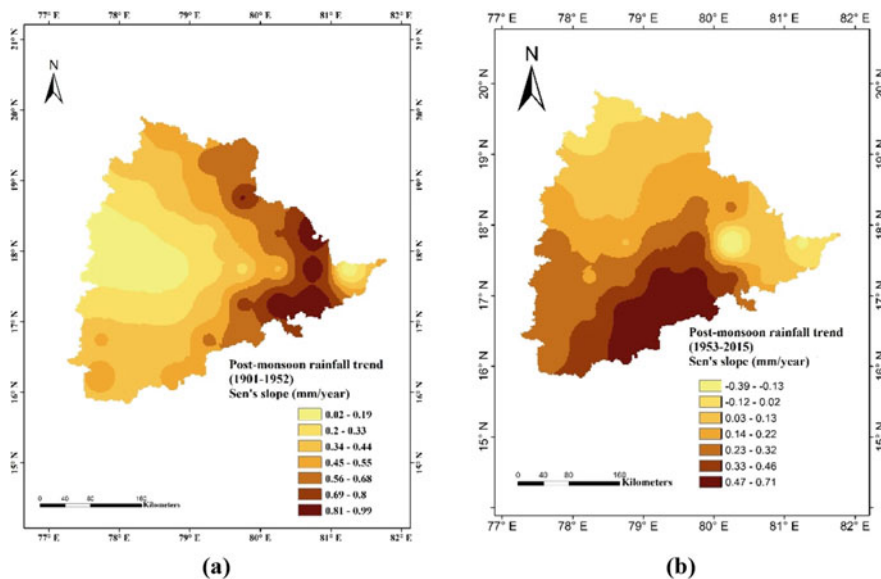
Fig. 15.9 Post-monsoon rainfall trend: (**a**) 1901–1952 and (**b**) 1953–2015

Conclusion

The rainfall analysis for the state of Telangana for the period of 115 years (1901–2015) was carried out to understand the spatial and temporal shifts in the rainfall. The annual mean rainfall for the entire state was found to be 927.87 mm, and the average seasonal rainfall values for winter, pre-monsoon, monsoon, and post-monsoon were 11.3 mm, 59.45 mm, 738.65 mm, and 118.47 mm, respectively. The annual and monsoon precipitation values were higher in Telangana's north and northeastern grids than its southern counterparts. In contrast, the post-monsoon rainfall values were higher in the south and southeast regions. Departure analysis showed the percentage occurrence of normal, excess, deficient, and scanty years as 67%, 12%, 19%, and 2%, respectively. The Mann–Kendall test showed a significant increase in the annual and monsoonal rainfall, with a maximum slope being 1.91 mm/year and 1.43 mm/year, respectively, for the entire period. Although an insignificantly decreasing trend was noticed in most grids for the winter season, its contribution to the overall annual rainfall is negligible. The majority of the grid points experienced an insignificantly increasing trend in the pre-monsoon season and a significantly increasing trend in the post-monsoon season. Pettitt's test, SNHT, and Buishand's test provided the most probable change point year as 1952. The percentage change in the average annual rainfall before and after the change point year was not much higher, but the annual and seasonal averages of all the grid points in the second part of the series (1953–2015) except for winter surpassed the first part (1901–1952).
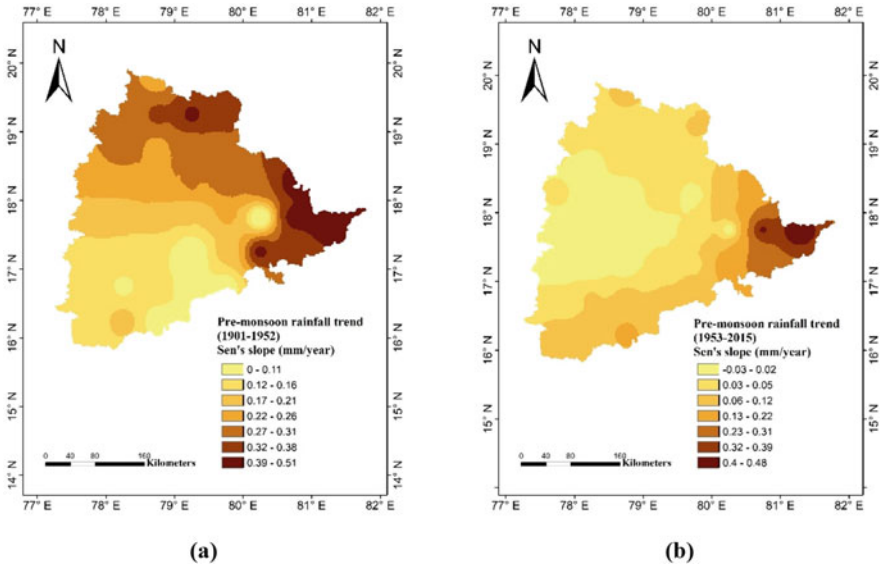
Fig. 15.10 Pre-monsoon rainfall trend: (**a**) 1901–1952 and (**b**) 1953–2015

Further, the trend analysis for the two split series revealed an insignificantly increasing trend before the shift point, which got reversed in the latter half, resulting in an insignificantly decreasing trend in all the grids. The comparatively lower slope of the rainfall trend and the improved lower extrema for the second period (1953–2015) and the negative percentages of all the grid points by the percentage change analysis validate the claim of the overall rainfall trend as increasing. The findings show that due to the increase in rainfall the cultivation of rainfed and irrigated crops may not get affected in the Telangana region.

Conflict of Interest On behalf of all authors, the corresponding author states that there is no conflict of interest.

Data Availability Statement All rainfall data used during the study are available online in accordance with funder data retention policies (https://doi.org/10.1038/s41597-020-0453-3).

References

Alexandersson H, Moberg A (1997) Homogenization of Swedish temperature data. Part I: homogeneity test for linear trends. Int J Climatol 17(1):25–34. https://doi.org/10.1002/(SICI)1097-0088(199701)17:1%3C25::AID-JOC103%3E3.0.CO;2-J

Bari SH, Rahman MTU, Hoque MA, Hussain MM (2016) Analysis of seasonal and annual rainfall trends in the northern region of Bangladesh. Atmos Res 176:148–158. https://doi.org/10.1016/j.atmosres.2016.02.008

Buishand TA (1982) Some methods for testing the homogeneity of rainfall records. J Hydrol 58:11–27. https://doi.org/10.1016/0022-1694(82)90066-X

Chandra R, Jain SK, Singh AK (2018) Assessment of ground water resources for irrigation in Nalanda District of South Bihar, India. Int J Curr Microbiol App Sci 7:1223–1232. https://doi.org/10.20546/ijcmas.2018.702.150

Chatterjee R, Gupta BK, Mohiddin SK, Singh PN, Shekhar S, Purohit R (2009) Dynamic groundwater resources of National Capital Territory, Delhi: assessment, development and management options. Environ Earth Sci 59:669. https://www.jstor.org/stable/24104886

Chatterjee S, Khan A, Akbari H, Wang Y (2016) Monotonic trends in spatio-temporal distribution and concentration of monsoon precipitation (1901–2002), West Bengal, India. Atmos Res 182:54–75. https://doi.org/10.1016/j.atmosres.2016.07.010

Duhan D, Pandey A (2013) Statistical analysis of long term spatial and temporal trends of precipitation during 1901–2002 at Madhya Pradesh, India. Atmos Res 122:136–149. https://doi.org/10.1016/j.atmosres.2012.10.010

Fischlin A, Midgley GF, Price JT, Leemans R, Gopal B, Turley C, Rounsevell MDA, Dube OP, Tarazona J, Velichko AA (2007) Ecosystems, their properties, goods, and services. In: Parry ML, Canziani OF, Palutikof JP, Hanson CE (eds) Climate change 2007: impacts, adaptation and vulnerability. Contribution of working group II to the fourth assessment report of the intergovernmental panel on climate change. Cambridge University Press, Cambridge, pp 212–272. http://plymsea.ac.uk/id/eprint/4614

Gitay H, Suárez A, Watson RT, Dokken DJ (2002) Climate change and biodiversity Intergovernmental Panel on Climate Change. Geneva, Switzerland. https://archive.ipcc.ch/pdf/technical-papers/climate-changes-biodiversity-en.pdf

Goswami BN, Venugopal V, Sengupta D, Madhusoodanan MS, Xavier PK (2006) Increasing trend of extreme rain events over India in a warming environment. Science 314:1442–1445. https://doi.org/10.1126/science.1132027

Goutam Kumar Ghosh and Kapil Ghosh (2019) Spatio-temporal analysis of rainfall pattern in North District, Sikkim, India. Int Adv Res J Sci Eng Technol 6:87–92

Goyal MK (2014) Statistical analysis of long term trends of rainfall during 1901–2002 at Assam, India. Water Resour Manag 28:1501–1515

Guhathakurta P, Rajeevan M (2008) Trends in the rainfall pattern over India. Int J Climatol 28:1453–1469. https://doi.org/10.1002/joc.1640

Hamed KH (2008) Trend detection in hydrologic data: the Mann–Kendall trend test under the scaling hypothesis. J Hydrol 349:350–363. https://doi.org/10.1016/j.jhydrol.2007.11.009

Harris I, Osborn TJ, Jones P, Lister D (2020) Version 4 of the CRU TS monthly high-resolution gridded multivariate climate dataset. Sci Data 7:1–18. https://doi.org/10.1038/s41597-020-0453-3

IMD (India Meteorological Department) (2017) Terminologies and glossary, August 5. http://imd.gov.in/section/nhac/termglossary.pdf

IPCC, 2007: Climate Change (2007) Synthesis Report. Contribution of Working Groups I, II and III to the Fourth Assessment Report of the Intergovernmental Panel on Climate Change [Core Writing Team, Pachauri, R.K and Reisinger, A. (eds.)]. IPCC, Geneva, Switzerland, 104 pp.

Inkley DB, Anderson MG, Blaustein, AR, Burkett V, Felzer B, Griffith B, Price J, Root TL (2004) Global climate change and wildlife in North America (No. 04-2, pp 1–26). Technical Review Committee on Global Climate Change and Wildlife, Wildlife Society. http://wildlife.org/wp-content/uploads/2014/05/ClimateChange04-2.pdf

Jain SK, Kumar V, Saharia M (2013) Analysis of rainfall and temperature trends in northeast India. Int J Climatol 33:968–978. https://doi.org/10.1002/joc.3483

Joshi MK, Pandey AC (2011) Trend and spectral analysis of rainfall over India during 1901–2000. J Geophys Res D: Atmos 116(D6). https://doi.org/10.1029/2010JD014966

Kant S, Meshram S, Sahu KC (2014) Analysis of rainfall data for drought investigation at Agra U.P. Recent Res Sci Technol 6:62–64. https://updatepublishing.com/journal/index.php/rrst/article/view/1166

Kendall MG (1975) Rank correlation methods. Charles Grifn and Co. Ltd, London

Kishtawal CM, Krishnamurti TN (2001) Diurnal variation of summer rainfall over Taiwan and its detection using TRMM observations. J Appl Meteorol 40:331–344. https://doi.org/10.1175/1520-0450(2001)040%3C0331:DVOSRO%3E2.0.CO;2

Kocsis T, Kovács-Székely I, Anda A (2020) Homogeneity tests and non-parametric analyses of tendencies in precipitation time series in Keszthely, Western Hungary. Theor Appl Climatol 139:849–859. https://doi.org/10.1007/s00704-019-03014-4

Kumar CP (2013) 3-Assessment of groundwater potential. Int J Eng Sci 1:64–79. http://doi.ord/117.252.14.250

Kumar V, Jain SK, Singh Y (2010) Analysis of long-term rainfall trends in India. Hydrol Sci J 55:484–496. https://doi.org/10.1080/02626667.2010.481373

Kumar A, Anand S, Kumar M, Chandra R (2017) Groundwater assessment: a case study in Patna and Gaya District of Bihar, India. Int J Curr Microbiol App Sci 6:184–195

Kundu S, Khare D, Mondal A, Mishra PK (2014) Long term rainfall trend analysis (1871–2011) for whole India. In: Climate change and biodiversity. Springer, Tokyo, pp 45–60. https://doi.org/10.1007/978-4-431-54838-6_4

Liu CH, Ma X, Li F, Wang YJ, Tie CL, Li SF, Chen TL, Fan TT, Zhang Y, Dong J, Yao L (2012) Regional homogeneity within the default mode network in bipolar depression: a resting-state functional magnetic resonance imaging study. PLoS One 7(11):e48181. https://doi.org/10.1371/journal.pone.0048181

Maragatham RS (2012) Trend analysis of rainfall data – a comparative study of existing methods. Int J Phys Math Sci 2:13–18

Mawdsley JR, O'malley R, Ojima DS (2009) A review of climate change adaptation strategies for wildlife management and biodiversity conservation. Conserv Biol 23:1080–1089. https://doi.org/10.1111/j.1523-1739.2009.01264.x

Meshram SG, Singh VP, Meshram C (2017) Long-term trend and variability of precipitation in Chhattisgarh State, India. Theor Appl Climatol 129:729–744. https://doi.org/10.1007/s00704-016-1804-z

Mishra AK, Singh VP (2011) Drought modeling: a review. J Hydrol 403:157–175. https://doi.org/10.1016/j.jhydrol.2011.03.049

Mohammad P, Goswami A (2019) Temperature and precipitation trend over 139 major Indian cities: an assessment over a century. Model Earth Syst Environ 5:1481–1493. https://doi.org/10.1007/s40808-019-00642-7

Mondal A, Khare D, Kundu S (2015) Spatial and temporal analysis of rainfall and temperature trend of India. Theor Appl Climatol 122:143–158. https://doi.org/10.1007/s00704-014-1283-z

Murari K, Kumar G, Pandey V (2016) Ground water recharge potential of the Dhanbad District, Jharkhand – a case study. Int J Sci Technol Eng Technol 2:29–37

Nicholls RJ, Cazenave A (2010) Sea-level rise and its impact on coastal zones. Science 328:1517–1520. https://doi.org/10.1126/science.1185782

Nicholls RJ, Hanson SE, Lowe JA, Warrick RA, Lu X, Long AJ (2014) Sea level scenarios for evaluating coastal impacts. Wiley Interdiscip Rev Clim Chang 5:129–150. https://doi.org/10.1002/wcc.253

Nico W, Van Lanen AJ, Loon AF (2010) Indicators for drought characterization on a globalscale, Wageningen, Netherlands. Water Global Change 24:80–93

Parthasarathy B, Dhar ON (1974) Secular variations of regional rainfall over India. Q J R Meteorol Soc 100:245–257. https://doi.org/10.1002/qj.49710042411

Patra JP, Mishra A, Singh R, Raghuwanshi NS (2012) Detecting rainfall trends in twentieth century (1871–2006) over Orissa State, India. Clim Chang 111:801–817. https://doi.org/10.1007/s10584-011-0215-5

Pettitt AN (1979) A non-parametric approach to the change point problem. J R Stat Soc 28:126–135. https://doi.org/10.2307/2346729

Piao S, Ciais P, Huang Y, Shen Z et al (2010) The impacts of climate change on water resources and agriculture in China. Nature 467:43–51. https://doi.org/10.1038/nature09364

Pingale SM, Khare D, Jat MK, Adamowski J (2014) Spatial and temporal trends of mean and extreme rainfall and temperature for the 33 urban centers of the arid and semi-arid state of Rajasthan, India. Atmos Res 138:73–90. https://doi.org/10.1016/j.atmosres.2013.10.024

Praveen B, Talukdar S, Mahato S, Mondal J, Sharma P, Islam ARMT, Rahman A (2020) Analyzing trend and forecasting of rainfall changes in India using non-parametrical and machine learning approaches. Sci Rep 10:1–21

Rangarajan S, Thattai D, Yellasiri SRR, Vytla R, Tedla N, Mandalemula B (2018) Detecting changes in annual and seasonal rainfall patterns for Chennai, India. J Hydrol Eng. https://doi.org/10.1061/(ASCE)HE.1943-5584.0001630

Rangarajan S, Thattai D, Cherukuri A, Borah TA, Joseph JK, Subbiah A (2019) A detailed statistical analysis of rainfall of Thoothukudi District in Tamil Nadu (India). In: Water resources and environmental engineering II. Springer, Singapore, pp 1–14. https://doi.org/10.1007/978-981-13-2038-5_1

Rao BB, Chowdary PS, Sandeep VM, Rao VUM, Venkateswarlu B (2014) Rising minimum temperature trends over India in recent decades: implications for agricultural production. Glob Planet Chang 117:1–8. https://doi.org/10.1016/j.gloplacha.2014.03.001

Reddy DR, Sreenivas G (2016) Agricultural drought monitoring and management at sub district level in Telangana. Mausam 67:259–266. https://metnet.imd.gov.in/mausamdocs/167121_F.pdf

Reddy DR, Sreenivas G, Mahadevappa SG, Lata AM, Rao SBSN, Varma N, Gopala R (2007) Rainfall variability and its impact on agriculture in north Telangana regions of Andhra Pradesh. J Agrometeorol 9:253–258

Rohan SG, Purandar BK, Jasmin (2017) Estimation of groundwater balance of Bailhongal Taluk Belagavi district. Int J Innov Res Sci Eng Technol 6(8). https://doi.org/10.15680/IJIRSET.2017.0608128

Root TL, Schneider SH (2002) Climate change: overview and implications for wildlife. In: Wildlife responses to climate change: North American case studies, 10, pp 765–766. https://stephenschneider.stanford.edu/Publications/PDF_Papers/Overview%281-56%29.pdf

Root TL, Price JT, Hall KR, Schneider SH, Rosenzweig C, Pounds JA (2003) Fingerprints of global warming on wild animals and plants. Nature 421:57–60. https://doi.org/10.1038/nature01333

Sarkar S, Kafatos M (2004) Interannual variability of vegetation over the Indian sub-continent and its relation to the different meteorological parameters. Remote Sens Environ 90:268–280. https://doi.org/10.1016/j.rse.2004.01.003

Sathyanathan R, Bhutia SY, Jyrwa KL, Jewel TR (2020) Precipitation analysis for the East and South districts of Sikkim, India. In: IOP Conference Series: Materials Science and Engineering. https://doi.org/10.1088/1757-899X/912/6/062071

Schwartz MW, Iverson LR, Prasad AM, Matthews SN, O'Connor RJ (2006) Predicting extinctions as a result of climate change. Ecology 87:1611–1615. https://doi.org/10.1890/0012-9658(2006)87[1611:PEAARO]2.0.CO;2

Sen PK (1968) Estimates of the regression coefficient based on' Kendall's tau. J Am Stat Assoc 63:1379–1389. https://doi.org/10.2307/2285891

State Profile at http://www.telangana.gov.in/

Stenseth NC, Mysterud A, Ottersen G, Hurrell JW, Chan KS, Lima M (2002) Ecological effects of climate fluctuations. Science 297:1292–1296. https://doi.org/10.1126/science.1071281

Talaee PH (2014) Iranian rainfall series analysis by means of non-parametric tests. Theor Appl Climatol 116:597–607. https://doi.org/10.1007/s00704-013-0981-2

Taxak AK, Murumkar AR, Arya DS (2014) Long term spatial and temporal rainfall trends and homogeneity analysis in Wainganga basin, Central India. Weather Clim Extremes 4:50–61. https://doi.org/10.1016/j.wace.2014.04.005

Terminologies and glossary at http://www.imdhyderabad.gov.in

Theil, H. (1950) A rank-invariant method of linear and polynomial regression analysis. Indagationes mathematicae 12(85), 173.

Tian Y, Bai X, Wang S, Qin L, Li Y (2017) Spatial-temporal changes of vegetation cover in Guizhou Province, Southern China. Chin Geogr Sci 27:25–38. https://doi.org/10.1007/s11769-017-0844-3

Villarini G, Serinaldi F, Smith JA, Krajewski WF (2009) On the stationarity of annual flood peaks in the continental United States during the 20th century. Water Resour Res 45(8). https://doi.org/10.1029/2008WR007645

Xia J, She D, Zhang Y, Du H (2012) Spatio-temporal trend and statistical distribution of extreme precipitation events in Huaihe River Basin during 1960–2009. J Geogr Sci 22:195–208. https://doi.org/10.1007/s11442-012-0921-6

Yang P, Ren G, Yan P (2017b) Evidence for a strong association of short-duration intense rainfall with urbanization in the Beijing urban area. J Clim 30:5851–5870. https://doi.org/10.1175/JCLI-D-16-0671.1

Yue S, Hashino M (2003) Long term trends of annual and monthly precipitation in Japan 1. JAWRA J Am Water Resour Assoc 39:587–596. https://doi.org/10.1111/j.1752-1688.2003.tb03677.x

Chapter 16
Causes, Effects, and Remedial Measures of Climate Change in the East Coast of India with Special Reference to the State of Odisha

Tarun Kumar Lohani

Abstract Climate change has put tremendous impact on the environment in the current scenario. The consequences are extensive consequences on the atmosphere, agronomy, water resources, biome, natural reserves, budget, biodiversity, and social security. Odisha, lying in the Eastern Coast of India connecting the Bay of Bengal, has a stretch of 480 km of coastline and is always vulnerable to climate change in terms of heavy storm like cyclones, beach erosion, coastal flooding, storm swell, and denudation. This state has scores of agro-climatic sectors which require improvement in the shape of diverse reworking approaches keeping pace with the ongoing scenario of climate change. Adaptation strategies such as agriculture, fisheries and animal husbandry, water, health, and coastal and disaster risk management have been formulated looking at the vulnerability, food security, and other parameters. Major steps have been initiated to mitigate the impact of climate change; still a lot of further strategies need to be dealt with to keep the region safe and disaster free. These include energy, urban development, transport, industries, and waste disposal. Proper attention must be adhered to embracing judicious policies on energy efficiency based on enactment, modifying state building codes and development codes to improve LULC, transportation, and energy productivities, establishment of new renewable energy policies, assortment and related criterions and reinforce multi-segment parameters to cater to the upcoming challenges related to reduction in poverty and increasing the adaptive capacity. Several initiatives have been undertaken in the government, private, and NGO sectors, but still lack of proper vision, appropriate mission, and slow pace of implementation has jeopardized the entire development.

Keywords Coastal tract · Climate change · Disaster management · Odisha · Vulnerability

T. K. Lohani (✉)
Hydraulic & Water Resources Engineering, Water Technology Institute, Arba Minch University, Arba Minch, Ethiopia
e-mail: tarun.kumar@amu.edu.et

Introduction

Agriculture and rotational farming are the primary sources of livelihood of 70% of the population in the state of Odisha. Though in recent years there has been high growth in industries, but that too is limited in some parts of the region, and hence most of the rural community rely on cultivation and allied sectors. It has been estimated that nearly 40% of the land of the state is used for agronomy, but due to lack of proper irrigation facilities and erratic rainfall, the farmers are compelled to go for a single farming except in a few areas which have been facilitated by irrigation canals (Mishra et al. 2015). This has activated a challenge to ensure food, livelihood, and nutritional security to meet the demand. In spite of the state enjoying significant rainfall due to the advantage of its long coastal tract (Kumar et al. 2010), its uneven distribution of monsoonal rainfall and inconsistency due to the prevailing climate changes have become a challenge (Jena and Dibiat 2020). This results in flood and drought of varying intensity on regular intervals. Due to extreme climatic conditions, the crops face substantial damage due to erratic rainfall (Guhathakurta and Rajeevan 2008). Incidence of frequent natural calamities has put adverse effect on the production of kharif rice, which is the primary crop production of the state. When the region faces acute drought, substantial loss in the production of pulses and oilseeds during both kharif and rabi seasons threaten the state's food reserve. Different plans proposed by various government departments are defined as increase knowledge and capacity, promotion of System of Rice Intensification (SRI), developing efficient micro and drip irrigation, and creation of awareness among farmers on climate change adaptation. The state is rich in minerals and mining which congregates large-scale excavation activities across the state excluding the coastal region. Mining activities on a regular basis trigger global warming, increasing the risk of climate change.

Area Under Study

Odisha is situated in the eastern part of the country endowed with a vast 480 km of coastal tract that starts from the state of West Bengal in the northeast to Andhra Pradesh in the southwest, bounded by the states of Chhattisgarh in the west, Jharkhand in the north, and Andhra Pradesh in the south. Odisha stands as the eighth state by its area comprising 4.7% land mass of India, nearly 3.5% of population, of which 5% are below the poverty line. Although poverty level has reduced from 57% to around 33% in the last decade, the percentage of people living below the poverty line still remains far more than the countrywide average of around 22%. Frequent change in climatic conditions, high rate of poverty, and higher fraction of aboriginal communities with maximum dependency on natural resource have made the state enormously susceptible to climate change. Fast-growing economy and rapid increase in urbanization in numerous clusters too nurture a challenge for mitigation. Odisha has a geographical area of 0.16 million km^2, constituting less than 5% of the
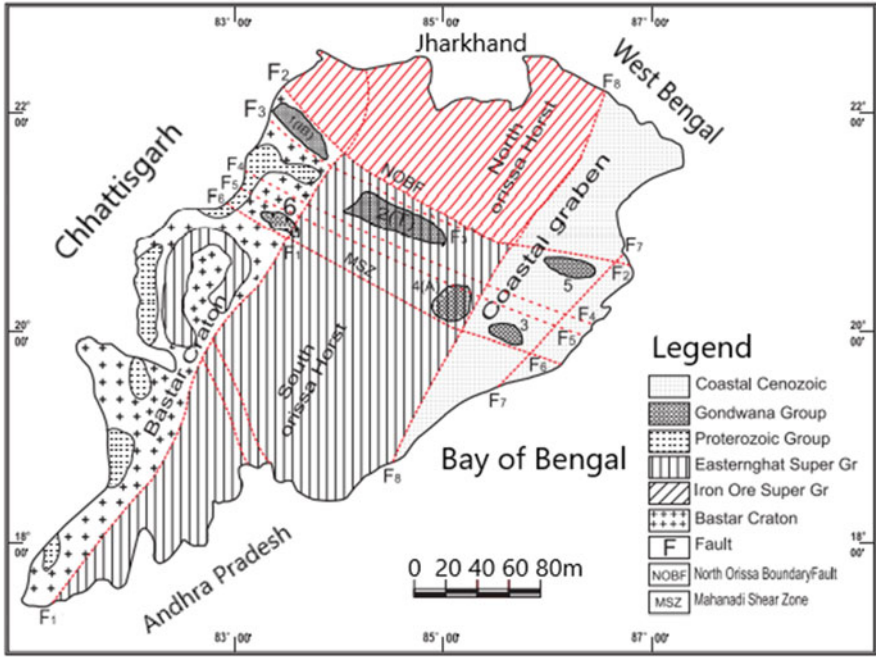
Fig. 16.1 Map of the study area with its geological distribution

total land mass of India. The state of Odisha stretches between 81°31′E to 87°30′E longitudes and 17°31′N to 22°31′N latitudes. It occurs in the eastern region of India surrounded by the states West Bengal, Jharkhand, Andhra Pradesh, Chhattisgarh, and open to the Bay of Bengal on the east, having a coastline of 480 km (Fig. 16.1). The state can be divided into four geographical regions, that is, the Northern Plateau, Eastern Ghats, Central Tableland, and Coastal Plains. A number of imperative rivers like Mahanadi, Brahmani, and Baitarani drain through the state. The state occupies the eleventh position in terms of population in India, with an approximate estimated population of 46.8 million and population density of 270 per km^2. Out of the 41.97 million population, scheduled caste and scheduled tribe communities have strong natural resource dependency and are highly vulnerable to climate change. The geographical location including the coastal tract in the east and Eastern Ghat mountain ranges in the north and northwest make the region more vulnerable to natural calamities, followed by aggressive climate change. The geology of the region also plays a vital role in adding fuel to the calamities. The geological map of Odisha shows the major geological units and structures such as the Gondwana Graben (Mahanadi Graben) running west to east and containing many sedimentary basins, some accommodating the most important coal deposits of the state.

The coal-bearing graben is cut across by the coastal graben which formed subsequently. The eastern border comprises a long coastline with the offshore coastal tract beneath the Bay of Bengal and the onshore coastal tract landward to its west.
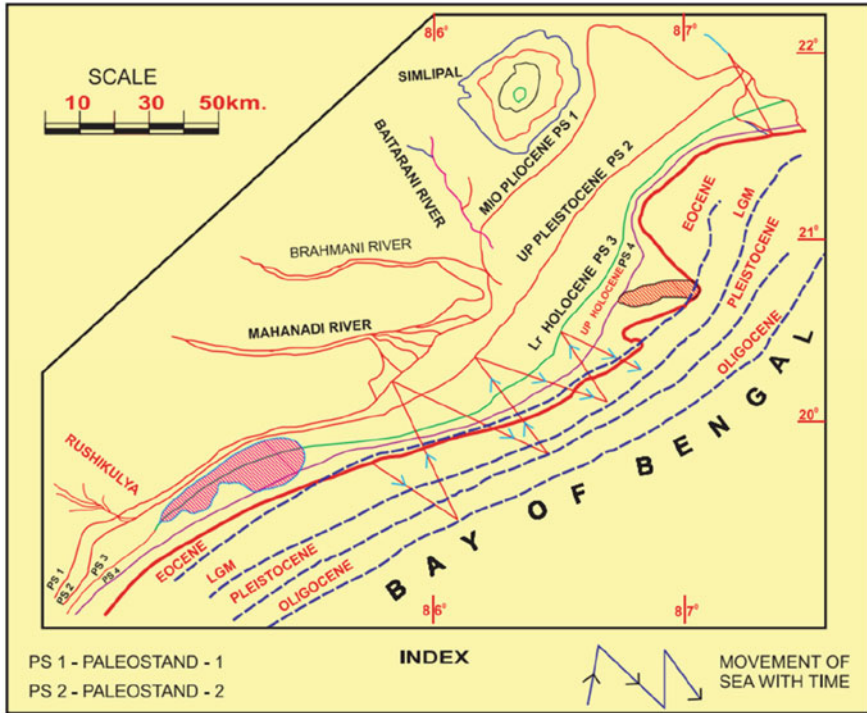
Fig. 16.2 Evolution of coastal tract of Odisha

The structures of ridges and depressions bounded by several west-to-east-running faults cut across by a later set of NE–SW running fault system (Mahalik 2006). The major tectonic features are the North Orissa Boundary Fault, Mahanadi Shear Zone, the Daitari Ridge, the Talcher–Jajpur Depression, the Chandikhol ridge, the Athgarh–Salepur Depression, the Southern ridge, and the Konark Puri Depression (Fig. 16.2). The state is gifted with numerous rivers flowing in every part of the region. Those are the lifeline for the farming community, but on the other hand the low pressure that often occurs in the Bay of Bengal triggers continuous rain for a longer period, increasing the water level in the rivers and aggravating massive flood. Alteration in pressure along the coast that frequently occurs is due to the impact of concurrent climatic changes.

Vulnerability Factors

Climate

It has been studied by different researchers that erratic rainfall has been recorded after 1960, with reducing rainfall across all over the areas every year. Monsoonal

rain normally prevails for 120 days, but due to various factors, including climate change, it has shrunk to a maximum of 60–70 days, yet sometimes there is a heavy shower of rainfall, with severity recorded as 200 mm/day to 250 mm/day that triggers the possibility of flood in all the major drainages. This exhibits a negative impact on agriculture (Khan et al. 2009) because of the reduced residual moisture, especially during the rabi season. The same is the case when there is a possibility of increase in average global temperature of 1−5 °C by 2100. As per the study from RCP 4.5 and RCP 8.5, the mean annual maximum temperature for RCP 4.5 scenario is projected to increase by about 0.4–1.2 °C in near term and 0.8–2.8 °C by mid-century. For RCP 8.5 scenario, it is projected to increase by about 0.7–1.4 °C in near term and 2.0–3.3 °C by mid-century; the mean annual minimum temperature for RCP 4.5 scenario is projected to increase by about 10.3–2.7 °C by near term and 1.6–4.2 °C by mid-century. For RCP 8.5 scenario, it is projected to increase by about 0.6–3.9 °C by near term and 2.0–4.9 °C by mid-century, and the mean annual rainfall for RCP 4.5 scenario is projected to decrease by 4.6% to an increase of 25.7% in the near term and a decrease of 8.2% to an increase of 55.7% towards mid-century in the districts (OCCAP 2018).

The six coastal districts and two northern districts of the state are high in combined risk index. Coastal Odisha remains comparatively less hot than the rest of the areas, even though it is higher by 2 °C. Due to being landlocked and global warming, the north–west, west, and south–west Odisha demonstrate the maximum rise in temperature. This causes negative effect on terrestrial and marine ecosystems. As per the costal vulnerability index (CVI), vulnerability, loss, and damage due to rise in sea level, geomorphology of the coast, tidal array, and increase in the coastal tract varied from low (76 km) of the coastline to medium (297 km) and high (107 km). In the coming 30 years, rise in sea level may adversely affect the long coast of Odisha with high surge and inundation, affecting millions of people residing along the coastline. According to a recent study, it has been projected that the sea level may rise between 2 and 7 feet probably in the next three decades, resulting in medium to severe flood, changing the entire scenario of the coastal areas and the ecosystems prevailing in the coastal region which may reflect by 2050.

Water Resources Management

The hydrological cycle that provides a rhythmic movement of water from one form to the other is considered as the lifeline of the earth system. There is a continuous process of evaporation, transpiration, condensation again precipitation in a cyclic pattern. Due to the imminent cause of global warming and its consequence on climate change in the near future, the natural water cycle perhaps may change whose repercussion may be felt by alterations in climate patterns aggravating from anthropogenic emissions, soil moisture, and river flow. The result will be replicable through severe floods and intermittent droughts. Since 1950, the adverse effects on nature imparts through spatiotemporal scales in several regions. Frequent flood and

drought may aggravate the rise in sea level. The primary source of water reserve in the state calculated to be 3/4th is monsoon dependent, and hence any change in climatic conditions will directly affect the vulnerability through floods and droughts. Demand and supply of water resources get hindered due to unevenness of erratic monsoonal rain. High rate of urbanization and massive growth of industries in recent years have increased the demand for water. Besides, water requirement is also a major necessity for aquaculture. Ultimately, decrease in rainfall will undesirably affect all those who are rain dependent. During flood, there occurs an imbalance in the ecosystem of water bodies. In order to mitigate the water resources issues, there must be an action plan to use water efficiently in the agriculture sector, protection from flood and prevention from erosion, non-infrastructural works, drainage system improvement, flood control, river training, flood modelling, non-structural work, erosion control, drainage improvement, and coastal and disaster risk management. The coastline and oceanic environment play a vital role in the socio-economic, cultural, and environment of the state (Mishra 2017). It is directly related to the development of industries, agrarian, aquaculture, water activities, and ports and harbours. This causes erosion of coastal landmass, which in due course of time gets submerged into the sea. Ocean currents and shore processes are directly related to climate change phenomena which are directly related to various natural disasters. The prioritized activities proposed by the Coast and Disaster Management sector have been considered by the authority, and processes have been initiated to reduce the effect of such calamities.

Coastal and Disaster Management

Proper planning and timely execution of coastal and disaster management have to be taken into priority. Construction of disaster-resilient public infrastructure creates an integrated capacity-building etiquette for shelter and a support group, a strong and efficient team of volunteers who can be used at the time and after the disaster specifically in coastal inundations, and a team of trained officials must be created to look into the upcoming disasters in the entire region.

Energy

Odisha is gifted with a strong resource of water to produce hydropower and a substantial amount of coal deposits in the Gondwana terrain to generate thermal power. The bimodal power-generating capability has helped the state to produce enough power which after its requirement is distributed to the neighbouring states, but on the other hand it provides risk factors to the environment, creating climate change. Hazardous gas emission from the thermal power plants generates continuous environmental issues to the localities residing in the nearby areas. The result is

increasing global warming and substantial environmental pollution followed by climate change. Erratic rainfall during monsoon affects the reservoir capacities hampering hydropower generation, agriculture, and industrial water supply. It seems that the probability of major change in precipitation level at a collective level will be negligible. Plant load factor (PLF) of the power plants will be affected by the increasing temperature, increasing the cooling stresses in addition to the already overloaded distribution network. There is always a power network failure which has been noticed frequently whenever severe cyclones occur. The state has taken major initiatives for alternate energy sources like wind and solar, but problem exists when cyclonic storms occur in the coastal areas, damaging the high invested wind mills. The solar power generators also fail due to continued rainy days and regular cloudy weather. In spite of such demerits, wind and solar power units can be installed in faraway regions from the coast that can improve efficiency in energy, adding more healthy power generation without putting any impact to global warming affecting climate change.

Urban Development

The urban population of Odisha was nearly 17% before the last decade but has gigantically increased to 27% during the last decade. In view of the population growth in the recent five years, it has been noticed that smaller towns have been growing faster than the already developed cities. They experience higher growth of population in expanding towns and cities and are more vulnerable to natural calamities. High rate of migrating labourers and daily-wage workers for their livelihood use to live in thatched roof houses, increasing the slum population in developed cities and towns which can be considered as vulnerable pockets. In due course of time, there exists the problem of encroachment hindering the natural drainage and municipal sewerage distribution system, leading to hygienic problems activating epidemics among the unhealthy community (Kalapahad et al. 2020). In order to keep the problems under control, augmentation of integrated sewerage project for bigger cities, frequent availability of public transport, development of Infrastructure for bus terminals, energy efficiency in providing products and services like street lights, developing urban storm water drainage based on the climate change, housing for all, and development of green space including smart cities should be taken care of.

Transport

The transport sector in the state consumes a huge quantity of fossil fuel as the number of vehicles, both two-wheelers and four-wheelers, and even the heavy vehicles, is increasing day by day. Since most of the vehicles are petrol or diesel

driven, emission of CO_2 increases the ozone layer, creating NO_2 and suspended particulate matter in the atmosphere. The high rate of consumption of fossil fuel has aggravated the environmental issues, becoming a threat to the climate change. This creates rising temperatures and extended heat wave in the atmosphere even if it expedites damage to roads and pavements. To enjoy comfort and to save themselves from the heat waves, vehicle users often turn on their air conditioning, which in turn emits hazardous gas. The heat island effect has compelled the city duellers to use air conditioning units frequently since cities are always at a higher temperature than the rural areas due to heavy pollution and gas emissions from the transportation. Thermal expansion is also a root cause of increased temperature in the railway sector. In recent times, the government has taken various steps to prevent air and noise pollution in order to prevent climate change. The prioritized activities are encouraging e-rickshaw and electric vehicles, policy and implementation of phasing out old and outdated vehicles, and strengthening enforcement wing for emission-level check-up in factories including heavy penalty for polluting vehicles and industries. Though industries contribute one-third of the state's gross domestic product and service sector, which is the backbone of the state's economy, temperature increase in the industrial belts has reduced the industrial activities, decreasing the production capabilities and putting direct impact on the service sector.

Besides, water scarcity, recurring cyclones, and floods damage the infrastructure of the industries, affecting their productivity. Industries along the coast related to chemical, aquaculture, and fertilizer are most vulnerable. To overcome these devastating factors, proper mechanism for the development of green belt, instantaneous maintenance for industrial installations, and formulation of regional environmental management plans for major industrial clusters have been taken up by government platforms.

Mining

Mineral reserves in Odisha constitute 28% of iron ore, 24% of coal, 59% bauxite, and 98% of its chromite of the total percentage of ores that the country produces. The mining sector alone contributed around 7.4% of GDP during the last decade which is continuously declining in the successive years. During the post-excavation period of mining, the area is abandoned and contaminated water which piles up in those excavated areas, incurring an opportunity to infiltrate into the subsurface zone making a passage to pollute the groundwater of the aquifers. This usually happens in all open cast mining regions that even do not spare the nearby streams, lakes, and surface runoff. Intense rainfall also escalates the risk of mining operations and damages the transportation of ores from the source. Mining operations correspondingly get affected by changes in the frequency and intensity of storm. Drastic increase in temperature, especially during summer (April–July) in the northern and western parts of the state, increases the risk of heat strokes among the workers, causing mining accidents, reducing the working hours, and decreasing productivity.

A sensible mechanism to provide green belt development and maintenance in and around the mines, creating green zones in major mining areas, and developing a methodology to measure, monitor, and verify the amount of carbon confiscated by plantation programmes, is to be taken into consideration, which the government is working on an emergency basis.

Waste Management

Rapid growth of population, massive industrialization, and large-scale mining activities have caused waste generation, creating environmental issues on a larger perspective. The average municipal solid waste generation in Odisha has been around thousands of tons per day in all major cities of the state. Improper management of solid and liquid waste discharged from households may lead to serious health hazards and spread of diseases. Waste disposed randomly all over the places in different localities attracts rats, flies, and other insects that may spread disease. Usually, the foul smell that exits from bacterial action of wet waste disposal leads to unhealthy conditions, creating several health problems. Awareness for waste management in the community level, scientific methods of waste disposal, and incineration and safe disposal of municipal solid waste may mitigate pollution, indirectly benefitting to prevent climate change.

The geographical location of the state makes the state more vulnerable that directly or indirectly affects the economic growth supplemented by increasing poverty. Various measures like coastal and disaster management, agrarian and forest, fishery and animal husbandry, mining and industry, water resources, and urban transport have been seriously considered to prevent recurrently occurring climate change. The entire responsibility is shouldered by the Department of Forest and Environment to monitor the positive activities taken by different departments. Policies have been formulated, and in coordination with other technical teams, measures have been executed for low carbon emission development, vulnerability reduction, and evaluation of progress (Fig. 16.3).

Climate Profile of the State

Climate

Hot subtropical climatic condition is the characteristic of the climatic scenario of the state (Ghosh and Majumdar 2007). Normally the temperature remains high, with high humidity index and high and winter prevailing for a shorter period including extreme to medium rainfall. Heavy rainfall is recorded from June to September due to the impact of southwest monsoon. Winter remains for a shorter period extending from November to February. Due to high vulnerability of climate change, the
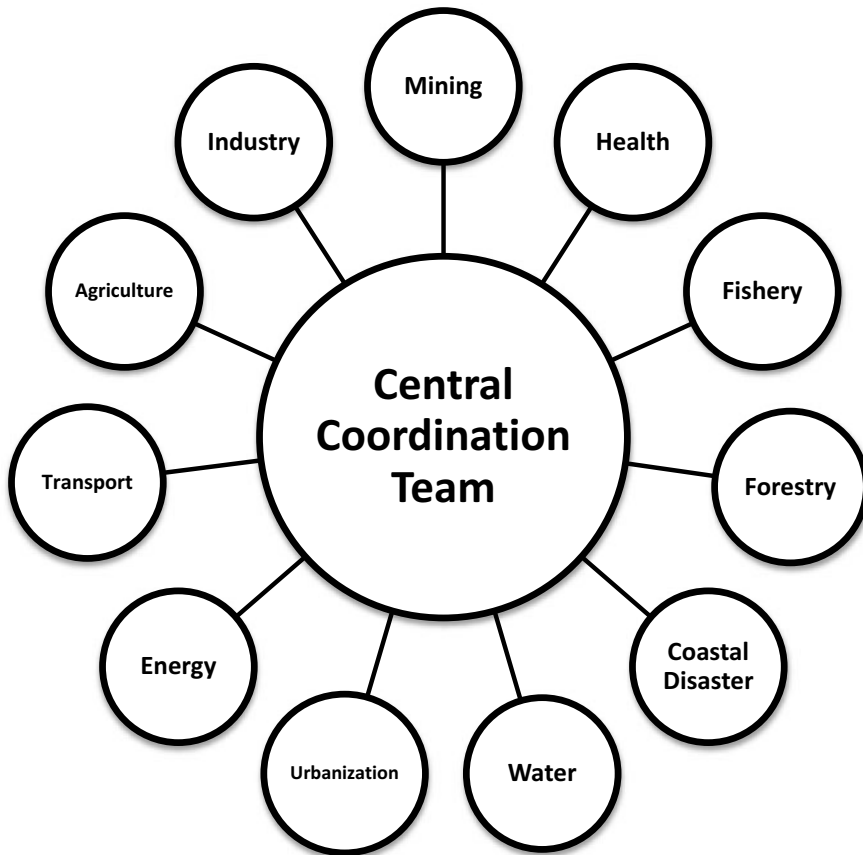
Fig. 16.3 Implementing departments for climate action plan

frequency goes on changing from year to year. Temperatures of the coastal areas always remain high in comparison to the western parts with a high rate of humidity. Similarly, rainfall in the coastal districts often remains alluring, primarily due to climate change effects stirring through frequently occurring low pressures in the Bay of Bengal. Climate change that occurs intermittently has put an alarming note to the maximum and minimum temperatures (Figs. 16.4 and 16.5) across the state. In summer, the western and northwestern parts of Odisha record a temperature of more than 44 °C with complete dry and arid climatic condition. Similar conditions exist during winter, when southern, northern, and southwestern parts record lower temperature in comparison to the other parts. Overall, it can be explained in a nutshell that there is a longer summer, followed by rainy and short summer seasons. Other seasons are almost missing from the seasonal chart.
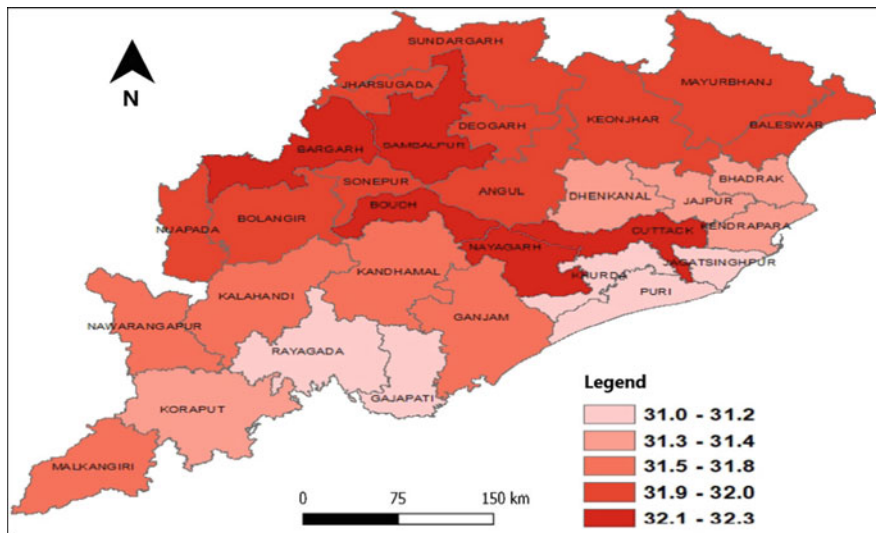
Fig. 16.4 Maximum trend of baseline temperature

Temperature

The maximum average temperature in the past was observed in the western parts of the area, and the lowest average minimum temperature was recorded in the northern districts. The maximum trend of baseline temperature varies from 31 to 32.3 °C, whereas the minimum trend starts from 18.6 °C to 22 °C. A detailed analysis of daily temperature has been projected under climate change scenarios of RCP 4.5 (Meinshausen et al. 2011). In the near term, the temperature may rise by around 0.4–1.2 °C and in mid-century it may go up by 0.8–2.8 °C, whereas under RCP 8.5, the projection is more alarming. In near term, it may increase by 0.7–1.4 °C and by mid-century 2.0–3.3 °C. The maximum deviation in the near century is least in the northeast and maximum in the southwest parts of the state. The minimum deviation in the temperature in the near future is 0.4 °C across the northeast and 1.2 °C, whereas mid value is around 0.8 °C in the western and eastern coastal region. The near century is taken from 2020 to 2039 under RCP 4.5 (Figs. 16.6 and 16.7).

Rainfall

Analysing the annual rainfall of the entire state, it has been noted that a negative trend is prevailing in the area. There is a decline of nearly 0.24 mm during the last decade. In the last half of the century, an increasing trend was recorded, but subsequently, there was a sign of climate change which puts an impact on the
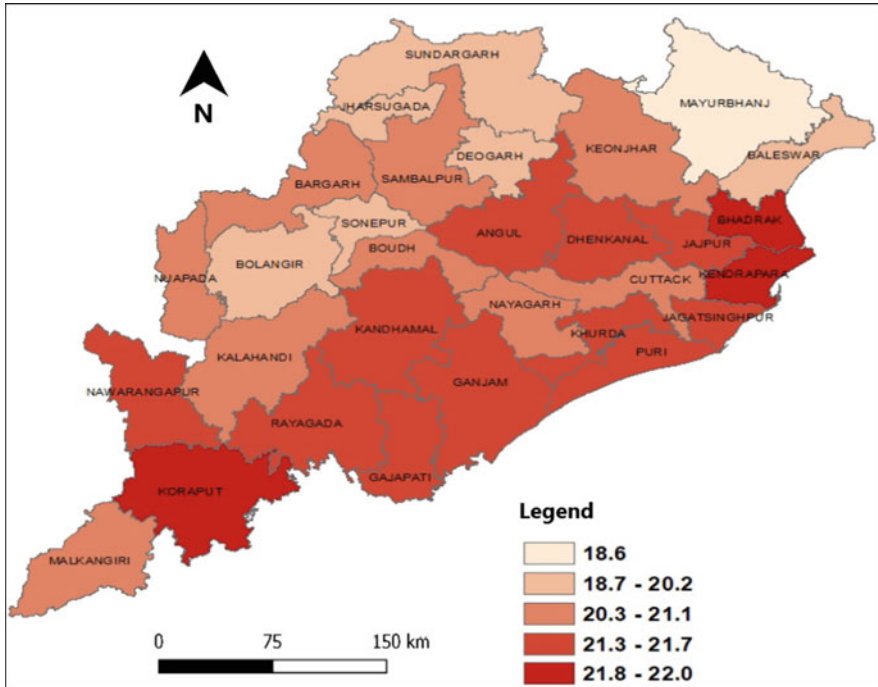
Fig. 16.5 Minimum trend of baseline temperature

trend and started decreasing. The situation is so aggravated that it can be termed as a deficit rainfall. Though during low pressure wherever exerted in the Bay of Bengal, there is heavy shower of rainfall, but that does not suffice the water requirement of the state either for domestic or agricultural need. According to RCP 4.5 scenario, the mean annual rainfall in the near term by mid-century is anticipated to decrease by 4.6 to a maximum increase of 25.7% and a decrease of 8.2% to an increase of 55.7% (Figs. 16.8 and 16.9). The variation is quite high, which may affect the rainfall, creating adverse effect on irrigation as well as flood control. For RCP 8.5 scenario, rainfall in the mid-century scenario is projected to decrease by 5% to nearly 31% and increase to 1.7% to around 65%.

Energy demand for cooling, evaporation, and evapotranspiration losses are the wide-ranging consequences if the temperature soars, producing heat stress and resulting in enhanced irrigation water requirement for crops. Erratic and untimely rainfall may lead to floods, runoff storms, vector-related diseases, loss in working hours, and disruption of traffic, factory, and warehouse issues. There might be more number of issues, but due to limited data availability, only a few of the related problems have been discussed and analysed.
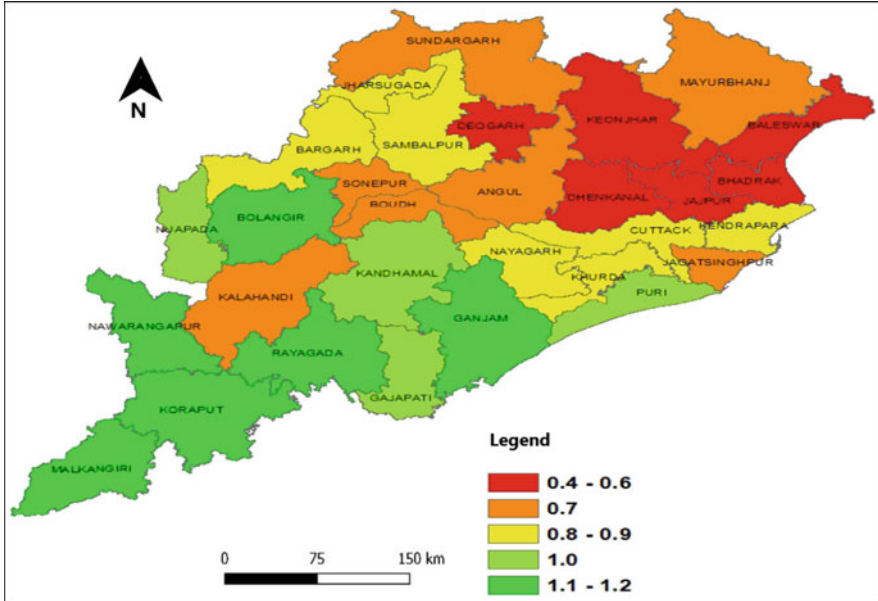
Fig. 16.6 Maximum temperature deviation in the near century under RCP 4.5 scenario
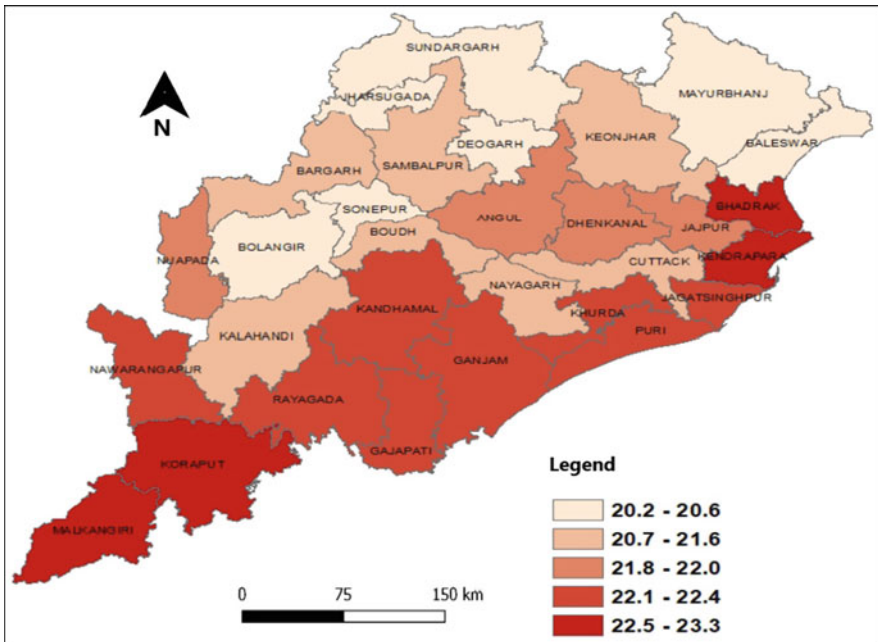
Fig. 16.7 Minimum temperature (in °C) deviation in the near century under RCP 4.5 scenario
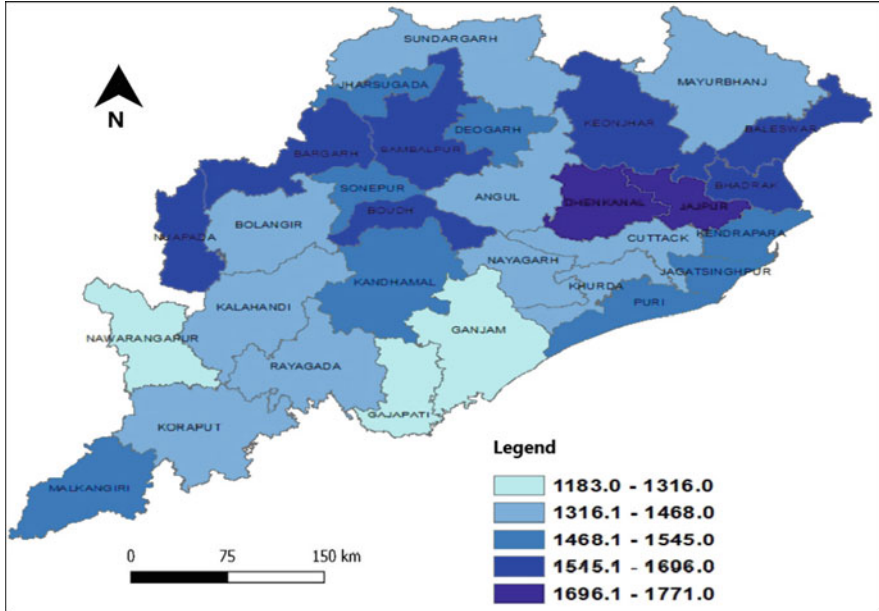
Fig. 16.8 Near century rainfall (in mm) pattern under RCP 4.5 scenario
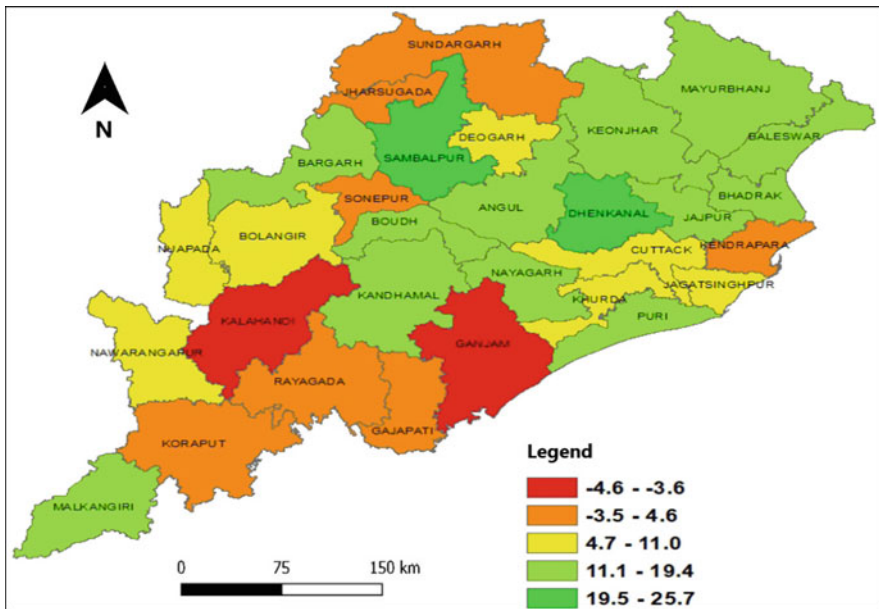
Fig. 16.9 Near century rainfall (in mm) deviation from baseline under RCP 4.5 scenario

Vulnerability Assessments

To recognize measure and prioritize, susceptibility can be defined as the assessment of vulnerability. It helps in present and future vulnerability, comparative analysis of vulnerability from one to the other, proper communication among the stakeholders, selecting right strategies, and some other miscellaneous factors. Under RCP 4.5 scenario, during the last decade, the hazard from temperature and precipitations remains the same. Drought proneness and incidence of dry spell changes are the other factors for vulnerability assessment (Mishra and Singh 2010). In other words, vulnerability is a function of sensitivity and adaptive capacity. The combined risk has been computed using hazard, exposure, and vulnerability as the three dimensions. 36 different parameters are considered as indicators in order to compute the index. In essence, the data shows the change in vulnerability as well as the change in risk over the last five years. As per the available data, baseline composite vulnerability index in the last decade is compared and analysed in a sensible manner (Figs. 16.10 and 16.11). The combined risk index is created for the end of the decade (Fig. 16.12).

Sea-Level Rise and Coastal Vulnerability

Coastal flooding, sea coast erosion, and saline water intrusion to the freshwater aquifers are expected to occur in the future as sea level starts rising. This may also trigger frequent cyclones and intensity of erratic rainfall with increase in hazard rates. Cyclonic effect in the coastal region may devastate the mangroves, changing the ecological balance. Aquaculture may also hit very badly. Sea-level rise, coastal geography, tidal range, and elevation are the major impacts in the vulnerability section. The effect on the long coastline may be high, medium, or low depending on the intensity they face. The severity of damage considered as low with an extension of 76 km is noted from Kendrapara to Gangam, including the brackish lake Chilka. Medium class extends up to 297 km parts of central coastline, whereas high rate of vulnerability may be recorded for 107 km in the remaining coastal areas.

Flood

Odisha stands in the fifth position as far as flood is considered among all the states of India, with a sensitized area of approximately 33,500 km^2. The whole coastline of 480 km is always under the threat of repeated floods and waterlogging. Flooding becomes more severe when cyclonic winds and tidal flows generate heavy rainfall lasting more or less for 5–15 days along the coastal belt. It causes cost of life and damage to property and crops affecting food security and livelihoods. Saline water
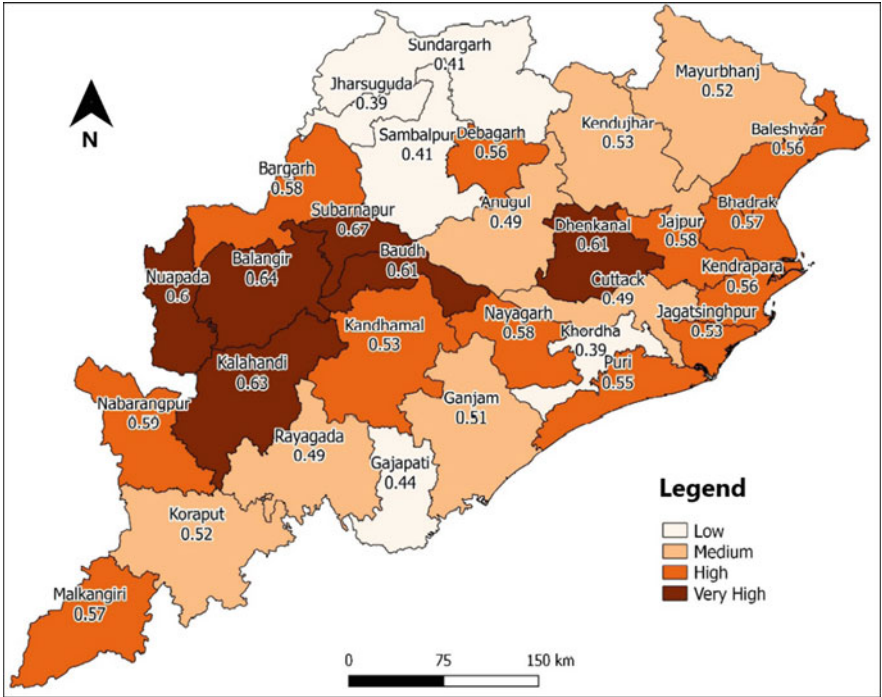
Fig. 16.10 Baseline composite vulnerability index in the beginning of the last decade
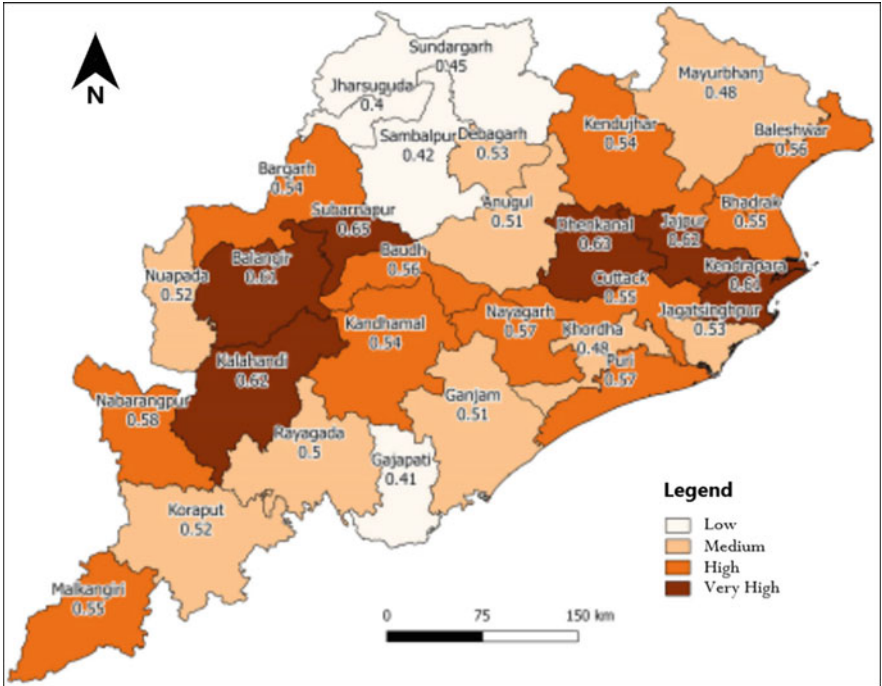
Fig. 16.11 Composite vulnerability index in the end of the last decade
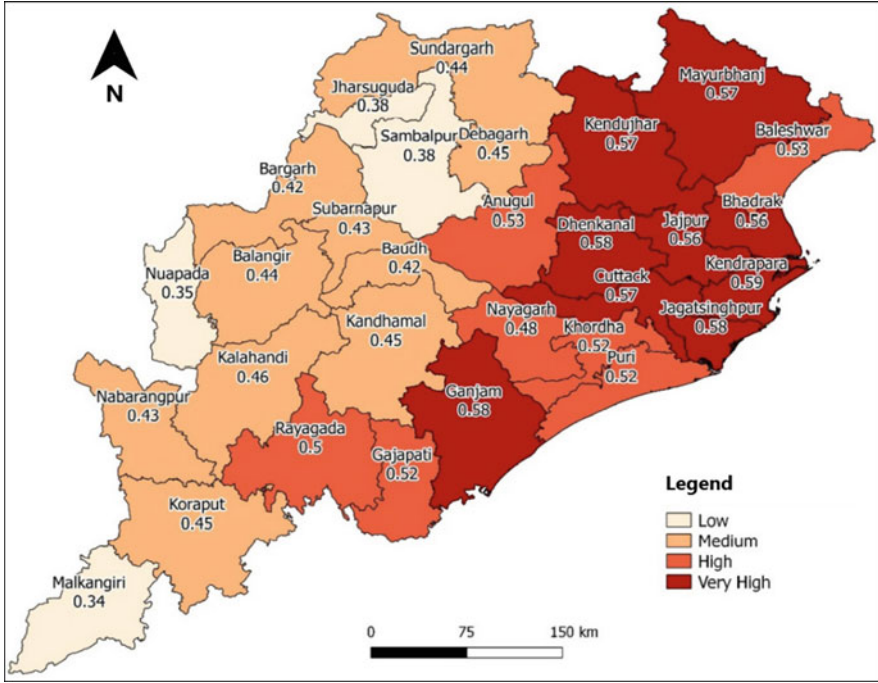
Fig. 16.12 Combined risk index at the end of the last decade

incursion to the coastal fertile lands destroys the paddy fields and converts the agricultural-friendly fields to barren lands. If deforestation, faulty flood control planning, and climate change continue in the similar pattern, Odisha may worsen itself for more severe flooding. The aftereffect will be huge migration of people from the coastal region to the already existing densely populated areas affecting the already disturbed civic amenities and resources. In the recent period, more areas are facing the threat of flooding, and it is rising from year to year (Fig. 16.13). The same is the case for cyclone. The brutality of nature is unbearable in the areas that are prone to cyclone as well as flood though this covers a small patch of the state. In most instances, flood has a direct relation to the cyclonic effect in Odisha. Once there exists a severe cyclone, it tends to rise in the intensity of rainfall, resulting in the rise in surface runoff of the natural streams, increasing the volume of water in the rivers.

The inhabitants residing along the river bank of Mahanadi, Brahmani, and Baitarani, the three major rivers of the state, are accustomed to the flood generated during monsoon, but when those rivers merge with the Bay of Bengal, it creates a huge deltaic zone. The flood water amalgamates and produces a flood zone which creates havoc if tidal waves support them. The water rises drastically, and loss of human life, property, and submergence of agricultural lands are destroyed.
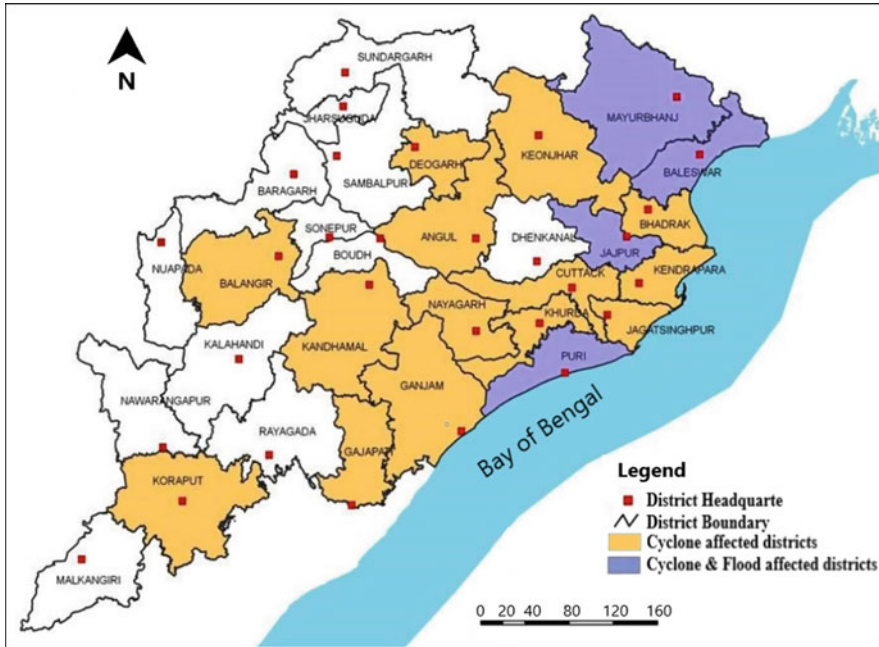
Fig. 16.13 Cyclone and flood-affected areas

Drought

Due to continuity in change of climate across the globe, areas affected by drought have been increasing from year to year starting from 1970. This was created due to the impact of sea-level rise and land and seawater warming. Such a repercussion has been reflected in the state of Odisha by continuous incidence of cyclones and floods. The severity of drought has increased with global warming on both land and ocean, and Odisha is the most affected due to the disadvantage of its geographical location.

It is evident from different researches that global warming has been tremendously increasing and so is the seawater rise. The severity of drought is its direct effect which is caused due to a rise in temperature of the land mass. Vulnerability increases in Odisha due to its geographical location. The aftereffect due to global warning will be more severe, which in turn may tend to drought and famine if timely precautions are not taken. Specifically, the interior areas of the state are more likely to get affected in the long term due to drought.

Cyclone

Odisha embraces tropic cyclones than any other category with high intensity. This is usually felt in the coastal regions, which are at high-risk zone. Since the areas are

highly fertile lands, so the population in those areas is also dense. A low-scale cyclonic effect even creates havoc due to the high rate of people living in these areas. Many people living close to the sea coastline suffer the maximum. Those populations depend on fishing as their livelihood and lose everything when they face cyclonic winds of intensity 100 km/hr. or more. An unforgettable example is the 1999 super cyclone when thousands lost their lives, millions became homeless, and same numbers were displaced with thousands of acres of highly cultivable lands submerged under the tragic effect of seawater incursion. The loss of life and property was due to the failure of the state mechanism, which was not prepared at all to face such calamity, and there were no programmes for any mitigation structure. The state took months to recover from the calamities and years to rebuild. Learning from the past, now the state is completely prepared and equipped with all sorts of mechanisms to face any such challenge. Recently occurred cyclones are smartly dealt with by the administration with minimum casualties and loss of properties, reducing the magnitude of vulnerability to disasters (Patel 2016). The coastal areas are most vulnerable followed by the central part of the state (Fig. 16.14). The least-susceptible areas are the extreme west and southern parts of the landmass.
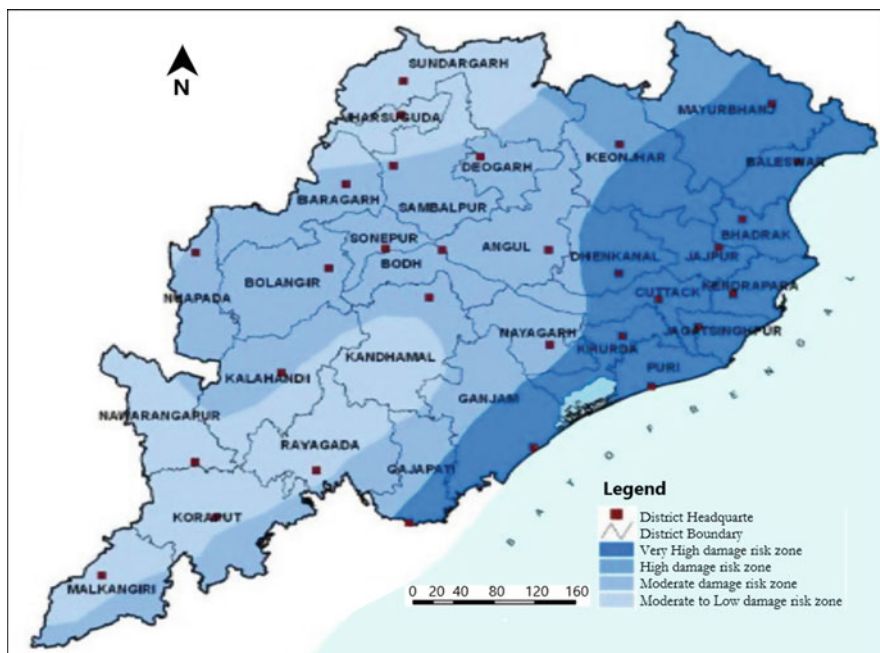
Fig. 16.14 Wind and cyclone zones of Odisha

Heat Effect

The state of Odisha has a long 4–5 months of summer which starts from March–April to August till monsoon breaks in the state. During this period, the temperature soars up to 45 °C in the inner land mass towards the western part of the state. The climatic condition of this region becomes completely arid by which the heat increases enormously. Loss of life is usually recorded in hundreds due to the heat wave termed as 'Loo'. Though the coastal region is even not spared, but the difference between the extreme west and coastal region is the coastal regions do have a high humidity during this period. Globally, the term more often is called urban heat island (UHI). The phenomenon is the urban areas are more heated during summer than the rural areas. Not only it affects the health of the people but also indirectly shakes the economy (Jena 2017). The rise in surface air temperature increases the demand of electricity, escalating air pollution, ultimately enhancing the air temperature. Due to high rate of mining activities along all the mines, the temperature even becomes more overwhelming, especially in the coal and iron mines areas of Gondwana and Iron ore series located in the central western and northeastern parts of the state, respectively. The same is the condition of the industrial belts of the area. Serious measures and targeted obligations are being initiated by the administration to overcome from such calamity, but unless the upsurge of global warming does not ease, it is mere difficult to comply and implement the required measures for mitigation of UHI.

Forestry

Large-scale deforestation for the purpose of expanding industrialization, increasing cultivable area, and enlargement of urban civilization are the major factors in reduction of forest land in the area (Gopalakrishnan et al. 2011). Schedule tribes who are the inhabitants of remote areas and dependent on forests suffer the most. During the last decade, CO_2 level in the atmosphere has increased by some fold, posing threat to the ecology. Almost 33% of the land mass in Odisha is covered by forest, comprising very dense forest, moderate forest, open forest, and scrub. During the 1980s, the forest land mass was severely affected, and in recent times forest land is expanding due to the initiative taken by the local government by conservation and plantation drive. Once Odisha was considered as the land of forests but now has become barren in many patches (Fig. 16.15). In the present scenario, dense forest is found in the northeast part of the state and in the extreme south, whereas some patches can be seen across the state. Many of the areas which were covered by forests have now been converted to non-forest areas. This causes a change in environment, reducing the intensity of rainfall, in turn increasing the percentage of CO_2. Concerns arise with the impact on the surface runoff of the major rivers of the state.
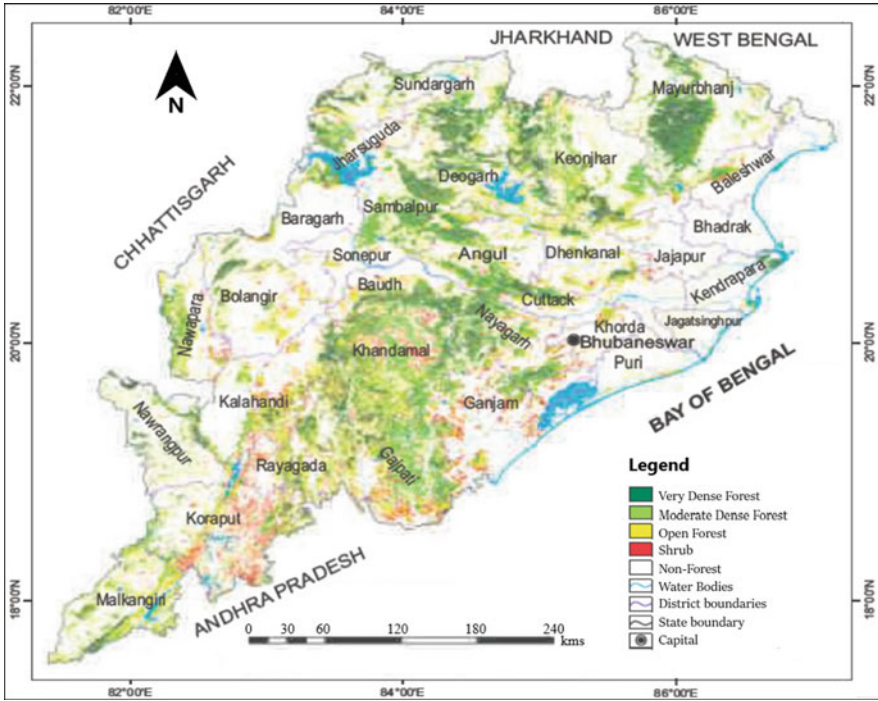
Fig. 16.15   Forest mix cover of Odisha

Impact of Climate Change

Recurrent change in climate has a long-standing repercussion to the present development of the state in various aspects. The primary factor lies with mass scale deforestation, which needs to be addressed earnestly. Large-scale plantation and awareness among the communities are the prime practices to reduce forest degradation. This will reduce carbon emissions, improving the quality of air, enhancing consistent rainfall, and increasing the probability of stable rainfall. To achieve this goal is merely difficult but not impossible. Robust management and dedicated administration may be implemented at the earliest. The risk is more aggravated from the research, which predicts a nearly 10% change in forest land by 2035 and 14% by 2085. This is no doubt an early warning for the safety of the forest land. Rise in temperature may have adverse effects on the flora and fauna along the northern territory and southwestern region of the state. If the forest is not protected before it slips from the hand, the temperature in the urban area may further increase and reach 50–55 °C. At that point of time, it may cause irreversible damage to the entire ecosystem. Geoclimatic conditions of the state will further aggravate the situation, generating a massive climate change to the already existing unbalanced climate. From the past experiences, it is a fact that the cyclones, floods, tornadoes, droughts,

and heat waves mostly prevail from March to October. Around 60% of the state always faces the bean of mass casualties and huge property loss due to frequently occurring natural calamities. The reverberation lies with spread of epidemic, water and airborne diseases. Extreme heat during summer brings more pain to the people with scores of deaths every year. Heat stroke, heat exhaustion, heat cramps, and heat syncope are caused due to heat waves; mass casualty, population displacement or migration, and water and vectorborne diseases due to flood; food scarcity, malnutrition, and psychological disorders due to drought; respiratory and related health issues due to air pollution are some of the major concerns due to the impact of climate change.

Mechanisms to Be Executed

A strong and successful mechanism has been developed by the central government known as the National Action Plan on Climate Change which is based on a long-term strategy (Jogesh and Dubash 2014). Odisha is also following the same plan to mitigate the vulnerability that may incur due to several natural distresses. Planning and execution is one part of this action plan, but continuous monitoring of the entire system is the major initiative that needs to be followed. To make the entire system a success, interdepartmental coordination must be active to bring all issues in one table and address each issue separately to accomplish proper and fruitful execution. Strategies must be clear; discussion should be open-minded to ensure a significant development. Major support should be provided by the collaborative departments to the principal implementing organization. There is no harm in connecting more departments who seldom get affected due to climate change. Sincere help from local communities and NGOs working during and after any disaster may also be incorporated into the forum.

Conclusion

The Forest and Environment Department is the nodal unit that controls and implements the entire project after detailed discussion from the supporting departments. The main focus is how to face the challenge due to climate change. With a controlled budget, mitigation planning is executed as per the vulnerability. After some of the unsuccessful attempts made in the past decade, the state machineries are now far more active to face any challenge from the issues related to change in climate. As of now different school of thoughts have put forth that climate change is inevitable, but mitigation by proper planning and implementation can reduce the sorrows of the state which it has faced several times in the past. Disaster rapid force in the last decade has been modernized and equipped with modern amenities 24/7 in active mode to face any consequences occurred due to disasters. The Climate Change Cell

is adequately empowered by the government to work as a driving force on climate change. To make things more technical savvy, a number of satellite data from geosatellites have been procured to prepare a long-term strategy for a successful implementation of different projects undertaken for a deep study on climate change. Though there is an issue of fund, this cannot be any hindrance to the implementation and execution of adaptive policies collaboratively taken by various organizations together. The central coordination committee has vibrant objective to create and maintain a climate change knowledge source, provide a forum for climate change knowledge access and transfer, manage climate change-related knowledge as an asset, promote research on policies, plans, and programmes in key sectors that has relevance to climate change to mainstream climate agenda, and promote regional research on climate change which can help in identifying regional adaptation options. In order to make things more transparent, a huge database is a need of today which can be exchanged with national and international forums who are working in the field of climate change for several decades.

It is promising to note that the state has taken a major initiative for a huge allocated budget to meet the climate change activities. It is really a commendable task that the state has undertaken to face the climate change issues seriously. On the contrary, it is also a naked truth that the mechanism must be mobilized more aggressively so that the region will be free from any further climate change scenarios.

References

Ghosh S, Majumdar PP (2007) Nonparametric methods for modelling GCM and scenario uncertainty in drought assessment. Water Resour Res 43(7)

Gopalakrishnan R, Jayaraman M, Bala G, Ravindranath NH (2011) Climate change and Indian forests. Curr Sci (Bangalore) 101(3):348–355

Guhathakurta P, Rajeevan M (2008) Trends in the rainfall pattern over India. Int J Climatol 28(11): 1453–1469

Jena DP (2017) Impact of climate change on Odisha, economic development-a comparative analysis. IOSR J Human Soc Sci 22(6):21–25. https://doi.org/10.9790/0837-2206012125

Jena D, Dibiat N (2020) Climate change patterns in two districts of Odisha: a trend analysis. Int J Adv Sci Technol 29(3):11498–11512

Jogesh A, Dubash NK (2014) Mainstreaming climate change in state development planning: an analysis of the Odisha Climate Change Action Plan. Centre for Policy Research (CPR), Climate Initiative, working paper. CPR, New Delhi, February 2014

Kalapahad BC, Acharya S, Kar P (2020) Effect of climate change on public health in Bhubaneswar Smart City, Odisha, India: risks and responses. Int J Res Eng Appl Manage 5(11):29–34. https://doi.org/10.35291/2454-9150.2020.0056

Khan SA, Kumar S, Hussain MZ, Kalra N (2009) Climate change, climate variability and Indian agriculture: impacts vulnerability and adaptation strategies. In: Climate change and crops. Springer, Berlin, pp 19–38

Kumar TS, Mahendra RS, Nayak S, Radhakrishnan K, Sahu KC (2010) Coastal vulnerability assessment for Odisha State, East Coast of India. J Coast Res:523–534

Mahalik NK (2006) A study of morphological features and borehole cuttings in understanding the evolution of and geologic processes in Mahanadi Delta, East Coast of India. East Coast Deltas of India. J Geol Soc India 67:595–603

Meinshausen M, Smith SJ, Calvin K, Daniel JS, Kainuma MLT, Lamarque JF et al (2011) The RCP greenhouse gas concentrations and their extensions from 1765 to 2300. Clim Chang 109(1–2): 213–241

Mishra AK, Singh VP (2010) A review of drought concepts. J Hydrol 391(1):202–216

Mishra D, Sahu NC, Sahoo D (2015) Impact of climate change on agricultural production of Odisha (India): a Ricardian analysis. Reg Environ Chang. https://doi.org/10.1007/s10113-015-0774-5

Mishra PK (2017) Socio-economic impacts of climate change in Odisha: issues, challenges and policy options. J Clim Change 3(1):93–107. https://doi.org/10.3233/JCC-170009

Odisha Climate Change Action Plan (OCCAP) 2021–30 (2018) Forest and Environment Department Government of Odisha, Report, 1–228

Patel SK (2016) Climate change and climate-induced disasters in Odisha, Eastern India: impacts, adaptation and future policy implications. Int J Human Soc Sci Invent 5(8):60–63

Chapter 17
Statistical Approach to Detect Rainfall Trend Over Tamil Nadu State, India

Sathyanathan Rangarajan [ID]**, R. Karthik Raja, Aravind Murali** [ID]**,**
Deeptha Thattai [ID]**, Manikandan Kamaraj, and Md. Nazrul Islam**

Abstract Analysis of long-term rainfall data set is being widely employed by the research community to study temporal variations in annual and seasonal rainfall series. This study aims to determine the spatial and temporal variability of precipitation in the southern part of Tamil Nadu over a period of 115 years (1901–2015) on an annual and seasonal basis. Forty-five gridded rainfall data of $0.5 \times 0.5°$ resolution (CRU TS 4) falling in Tamil Nadu was taken into account. The data were preprocessed using MATLAB software to convert the data into 12×115 matrix form. The processed data is then formulated into seasonal and annual series. Seasonal series were prepared based on the guidelines given by IMD, Chennai. For each grid points, the Mann–Kendall test and Sen's slope analysis were performed for annual and seasonal series using Minitab software to determine the spatial and temporal trends. Rainfall departure analysis and the percentage contribution between annual and seasonal rainfall were arrived for all the grid points. The year 1962 was the most probable year of change in annual and monsoonal precipitation. Spatial analysis of precipitation after the change point (1963–2015) showed

S. Rangarajan (✉) · R. Karthik Raja · M. Kamaraj
Department of Civil Engineering, SRM Institute of Science and Technology, Kattankulathur, Chennai, Tamil Nadu, India
e-mail: sathyanr5@srmist.edu.in

A. Murali
Department of Civil and Environmental Engineering, Carleton University, Ottawa, Ontario, Canada

D. Thattai
Independent Researcher, Chennai, Tamil Nadu, India

Md. N. Islam
Department of Geography and Environment, Jahangirnagar University, Savar, Dhaka, Bangladesh
e-mail: nazrul_geo@juniv.edu

an increase in NEM precipitation in the full extent of the Western Ghats region. Eventually, increase in annual precipitation was 4.97% during the period of 1901–2015.

Keywords Tamil Nadu · Mann · Kendall test · Sen's slope test · Precipitation · Departure analysis · Rainfall trend

Data Availability Statement
All rainfall data used during the study are available online in accordance with funder data retention policies (Harris et al. 2020).

Introduction

Hydro-meteorological variables are experiencing a drastic shift in their pattern due to various environmental and anthropogenic alterations, which must be immediately attended to address the anticipated issues of demand–supply chain imbalance. Rainfall is one of the fundamental climatic variables and an in-demand natural source of water supply to living creatures worldwide, whose variation and timely arrival directly affect the demography of a country. The rapid increase in the average global temperature over the past few decades, as reported by the Intergovernmental Panel on Climate Change (IPCC 2018), has resulted in an unevenness to the weather extrema causing ups and downs in the rainfall pattern. Hence, it becomes essential to understand the spatiotemporal variability of rainfall, which governs the major needs of the socioeconomical, agricultural, and industrial sectors.

Analysis of rainfall occurrence and its distribution has been the most research topic worldwide, and the outcomes of which are useful in bringing up sustainable watershed development and management. The predicted increase in the global population threatens the availability and storage of water day by day, making researchers nurture innovative solutions to augment water resources, which requires accurate knowledge of long-term rainfall trends and variability. Also, the variation in the precipitation must be given rigorous and practical importance as it directly affects the agricultural production and freshwater supply, which forms a major part of the country's economy.

In the recent decade, several parametric and nonstatistical approaches have been incorporated in analyzing the spatiotemporal trends in the time-series data of different climatic variables, both on regional and national scales. These approaches include regression analysis (Piao et al. 2010), Kendall rank correlation test (Kendall 1975), Mann–Kendall (MK) test, modified Mann–Kendall test, Spearman's rho correlation test (Spearman 1904, 1906), Sen's slope approach (Sen 1968), and many other graphical representation methods. Many researchers worldwide have

concluded major outcomes on how the pattern of rainfall trends varied over the years using these methodologies (Yue and Hashino 2003; Smith 2004; Joshi and Rajeevan 2006; Beecham and Chowdhury 2010; Piao et al. 2010; Tabari et al. 2011; Maragatham 2012; Mondal et al. 2012; Shifteh Some'e et al. 2012; Xia et al. 2012; Jain et al. 2013; Fu et al. 2013; Dinpashoh et al. 2014; Pingale et al. 2014; Rao et al. 2014; Talaee 2014; Goyal 2014; Gajbhiye et al. 2016; Khatiwada et al. 2016; Bari et al. 2016; Chatterjee et al. 2016; Amirataee and Montaseri 2017; Yang et al. 2017; Tian et al. 2017; Chandniha et al. 2017; Meshram et al. 2018; Bisht et al. 2018; Chang et al. 2018; Sa'adi et al. 2019; Machiwal et al. 2019; Rangarajan et al. 2019; Malik and Kumar 2020; Praveen et al. 2020; Sathyanathan et al. 2020; Singh et al. 2021). There must have been an abrupt shift in the rainfall quantum from a particular period if there is a trend over the time series. Detecting this change point plays a significant role in analyzing the trend before and after the shift point, thereby helping in predicting the future rainfall patterns. For a given time series, these shift points are determined using change detection methods such as the Standard Normal Homogeneity Test (SNHT) (Alexandersson and Moberg 1997), Buishand range test (Buishand 1982), and Pettitt's test (Pettitt 1979). Although these methods are most widely incorporated in trend detection studies, they restrict their applications in the absence of independent time series and the normality in their distribution (Yue and Hashino 2003). But the application of more than two trend detection methods for the same time series revealed satisfactory conclusions (Sonali and Nagesh Kumar 2013; Machiwal and Jha 2017).

Indian agriculture is predominantly rainfed, encompassing 68% of the cultivated area (Meshram et al. 2017). The states are thickly urbanized and ultimately rely on the monsoon and their storage to satisfy the daily water demands. India is categorized as the most unsafe drought-prone country, and the frequency of risk is intensifying every three years (FAO 2002; World Bank 2003; Mishra and Singh 2010; Meshram et al. 2017; Praveen et al. 2020). Even Cherrapunji in Meghalaya, India, which is among the world's highest rainfall zones, was also affected by drought in recent years (Thomas et al. 2015). Hence, it is significant to evaluate the precipitation trend for the Indian context to plan the water augmentation and proper distribution accurately.

Recent studies have focused on identifying the precipitation trends in India at varying spatial scales (Sarkar and Kafatos 2004; Guhathakurta and Rajeevan 2008; Kumar and Jain 2011; Duhan and Pandey 2013; Taxak et al. 2014; Thomas and Prasannakumar 2016; Mohammad and Goswami 2019; Rangarajan et al. 2018). Guhathakurta, P. and Rajeevan, M. (2008) identified a wet decadal change in the Indian rainfall pattern followed by a drought period from 1961 to 1990. A significant increase in annual rainfall trends was observed over central India (Goswami et al. 2006) and a nonsignificant increasing trend over the western and southern regions (Mondal et al. 2015; Joshi and Pandey 2011; Praveen et al. 2020). A similar observation for monsoon rainfall was made where increasing rainfall of 2.06 mm/ year was noticed in the southwest Indian regions of Konkan and Goa. Of all the

spatial scales, a regional-scale analysis proves its efficiency in examining the aspects of the water resource and its risk management. Rangarajan et al. (2018) have identified an insignificant increasing trend in the Chennai district's annual rainfall pattern and concluded that if the southwest monsoon provides excess rainfall, the northeast monsoon gets subdued vice versa. Based on the Mann–Kendall trend analysis over Assam, Goyal (2014) found that the state depicted no significant trend on the seasonal distribution patterns. Rainfall trends in the Indian Himalayas were investigated by Basistha et al. (2009). The rainfall trend and pattern analysis for the Kongu upland of Tamil Nadu (TN) were carried out by Rathod and Aruchamy (2010). They observed that the Upper Niradam recorded the highest rainfall and the Krishnapuram received the lowest rainfall. Hence, it is understood that the spatial and temporal trend analysis varies for different Indian regions.

Assessment of rainfall trend analysis and its outcomes are useful in establishing the effective control of available water resources (Rana Chatterjee et al. 2009). While considering India's southern regions, there are numerous nonperennial rivers depending solely on monsoonal rainfalls. Due to the lack of water resource management, the farmers and agricultural workers depending on rainfall are getting affected (Bhushra Praveen et al. 2020).

In this study, a detailed statistical analysis of rainfall was accomplished for Tamil Nadu state to detect the trend and pattern on seasonal and annual time scales. The results of the analysis will support the administration of the state to manage the available water resources in a judicial way.

Study Area

The state of Tamil Nadu (TN) lies in the southernmost part of the Indian Peninsula between latitudes $8° 5'$ and $13° 53'$ N and longitudes $76° 15'$ and $80° 20'$ E (Fig. 17.1). It is the eleventh largest state in India, with an area of 130,058 km^2. The Bay of Bengal bounds it in the east, the Indian Ocean and Sri Lanka on the south, the state of Andhra Pradesh on the north, and the Western Ghats and Kerala state on the west. The capital of Tamil Nadu is the city of Chennai. Agriculture is the primary occupation of the state, and rice is the staple food. Other principal food crops include millets and pulses. Approximately 58% of the total geographical area is cultivated, while nearly 17% of the land is under nonagricultural uses.

According to the Indian Meteorological Department (IMD 2017) definition, the four seasons of Tamil Nadu are classified as follows: winter (January–February), pre-monsoon (summer) (March–May), southwest monsoon (June–September), and northeast monsoon (October–December). The southwest monsoon (SWM) period is the principal rainy season for the most Indian subcontinent. However, Tamil Nadu gets its significant share of rainfall from the northeast monsoon (NEM). The SWM usually begins in the first week of June in Kerala and West Bengal and progresses inland in stages; it covers most of the country by the middle of July and contributes 75% of India's rainfall. The monsoon starts receding from the northwest by the beginning of
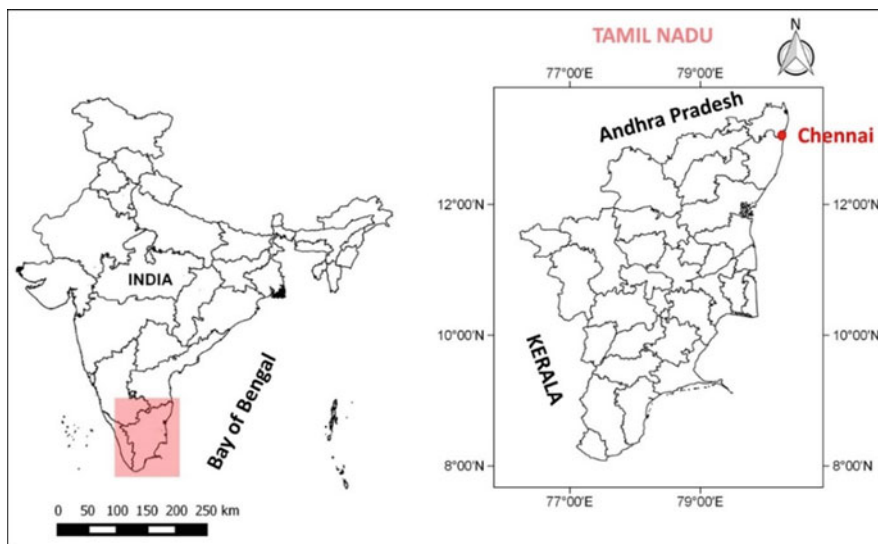
Fig. 17.1 Map of the study area

September, progressively receding southward. The retreating SWM season is referred to as the NEM season, which usually begins around 20th October (±1 week) in Tamil Nadu. During this period, the interior and coastal districts of Tamil Nadu get about 40–50% and 60% of the annual rainfall, respectively. The precipitation occurs in about 3–4 days, with intermittent long dry periods that see little or no rain.

Methodology

The methodology followed for this research can be exclusively divided into four major steps and are elaborated in the following sections in detail.

Data Used

CRU TS 4 data set comprises more than 4000 weather stations distributed around the world. The data set contain nine climatic variables: cloud cover, diurnal temperature range, frost day frequency, rainfall, daily mean temperature, monthly average daily maximum temperature, vapor pressure, potential evapotranspiration, and wet day frequency. The data was downloaded from the Centre of Environmental Data Archival (https://crudata.uea.ac.uk/cru/data/hrg/). For this analysis, 45 grid points with a regular $0.5 \times 0.5°$ resolution falling within the boundary of Tamil Nadu (Fig. 17.2) were considered for the analysis for 115 years from 1901 to 2015.
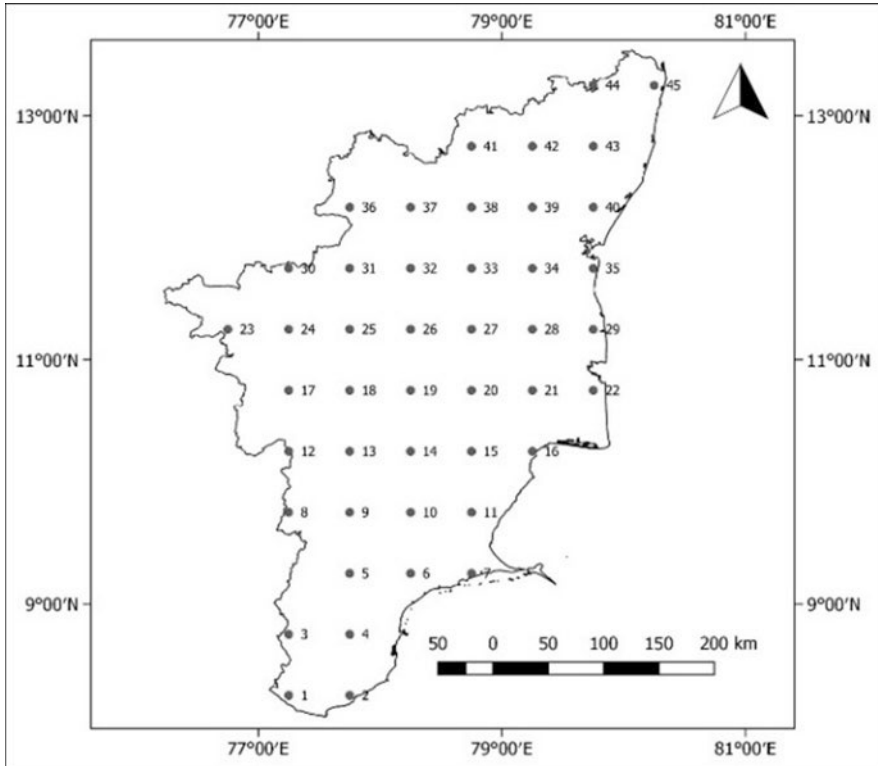
Fig. 17.2 Map of the grid points in the state of Tamil Nadu, India

Rainfall Analysis

The complete rainfall data sets were merged into four different sets, that is, winter, summer, northeast monsoon, and southwest monsoon, which were prescribed by the Indian Metrological Department (IMD) (www.mausam.imd.gov.in). The most common statistical parameters such as average, standard deviation, and coefficient of variation of the annual and seasonal rainfall data sets were determined to crosscheck the closeness of individual data with its total average. Homogeneity tests were done to authenticate the given prediction with Pettitt's, Buishand's, and Standard Normal Homogeneity Tests, which directly determine the breakpoint of the homogeneity at any given point of the series. This outcome explains the change in shift points, which illustrates the knowledge of the trend analysis. The obtained shift point year will help in breaking the entire data into two sets; trends before and after the shift point would help to determine the overall trend pattern.

Trend Detection

Mann–Kendall (MK) Test

The sinusoidal change can be precisely determined with the help of the MK test, which was utilized to find the trends in yearly and seasonal precipitation data sets. A null hypothesis stating that there is no possible occurrence of trend is assumed in this test, while an alternate hypothesis of either double-sided test having a trend or single-sided test having an increasing or decreasing trend was considered. Equation 17.1 provides the information on the test statistics to envisage the trend for the time series of $x_1, x_2, \ldots, x_n$.

$$S = \sum_{i=1}^{n-1}\sum_{j=i+1}^{n} \text{sgn}\left[x_j - x_i\right] \qquad (17.1)$$

where x_j are the sequential data values, n is the length of the data set, and sgn is given by Eq. 17.2:

$$\text{sgn}(y) = \left\{ \begin{array}{l} 1 \ldots \text{if}(y > 0) \\ 0 \ldots \text{if}(y = 0) \\ -1 \ldots \text{if}(y = 0) \end{array} \right\} \qquad (17.2)$$

The statistic S varies for $n \geq 8$. Equation 17.3 provides the variance and is followed as normal distribution for the same with its mean considered $E(S) = 0$:

$$V(S) = \frac{n(n - 1)(2n - 1) - \sum_{i=1}^{m} t_i(t_i - 1)(2t_i + 5)}{18} \qquad (17.3)$$

where m is the number of tied groups and t_i is the size of the ith knotted group.

In the final step with the help of Eq. 17.4, the standardized test statistic Z from the MK test is calculated:

$$Z_{MK} = \left\{ \begin{array}{l} \dfrac{s - 1}{\sqrt{var(S)}} \text{ when } S > 0 \\ 0 \cdots \text{when } S = 0 \\ \dfrac{S + 1}{\sqrt{var(S)}} \text{ when } S < 0 \end{array} \right\} \qquad (17.4)$$

Sen's Slope Estimator

Sen's slope estimator provides the extent of the trend of the single-variable time series. This method is completed in two steps with computing the slopes of each and every pair of ordinal time instant, followed by the calculation of the overall slope by considering the median of the initial slopes. It is used to determine if any trend is present in the provided data and cannot process if the data is situated away from the main set.

Equation 17.5 shows the Theil–Sen's estimator, which was used to estimate the slope of n pairs of data:

$$Q_i = \frac{x_j - x_k}{j - k} \text{ for } i = 1, \cdots N \tag{17.5}$$

where x_j and x_k are the data values at times j and k, $(j > k)$, respectively.

The median of the abovementioned N values of Q is called Sen's estimator of the slope. If the provided data consists of one data in each time period, then N is given by Eq. 17.6:

$$N = \frac{n(n-1)}{2} \tag{17.6}$$

where n is the number of time periods.

The N values are ranked first and the Sen's estimator (β) is calculated using Eq. 17.7:

$$\beta = \begin{cases} Q_{\frac{N+1}{2}} & \text{if N is odd} \\ \left(\frac{1}{2}\right)\left(Q_{\frac{N}{2}} + Q_{\frac{(N+2)}{2}}\right) & \text{if } N \text{ is even} \end{cases} \tag{17.7}$$

The product of number of years (115) and the Sen's slope value will provide a value, which is divided by the mean annual rainfall for each of the 45 grid points, resulting in the percent change in trend.

Homogeneity and Change Point Test

On a general note, in the homogeneity test, the null hypothesis will be considered by assuming the homogenous distribution for the categorical values. In the present study, a homogeneity test was conducted for the overall trend to determine the shift year with the help of the XLSTAT tool. Pettitt's, Standard Normal Homogeneity, and Buishand's tests were considered to determine the exact shift point between the two halves of the overall time data sets (Kocsis et al. 2020). However, Pettitt's test requires no such assumption regarding the null hypothesis to obtain the results

(Pettitt 1979). The SNHT deals with the series of ratios, while in comparison with the observing period to that of the average of the total time considered, which would show the details of the shift point, proving the results in Pettitt's test. The Buishand's test infers the change in shift point by considering the most recurring year and detects the change in its distribution mean.

Results

Percentage Rainfall Contribution for the Seasonal Series

The interdependence between annual and seasonal rainfall was explored by computing percentage rainfall contribution for each grid point by dividing the seasonal rainfall with the annual rainfall values. The results of the percentage rainfall contribution for the entire Tamil Nadu (TN) are listed in Table 17.1. TN is dominated by NEM with 46.40%, followed by SWM with 36.26%, summer with 13.98%, and winter with 3.37%. Grids #4, #7, #22, #29, #35, and #45 falling near the Bay of Bengal coast had more than 60% rainfall in NEM. Grids #3, #8, #9, #12, #18, #19, #23, #25, #26, #31– #33, #36–38, #41 and #42 falling near the Western Ghats region had more than 40% in SWM. Grids #3, #5, #17, #18, and #30 showed more than 20% in the summer season, and only grid #4 had more than 10% in the winter season. The grids (#2, #4, #6, #7, #11, #16, #22, #29, #35) nearer to the eastern coastal belt experience 50% higher NEM than SWM, and the grids (#3, #8, #12, #18, #23, #25, #31, #32, #36, #37, and #41) closer to the western ends of TN showed nearly10% higher SWM than NEM. The former is due to the influence of cyclonic precipitation, and the latter is due to the influence of the windward side of the Western Ghats.

Descriptive Statistical Analysis

The descriptive statistical analysis (Table 17.2) of the rainfall data depicts that the average annual rainfall varies from 756.59 mm in the northwestern part (grid #30) to 1604.86 mm in the southwestern part (grid #08), and the average for the entire TN being 1044.75 mm. The standard deviation varies from 121.99 mm (grid #24) to 279 mm (grid #45), with an average standard deviation of 175.98 mm for the state. The coefficient of variation varies from 12.22 % to 22.86 % for grid #3 and grid #45, respectively, with an average coefficient of variation of 16.88% for the entire state, which signifies the spatial interannual variability among the grids. The skewness is predominantly positive and varies between 0.613 and 0.03 except in grid #3 (-0.04) and grid #8 (-0.05), which shows that the annual rainfall is asymmetric with the distribution moderately skewed and lies to the right of the mean for the majority of the stations. Kurtosis varies from -0.84 to 1.19 for the entire state; for 18 grid points,

Table 17.1 Percentage rainfall contribution between annual and seasonal precipitation for grids #1–45

Grids	Annual – winter	Annual – summer	Annual – SWM	Annual – NEM
1	3.80	19.43	38.25	38.53
2	6.31	19.86	21.73	52.11
3	3.89	20.07	40.83	35.21
4	10.39	18.27	10.05	61.30
5	2.20	24.74	31.67	41.39
6	6.76	15.42	18.98	58.83
7	7.74	13.65	10.83	67.77
8	2.74	18.29	47.61	31.36
9	3.35	17.02	41.55	38.08
10	3.81	13.95	31.44	50.80
11	5.23	11.28	24.53	58.95
12	2.40	18.45	45.08	34.07
13	2.88	18.11	38.95	40.06
14	2.72	14.31	38.00	44.97
15	3.21	10.43	39.85	46.51
16	4.99	9.00	27.33	58.68
17	0.61	25.41	37.48	36.50
18	0.84	23.21	40.25	35.70
19	2.74	14.84	41.08	41.34
20	4.07	12.40	38.06	45.47
21	4.56	9.17	31.07	55.19
22	5.60	5.38	20.20	68.82
23	1.16	17.21	53.06	28.56
24	1.44	19.09	38.13	41.34
25	1.48	17.17	44.00	37.35
26	2.28	16.25	42.39	39.08
27	3.22	12.75	37.96	46.07
28	4.34	8.27	32.15	55.25
29	5.49	5.20	24.74	64.57
30	1.13	22.70	38.08	38.09
31	1.12	18.44	46.15	34.30
32	1.77	16.79	44.88	36.56
33	2.82	12.79	40.06	44.33
34	3.94	7.85	35.83	52.38
35	5.32	4.52	28.64	61.52
36	1.04	19.47	46.45	33.04
37	1.31	15.72	48.94	34.04
38	2.55	13.02	42.42	42.01
39	3.35	8.05	38.90	49.70
40	3.94	4.73	33.85	57.48
41	1.87	13.04	47.83	37.26
42	2.85	8.72	43.01	45.42

Table 17.1 (continued)

Grids	Annual – winter	Annual – summer	Annual – SWM	Annual – NEM
43	2.52	5.10	38.15	54.24
44	2.53	5.56	38.54	53.38
45	3.28	3.74	32.56	60.43
% Contribution	**3.37**	**13.98**	**36.26**	**46.40**

the distribution is leptokurtic, implying the peaks are higher and sharper than the peak of the normal distribution, and for the remaining 27 grid points, the distribution is platykurtic, signifying the distribution has its peak shallower than the normal distribution.

Figures 17.3 and 17.4 depict the spatial mean annual and mean monsoonal rainfall variation spread over the entire state of Tamil Nadu. The average yearly rainfall of TN is high in the southwestern belt and northeastern coastal belt, and it is less in the central and northwestern regions. It is also well understood that the concentration of NEM is more in northern and central coastal areas in the east and gradually shows a decline on the way to the northwestern regions of TN. At the same time, SWM is dominated on the western and southwestern sides of TN, which spreads across the ridges of the Western Ghats, and its contribution is less on the eastern and coastal areas in TN.

Trend Analysis for Annual and Seasonal Rainfall During 1901–2015

The MK trend results and the percentage change in the rainfall per year for annual and seasonal series are presented in Tables 17.3 and 17.4. For the annual series, the majority of grids depicted an insignificant increasing trend with only four grid locations (#32, #36, #37, and #41) exhibiting significance in its positive trend. Parallelly grids #3, #5, #8, #9, #12, and #13 showed an insignificant decreasing trend in its annual series. The gradational image of the annual rainfall variation per year is pictured in Fig. 17.5. Almost all the gridded locations fall under positive slopes with a considerable number of negative slopes in the southern and southwestern regions. There is a gradual hike in the overall trend from southwest regions to northeastern tip with only the central northern region having the peak rainfall rates (0.83–1.12 mm/year). Most of the grid points falling in this red band had received a minimum rainfall average and hence did not significantly contribute to the overall rainfall trend.

On the seasonal trend analysis, around 40 grid points exhibited a significant decreasing trend, and the remaining 5 grids (#1–#5) show an insignificant decreasing trend for the winter season. There were no considerable increasing or decreasing trends noticed for the summer season across the grids. Figure 17.6 represents the variation of the overall trend of the SWM and NEM, respectively. Although these

Table 17.2 Descriptive statistical analysis

Grids	Mean	Std dev	CV	Kurtosis	Skewness
1	1310.05	166.65	12.72	−0.28	0.03
2	938.02	127.65	13.61	−0.05	0.23
3	1534.54	187.45	12.22	−0.27	−0.04
4	779.81	130.41	16.72	−0.10	0.25
5	1128.08	152.87	13.55	−0.04	0.22
6	872.64	135.68	15.55	0.40	0.43
7	882.55	152.61	17.29	0.14	0.21
8	1604.85	198.72	12.38	−0.17	−0.05
9	1164.73	164.33	14.11	−0.25	0.17
10	872.75	144.93	16.61	0.38	0.36
11	923.49	161.98	17.54	0.66	0.35
12	1331.64	181.28	13.61	−0.15	0.07
13	1015.02	152.45	15.02	−0.23	0.12
14	871.47	149.33	17.14	0.23	0.38
15	987.96	181.22	18.34	0.37	0.50
16	1059.37	191.75	18.10	0.33	0.27
17	1007.49	145.07	14.40	−0.47	0.06
18	908.54	138.93	15.29	−0.47	0.18
19	887.96	148.03	16.67	−0.15	0.36
20	915.53	166.10	18.14	0.00	0.43
21	1029.32	183.88	17.86	0.06	0.26
22	1305.59	257.42	19.72	−0.15	0.05
23	1219.93	181.26	14.86	−0.64	0.01
24	768.65	122.00	15.87	−0.61	0.24
25	866.61	132.10	15.24	−0.74	0.25
26	909.68	150.07	16.50	−0.57	0.27
27	959.41	161.49	16.83	−0.29	0.35
28	1107.90	198.57	17.92	−0.07	0.22
29	1296.53	261.22	20.15	−0.02	0.18
30	756.59	127.13	16.80	−0.84	0.20
31	875.91	143.86	16.42	−0.64	0.33
32	924.10	160.59	17.38	−0.59	0.25
33	989.76	168.32	17.01	−0.13	0.31
34	1166.94	201.59	17.28	0.26	0.28
35	1329.51	262.75	19.76	0.22	0.23
36	838.91	146.66	17.48	−0.57	0.28
37	934.95	168.80	18.05	−0.06	0.36
38	946.35	167.33	17.68	0.56	0.54
39	1118.12	206.62	18.48	1.20	0.61
40	1248.56	248.21	19.88	0.84	0.51
41	887.50	158.19	17.82	0.53	0.53
42	1038.20	190.79	18.38	0.87	0.49

Table 17.2 (continued)

Grids	Mean	Std dev	CV	Kurtosis	Skewness
43	1171.28	237.90	20.31	1.10	0.61
44	1106.16	225.93	20.42	0.85	0.57
45	1220.73	279.00	22.86	0.63	0.52
Average	**1044.75**	**175.98**	**16.89**		

Fig. 17.3 Average annual rainfall of Tamil Nadu (1901–2015)
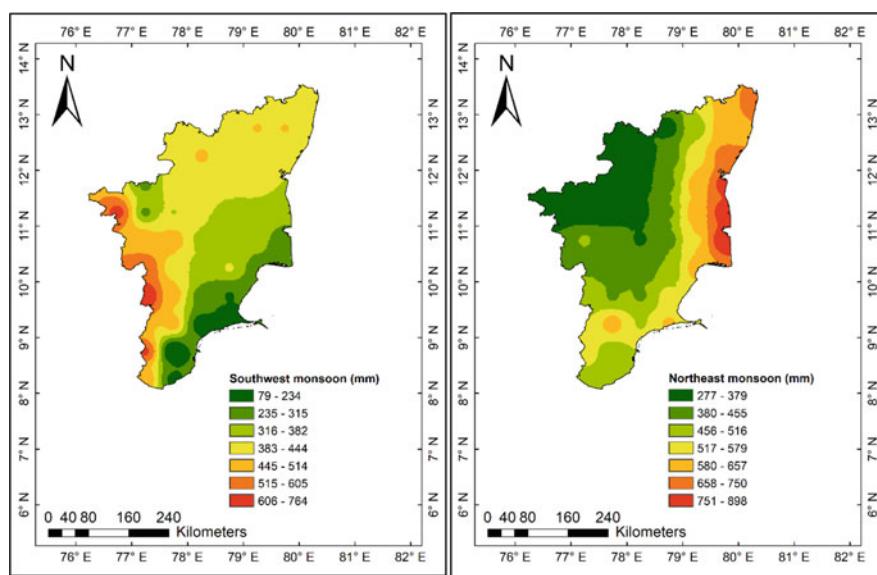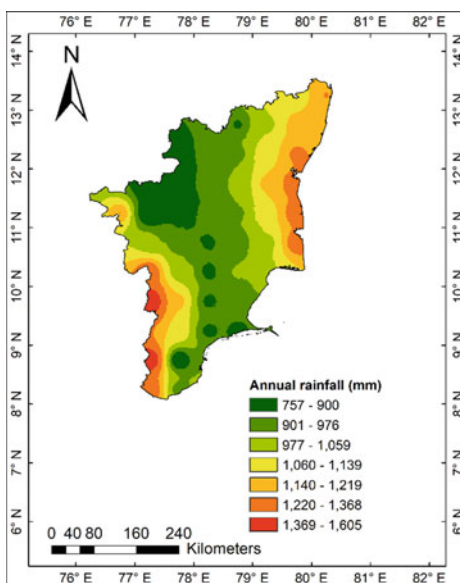
Fig. 17.4 Average NEM and SWM monsoon rainfall of Tamil Nadu (1901–2015)

Table 17.3 Values of MK trend and Sen's slope (β) for grids #1–23

	Precipitation (mm)														
	Annual			Seasonal											
				Winter			Summer			SWM			NEM		
Grids	Z	β	%	Z	β	%	Z	β	%	Z	β	%	Z	β	%
1	0.01	0.00	0.04	−0.48	−0.05	−10.82	0.80	0.20	8.90	−1.45	−0.51	−11.71	0.09	0.04	0.93
2	0.38	0.13	1.65	−0.35	−0.04	−8.04	0.73	0.14	8.38	−1.23	−0.19	−10.62	0.45	0.16	3.70
3	−0.44	−0.25	−1.89	−1.08	−0.13	−24.25	0.37	0.10	3.73	−1.19	−0.47	−8.55	−0.34	−0.11	−2.27
4	0.17	0.08	1.23	−1.32	−0.18	−25.80	0.43	0.06	5.12	−0.39	−0.03	−4.36	0.27	0.14	3.32
5	−0.40	−0.21	−1.57	−1.41	−0.15	−49.98	0.42	0.09	2.57	−0.73	−0.23	−5.38	0.29	0.11	2.03
6	0.00	0.00	0.04	−2.20	−0.24	−46.40	0.35	0.06	4.80	−0.99	−0.15	−10.55	0.67	0.33	7.43
7	0.93	0.40	5.16	−2.36	−0.32	−53.22	0.87	0.14	13.30	−0.19	−0.03	−3.34	1.17	0.59	11.26
8	−1.04	−0.49	−3.53	−2.36	−0.16	−42.79	−0.55	−0.04	−1.75	−0.79	−0.13	−1.94	0.23	−0.14	−3.16
9	−1.04	−0.48	−4.76	−2.36	−0.18	−52.47	−0.55	−0.08	−4.47	−0.79	−0.26	−6.18	0.23	0.07	1.76
10	0.35	0.14	1.86	−2.63	−0.16	−56.07	−0.08	−0.01	−0.94	−0.66	−0.17	−6.95	1.44	0.49	12.73
11	0.59	0.27	3.41	−2.89	−0.27	−64.70	0.24	0.03	3.15	−0.70	−0.15	−7.65	1.50	0.73	15.37
12	−0.06	−0.02	−0.20	−2.19	−0.14	−49.41	−0.35	−0.06	−2.78	0.22	0.08	1.62	0.42	0.13	3.37
13	−0.23	−0.09	−0.98	−2.73	−0.16	−62.58	−0.91	−0.14	−8.71	−0.34	−0.09	−2.49	1.36	0.39	11.03
14	0.53	0.21	2.76	−2.90	−0.15	−73.26	−1.06	−0.10	−9.33	−0.27	−0.07	−2.32	1.90	0.56	16.52
15	0.14	0.06	0.68	−2.94	−0.18	−66.36	−0.48	−0.05	−5.31	−0.53	−0.20	−5.70	1.89	0.69	17.37
16	0.84	0.49	5.34	−2.83	−0.28	−61.79	−0.03	0.00	−0.42	0.10	0.03	0.99	1.70	0.92	17.02
17	0.21	0.09	0.97	−2.56	−0.09	−59.27	−0.87	−0.13	−9.05	0.02	0.01	0.15	1.10	0.30	9.56
18	0.53	0.20	2.53	−2.91	−0.11	−67.84	−1.54	−0.18	−13.30	0.38	0.48	14.24	1.76	0.10	3.22
19	1.13	0.47	6.02	−2.78	−0.14	−67.45	−1.37	−0.16	−13.60	0.51	0.14	4.47	2.26	0.62	19.57
20	1.04	0.48	6.06	−2.59	−0.21	−64.87	−1.27	−0.14	−14.13	0.35	0.10	3.30	2.35	0.74	20.50
21	1.20	0.70	7.80	−2.53	−0.23	−56.57	−0.28	−0.03	−3.04	0.28	0.07	2.41	2.04	0.94	19.10
22	1.51	1.06	9.35	−2.57	−0.33	−52.52	−0.08	−0.01	−0.83	0.75	0.16	7.13	1.91	1.46	18.65
23	0.88	−0.45	−4.24	−3.07	−0.09	−71.83	−0.82	−0.17	−9.43	−1.09	−0.39	−6.95	0.11	0.03	0.95

Table 17.4 Values of MK trend and Sen's slope (β) for grids #24–45

Grids	Precipitation (mm)														
	Annual			Seasonal											
				Winter			Summer			SWM			NEM		
	Z	β	%	Z	β	%	Z	β	%	Z	β	%	Z	β	%
24	0.47	0.19	2.79	−2.84	−0.07	−67.62	−0.42	−0.05	−4.26	0.53	0.10	3.78	1.02	0.25	8.91
25	1.12	0.45	5.96	−2.81	−0.08	−67.61	−0.97	−0.11	−8.77	0.94	0.24	7.12	1.63	0.41	14.45
26	1.56	0.70	8.80	−2.56	−0.12	−64.34	−1.09	−0.12	−9.53	0.99	0.29	8.63	2.38	0.62	19.92
27	1.54	0.76	9.07	−2.42	−0.16	−61.36	−1.06	−0.10	−9.08	0.90	0.26	8.26	2.07	0.72	18.81
28	1.57	0.92	9.55	−2.53	−0.25	−60.46	−0.58	−0.05	−6.63	1.10	0.31	10.12	1.96	0.96	17.96
29	1.62	1.12	9.97	−2.54	−0.37	−59.05	−0.57	−0.04	−6.68	1.19	0.28	10.10	1.76	1.30	17.82
30	1.29	0.50	7.58	−2.63	−0.05	−61.24	−0.19	−0.03	−1.67	1.29	0.28	11.28	0.91	0.24	9.46
31	1.64	0.70	9.17	−2.49	−0.05	−57.45	−0.33	−0.04	−2.93	1.28	0.40	11.28	1.55	0.35	13.56
32	2.39	1.12	13.94	−2.27	−0.08	−54.07	−0.36	0.03	2.12	1.66	0.54	15.01	2.45	0.66	22.44
33	1.86	0.92	10.73	−2.64	−0.15	−61.12	−0.46	−0.05	−4.54	1.78	0.50	14.40	1.86	0.66	17.28
34	1.52	0.87	8.53	−2.73	−0.26	−65.76	−0.33	−0.03	−3.59	1.53	0.40	10.95	1.56	0.82	15.39
35	1.38	1.05	9.08	−2.67	−0.40	−65.01	0.32	0.02	4.29	1.82	0.51	15.28	1.31	0.85	11.90
36	2.15	0.94	12.84	−2.80	−0.05	−61.28	0.36	0.05	3.31	1.90	0.55	16.27	1.30	0.32	13.09
37	2.20	1.12	13.79	−2.25	−0.06	−55.98	0.66	0.08	6.57	2.07	0.73	18.28	1.56	0.46	16.45
38	1.91	0.93	11.29	−2.58	−0.14	−65.10	0.59	0.07	6.10	1.84	0.54	15.37	1.47	0.51	14.71
39	1.42	0.82	8.40	−2.96	−0.18	−54.75	0.84	0.13	17.00	1.75	0.64	16.83	0.80	0.22	4.52
40	1.06	0.66	6.10	−3.06	−0.32	−75.71	0.79	0.05	10.68	1.76	0.56	15.10	0.52	0.34	5.37
41	2.35	−0.09	−1.17	−2.56	0.08	52.33	0.66	0.64	63.40	2.18	0.37	10.14	1.33	1.04	36.12
42	1.59	0.74	8.23	−2.82	−0.19	−74.33	1.17	0.07	9.40	2.11	0.64	16.60	0.50	0.19	4.53
43	1.21	0.74	7.30	−2.88	−0.19	−74.72	0.96	0.07	14.25	2.01	0.64	16.59	0.29	0.19	3.36
44	1.17	0.67	6.95	−2.92	−0.18	−74.84	1.30	0.13	23.43	2.08	0.66	17.73	0.00	0.00	0.00
45	0.94	0.73	6.87	−3.08	−0.27	−77.99	1.44	0.11	28.75	2.28	0.70	20.25	−0.09	−0.05	−0.81

Fig. 17.5 Annual rainfall trend of Tamil Nadu (1901–2015)
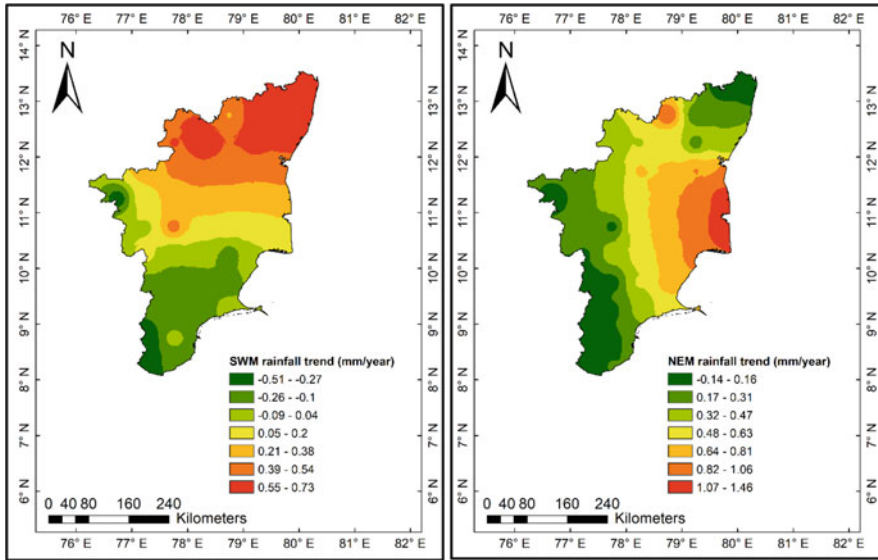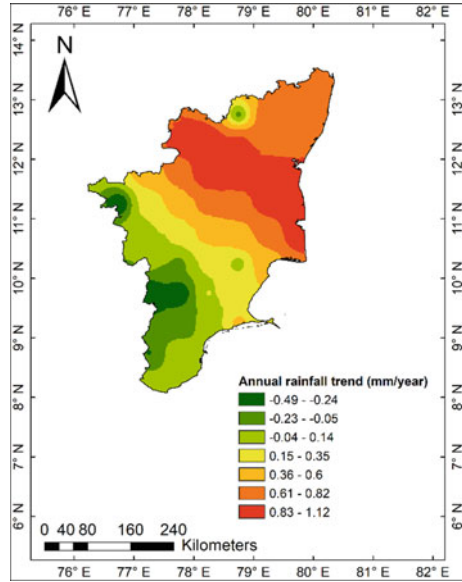
Fig. 17.6 SWM and NEM rainfall trend of Tamil Nadu (1901–2015)

two seasons were the major contributors to the annual precipitation, almost every grid points showed an insignificant increasing trend with no points having a significant decreasing trend. The SWM exhibited a significant increasing trend over the northern regions of Tamil Nadu (grids #37, #41–45), which gradually got swapped to an insignificant decreasing trend (grids #1–15) along the southern sections. The result signifies how spatially the significant rising trend is noticed for SWM from the farthest northern end grids, and the trend got reversed for the grids lying south. While considering the NEM, grids falling in the eastern and central Tamil Nadu (#19–21, #26–28, and #32) experienced a significant increasing precipitation pattern that got backed to insignificant decreasing trends only in grids #3 and #45. The remaining 36 grids exhibited an insignificantly increasing trend over the 115 years. As a concluding remark, around 77.77%, 53.33 %, and 80% of the grids displayed an insignificant increasing trend for annual, SWM, and NEM, respectively, with only countable number (<17%) of grids exhibiting either significantly increasing or decreasing trend for the three series. Since the contribution of rainfall during winter and summer is meager, the increasing/decreasing trend has no effect on water availability in the region.

Tables 17.3 and 17.4 also depict the percentage of changes over mean values in annual and seasonal rainfall. Only one grid (#41) exhibits more than 10% changes in all four series. Decreasing the magnitude of change in rainfall is witnessed in all grids for the winter season. More than 10% of changes in three and two monsoonal series are 13% and 42%, respectively. More than 10% of changes are observed in northbound grids in SWM, and on the contrary, southbound grids experience a decrease in magnitude.

Change Point Analysis

Pettit's test, SNHT test, and Buishand's test were employed to determine the homogeneity of the rainfall series. Table 17.5 reveals the outcome of the probable change point year in the annual rainfall. Since Buishand's and Pettit's tests hold useful for detecting the change point in the middle of the series (Angulo-Martínez et al. 2009), by considering the outputs, 1962 was taken as the most probable change point year.

Comparisons in Mean Annual Precipitation Between Two Time Periods

Based on the probable change point year, that is, 1962, the annual and seasonal series were divided, and the basic statistical and trend detection analysis was done for the periods 1901–1962 and 1963–2015, respectively. The average values of annual, SWM, and NEM precipitation before and after the change point for each station were

Table 17.5 Pettit's test, SNHT test, and Buishand's test to find out the most probable change year

	Pettit's test			SNHT			Buishand's test		
Grids	K value	Year	Tread	T_0	Year	Tread	Q value	Year	Trend
1	254	1986	H_0	6.55	2014	H_0	3.88	1925	H_0
2	397	1991	H_0	7.76	2014	H_0	6.86	1991	H_0
3	348	1963	H_0	6.73	2014	H_0	5.15	1933	H_0
4	468	1996	H_0	5.53	2014	H_0	8.20	1996	H_0
5	334	1963	H_0	7.62	2014	H_0	4.85	1996	H_0
6	410	1996	H_0	7.15	2014	H_0	7.51	1996	H_0
7	444	1977	H_0	6.26	2014	H_0	6.09	1977	H_0
8	444	1977	H_0	6.26	2014	H_0	6.09	1977	H_0
9	520	1957	H_0	6.39	2014	H_0	5.73	1957	H_0
10	368	1996	H_0	7.71	2014	H_0	7.88	1996	H_0
11	438	1976	H_0	6.46	2014	H_0	9.04	1976	H_0
12	379	1964	H_0	5.37	2014	H_0	5.04	1996	H_0
13	368	1964	H_0	6.46	2014	H_0	6.00	1996	H_0
14	374	1996	H_0	7.83	2014	H_0	8.47	1996	H_0
15	256	1996	H_0	7.01	2014	H_0	7.53	1976	H_0
16	552	1962	H_0	5.19	2014	H_0	10.91	1976	H_0
17	304	1996	H_0	3.79	1903	H_0	5.58	1996	H_0
18	432	1996	H_0	6.05	2014	H_0	8.31	1996	H_0
19	443	1996	H_0	7.13	2014	H_0	9.49	1996	H_0
20	532	1962	H_0	6.44	2014	H_0	9.42	1962	H_0
21	660	1962	H_0	5.21	2013	H_0	11.40	1962	H_0
22	762	1962	H_0	5.60	1976	H_0	12.06	1976	H_0
23	592	1964	H_0	3.84	1903	H_0	9.37	1964	H_0
24	454	1996	H_0	4.91	1903	H_0	7.19	1996	H_0
25	584	1996	H_0	5.86	1996	H_0	9.69	1996	H_0
26	620	1996	H_0	6.69	1996	H_0	10.34	1996	H_0
27	660	1962	H_0	6.61	1996	H_0	11.19	1962	H_0
28	856	1962	H_0	6.18	1962	H_0	13.35	1962	H_0
29	920	1962	H_0	5.68	1962	H_0	12.79	1962	H_0
30	610	1952	H_0	4.98	2006	H_0	8.67	1938	H_0
31	676	1996	H_0	6.83	2003	H_0	9.94	1996	H_0
32	866	1961	H_0	8.45	2003	H_0	12.93	1961	H_0
33	862	1961	H_0	7.43	2003	H_0	12.76	1962	H_0
34	847	1962	H_0	6.10	2003	H_0	12.75	1962	H_0
35	900	1959	H_0	5.54	1959	H_0	12.67	1959	H_0
36	826	1952	H_0	7.17	2003	H_0	11.34	1952	H_0
37	808	1952	H_0	7.72	2003	H_0	11.30	1952	H_0
38	828	1961	H_0	7.50	2003	H_0	11.51	1961	H_0
39	834	1959	H_0	6.24	1903	H_0	10.18	1959	H_0
40	833	1959	H_0	5.68	1903	H_0	10.50	1959	H_0
41	916	1961	H_0	7.92	2003	H_0	12.12	1961	H_0

Table 17.5 (continued)

Grids	Pettit's test			SNHT			Buishand's test		
	K value	Year	Tread	T_0	Year	Tread	Q value	Year	Trend
42	860	1959	H_0	6.27	1903	H_0	10.92	1959	H_0
43	826	1959	H_0	6.35	1903	H_0	10.67	1959	H_0
44	798	1955	H_0	6.01	1903	H_0	9.80	1959	H_0
45	710	1955	H_0	5.63	1903	H_0	9.20	1959	H_0

got. The difference between average precipitations of the two periods as a percentage of the averages of the first period was calculated and is summarized in Table 17.6.

The result demonstrates a smaller number of grids showing a decrease in rainfall in the second period with relatively less magnitude in both annual (22%) and monsoonal series [SWM (8.89%) and NEM (4.44%)]. In contrast, a greater number of grids show an increase in rainfall in both annual and monsoonal series. No grid shows more than 10% increase in annual precipitation. The central, northern, and mid-coastal TN, except the western and southern regions, exhibit more than a 10% increase in rainfall during SWM. However, in NEM, only grids falling in the central area show this magnitude.

Pre- and Post-change Point Trend Analysis for the Periods 1901–1962 and 1963–2015

Rainfall trend analysis for the periods 1901–1962 and 1963–2015 is provided in Tables 17.7 and 17.8. No significant increasing or decreasing trend is found in annual and seasonal series for both the periods. An insignificant positive trend is observed for all grid points during the winter 1963–2015 period, while most of the grid points show an insignificant negative trend during the winter 1901–2015 period. As seen in Fig. 17.7, the SWM shows equal numbers of insignificant positive and negative trends during the second period, whereas only the northeastern tip revealed an insignificant positive trend for the first period. This pattern of rainfall will not have any diverse effect on the overall trend of the annual rainfall since the location that has to be fed during this particular season is at a declining pattern. Even the second part of the series had a majority of declining pattern with the northern belt owing insignificant positive trend. The Western Ghats region had seen a recession in its trend in the latter half of the series, thereby reducing the rainfall to 1.2 mm/year.

Contradicting the usual fed locations (grids #35, #39, #40, #42–45), other gridded regions owed an insignificant increasing trend in its NEM during 1963–2015. As depicted in Fig. 17.8, the first part of the series rendered an insignificantly increasing trend in the western and west-central regions, momentously reaching a significantly decreasing trend as driven toward the northeastern tip. The vulnerability of the insignificant decreasing trend in the second half of the series resulted in declination of the overall annual rainfall quantum.

Table 17.6 Percentage change in mean rainfall over the period of 1901–1962 and 1963–2015

Grids	Annual	SWM	NEM
1	−1.28	−4.02	3.06
2	0.30	−2.66	4.30
3	−1.98	−2.00	0.67
4	−0.29	6.49	4.07
5	−1.10	0.12	2.67
6	0.40	3.81	5.21
7	3.55	11.79	8.35
8	−2.07	0.66	−1.07
9	−2.21	0.72	1.25
10	2.75	5.65	8.11
11	4.13	8.03	9.92
12	−1.00	1.64	1.56
13	−0.69	3.48	4.67
14	3.66	7.71	9.88
15	4.51	6.67	11.39
16	6.67	11.98	12.09
17	−0.51	0.80	4.03
18	1.51	5.43	6.89
19	4.83	10.60	10.89
20	6.12	12.55	13.66
21	7.34	9.94	14.08
22	8.50	13.55	13.68
23	−4.29	−3.45	−0.66
24	0.51	2.78	3.82
25	2.98	6.02	8.03
26	5.54	10.21	11.91
27	6.76	11.73	13.17
28	8.67	12.08	15.11
29	9.37	12.68	15.53
30	1.32	6.23	2.49
31	3.28	7.19	5.30
32	7.98	11.54	14.15
33	7.83	12.14	13.61
34	7.95	10.39	14.21
35	8.91	12.74	13.65
36	4.87	9.88	5.30
37	6.58	10.61	1.63
38	7.02	10.32	11.09
39	6.26	9.34	9.74
40	7.00	10.36	10.27
41	7.37	11.54	9.20
42	6.52	10.26	8.37
43	7.15	10.48	8.73
44	5.68	10.20	5.53
45	5.89	12.20	5.37

Table 17.7 Results of MK test (Z) and % change for the period 1901–1962

Grids	Annual		Seasonal Winter		Summer		SWM		NEM	
	Z	% Change	Z	% Change	Z	% Change	Z	% Change	Z	% Change
1	0.67	4.10	1.65	48.32	3.17	50.99	−0.85	−7.06	−1.17	−13.97
2	0.43	2.76	1.51	48.86	3.10	46.69	−1.12	−12.48	−0.97	−13.28
3	0.30	1.42	1.22	33.42	3.06	43.28	−0.98	−8.72	−1.21	−12.85
4	0.11	1.56	1.01	32.08	2.59	42.29	−1.54	−18.67	−1.08	−13.85
5	−0.07	−0.51	0.74	24.43	2.75	40.80	−1.00	−7.67	−0.83	−9.57
6	−0.19	−1.40	0.13	3.23	2.51	42.92	−1.38	−17.62	−0.68	−9.40
7	−0.33	−2.63	−0.09	−2.12	2.65	45.58	−1.43	−21.09	−0.77	−9.50
8	0.34	2.01	0.51	15.30	2.75	30.85	−0.48	−3.26	−0.63	−5.59
9	−0.16	−0.79	0.13	4.13	2.41	33.01	−0.81	−7.34	−0.28	−3.47
10	−0.40	−3.02	−0.21	−4.37	2.11	−37.50	−1.36	−17.86	−0.06	−0.84
11	−0.73	−4.60	−0.41	−32.82	2.31	44.01	−1.02	−16.68	−0.43	−4.60
12	0.67	2.32	−0.67	−15.87	2.50	26.31	−0.90	−4.16	0.70	6.75
13	0.67	3.04	−0.67	−16.75	2.50	34.18	−0.90	−6.37	0.70	7.63
14	−0.33	−2.48	−0.54	−19.48	1.85	28.69	−1.28	−14.84	0.07	1.01
15	−1.02	−6.65	−0.50	−12.20	2.22	36.25	−1.11	−13.77	−0.19	−2.77
16	−1.32	−7.78	−0.42	−13.38	2.17	40.39	−0.77	−11.20	−0.64	−10.45
17	0.75	4.99	−0.38	−10.72	2.16	28.56	−0.67	−5.28	0.27	3.15
18	0.33	2.14	−0.58	−16.96	1.79	23.13	−0.66	−6.82	0.50	5.90
19	0.02	0.30	−0.60	−17.89	1.91	23.76	−1.08	−11.29	0.22	1.49
20	−0.67	−4.63	−0.53	−24.69	2.16	32.97	−1.40	−20.35	−0.18	−2.55
21	−1.09	−8.24	−0.57	−18.53	1.68	28.97	−0.86	−9.85	−0.66	−9.03
22	−0.97	−9.56	−0.53	−14.56	2.05	34.39	−0.80	−9.75	−0.57	−11.74
23	0.23	1.72	−0.83	−27.00	1.69	26.84	−1.23	−10.02	−0.21	−2.73

(continued)

Table 17.7 (continued)

Grids	Annual		Seasonal							
			Winter		Summer		SWM		NEM	
	Z	% Change	Z	% Change	Z	% Change	Z	% Change	Z	% Change
24	0.22	1.98	−0.69	−19.68	1.79	24.67	−0.94	−8.57	0.09	1.05
25	0.22	1.56	−0.53	−15.09	1.68	23.96	−0.46	−5.94	0.06	1.15
26	0.05	0.60	−0.40	−10.87	1.48	13.62	−1.05	−12.85	0.17	1.45
27	−0.37	−2.52	−0.36	−16.04	1.43	23.78	−1.09	−9.69	−0.33	−5.15
28	−1.31	−9.65	−0.63	−18.57	1.39	22.74	−0.94	−11.03	−0.92	−14.08
29	−1.30	−12.89	−0.77	−23.29	1.25	25.47	−0.81	−7.69	−1.24	−16.96
30	1.23	8.32	−0.53	−14.75	1.96	24.59	−0.06	−0.69	1.07	13.44
31	0.83	5.33	−0.38	−8.47	1.25	17.38	−0.19	−1.35	0.92	11.94
32	0.05	0.47	−0.16	−5.02	0.88	13.81	−0.90	−10.95	0.19	2.58
33	−0.71	−5.27	−0.38	−11.48	1.20	20.02	−0.70	−8.56	−0.80	−8.98
34	−1.25	−9.19	−0.62	−21.21	1.26	21.85	−0.75	−6.60	−1.02	−18.27
35	−1.43	−13.43	−0.81	−28.83	1.08	22.95	−0.39	−3.15	−1.45	−22.77
36	1.00	7.86	−0.49	−10.13	1.46	19.45	0.00	0.28	1.01	15.67
37	0.52	5.44	−0.46	−10.59	1.36	20.98	−0.11	−1.94	0.43	7.32
38	−0.39	−3.22	−0.58	−18.86	1.28	−20.79	−0.44	−6.70	−0.39	−7.26
39	−0.97	7.89	−0.77	27.65	1.56	−33.83	−0.21	2.14	−1.25	20.33
40	−1.57	−14.37	−1.11	−34.22	1.84	43.74	−0.10	−0.74	−1.75	−28.83
41	−0.08	−0.69	−0.59	−17.42	1.26	21.98	−0.35	−4.43	−0.30	−6.08
42	−0.79	−6.15	−0.91	−115.26	1.91	38.93	0.09	1.00	−1.25	−21.45
43	−1.31	−12.04	−1.04	−33.58	1.90	38.24	0.19	1.82	−1.64	−26.36
44	−0.84	−7.94	−1.25	−38.71	1.83	40.17	0.36	3.26	−1.38	−25.38
45	−0.89	−10.06	−1.59	−46.66	1.69	38.64	0.85	10.68	−1.57	−28.19

Table 17.8 Results of MK test (Z) and % change for the period 1963–2015

Grids	Annual		Seasonal									
			Winter		Summer		SWM		NEM			
	Z	% Change	Z	% Change	Z	% Change	Z	% Change	Z	% Change		
1	0.88	6.28	0.60	22.86	0.12	2.51	−0.81	−9.55	1.29	18.01		
2	1.34	8.67	0.91	29.25	0.29	5.85	−0.89	−11.02	1.18	18.17		
3	0.79	4.94	0.40	16.59	0.09	1.33	−0.87	−9.71	1.22	18.94		
4	1.59	13.37	0.75	24.68	0.41	6.56	−0.15	−1.69	1.06	13.94		
5	0.77	4.27	0.75	26.91	0.66	10.58	−0.61	−8.97	1.00	14.61		
6	0.99	7.90	0.82	27.67	0.62	9.41	−0.66	−10.65	1.07	14.25		
7	1.08	9.63	0.82	30.79	0.53	10.92	−0.32	−8.02	0.85	12.76		
8	0.28	1.65	0.64	16.77	0.41	5.82	−0.71	−7.60	1.08	14.06		
9	0.22	1.88	0.58	25.71	0.81	9.41	−0.77	−11.42	0.93	12.04		
10	0.56	5.81	0.84	35.84	0.87	14.66	−0.61	−10.38	0.93	12.55		
11	0.21	2.44	1.01	32.92	0.93	18.78	−0.78	−14.61	0.88	11.48		
12	0.83	6.66	0.72	22.41	0.33	4.86	−0.01	−0.13	1.08	14.36		
13	0.52	4.55	1.11	31.45	0.83	11.87	−0.35	−3.95	0.93	12.61		
14	0.33	3.68	1.22	36.66	1.08	16.30	−0.50	−8.71	0.94	11.38		
15	−0.21	−1.93	1.47	49.01	1.22	18.73	−0.77	−15.13	0.80	10.31		
16	0.11	0.87	1.25	40.97	0.74	15.58	−0.55	−8.06	0.79	9.38		
17	0.93	6.57	0.95	29.57	0.15	2.02	0.46	5.87	0.91	11.70		
18	0.82	6.19	1.08	31.03	0.71	11.24	0.02	0.54	0.73	11.80		
19	0.27	1.89	1.27	38.65	1.08	14.33	−0.36	−6.71	0.70	9.14		
20	0.08	0.92	1.47	46.38	1.14	18.11	−0.41	−8.33	0.81	8.00		
21	0.14	2.18	1.23	38.76	0.68	10.96	−0.58	−8.68	0.62	5.76		
22	0.18	1.74	1.24	38.26	0.63	13.96	−0.12	−1.46	0.30	3.30		
23	1.07	7.53	0.95	21.50	−0.43	−6.18	0.91	8.27	1.18	15.54		

(continued)

Table 17.8 (continued)

| Grids	Annual		Seasonal				SWM		NEM	
			Winter		Summer					
	Z	% Change	Z	% Change	Z	% Change	Z	% Change	Z	% Change
24	1.33	11.71	1.17	26.09	0.38	3.39	1.11	12.96	1.02	11.85
25	0.98	8.81	1.30	35.15	0.84	10.51	0.50	6.39	0.73	7.60
26	0.58	4.98	1.32	38.93	1.19	12.56	0.08	1.92	0.62	8.23
27	0.31	2.44	1.37	42.52	1.07	15.82	-0.27	-4.29	0.41	4.77
28	0.07	0.88	1.05	33.57	0.64	11.92	-0.29	-3.90	0.27	3.34
29	-0.07	-0.32	1.00	36.20	0.43	9.31	-0.29	-3.71	0.08	0.74
30	1.37	13.33	1.25	26.47	0.56	6.81	0.94	14.21	0.84	10.55
31	1.48	13.57	1.11	24.85	1.27	16.81	0.81	9.69	1.14	13.09
32	1.02	9.53	1.40	33.21	1.20	16.81	0.35	7.11	0.53	8.19
33	0.28	2.79	1.01	31.80	0.96	12.73	0.31	2.30	0.48	4.75
34	-0.07	-0.49	0.79	26.43	0.81	13.24	0.13	1.35	0.00	-0.02
35	-0.44	-3.47	0.83	30.39	0.29	4.41	0.31	6.41	-0.17	-1.86
36	1.37	13.79	1.03	19.05	0.65	21.62	0.73	9.43	0.54	10.07
37	1.05	9.25	1.37	27.79	1.62	24.91	0.75	8.45	0.62	10.40
38	0.56	3.83	0.81	20.46	1.32	20.78	0.56	8.03	0.53	7.57
39	-0.10	-0.71	0.43	14.54	0.57	9.46	0.74	9.45	-0.10	-1.60
40	-0.44	-3.48	0.33	10.88	0.31	5.09	0.41	5.93	-0.44	-6.48
41	0.94	7.32	0.87	20.06	1.27	21.88	0.75	7.75	0.64	8.51
42	0.16	0.71	0.52	13.66	0.71	14.88	0.68	9.46	-0.02	-0.32
43	-0.21	-2.37	0.44	8.16	0.25	7.43	0.47	5.13	-0.57	-6.74
44	0.09	0.61	0.47	11.80	0.36	11.10	0.59	7.65	-0.05	-0.56
45	-0.08	-0.81	0.21	6.58	0.34	15.40	0.35	4.79	-0.33	-4.49
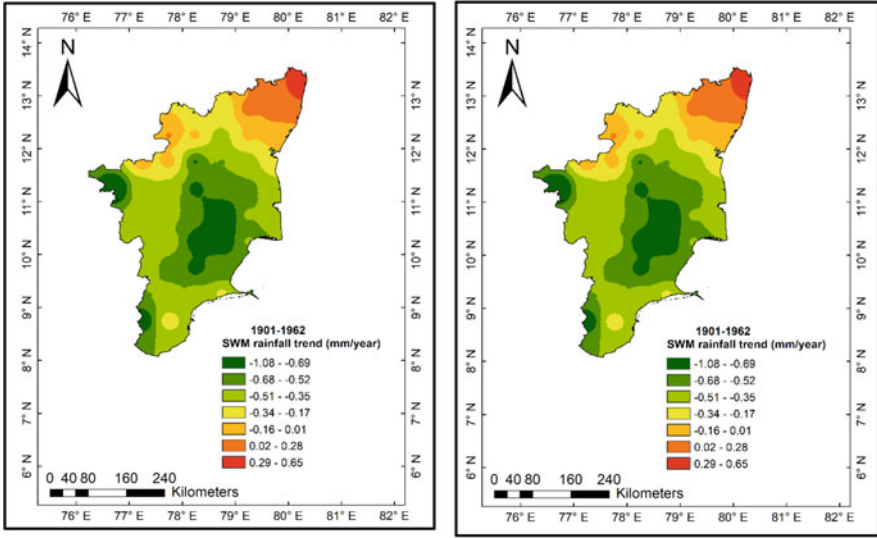
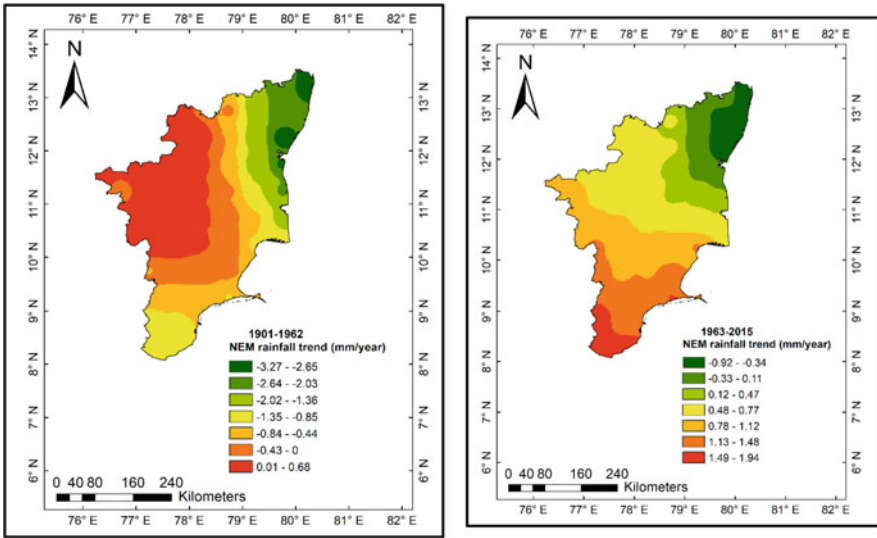**Fig. 17.7** SWM rainfall trend for the periods 1901–1962 and 1963–2015

Fig. 17.8 NEM rainfall trends for the periods 1901–1962 and 1963–2015

The collective effects of NEM and SWM are clearly seen in the annual rainfall trend, as could be seen from Fig. 17.9. In the first part of the series, only the western fringes exhibited an insignificant increasing trend and the rest part of the state exhibits a decreasing trend; the northeastern part of TN showed a significant decreasing trend. Even for the second half of the series (1963–2015), the
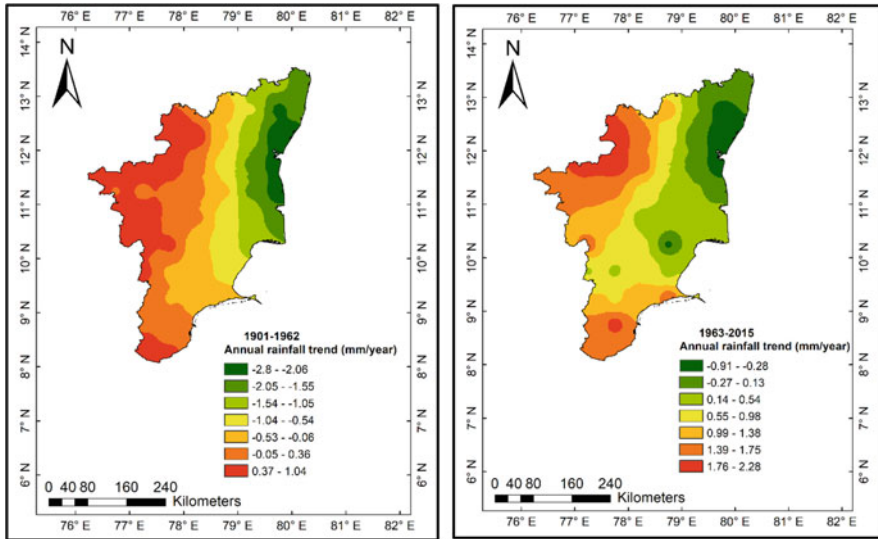
Fig. 17.9 Annual rainfall trends for the periods 1901–1962 and 1963–2015

northeastern part of TN showed a decreasing trend when compared to other areas of the state. Due to the majority of grids exhibiting a negative trend in the SWM, the justification for the overall annual trend to be insignificantly increasing is acceptable.

Grids #24 and 30 show more than a 10% increase in case of both SWM and NEM during 1963–2015. Grids in the southeast coastal region and northwestern region (#4, #24, #30, #31, and #36) witness more than a 10% increase in change, and grids in the central and north coastal regions (grids #15, #29, #34, #35, #39, #40, #43, and #45) exhibit less than 10% decrease in change for annual rainfall during 1963–2015. For SWM series, grids in the northwestern region (grids #24 and #30) and southern regions (grids #2, #6, #9, #10, #11, and #15) exhibit more than 10% increase and decrease in change, respectively. For NEM, the grids covering the full extent of Western Ghats (grids #1, #3, #8, #12, and #23) show more than 10% changes, and the grids in the north coastal regions (grids #34, #35, #39, #40, and #42–45) exhibit a decrease in percentage change. Maximum percentage increasing change and maximum decreasing percentage change in annual rainfall are found at grids #36 (13.79% during 1963–2015) and #40 (−14.37 during 1901–1962), respectively.

Trend Analysis of Mean Rainfall Data Over Entire Tamil Nadu

To examine the trend analysis of mean annual and seasonal rainfall data over the entire Tamil Nadu, data were prepared by considering all the grids for the three time periods 1901–2015, 1901–1962, and 1963–2015. MK test, Sen's slope test, and % change were experimentally performed for the three periods, and results are given in Table 17.9.

Table 17.9 Results of trend analysis of mean rainfall data for three time periods 1901–2015, 1901–1962, and 1963–2015

Series	Mean	MK-Trend	Sen's slope	% Change
(i) 1901–2015				
Annual	1044.75	1.08	0.45	4.97
Winter	36.73	−2.75	−0.20	−61.84
Summer	137.80	−0.08	−0.01	−0.50
SWM	383.42	0.99	0.25	7.46
NEM	486.79	1.06	0.37	8.71
(ii) 1901–1962				
Annual	978.76	−0.47	−0.47	−2.97
Winter	41.73	−0.35	−0.07	−1.08
Summer	138.55	2.41	0.69	30.88
SWM	353.53	−0.46	−0.21	−3.61
NEM	444.95	−1.01	−0.81	−11.34
(iii) 1963–2015				
Annual	1065.44	0.56	0.82	4.07
Winter	28.47	0.51	0.11	20.51
Summer	132.17	0.85	0.24	9.53
SWM	396.71	0.07	0.15	2.01
NEM	508.09	0.44	0.59	6.17

A statistically insignificant increase in trend was found in annual, SWM, and NEM series for the entire state during 1901–2015. There is a statistically insignificant decrease in trend for annual, winter, SWM, and NEM series during the period 1901–1962, and the trend got reversed with an insignificant increase in trend during 1963–2015. A marginal increase of 2.01% and 6.17% is witnessed for SWM and NEM, respectively, during the second period. Though a 20% increase in winter rainfall is observed during 1963–2015, it has no impact on the water resource potential of TN since its contribution is only 3.37% of the annual mean. A marginal increase of 4.97% is observed for the annual series, and a steep decrease (−61.84%) is found for the winter series from 1901 to 2015 for the entire Tamil Nadu.

Rainfall Departure Analysis

Departure analysis is carried out to represent the drought better and understand the drought years. Table 17.10 depicts the departure analysis of rainfall for the 115 years from 1901 to 2015 for TN. Grids #22, #44, and #45 exhibit no rain for a year; 44% of the grids experience scanty rain for a few years, ranging 1–5 years; grids falling near the northeastern coastal belt experience more excess rainfall than other grids, which may be due to the influence of cyclonic precipitation. The number of normal years outweighs the other categories in all the grids. The average values for the entire TN from 1901 to 2015 are 9 excess years, 88 normal years, 18 deficient years, 1 scanty year, and 0 for no rain category.

Table 17.10 Rainfall departure analysis

Grids	Excess	Normal	Deficient	Scanty	No rain
1	4	98	13	0	0
2	6	95	14	0	0
3	2	104	9	0	0
4	12	85	17	1	0
5	6	99	10	0	0
6	7	91	16	1	0
7	11	85	17	2	0
8	2	103	10	0	0
9	5	96	14	0	0
10	9	89	15	2	0
11	8	88	17	2	0
12	3	101	11	0	0
13	4	93	18	0	0
14	8	88	19	0	0
15	9	85	20	1	0
16	10	87	16	2	0
17	8	93	14	0	0
18	6	92	17	0	0
19	10	87	18	0	0
20	15	84	15	1	0
21	12	84	17	2	0
22	16	78	17	3	1
23	4	96	15	0	0
24	10	83	22	0	0
25	7	91	17	0	0
26	9	90	16	0	0
27	11	87	17	0	0
28	10	85	18	2	0
29	15	79	17	4	0
30	10	80	25	0	0
31	9	85	21	0	0
32	10	85	20	0	0
33	11	84	20	0	0
34	10	89	15	1	0
35	12	81	17	5	0
36	11	81	23	0	0
37	10	83	21	1	0
38	8	90	17	0	0
39	8	84	22	1	0
40	11	82	21	1	0
41	9	87	19	0	0
42	10	84	20	1	0
43	13	79	22	1	0
44	12	78	24	0	1
45	15	71	27	1	1

Conclusion

Precipitation is one of the most important variables that has a major impact on ecosystems and agriculture. Spatial and temporal variability of precipitation was investigated at 45 stations of Tamil Nadu state, India, over the period of 115 years (1901–2015) on an annual and seasonal basis. Seasonal series were prepared based on the guidelines given by IMD, Chennai. In this study, homogeneity and trend analysis were performed for annual and seasonal rainfall series for the entire Tamil Nadu during the period 1901–2015 using CRU 0.5 × 0.5 gridded rainfall data. From Mann–Kendall test, four grids of annual series, six grids of SWM series, and seven grids of NEM series showed a significant increasing trend. In winter series, 40 grids showed a significant decreasing trend. It is concluded that the grids #32, #33, #36, #37, and #38 have a positive percentage deviation of greater than 10.0 and the grid points #9 and #23 have a negative percentage deviation of lesser than 4.0 in the annual series. The parts of Cauvery delta region and northern coastal region have excess rainfall contribution in the order of more than or equal to 15. In most of the grid points, the number of normal rainfall is more than the other categories. From the percentage difference in mean rainfall over the period of 1901–1962 and 1963–2015, increase in rainfall for annual (8.86 %), SWM (12.22 %), and NEM (14.19%) was observed. Decrease in rainfall for winter (−31.79%) and summer (−4.61%) was realized. The percentages of rainfall contribution for the seasonal series for the entire Tamil Nadu are winter (3.37%), summer (13.98%), SWM (36.26%), and NEM (46.4%). The average annual rainfall of Tamil Nadu is high in southern parts of Western Ghats and northern coastal extent, but it is deficient in southern coastal regions, central regions, and northwestern regions. From the observation, the average annual and seasonal rainfall of Tamil Nadu in mm are annual (1044.75), winter (36.73), summer (137.80), SWM (383.42), and NEM (486.79). From homogeneity analysis, the year 1962 is found as the probable change point period. From the result of percentage change in mean rainfall over the period of 1901–1962 and 1963–2015, it is understood that annual rainfall had increased in the coastal belt of Cauvery delta region and had decreased in the extent of Western Ghats in the second half of the time series. While comparing the period of 1901–1962 and 1963–2015, increase in NEM is witnessed in regions of Western Ghats, increase in SWM is realized in the northwestern regions, and annual rainfall has increased in the southeast coastal region and also in the northwestern region of Tamil Nadu. From the trend analysis of mean rainfall data over entire Tamil Nadu, it is found that there is an overall increase (4.97%) in the annual rainfall during the period 1901–2015. Spatial analysis of precipitation after the change point (1963–2015) showed an increase in NEM and a decrease in SWM for the entire extent of Western Ghats region. It was also observed that NEM had decreased in the north coastal region and showed an increase in the southern coastal belt.

Conflict of Interest On behalf of all the authors, the corresponding author states that there is no conflict of interest.

References

Alexandersson H, Moberg A (1997) Homogenization of Swedish temperature data. Part I: homogeneity test for linear trends. Int J Climatol 17(1):25–34

Amirataee B, Montaseri M (2017) The performance of SPI and PNPI in analyzing the spatial and temporal trend of dry and wet periods over Iran. Nat Hazards 86(1):89–106

Angulo-Martínez M, Beguería S (2009) Estimating rainfall erosivity from daily precipitation records: A comparison among methods using data from the Ebro Basin (NE Spain). J Hydrol 379(1–2):111–121. https://doi.org/10.1016/j.jhydrol.2009.09.051

Bari SH, Rahman MTU, Hoque MA, Hussain MM (2016) Analysis of seasonal and annual rainfall trends in the northern region of Bangladesh. Atmos Res 176:148–158. https://doi.org/10.1016/j.atmosres.2016.02.008

Basistha A, Arya DS, Goel NK (2009) Analysis of historical changes in the Indian Himalayas. Int J Climatol 29:555–572

Beecham S, Chowdhury RK (2010) Temporal characteristics and variability of point rainfall: a statistical and wavelet analysis. Int J Climatol 30(3):458–473

Bisht DS, Chatterjee C, Raghuwanshi NS, Sridhar V (2018) Spatio-temporal trends of rainfall across Indian river basins. Theor Appl Climatol 132(1):419–436

Buishand TA (1982) Some methods for testing the homogeneity of rainfall records. J Hydrol 58:11–27. https://doi.org/10.1016/0022-1694(82)90066-X

Chandniha SK, Meshram SG, Adamowski JF, Meshram C (2017) Trend analysis of precipitation in Jharkhand state, India. Theor Appl Climatol 130(1):261–274

Chang Y, Huang K, Xie M, Deng C, Zou Z, Liu S, Zhang Y (2018) First long-term and near real-time measurement of trace elements in China's urban atmosphere: temporal variability, source apportionment and precipitation effect. Atmos Chem Phys 18(16):11793–11812

Chatterjee R, Gupta BK, Mohiddin SK, Singh PN, Shekhar S, Purohit R (2009) Dynamic groundwater resources of National Capital Territory, Delhi: assessment, development and management options. Environ Earth Sci 59:669, https://www.jstor.org/stable/24104886

Chatterjee S, Khan A, Akbari H, Wang Y (2016) Monotonic trends in spatio-temporal distribution and concentration of monsoon precipitation (1901–2002), West Bengal, India. Atmos Res 182:54–75. https://doi.org/10.1016/j.atmosres.2016.07.010

Dinpashoh Y, Mirabbasi R, Jhajharia D, Abianeh HZ, Mostafaeipour A (2014) Effect of short-term and long-term persistence on identification of temporal trends. J Hydrol Eng 19(3):617–625

Duhan D, Pandey A (2013) Statistical analysis of long term spatial and temporal trends of precipitation during 1901–2002 at Madhya Pradesh, India. Atmos Res 122:136–149. https://doi.org/10.1016/j.atmosres.2012.10.010

FAO (2002) Report of FAO-CRIDA expert group consultation on farming system and best practices for drought-prone areas of Asia and the Pacific region. Food and Agricultural Organisation of United Nations, Central Research Institute for Dry Land Agriculture, Hyderabad

Fu G, Yu J, Yu X, Ouyang R, Zhang Y, Wang P et al (2013) Temporal variation of extreme rainfall events in China, 1961–2009. J Hydrol 487:48–59

Gajbhiye S, Meshram C, Mirabbasi R, Sharma SK (2016) Trend analysis of rainfall time series for Sindh river basin in India. Theor Appl Climatol 125(3):593–608

Goswami BN, Venugopal V, Sengupta D, Madhusoodanan MS, Xavier PK (2006) Increasing trend of extreme rain events over India in a warming environment. Science 314:1442–1444

Goyal MK (2014) Statistical analysis of long term trends of rainfall during 1901–2002 at Assam, India. Water Resour Manag 28:1501–1515

Guhathakurta P, Rajeevan M (2008) Trends in the rainfall pattern over India. Int J Climatol 28: 1453–1469. https://doi.org/10.1002/joc.1640

Harris I, Osborn TJ, Jones P, Lister D (2020) Version 4 of the CRU TS monthly high-resolution gridded multivariate climate dataset. Sci Data 7:1–18. https://doi.org/10.1038/s41597-020-0453-3

IMD (India Meteorological Department) (2017) Terminologies and glossary, http://imd.gov.in/section/nhac/termglossary.pdf (Aug. 5, 2017)

IPCC (2018) Summary for policymakers

Jain SK, Kumar V, Saharia M (2013) Analysis of rainfall and temperature trends in Northeast India. Int J Climatol 33:968–978. https://doi.org/10.1002/joc.3483

Joshi MK, Pandey AC (2011) Trend and spectral analysis of rainfall over India during 1901–2000. J Geophys Res D Atmos 116(D6). https://doi.org/10.1029/2010JD014966

Joshi UR, Rajeevan M (2006) Trends in precipitation extremes over India. National Climate Centre, India Meteorological Department, Pune

Kendall MG (1975) Rank correlation methods. Charles Grifn and Co. Ltd., London

Khatiwada KR, Panthi J, Shrestha ML, Nepal S (2016) Hydro-climatic variability in the Karnali River basin of Nepal Himalaya. Climate 4(2):17

Kocsis T, Kovács-Székely I, Anda A (2020) Homogeneity tests and non-parametric analyses of tendencies in precipitation time series in Keszthely, Western Hungary. Theor Appl Climatol 139:849–859. https://doi.org/10.1007/s00704-019-03014-4

Kumar V, Jain SK (2011) Trends in rainfall amount and number of rainy days in river basins of India (1951–2004). J Hydrol Res 42(4):290–306

Machiwal D, Jha MK (2017) Evaluating persistence and identifying trends and abrupt changes in monthly and annual rainfalls of a semi-arid region in western india. Theor Appl Climatol 128 (3–4):689–708. https://doi.org/10.1007/s00704-016-1734-9

Machiwal D, Gupta A, Jha MK, Kamble T (2019) Analysis of trend in temperature and rainfall time series of an Indian arid region: comparative evaluation of salient techniques. Theor Appl Climatol 136(1):301–320

Malik A, Kumar A (2020) Spatio-temporal trend analysis of rainfall using parametric and non-parametric tests: case study in Uttarakhand, India. Theor Appl Climatol 140(1):183–207

Maragatham RS (2012) Trend analysis of rainfall data: a comparative study of existing methods. Int J Phys Math Sci 2(1):13–18

Meshram SG, Singh VP, Meshram C (2017) Long-term trend and variability of precipitation in Chhattisgarh state, India. Theor Appl Climatol 129:729–744. https://doi.org/10.1007/s00704-016-1804-z

Meshram SG, Singh SK, Meshram C, Deo RC, Ambade B (2018) Statistical evaluation of rainfall time series in concurrence with agriculture and water resources of Ken River basin, Central India (1901–2010). Theor Appl Climatol 134(3):1231–1243

Mishra AK, Singh VP (2010) A review of drought concepts. J Hydrol 391(1–2):202–216

Mohammad P, Goswami A (2019) Temperature and precipitation trend over 139 major Indian cities: an assessment over a century. Model Earth Syst Environ 5:1481–1493. https://doi.org/10.1007/s40808-019-00642-7

Mondal A, Kundu S, Mukhopadhyay A (2012) Rainfall trend analysis by Mann-Kendall test: a case study of north-eastern part of Cuttack district, Orissa. Int J Geol Earth Environ Sci 2(1):70–78

Mondal A, Khare D, Kundu S (2015) Spatial and temporal analysis of rainfall and temperature trend of India. Theor Appl Climatol 122:143–158. https://doi.org/10.1007/s00704-014-1283-z

Pettitt AN (1979) A non-parametric approach to the change point problem. J R Stat Soc 28:126–135. https://doi.org/10.2307/2346729

Piao S, Ciais P, Huang Y, Shen Z et al (2010) The impacts of climate change on water resources and agriculture in China. Nature 467:43–51. https://doi.org/10.1038/nature09364

Pingale SM, Khare D, Jat MK, Adamowski J (2014) Spatial and temporal trends of mean and extreme rainfall and temperature for the 33 urban centers of the arid and semi-arid state of Rajasthan, India. Atmos Res 138:73–90. https://doi.org/10.1016/j.atmosres.2013.10.024

Praveen B, Talukdar S, Mahato S, Mondal J, Sharma P, Islam ARMT, Rahman A (2020) Analyzing trend and forecasting of rainfall changes in India using non-parametrical and machine learning approaches. Sci Rep 10:1–21

Rangarajan S, Thattai D, Yellasiri SRR, Vytla R, Tedla N, Mandalemula B (2018) Detecting changes in annual and seasonal rainfall patterns for Chennai, India. J Hydrol Eng. https://doi.org/10.1061/(ASCE)HE.1943-5584.0001630

Rangarajan S, Thattai D, Cherukuri A, Borah TA, Joseph JK, Subbiah A (2019) A detailed statistical analysis of rainfall of Thoothukudi District in Tamil Nadu (India). In: Water resources and environmental engineering II. Springer, Singapore, pp 1–14. https://doi.org/10.1007/978-981-13-2038-5_1

Rao BB, Chowdary PS, Sandeep VM, Rao VUM, Venkateswarlu B (2014) Rising minimum temperature trends over India in recent decades: implications for agricultural production. Glob Planet Change 117:1–8. https://doi.org/10.1016/j.gloplacha.2014.03.001

Rathod IM, Aruchamy S (2010) Rainfall trends and pattern of Kongu upland, Tamil Nadu, India using GIS techniques. Int J Environ Sci 1(2):109–122

Sa'adi Z, Shahid S, Ismail T, Chung ES, Wang XJ (2019) Trends analysis of rainfall and rainfall extremes in Sarawak, Malaysia using modified Mann–Kendall test. Meteorog Atmos Phys 131(3):263–277

Sarkar S, Kafatos M (2004) Interannual variability of vegetation over the Indian sub-continent and its relation to the different meteorological parameters. Remote Sens Environ 90:268–280. https://doi.org/10.1016/j.rse.2004.01.003

Sathyanathan R, Bhutia SY, Jyrwa KL, Jewel TR (2020) Precipitation analysis for the East and South districts of Sikkim, India. In: IOP conference series: materials science and engineering. https://doi.org/10.1088/1757-899X/912/6/062071

Sen PK (1968) Estimates of the regression coefficient based on Kendall's tau. J Am Stat Assoc 63:1379–1389. https://doi.org/10.2307/2285891

Shifteh Some'e B, Ezani A, Tabari H (2012) Spatiotemporal trends and change point of precipitation in Iran. J Atmos Res 113:1–12

Singh RN, Sah S, Das B, Vishnoi L, Pathak H (2021) Spatio-temporal trends and variability of rainfall in Maharashtra, India: analysis of 118 years. Theor Appl Climatol 143(3):883–900

Smith I (2004) An assessment of recent trends in Australian rainfall. Aust Meteorol Mag 53(3):163–173

Sonali P, Kumar DN (2013) Review of trend detection methods and their application to detect temperature changes in India. Journal of Hydrology 476:212–227, https://doi.org/10.1016/j.jhydrol.2012.10.034

Spearman C (1904) The proof and measurement of association between two things. Am J Psychol 15:72–101

Spearman C (1906) 'Footrule' for measuring correlation. Br J Psychol 2:89–108

Tabari H, Somee BS, Zadeh MR (2011) Testing for long-term trends in climatic variables in Iran. Atmos Res 100:132–140. https://doi.org/10.1002/(SICI)1097-0088(199701)17:1%3C25::AID-JOC103%3E3.0.CO;2-J

Talaee PH (2014) Iranian rainfall series analysis by means of non-parametric tests. Theor Appl Climatol 116:597–607. https://doi.org/10.1007/s00704-013-0981-2

Taxak AK, Murumkar AR, Arya DS (2014) Long term spatial and temporal rainfall trends and homogeneity analysis in Wainganga basin, Central India. Weather Clim Extremes 4:50–61. https://doi.org/10.1016/j.wace.2014.04.005

Thomas J, Prasannakumar V (2016) Temporal analysis of rainfall (1871–2012) and drought characteristics over a tropical monsoon-dominated state (Kerala) of India. J Hydrol 534:266–280

Thomas T, Jaiswal RK, Nayak PC, Ghosh NC (2015) Comprehensive evaluation of the changing drought characteristics in Bundelkhand region of Central India. Meteorol Atmos Phys 127(2): 163–182

Tian Y, Bai X, Wang S, Qin L, Li Y (2017) Spatial-temporal changes of vegetation cover in Guizhou Province, Southern China. Chinese Geog Sci 27:25–38. https://doi.org/10.1007/s11769-017-0844-3

World Bank (2003) Report on financing rapid onset natural disaster losses in India: a risk management approach, Report no. 26844-IN. World Bank, Washington, DC

Xia J, She D, Zhang Y, Du H (2012) Spatio-temporal trend and statistical distribution of extreme precipitation events in Huaihe River basin during 1960–2009. J Geogr Sci 22:195–208. https://doi.org/10.1007/s11442-012-0921-6

Yang P, Ren G, Yan P (2017) Evidence for a strong association of short-duration intense rainfall with urbanization in the Beijing urban area. J Clim 30:5851–5870. https://doi.org/10.1175/JCLI-D-16-0671.1

Yue S, Hashino M (2003) Long term trends of annual and monthly precipitation in Japan 1. JAWRA 39:587–596. https://doi.org/10.1111/j.1752-1688.2003.tb03677.x

Conclusion

In parts of peninsular India and Southeast Asia that have a seasonal monsoon climate (with 4–8 dry months per year), moist and dry deciduous forests thrive. In the past two decades, more than half of all South Asians, or 750 million people, have been affected by at least one natural disaster such as flooding, drought, or cyclones. Based on current trends, losses in the region will average $160 billion annually by 2030. Variability in the annual monsoon season, which delivers more than 70% of South Asia's rainfall, affects farm production as well as aviation, hydropower, urban infrastructure, and tourism. However, there is limited access to weather information tailored to economic sectors. Targeted weather information can save lives, improve the livelihoods of farmers and business owners, and strengthen the resilience of vulnerable communities (World Bank 2020; https://www.worldbank.org/en/programs/south-asia-regional-integration/climate-change). On the international front, India is leading efforts with the International Solar Alliance (ISA), Kigali Amendment to the Montreal Protocol, International Coalition for Disaster Resilient Infrastructure (CDRI), and Leadership Group for Industry Transition to build a smart climate policy. Particularly in the Bay of Bengal regions, the loss of land is damaging economies, agriculture, and habitats, and constricting livelihood opportunities, particularly of the rural poor.

Mangrove covers 75% of tropical coastlines throughout the world and supports around 80 species of flora and 1300 faunal species. However, recently, the mangroves of the Sundarbans region are showing a declining trend globally in terms of biodiversity. The Sundarbans, which is the world's largest mangrove forest, extending from India to Bangladesh, is facing a similar problem. It is observed that the maximum changes in land use and land cover classes had occurred from May to December 2020. In this time frame, the rapid population increase is noticed in the coastal blocks of the Indian Sundarbans region, which is a biological threat to biological diversity. There are many rivers in the Duars and Barind regions of West Bengal and its lowlands which cause severe flooding during the monsoon season. However, due to the changing and complex nature of this flood, it is not

possible to measure and predict it. Various models have been used by many researchers and government policymakers to understand the real causes, nature, and extent of floods. However, various conventional hydrological models do not accurately comprehend the nature and extent of floods.

Saltwater intrusion into the coastal areas is the main directing fact today in India. Due to climate change, coastal areas have become environmentally vulnerable and are affected by several natural hazards, which impacts agricultural productivity, the natural environment, and food safety and results in massive economic loss. The super cyclone Aila affected the southern parts of West Bengal and other regions where Gosaba is a riverine island, where tide and natural phenomenon were occurring gradually. That is why people can change crop production and adopt new strategies for sustainable livelihood. Mangrove is a natural barrier to protect the coastal areas; due to climate change mangrove trees today are much affected, and the results are flood, hazards, environmental degradation, and cropping pattern change. The coastal areas were struggling much from natural environmental conditions. The Pindar basin is situated at the higher ranges of Kumaun Himalaya and comparatively less worked up from a climate change point of view. This basin's main glaciers are Pindari, Kafni, Bidalgwar, Mrigthuni, and Buriagal. The current trend of the surrounding basins shows that a majority of glaciers have sustained a decrease in this area at an accelerating rate. It is evident from the analysis that the average retreat rate of Pindar glacier was higher at 38.19 m/year from 2000 to 2010 but reduced to 55.41 m/year during 2010–2018. Also, due to climate changes and human interference into the river systems, flood risks have also increased. Flood losses can be reduced by proper floodplain management.

The scientific consideration of wetland services has exploded, but few studies have been conducted on wetland ES and ES for conservation and management. Wetland types and locations will be necessary to strengthen the basis for decision-making for conservation and management aspects. Apart from government regulation, an improved monitoring method is required to raise awareness of the physical, chemical, and biological characteristics of the wetland assets in India. Also, creating awareness about wetlands will create a better understanding and management of wetlands. The main challenge in the assessment of climate change impacts on the estimation of extreme rainfalls (ERs) for urban drainage systems design is how to establish the linkages between the climate projections given by global climate models (GCMs) at global scales and the observed extreme rainfalls at the affected areas in India. In this book, many researchers have applied some approaches of design standards of climate change mitigation and adaptation options that are based on the historic climate information only, but under changing climate and nonstationary extreme rainfall intensity hydrological engineers, planners, and various stakeholders need to understand the possible effects of developing suitable management decisions for the future.

Despite several steps in a positive direction, India's efforts are widely seen as a long way from the drastic measures needed to respond to the climate emergency. India is the only major country to be on track to achieve its targets set out in the landmark Paris Climate Agreement, according to the UN Environment

Program's Emission Gap Report. For instance, India plans to reduce the emissions intensity of GDP, the volume of carbon emissions emitted for every unit of GDP, by around 35% by 2030 from 2005 levels. India emits about 3 gigatonnes (Gt) CO_2 eq of greenhouse gases each year, about two and a half tons per person, which is less than the world average. The country emits 7% of global emissions. The Indian government has been trying to address the problem through the National Action Plan and State Action Plans on Climate Change. These Action Plans aim to work through eight missions covering agriculture, habitat, energy efficiency, water, afforestation, the Himalayan ecosystems, solar energy, and strategic knowledge.